DIRECT DESIGN OF

REINFORCED CONCRETE SLABS

A study of the Ultimate and Serviceability Behaviour of

R.C. Slabs and Slab-Beam Systems Designed

Using Elastic Stress Fields

by

ABDEL WAHID HAGO MOHAMMED

A Thesis Submitted for the Degree of

Doctor of Philosophy

Department of Civil Engineering

University of Glasgow

May, 1982

بسم الله الرحمن الرحيم

By the name of Allah, the Compassionate, the Merciful.

To my Parents and my family.

C O N T E N T S

ACKNOWLEDGEMENTS

The work described herein was carried out in the Department of Civil Engineering at the University of Glasgow, under the general guidance of Professor A. Coull. The author would like to express his appreciation to Professor Coull, and to Professor H. B. Sutherland for the facilities of the department.

The author is indebted to Dr. P. Bhatt for his valuable supervision, encouragement and advice throughout the course of this study.

Grateful thanks are also due to:-

Dr. P. D. Arthur, Senior Lecturer in Civil Engineering for his help with the concrete mixes.

Dr. W. Duncan, Lecturer in Civil Engineering - University of Strathclyde - for his help with the Computer program.

Dr. D. V. Phillips, Lecturer in Civil Engineering, for his help with the Computer program.

Dr. I. A. Smith, Senior Lecturer, for his help with the data logger.

Mr. J. Thomson, Mr. J. Coleman, Mr. A. Galt and Mr. P. Hawthorn for assisting in the experimental work and for all the tedious work involved in the preparation of the specimens.

Mr. J. Love, Mr. R. Thornton, Mr. W. Thomson and Mr. T. Montgomery for their help in the fabrication of the testing rig.

Mr. I. Todd and Mr. A. Yuill for their help with the electrical connections and the operation of the data logger.

The Staff of the University Library for all the trouble taken in procuring some references on inter library loan system.

Mrs. Carol John for her help with the computer.

The Staff of the Computer Centre.

Mrs. Williamson (Astronomy Department) for the neat typing of the thesis.

My wife Eitidal and my daughter Amal for their cooperation and moral support.

The Sudan Government for the financial support during the period of the research.

SUMMARY

This research work is concerned with the service and ultimate behaviour of reinforced concrete slabs and slab-beam systems designed in accordance with a predetermined stress field. The elastic stress distribution (N_x, N_y, N_{xy}, M_x, M_y, M_{xy}) in the slab at the ultimate load was calculated by the finite element method, using the initial elastic uncracked stiffnesses for the slab.

Design moments (M^*_x , M^*_y) for flexure were based on Wood-Armer equations which were derived from the general yield criterion for orthotropically reinforced concrete slabs given by

$$(M^*_x - M_x)(M^*_y - M_y) = M^2_{xy} .$$

The reinforcement was provided parallel to slab edges.

Design forces (M^*_x , M^*_y , N^*_x , N^*_y) for combined flexure and membrane forces were calculated using a sandwich model. The core of the sandwich was ignored in the design, and the equations of Nielsen-Clark were used to calculate the design forces. In all cases the reinforcement was designed to withstand the design forces using the appropriate uniaxial ultimate limit state of stress.

A nonlinear layered finite element model was used to study the behaviour of the slabs designed by this method, and results were checked against laboratory tests on large scale models with various boundary conditions.

Results indicated that all the slabs designed by this method behaved satisfactorily under service loads. Both deflections and crack widths were within acceptable limits (span/250 for deflections and 0.3 mm for cracks), and crack spread in an evenly distributed

pattern. All slabs recorded failure loads in excess of their design loads. The average enhancement in the design loads for the slabs without edge beams was about 16%, and for slab-beams systems about 48%.

It is then concluded that the proposed method provides designs with good service and ultimate behaviour, with a reserve of strength at least 10% above the design loads.

N O T A T I O N S

A_s	Area of Steel
A_{ct}	Effective area per unit width in tension
A_x	Steel area in x direction per unit width
A_α	Steel area in α direction per unit width
a	Length of a plate
a_1, a_2	Steel areas in principal directions per unit width
a_{max}	Maximum crack spacing
b	Width of a section
b_w	Width of a rib of a beam
C.L.	Centre Line
[B]	The Strain matrix
[D]	The Constitutive matrix
{d}	displacement vector
d	Effective depth
d_n	Depth to the neutral axis
E	Young's modulus
E_c	Young's modulus for concrete
E_s	Young's modulus for steel
E_i	Instantaneous Secant modulus
E_{se}	Secant modulus at peak stress
E'_c	Reduced modulus for cracked concrete
E_x, E_y	Young's moduli in x and y directions in an anisotropic plate
F	Yield function
f_b	Bond stress
f_{bb}	Bearing stress
f_c	Compressive strength of concrete
f'_c	Cylinder compressive strength of concrete
f_{co}	Discontinuity stress
F^{ex}, R^{ex}	Excess & External load vectors
f_u	Ultimate stress

f_{cu}	Cube compressive strength of concrete
f_d	Equivalent biaxial compressive strength of concrete
f_r	Modulus of rupture
f_s	Yield strength of steel in tension
f'_s	Yield strength of steel in compression
f_{st}	Yield strength of steel
f_t	Tensile strength of concrete
f_p	Plastic load increment vector
f_x	Stress in x direction steel
f_y	Yield strength of steel
f_α	Stress in steel laid at angle α to the x axis
G	Shear Modulus
GP	Gauss Point
G_{red}	Reduced shear modulus
h	Plate thickness
H	Torsional rigidity of an anisotropic plate
I	Grid index
I_{cr}	Moment of inertia of a cracked section
I_g	Gross moment of inertia of uncracked section
I_{eff}	Effective moment of inertia of a section
I_1, I_2, I_3	First, second and third invariants of stress
[K]	Stiffness matrix
K_b	Constant to account for the distribution and surface characteristics of bar for the bond stress
K_1,K_2	Principal curvatures at a point on a plate
K_x	Curvature in x direction = $-\frac{\partial^2 w}{\partial x^2}$
K_y	Curvature in y direction = $-\frac{\partial^2 w}{\partial y^2}$

K_{xy} Torsional curvature = $\frac{\partial^2 w}{\partial x \partial y}$

K_t A constant to account for the distribution of tensile stress

K_o Initial stiffness matrix

L Short span length

L_x, L_y Span lengths in X and Y directions

m Ratio between tensile and compressive strengths of concrete

M Bending moment at any stage of loading

M_{cr} Cracking moment of a section

M_p Ultimate moment of a section

M_x, M_y, M_{xy} Applied moment component at a point in Cartesian Coordinates.

M_{el} Design normal moment based on elastic analysis system

M_x^*, M_y^* Design moments in X and Y directions respectively

M_n, M_t, M_{nt} Applied moment components at a point in the n-t Coordinate System

M_n^*, M_t^*, M_{nt}^* Component of resisting moments at a point in the n-t Coordinate system

N_{el} Design membrane force based on elastic analysis

M, N Stress resultants

N.A. Neutral Axis

N_x, N_y, N_{xy} Membrane force components at a point in the Cartesian Coordinate System

N_x^*, N_y^* Design membrane forces in X and Y directions

[P] Load vector

p Mean normal stress

P Total load at any stage of a monotonic loading

P_{cr}	Cracking load
P_d	Design load
$P_{\delta L}$	Service deflection load
P_y	First yield load
P_u	Ultimate load
q	Design uniform load
q_{cr}	Cracking uniform load
q_j	Johansen load
Q_x, Q_y	Shear force components in Cartesian Coordinates
q_{ij}	Intensity of uniform load in element ij
q_x	Intensity of load on x strips
q_y	Intensity of load on y strips
R	Transformation matrix
R_c	Cover ratio
R	Total force imbalance vector
p	
R_u	Flexural rigidity of a section
S_t	Bar spacing in transverse direction
T	Transformation matrix
u	Displacement along the X-axis
v	Displacement along the Y-axis
V	Total moment volume
V_s	Total steel volume
W	Vertical displacement along the Z-axis
W_{max}	Maximum crack width
X,Y,Z	Rectangular Cartesian Coordinates
Z_{xx}	Section modulus
x,y,z	Distances along X,Y and Z respectively
x_1	Depth of stress block

α	Angle of skew
α_{sx},α_{sy}	Moment coefficients
β	Shear retention factor
γ	Mass density
$\{\delta\}$	Nodal displacement vector
δ	Displacement at a point
δ_{cr}	Displacement at the cracking load
Δ	Total displacement at a point
ε	Strain at a point
$\varepsilon_x,\varepsilon_y,\varepsilon_{xy}$	Strain components in Cartesian Coordinates
ε_{cr}	Strain corresponding to a stress of f_t in concrete
ε_p	Peak strain
ε_s	Steel strain
$\{\varepsilon_m\}$	Middle Plane strain vector
$\{\varepsilon_z\}$	Strain vector at a point distant Z from the middle plane of a plate
ε^b	Bending strains components
ε^p	Plastic strain vector
ξ,η	Nondimensional local coordinate system
θ	Angle of principal plane
θ_x	Rotation about X-axis $= -\frac{\partial\omega}{\partial y}$
θ_y	Rotation about Y-axis $= \frac{\partial\omega}{\partial x}$
θ_t	Rotation about t-axis $= \frac{\partial\omega}{\partial n}$
θ_{cr}	Angle of crack
μ	Degree of orthotropy
ρ	Sides ratio of a slab (<1.0)
ε_y	yield Strain

ρ_x, ρ_y	Steel ratios in X and Y directions
ρ_α	Steel ratio in the α direction
σ	Stress at a point
$\sigma_x, \sigma_y, \tau_{xy}$	Stress components in Cartesian Coordinates
σ_1, σ_2	Principal stresses
σ_{eq}	Equivalent stress
σ_o	Mean normal stress
σ_p	Peak stress
τ_{oct}	Octahedral shear stress
ϕ	Bar diameter
χ	Curvature vector

CHAPTER ONE

I N T R O D U C T I O N

Present designs of reinforced concrete slabs are based on Limit States concepts. The object of such designs is to ensure that the structure satisfies the prescribed requirements at any stage of loading. Accordingly, two limit state criteria have to be satisfied by such designs, viz: the ultimate limit state and the serviceability limit state. Most of the existing methods of slabs design, which are based on Limit analysis concepts concentrate exclusively on the ultimate limit state. Thus the main concern of these methods is the ultimate load for the slab, with empirical rules (e.g. span/depth ratio...etc.) to ensure satisfactory performance at the Serviceability Limit State.

According to limit analysis, it is generally difficult to calculate the exact value for the limit load of a reinforced concrete slab. The methods either

(a) Postulate a number of collapse mechanisms compatible with the edge conditions of the slab, and derive the limit load accordingly. The true collapse load corresponds to the collapse mechanism giving the least load. Such methods thus provide an upperbound to the ultimate load. The yield line method for slabs is of this nature.

or (b) Postulate a stress field which is in equilibrium with the externally applied load, and does not exceed the strength of the slab at any point on the slab. Such stress fields are called admissible stress fields. The load corresponding

to an admissible stress field will always be less than or equal to the true collapse load of the slab. Such methods provide a lower bound to the ultimate load. The Hillerborg's Strip Method is of this nature.

An exact value for the true collapse load will obviously exist when the loads obtained by upper and lower bound methods coincide - Upper bound solutions can thus be unsafe, in contrast with those of lower bound, which are always safe.

The basic requirement by this approach is to satisfy the equilibrium and the yield conditions. For concrete slabs, the equilibrium equation to be satisfied (see Chapter 2) is

$$\frac{\partial^2 M_x}{\partial x^2} - 2\frac{\partial^2 M_{xy}}{\partial x\, \partial y} + \frac{\partial^2 M_y}{\partial y^2} = -q \qquad (1.1)$$

where (M_x, M_y, M_{xy}) are the moments components at any point on the slab and q is the load. Unless the Hillerborg's method is employed (Section 2.2.2.2), it is not directly possible to obtain a non-trivial solution to equation (1.1), since it contains three independant variables (M_x, M_y, M_{xy}). However, by adopting linear elastic moment-curvature relationships (section 2.2.1) in equation (1.1) we will have:

$$D_x \frac{\partial^4 \omega}{\partial x^4} + 2H \frac{\partial^4 \omega}{\partial x^2 \partial y^2} + D_y \frac{\partial^4 \omega}{\partial y^4} = q \qquad (1.2)$$

Where D_x, D_y and H are the anistropic stiffnesses of the plate. A solution to (1.2) can be obtained since it involves only one variable. And hence a solution to (1.1) can be found, by using any values for the flexural stiffnesses in the moment-curvature relationships. Of course different values of these stiffnesses will give different reinforcement patterns. From the ultimate Limit State point of view, all such

distributions are acceptable, since they are all derived from equilibrium considerations, and are followed in design. The major question is which of all these solutions is acceptable and the criterion to be satisfied will be of serviceability and economy.

In the present study, the initial uncracked stiffnesses are used to obtain the elastic stress distribution under the ultimate load. This elastic analysis under the ultimate load will be done using the finite element method. A yield criterion will then be used to provide the necessary strength to resist the predicted stress distribution. Both criteria of Limit analysis for a safe admissible stress field are satisfied in this way, and accordingly the method is expected to yield a lower bound on the ultimate load, with minimum reserve of strength.

Since the design will be based on the ultimate limit state, it becomes essential to check on the serviceability of the slabs designed by this method. A nonlinear layered finite element model will be used to analyse the slab under monotonic loading till failure. Experimental work on large scale slabs will be used to check against the theoretical predictions.

CHAPTER TWO

LITERATURE REVIEW

2.1 INTRODUCTION:

In this chapter, the various methods of reinforced concrete slab design are discussed. In normal practice, loads to which the structure will be subjected are normally known, and it is first desirable to find the stress distribution in the slab for calculating the steel areas. The stress distribution in the slab is dependant upon the geometry, boundary conditions and the state of the material in the slab whether elastic or plastic. Accordingly, the design methods can be classified into two main categories, viz: elastic and plastic methods of design.

The stress distribution can be found by analytical or numerical procedures, and in the latter, both elastic and plastic effects can be conveniently included. The most popular procedure used in obtaining stress distributions is the finite element method. Accordingly, the finite element method, which is used extensively in this study, will also be reviewed.

2.2 METHODS OF SLAB DESIGN

2.2.1 Elastic Methods:

In these methods, classical plate theory is used to obtain the stress distribution. Such methods are adequate for elastic slabs in which shear deformations and inplane effects due restraints at the boundaries can be ignored. In most cases, the first order theory of bending is adopted, with the prerequisite that the lateral deflections should be sufficiently small compared to the slab thickness. The stress distribution obtained using elastic methods satisfies both equilibrium

of stresses and compatibility of deformations.

By considering the equilibrium of forces acting on the slab element in Figure (2.1), with side lengths dx and dy in the x and y directions respectively, the following equilibrium equations can be derived:

$$\frac{\partial Q_x}{\partial x} + \frac{\partial Q_y}{\partial y} + q = 0$$

$$\frac{\partial M_x}{\partial x} + \frac{\partial M_{yx}}{\partial y} - Q_x = 0 \qquad (2.1)$$

$$-\frac{\partial M_y}{\partial y} + \frac{\partial M_{xy}}{\partial y} + Q_y = 0$$

Eliminating Q_x and Q_y between the three equations, they can be combined in one equation of the form

$$\frac{\partial^2 M_x}{\partial x^2} - 2\frac{\partial^2 M_{xy}}{\partial x\, \partial y} + \frac{\partial^2 M_y}{\partial y^2} = -q \qquad (2.2)$$

Equation (2.2) is known as the plate equilibrium equation. The equation can be transformed to one in terms of displacements, by relating the moments to the lateral deflection w through the slab curvatures, and Hook's law for stress and strains. Thus, if Z is the distance of any point normal to the plate middle plane, then

$$\varepsilon_x = -Z\frac{\partial^2 w}{\partial x^2}\ ,\quad \varepsilon_y = -Z\frac{\partial^2 w}{\partial y^2}$$

$$\varepsilon_{xy} = -2Z\frac{\partial^2 w}{\partial x\ \partial y} \qquad (2.3)$$

where ε_x, ε_y, ε_{xy} are the normal and shearing strains at the point in the x,y cartesian system of coordinates. And from Hook's law, the stresses σ_x, σ_y, τ_{xy} are related to strains by

$$\sigma_x = E_x \varepsilon_x + E_{x1} \varepsilon_y \qquad (2.4)$$

with similar expressions for σ_y and τ_{xy}. The moments are given by

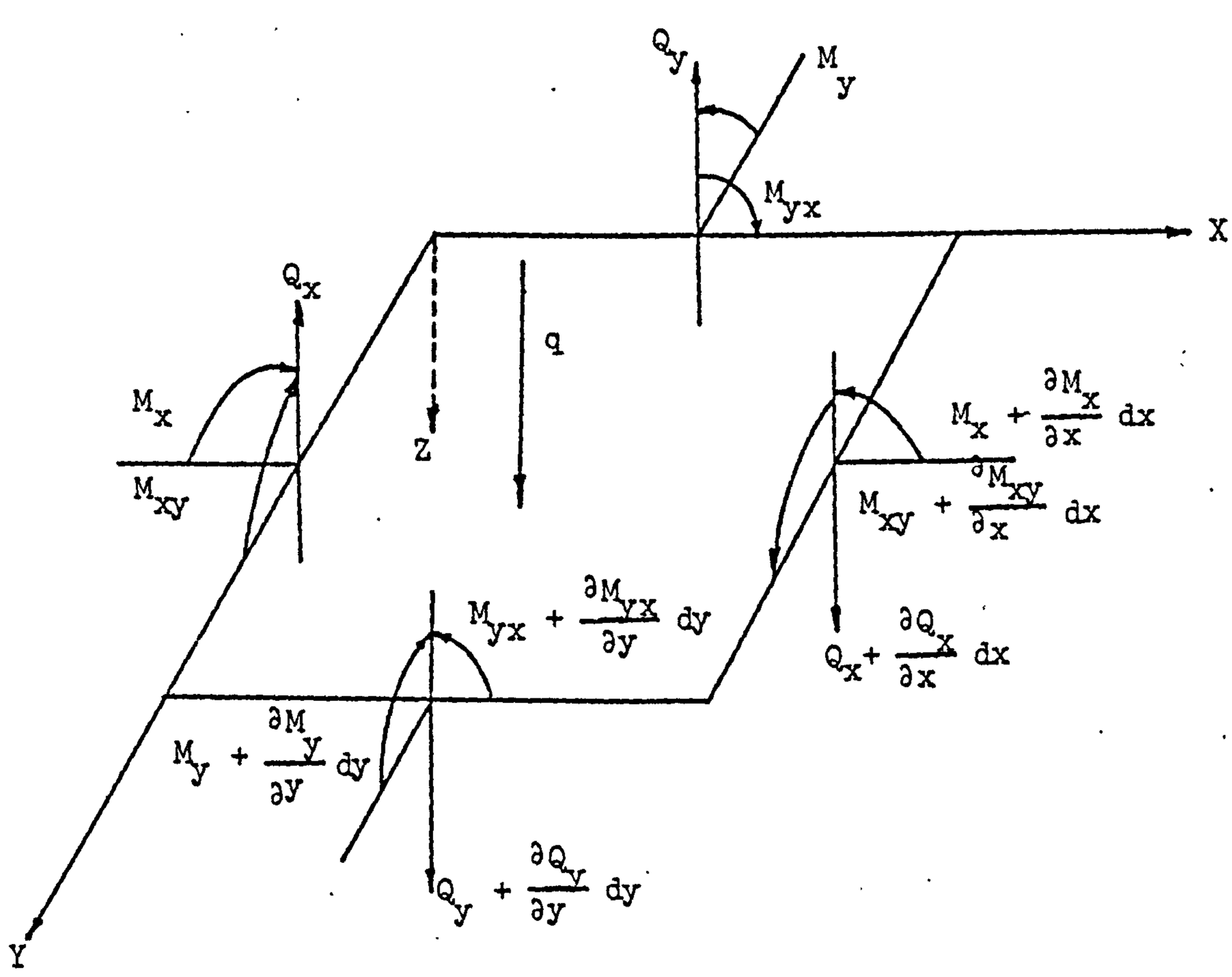

Figure (2.1) Equilibrium of a slab element

$$M_x = \int_{-h/2}^{h/2} \sigma_x \, z \, dz$$

where h is the thickness of the plate.

$$\therefore \quad M_x = -\int_{-h/2}^{h/2} \left(E_x \frac{\partial^2 w}{\partial x^2} + E_{x1} \frac{\partial^2 w}{\partial y^2}\right) z^2 dz$$

$$= -\left(D_x \frac{\partial^2 w}{\partial x^2} + D_1 \frac{\partial^2 w}{\partial y^2}\right) \qquad (2.5)$$

Similarly

$$M_y = -\left(D_y \frac{\partial^2 w}{\partial y^2} + D_1 \frac{\partial^2 w}{\partial x^2}\right)$$

$$M_{xy} = -M_{yx} = 2 D_{xy} \frac{\partial^2 w}{\partial x \, \partial y}$$

in which

$$D_x = \frac{E_x h^3}{12}, \quad D_y = \frac{E_y h^3}{12}$$

$$D_1 = \frac{E_{x1} h^3}{12}, \quad D_{xy} = \frac{G h^3}{12} \qquad (2.6)$$

Substituting expressions (2.5) in the equilibrium equation (2.2), we obtain

$$D_x \frac{\partial^4 w}{\partial x^4} + 2(D_1 + 2D_{xy}) \frac{\partial^4 w}{\partial x^2 \partial y^2} + D_y \frac{\partial^4 w}{\partial y^4} = q \qquad (2.7)$$

introducing the notation

$$H = D_1 + 2 D_{xy}$$

we obtain

$$D_x \frac{\partial^4 w}{\partial x^4} + 2H \frac{\partial^4 w}{\partial x^2 \partial y^2} + D_y \frac{\partial^4 w}{\partial y^4} = q \qquad (2.8)$$

In the particular case of isotropy we have

$$E_x = E_y = \frac{E}{1 - \nu^2}, \quad E_{x1} = \frac{\nu E}{1 - \nu^2}$$

and $$G = \frac{E}{2(1+\nu)}$$

and (2.8) reduces to

$$\frac{\partial^4 w}{\partial x^4} + 2 \frac{\partial^4 w}{\partial x^2 \partial y^2} + \frac{\partial^4 w}{\partial y^4} = q/D \qquad (2.8a)$$

where $D = \dfrac{E h^3}{12(1-\nu^2)}$.

Thus if a solution to (2.8) can be found, then the stress distribution is readily obtained from the moment-curvature relationships, equations (2.5). Such an approach is quite common to both the approximate analytical procedures, and to the numerical methods of finite differences and finite elements.

In the analytical procedures, the deflected surface of the plate is represented by either a double infinite Fourier series (Navier Solutions), or by a single infinite sine series (Levy's solutions)[1]. A detailed account of such methods can be found in text books on Plate Theory[1,2].

The concept of energy solutions applied to plates was developed by Ritz based on the principle of minimization of the total potential. The solutions are usually of series solution form, but here more freedom in selecting the series type is given, as long as the function satisfies the boundary conditions of the problem. Coefficients for the successive terms in the series are selected to minimize the total potential in the system. The Galerkin method of solution falls within this general class. The terms in the series may be polynomial or trigonometric, and sometimes, Bessel and Hankel functions have been used[3]. The discovery of suitable series solutions which satisfies both the boundary conditions and approximates the deflected shape has been generally difficult.

An alternative to these analytical procedures for the solution of the plate equation is the use of the numerical method of the finite differences. The method replaces the fourth order partial differential equation of the plate by a series of linear simultaneous algabraic equations

in the deflections at a finite number of points on the slab. Once the deflections at these grid points are found, moments can be obtained from equations (2.5), by replacing the curvatures by its equivalent finite difference operators. The derivation of the method and its application can be found elsewhere [1,2,3,4]. The accuracy of the finite difference solutions depends on the number of grid points used, the larger the number, the better the accuracy obtained. Accordingly, the number of simultaneous equations increases, and thus, requires a large space in the computer, even for small problems. The effort involved in setting these equations also increases, and the method is difficult to automate.

For the design engineer, all the methods described are inappropriate, and simplified methods have always been resorted to, unless of course design tables and charts are available. The simplified methods generally approximate the slab to a set of parallel beams, and thus the load is carried by bending action, in which torsional moments are ignored. Compatibility is only approximately satisfied. For a uniform load q, the proportions of the load carried by orthogonal strips in x and y directions are such that

$$q_x + q_y = q \qquad (2.9)$$

The actual distributions q_x and q_y are determined by the compatibility of deflections at the centre strips. Thus using simple beams deflections:

$$\frac{5}{384}\,\frac{q_x L_x^4}{E_x I_x} = \frac{5}{384}\,\frac{q_y L_y}{E_y I_y} \qquad (2.10)$$

and assuming equal flexural rigidities in the two strips, and solving (2.9) and (2.10), we have

$$q_x = \left[\frac{L_y^4}{L_x^4 + L_y^4} \right] q \qquad (2.11)$$

and

$$q_y = \left[\frac{L_x^4}{L_x^4 + L_y^4} \right] q \qquad (2.12)$$

The bending moments in the x and y directions can thus be obtained as for simple beams:

$$M_x = q L_x^2 \left[\frac{L_y^4}{8(L_x^4 + L_y^4)} \right] = \alpha_{sx} q L_x^2$$

$$M_y = q L_x^2 \left[\frac{L_x^2 L_y^2}{8(L_x^4 + L_y^4)} \right] = \alpha_{sy} q L_x^2 \qquad (2.13)$$

Coefficients α_{sx} and α_{sy} corresponding to the bracketed terms in (2.13) can be evaluated for various side ratios, and are given in Table 12 of Cp 110[5].

The method is known as Rankine-Grashof method, and applies to rectangular simply supported slabs under uniform loads. For concentrated loads, loads are assumed to be distributed over a finite area, and similar analytical procedures are used. The moment distribution depends on the dimensions of the finite area and its sides ratios to be the respective plate dimensions. The method becomes complex if a group of separate concentrated loads are acting. In such cases, superposition principle can be applied.

This section shows clearly the difficulty of obtaining analytical elastic solutions. In most cases, the methods lack generality. The methods are further restricted by the inability to account of plasticity at high loads, and the wide variability of support conditions encountered in practice.

2.2.2 Plastic (or Limit States) Methods:

The assumption of the classical plate theory that the slab material is elastic and homogeneous is limited to low levels of stress. As the load is increased, concrete slabs crack due to the limited strength of concrete in tension, and accordingly, the slab flexural rigidity deteriorates. Cracking induces nonlinearity, and at higher loads, the degree of nonlinearity is increased by plastification of reinforcing steel. To account for these material changes, plasticity theory is used. The plasticity theory assumes that the material of the slab is perfectly plastic, which means that the material of the slab is capable of indefinite plastic straining, once the conditions of yield have been reached.

The plastic methods of concrete slabs design can be broadly classified in two groups - according to the theory of plasticity - viz: upper bound and lower bound methods (Chapter 1). These methods include:-

1. The Yield Line Theory.
2. Hillerborg Strip Method.
3. The Strip Deflection Method.
4. Minimum Weight Designs.
5. Lower Bound Solutions.

of which only the first is an upper bound method.

2.2.2.1 The Yield Line Theory

The yield line theory of slabs was first introduced by Johansen [7,8,9]. The method derives the slab ultimate load based on a pre-postulated failure mechanism. It is assumed that all the reinforcement crossing the yield lines defining the postulated mechanism is yielding.

The shape of the assumed mechanism depends on the slab geometry, support conditions and the type of loading. Several modes of failure are thus possible even for one problem, and according to the theory of plasticity, the correct mechanism which determines the ultimate capacity of the slab corresponds to the one giving the smallest load. The method thus provides an upper bound to the ultimate load, and the designer is forced to seek all possible modes, for correct analysis. This would create some difficulty especially in case of slabs of uncommon shapes.

In spite the method being an upper bound approach, the effects of strain hardening and membrane forces, in general, tend to make the experimental load higher than the calculated ultimate load.

Although the yield line theory applies to any shape of slab, any load and any edge conditions, it is restricted - in practice - to slabs of constant thickness, uniformly reinforced in each of the two mutually perpendicular or skew directions. The method does not give any information on the best steel distribution within the slab, but can be used to analyse a slab with a predetermined distribution of steel. Furthermore, the method provides no information on the slab deflections or cracking at any stage of loading. Prediction of the mechanism with a combination of concentrated loads can be very difficult, especially when uniform loads are also acting.

2.2.2.2 Hillerborg Strip Method:

According to the lower bound theorem of plasticity (Chapter 1), any combination of M_x, M_y and M_{xy} which satisfy the equilibrium equation (2.2) at all points on the slab, and the boundary conditions of the problem, is a valid solution. Hillerborg[13] made use of the

strip action in the slab, and chose his solution so that $M_{xy} = 0$, everywhere in the slab. The load is thus carried by bending action created by parallel strips spanning in two orthogonal directions X and Y. Thus, if α is the proportion of the load carried in the X direction strips, equation (2.2) gives

$$\frac{\partial^2 M_x}{\partial x^2} = \alpha q$$

and

$$\frac{\partial^2 M_y}{\partial y^2} = (1-\alpha)\, q \qquad (2.14)$$

with the proviso that $M_{xy} = 0$.

The factor α is arbitrarily chosen, and can vary throughout the slab, if $\alpha = 1.0$, all the load is carried by bending of x strips, and if equal to zero, then all the load is carried by bending of y strips. Of course, different ways of dividing the load will, however, lead to different reinforcement patterns, although all such solutions are valid, as far as equilibrium is concerned. The designer needs some experience to arrive at the most economical distribution, and in practice, several cases have to be considered.

For rectangular slabs under uniform loads, the method is easy and straightforward. Once the load distribution is determined, each strip acting as a beam, can be designed according to the bending moments in the strip. In cases when the moments are rapidly changing (e.g. strips with discontinuity lines), Hillerborg suggests the use of banded reinforcement based on average moments across the band. Each band is composed of a number of strips. Design on basis of average moments is strictly not in accordance with the lower bound theory, because at ultimate load, the theoretical moments will exceed the ultimate moments of resistance over a part of each band. However,

once yielding occurs, it is reasonable to expect the moments to redistribute themselves. Also, the total available ultimate moment of resistance across a band is equal to the required value[3].

Figure (2.2) is an example of a simply supported square slab under uniform load, and is intended to show some possible load distributions. In this case, two distributions are considered. However, both distributions are valid, but the first distribution is impractical as it requires varying layout of steel. From a design point of view, the second is more suitable, as it gives an even distribution over large areas, and therefore can be recommended from a theoretical as well as a practical point of view, although it requires 12% more steel, than the first distribution.

This simple strip method thus presented is restricted to certain slab problems. For cases involving point loads or supports (flat slabs), the simple strip method utterly fails. Hillerborg suggested the use of what is known as the "Advanced Strip Method"[13]. In this method, the slab is divided into elements bounded by lines of zero shear force. The design moments are the bending moments found throughout the slab which are compatible with zero shear lines, and which are in equilibrium with the applied design loading. The slab can be divided into three different types of elements as shown in Figure (2.3). Element Types (1) and (2) can be designed by the simple strip method. But Type (3) is more complex. Hillerborg uses a radial stress field and secondary load actions to transfer the loads from the element to the column. Finally he achieves his solution by proposing a set of rules for reinforcing the element.

Hillerborg has devoted considerable effort to overcome the problem of point supports by the use of Type (3) elements. Nevertheless,

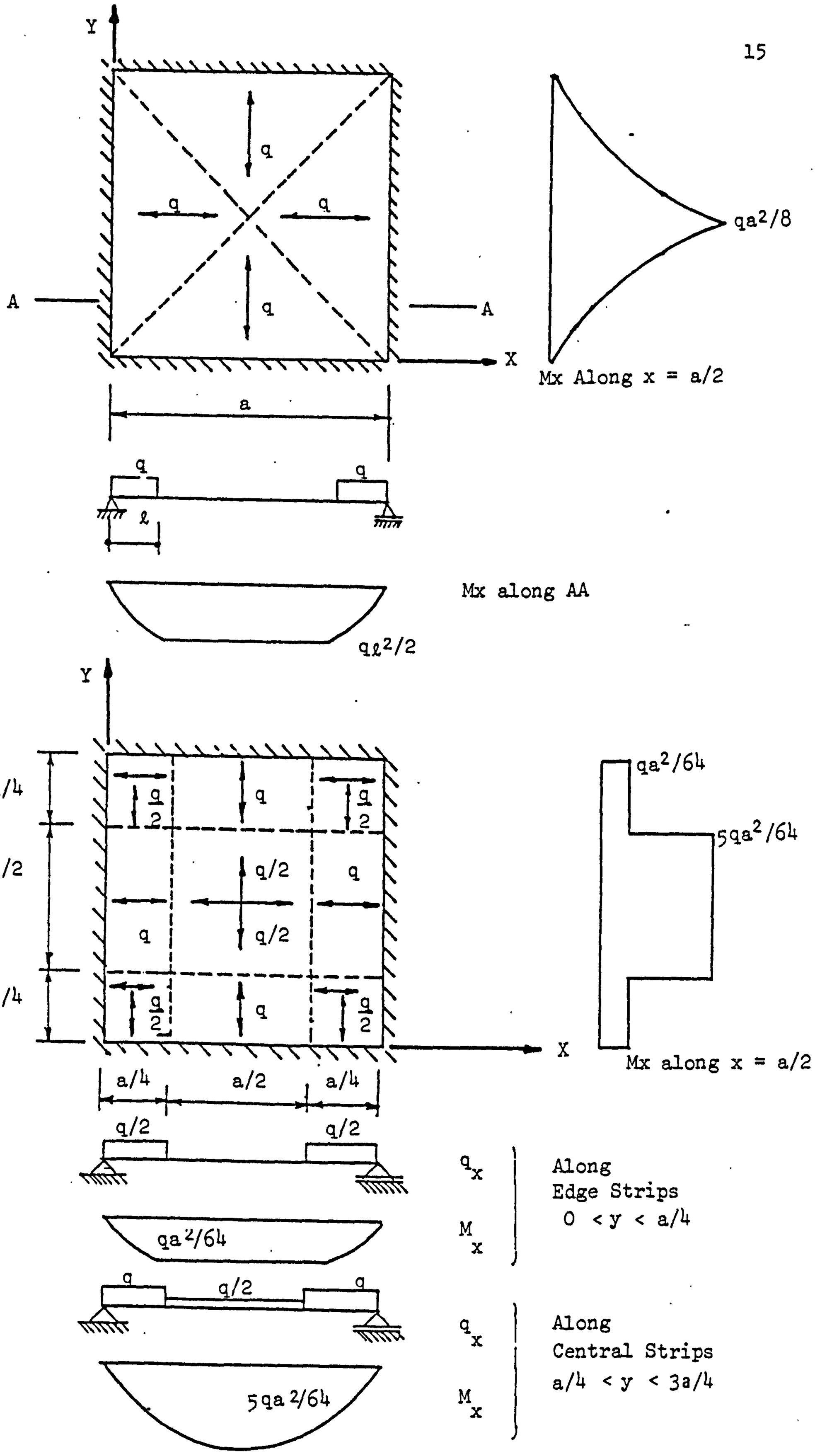

Figure (2.2) Strip Method Solutions for a Simply Supported Slab (13)

the simplicity of the strip method is lost and this approach is not satisfactory as a design procedure. The method as described is for the case of a uniform load within the element, and it will be increasingly difficult to find a suitable stress field for any other type of loading.

A further drawback of the strip method (in general) is that, on pursuit of simple solutions, the designer may choose stress distributions which depart far from those required for a good service behaviour, which impairs the function of the slab at early stages of loading.

2.2.2.3 The Strip-Deflexion Method:

To overcome the difficulty in choosing suitable load dispersion factors α in the strip method, Fernando and Kemp[15] developed the generalized strip-deflection method. The method can be considered as a development of the Hillerborg strip method, in the sense that torsional moments are ignored everywhere on the slab and the load is resisted by bending action created by a set of orthogonal strips.

Considering the rectangular slab under uniform load q shown in Figure (2.4), the slab is first divided into four strips in each direction giving 16 grid rectangles. The load intensity q_{ij} on each grid (ij) must theoretically be uniform, but can vary from grid to another. For any grid (ij), the unknown load distribution in x direction is $(q_x)ij$, and from equilibrium, the corresponding load distribution in the y direction will be $(q_y)ij = q - (q_x)ij$.

Any arbitrarily selected values of such distributions will satisfy equilibrium conditions. However, in the strip-deflection method, one chooses the distributions q_x and q_y by considering compatibility of deflections at points of intersection of the centre lines of the X and

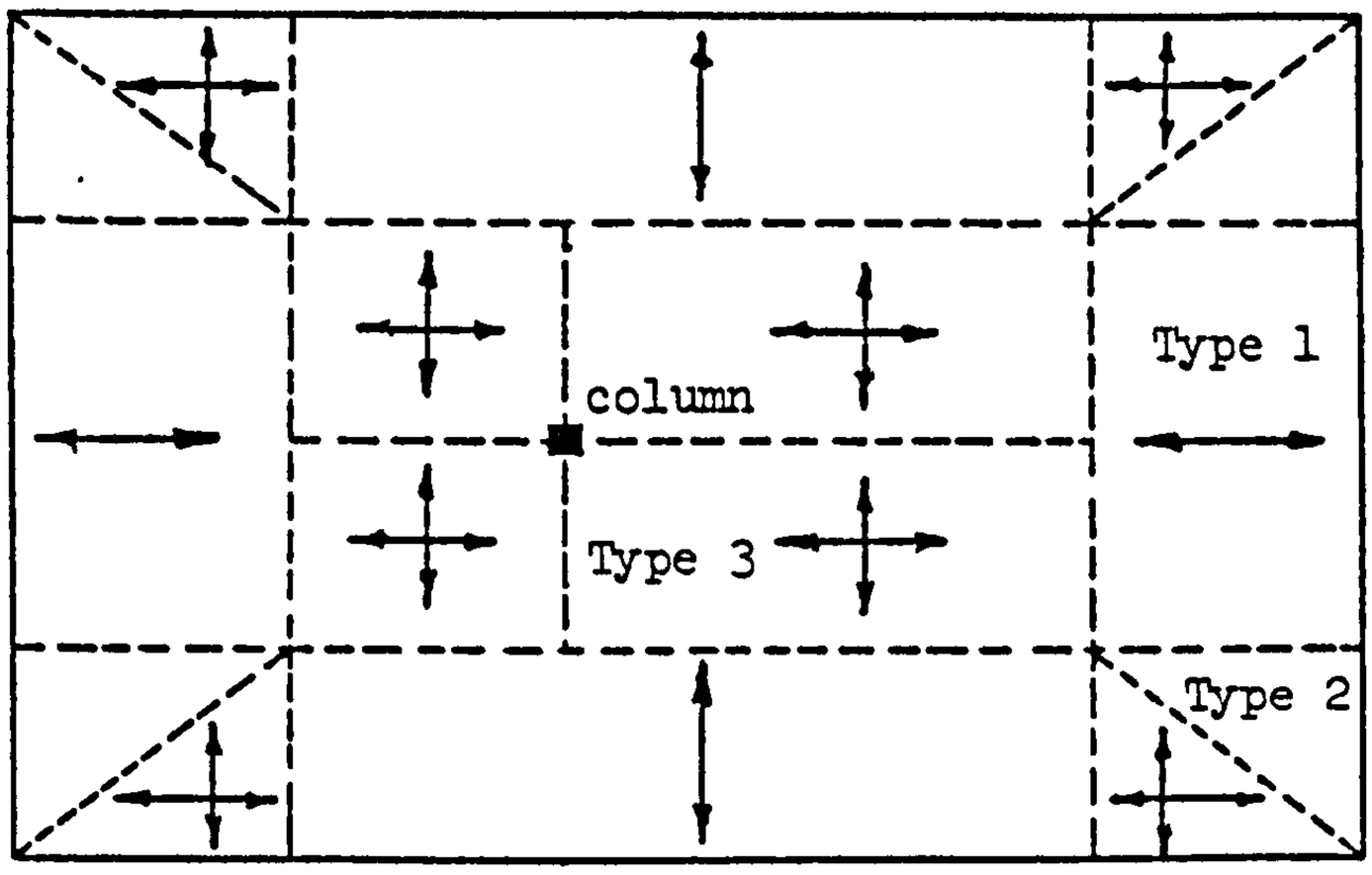

Figure (2.3) Elements Types in the Advanced Strip Method

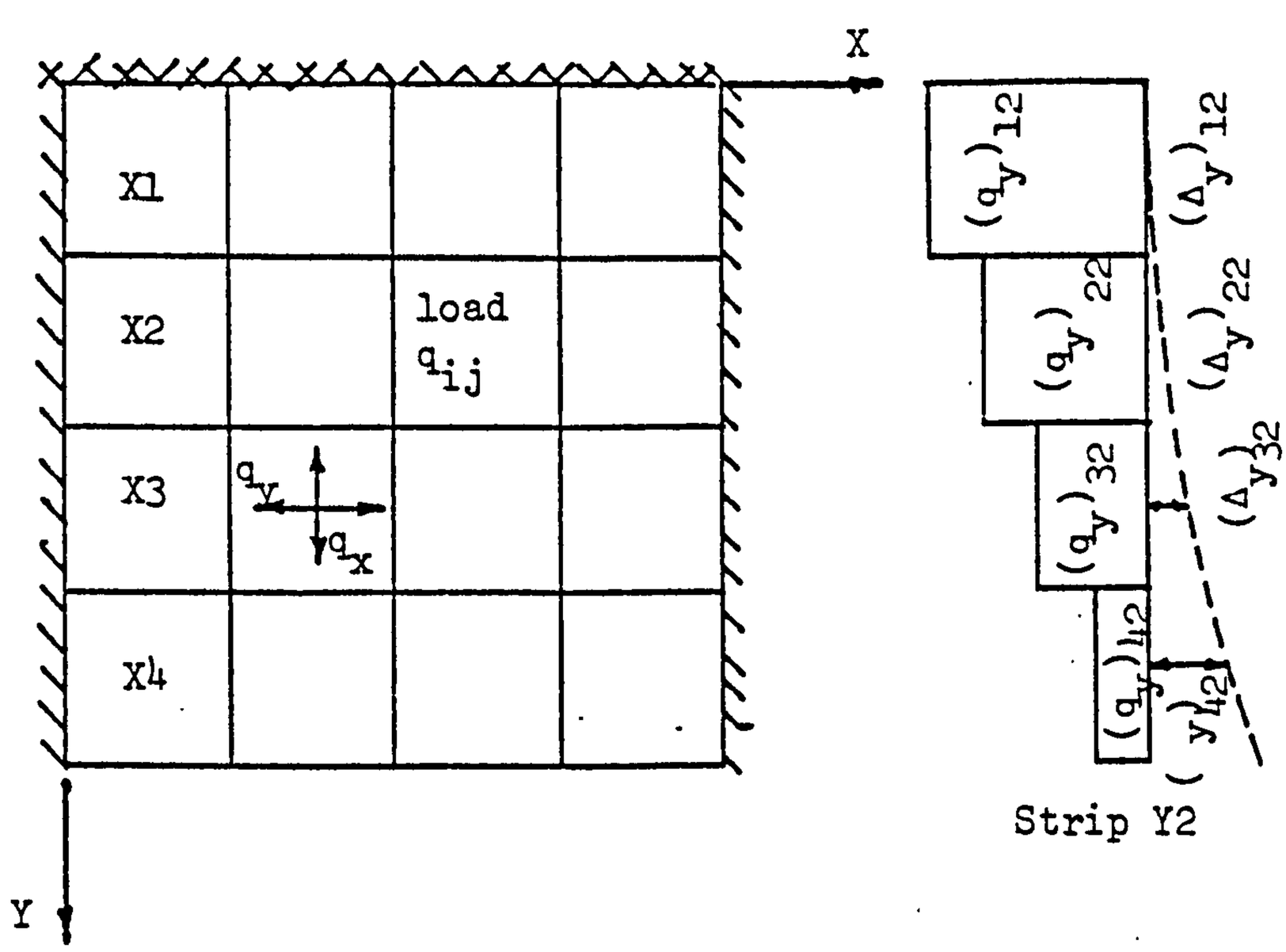

Figure (2.4) The Strip-deflection Method

Y strips. The method uses flexibility coefficients, which are independent of loading, but depend on the geometry and the boundary conditions of the problem. The elastic deflection at the intersection points due to X loading on X strips is obtained from these coefficients as

$$\Delta x_{ij} = \sum_{n=1}^{k} Fx_{in}\, qx_{in} \qquad (2.15)$$

where

Δx_{ij} = the deflection due to x loading on x strips

Fx_{in} = the flexibility coefficient of x strip at node i

qx_{in} = x load on x strips

k = number of intersection points on x strip.

Similar expressions to (2.15) can be written for the deflection at the same points due to Y loading on Y strips. Equating such deflections results in a set of linear simultaneous equations in terms of the load distributions q_x and q_y on each grid element.

For patch loads covering extensive areas of the slab, the strip system can be chosen so that the load is contained within one grid area, and the analysis is identical to that described for uniformly distributed loading. If the loaded area is small, the strip system is chosen so that the concentrated load is centrally positioned within the grid rectangle. It can then be assumed to be uniformly distributed over the whole grid area, and the analysis for load distributions and bending moments would proceed exactly as for distributed loading (Figure (2.5)).

The bending moments so derived do not satisfy equilibrium in the local region of the grid containing the concentrated load due to the initial assumption of spreading the load over the whole grid area. To

obtain an exact solution for the plastic collapse load, additional moments must be added within the grid element containing the concentrated load, using a simple equilibrium spreader system[16].

Such a system is shown in Figures (2.5b) and (2.5c). The concentrated load is first uniformly distributed equally to the two strips AA and BB in Figure (2.5b), giving the bending moments shown within these two strips. The load from the two strips AA and BB is then distributed uniformly to the whole grid area which produces the bending moments shown in Figure (2.5c) within the grid area. By the use of these spreader systems, equilibrium is satisfied within the grid element containing the concentrated load. Additional reinforcement has then to be provided in accordance with the moments in both of the two spreader systems. Similar procedures can be used for concentrated supports.

The method is simple for simple grid numbers, but it requires the formation of special flexibility coefficients dealing with patch loads rather than point loads. In addition, increasing the number of strips improves the accuracy, but at the expense of increasing the number of simultaneous equations to be solved, which renders the method to be computer oriented, and thus the simplicity of the method is lost [17]. The method resembles the grid analogy method and the Rankine-Grashof's method.

The strip methods (both Hillerborg and Fernándo and Kemp) would be unsuitable for cases involving high torsional moments. In such cases, both methods would give solutions which are far from the elastic solutions[18]. The only reason for neglecting torsion in the strip methods is because it leads to a simple procedure for hand

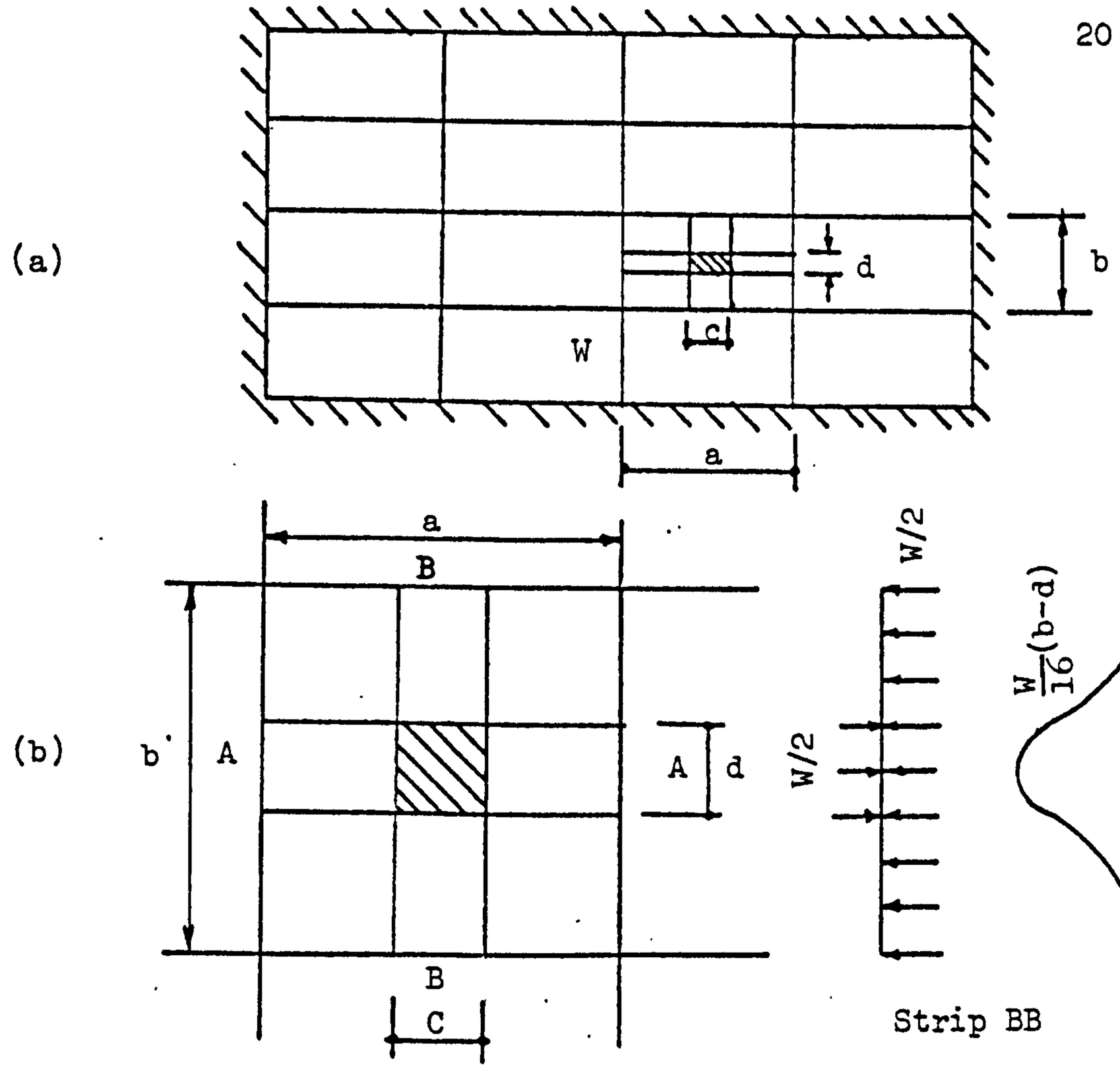

Figure (2.5) Spreader System for Concentrated Loads

calculations. The main disadvantage is that it is difficult to decide the appropriate load distribution factors without jeopardizing the behaviour at working loads. If one has to use a computer program to analyse the slab, the best procedure is to include torsional moments as well, whether the analysis is done by the grid analogy method or the finite element method.

2.2.2.4 Minimum Weight Designs:

By assuming a uniform slab thickness, and neglecting the ability of concrete to resist tensile forces, Morley[10] derived the sufficient conditions for minimum reinforcement in concrete slabs. If a_1 and a_2 are the distributed areas of the reinforcing steel in the direction of the principal moments M_1 and M_2 respectively, then the volume of steel V_s required over an area A is given by

$$V_s = \int_A (a_1 + a_2)\, dA \qquad (2.16)$$

where the steel areas are given by

$$a_1 = \frac{|M_1|}{f_y\, d} \; ; \quad a_2 = \frac{|M_2|}{f_y\, d}$$

where f_y is the yield stress for the steel, and d is the lever arm. Substituting for the steel areas a_1 and a_2 in (2.16) we have

$$V_s = \frac{1}{f_y\, d} \int_A (|M_1| + |M_2|)\, dA \qquad (2.17)$$

Accordingly the steel volume is proportional to the moment volume on the slab. Hence the problem of minimizing the reinforcement reduces to that of finding the minimum volume V which is given by

$$V = \int_A (|M_1| + |M_2|)\, dA \qquad (2.18)$$

A moment field is said to "correspond" if the principal moments M_1 and M_2 and the principal curvatures k_1 and k_2 have the same sign and direction. Morley[10] proved that the moment volume for a corresponding field is less than or equal to that of a non corresponding one. The sufficient conditions can be summarized as follows:

If for a slab a particular moment distribution "0" corresponds to the displacement field which has

(a) The curvatures $|k_1| = |k_2| = K$ throughout except in regions where

(b) $|k_1| = k$, $|k_2| \leq k$ and $M_2 = 0$ or

(c) $|k_2| = k$, $|k_1| \leq k$ and $M_1 = 0$

then that field has a minimum moment volume. The problem of finding such a distribution field is purely geometrical.

In a neutral area where $|k_1| = |k_2| = + k$, it is possible that $M_1 \neq 0$ and $M_2 \neq 0$. M_1 and M_2 can be in any direction and the loads too can be distributed in any direction. For the simply supported slab shown in Figure (2.6) the regions JEH and FKG are such neutral areas.

If $k_1 = - k_2 = \pm k$, the deformation surface is anticlastic, and there is less freedom since for correspondence the loads must be distributed in the directions of the principal curvatures, i.e. for regions such AEJ, loads must be distributed parallel or perpendicular to side EJ as shown, though the ratio of such distributions can be arbitrary.

In the regions where $|k_1| = k$ and $|k_2| \leq k$ the moment M_2 must be zero. The region EFGH is such an example and the loads must be carried only in the direction of k_1 (i.e. EH or FG) and the signs

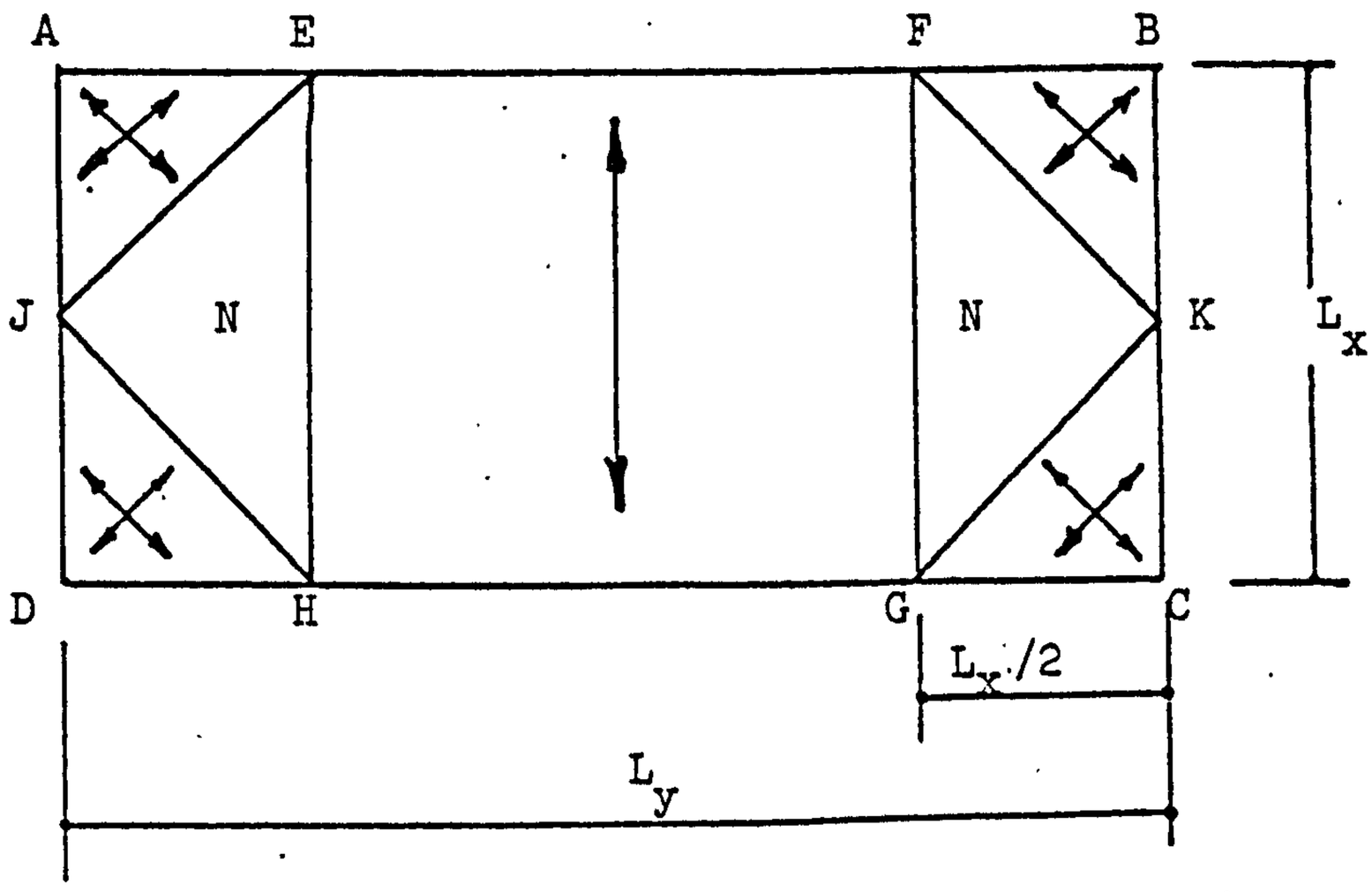

Figure (2.6) Minimum Weight Solution for a Rectangular Simply Supported Slab

of M_1 and k_1 must be the same.

Figure (2.6) shows the solution for the slab ABCD and illustrates the three types of displacement fields which are sufficient for a minimum weight solution. The moment volume due to a uniform load q is

$$V = (0.0834\ L_y - 0.0313\ L_x)\ q\ L_x^3 \qquad (2.19)$$

which reduces to $0.0521\ q\ L_x^4$ or $\frac{5}{96}\ q\ L_x^4$ for a simply supported slab.

The method assumes no constraints on the reinforcement directions. Such methods are likely to be impractical, as they could yield curvilinear reinforcement patterns. The method is also deficient in providing any information on the serviceability of the slab.

2.2.2.5 Lower Bound Solutions:

In this method, simple polynomials in moment components are chosen to fulfil the equilibrium equation (2.2) and the boundary conditions of the problem. To determine the slab ultimate capacity, the moment fields are intuitively assumed. Wood [4] gives a good account of the method and shows how the procedure can be used to determine the ultimate capacity of reinforced concrete slabs. The concept was later extended by Vijaya Rangan [11,12] to cover continuous slabs. In general terms, it has been shown that the collapse loads for such slabs can be written in the form

$$\frac{q\ L_x^2}{M} = (8\ \mu + 2\lambda\rho + 16\rho^2) \qquad (2.20)$$

in which: L_x = short span length of the slab (along the Y-axis)

μ = degree of orthotropy

ρ = sides ratio of the slab = L_x/L_y ,

L_y = Long span,

M = yield moment in the X direction

λ = a constant

The value of the constant λ depends on the sides ratio and the degree of orthotropy μ . The value which satisfies the yield criterion is approximated by

$$\lambda = 4\sqrt{\mu}\ \sqrt[3]{\rho} \qquad (2.21)$$

The collapse load given by (2.20) was compared with the corresponding upper bound solution

$$\frac{q\ L_x^2}{M} = \frac{24\mu}{\left(\sqrt{3 + \frac{2\rho^2}{\mu}} - \frac{\rho\sqrt{2}}{\mu}\right)^2} \qquad (2.22)$$

after the latter has been reduced by 4%, to account for the corner effects. The two solutions agree within 10% of the reduced upper bound solution.

In obtaining the solution (2.20), Vijaya Rangan [11,12] used a truncated sixth order polynomials to define the lower bound moment fields. It is evident from the approach in the paper how difficult it is to obtain such solutions, and they can be produced only for limited cases of end conditions and load combinations. Point loads or supports present great difficulty in selecting simple moment fields. The method has the advantage over the yield line method in that conditions of yield are considered at every point on the slab, and not just at the yield lines. But the method, in addition to the difficulty encountered in obtaining the stress fields, does not provide any information on the serviceability of the slab.

To overcome this difficulty, recently Vijaya Rangan[12] has derived expressions to limit crack widths by choosing the reinforcement diameter and spacing to satisfy the code limits. Deflections can then be limited by a suitable choice of depth.

2.3 ASSESSING SERVICEABILITY OF REINFORCED CONCRETE SLABS:

In the context of limit state design, the two main criteria for design are ultimate strength and serviceability. The latter may, as a first approximation, be related to the slab stiffness. The stiffness of the slab as a function of the load may be obtained in many ways. For design purposes, empirical values may be used. For elaborate analysis, the numerical methods of the finite difference and finite element are employed.

2.3.1 Analytical Procedures:

2.3.1 Deflections:

In a macroscopic slab model in which only flexural failures are permissible, the slab stiffness at any stage of loading is represented by the slope of the moment-curvature diagram of Figure (2.8). Before cracking, the slab material is linear elastic, and hence deflections can be calculated using the elastic theory, with the gross moment of inertia. Ig of the section. After cracking, the behaviour is also approximated by a linear reduced flexural rigidity up to the yield moment. This implies the use of a bi-linear moment-curvature relationship in the working load range. The reduced rigidity after cracking is the fully cracked transformed section rigidity in the Beeby's method[21]. Thus

$$R_u = E'_c I_{cr} \qquad (2.23)$$

where

R_u = The flexural rigidity of the section

$E'_c = 0.57\ Ec$

E_c = Youngs modulus for concrete

I_{cr} = moment of inertia of a fully cracked transformed section.

While in the Branson's method [21], an effective moment of inertia is used. The effective moment of inertia depends of the stage of loading, and is given by:

$$I_{eff} = I_g \left(\frac{M_{cr}}{M}\right)^3 + I_{cr}\left[1 - \left(\frac{M_{cr}}{M}\right)^3\right] \qquad (2.24)$$

where

I_{eff} = Effective moment of inertia

I_g = Gross moment of inertia

M = The maximum applied moment in the span

M_{cr} = The cracking moment.

The cracking moment is calculated from the flexural formula as

$$M_{cr} = f_r I_g / y \qquad (2.25)$$

where f_r = modulus of rupture.

The Branson's method is more realistic than the Beeby's, and hence, it is recommended for use in the ACI Code[3].

The applicability of such methods is well established for reinforced concrete beams and one-way slabs. For two-way slabs, Desayi and Muthu[22] proposed a method for estimating short-time deflections. The load-deflection curve is predicted in two stages: prior to and after cracking. In the uncracked stage, the deflections are calculated using elastic plate theory. Thus

$$\delta = \beta \frac{q\, L_x^4}{E_c\, I_g} \qquad (2.26)$$

where β is a constant depending on the boundary conditions of the problem.

At the initiation of cracking, the deflection δ_{cr} under the cracking load q_{cr} is estimated from

$$\delta_{cr} = \beta \frac{q_{cr} L_x^4}{E_c I_g} \qquad (2.27)$$

After cracking, due to the continuous decay of the flexural rigidity of the slab, an effective moment of inertia can be used. The proposed equation is

$$I_{eff} = I_g \left[1 - k_1 \left(\frac{q - q_{cr}}{q_J - q_{cr}} \right)^{k_2} \right] \qquad (2.28)$$

where q_J is the Johanson load, k_1 and k_2 are constants to be determined. Using the effective moment of inertia after cracking (equation 2.28), the deflection in this range can be calculated as

$$\Delta - \delta_{cr} = \beta \frac{(q - q_{cr}) L_x^4}{E_c I_{eff}} \qquad (2.29)$$

The expression for I_{eff} in (2.28) depends on the constants k_1 and k_2. Experimental results of Desayi and Muthu[22] have shown that

$$k_1 = 0.87761 - 4.1604 \times 10^{-4} X_o \qquad (2.30)$$

$$k_2 = 0.025227 + 8.28 \times 10^{-4} X_o \qquad (2.31)$$

where

$$X_o = (\rho_x + \rho_y)\left(\frac{f_y}{f'_c}\right)\left(\frac{L_x}{L_y}\right)\left(\frac{L_x}{h}\right)^2$$

where

ρ_x and ρ_y = percentage of steel in X and Y directions respectively

L_x , L_y = short and long spans

h = slab thickness

f'_c = compressive strength of concrete

f_y = yield strength of steel

Equations (2.30) and (2.31) are said to be valid in the range $40 \leq x_o \leq 270$.

The method predicts the maximum deflections in two-way reinforced concrete slabs with excellent accuracy, but is restricted in its application to uniformly loaded, uniformly reinforced concrete slabs. Up till now, it is the only method known for estimating deflections of two-way rectangular simple slabs. Recently, the method has been extended to cover fixed slabs by Desayi et al[23]. The method still needs further investigation to cover other types of supports and loading conditions.

2.3.1.2 Cracking:

The problem of predicting the maximum crack width is very complex. Due to its stochastic nature, assessment of crack widths can only be made using empirical means derived using statistical procedures. Although a lot of work has been done and is still continuing, the suggestions for design are far from being conclusive.

At present, two theories are known, which deal with the prediction of crack widths in structural members. These are:-

1. The "Slip" Theory, which assumes that the crack widths depend on the amount of bond slip in the reinforcement. Here crack widths are normally expressed in terms of steel stresses.

2. The "No Slip" Theory which considers the crack width to be effectively zero at the face of the reinforcing bar. Here crack widths are expressed in terms of strains.

Beeby[24] investigated cracking in one-way slabs and concluded that, the "no slip" theory gives better prediction of crack widths. He also found that the crack width and spacing are both linearly related to the distance from the point where the crack is measured to the surface of the nearest bar.

For two-way slabs, extensive work has been done by Orenstien and Nawy[25] and Nawy et al[26]. Their proposed equation to estimate the maximum crack width is

$$W_{max} = k\, R_c \sqrt{I}\ f_s \qquad (2.32)$$

where

W_{max} = The maximum crack width

k = A constant depending on the support conditions, the sides ratios and the type of loading

R_c = Cover ratio = $(h - d_n)/(d - d_n)$

f_s = steel stress

I = The grid index = $\phi S_t/\rho_t$

ϕ = Bar diameter in longitudinal direction.

S_t = Bar spacing in transverse direction

ρ_t = Steel ratio in the longitudinal direction.

d, d_n = effective and neutral axis depths, respectively.

It has been found that the grid index is a good indication in checking whether wide cracks would form or not. Only if the grid index (I) > 160 in^2 the slab would develop a pronounced yield line cracks early in the loading history. Cracks tend to be finer in width for low values of the grid index.

Orenstien and Nawy's equations are restricted to very special cases of uniformly loaded, simply supported, and fixed slabs with central point loads. In their experiments, welded wire meshes were used, which is not the case in most practical situations.

Desayi and Kulkarni[27] also did extensive work on two-way reinforced concrete slabs. On the same principles, Desayi and

Prabhakara[28] extended their work to cover skew slabs. The work rests on estimating the maximum crack spacing at the cracking moment.

Assuming that the reinforcement is laid along the directions 1 and 2, Figure (2.7), then the spacing of the cracks formed in direction 2 is

$$a_1 = \frac{k_t f_t A_{ct_1}}{(\pi \phi_1 k_b f_b/s_1)+(\phi_2 f_{bb}/s_2)} \qquad (2.33)$$

similarly the spacing of the cracks formed in direction 1 is

$$a_2 = \frac{k_t f_t A_{ct_2}}{(\pi \phi_2 k_b f_b/s_2)+(\phi_1 f_{bb}/s_1)} \qquad (2.34)$$

where

A_{ct_1}, A_{ct_2} = Effective area per unit width in tension in directions 1 and 2 = $2(h-d)-A_s$

f_t = tensile strength of concrete

ϕ_1 , ϕ_2 = bar diameters in directions 1 and 2

s_1 , s_2 = spacing between bars in directions 1 and 2

k_t = a constant to account for distribution of tensile stress

f_b = bond stress

f_{bb} = bearing stress

The maximum crack width is then estimated at any stage of loading from

$$W_{max} = a_{max} \varepsilon_s R_c \qquad (2.35)$$

where a_{max} is the maximum crack spacing, ε_s = steel strain at the stage of loading considered, and R_c = the cover ratio as defined in equation (2.32) before.

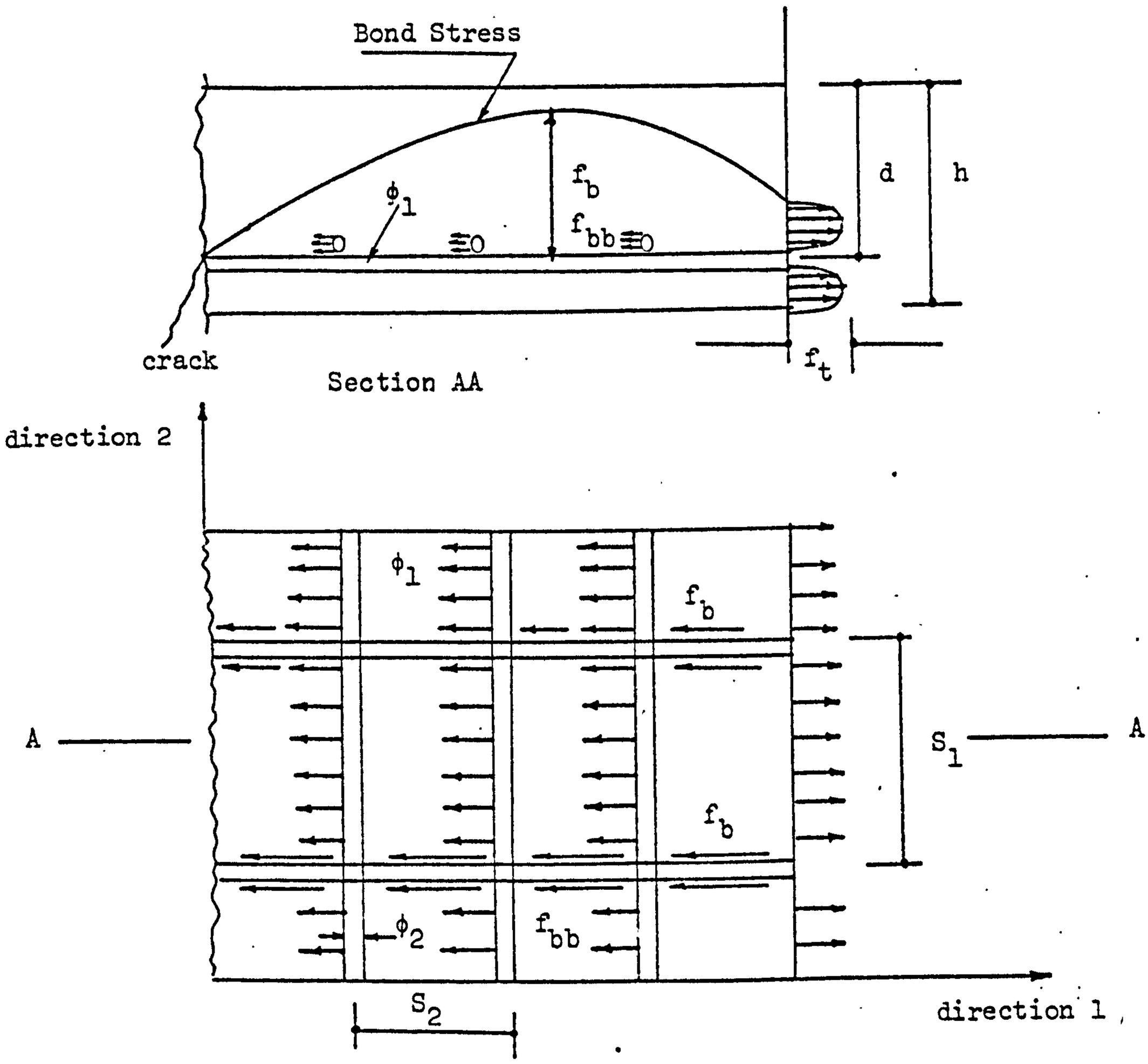

Figure (2.7) Distribution of Bond Stress and Tensile Stress over a Section

Test results have indicated that the constants $k_b = 1.0$, $f_{bb} = \frac{1}{2} f_t$, $f_b = f_{ub} M/M_p$ for rectangular slabs, and f_{ub} = the ultimate bond stress can be taken from CP 110[5] (Section 3.11.6). M and M_p are the applied and ultimate moments in the direction of reinforcement.

The proposed method estimates crack widths with reasonable accuracy. One good aspect of the method is that it is independent of the type of loading and the aspect ratio of the slab. The method is established for simply supported slabs and fixed slabs, and thus needs further investigation to cover other types of supports.

2.3.2 Numerical Procedures:

Deflections and cracking of reinforced concrete slabs can be calculated using the numerical methods of finite difference and finite elements. Due to nonlinearity in material behaviour caused by progressive cracking and yielding of reinforcement, a nonlinear procedure is used in conjunction with these methods. The finite difference had been used to analyse plates by Bhaumik et al[29] and May et al[30] using the Tresca and Von Mises Criteria. Concrete slabs had been analysed using the finite element method, accordingly it will be reviewed here.

2.4 NONLINEAR FINITE ELEMENT MODELS:

To account for nonlinearity due to cracking etc., two types of models are normally adopted, viz. a macroscopic model employing a moment-curvature relationship to reflect stiffness degradation at various stages of loading, or, a microscopic model treating nonlinearities in each constituent material individually as they occur. Such models adopt either uniaxial or biaxial stress-strain properties for plain concrete,

and the uniaxial properties of steel to treat individual nonlinearities arising from progressive microcracking in concrete, yielding of steel, and plastic flow under compressive states of stress in concrete.

2.4.1 Macroscopic Models:

In this case, the reinforced concrete element is assumed to be homogeneous and initially isotropic. For low steel percentages, which is usually the case in reinforced concrete slabs, the reinforcement contributes little to the moment of resistance of uncracked sections[21], thus the assumption is quite logical. In this case, the material behaviour is linear elastic, with the initial elastic matrix derived in the normal way[31].

On the onset of cracking in the element, the stiffness of the element starts to decrease. The new stiffness at any stage of loading can be derived from the moment-curvature diagram shown in Figure (2.8a). Jofriet and McNiece[21] used a bilinear relationship of the type

$$R_u = E_c I_g \qquad \text{prior to cracking} \qquad (2.36)$$

$$R_u = E_c' I_{cr} \qquad \text{after cracking} \qquad (2.37)$$

where $E_c' = 0.57 E_c$.

This method of calculating the rigidity is due to Beeby. In their analysis, they did not consider yielding of steel, and thus, could not give any information about ultimate behaviour.

Macroscopic models were also used by Bell and Elms[6,32]. In their model, the behaviour is idealised by a four stage moment curvature relationship, Figure (2.8a). Using the square yield assumption several intermediate loading surfaces were defined as shown in Figure (2.8b). The point on the moment-curvature curve corresponding to each surface is

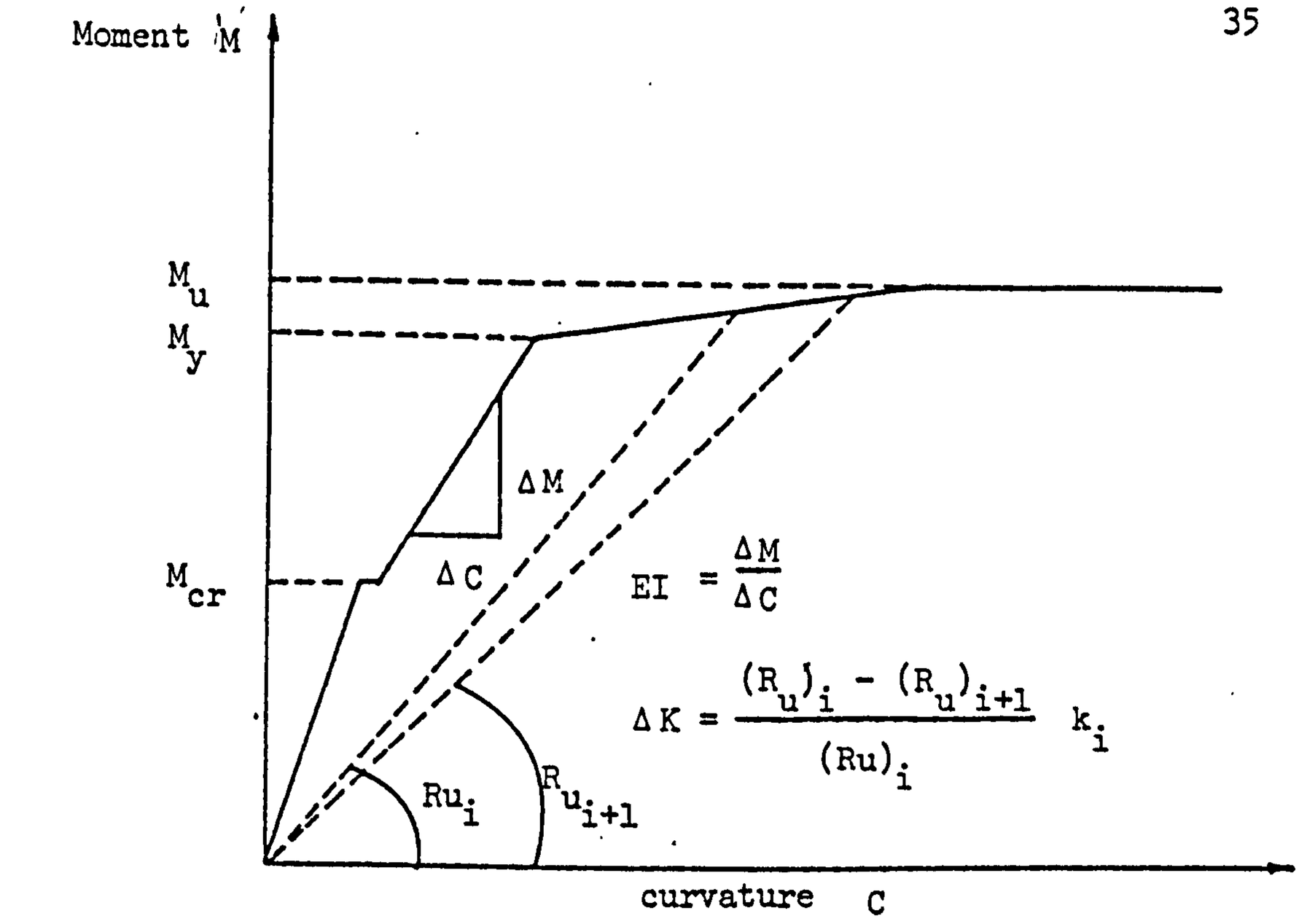

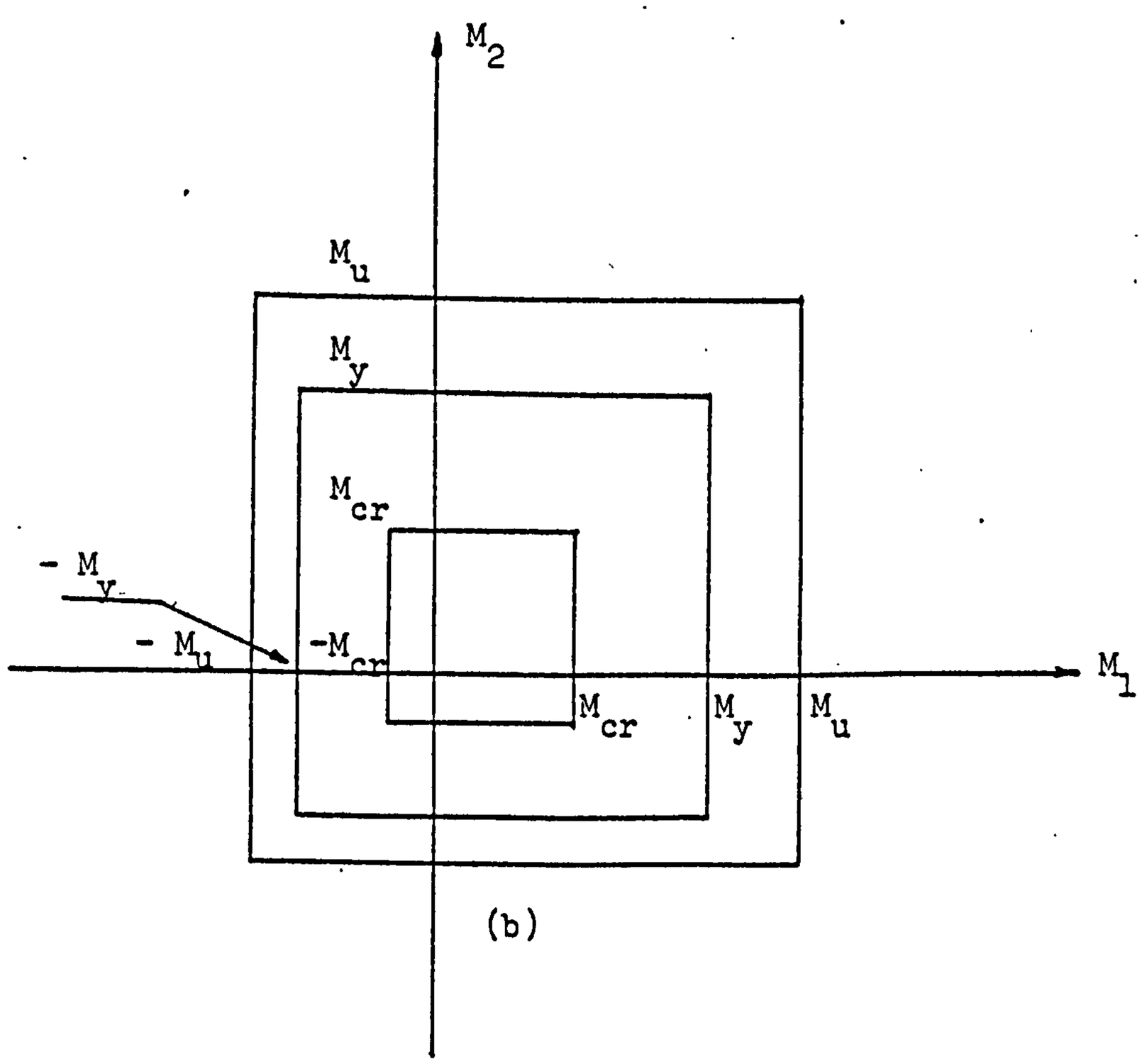

Figure (2.8)(a) - Moment-Curvature Relationship for an Under-Reinforced Section

(b) Square Yield Surfaces

established, and using the relative change of rigidity, the stiffness of an element satisfying a yield criterion is appropriately modified. A secant modulus approach is used in making the stiffness reduction. A direct iteration procedure[31,34] was used in the analysis, in which the structure is solved successively under the load while stiffnesses are changed, until equilibrium is reached.

The use of a moment-curvature relationship is an extension of the elementary theory of bending. The behaviour of concrete is not being investigated in detail, but only treated grossly in the tensile and compressive zones along two principal directions. Furthermore, if reinforcement patterns vary, several moment-curvature curves may be needed for a single analysis. Load enhancement due to biaxial effects, effects of constraints in the plane of the structure, are both neglected. In most elements, the behaviour of the whole element is judged by the state of stress at one point in the element. Recent developments in these models involved the use of numerically integrated high order elements for discretization, so that the variability of material properties within the element can be traced[35]. Although all these models do not reflect the true variation of stress through the slab depth, the response can in most cases be predicted in a satisfactory manner.

2.4.2 Microscopic models:

In such models the slab thickness is divided hypothetically into a finite number of layers parallel to its middle plane, Figure (2.9). Each layer is assumed to be in a state of plane stress condition, and a linear strain variation with the slab depth is assumed for the small deflection theory. Each layer can be of a different material. Thus for a reinforced concrete element, each constituent material is assigned

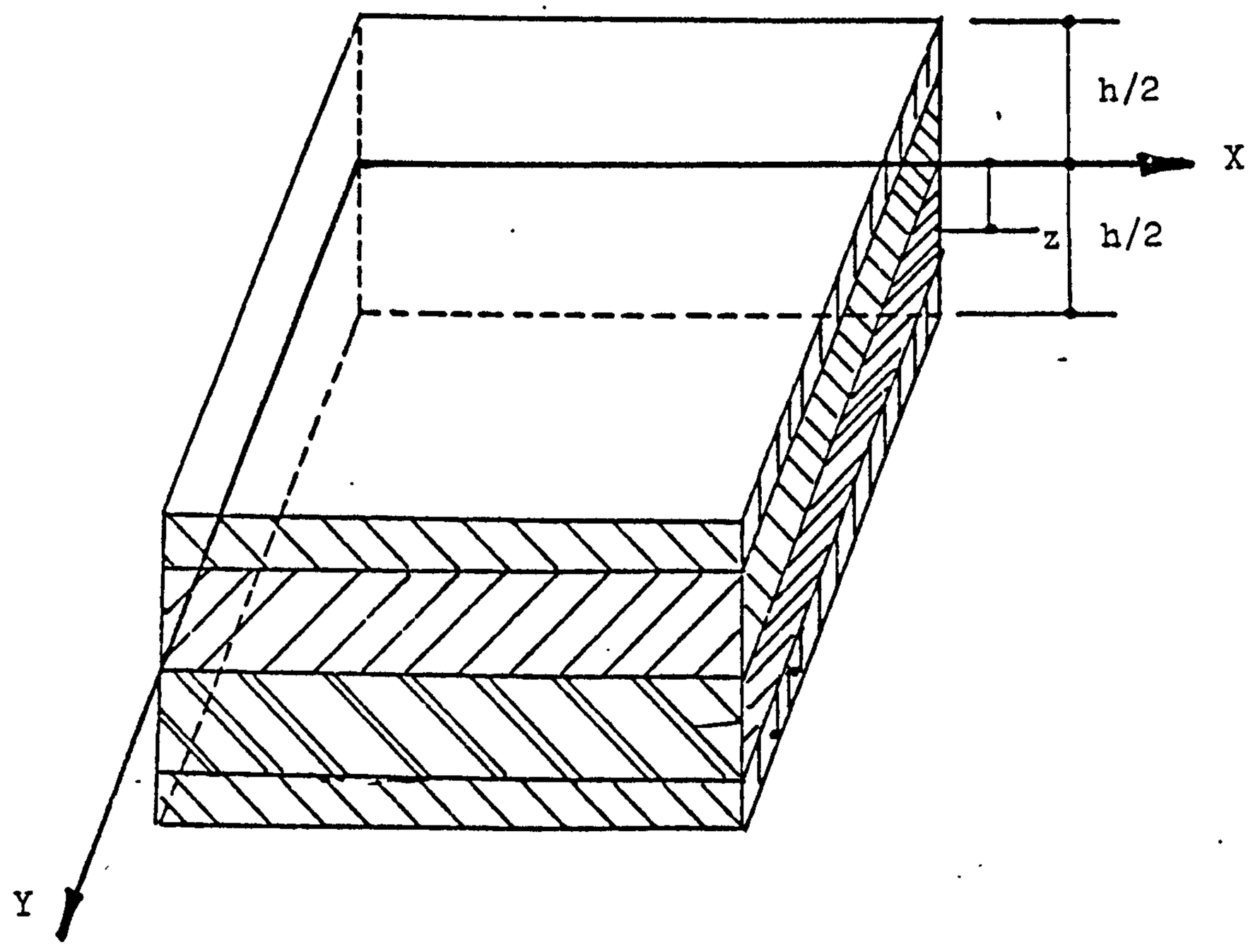

Figure (2.9) Layered Plate Model

a different layer. Perfect bond between all layers is normally assumed, although in some cases, bond slip relations can easily be accommodated.

The deterioration in the slab stiffness is represented by appropriately changing the layers properties, whenever nonlinearities occur. Crack penetration through the slab can thus be conveniently reflected by this model. The basic requirements for this model in analysing plate bending problems are a stress-strain relationships for concrete and steel layers separately, and a yield criterion (Section 2.4.5) for concrete layers, expressed in terms of principal stresses.

2.4.3 Review of Layered Finite Element Models:

Various types of elements have been used by different investigators, and Table (2.1) gives the types of layered elements used, number of degrees of freedom and the reference in each that had been used. All the elements given are two-dimensional, except the one used by Schnobrich[36,37] and Mubbad/Suidan et al[38], which is a three-dimensional numerically integrated isoparametric element. The element computes the shear stresses in planes normal to the plate middle plane in addition to the normal and torsional bending stresses. Accordingly, the element was developed to solve the three-dimensional punching shear failure around columns heads. For such problems, an ordinary two-dimensional element with a plane stress assumption fails to recognize such failures, but is quite good for other problems in which such failures are prevented, and accordingly, the element can only fail in flexure.

All the two-dimensional elements given in Table (2.1) assume that the stress in each layer is constant, and do not allow variations of stress within the element, except the one developed by Rao[39]. The assumption of constant stress is a crude idealization, especially after cracking.

Table (2.1) Layered Plate Bending Elements

No.	Element	Nodal Degrees of Freedom	Total degrees of freedom	References
1	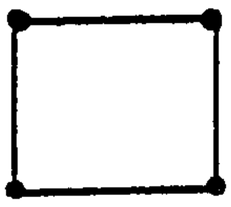	w, θ_x, θ_y	12	40
2	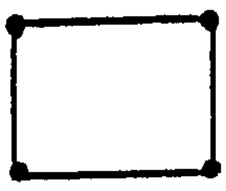	u, v, w, θ_x , θ_y	20	39, 41, 42, 43, 44, 45
3	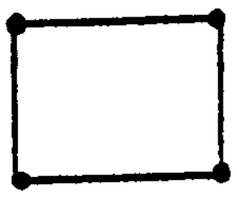	u, v, w θ_x , θ_y Reduced bending stiffness	12	46
4	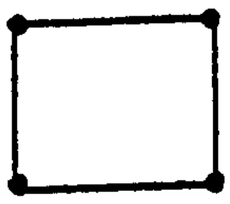	w, θ_x, θ_y k_{xy}	16	47, 48
5	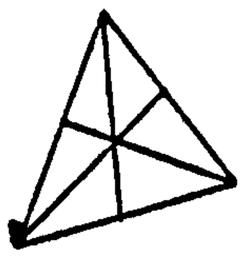	corners: u, v, w, θ_x, θ_y k_x, k_y, k_{xy} Midside nodes: u, v, θ_t	33	49
6	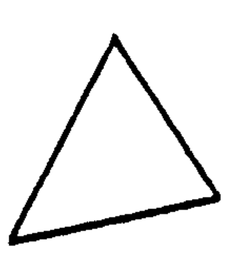	u, v, w, θ_x, θ_y	15	50
7	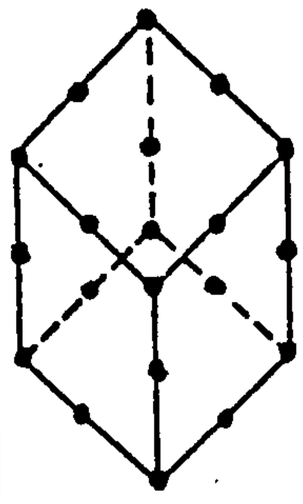	u, v, w three dimensional	60	36, 37, 38

In the finite element models which rely mainly on the released imbalanced forces to simulate stiffness degradation, such an assumption would lead to underestimation of these forces. Because variability of stress is not allowed, convergence problems can arise and in such cases, equilibrium can hardly be satisfied. This problem will be treated in depth in this research.

The first element used by Wegmuller[40] is the simplest, as only three-degrees of freedom per node were used. The element ignores inplane effects, and thus assumes a fixed position for the middle plane of the plate. Such an assumption would be restricted only to problems in which membrane forces are negligible.

For concrete slabs in bending the neutral axis shifts from its initial position towards the compression face due to cracks progressing deeper into the slab depth. The normal procedure adopted in nonlinear layered finite element models, is to simulate this shift by prefixing the position of the neutral axis, and superimposing an inplane action on the section. This would of course require additional inplane degrees of freedom to be incorporated in the element derivation.

In such models once cracking occurs, the constitutive relations exhibit coupling between inplane and flexural components, similar to that which occurs in unsymmetrically laminated plates. A consequence of this is that inplane and bending effects are no longer uncoupled, and membrane boundary conditions must be specified even for pure bending problems. Hand et al[42] has shown that inplane boundary conditions have a large effect on computed load deflection response. Cope and Rao[45] also studied this effect on fixed slabs and concluded that the neglect of inplane boundary conditions has greater effects than relaxing

restraints to flexural boundary conditions. The effects of inplane boundary conditions will be further investigated in this study.

In an attempt to reduce the computational effort, Dotreppe et al[46] used a reduced bending stiffness approximation in their layered finite element model. In this approach, it has been assumed that membrane forces are zero, and the bending stiffness was derived accordingly. Responses of a simply supported slab using this model underestimated the ultimate load by 10%. However, the assumption cannot be applied to problems in which there are inplane restraints.

2.4.4 Materials Idealization

2.4.4.1 Concrete in Tension:

When loaded in tension, concrete can resist only low stresses, up to about 10% of its ultimate strength in compression. Up to this loading stage, the material behaves as a linear elastic isotropic material. Upon cracking, anisotropic properties are created. In the direction normal to the crack, concrete is given a null stiffness. However, due to aggregate interlock, concrete is still capable of resisting shear stresses in cracked zones. In such cases, shear stresses are calculated using a reduced shear modulus βG. The constant reducing factor β is called the shear retention factor, and lies between unity for uncracked sections and zero for extensively cracked sections.

The value of β to be used is still uncertain, and in most cases, it is arbitrarily assumed. It has been postulated that variations in the numeric value of β produced little differences in the computed response of reinforced concrete slabs [42, 48]. This might not be the case for problems in which the response is largely influenced by

shear. Values as high as 0.5 [38] or 0.6 [48] had been used for both plane stress and plate bending problems. Labib and Edwards [51] investigated several values of β in the range 0.2 to 0.5 and used a value of 0.4 in their study of cracking in concentric and eccentric concrete members.

The reduced shear modulus in cracked concrete is sometimes computed using empirical equations, such as[52]:

$$G_{red} = G\left[0.4 + (1 - \varepsilon/\varepsilon_{tmax}) \times 0.6\right] \qquad (2.38)$$

$$\text{for } \varepsilon_{cr} < \varepsilon < \varepsilon_{tmax}$$

$$G_{red} = 0.4 \text{ for } \varepsilon > \varepsilon_{tmax} \qquad (2.39)$$

In the paper the terms are not defined, but it is logical that

G_{red} = reduced shear modulus in cracked concrete

G = initial shear modulus in concrete

ε = strain in concrete at any load level

ε_{cr} = cracking strain of concrete

ε_{tmax} = yield strain of steel

A zero value for β is also common[43, 46, 47]. However in all these models, a definite value is difficult to determine, due to differences in idealizations, and the nature of the structural problem at hand. The problem needs further investigation.

2.4.4.2 Bond Between Concrete and Steel:

Due to bond effects between concrete and steel, concrete between cracks offers some resistance to normal stresses in cracked elements. To account for this "stiffening" effect, the stress-strain curve for

concrete in tension is modified so that, some stresses will be transferred by concrete after cracking. Ignoring tension stiffening effect has been known to produce up to 100% errors in the computed slab deflections[48]. Various theories can be used to incorporate tension stiffening effects in layered finite element models. All such theories are based on the fact that the average stress over the element is not zero, and accordingly, an average stress-strain curve with an unloading portion (Figure 2.10) can be used for concrete after cracking. Such a concept is due to Scanlon [50]. The only difference between the various theories is the shape of this descending portion and its length. Various theories are shown in Figure (2.10) and include:

(a) Stepped response after cracking.

(b) Gradually unloading response.

(c) Discontinuous unloading after cracking.

Gilbert and Warner[48] investigated the three theories in connection with plate bending problems. They found that while the first theory produced very good correlation with experimental results, the gradual unloading response predicted an overstiff behaviour. Results obtained using the third theory produced good results, but at the expense of slow convergence and high cost.

The strain up to which tension stiffening is considered effective is arbitrarily selected. Gilbert and Warner [48] used 10 ε_{cr}, where ε_{cr} is the strain corresponding to a stress of ft. Shirai[53] et al used the strain at which bond between concrete and steel is lost, and this was taken as the yield strain of steel. For the shape of the unloading curve, they used a polynomial function in the form

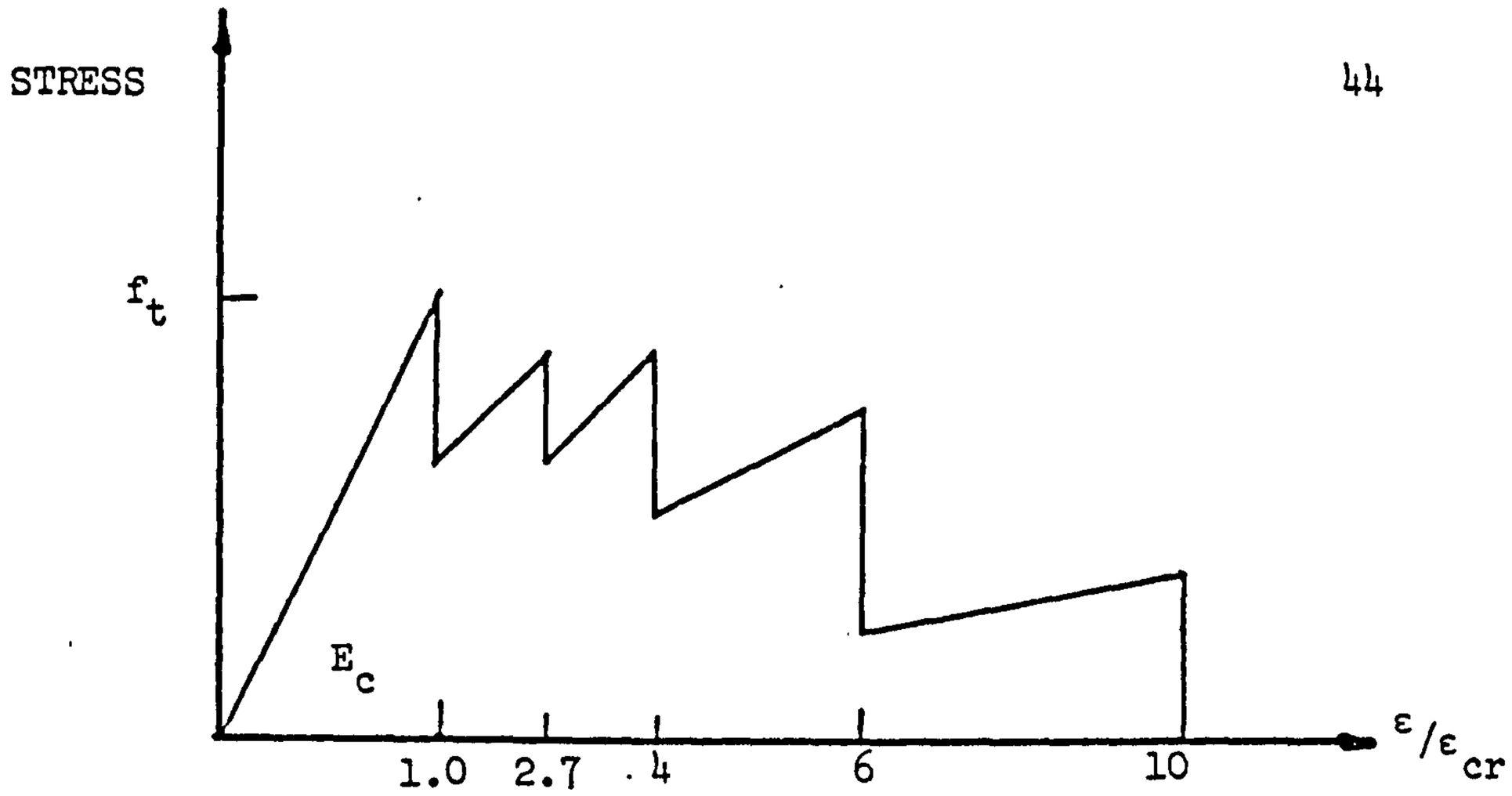

(a) Stepped Response After Cracking

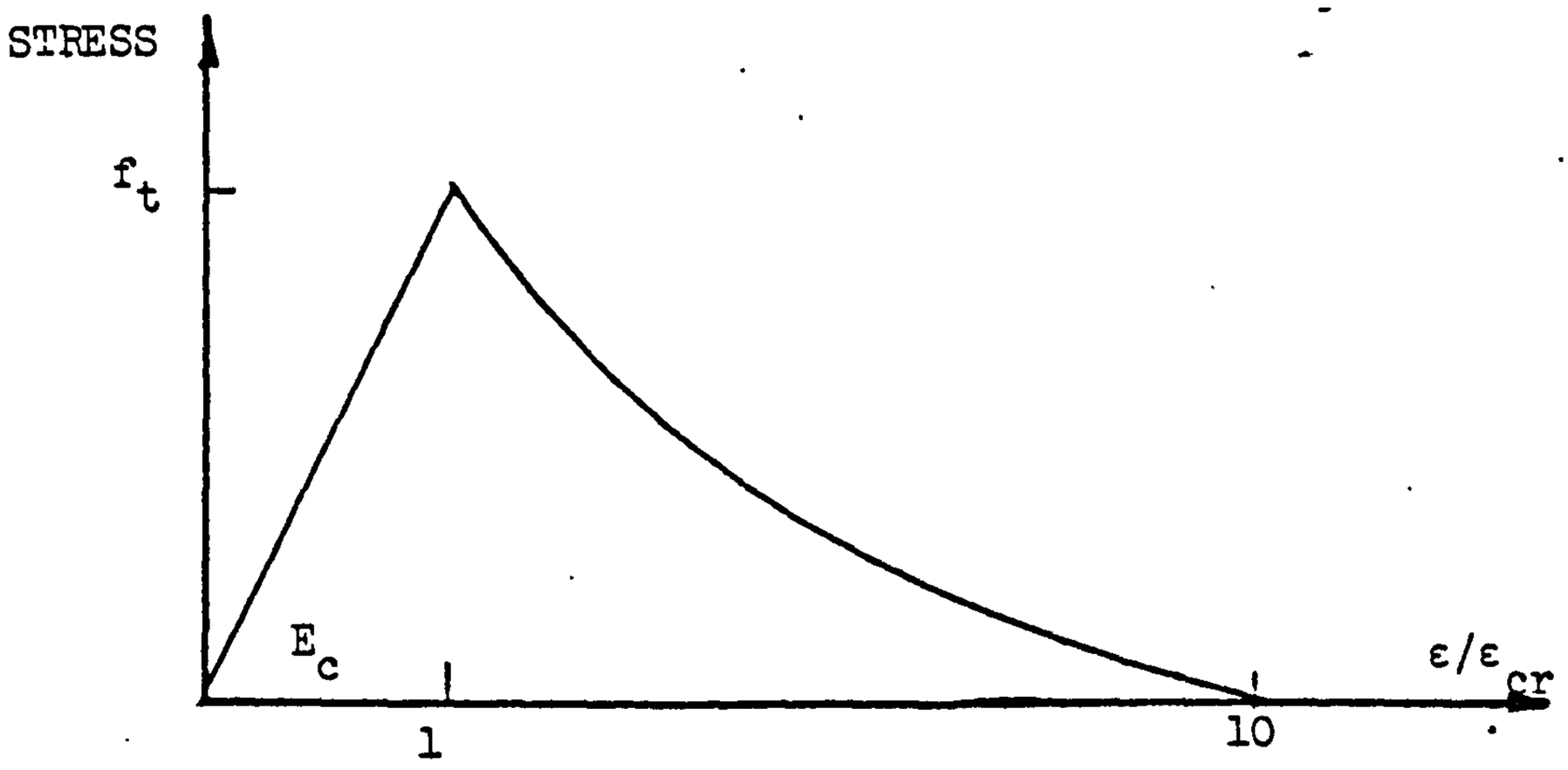

(b) Gradually Unloading Response After Cracking

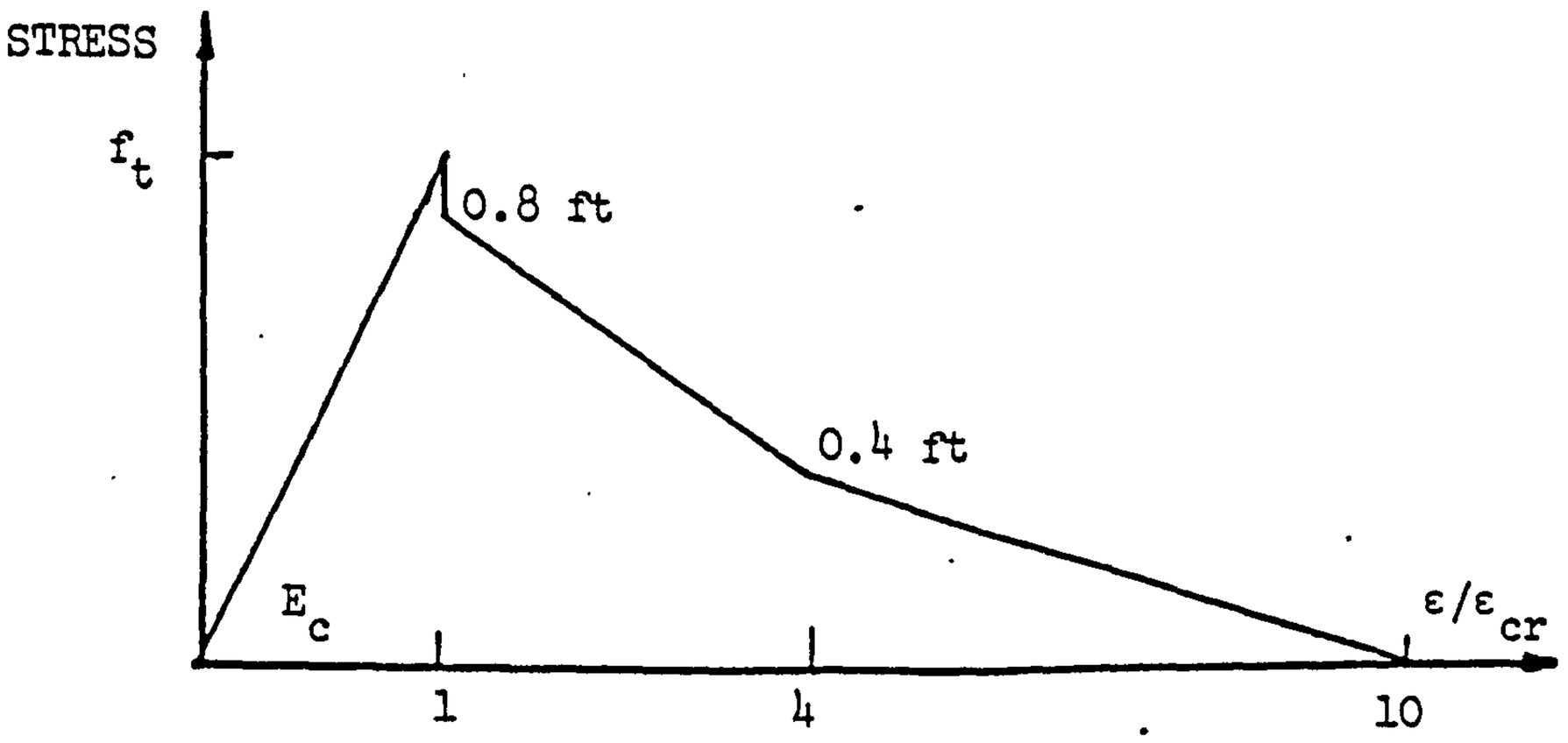

(c) Discontinuous Unloading Response After Cracking

Figure (2.10) Tensile Stress-Strain Curves for Concrete

$$\sigma_{eq} = (a_o + a_1 x + a_2 x^2 + a_3 x^3)\, f_t \qquad (2.40)$$

Razaqpur and Ghali[54] used a linear unloading curve, with an ultimate strain of 10 ε_{cr}, in studying shear lag in reinforced concrete T-beams. Values as high as 25 ε_{cr} had also been used in some cases[55].

This reflects the lack of objective criteria to treat cracking of reinforced concrete under biaxial stresses. The effects of the factor discussed in this section can not be separated from other numerical aspects involved in the discretization e.g. method of solution, convergence criteria etc., which in general, depend on the problem at hand.

2.4.4.3 Concrete in Compression:

Under compression, concrete diviates from linearity very early in the loading history. Tests results[56, 57, 58, 59] have indicated that the ultimate strength of concrete under biaxial compression is greater than in uniaxial compression, and is dependant on the ratio of the principal stresses.

The earlier works in obtaining biaxial stress-strain curves for concrete were those due to Liu et al[60]. His proposed equation is

$$\sigma = \frac{A + B E_c \varepsilon}{(1-\nu\alpha)(1 + C\varepsilon + D\varepsilon^2)} \qquad (2.41)$$

where

σ , ε = stress and strain in concrete

E_c, ν = Youngs modulus and Poisson's ratio for concrete, respectively.

α = ratio of the principal stresses in concrete.

The constants A, B, C and D are found from the following conditions on the stress-strain curve in compression (Figure (2.11)):

(a) For $\varepsilon = 0$, $\sigma = 0$

(b) For $\varepsilon = 0$ $\frac{d\sigma}{d\varepsilon} = \frac{E_c}{1-\nu\alpha}$

(c) For $\varepsilon = \varepsilon_p$, $\sigma = \sigma_p$

(d) For $\varepsilon = \varepsilon_p$, $\frac{d\sigma}{d\varepsilon} = 0$

where σ_p and ε_p are the peak stress and peak strain in biaxial compression, respectively. Substituting these in (2.41) and introducing the secant modulus at peak stress $E_{se} = \sigma_p/\varepsilon_p$ we have

$$\sigma = \frac{E_c\,\varepsilon}{(1-\nu\alpha)\left[1 + \left(\frac{1}{1-\nu\alpha}\frac{E_c}{E_{se}} - 2\right)\left(\frac{\varepsilon}{\varepsilon_p}\right) + \left(\frac{\varepsilon}{\varepsilon_p}\right)^2\right]} \qquad (2.42)$$

Later this equation was further investigated by Tasuji et al[59] and was found to represent the behaviour of concrete in both tension and compression. For uniaxial cases $\alpha = 0$. The material constants E_c, ν, ε_p, σ_p to be used in equation (2.42) are found from:

1. E_c from CP110 or the ACI code equations

$$E_c = 5.5\sqrt{\frac{f_{cu}}{1.5}} \quad \text{in KN/mm}^2 \qquad (2.43)$$

or

$$E_c = 0.043\,\gamma_c^{3/2}\,\sqrt{f'_c} \quad \text{in N/mm}^2 \qquad (2.44)$$

where γ_c = unit mass of concrete in kg/m^3.

The two equations differ by only 0.5% for 2400 kg/m^3 concrete and $f'_c = 0.78\,f_{cu}$.

2. Poisson's ratio ν ranges between 0.11 - 0.21[61]. An average of 0.19[59] or 0.15[43] has extensively been used.

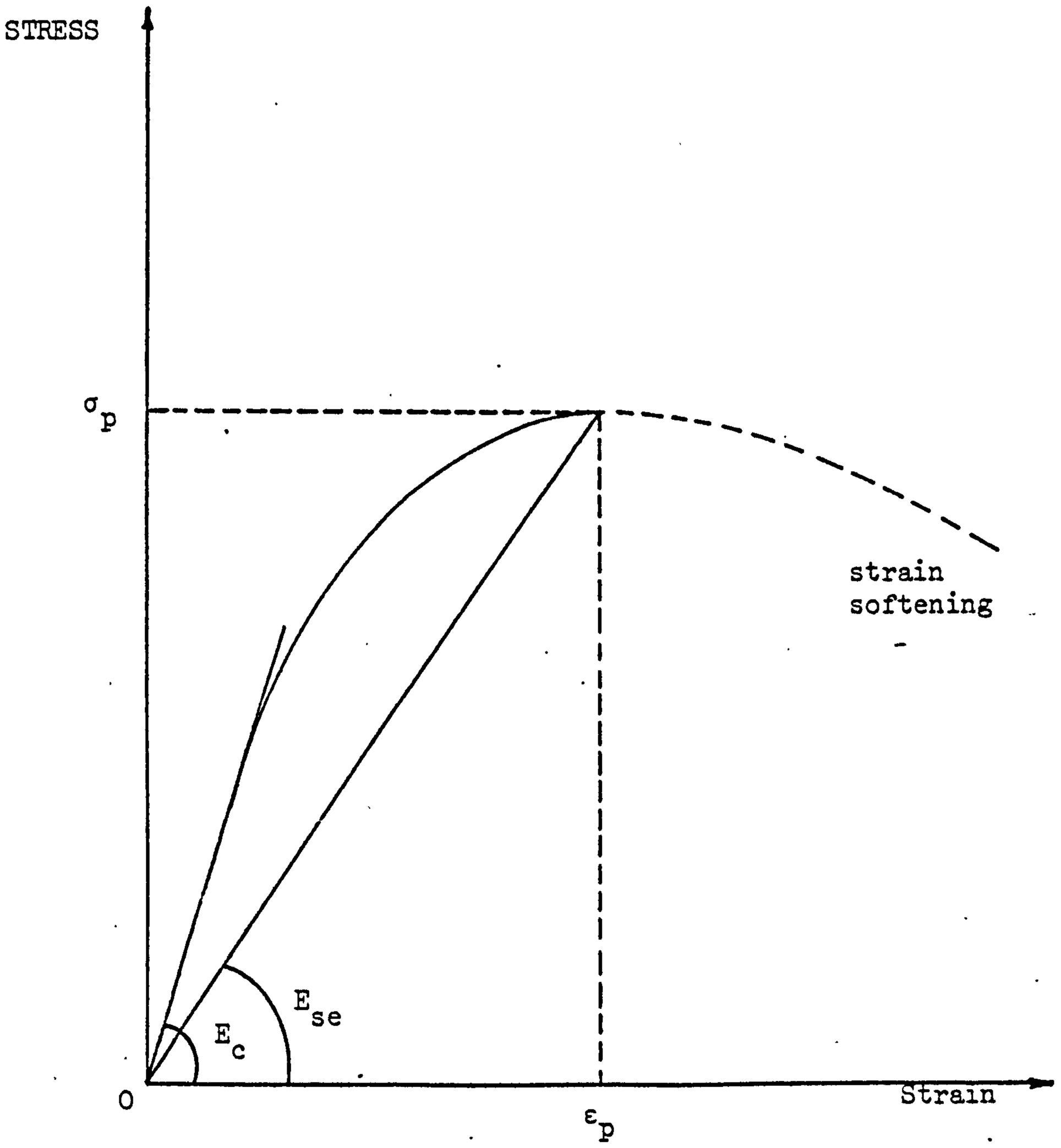

Figure (2.11) Stress-Strain Curve for Concrete in Compression

3. The peak strain ε_p :

Test results by Liu et al[60] indicated that for biaxial compression

ε_p = - 2500 microstrains (major direction)

ε_p = 500 + 79.8 σ_p" (minor direction)

where σ_p is the peak stress.

4. The peak stress σ_p:

This can be obtained from the biaxial strength envelope (see Section 2.4.5).

Finally, equation (2.42) can then be used to describe the stress-strain behaviour of concrete in compression up to the peak stress. Beyond peak, the equation ceases to hold due to the strain softening of concrete. At present, little is known about this descending branch of the stress-strain curve of concrete.

For plate benging problems, strain softening effects can safely be neglected, and in most cases, the stress-strain curve is assumed to possess a horizontal plateau[36]. Due to the fact that the major effect on the response of under-reinforced flexural members is due to cracking, post-peak behaviour of concrete in compression can safely be ignored.

2.4.4.4 Idealization of Reinforcement

In most layered finite element models, each layer of reinforcement is represented by an equivalent smeared layer, which can carry stresses only in the direction of the original bars. The equivalent thickness of the steel layer is determined such that the corresponding area of the reinforcement in the element remains unchanged. The steel layer

is then assumed to be elastic-plastic in both tension and compression and to have a definite yield point with or without strain hardening. In some cases, two reinforcing steel layers can be represented by an equivalent orthotropic layer with two-dimensional properties. In such cases, the layer is treated as a two-dimensional steel plate, which obeys the Von Mises yield criterion [43,44]. Such an assumption is very useful in treating skew reinforcement. Even in orthogonal reinforcement, two layers of steel can be represented by one, but in this case, no interaction between the orthogonal directions is assumed. In such cases, care has to be taken in treating yielding of steel in one direction not to influence the state of stress in the other direction.

Steel can also be modelled as discrete bar elements[39,63,64]. Such steel representation is restricted by the fact that steel bars have to be laid along certain directions, normally the element local coordinate system[64]. In addition, a special element stiffness derivation is needed, in contrast to the smeared approach in which the same element stiffness derivation is used for both concrete and steel layers.

In both idealizations, perfect bond between steel and concrete is assumed. Bond slip is also sometimes represented by reducing the modulus of steel[52].

2.4.5 Yield Criteria for Plain Concrete:

In layered finite element models, each layer is treated as being in a state of plane stress condition. And since each material is separately treated, yield criteria in plane stress condition are required for both concrete and the reinforcing steel. For the latter,

owing to its unlimited plasticity, the Von Mises yield criterion is usually adopted. For concrete, the problem is more complex, since concrete is brittle in tension and of limited ductility in compression. Accordingly, at least two criteria are required (or an equivalent) for yielding under tensile and compressive states of stress.

As a criterion for cracking, two theories are known:

(a) The maximum stress theory, which assumes that cracking in concrete occurs whenever the maximum principal stress exceeds the tensile strength of concrete. Test results by Kupfer et al[56] indicated that the latter has the same value in both uniaxial and biaxial stress states.

(b) Maximum strain theory, assumes that cracking occurs whenever the maximum principal strain exceeds the limited tensile strain of concrete.

The first theory, however, is more popular than the second: However, Phillips[65] found that the second theory predicts stiffer behaviour than the first.

For yielding under biaxial compression states of stress, various criteria had been used by many researchers. The Von Mises yield criterion was used by Valliappan et al[63], Lin et al[50], Gilbert and Warner[48], Wanchoo et al[47], Suidan et al[38] and Hinton et al[55]. The applicability of this criterion to concrete is debatable, because nonlinear action in concrete is not caused by actual plastic flow as in metals, but is dictated by the cumulative effect of microcrack propagation. In such applications, the associated flow rule of plasticity is normally adopted, and the limited plasticity in concrete

is represented by the use of a crushing surface analogous to the yield surface, but expressed in terms of strains[50].

The modified Columb-Mohr law is more popular, because it represents well the behaviour of concrete. Following Nadai[66], failure can be expressed in terms of the octahedral shear and normal stresses in the following manner

$$I_1 = \sigma_1 + \sigma_2 + \sigma_3$$
$$I_2 = \sigma_1 \sigma_2 + \sigma_2\sigma_3 + \sigma_3 \sigma_1 \qquad (2.45)$$
$$I_3 = \sigma_1 \sigma_2 \sigma_3$$

with the generalized failure criterion $F(I_1, I_2, I_3) = 0$. If one of the principal stresses is zero, then $I_3 = 0$. I_1, I_2 and I_3 are called the stress invariants. Now the octahedral shear stress is given by

$$\tau_{oct} = \frac{1}{3}\left[(\sigma_1 - \sigma_2)^2+(\sigma_2 - \sigma_3)^2+(\sigma_3 - \sigma_1)^2\right]^{\frac{1}{2}} \qquad (2.46)$$

and the mean normal octahedral stress σ_o is

$$\sigma_o = \frac{1}{3}(\sigma_1 + \sigma_2 + \sigma_3) = I_1/3 \qquad (2.47)$$

i.e.

$$\tau_o = F(I_1, I_2) \qquad (2.48)$$

Octahedral stresses are so named because they occur on the sides of an octahedral element formed by planes whose normals make equal angles with the principal stress axes. In general form, the octahedral shear stress failure criterion can be written in the form

$$\tau_{oct} - a\sigma_o - b = 0 \qquad (2.49)$$

The constants a and b are normally determined from

experimental data. Test results by Kupfer et al[56] had been used by many researchers in connection with this criterion[42,44]. The problem will further be treated in Chapter (4) of this thesis.

2.4.6 Methods of Solution for Nonlinear Analysis:

The structural problem to be solved at any stage of loading is

$$[k][d] - [P] = 0 \qquad (2.50)$$

where

$[k]$ = the stiffness matrix of the structure

$[P]$, $[d]$ = Load and displacement vectors, respectively.

In equation (2.50), the stiffness matrix of the structure is a stress-dependant. The equation is thus nonlinear, and for solution, it is preferable to proceed along a sequence of linearized steps. Such an approach is common to solutions of nonlinear algabraic equations, such as the Newton-Raphson technique or its modified version[31]. For simplicity, a one degree of freedom system will be examined:-

Let the root of the nonlinear equation $f(x) = 0$ be required. The Newton-Raphson procedure states that

$$x_{i+1} = x_i + \Delta x \qquad (2.51)$$

where x_i and x_{i+1} are two successive iterates, and Δx, the correction to x_i is given by

$$\Delta x = - f(x_i)/f'(x_i) \qquad (2.52)$$

In Newton-Raphson procedure, the gradient $f'(x_i)$ is evaluated in each iteration. In the modified Newton-Raphson procedure, at the expense of slow-down in rate of convergence, the initial gradient

$f'(x_o)$ is used throughout, thus

$$\Delta x = - f(x_i)/f'(x_o) \qquad (2.53)$$

The approach,is schematically shown in Figure (2.12), where the tangents drawn as continuous lines are instantaneous gradients. The dotted lines are parallel to the initial tangent, and represent the modified Newton-Raphson procedure[31].

Referring to the structural problem, the nonlinear equation can be written in the form

$$f(d) = [k][d] - [P] = 0 \qquad (2.54)$$

The stiffness $[k]$ corresponds to the gradient in equation (2.52) above. Accordingly, if a variable stiffness approach is used, then it is analogous to a Newton-Raphson procedure, while a solution employing the initial stiffness matrix (constant stiffness) corresponds to the modified Newton-Raphson technique. The"initial stiffness" method[68] is also identical to the modified Newton-Raphson procedure.

Both methods have been extensively used by research workers. The variable stiffness approach had been employed by Hand et al[42], Dotreppe et al[46], Schnobrich[37], Bell and Elms[32], Jofriet and McNiece[21], Darwin and Pecknold[67], and Johnarry[43].

Although the rate of convergence of the variable stiffness method is fast, a long time is spent in each load increment in the updating process. Most of the time is lost in the housekeeping, as normally such procedures call for extensive use of backing stores in most computers.

On the other hand, the initial stiffness method converges very slowly to the correct solution, and depending on the severity of nonlinearity in the structure, it might need a very large number of iterations to achieve an equilibrium position. Johnarry[43] and Duncan et al[44] have claimed that demanding static equilibrium at each load level normally leads to expensive analysis and poor results, although their statement was not supported by any numerical evidence.

Constant stiffness methods have been used by Valliappan and Doolan[63], Shirai et al[53], Suidan and Schnobrich[38], Dietrich et al[49], Cope and Rao[45], Rao[39], Duncan[44] and Johnarry[43], and Hinton et al[55].

Johnarry[43] compared the constant and variable stiffness methods in plate bending applications. He concluded that for such problems, the constant stiffness is the best and least expensive. Cope et al[97] had also undertaken similar study, and concluded that no significant increase in computational efficiency could be achieved by recomputing the stiffness matrix. Similar conclusions were also arrived at by Hinton et al[55].

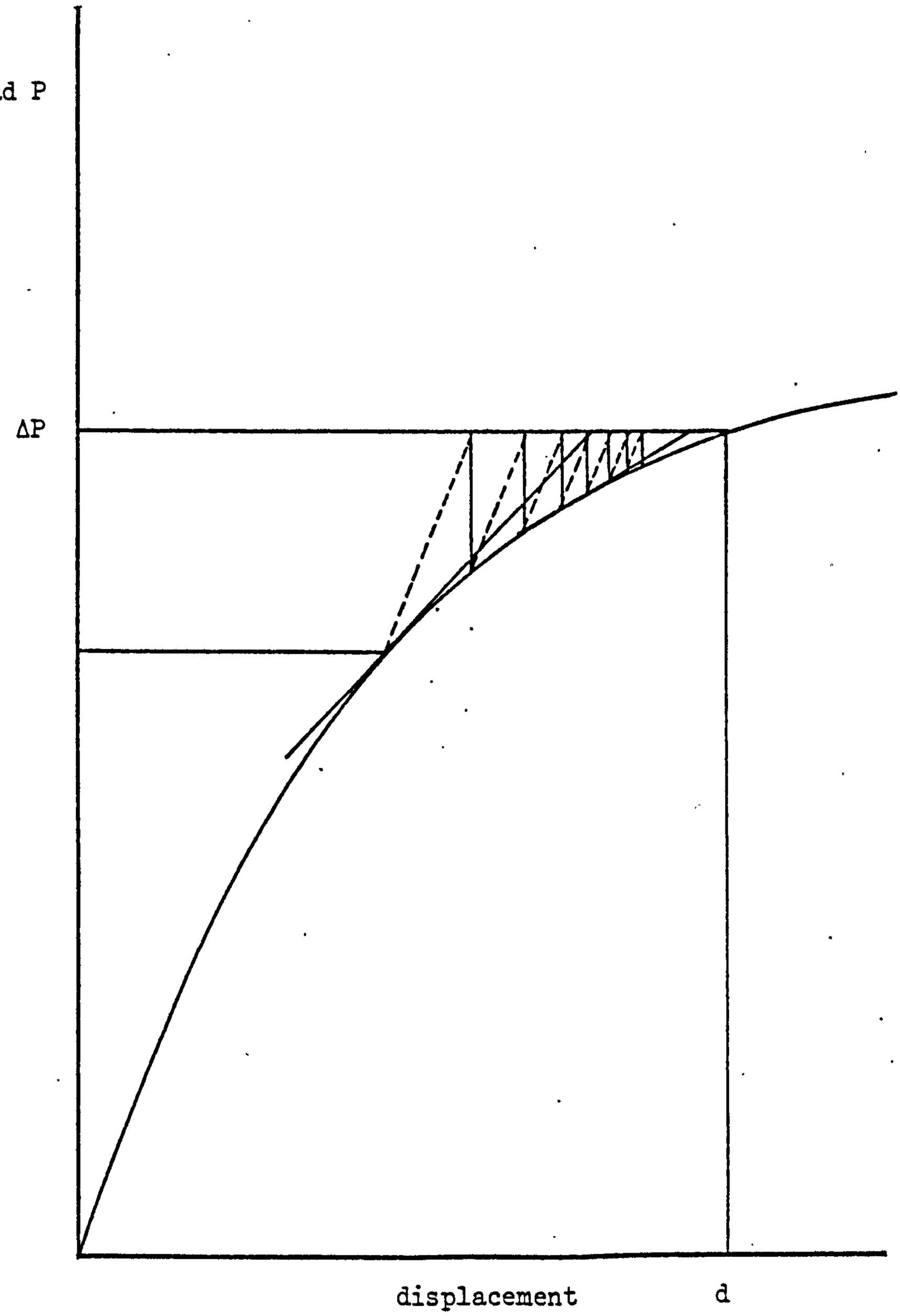

Figure (2.12) The Newton-Raphson Procedures

CHAPTER THREE

DESIGN OF REINFORCED CONCRETE SLABS

3.1 INTRODUCTION

In the previous chapter, the various methods available for the design of reinforced concrete slabs have been discussed. Most of these methods concentrated exclusively on ultimate loads, and were all unsatisfactory, either in terms of the information they provide on the distribution of steel (e.g. the Yield Line Theory - with no information about the rigid regions), or the best distribution for a satisfactory service behaviour under working loads.

A design procedure based on realistic understanding of material behaviour both at service and ultimate loads is now suggested. The proposed direct design approach is based on the theory of plasticity, and will be discussed in this chapter.

3.2 THEORY OF PLASTICITY IN SLAB DESIGN

Any solution to the ultimate load has to satisfy the conditions of classical plasticity. This can be stated in the following manner:-

1. The Equilibrium Condition:- The internal stresses must be in equilibrium with the externally applied loads.
2. The Mechanism Condition:- Under the ultimate load, sufficient plastic hinges must exist to transform the structure into a mechanism.
3. The Yield Criterion:- The ultimate strength of the member must nowhere be exceeded.

For reinforced concrete slabs, it is very difficult (if not

impossible) to find a design procedure satisfying the three conditions. Existing methods are either:

(a) satisfying conditions (1) and (2) by assuming a suitable collapse mechanism. Such methods usually render loads higher or equal to the true collapse load. Accordingly, such methods provide an upper bound on the true collapse load of the slab, which may be unsafe. The yield line method of reinforced concrete slabs is of this nature. However such methods do not check condition (3) on the "rigid" portions of the slab.

or (b) Satisfying conditions (1) and (3) by assuming a suitable stress field (safe admissible stress fields). Such methods render a load which is lower or equal to the true collapse load of the slab, and thus,one of lower bound nature. Accordingly, the load calculated is a safe load i.e. the true ultimate load is greater than the calculated load.

3.3 THE PROPOSED DIRECT DESIGN APPROACH:

For a safe design, it is well advised to use a lower bound approach. The proposed design approach is very simple and straightforward. The method suggested here will be shown to satisfy the three conditions of the theory of plasticity. The steps in the method will be discussed in relation to these conditions in the following manner:

3.3.1 The Equilibrium Condition:

The stress distribution under the design loads will be obtained using the elastic analysis by the finite element method. Accordingly, such a distribution will automatically satisfy the equilibrium condition, as the method is derived from equilibrium considerations. Owing to its

simplicity and versatility, the method can be applied to any type of slab problem - with any edge conditions.

The analysis will be made assuming elastic properties for the slab. Although the stress distribution is greatly affected by cracking in the slab at high loads, the distribution of stresses at ultimate conditions is dependant on the amount of steel provided for under reinforced sections. Accordingly, it is proposed here to reinforce the slab so that the strength at any section will follow the elastic distribution of stresses.

The actual ultimate load for the slab so designed should at least reach the ultimate load predicted by the elastic analysis.

3.3.2 The Yield Criterion:

The yield condition defines the combination of stresses necessary to cause plastic flow at a point. The condition will be satisfied if the strength at any point is made equal to or greater than the applied stresses.

An elastic analysis on the slab under the ultimate loads by the finite element method provides the stress resultants M_x, M_y, M_{xy} for laterally loaded plates. To provide the reinforcement to fit the predicted moment field at ultimate Limit state, the steel should be proportioned as required by the yield criterion. Accordingly, it becomes necessary to derive the yield criterion in terms of the three moments components.

Considering the slab element in Figure (3.1), under the moment field M_x, M_y, M_{xy} with anisotropic properties. The sign convention adopted here is such that all moments acting in the element are positive.

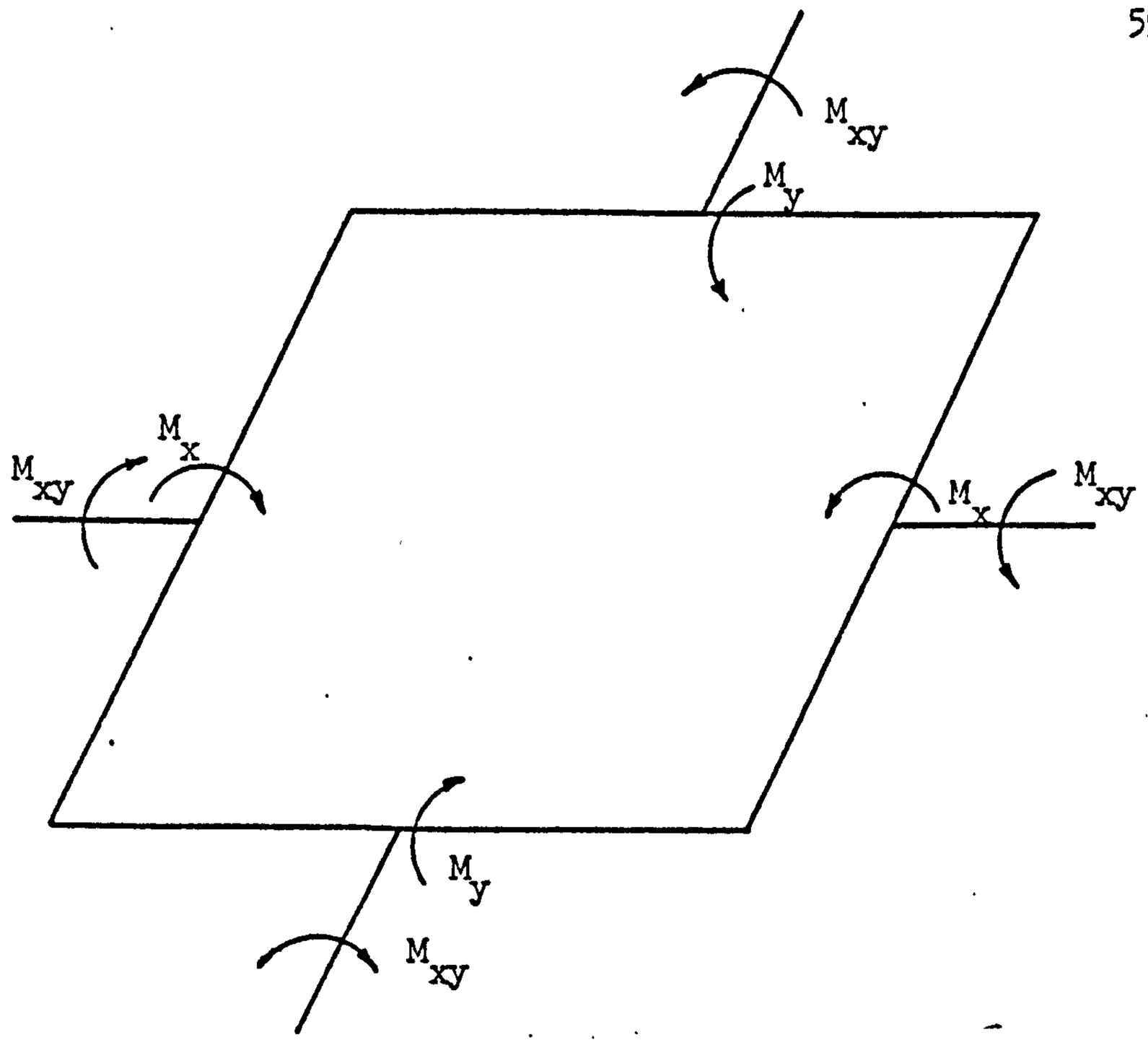

Figure (3.1) Notation for Moments on an Element
(Positive as shown)

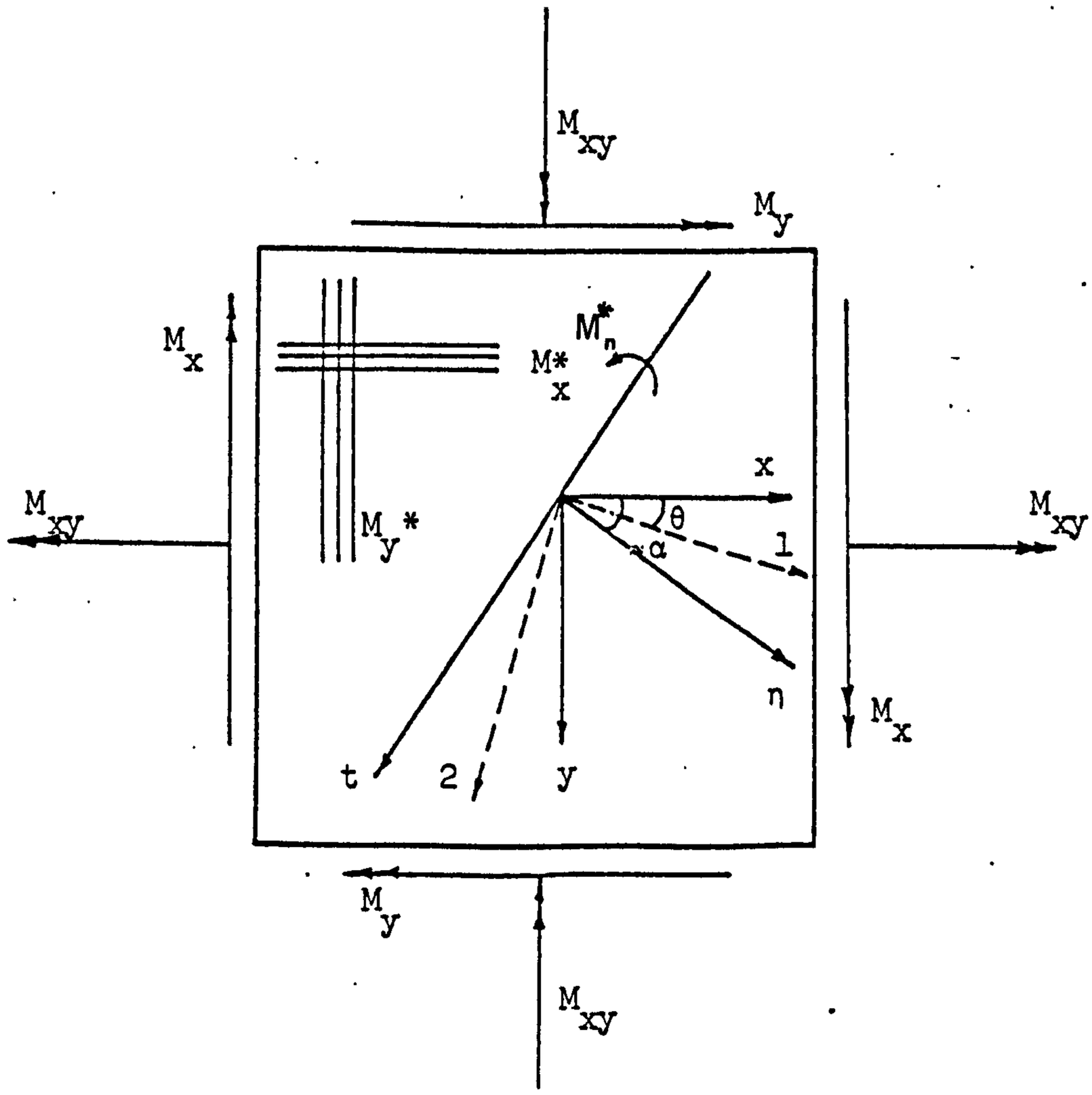

Figure (3.2) Element with Orthogonal Reinforcement

Simplifying assumptions are further made, and these can be summarized in the following:

1. The concrete is assumed to have a tensile strength equal to zero.
2. Bar diameters are small in comparison with the slab depth, and that they can carry stresses only in their original direction. Accordingly, kinking of bars across a yield line is not considered.
3. The slab element is lightly reinforced, so that compression failures are not permissible and only ductile failures are allowed. This is necessary for moment redistribution, so that the slab elements can reach their ultimate strength at sufficient number of sections, to convert the slab into a mechanism.
4. Membrane forces do not exist. It is acknowledged that the co-existence of such forces with flexural fields on the slab elements, will considerably enhance or reduce the resisting moment of the slab element, depending on whether they are compressive or tensile, respectively.

(Membrane forces will be treated later in Sections 3.6 and 3.7).

For simplicity, the anisotropic reinforcement in the element will be assumed to lie parallel to the element sides (Figure 3.2). The element may be reinforced on the top and bottom surfaces, although the degree of orthotropy in the two faces may be different.

The basic idea is that, if at any point in the slab element (Figure 3.2), a line with a normal n and direction t is examined,

then the normal moment M_n must not exceed the value M_n^*, where M_n^* is the moment of resistance that the reinforcement in the slab could develop in direction n. This is therefore a normal moment criterion which is tested in every direction, as has been shown by Kemp[72].

It should be noted that a lower bound stress field with variable reinforcement at different points must make provision for yield lines in any conceivable direction, because there may be simultaneous multiple modes of collapse[19].

Taking the normal to the yield line at an angle α to the x-axis, and considering the equilibrium of the element shown in Figure (3.3), we will have

$$M_n = M_x \cos^2\alpha + M_y \sin^2\alpha - M_{xy} \sin 2\alpha \qquad (3.1)$$

$$M_t = M_x \sin^2\alpha + M_y \cos^2\alpha + M_{xy} \sin 2\alpha \qquad (3.2)$$

$$M_{nt} = (M_x - M_y)\sin 2\alpha/2 + M_{xy} \cos 2\alpha \qquad (3.3)$$

The resisting moments at the yield line can be expressed as follows

$$M_n^* = M_x^* \cos^2\alpha + M_y^* \sin^2\alpha \qquad (3.4)$$

$$M_t^* = M_x^* \sin^2\alpha + M_y^* \cos^2\alpha \qquad (3.5)$$

$$M_{nt}^* = (M_x^* - M_y^*) \sin 2\alpha/2 \qquad (3.6)$$

Therefore, when designing the steel, the resistance to normal moment should be checked in every direction. Accordingly

$$(M_n^* - M_n) \geq 0 \qquad (3.7)$$

substituting (3.1) and (3.4) in (3.7) we have

$$(M_x^* - M_x) \cos^2\alpha + (M_y^* - M_y) \sin^2\alpha - M_{xy} \sin 2\alpha \geq 0$$

dividing by $\cos^2\alpha$ and putting $k = \tan\alpha$

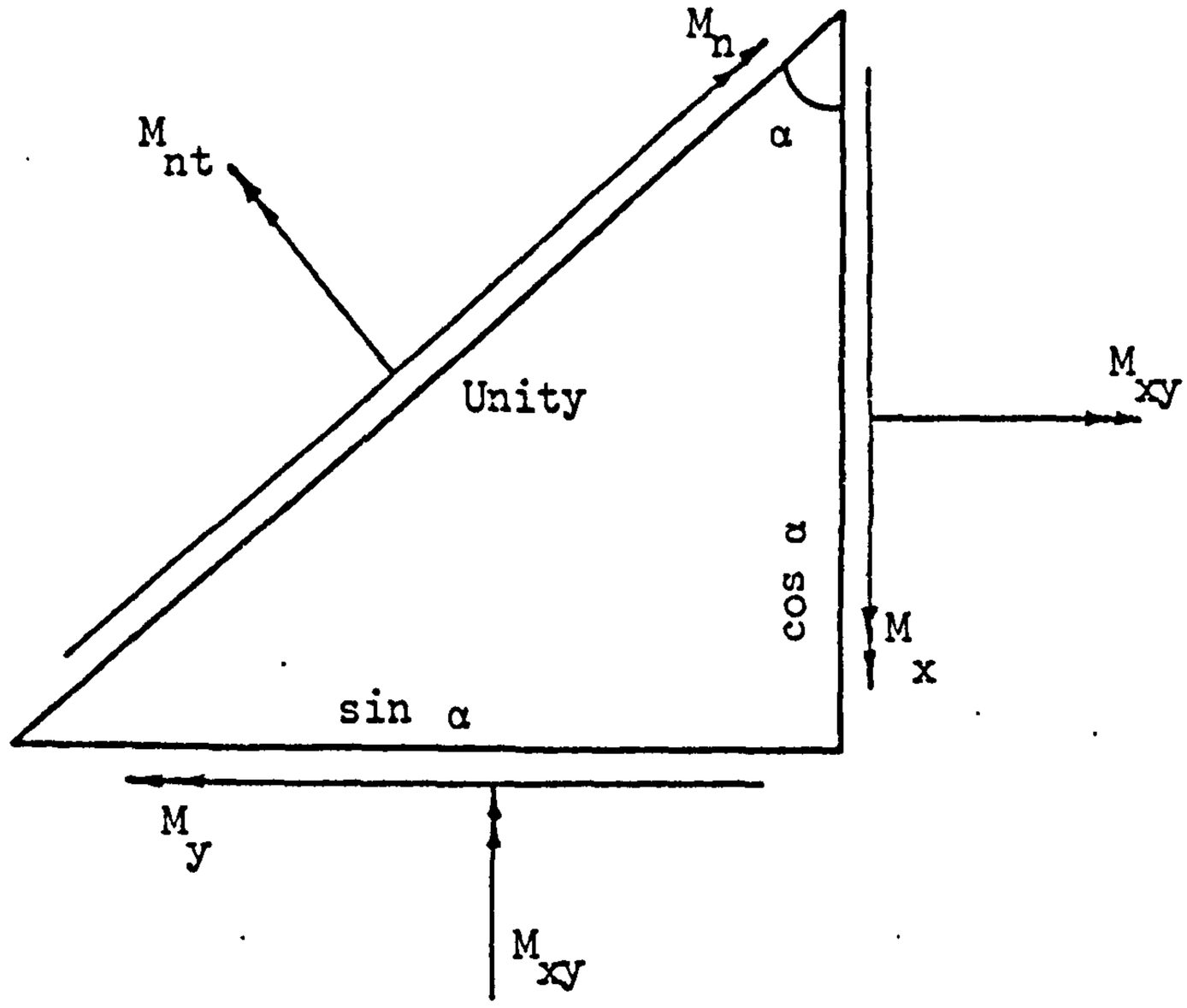

Figure (3.3) Equilibrium of a Slab Element under Applied Moment Field

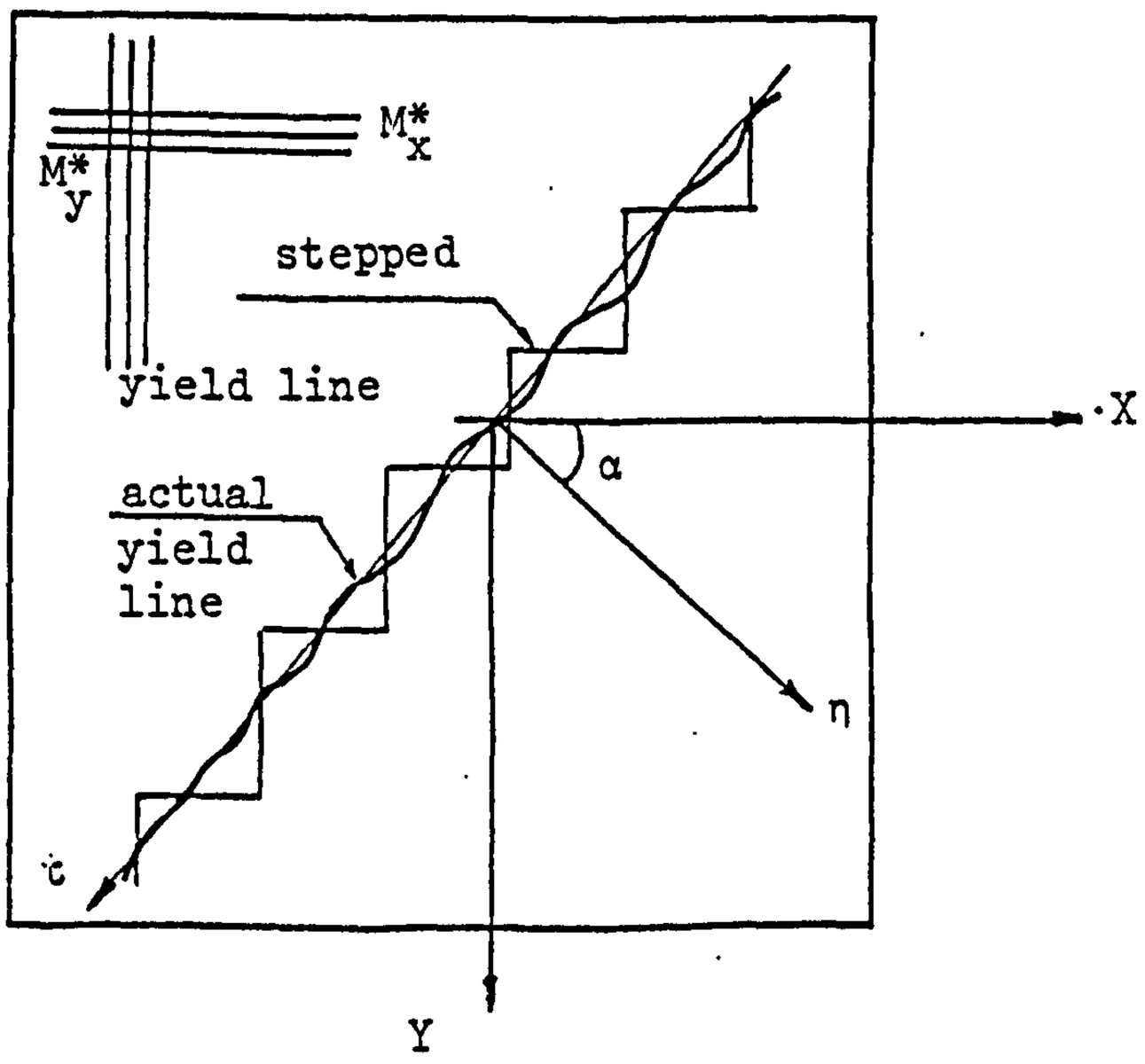

Figure (3.4) Idealized Yield Line (Johansen's stepped yield criterion)

$$(M_x^* - M_x) + k^2(M_y^* - M_y) + 2k\, M_{xy} \geq 0 \qquad (3.8)$$

If the left hand side of equation (3.8) is denoted by f(k), then f(k) is related to the excess normal resistance provided by the reinforcement over the required normal moment in the stress field. As has been shown by Lenschow and Sozen[77], yield is liable to occur along lines with least reistance. Accordingly, along such lines

$$df(k)/d\alpha = \frac{d\, f(\tan\alpha)}{d\alpha}$$

$$= \frac{d\, f(\tan\alpha)}{d\, \tan\alpha} \cdot \frac{d\, \tan\alpha}{d\, \alpha}$$

$$= \frac{d\, f(k)}{dk} \cdot \sec^2\alpha$$

$$= 0 \qquad (3.9)$$

Since sec α cannot be zero, hence from (3.8) and (3.9)

$$\frac{d\, f(k)}{dk} = 2\, k\, M_y^* - 2k\, M_y + 2\, M_{xy} = 0$$

or

$$(M_y^* - M_y) = -\frac{1}{k} M_{xy} \qquad (3.10)$$

If f(k) is to represent a minimum excess moment of resistance then

$$\frac{d^2 f(k)}{dk^2} = 2\, M_y^* - 2M_y \geq 0$$

Hence $M_y^* \geq M_y$ (3.11)

and accordingly, in (3.10), $M_{xy}/k \leq 0$ (3.12a)

and from (3.10)

$$k = \tan\alpha = \frac{-\, M_{xy}}{M_y^* - M_y} \qquad (3.12b)$$

This gives the orientation of the plane of minimum resistance. As has been shown by Lenschow and Sozen[77], at the yield line resulting in the minimum resistance, the components of the external normal moments is equal to the moment capacity across the yield line, while the internal twisting moment is in equilibrium with the external twisting moment. The variation of the normal moments with the yield line orientation is given in Figure (3.5).

Substituting (3.12b) in (3.8) and using the equality sign for minimum resistance, then

$$(M_x^* - M_x) + \left[\frac{-M_{xy}}{M_y^* - M_y}\right]^2 (M_y^* - M_y) - \frac{2 M_{xy}^2}{(M_y^* - M_y)} = 0 \qquad (3.13)$$

Rearranging, we have

$$(M_x^* - M_x)(M_y^* - M_y) = M_{xy}^2 \qquad (3.14)$$

which is the same equation arrived at by Save[73], Nielsen[94], Lenschow et al[77], and Kemp[72].

Equation (3.14) is the yield criterion for orthotropically reinforced concrete slabs. If $M_x^* = M_y^* = M$ (isotropic reinforcement), then the equation reduces to that of isotropic slabs [72]. The Johansen (or Prager's) square criterion (Figure 3.6) is readily obtained from equation (3.14) for isotropic slabs.

It is evident from the yield condition (3.14) that twisting moments do exist on the yield lines. This has been confirmed by the works of Lenschow et al[77], Cardenas and Sozen[92], Lenkei[95], and Satish Jain et al[90]. The extensive experimental work on the above yield criterion provided by the above mentioned research workers

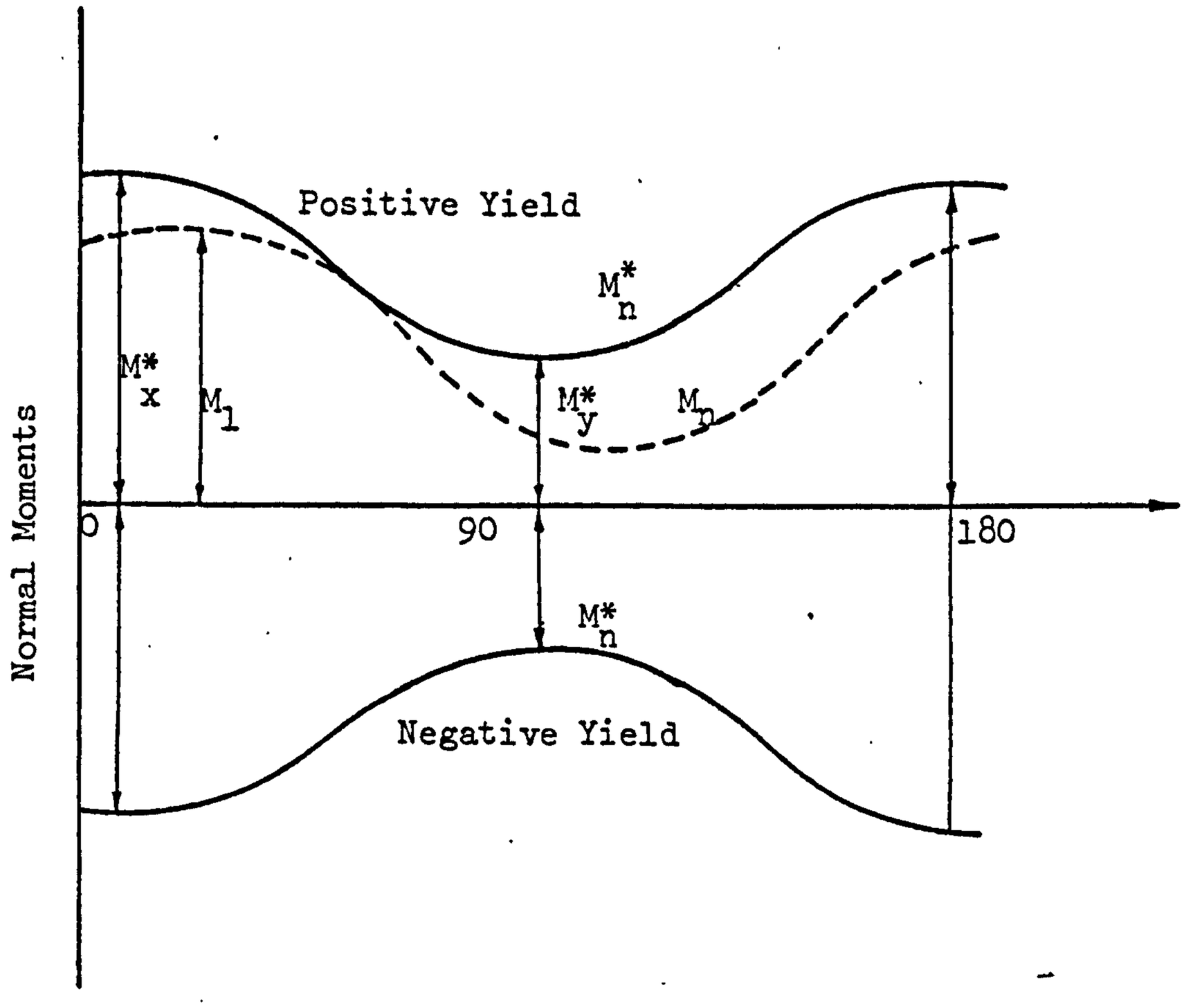

Figure (3.5) Variation of Applied and Yield Moments with Yield Line Orientation

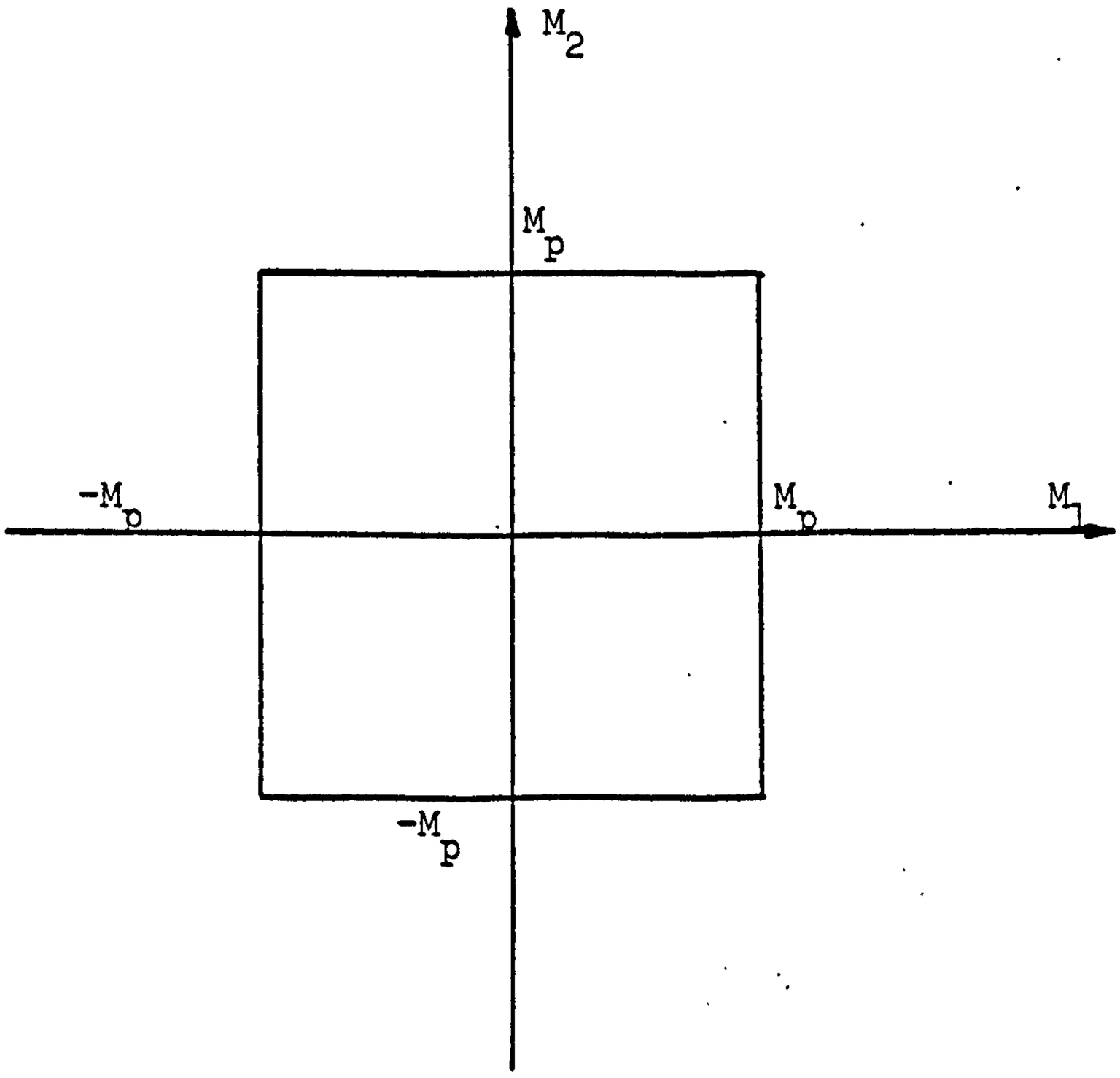

Figure (3.6) The Square Yield Criterion

confirmed the validity of this criterion. It has further been established that the yield line orientation will not in general coincide with the principal directions of neither the applied nor the resisting moments, except for isotropic reinforcement. Consequently, twisting moments do exist at the yield lines, but their existence do not reduce the flexural yield capacity due to the interaction between flexural and torsional moments. Equation (3.14) represents a pair of intersecting cones in the M_x, M_y, M_{xy} space, Figure (3.7). The derivation of the yield criterion in terms of principal moments on similar lines has been given by Kemp[72].

For yield in the negative steel at the top of the slab, similar procedure to the one just described for positive yield, can be applied. If the top steel layers are laid in the x and y directions to provide the resisting moments $M_x^{*\prime}$ and $M_y^{*\prime}$ respectively,then the yield condition with negative steel can be written as

$$(M_x^{*\prime} + M_x)(M_y^{*\prime} + M_y) = M_{xy}^2 \qquad (3.15)$$

where both M_x and M_y are negative moments (see Figure (3.1)).

3.3.3 The Mechanism Condition

The elastic analysis under the ultimate load by the finite element will be linked with the yield conditions just derived to provide the necessary strength according the elastic moment field. The derivation of such design equations will be outlined in subsequent sections.

Because the necessary resistance is made equal to the calculated stress at every point in the slab, it is anticipated that all slab

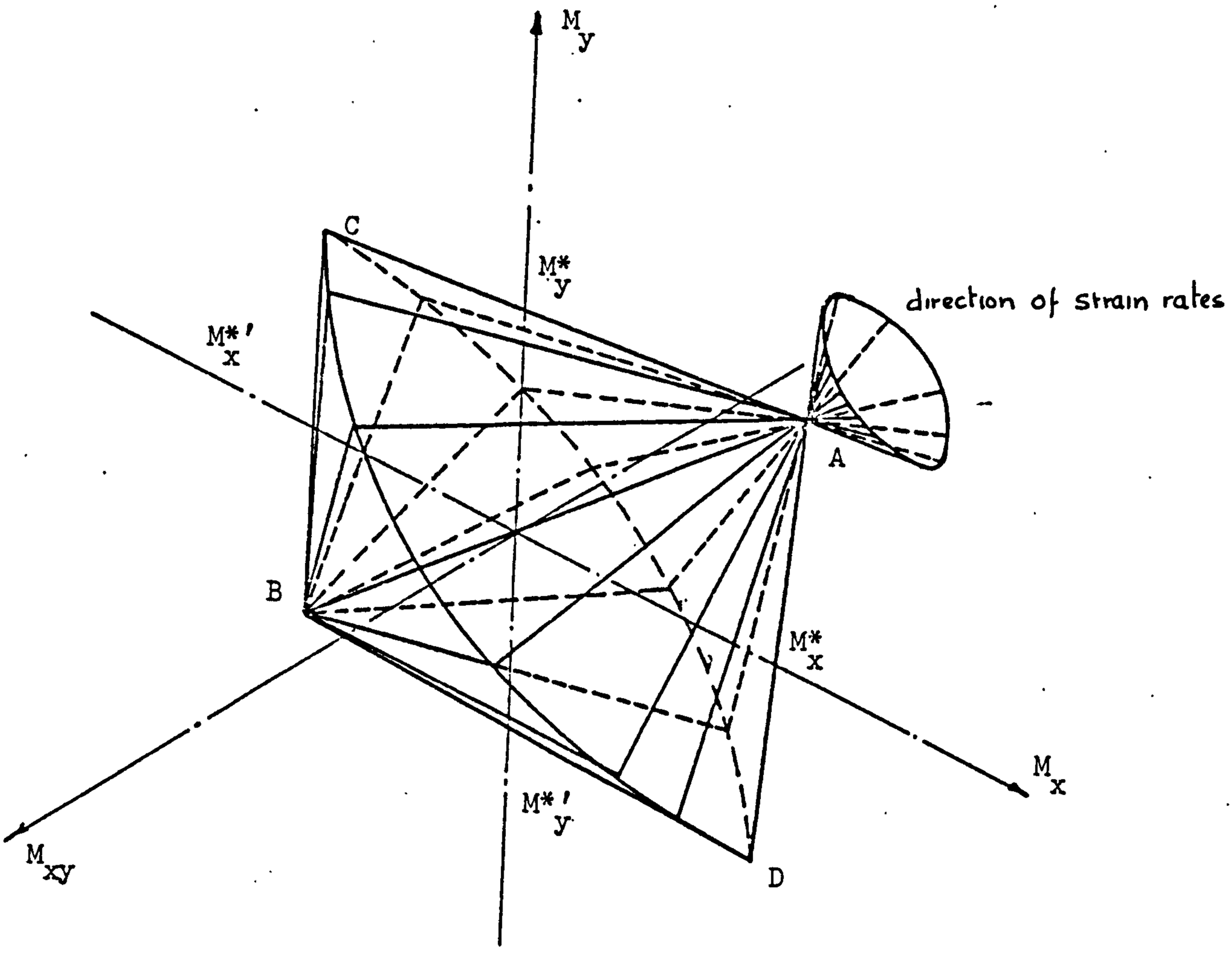

Figure (3.7) Yield Surface for an orthotropically Reinforced Concrete Slab

parts will attain their ultimate strength under the design load. Accordingly, with minimum amount of redistribution, every point will turn into a plastic hinge at the design load, thus converting the slab into a mechanism. Because of the minimum redistribution to achieve collapse by this method, the demand for ductility as normally emphasized by the classical theory of plasticity will obviously drop.

3.4 DESIGN OF ORTHOGONAL REINFORCEMENT

3.4.1 Positive Moment Fields:

Referring to equation (3.10), substituting it into equation (3.8) we will have

$$M_x^* = M_x - k\, M_{xy} \qquad (3.16)$$

and from (3.12a), if $M_{xy} > 0$ then $k < 0$ and vice versa. Equations (3.10) and (3.16) then become

$$M_x^* = M_x + K\,|M_{xy}| \qquad (3.17)$$

$$M_y^* = M_y + K\,|M_{xy}| \qquad (3.18)$$

in which $K = |k|$ is now taken to be a positive arbitrary constant.

The value of K may be determined so that the total amount of steel is minimum. As has been shown in Section (2.2.2.4), the volume of steel to be used is proportional to the total moment volume. Accordingly, at any point on the slab, this will be minimum if the sum $(M_x^* + M_y^*)$ is minimum. Using equation (3.17) and (3.18) we will have

$$M_x^* + M_y^* = M_x + M_y + |M_{xy}|\,(K + \frac{1}{K})$$

so that for a minimum

$$\frac{d}{dk}(M_x^* + M_y^*) = |M_{xy}|\,(1 - \frac{1}{K^2}) = 0$$

whence $K = 1.0$.

Hence the most effective arrangement of reinforcement would be

$$M_x^* = M_x + |M_{xy}| \qquad (3.19)$$

$$M_y^* = M_y + |M_{xy}| \qquad (3.20)$$

3.4.2 Negative Moment Fields:

In this case, f(k) in equation (3.8) must be algabraically less than or equal to zero. This would yield $M_x^* \leq M_x$ and $M_y^* \leq M_y$. And as before, $df(k)/dk = 0$, but in this case $d^2f(k)/d\,k^2 \leq 0$ for an algabraic maximum. The value of k is still given by equation (3.13), and hence the corresponding equations to (3.19) and (3.20) would become

$$M_x^{*\prime} = M_x - |M_{xy}| \qquad (3.21)$$

$$M_y^{*\prime} = M_y - |M_{xy}| \qquad (3.22)$$

In which M_x and M_y are both negative. The value of k had also been taken unity for most economical steel, although a different value could have been used.

3.4.3 Mixed Moment Fields:

Awkward cases occur when one of the applied moments is positive, the other is negative. Thus if equations (3.19) or (3.20) is used to calculate the design moments M_x^* or M_y^*, a negative value may result, for which a positive (bottom) steel is useless. Accordingly, resisting normal moment can be set equal to zero and . steel will then be provided in one direction. Thus two cases may arise:

(a) Case of steel in x direction only:

In this case $M_y^* = 0$.

Using this in (3.8) and adopting the equality for minimum resistance, then

$$(M_x^* - M_x) - k^2 M_y + 2k M_{xy} = 0$$

and as before d f(k)/dk = 0 and insisting on $M_y^* = 0$ then $k = M_{xy}/M_y$ so that

$$M_x^* = M_x + \left|\frac{M_{xy}^2}{M_y}\right| \qquad (3.23)$$

with $$M_y^* = 0.0 \qquad (3.24)$$

(b) Case of steel in Y direction only:

In this case $M_x^* = 0$.

Again using (3.8), and following the normal procedure with df(k)/dk = 0 we will have

$$k = -M_{xy}/(M_y^* - M_y)$$

then

$$M_y^* = M_y + \left|\frac{M_{xy}^2}{M_x}\right| \qquad (3.25)$$

with

$$M_x^* = 0 \qquad (3.26)$$

Similar procedures can be used when positive moments occur with negative ones. Again no top steel will then be needed for the positive moments, and similar equations to those derived can be established, and will be listed below.

3.4.4 Rules for Placing Orthogonal Reinforcement:

Given the stress field (M_x,M_y,M_{xy}) at any point on the slab, the reinforcement in the X, Y directions will be placed according to the following rules:

3.4.4.1 Bottom Steel

(1) Compute the normal moments

$$M_x^* = M_x + |M_{xy}|$$
$$M_y^* = M_y + |M_{xy}| \qquad (3.27)$$

if $M_x^* < 0$ then

$$M_y^* = M_y + \left|\frac{M_{xy}^2}{M_x}\right| \quad \text{with } M_x^* = 0 \qquad (3.28)$$

if $M_y^* < 0$ then

$$M_x^* = M_x + \left|\frac{M_{xy}^2}{M_y}\right| \quad \text{with } M_y^* = 0. \qquad (3.29)$$

(2) If still in (3.28) or (3.29) one gets a negative sign, then put such normal moment equal to zero i.e. no reinforcement is required.

(3) If both M_x^* add M_y^* are negative, then no bottom steel is required.

3.4.4.2 Top Reinforcement

(1) Compute the normal moments

$$M_x^* = M_x - |M_{xy}|$$
$$M_y^* = M_y - |M_{xy}| \qquad (3.30)$$

if $M_x^* > 0$ then

$$M_y^* = M_y - \left|\frac{M_{xy}^2}{M_x}\right| \quad \text{with } M_x^* = 0 \qquad (3.31)$$

If $M_y^* > 0$ then

$$M_x^* = M_x - \left|\frac{M_{xy}^2}{M_y}\right| \quad \text{with } M_y^* = 0 \qquad (3.32)$$

(2) If still in (3.31) or (3.32) one gets a positive sign, then put such normal moment equal to zero, i.e. no reinforcement is required.

(3) If both M_x^* and M_y^* are positive, then no top steel is required.

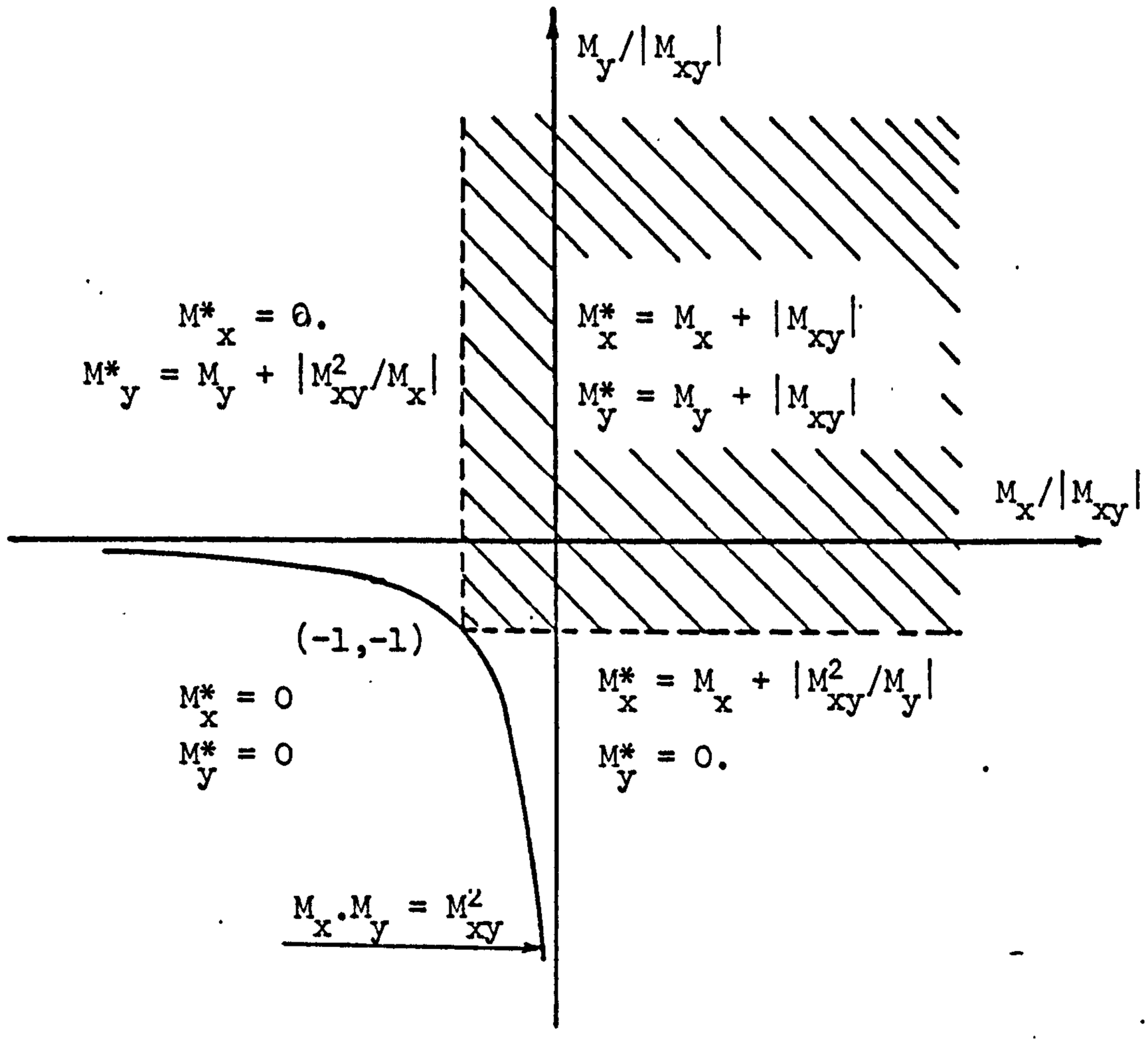

Figure (3.8) Design Equations for Bottom Steel

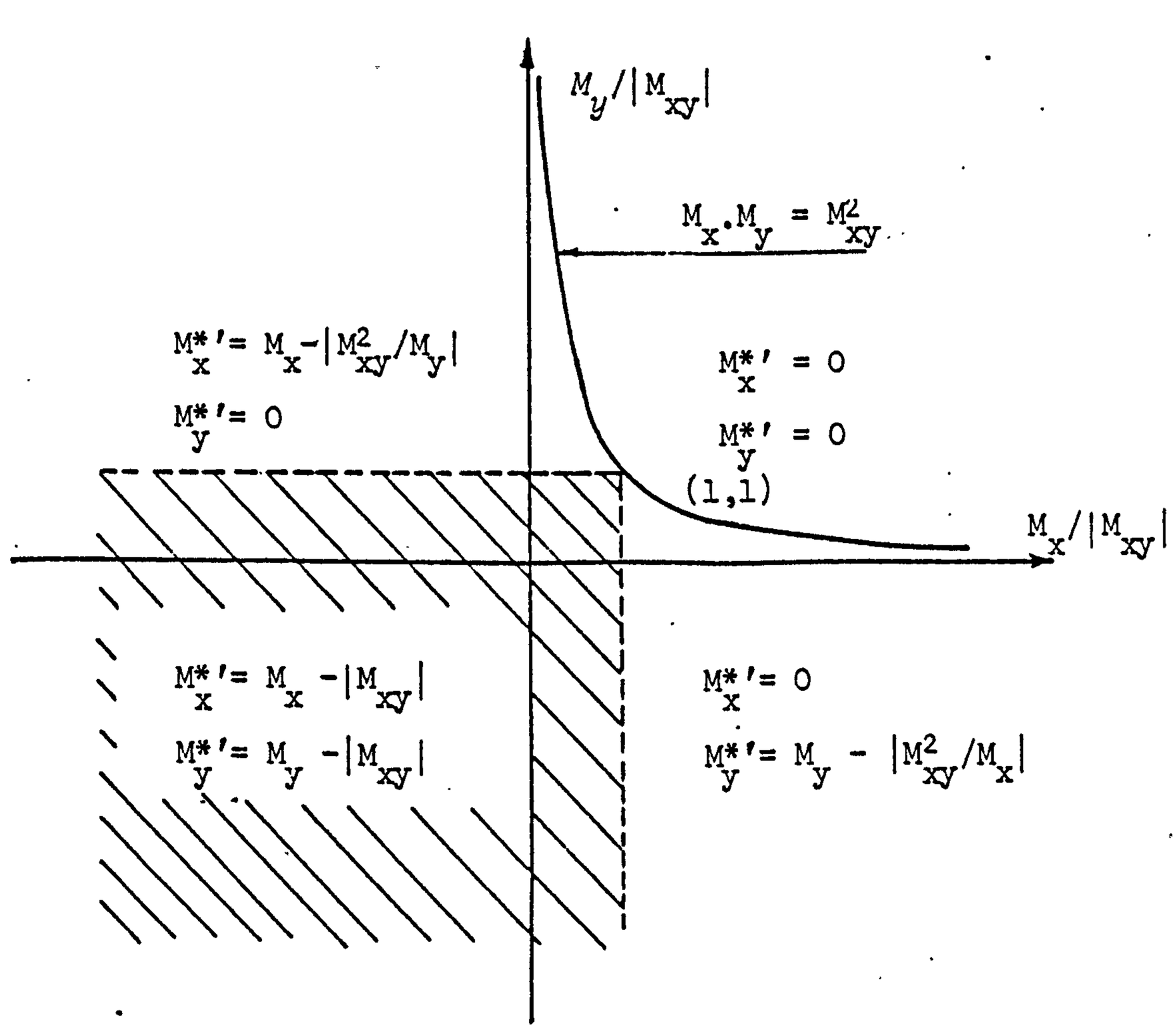

Figure (3.9) Design Equations for top Steel

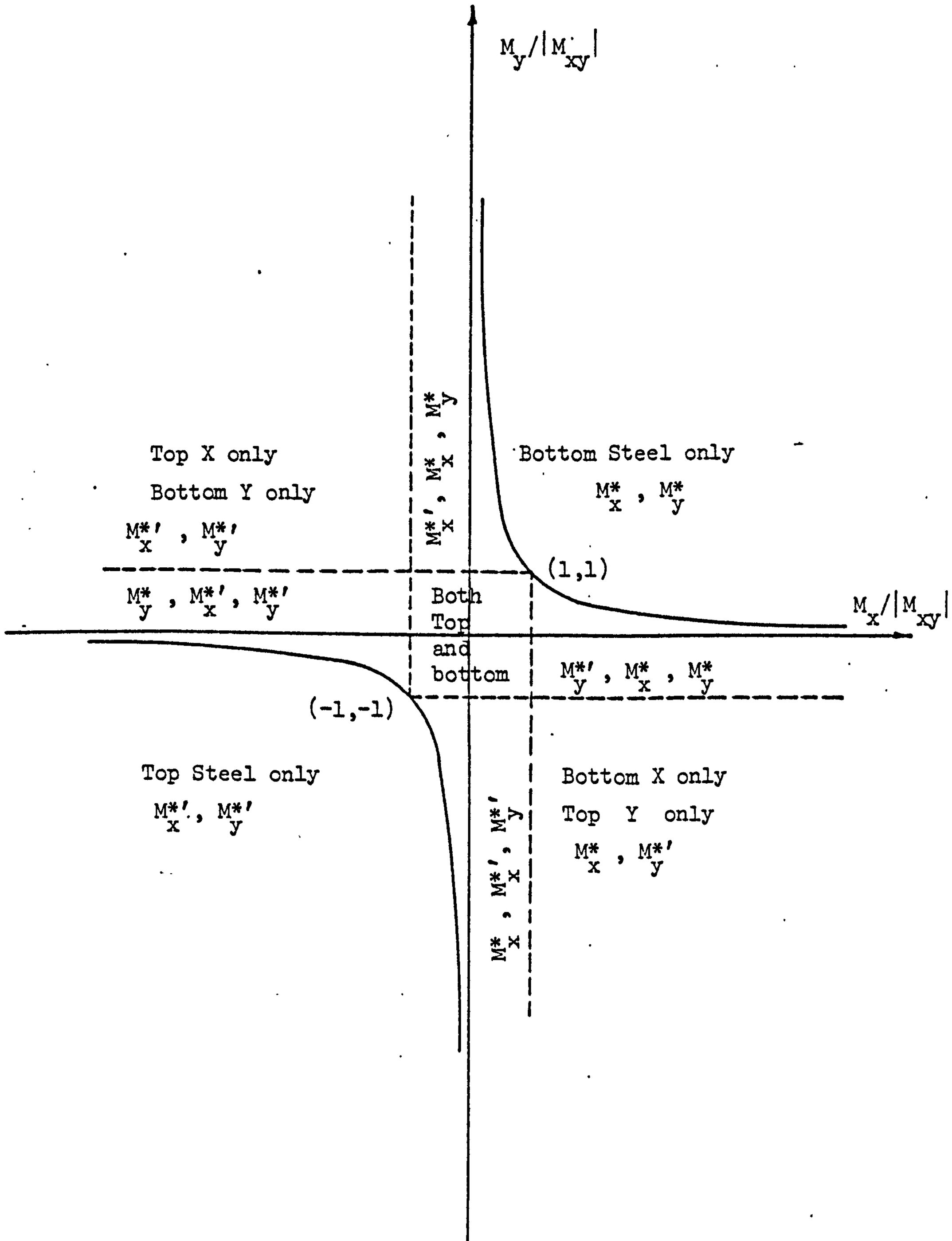

Figure (3.10) Reinforcement required for a given Moment Triad

Figures (3.8) to (3.10) give a detailed picture of these rules. For general use, the diagrams are sketched in a nondimensional form[71]. The designer, after establishing the point $(\left|\frac{M_x}{M_{xy}}\right| , \left|\frac{M_y}{M_{xy}}\right|)$ on the diagram, can easily know which equation to use to get the required design normal moments. Bottom steel equations are given in Figure (3.8), while those for top steel in Figure (3.9). Figure (3.10) shows the two branches of the yield hyperbola, and indicates the directions of the steel to be provided at any point. Primed moments refer to top steel.

The equations in this section had been derived by Wood[19], and on a similar basis were extended to skew reinforcement by Armer[20].

3.5 MULTIPLE LOADING CASES:

The above rules apply only when the slab is subjected to a moment field resulting from a single load case. In practice, however, many slabs and particularly bridge decks are subject to multiple loading. The reinforcement must then be proportioned to satisfy the multiple moment triads $(M_{xi}, M_{yi}, M_{xyi})$ i=1,n, produced by the multiple loading, where n is the number of such loading cases.

If the slab is reinforced to resist the severest load case, then an upper bound solution to the minimum reinforcement is thus provided, which is economical only if the solution lies close to some stationary minimum value of the sum $(M^*_x + M^*_y)$ for all load cases. Such a stationary minimum value is represented by point p of Figure (3.11), which represents the reinforcement needed for one loading case.

For multiple loading cases, the problem can be attacked in the following steps. The solution presented can be viewed with respect to

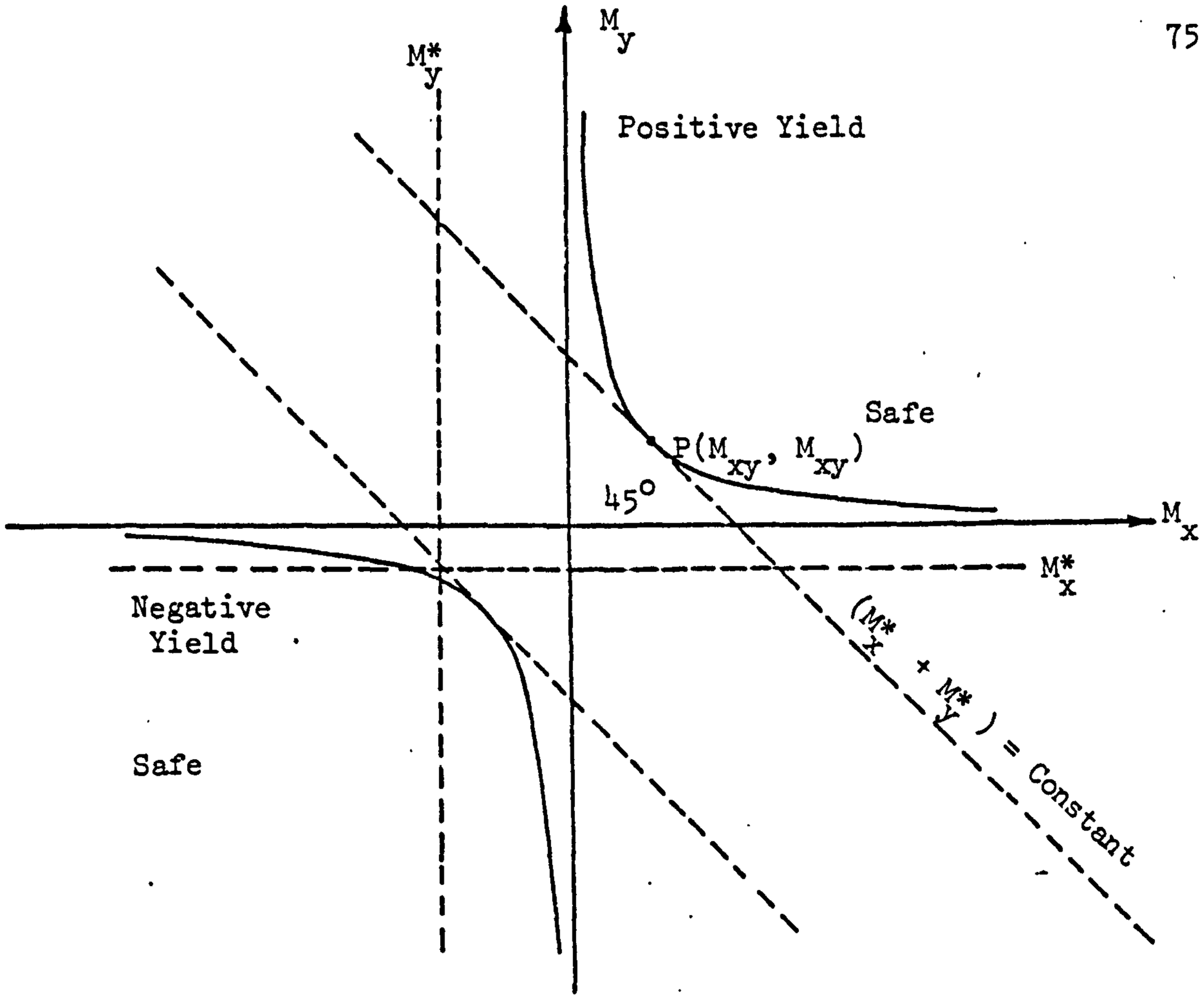

Figure (3.11) Yield Curve for Orthogonal Reinforcement

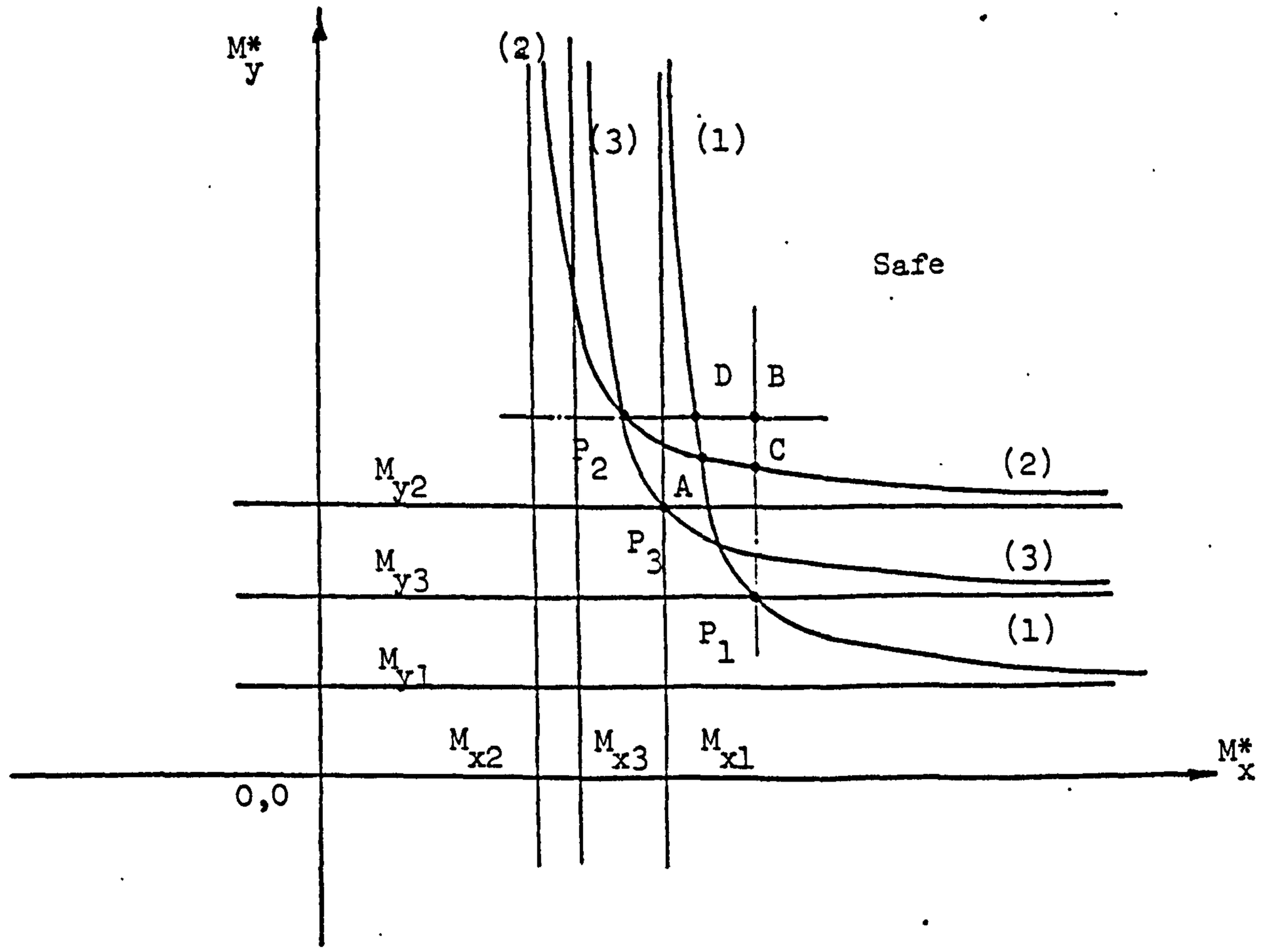

Figure (3.12) Optimum Yield Moments for Multiple Moment Triads

the case of the three loading cases shown in Figure (3.12). For simplicity, only design moments for bottom steel will be considered. It is assumed that a moment field has been established for each load case separately, and will be designated by $(M_{xi}, M_{yi}, M_{xyi})$. The steps in the solution are as follows:

(1) For each load case, find the design moments using equations (3.27) to (3.29). This will define a stationary minimum value of $(M_x^* + M_y^*)$ for each individual load case as points p_1, p_2 and p_3 in Figure (3.12).

(2) Find the maximum values of the design moments for all load cases i.e. $[M_x^* , M_y^*]_{max}$. This will represent an upper bound on the optimum yield moments, and is represented by point B in Figure (3.12). This point will always lie on the safe region.

(3) Closer upper bounds are given by points C and D in Figure (3.12).

To find the design moments values at such points, then proceed as follows: for point C, the x coordinate is $[M_x^*]_{max}$ of point B. Its y-coordinate is found by substitution of this value into the yield equation of each load case, and selecting the maximum. Whence, for point C

$$M_x^* = [M_x^*]_{max} \qquad (3.33)$$

$$M_y^* = \max \left[M_y + \frac{M_{xy}^2}{(M_x^* - M_x)} \right] \qquad (3.34)$$

Similarly for point D

$$M_y^* = [M_y^*]_{max} \qquad (3.35)$$

$$M_x^* = \max \left[M_x + \frac{M_{xy}^2}{(M_y^* - M_y)} \right] \qquad (3.36)$$

(4) A further optimization is done by looking for the minimum of $(M_x^* + M_y^*)$, and satisfy the yield criterion at all grid points in the region CBD.

However, the same procedure can be adopted for negative steel, in which case, the minimum replaces the maximum in the above steps. The problem can also be solved graphically, by drawing the yield curve for each load case, and then selecting the least value of $(M_x^* + M_y^*)$, as point A in Figure (3.12) by inspection, which is the intersection of two yield curves.

The above procedure can also be used in case of skew reinforcement, as explained by Kemp[69].

3.6 DESIGN OF REINFORCEMENT FOR MEMBRANE FORCES:

Equations analogous to those given for flexural reinforcement were also derived by Nielsen[74] to design orthogonal reinforcement to resist tensile membrane forces. He assumed that, if both principal inplane forces are compressive, then all such forces can be supported by concrete only, and no reinforcement is needed. He also considered skew reinforcement, and the procedure adopted is similar to that used for flexural reinforcement. ( ) Clark[75] extended the Nielsen approach to cover a general state of stress. Clark pointed out that it may be of practical interest to provide reinforcement even for inplane compressive forces. Clark equations are thus more general than those of Nielsen or Morley[88], who considered the case of combined flexure and membrane forces. This problem will be discussed later in section (3.7).

3.6.1 Rules for Designing for Inplane Forces:

Given the stress triad (N_x, N_y, N_{xy}) at any point in the slab, and is required to design reinforcement according to the lower bound theory of plasticity. In this research, the stress vector will be obtained using the finite element program described in Chapter 4. In addition to assumptions (1) and (2) of Section (3.3.2), it will further be assumed that under plane stress conditions, concrete obeys the square yield criterion shown in Figure (3.13), and that failure occurs by unrestricted plastic flow and not by buckling of the section.

Sign convention for membrane forces is tension positive, Figure (3.14). A general case of providing reinforcement in the two directions x and α will be considered. The reinforcement in these directions and their associated stresses will be A_x, A_α and f_x and f_α respectively. The principal concrete stresses are taken to be σ_1 and σ_2 with the major principal stress at θ to the x-axis, as shown in Figure (3.15). σ_1 is always algabraically greater than σ_2.

By considering Figures (3.15) and (3.16), the following equilibrium equations may be written:

$$N_x = A_x f_x + A_\alpha f_\alpha \cos^2 \alpha + \sigma_1 h \cos^2 \theta + \sigma_2 h \sin^2 \theta$$

$$N_y = A_\alpha f_\alpha \sin^2 \alpha + \sigma_1 h \sin^2 \theta + \sigma_2 h \cos^2 \theta \qquad (3.37)$$

$$N_{xy} = - A_\alpha f_\alpha \sin \alpha \cos \alpha - \sigma_1 h \sin \theta \cos \theta + \sigma_2 h \sin \theta \cos \theta$$

On dividing through by the slab thickness (h) and defining the normal and shear stresses as

$$\sigma_x = N_x/h \ , \quad \sigma_y = N_y/h \ , \quad \tau_{xy} = N_{xy}/h \qquad (3.38)$$

and the reinforcement ratios as

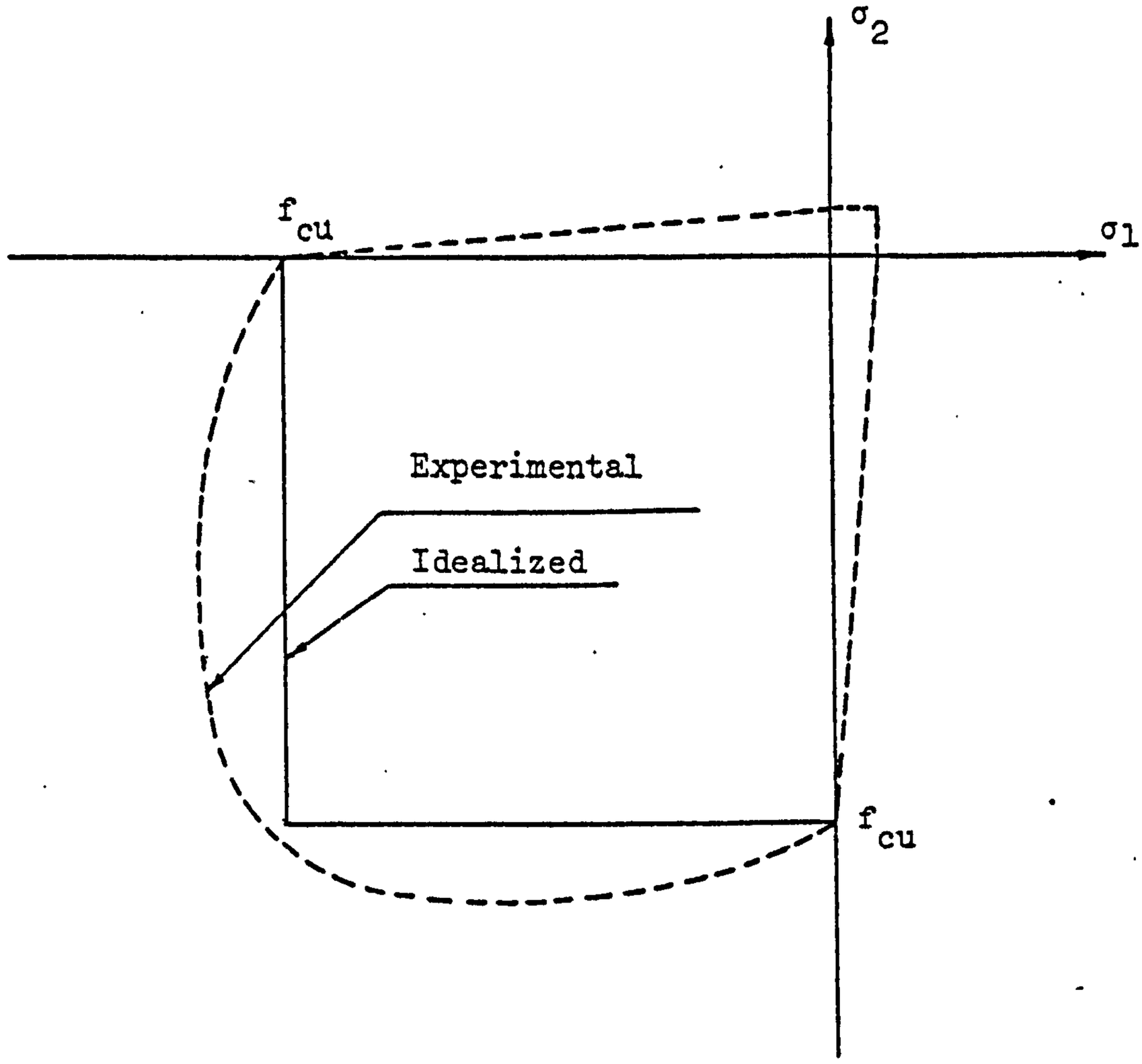

Figure (3.13) Yield Criterion for Concrete in Plane Stress

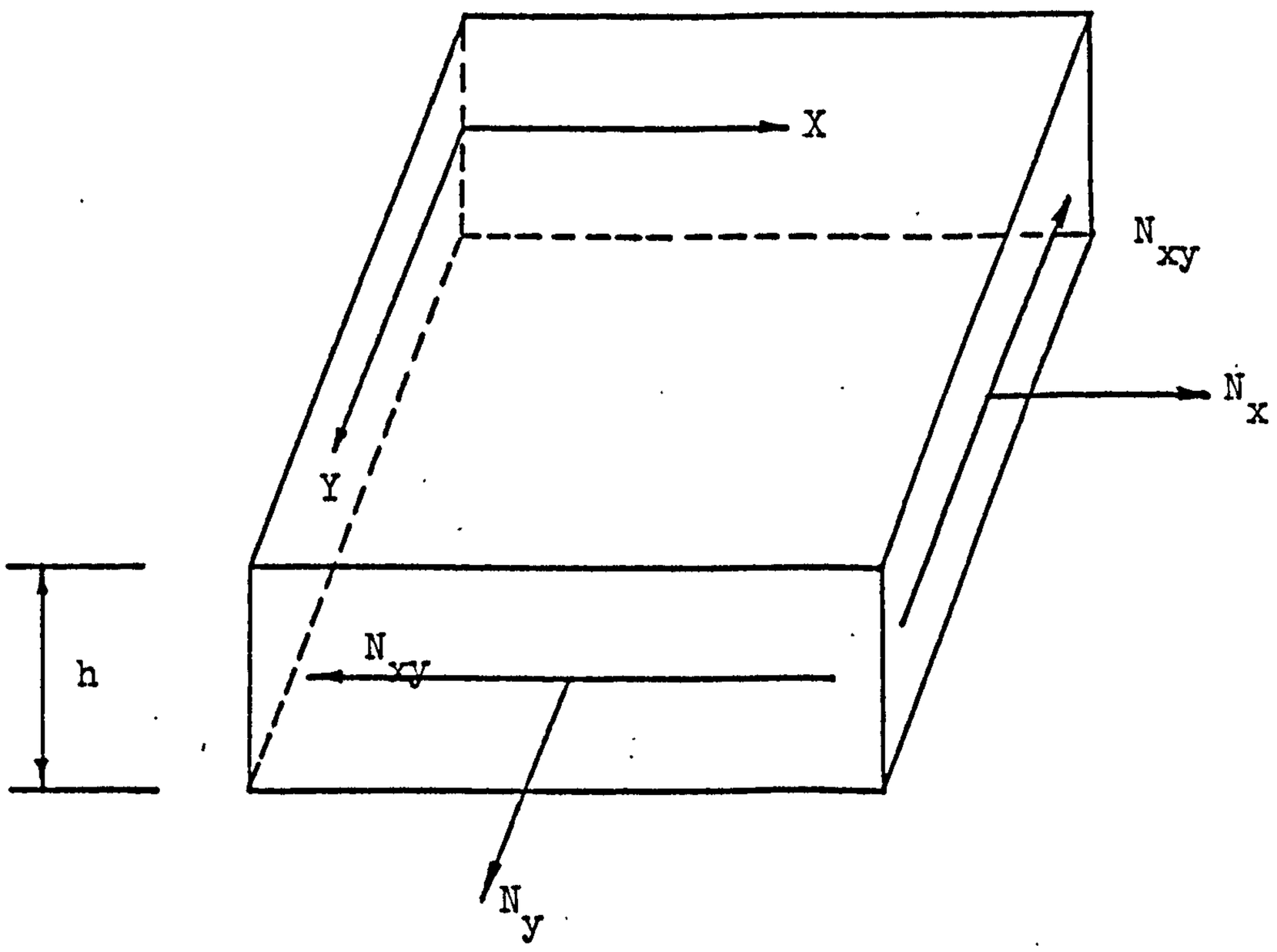

Figure (3.14) Sign Convention for Direct and Shear Inplane Forces per Unit Length

$$\rho_x = A_x/h \quad , \qquad \rho_\alpha = A_\alpha/h \tag{3.39}$$

we obtain

$$\begin{aligned}
\sigma_x &= \rho_x f_x + \rho_\alpha f_\alpha \cos^2\alpha + \sigma_1 \cos^2\theta + \sigma_2 \sin^2\theta \\
\sigma_y &= \rho_\alpha f_\alpha \sin^2\alpha + \sigma_1 \sin^2\theta + \sigma_2 \cos^2\theta \qquad (3.40) \\
\tau_{xy} &= -\rho_\alpha f_\alpha \sin\alpha \cos\alpha - (\sigma_1 - \sigma_2) \sin\theta \cos\theta
\end{aligned}$$

There are seven unknowns in equations (3.40). By considering the yield criterion for a certain state of stresses, some of the variables can be predetermined for nine possible cases summarized in Table (3.1). It can be seen that a direct solution can be obtained except for cases (1) and (4), where four unknowns are to be determined from the three equations of (3.40). The fourth equation can be obtained by minimizing the total reinforcement in the element thus

$$\frac{\partial (\rho_x + \rho_{\alpha,y})}{\partial \tan\theta} = 0 \tag{3.41}$$

In Table (3.1), σ_1 is given as zero when tension reinforcement is provided because of the assumption that concrete does not carry tensile forces, and $\sigma_2 = f_c$ when compression reinforcement is provided to make the optimum use of concrete.

Table (3.2) summarizes the expressions for the areas of reinforcement, principal stresses in concrete, and θ for each case. The following symbols are used in Table (3.2)

$$\begin{aligned}
\sigma_{xf} &= \sigma_x - f_c \\
\sigma_{yf} &= \sigma_y - f_c
\end{aligned}$$

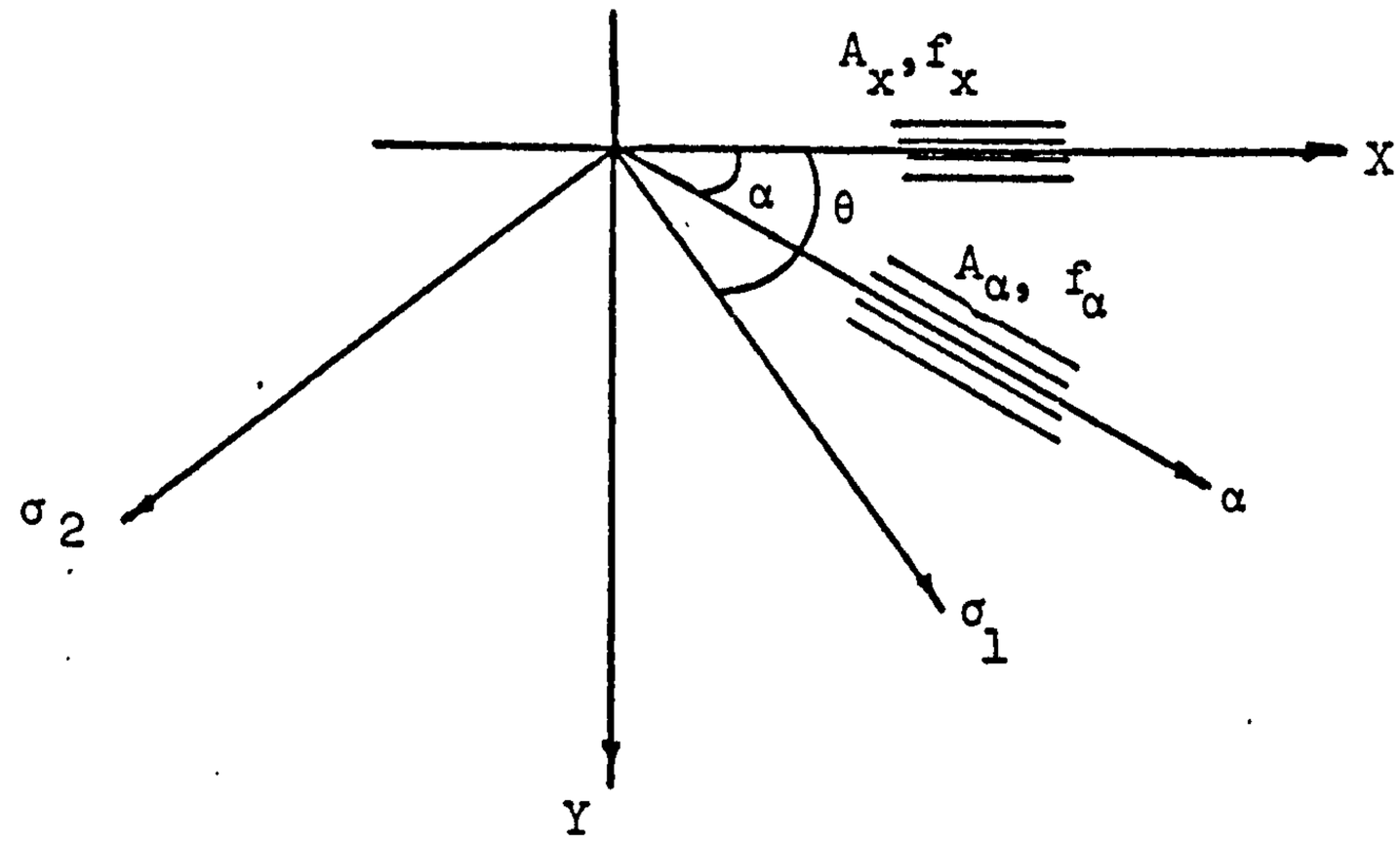

Figure (3.15) Directions of Reinforcement and Principal Stresses in Concrete

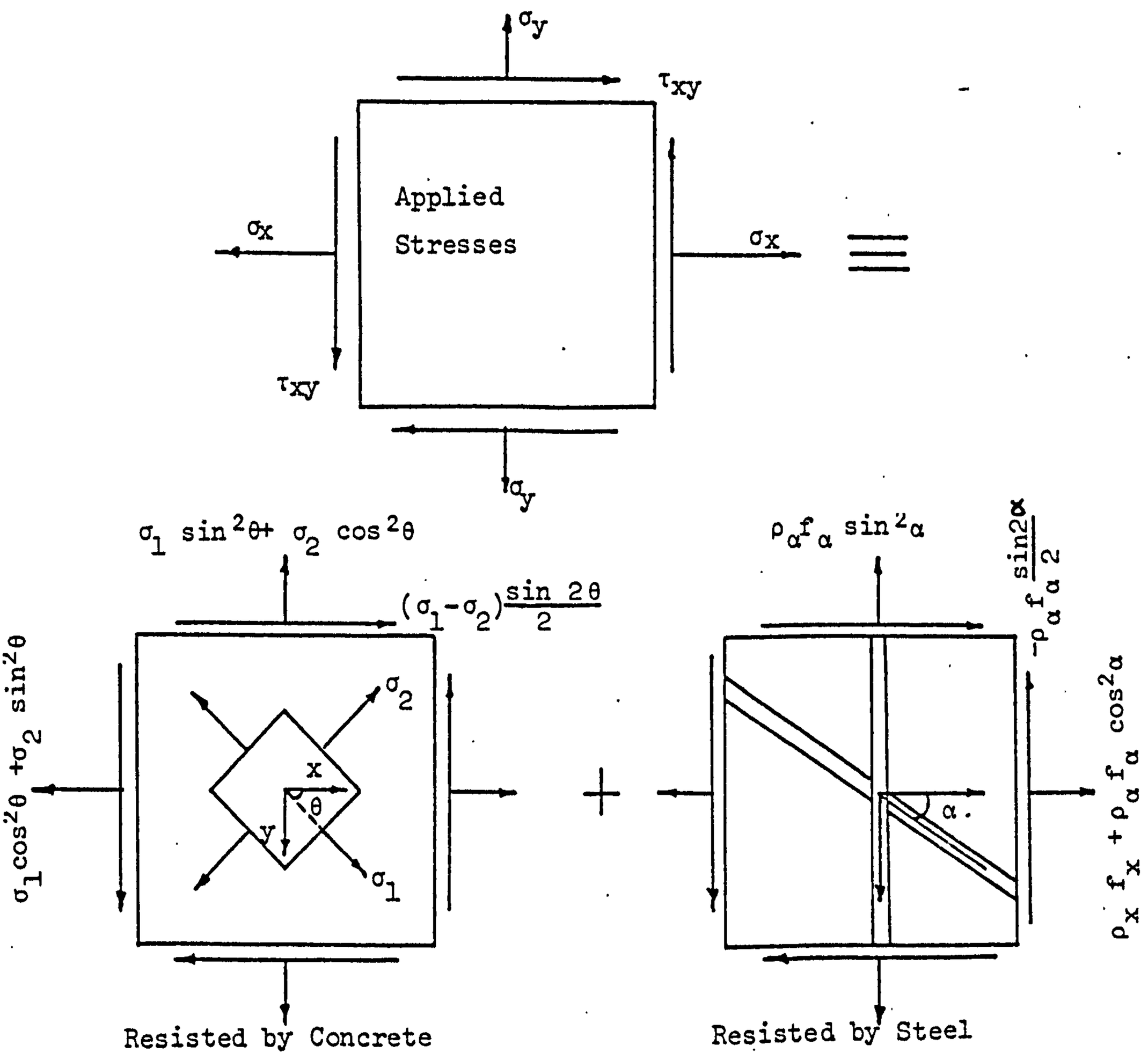

Figure (3.16) Equilibrium of a slab element under Membrane Forces

$$\beta = \sqrt{1 - \frac{4}{f_c^2}(\tau_{xy} + \sigma_y \cot \alpha)(\tau_{xy} + \sigma_{yf} \cot \alpha)} \ .$$

Having established the equations relevant to each case in Table (3.1), it is necessary to establish a means of determining which set of equations should be used for a particular stress triad. This can be achieved by deriving the surfaces in stress space which form the boundaries to regions pertinent to each case. Following the procedure adopted for flexural reinforcement (Section 3.4.4), the design equations can be plotted on the non-dimensional plane $\sigma_x/|\tau_{xy}|$, $\sigma_y/|\tau_{xy}|$. Typical curves are shown in Figure (3.17) for $\alpha = 60^\circ$ and $f_c/|\tau_{xy}| = -4$. The equations of the boundary curves are given in Table (3.3).

To cover all the cases with real boundary curves, it is required that

$$f_c \leq -2\,|\tau_{xy}|\ \text{cosec}\ \alpha$$

The boundary line parallel to $\sigma_x/|\tau_{xy}|$ axis extends to $\pm \infty$.

When $\alpha = \pi/2$, we have the case of orthogonal reinforcement, and the complex expressions in Table (3.2) and (3.3) reduce those given in Table (3.4) and (3.5) respectively. In addition, the case boundary graphs illustrated in Figure (3.17) reduce to one graph of Figure (3.18).

3.7 COMBINED BENDING AND MEMBRANE FORCES:

The stress triad in this case becomes (N_x, N_y, N_{xy}, M_x, M_y, M_{xy}), and to design for all six components, a filled sandwich element is used[74, 75, 76]. In such an approach, all six stress resultants are resolved into a set of inplane stress resultants acting in the outer

shells of the sandwich. Figure (3.19) shows such an element, whereas Figures (3.20) and (3.21) show the resolution of these forces and how they are all lumped at the level of the reinforcements. The basic assumption behind such methods is that the reinforcement will be centrally positioned in the outer shells of the element. Further to simplify the problem for designers, it is best to assume that

$$Z_x = Z_y = Z_{xx}$$

$$X_x = X_y = X_{xx}$$

$$Y_x = Y_y = Y_{xx}$$

where X_{xx}, Y_{xx} and Z_{xx} are some reasonable average values of the distances of the steel layers from the middle plane of the plate.

When all stress resultants are summed up as membrane forces at the reinforcement level, the problem reduces to the problem of designing for membrane forces only. And the equations described in the previous section can then be used.

3.8 CLOSURE

The rules set in this chapter provide either an optimum reinforcement or a close upper bound to the minimum reinforcement in concrete slabs. These rules will ensure that the yield criteria are nowhere exceeded, and that a state of yield will exist in most slab portions, sufficient to convert it into a mechanism at failure. The other conditions of equilibrium and boundary conditions will be satisfied by a stress field obtained from a finite element program, and this will be discussed in the following chapter.

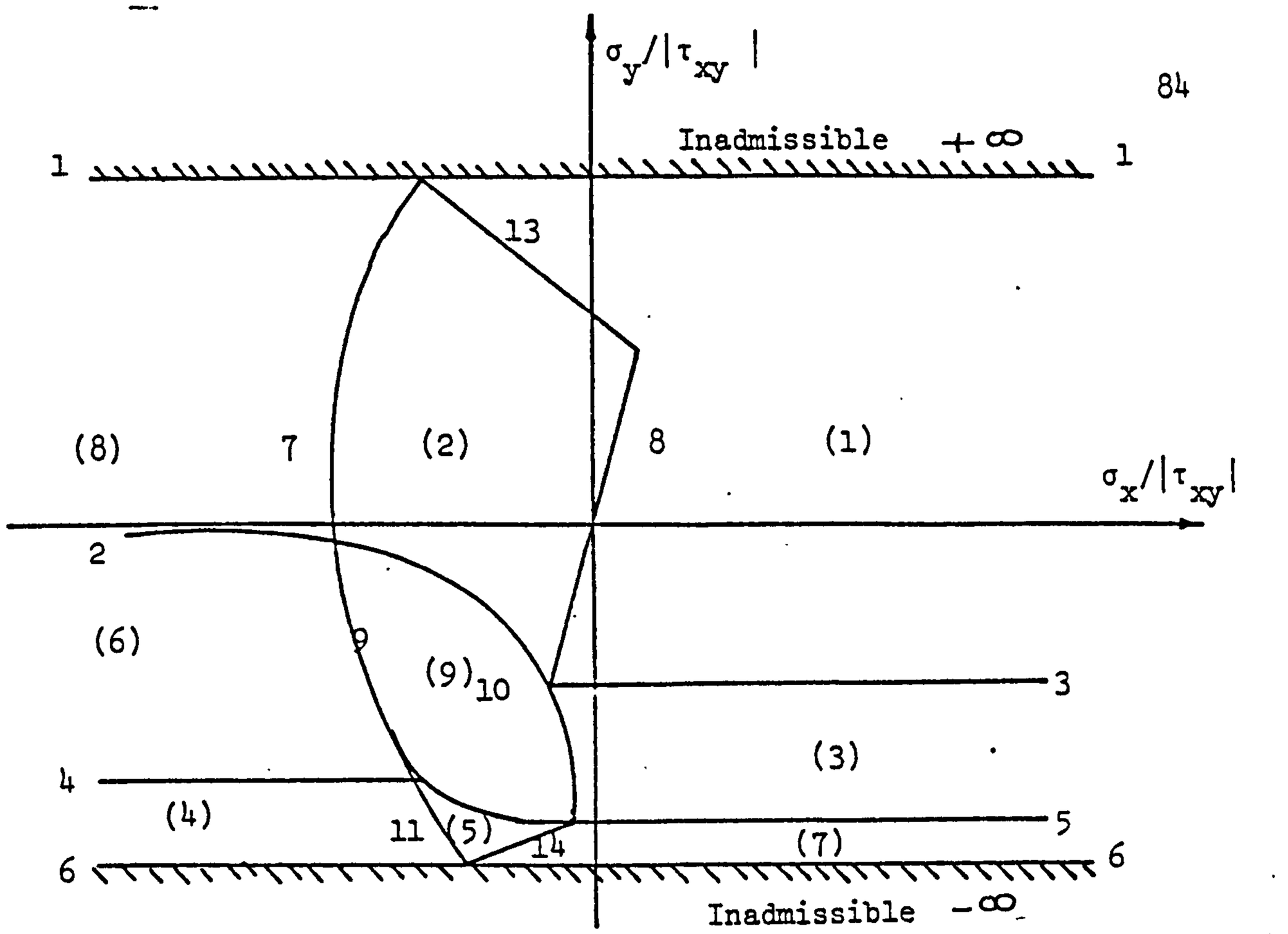

(a) Negative Shear Stress τ_{xy}

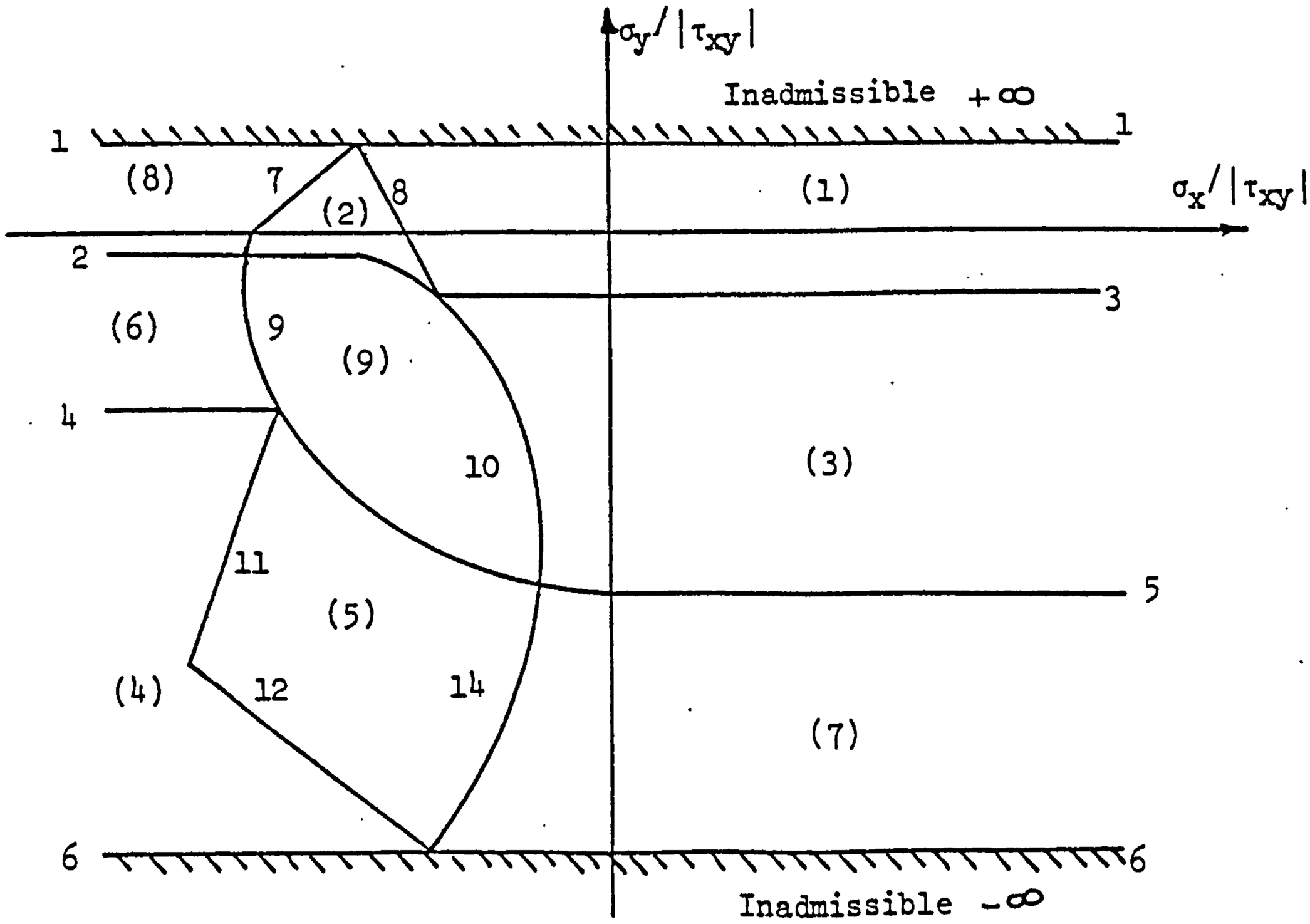

(b) Positive Shear Stress τ_{xy}

Figure (3.17) Case Boundary Graphs for $\alpha = 60^{\circ}$; $f_c = -4\ (\tau_{xy})$.

Plain Numerals Represent Boundary Curves Nos.
bracketed numerals for case nos.

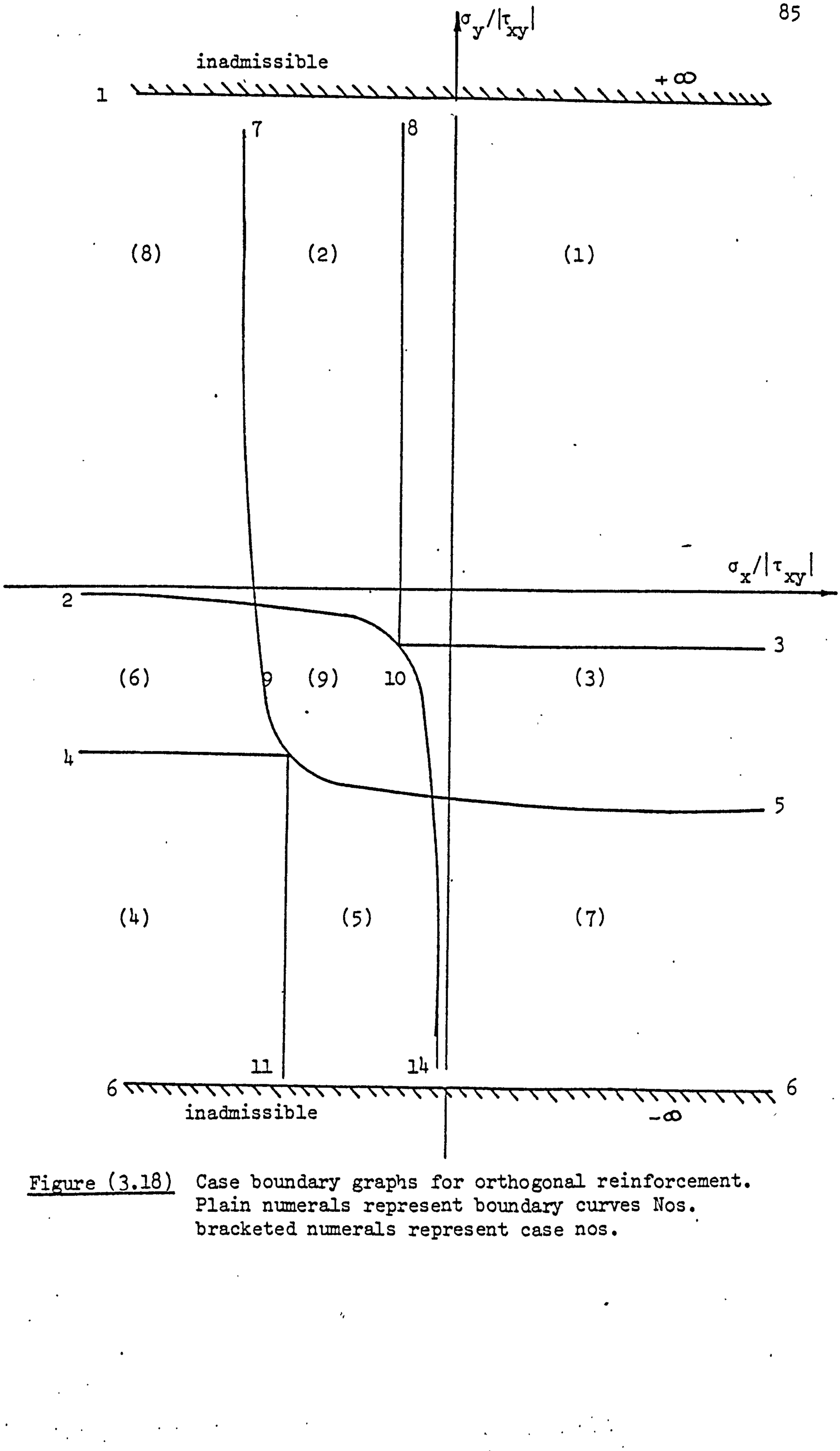

Figure (3.18) Case boundary graphs for orthogonal reinforcement. Plain numerals represent boundary curves Nos. bracketed numerals represent case nos.

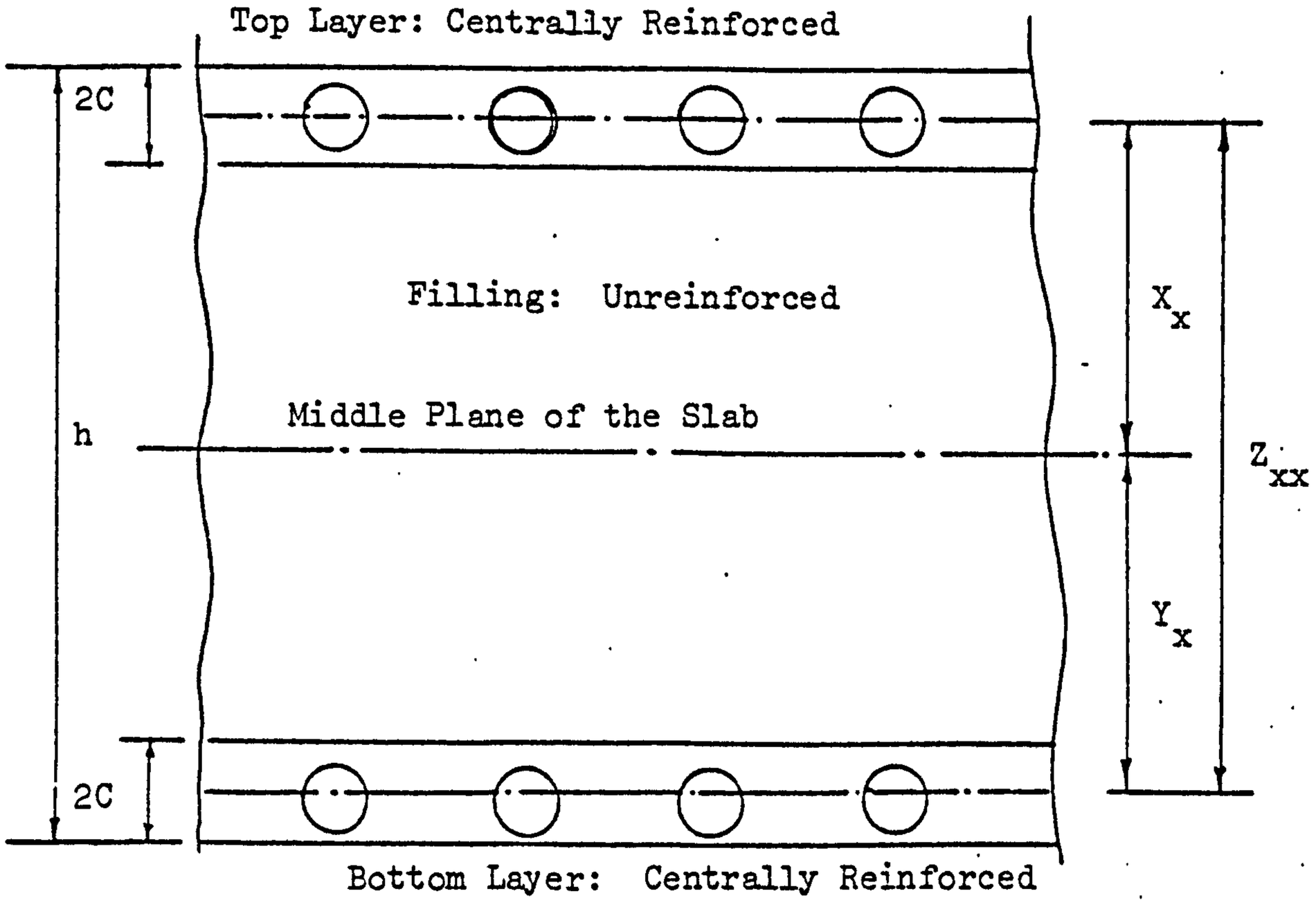

Figure (3.19) Filled Sandwich Model

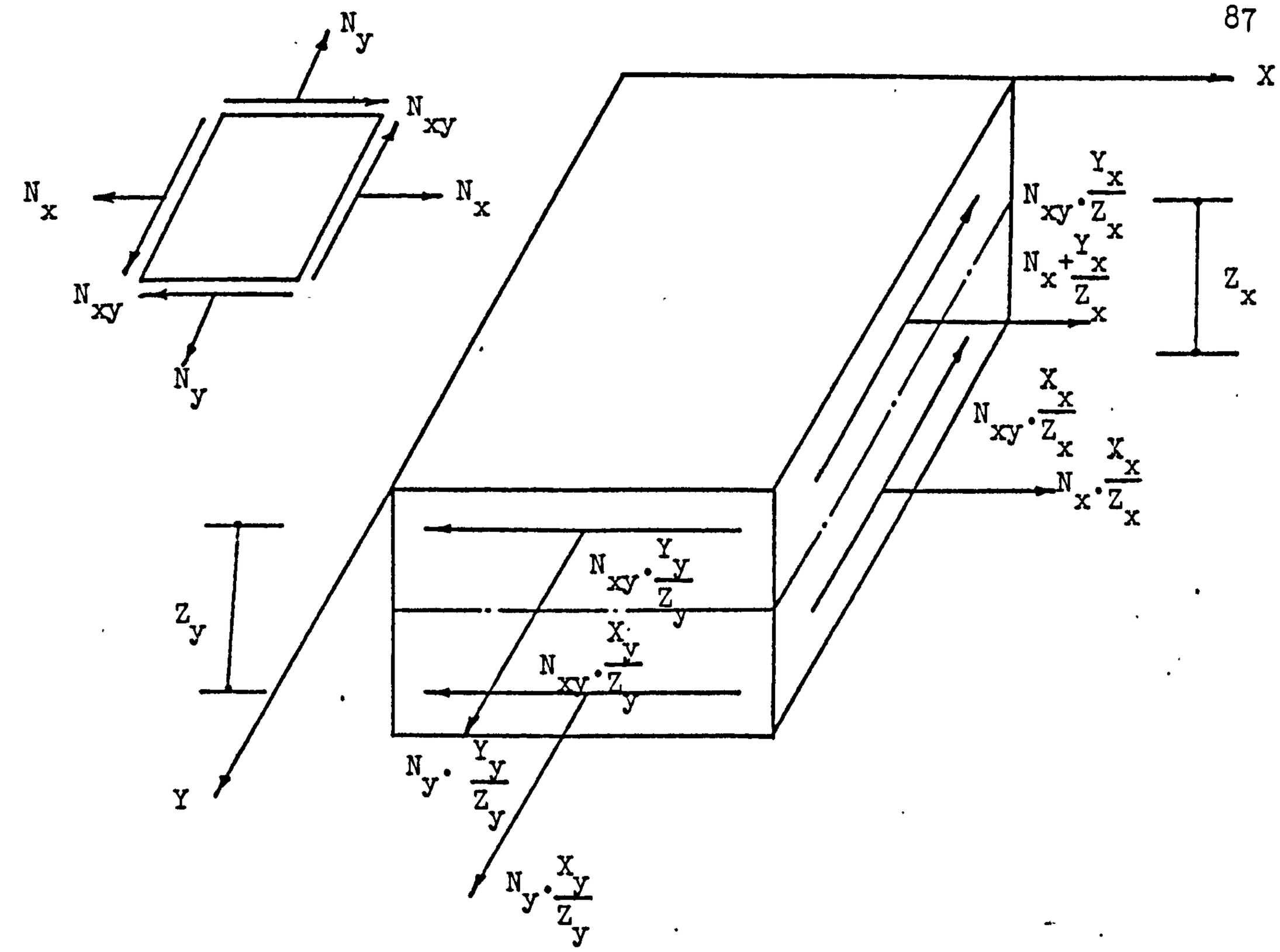

Figure (3.20) Membrane Stress Resultants on a Filled Sandwich Element

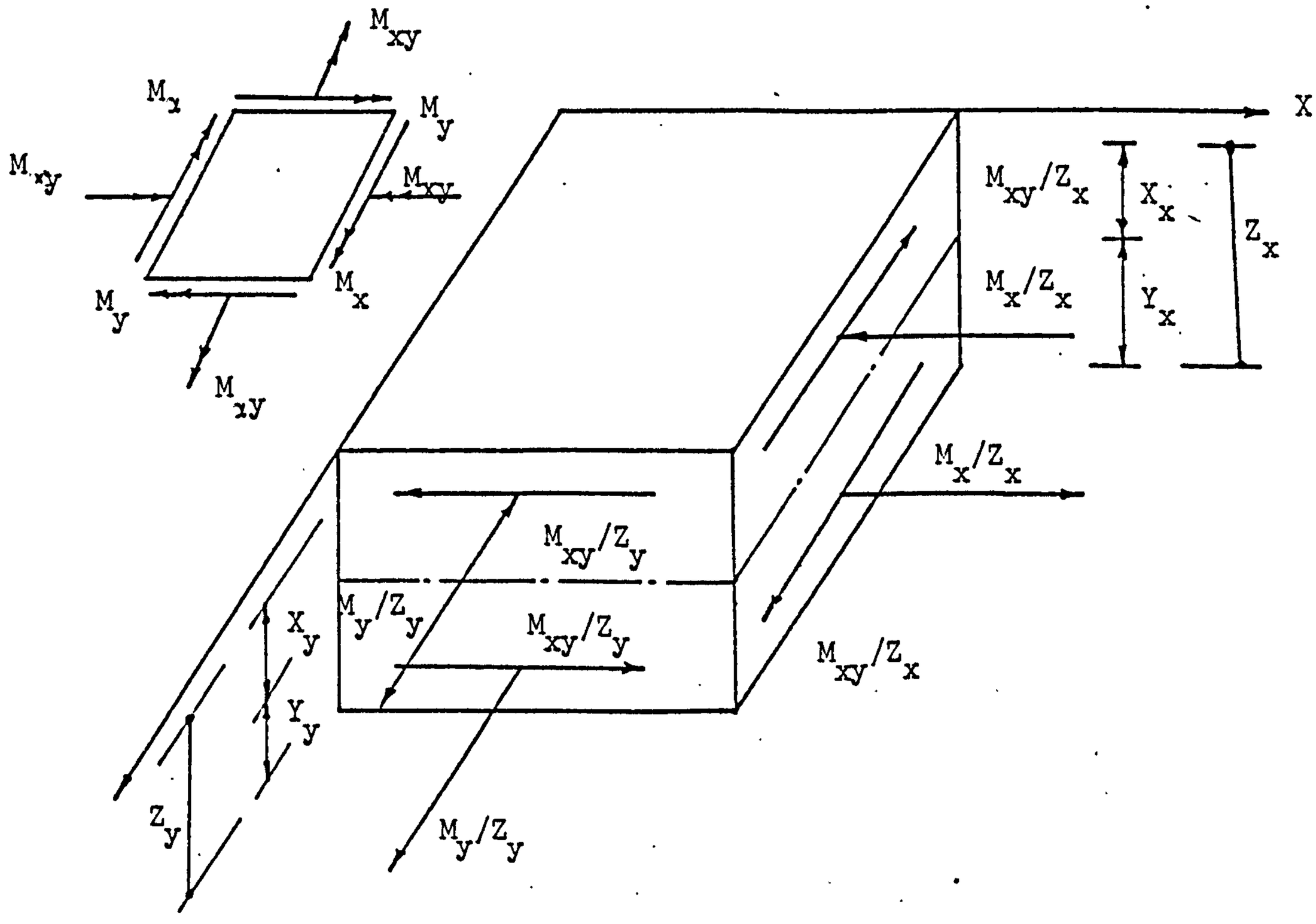

Figure (3.21) Bending Stress Resultants on a Filled Sandwich Element.

Table 3.1 Summary of Various Possible Combinations of Reinforcement.

Case	Reinforcement description	Known values	Method of Solution
1	Both tension	$f_x = f_\alpha = f_s$, $\sigma_1 = 0$	minimization of $(\rho_x + \rho_y)$
2	No x α tension	$f_\alpha = f_s$, $\rho_x = 0$, $\sigma_1 = 0$	direct solution
3	No α x tension	$f_x = f_s$, $\rho_\alpha = 0$, $\sigma_1 = 0$	direct solution
4	Both compression	$f_x = f_\alpha = f'_s$, $\sigma_2 = f_c$	minimization of $(\rho_x + \rho_y)$
5	No x α compression	$f_\alpha = f'_s$, $\rho_x = 0$, $\sigma_2 = f_c$	direct solution
6	No α x compression	$f_x = f'_s$, $\rho_\alpha = 0$, $\sigma_2 = f_c$	direct solution
7	x tension α compression	$f_x = f_s$, $f_\alpha = f'_s$, $\sigma_1 = 0$, $\sigma_2 = f_c$	direct solution
8	x compression α tension	$f_x = f'_s$, $f_\alpha = f_s$, $\sigma_1 = 0$, $\sigma_2 = f_c$	direct solution
9	No reinforcement	$\rho_x = \rho_\alpha = 0$	direct solution

Case	ρ_x	ρ_α	σ_1	σ_2	tan θ
1	$\frac{1}{f_s}(\sigma_x+2\tau_{xy}\cot\alpha+\sigma_y\cot\alpha+[(\tau_{xy}+\sigma_y\cot\alpha)/\sin\alpha])$	$\frac{1}{f_s}(\sigma_y\,\mathrm{cosec}^2\alpha+[(\tau_{xy}+\sigma_y\cot\alpha)/\sin\alpha])$	0	$-2(\tau_{xy}+\sigma_y\cot\alpha)(\cot\alpha\pm\mathrm{cosec}\,\alpha)$	$-(\cot\alpha\pm\mathrm{cosec}\,\alpha)$
2	0	$\frac{\mathrm{cosec}^2\alpha}{f_s}\left(\frac{\sigma_x+\sigma_y-\tau_{xy}^2}{\sigma_x+2\tau_{xy}\cot\alpha+\sigma_y\cot^2\alpha}\right)$	0	$[(\sigma_x+\tau_{xy}\cot\alpha)^2+(\tau_{xy}+\sigma_y\cot\alpha)^2]/[\sigma_x+2\tau_{xy}\cot\alpha+\sigma_y\cot^2\alpha]$	$\frac{\sigma_x+\tau_{xy}\cot\alpha}{\tau_{xy}+\sigma_y\cot\alpha}$
3	$\frac{1}{f_s}(\sigma_x-\frac{\tau_{xy}^2}{\sigma_y})$	0	0	$\sigma_y+\frac{\tau_{xy}^2}{\sigma_y}$	$\frac{\tau_{xy}}{\sigma_y}$
4	$\frac{1}{f'_s}(\sigma_{xf}+2\tau_{xy}\cot\alpha+\sigma_{yf}\cot^2\alpha-\lvert[(\tau_{xy}+\sigma_{yf}\cot\alpha)/\sin\alpha]\rvert)$	$\frac{1}{f'_s}(\sigma_{yf}\,\mathrm{cosec}^2\alpha-\lvert[(\tau_{xy}+\sigma_{yf}\cot\alpha)/\sin\alpha]\rvert)$	$f_c+2(\tau_{xy}+\sigma_{yf}\cot\alpha)(-\cot\alpha\pm\mathrm{cosec}\,\alpha)$	f_c	$-(-\cot\alpha\pm\mathrm{cosec}\,\alpha)^{-1}$

Table 3.2 Design Equation for Skew Reinforcement

Note: Case 1: alternative sign is the same as that of $(\tau_{xy}+\sigma_y\cot\alpha)$

Case 4: alternative sign is the same as that of of $(\tau_{xy}+\sigma_{yf}\cot\alpha)$

Case	ρ_x	ρ_α	σ_1	σ_2	$\tan\theta$
5	0	$\dfrac{\operatorname{cosec}^2\alpha}{f_s'\left(\dfrac{\sigma_{xf}\sigma_{yf}-\tau_{xy}^2}{\sigma_{xf}+2\tau_{xy}\cot\alpha+\sigma_{yf}\cot^2\alpha}\right)}$	$f_c+\left[(\sigma_{xf}+\tau_{xy}\cot\alpha)^2+(\tau_{xy}+\sigma_{yf}\cot\alpha)^2\right]/\left[\sigma_{xf}+2\tau_{xy}\cot\alpha+\sigma_{yf}\cot^2\alpha\right]$	f_c	$-\left(\dfrac{\tau_{xy}+\sigma_{yf}\cot\alpha}{\sigma_{xf}+\tau_{xy}\cot\alpha}\right)$
6	$\dfrac{1}{f_s'}\left(\sigma_{xf}-\dfrac{\tau_{xy}^2}{\sigma_{yf}}\right)$	0	$\sigma_y+\dfrac{\tau_{xy}^2}{\sigma_{yf}}$	f_c	$-\dfrac{\sigma_{yf}}{\tau_{xy}}$
7	$\dfrac{1}{f_s}\left[\sigma_x+\tau_{xy}\cot\alpha-\dfrac{f_c}{2}(1-\beta)\right]$	$\dfrac{1}{f_s'}\left[\sigma_y-\tau_{xy}\cot\alpha-\dfrac{f_c}{2}(1+\beta)\right]$	0	f_c	$\dfrac{\tau_{xy}+\sigma_y\cot\alpha-\frac{f_c}{2}(1+\beta)\cot\alpha}{\sigma_y\cot^2\alpha+\tau_{xy}\cot^2\alpha+\frac{f_c}{2}(1+\beta)}$
8	$\dfrac{1}{f_s'}\sigma_x+\tau_{xy}\cot\alpha-\dfrac{f_c}{2}(1+\beta)$	$\dfrac{1}{f_s}\sigma_y-\tau_{xy}\cot\alpha-\dfrac{f_c}{2}(1-\beta)$	0	f_c	$\dfrac{\tau_{xy}+\sigma_y\cot\alpha-\frac{f_c}{2}(1-\beta)\cot\alpha}{\sigma_y\cot\alpha+\tau_{xy}\cot+\frac{f_c}{2}(1-\beta)}$
9	0	0	$\dfrac{\sigma_x+\sigma_y+\sqrt{(\sigma_x-\sigma_y)^2+4\tau_{xy}^2}}{2}$	$\left(\sigma_x+\sigma_y-\sqrt{(\sigma_x-\sigma_y)^2+4\tau_{xy}^2}\right)/2$	$\dfrac{\sigma_x-\sigma_y-\sqrt{(\sigma_x-\sigma_y)^2+4\tau_{xy}^2}}{2}$

Table 3.2: Design Equation for Skew Reinforcement.

continued....

Notes: Case 1: alternative sign is the same as that of $(\tau_{xy}+\sigma_y\cot\alpha)$

Case 4: alternative sign is the same as that of $(\tau_{xy}+\sigma_y\cot\alpha)$

Table 3.3 Boundary Curves for Skew Reinforcement

Curve	Equation
1	$\left\lvert\frac{\sigma_y}{\tau_{xy}}\right\rvert = -\left[\pm\tan\alpha - \frac{f_c}{2\lvert\tau_{xy}\rvert}\,(1-\lvert\sec\alpha\rvert)\right]$
2	$\left\lvert\frac{\sigma_y}{\tau_{xy}}\right\rvert = \frac{1}{2}\left[\frac{f_c}{\lvert\tau_{xy}\rvert} + \sqrt{\left(\frac{f_c}{\lvert\tau_{xy}\rvert}\right)^2 - 4}\right]$
3	$\left\lvert\frac{\sigma y}{\tau_{xy}}\right\rvert = -\,(\operatorname{cosec}\alpha \pm \cot\alpha)^{-1}$
4	$\left\lvert\frac{\sigma_y}{\tau_{xy}}\right\rvert = \left\lvert\frac{f_c}{\tau_{xy}}\right\rvert - (-\operatorname{cosec}\alpha \pm \cot\alpha)^{-1}$
5	$\left\lvert\frac{\sigma_y}{\tau_{xy}}\right\rvert = \frac{1}{2}\left[\frac{f_c}{\tau_{xy}} - \sqrt{\left(\frac{f_c}{\lvert\tau_{xy}\rvert}\right)^2 - 4}\right]$
6	$\left\lvert\frac{\sigma_y}{\tau_{xy}}\right\rvert = -\left[\pm\tan\alpha - \frac{f_c}{2\lvert\tau_{xy}\rvert}\,(1+\lvert\sec\alpha\rvert)\right]$
7	$\left\lvert\frac{\sigma_x}{\tau_{xy}}\right\rvert = -\frac{1}{2}\left[-\left\lvert\frac{f_c}{\tau_{xy}}\right\rvert \pm 2\cot\alpha + \sqrt{\left[\frac{f_c}{\lvert\tau_{xy}\rvert}\right]^2 - 4\left(\frac{\sigma_y\cot\alpha}{\lvert\tau_{xy}\rvert} \pm 1\right)\left(\frac{\sigma_y\cot\alpha}{\lvert\tau_{xy}\rvert} \pm 1\right)}\right]$
8	$\left\lvert\frac{\sigma_x}{\tau_{xy}}\right\rvert + \left\lvert\frac{\sigma_y}{\tau_{xy}}\right\rvert \cot\alpha(\cot \pm \operatorname{cosec}\alpha) + \operatorname{cosec}\alpha \pm 2\cot\alpha = 0$
9	$\frac{\sigma_{xf}}{\lvert\tau_{xy}\rvert}\;\frac{\sigma_{yf}}{\lvert\tau_{xy}\rvert} = 1$
10	$\frac{\sigma_x}{\lvert\tau_{xy}\rvert}\;\frac{\sigma_y}{\lvert\tau_{xy}\rvert} = 1$
11	$\frac{\sigma_x}{\lvert\tau_{xy}\rvert} - \frac{\sigma_y}{\lvert\tau_{xy}\rvert}\cot\alpha\,(-\cot\alpha \pm \operatorname{cosec}\alpha) - \operatorname{cosec}\alpha \pm 2\cot\alpha + \frac{f_c}{\lvert\tau_{xy}\rvert}\operatorname{cosec}\alpha\,(-\operatorname{cosec}\alpha \pm \cot\alpha) = 0$
12	$\frac{\sigma_x}{\lvert\tau_{xy}\rvert} + \frac{\sigma_y}{\lvert\tau_{xy}\rvert}\cot\alpha\,(\cot\alpha \pm \operatorname{cosec}\alpha) + \operatorname{cosec}\alpha \pm 2\cot\alpha - \frac{f_c}{\lvert\tau_{xy}\rvert}\operatorname{cosec}\alpha\,(\operatorname{cosec}\alpha \pm \cot\alpha) = 0$
13	$\frac{\sigma_x}{\lvert\tau_{xy}\rvert} - \frac{\sigma_y}{\lvert\tau_{xy}\rvert}\cot^{\alpha}\,(-\cot\alpha \pm \operatorname{cosec}\alpha) - \operatorname{cosec}\alpha \pm 2\cot\alpha = 0$
14	$\frac{\sigma_x}{\lvert\tau_{xy}\rvert} = -\frac{1}{2}\left[-\left\lvert\frac{f_c}{\tau_{xy}}\right\rvert \pm 2\cot\alpha - \sqrt{\left(\frac{f_c}{\lvert\tau_{xy}\rvert}\right)^2 - 4\left(\frac{\sigma_y\cot\alpha}{\lvert\tau_{xy}\rvert} \pm 1\right)\left(\frac{\sigma_y\cot\alpha}{\lvert\tau_{xy}\rvert} \pm 1\right)}\right]$

Note: Alternative sign is the same as that of τ_{xy}.

Case	ρ_x	ρ_y	σ_1	σ_2	tan θ
1	$\frac{1}{f_s}(\sigma_x + \lvert\tau_{xy}\rvert)$	$\frac{1}{f_s}(\sigma_y + \lvert\tau_{xy}\rvert)$	0	$-2\lvert\tau_{xy}\rvert$	$-\frac{\tau_{xy}}{\lvert\tau_{xy}\rvert}$
2	0	$\frac{1}{f_s}(\sigma_y - \frac{\tau_{xy}^2}{\sigma_x})$	0	$\sigma_x + \frac{\tau_{xy}^2}{\sigma_x}$	$\frac{\sigma_x}{\tau_{xy}}$
3	$\frac{1}{f_s}(\sigma_x - \frac{\tau_{xy}^2}{\sigma_y})$	0	0	$\sigma_y + \frac{\tau_{xy}^2}{\sigma_y}$	$\frac{\tau_{xy}}{\sigma_y}$
4	$\frac{1}{f_s}(\sigma_{xf} - \lvert\tau_{xy}\rvert)$	$\frac{1}{f_s}(\sigma_{yf} - \lvert\tau_{xy}\rvert)$	$f_c + 2\lvert\tau_{xy}\rvert$	f_c	$-\frac{\tau_{xy}}{\lvert\tau_{xy}\rvert}$
5	0	$\frac{1}{f_s}(\sigma_{yf} - \frac{\tau_{xy}^2}{\sigma_{xf}})$	$\sigma_x + \frac{\tau_{xy}^2}{\sigma_{xf}}$	f_c	$\frac{\tau_{xy}}{\sigma_{xf}}$
6	$\frac{1}{f_s}(\sigma_{xf} - \frac{\tau_{xy}^2}{\sigma_{yf}})$	0	$\sigma_y + \frac{\tau_{xy}^2}{\sigma_{yf}})$	f_c	$-\frac{\sigma_{yf}}{\tau_{xy}}$
7	$\frac{1}{f_s}\left[\sigma_x - \frac{f_c}{2}(1-\beta)\right]$	$\frac{1}{f_s}\left[\sigma_y - \frac{f_c}{2}(1+\beta)\right]$	0	f_c	$\frac{2\tau_{xy}}{f_c(1+\beta)}$
8	$\frac{1}{f_s}\left[\sigma_x - \frac{f_c}{2}(1+\beta)\right]$	$\frac{1}{f_s}\left[\sigma_y - \frac{f_c}{2}(1-\beta)\right]$	0	f_c	$\frac{2\tau_{xy}}{f_c(1+\beta)}$
9	0	0	$\frac{\sigma_x+\sigma_y+\sqrt{(\sigma_x-\sigma_y)^2+4\tau_{xy}^2}}{2}$	$\frac{\sigma_x+\sigma_y-\sqrt{(\sigma_x-\sigma_y)^2+4\tau_{xy}^2}}{2}$	$\frac{\sigma_x-\sigma_y-\sqrt{(\sigma_x-\sigma_y)^2+4\tau_{xy}^2}}{2}$

Table 3.4 Design Equations for Orthogonal Reinforcement

Table 3.5 Boundary Curves for Orthogonal Reinforcement

Curve	Equation
1	$\frac{\sigma_y}{\lvert\tau_{xy}\rvert} = +\infty$
2	$\frac{\sigma_y}{\lvert\tau_{xy}\rvert} = \frac{1}{2}\left(\frac{f_c}{\lvert\tau_{xy}\rvert} + \sqrt{\left(\frac{f_c}{\lvert\tau_{xy}\rvert}\right)^2 - 4}\right)$
3	$\frac{\sigma_y}{\lvert\tau_{xy}\rvert} = -1$
4	$\frac{\sigma_y}{\lvert\tau_{xy}\rvert} = \frac{f_c}{\lvert\tau_{xy}\rvert} + 1$
5	$\frac{\sigma_y}{\lvert\tau_{xy}\rvert} = \frac{1}{2}\left(\frac{f_c}{\lvert\tau_{xy}\rvert} - \sqrt{\left(\frac{f_c}{\lvert\tau_{xy}\rvert}\right)^2 - 4}\right)$
6	$\frac{\sigma_y}{\lvert\tau_{xy}\rvert} = -\infty$
7	$\frac{\sigma_x}{\lvert\tau_{xy}\rvert} = \frac{1}{2}\left(\frac{f_c}{\lvert\tau_{x_y}\rvert} - \sqrt{\left(\frac{f_c}{\lvert\tau_{xy}\rvert}\right)^2 - 4}\right)$
8	$\frac{\sigma_x}{\lvert\tau_{xy}\rvert} = -1$
9	$\frac{\sigma_{xf}}{\lvert\tau_{xy}\rvert}\ \frac{\sigma_{yf}}{\lvert\tau_{xy}\rvert} = 1$
10	$\frac{\sigma_x}{\lvert\tau_{xy}\rvert}\ \frac{\sigma_y}{\lvert\tau_{xy}\rvert} = 1$
11	$\frac{\sigma x}{\lvert\tau_{xy}\rvert} = \frac{f_c}{\lvert\tau_{xy}\rvert} + 1$
12	Inapplicable
13	Inapplicable
14	$\frac{\sigma x}{\lvert\tau_{xy}\rvert} = \frac{1}{2}\left(\frac{f_c}{\lvert\tau_{xy}\rvert} + \sqrt{\left(\frac{f_c}{\lvert\tau_{xy}\rvert}\right)^2 - 4}\right)$

CHAPTER FOUR

THE FINITE ELEMENT METHOD

4.1 INTRODUCTION:

In the previous chapter, the rules for designing the reinforcement in concrete slabs for a given moment triad have been established. The moment triad is obtained by the elastic analysis using the finite element method. In this chapter, the finite element method, which will be used not only to obtain the elastic moment fields but also to carry out a detailed nonlinear analysis on the slab will be described. Some examples demonstrating the validity of the finite element model adopted will also be given.

4.2 THE FINITE ELEMENT USED:

4.2.1 The Stiffness of a Layered Finite Element:

In this study, a rectangular four noded layered finite element is used. In such models, plate bending problems are treated by dividing the plate thickness into a finite number of layers parallel to the plate middle plane. Each layer is assumed to be in a state of plane stress condition. The usual assumptions of the first order theory of plates are adopted in this research[1]. Accordingly, the layered element is built up as a combination of two standard elements.

1. A rectangular four noded plane stress element, with eight degrees of freedom. The two nodal degrees of freedom are the inplane deformations u and v, are represented by the following bilinear functions

$$u = a_1 + a_2x + a_3y + a_4xy \qquad (4.1)$$

$$v = a_5 + a_6x + a_7y + a_8xy \qquad (4.2)$$

with a linear strain variation within the element.

2. A rectangular four-noded plate bending element, originally developed by Adini-Clough and Melosh[68]. This non-conforming type element employing twelve degrees of freedom, has the vector of nodal deformations $\{\delta\} = \left[w, -\frac{\partial w}{\partial y}, \frac{\partial w}{\partial x} \right]^T$, and is defined by a truncated fourth order polynomial in the lateral deflection w given by

$$W = a_9 + a_{10}x + a_{11}y + a_{12}x^2 + a_{13}xy + a_{14}y^2 + a_{15}x^2 + a_{16}x^2y + a_{17}xy^2 + a_{18}y^3 + a_{19}x^3y + a_{20}xy^3 \qquad (4.3)$$

Accordingly, the layered element model defined by combining the above two elements will have the vector of nodal deformations

$$\{\delta\} = \left(u, v, w, -\frac{\partial w}{\partial y} \quad \frac{\partial w}{\partial x} \right)^T \qquad (4.4)$$

The constants of the polynomials a_1 to a_{20} can be evaluated by writing down the twenty simultaneous equations linking the nodal displacements when the coordinates take up their appropriate values. In matrix form, the nodal displacement vector for the element can be written as

$$\{\delta\}^e = [C] \{a\} \qquad (4.5)$$

where $[C]$ is a 20 x 20 matrix depending on nodal coordinates, and $\{a\}$ a vector of 20 unknown constants. Inverting

$$\{a\} = [C]^{-1} \{\delta\}^e \qquad (4.6)$$

The strain vector from the classical first order theory of plates will be given by

$$\{\varepsilon\} = \{ \frac{\partial u}{\partial x}, \frac{\partial v}{\partial y}, \frac{\partial u}{\partial y} + \frac{\partial v}{\partial x}, \varepsilon_x^b, \varepsilon_y^b, \varepsilon_{xy}^b \} \qquad (4.7)$$

in which the first three are inplane components. The bending strain components ε^b are obtained from the curvatures at the middle plane

of the plate. For a layer at a distance Z from the middle plane of the plate, the bending strains are $\varepsilon_x^b = -Z\frac{\partial^2 w}{\partial x^2}$ ... etc. Accordingly, the total strains in each layer at Z from the middle plane are

$$\varepsilon_x = \frac{\partial u}{\partial x} - Z\frac{\partial^2 w}{\partial x^2}$$

$$\varepsilon_y = \frac{\partial v}{\partial y} - Z\frac{\partial^2 w}{\partial y^2}$$

$$\varepsilon_{xy} = \frac{\partial u}{\partial y} + \frac{\partial v}{\partial x} + 2Z\frac{\partial^2 w}{\partial x\,\partial y}$$

which can be written in the form

$$\begin{bmatrix} \varepsilon_x \\ \varepsilon_y \\ \varepsilon_{xy} \end{bmatrix} = \begin{bmatrix} 1 & 0 & 0 & Z & 0 & 0 \\ 0 & 1 & 0 & 0 & Z & 0 \\ 0 & 0 & 1 & 0 & 0 & Z \end{bmatrix} \begin{bmatrix} \frac{\partial u}{\partial x} \\ \frac{\partial v}{\partial y} \\ \frac{\partial u}{\partial y} + \frac{\partial v}{\partial x} \\ -\frac{\partial^2 w}{\partial x^2} \\ -\frac{\partial^2 w}{\partial y^2} \\ 2\frac{\partial^2 w}{\partial x\,\partial y} \end{bmatrix} \qquad (4.8)$$

In matrix form, equation (4.8) can be written as

$$\{\varepsilon\} = [R]\ \{\varepsilon_m\} \qquad (4.9)$$

where ε is the vector of total strains at level z, and ε_m is the strain vector at the middle plane of the plate, and $[R]$ is 3 x 6 transformation matrix defined in (4.8) above.

The strain vector $\{\varepsilon_m\}$ is related to the element nodal displacement vector through the differential operators defined in (4.7). Thus operating on the displacement functions equations (4.1) to (4.3) we have:

$$\varepsilon_m = \begin{bmatrix} a_2 & a_4 y & & & \\ a_7 & a_8 x & & & \\ a_3 & a_4 x & a_6 & a_8 y & \\ -2a_{12} & -6a_{15}x & -2a_{16}y & -a_{19}xy & \\ -2a_{14} & -2a_{17}x & -6a_{18}y & -a_{20}xy & \\ 2a_{13} & 4a_{16}x & 4a_{17}y & 6a_{19}x^2 & 6a_{20}y^2 \end{bmatrix}$$

we can write

$$\{\varepsilon_m\} = [Q]\ \{a\} = [Q]\,[C]^{-1}\ \{\delta\}^e$$

$$= [B]\ \{\delta\}^e \qquad (4.10)$$

in which $[B]$ is a 6 x 20 matrix at each Gauss point, called the strain matrix, and $\{\varepsilon_m\}^e$ is a vector of middle plane strains.

Using (4.10) in (4.8) we will have

$$\{\varepsilon\} = [R]\ [B]\ \{\delta\}^e \qquad (4.11)$$

The stress vector in any layer is given by

$$\sigma = [D]\ \{\varepsilon\} \qquad (4.12)$$

where $[D]$ is given by Hooks law as

$$[D] = \frac{E}{1-\nu^2} \begin{bmatrix} 1 & \nu & 0 \\ \nu & 1 & 0 \\ 0 & 0 & \frac{1-\nu}{2} \end{bmatrix} \qquad (4.13)$$

called the constitutive matrix.

Following the standard procedures (68), the element stiffness matrix is given by

$$[K] = \iiint B^T D B\, dx\, dy\, dz \qquad (4.14)$$

and using equation (4.11) in (4.14), the element stiffness matrix is given by

$$[K] = \iiint (R\ B)^T D (R\ B) dx\, dy\, dz$$

$$= \iiint B^T (R^T D R)\ B\, dx\, dy\, dz \qquad (4.15)$$

only the bracketed term in (4.15) is dependent on the Z coordinate,

and the integration can be performed by summing the layers contributions. Accordingly, equation (4.15) becomes

$$[K] = \iint B^T D' B \, dx \, dy \qquad (4.16)$$

in which the constitutive matrix D' represents the equivalent constitutive matrix of the layered element and is given by

$$D' = \int [R]^T [D] [R] \, dz$$

$$= \sum_{i=1}^{N} \frac{E_i}{1-\nu_i^2} \left[\begin{array}{ccc|ccc} 1 & \nu_i & 0 & Z_i & \nu_i Z_i & 0 \\ \nu_i & 1 & 0 & \nu_i Z_i & Z_i & 0 \\ 0 & 0 & \frac{1-\nu_i}{2} & 0 & 0 & \frac{1-\nu}{2} Z_i \\ \hline Z_i & \nu_i Z_i & 0 & Z_i^2 & \nu_i Z_i^2 & 0 \\ \nu_i Z_i & Z_i & 0 & \nu_i Z_i^2 & Z_i^2 & 0 \\ 0 & 0 & \frac{1-\nu_i}{2} Z_i & 0 & 0 & \frac{1-\nu_i}{2} Z_i^2 \end{array}\right] (dZ)_i$$

$$= \sum_{i=1}^{N} \left[\begin{array}{c:c} D_i & Z_i D_i \\ \hline Z_i D_i & Z_i^2 D_i \end{array}\right] (d Z)_i \qquad (4.17)$$

where N is the total number of layers in the element.

Equation (4.17) dictates the important feature of this model in treating composite materials made up as a combination of various constituents. If the element is made up of layers with symmetric properties about the middle plane of the plate, the summation terms of ZdZ in (4.17) would vanish, and the constitutive matrix exhibits uncoupling between membrane and flexural effects. For reinforced concrete, such a coupling effect is bound to occur due to unsymmetric cracking, even if the slab element was initially isotropic.

The membrane terms $D_i dZ_i$ in (4.17) can be evaluated exactly using any number of layers across the thickness of the slab, even if the slab whole thickness is considered as one layer. But the flexural

terms $\left(\Sigma \frac{E_i}{1-\nu_i^2} Z_i^2 \, dZ_i \right)$ representing the flexural rigidity of the plate, depend on the number of layers used. Table (4.1) gives the accuracy obtained in computing the flexural stiffness as a function of the number of layers N. The convergence of the integral to the conventional plate flexural rigidity $Eh^3/12(1-\nu^2)$ is clear from the table, as the number of layers is increased.

Although increasing the number of layers would enable a close monitering of nonlinearities, it requires both a large space and time in the computer. The flexural stiffnesses can be corrected by the factors given in Table (4.1) which were derived assuming one material plate with layers of equal thicknesses.

Table (4.1) Flexural rigidities of a layered plate as a function of number of layers

N	% error	correction factor
2	25·0	1·333
4	6·25	1·066
6	2·78	1·028
8	1·56	1·015
10	1·00	1·010
12	0·70	1·007

The area integration of the stiffness matrix in (4.16) is performed using the Gaussian quadrature[68]. For the range of problems tested in this study, it is found that a reduced number of four station points is quite adequate to yield good results. It is true that a higher number of such points will enable a close monitor of plastification, but the stiffness integration is not affected, and the computation time is substantially increased.

4.2.2 Element Subdivision:

This element has been tested extensively by the author, and is found to converge very well with the increasing element subdivision. In bending, the case of a square simply supported slab under uniformly distributed load will be given as an example. The rate of convergence is very good, and the accuracy of both the deflections and moments can be seen even for the case of a rough mesh of 2 x 2 elements. Table (4.2) gives the results of this study, using six layers across the slab depth. The mesh subdivisions given in the table, are those used on a symmetric quadrant.

Table 4.2 Convergence study for the case of a Simply Supported Plate under uniform loading.

Mesh	Deflection x $10^3/\frac{qa^4}{D}$	Moment x 100 / qa^2
2 x 2	4·303	4·18
4 x 4	4·127	4·22
6 x 6	4·094	4·23
8 x 8	4·092	4·24
10 x 10	4·077	4·24
Exact[1]	4·060	4·57

The deflection and moments referred to are those measured at the centre of the plate. The boundary conditions are those of Type 3 in Figure (4.13b), and a reduced integration order of 2 x 2 was used in the computations.

The inplane element has also been tested by the author. As has been shown in the previous section, the stiffness of this element is independant of the number of layers, if the element is made up of

one material, and thus only one layer can be used. For more than one material, the number of layers may be taken equal to the number of constituting materials.

The problem considered for convergence is the cantilever problem under an edge point load. Table (4.3) reflects the excellent rate of convergence of the results to the exact solution as the mesh size is refined. The beam is assumed to be of one material, thus only one layer was adopted and a reduced integration of 2 x 2 was used. The maximum stress referred to in the table is that given at the Gauss point No.4 (Figure 4.1) of element No.1, near the support.

Table (4.3) Convergence study for the case of a cantilever beam carrying a point load P at the free edge.

Mesh	Maximum deflection/$\frac{PL^3}{EI}$	$\frac{\text{maximum stress at GP}}{PL/Z_{xx}^*}$
4 x 4	0·24774	0·55208
6 x 6	0·29896	0·72017
8 x 8	0·32260	0·82292
10 x 10	0·33507	0·88021
Exact[1]	0·33333	0·93497

$*Z_{xx}$ = the section modulus = $\frac{bd^2}{6}$

4.3 NONLINEAR ANALYSIS OF CONCRETE STRUCTURES.

4.3.1 General

The behaviour of concrete can be explained with the aid of the stress-strain curve of Figure (4.2). Under small compressive loads less than 30% of its ultimate strength, concrete behaves as a linear elastic material. Under increasing loads, concrete behaves in a non

linear way. The material has got but a limited ductility, and under high compressive stresses, the material fails by crushing when attaining a limiting strain value, normally taken as 0·0035 for design purposes.

On the other hand, concrete cracks at very early stages of loading owing to its small tensile strength. Once the material cracks, it also loses all its strength in a direction normal to the crack. The reinforcing layers are thus left to carry all such stresses. The latter will, under increasing states of stress, become plastic.

A valid nonlinear finite element model has thus to consider all these sources of nonlinearities. Other sources of nonlinearities like bond effects and dowel-action are still difficult to treat, and in most cases, they are probably unimportant in slab problems. Accordingly, they will not be considered in this study.

4.3.2.1 Biaxial Yield Criteria for Plain Concrete:

Under biaxial states of stress, concrete strength increases in comparison to uniaxial[56,57,58,77,78]. The increase in ultimate strength due to biaxial stressing depends on the ratio of the two principal stresses. A maximum increase in compressive strength of 25% is achieved at a stress ratio of lateral/axial stress of 0·5, whereas the minimum increase of 16% corresponds to equal biaxial compressive stresses. Under biaxial compression-tension, the compressive strength was found to decrease almost linearly as the applied tensile stress is increased. For biaxial tension, the strength is almost the same as that of the uniaxial strength.

In connection with finite elements applications the experimental results of Kupfer et al[56] has largely been employed, and is adopted in this study too, Figure (4.3). This biaxial failure envelope had

also been confirmed by the works of Buyokozturk[82], and Tasuji et al[58]. The Mohr-Coulomb failure surface is nearly the same (see the following section), except in the region of combined tension-compression stresses, a region over which the Kupfer's surface predicts a higher strength. The square yield criterion due to Johansen [16] and Prager[7] ignores any possible interaction between a set of orthogonal stresses, which implies that for failures under biaxial compressive states, the ultimate strength of concrete is the same as that under uniaxial states, Figure (4.4).

The use of uniaxial properties is thus more conservative, and hence justifiable from the design point of view. In cases where nonlinearities are largely dictated more by crack propagation than plastic action under compressive states of stresses, such differences in the yield conditions are insignificant, as in such cases, the concrete compressive strength may not be reached before the structure collapses.

4.3.2.2 The Yield Criterion:

A multi-linear fit for the yield surface of Figure (4.3) can be obtained in terms of the octahedral shear stress of the form[43]

$$\tau_{oct} = \frac{\sqrt{2}}{3} \left(\sigma_x^2 + \sigma_y^2 - \sigma_x\sigma_y + 3\,\tau_{xy}^2\right)^{\frac{1}{2}} \qquad (4.18)$$

as

$$\tau_{oct} - a - b\,\sigma_o = 0 \qquad (4.19)$$

where σ_o is the mean normal stress, a and b are constants, to be determined from experiments. Taking f_c as the uniaxial compressive strength of concrete and f_d as the equivalent compressive strength under biaxial compression, and defining the ratios

$$m = f_t/f_c \qquad \text{and} \qquad n = f_d/f_c \qquad (4.20)$$

equation (4.19) can be established in the following manner:

(a) compression yielding:

(i) For uniaxial compression $\tau_{oct} = \frac{\sqrt{2}}{3} f_c$ and the mean stress is $- f_c/3$, then by (4.19)

$$\frac{\sqrt{2}}{3} f_c = - b f_c/3 + a \qquad (4.21)$$

(ii) for biaxial compression $\tau_{oct} = \frac{\sqrt{2}}{3} f_d$ and the mean stress is $- 2 f_d/3$, then

$$\frac{\sqrt{2}}{3} f_d = - 2b f_d/3 + a \qquad (4.22)$$

Solving (4.21) and (4.22) and using (4.2) then

$$\tau_{oct} + \sqrt{2} \frac{(n - 1)}{(2n - 1)} \sigma_o - \frac{\sqrt{2}}{3} \frac{n}{(2n - 1)} f_c = 0 \qquad (4.23)$$

Taking n = 1·16 from Figure (4.3), then

$$\tau_{oct}/f_c + (0·1714\ \sigma_o/f_c) - 0·4143 = 0 \qquad (4.24)$$

(b) Tension-Compression

Using the same procedure, it can be shown that

$$\tau_{cct}/f_c + \sqrt{2} \left\{\frac{(1 - m)}{(1 + m)} \sigma_o/f_c - \frac{2\sqrt{2}}{3} \frac{m}{(1 + m)}\right\} = 0 \qquad (4.25)$$

(c) Tension-tension:

Since no increase in ultimate tensile strength due tc biaxial stressing, the simple circular condition:

$$(\sigma_1/f_t)^2 + (\sigma_2/f_t)^2 - 1 = 0 \qquad (4.26)$$

is sufficient, although equation (4.25) can also be used in this case.

4.3.3 Materials Modelling.

In the present layered finite element model, each layer is assumed to be in a state of plane stress. A layer is also assumed to be of one material whose properties are represented at the Gauss points, although using the present formulation, different materials properties can be assigned at each Gauss point.

Prior to cracking, a Gauss point in a concrete layer is assumed to be elastic and isotropic, having the following constitutive matrix

$$D = \frac{E_c}{1-\nu^2}\begin{bmatrix} 1 & \nu & 0 \\ \nu & 1 & 0 \\ 0 & 0 & \frac{1-\nu}{2} \end{bmatrix} \qquad (4.27)$$

Upon cracking, the x-coordinate axis is placed parallel to the crack (Figure (4.5)), and the stress normal to the crack direction is removed. The constitutive matrix is then modified accordingly, with the new orientation of the axes, to be

$$D^* = \begin{bmatrix} E_c & 0 & 0 \\ 0 & 0 & 0 \\ 0 & 0 & \beta G \end{bmatrix} \qquad (4.28)$$

in which β is the shear retention factor in cracked concrete. The numerical value of β ranges between 1 and 0 for uncracked and cracked concrete, respectively. In this study β is taken as 0.4 for all the problems investigated here. Literature reveals a good justification for the use of such a value, see section (2.4.4.1).

It is known that bond between concrete and reinforcing steel gives some resistance to stresses in concrete after cracking. To account for this tension stiffening effect, the modified stress-strain diagram for concrete in tension is used, Figure (4.6).

The direction of the principal stress responsible for the crack is given by

$$\text{Tan } 2\theta = \frac{2\sigma_{xy}}{\sigma_x - \sigma_y} \qquad (4.30)$$

However, the angle θ given by (4.30) will lie between 0 and 45°. The actual crack direction θ_{cr} is determined from a Mohr's circle.

The constitutive matrix D* is defined in the crack directions and thus has to be transformed to the global directions. The transformed matrix becomes

$$D' = T^T D T \qquad (4.31)$$

where the transformation matrix T is given by

$$T = \begin{bmatrix} C^2 & S^2 & CS \\ S^2 & C^2 & -CS \\ -2CS & 2CS & C^2-S^2 \end{bmatrix} \qquad (4.32)$$

where

$$C = \cos \theta_{cr}, \quad S = \sin \theta_{cr}$$

However, during the load history of the structure, an open crack might close, if the stress across the crack turns to a compressive one. On the yield surface, this behaviour is restricted to the region CB of Figure (4.7), where dowel action and cleavage behaviour exist they would also occur in this region of the yield surface. Since very little is understood about the behaviour of concrete in this region, it will be possible to allow for such features by a modification of the yield surface in this zone[43]. This is usually done by converting the tension-compression stresses to an effective compression, and using the corresponding intermediate compression yield surface (see section 4.3.3.1), thus

(i) dowel action is allowed for since the loss of stiffness is substantially less than the case of tensile failure.

(ii) the possibility of cracks closing can be avoided for the same reason.

The yield surface can thus be divided into four regions as shown in Figure (4.7):

1. Failure under combined tension - ED
2. Failure under tension compression stresses - DC
3. Cleavage failure - CB.
4. Biaxial compression failure - BA.

The term cleavage failure is used to describe a state of failure intermediate between splitting and crushing. In this study whenever cleavage yielding is detected, the point is treated as for compression yielding as far as the constitutive matrix is concerned.

4.3.3.1 Concrete:

It has already been established that an initial linear elastic behaviour for concrete under compression is limited only to small load range up to about 30 to 50% of the ultimate capacity[58,59]. Beyond this range, some plastic action is involved. Accordingly, two approaches can be defined, which deal with the analysis of concrete under compressive forces:

1. Perfect and work-hardening plasticity theorems
2. Representation of a given stress-strain relationship using curve fitting methods.

4.3.3.1(a) Perfect and work hardening plasticity:

In compression, concrete can flow like a ductile material on the yield surface, before it reaches its crushing strain. To account for its limited plastic flow ability before crushing, a perfectly plastic model can be introduced. The complete stress-strain relationship is developed in three parts: (1) before yield, (2) during plastic flow, and (3) after fracture.

Before yield, a linear elastic model can be used. During the plastic flow, a yield surface is needed to define the onset of yield. The famous Von Mises criterion defined in terms of an effective stress

as

$$F = (\sigma_x^2 + \sigma_y^2 - \sigma_x\sigma_y + 3\,\tau_{xy})^{\frac{1}{2}} - \sigma_o \qquad (4.33)$$

has been used by many investigators[47,48,50].

To construct the stress-strain relationship in the plastic range, the normality of the plastic deformation rate vector to the yield surface (known as the normality rule) is used. Thus

$$d\,\varepsilon^p = \lambda \frac{\partial F}{\partial \sigma} \qquad (4.33)$$

in which $\lambda > 0$ is a scalar proportionality factor. The onset of fracture can be defined using a crushing surface, analogous to (4.33) and expressed in terms of strains[50]. After fracture, concrete is assumed to lose all its strength.

One disadvantage of this approach is that nonlinear action is ignored until the yield surface is reached. In case of planar structures subjected in plane compressive forces, such an assumption may lead to stiff predictions[43].

4.3.3.1(b) Representation of a given stress-strain -

Curve using curve fitting methods:-

Various empirical stress-strain equations expressed in terms of their respective principal stress and strain values have been established by fitting curves to the large amounts of biaxial test data. Works by Liu et al[60], Tasuji et al[58,59] and Buyokoztuk[82] are all of this type. The following equation

$$\sigma = \frac{a\,\varepsilon}{1 + \left(\frac{a\,\varepsilon_p}{\sigma_p} - 2\right)\left(\frac{\varepsilon}{\varepsilon_p}\right) + \left(\frac{\varepsilon}{\varepsilon_p}\right)^2} \qquad (4.34)$$

represents a unixial stress-strain curve for concrete, and was

originally proposed by Liu . Experiments indicate that, the constants are

$a = E_c$ = initial elastic modulus

ε_p = 0·0025 for compression

$\sigma_p = f_{cu}$ for uniaxial compression.

Equation (4.34) may also be used for concrete in tension[58,78], and in this case ε_p = 0·00015, $\sigma_p = f_t$.

For the numerical procedure adopted in this study, equation (4.34) is incrementally linearized during the monotonic loading. This is usually done by using intermediate loading surfaces after Bell and Elms [6], and Chen et al[78]. Such surfaces are shown in Figure (4.7). The first loading surface corresponds to the initial discontinuity in the stress-strain diagram. Subsequent loading surfaces are assumed to have the shape of the limiting yield surface. Accordingly, the intermediate surfaces will be represented by equation (4.24) but with an intermediate strength f_{cc} replacing the ultimate strength f_c. An empirical form for f_{cc} has been suggested by Johnarry[43] as

$$f_{cc} = f_{co} - f_t + f_t\,(E_c/E_i) \qquad (4.35)$$

subject to $f_{cc} \nmid f_c$. E_c is the initial modulus. In this research, the instantaneous modulus is computed using (4.34). The discontinuity stress f_{co} is taken as 50% f_{cu}.

4.3.3.2 Reinforcing Steel:

In the present layered approach, steel bars are represented by a smeared layer, which can carry stresses only in the original direction of the bars. The stress-strain curve for steel bars is taken as a bilinear relationship in both tension and compression, Figure (4.8).

Steel bars are thus assumed to have a definite yield point f_y, and in case of high yield bars, a proof stress corresponding to 0.2% strain is used.

Prior to yielding, stresses are computed using the initial modulus. After yielding, a secant modulus is calculated and used in the subsequent load increment, as

$$E_i = f_y/\varepsilon_i \qquad (4.36)$$

Linear strain hardening can also be incorporated, if so desired.

4.3.4 Pseudo-load vector:

The out-of-balance forces resulting from lack of equilibrium during a certain load increment in a nonlinear analysis are used to supplement the current load vector. Such forces are obtained from:

$$F^{ex} = P - \int B^T \sigma \, dv \qquad (4.37)$$

where the stress vector is always kept within the material yield surface. Lack of equilibrium results whenever excess stresses beyond the yield surfaces are removed, and the stress state is brought back on the yield surface. Within any material, whenever such a stress state exists, the current constitutive matrix of the material is modified, for their use in the subsequent loading step.

In this study, the integration in (4.37) is performed using the Gauss quadrature[68], and for consistency, the same order of integration as that used for the stiffness computation, is also adopted.

The numerical procedure used in this study employs a total strain technique[43] at each load level. Using such procedures would eventually lead to large pseudo-forces, particularly when the structure is undergoing extensive plastification. And if the load increment is made

sufficiently small, these induced forces will lead to unacceptable predictions, especially if equilibrium is satisfied at each load level by allowing the required number of iterations. Accordingly, bounds can be set on the load increments, which depend on the degree of plastification in the structure. Following Johnarry[43], the derivation of such bounds is given in Appendix (C). However, analysis with such bounds on the load increment requires the load increment to be less than 0·15 P_{cr}[43], although acceptable predictions with a load increment of 0·2 P_{cr} have been obtained as will be shown in (4.4.1).

4.3.5 Details of the Numerical Procedure:

An incremental, total strain, iterative procedure using the initial stiffness matrix is used[43,68,45]. The load is applied in small increments, within each, an elastic problem is first tried, followed by a succession of linearized iterations until equilibrium is maintained. At any stage of loading, the equilibrium equation to be satisfied is represented by equation (4.37), with the excess forces F^{ex} tending to zero. The excess force representing the lack of equilibrium at any stage is recycled until equilibrium is achieved. At any moment, these excess forces are added to the load vector at the start of the next load increment. Accordingly, the elastic solution at the beginning of a load increment is obtained using a fictitious load vector, that contains all applied loads in addition to the accumulated nonlinear effects resulting from previous load increments.

The convergence of the residual load vector F^{ex} towards zero is generally slow, particularly when the initial stiffnesses are used.

Accelerators have been used, but since no universal procedure exists, these were not tried. Phillips[65] examined various techniques, but could not obtain successful results with any one type. However, during the course of this study, it was found that a limit between 10 to 15 iterations yields goods results for most of the problems considered in this research.

The solution proceeds along the following steps:

1. Elements stiffness matrices are formed from the layers stiffnesses, using Gauss quadrature. A reduced integration order of 2 x 2 is used for all the problems considered in this study.
2. The global stiffness matrix is formed from the elements matrices, using standard procedures[31]. The matrix is then decomposed using the Gaussian elimination procedure[68].
3. A small load increment is applied, and the structure is solved for nodal displacements. From nodal displacements, middle plane strains and curvatures are found at the Gauss points.
4. For each sampling point in a layer, the total strains are found from:-

$$\varepsilon = \varepsilon_o + Z\,\chi \qquad (4.38)$$

Using the current constitutive matrix D for the point, stresses and principal stresses are found.

5. The stress state at the point is checked against the relevant transition criteria. If none are violated, steps 4 and 5 are repeated for all sampling points in all layers in all elements.
6. If any of the criteria are violated, the constitutive matrix D at the sampling point is changed. The change in the stiffness matrix D is used to compute the excess stress, and the stresses

are then brought back to within the yield surface. The point contribution to the stress resultant vectors N,M is calculated from

$$N = \sigma \, dz \quad , \quad M = \sigma z \, dz \qquad (4.39)$$

7. Previous steps are repeated for all sampling points in all layers and in all elements.

8. For each element, numerical integration is used to evaluate the nodal forces resulting from the stress resultants N and M, thus

$$F = \int B^T \begin{Bmatrix} N \\ M \end{Bmatrix} dA \qquad (4.40)$$

The global force vector is assembled from elements contributions at the nodes, and equilibrium is then examined, using

$$[F^{ex}] = [P] - [F] \qquad (4.41)$$

9. The excess force vector F^{ex} is added to the load vector, and the structure is analysed using $[F^{ex}]$, and steps 4 to 8 are repeated, and convergence is checked, using the displacement norm

$$NORM = ([\delta d]^T \{\Delta d\} / [d]^T \{ d \})^{\frac{1}{2}} \qquad (4.42)$$

Iterations are assumed to converge when the iterate Norm $\leq 10^{-4}$.

10. If convergence is achieved, or a predefined limit on the iterations is exhausted, a new load increment is added to the load vector, and steps 3 to 9 are repeated. (For the required iterations limit, see section 4.5).

A schematic illustration for the numerical procedure is given in Figure (4.9). Details of the computer program are given in Appendix (B), together with the instructions for data preparation.

When failure is imminent, a large disparity between internal and

external forces can be seen. At such a stage, the reinforcement could have yielded at quite a large number of points, and displacements increase at faster rates. In most cases, convergence does not occur, when failure is approached.

4.4 RESULTS AND COMPARISONS.

To examine the validity of the developed model, various types of problems have been analysed, and the results were compared with existing reliable test data. The logic followed is that, if over a wide range of problems, this model could produce accurate predictions for both the deflections and the ultimate loads, the program can then be used to predict the behaviour of similar problems, when using different design procedures. In the end, the program is aimed at examining the validity of the design equations of Chapter 3 in this research.

4.4.1 A Square Simply Supported Slab under a Central Point Load.

A square simply supported slab 1828·8 mm side length and 139·7 mm deep with isotropic reinforcement 0·99% which was tested under a central point load by the Portland Cement Association and was analysed by Dotreppe et al[46]. The materials properties used were as follows

$f_{cu} = 47{\cdot}7\ N/mm^2$, $f_y = 303{\cdot}4\ N/mm^2$

$E_c = 27580\ N/mm^2$, $E_s = 206850\ N/mm^2$

$h = 139{\cdot}7\ mm$, $d_1 = 114{\cdot}3\ mm$.

Figure (4.10) gives the load-deflection curve for this slab. Due to symmetry, one quadrant with a mesh of 6 x 6 elements was analysed, using an integration order of 2 x 2. The slab was analysed using this model with and without considering tension stiffening.

The analysis considering tension stiffening shows the high

accuracy of the model in predicting both the displacements and the ultimate load. The analysis ignoring tension stiffening produced a more flexible behaviour. This is in good agreement with Gilbert and Warner[48], who concluded that by ignoring tension stiffening effects in concrete between adjacent cracks, errors in the calculated deflections can be as high as 100%.

Although neglecting tension stiffening effect must not affect the ultimate load, this model predicts an ultimate load 10% less than the actual ultimate load when tension stiffening is not considered. The computed deflections show that, if the analysis was not terminated, the ultimate load could have been reached, but at very high deflections. Dotreppe[46] using a different model also found that the ultimate load is underestimated by 10%. Although he did not attribute this to any one reason, the author is of the opinion that such an underestimation in the ultimate load is mainly due to the neglected tension stiffening effect (see Figure (4.10)).

Other numerical aspects of this model had also been investigated. Figure (4.11) compares the predictions of the response for the same slab with various mesh subdivisions using the same load increment size. As far as mesh refinement is concerned, no significant difference is obtained between the predictions made using a 4 x 4 and 6 x 6 elements. Materials nonlinearities are predicted to occur at exactly the same loads for the two mesh subdivisions.

The same slab was also reanalysed using different sizes of load increments. Figure (4.12) gives a comparison between the responses predicted by different sizes of load increments. It is apparent how the predictions improve with a reduced size of load increment. Experience with this model indicates its ability in producing

accurate predictions when the load increment is taken around 0.08 of the cracking load P_{cr}.

The effect of increasing the number of iterations has also been considered. Figure (4.13) gives the results of the predictions for the same slab, when the total number of iterations is increased from 5, 10, 15 and then 30. In any case, this would mean the static equilibrium is satisfied at any load level. The accuracy of the predictions is shown to improve with the increased number of iterations. This is in contradiction to what Duncan and Johnarry[44] have found. They claimed that"attempts to satisfy static equilibrium at each load level, lead to expensive analysis and poor results". It is obvious that demanding static equilibrium at each load level leads to expensive analysis, but should never lead to poor results. However, this model in its present formulation shows a very good desirable response with increasing number of iterations. As a compromise between cost and accuracy, a limit of 15 to 20 iterations normally produces acceptable results.

The effect of imposing various membrane boundary conditions have also been studied using this model. For a simply supported slab, the flexural boundary conditions are obvious, but the restraints to membrane movements are ambiguous. Such a slab can be supported in quite different ways, and each can be considered as a simple support. In this study, different restraints to inplane movements have been tried, to see their effect on the predictions made by this model. Four types of inplane boundary conditions are shown in Figure (4.14b). The problem investigated is the same simply supported slab under a central point load. The predicted response for the slab corresponding to each type of

boundary condition is shown in Figure (4.14a).

Figure (4.14a) compares the various predictions obtained in each case. The effect of increasing the restraint to inplane movements affected both the computed deflections and the ultimate load. However, for elastic solutions, usually the effect of various inplane restraints is insignificant. Even the cracking load is not affected by such variations.

From Figure (4.14a), it is clear that the boundary conditions type (3) gives accurate predictions for both the response and the ultimate load. Accordingly, this type will be adopted in analysing simply supported slabs.

4.4.2 The Slab Tested by McNeice:

This was a square slab simply supported at four corners, and was tested by Jofriet and McNeice[21]. The slab was 914.4 mm square and 44.7 mm deep, isotropically reinforced with 0.85% reinforcing steel. The slab was tested under a central point load, and had the following properties:

f_{cu} = 48.62 N/mm^2 $\quad$ f_y = 331 N/mm^2

E_c = 28614 N/mm^2 $\quad$ ES = 200000 N/mm^2

f_t = 2.413 N/mm^2 $\quad$ d_1 = 33.3 mm

ν = 0.15 N/mm^2

h = 44.7 mm

A mesh of 4 x 4 elements over asymmetric quadrant was used, together with a load increment size of 0.1 P_{cr}. Details of the slab are shown in Figure (4.16), and the results of the analysis in Figure (4.15). Two results of analyses had been given here, one for the slab with pin

supports at the corners, the other with roller supports. The agreement in both cases is quite good. Analysis with pin supports predicts stiffer behaviour at high loads, while the one with roller supports shows a flexible response at high levels. In both cases, the discrepancy with experimental results is not too serious. Hand[42], using a layered model in analysing this slab, also noticed the difference in the computed response due to variation in inplane boundary conditions. The results obtained by Dotreppe[46] using a reduced bending stiffness are identical to the one obtained here using pin supports. Since it had not been reported which inplane boundary condition was actually used in the test, the predictions obtained here are considered satisfactory.

4.4.3 Tee-Beam B1 Tested by Rao:

This problem was chosen to demonstrate the ability of this model to analyse complex structures. This beam was first tested and analysed by Rao[39] using a combination of beam elements for the web of the beam, and plain stress elements for the flanges. The data needed for the analysis were as follows:

$f_{cu} = 48\ N/mm^2$ $\quad f_y = 340\ N/mm^2$

$E_c = 35000\ N/mm^2$ $\quad E_s = 200000\ N/mm^2$

$f_t = 4.8\ N/mm^2$

$\nu = 0.2$

Other geometrical properties of the beam are given in Figure (4.18). The beam was analysed subject to a single point load at the centre.

Due to symmetry, only one quarter of the beam represented by half the span and half the flange width was analysed here. The mesh used here comprised of six elements along the span, and four across the flange.

The computed load-deflection curve for the central point of the beam is given in Figure (4.17). This analysis predicts a higher cracking load (of 16 kN) in comparison with the actual cracking load of 9 kN, but could predict exactly the ultimate load of the beam. Rao[39], in his analysis, also obtained such a high cracking load. He suggested that the low experimental cracking load could be due to the beam being already cracked prior to test, and suggested the use of 0.96 N/mm^2 for the tensile strength of concrete. This value he later used to analyse the beam, but still his predictions were too flexible, and could not predict the ultimate load correctly.

As for the present model, apart from the high cracking load, the predictions made are acceptable. The cracking load could have been reduced if a value of 5% f_{cu} is used for the tensile strength of concrete.

4.4.4 Hayes' Slab-Beam System

This is a square slab which is monolithically cast with its supporting beams. The slab was chosen from a series of tests on integral slab-beam systems conducted by Hayes et al. The present slab represents the slab-beam test designated A1 by Hayes et al[84]. The slab was supported by edge beams of the same flexural stiffness, which were simply supported at the corners. The relevant data is as follows:

f_{cu} = 35.3 N/mm^2 fy = 300 N/mm^2

f_t = 2.65 N/mm^2 E_s = 210000 N/mm^2

E_c = 24710 N/mm^2

ν = 0.15

Other dimensions and reinforcement data are given in Figure (4.19).

The slab reinforcement was uniformly spaced in each direction.

The slab was analysed using a mesh of 5 x 5 elements over a symmetric quadrant. The load was applied as a uniformly distributed load, and an increment size of 0.1 P_{cr} was used in the analysis. Tension stiffening effects were neglected, but bounds were set on the incremental plastic loads (see section 4.3.4). A maximum number of 30 iterations was allowed in the analysis.

The results are shown in Figure (4.19). The figure shows the excellent ability of the model in predicting the behaviour of slab-beam systems. The analysis predicts the first cracking of the slab and the beams to occur simultaneously at a load of 5 kN/m^2 (about 18 kN). This is exactly the cracking load reported by Hayes[84] in his experiments. In the post cracking range, and up to 75% of the ultimate load, only an average of 9 iterations were needed to achieve convergence. First yield of steel was detected at the centre of the supporting beams, at about 15.4 kN/m^2 (about 56 kN), which again agrees very well with the value of 54 kN reported in the paper. After yielding of the steel, convergence to the specified limits was not obtained, and the total number of iterations allowed was reached in each load increment. Although convergence to the desired levels was not achieved, the disparity was not great. The stiffening effects appearing after the first yield load in Figure (4.19) is caused by convergence problems. The solution would very much improve if the size of load increment was further reduced after attaining first yield. In any case, the present model could accurately predict the ultimate load of this slab-beam system. Under the ultimate load a mechanism had already formed, with the reinforcement in the supporting beams yielding, and also along

the two centre lines of the slab. Deflections were also very high, and at the slab centre, the deflection was greater than the slab thickness.

The state of mechanism just described represents the composite rectangular mode in which the slab-beam system actually failed. This supports the conclusion that the present model is able to predict accurately the behaviour of slab-beam systems.

Perhaps, the only disadvantage in the formulation of this model in the analysis of slab-beam systems lies in the assumption of plane stress state in the layer. The effect of such an assumption is the neglect of the vertical shear, normal to the middle plane. For thin plates, this shear has no effect. But for beams, the effect may be felt, if the beam will be subjected to high torsional stress, for example. In this case, this model would definitely underestimate the shear stresses in the beam (see Figure(4.20) below).

Actual Shear Flow

Predicted by The Layered Model

Figure (4.20) Shear Flow in a layered Plate Bending Model

4.5 CONCLUSIONS.

This element in its present formulation had been extensively tested by the author, and the following conclusions are arrived at:

1. A mesh division which is valid for an elastic analysis is also adequate for nonlinear analysis of concrete planar structures. Acceptable predictions can be obtained even with a rough mesh subdivision.

2. Inplane boundary conditions are very important for a successful nonlinear analysis. The computed response is found to be greatly affected by varying edge restraints to inplane movements.

3. A numerical integration of order 2 x 2 is adequate to produce acceptable results, for the range of problems considered in this chapter. It is true that a higher order would enable close monitoring of the nonlinearities, and can thus aid in achieving faster convergence. However, the cost of the analysis increases dramatically when using higher orders of numerical integration, in addition, no significant improvement on the computed response was observed.

4. Tension stiffening provided by concrete between adjacent cracks has very significant influences on the accuracy of the predictions. Taking this factor in consideration aids convergence, and thus reduces the cost of the analysis. Cracking and yielding initiation, though are not affected, would not produce the large imbalance forces which occur when neglecting tension stiffening. The same effect can be produced by setting bounds on the plastic load increments, in which case tension stiffening can be ignored.

5. In all cases, convergence is very fast when the load increment size is taken between 0.08 and 0.1 of the cracking load. Prior to yielding of reinforcement, convergence to very small tolerances of the order specified in section (4.3.5) can be achieved within 10 to 15 iterations, for most of the problems considered, with the load increment around 0.15 the cracking load. With a load increment of 0.08 the cracking load, convergence to small tolerances can be obtained with less than 10 iterations, in most cases. After yielding of reinforcement, large excessive forces are produced. If bounds are not set on the plastic loads, convergence cannot be achieved. The problem can further be treated by reducing the size of the load increment after the steel starts yielding. In the present program, the load increment is reduced to half its value prior to yield in steel.

6. The lack of convergence after yielding normally happens when the structure is undergoing extensive plastification. Experience with this model indicates that this occurs near ultimate conditions, and is indicative of the imminent failure of the structure.

7. Analysis with this model indicates the effect of attaining equilibrium at each load increment. The accuracy of the predictions is found to improve very much by demanding convergence to small tolerances. This is in contradiction to what Duncan and Johnarry[44] have found. The Duncan and Johnarry's[43,44] model was a crude one, because of the restricting assumption of constant stress over the layer. As their numerical procedure involving total strains (successive approximations) relied in its success on the released imbalance forces, the assumption of constant stress always under-

estimated these forces. Accordingly, it was not strange that their predictions were stiffer than what they should be, and their model was not able to achieve equilibrium in most cases. In the present formulation, stresses are sampled at the Gauss points, which allows for the variability of stresses over the layer. In this way, a good improvement in the element performance was achieved.

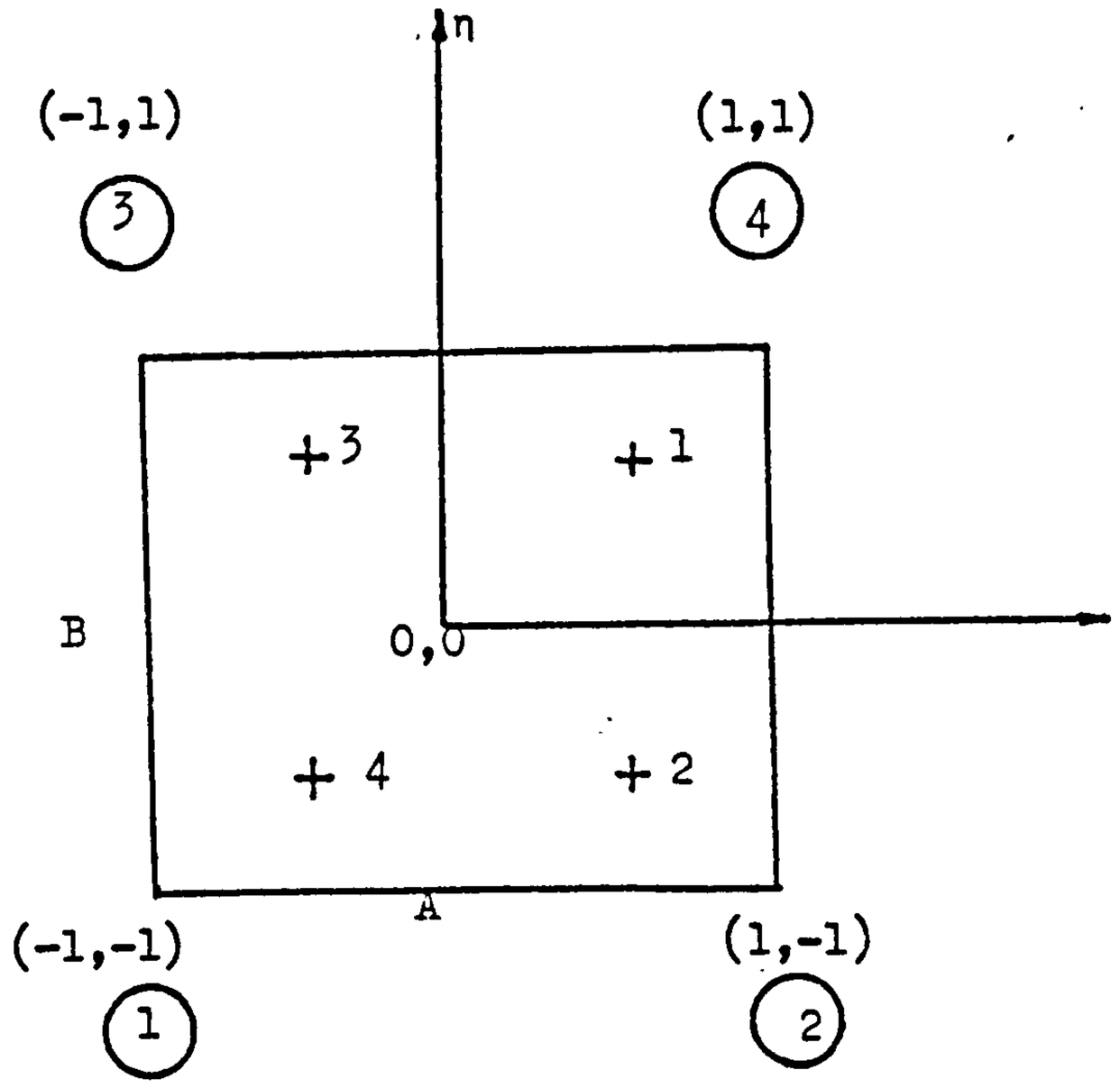

Gauss points in a finite element

N.B. Encircled are the nodal numbering in element local coordinate

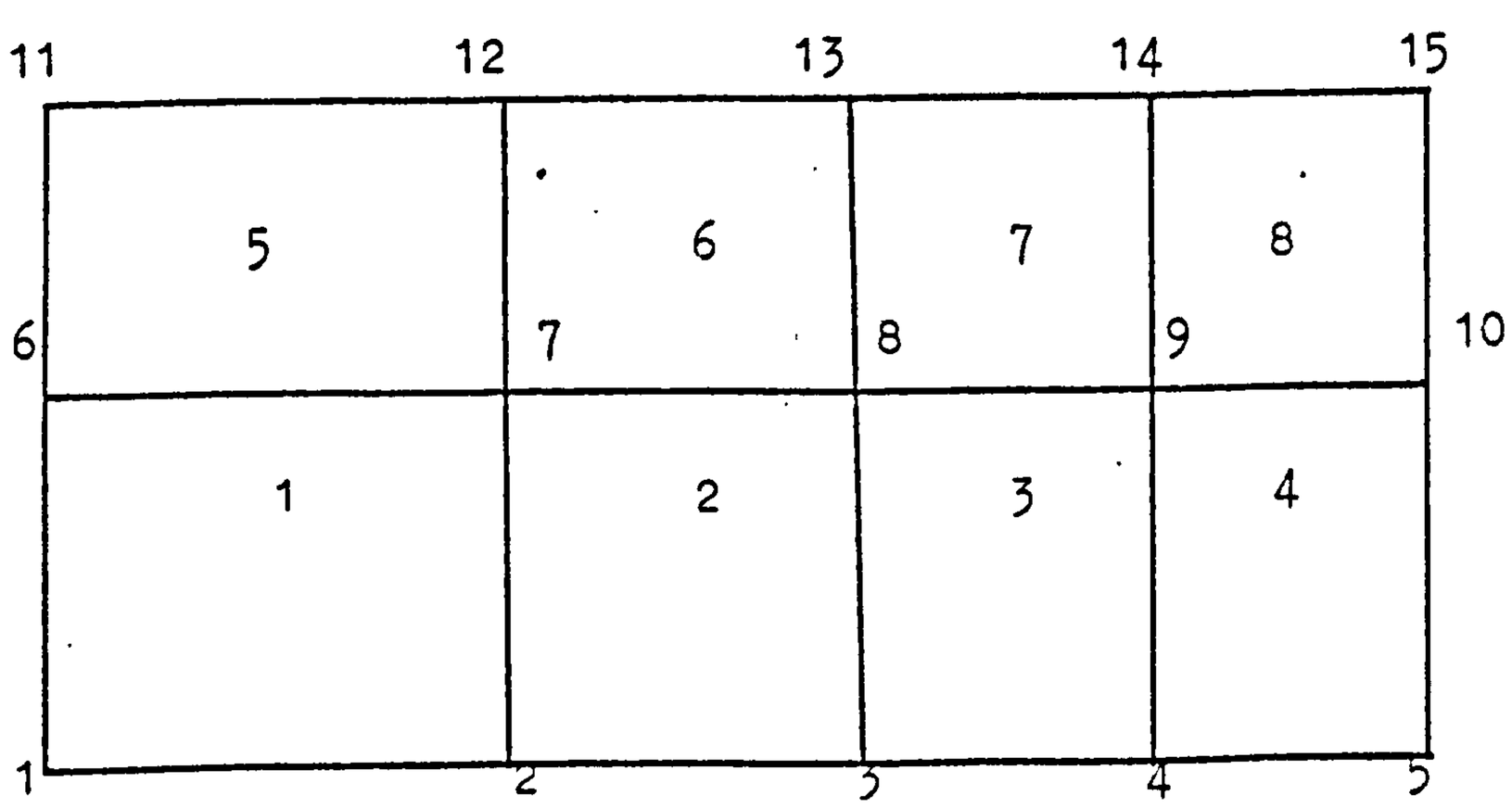

Figure (4.1) Elements and nodal numbering system in the finite element program

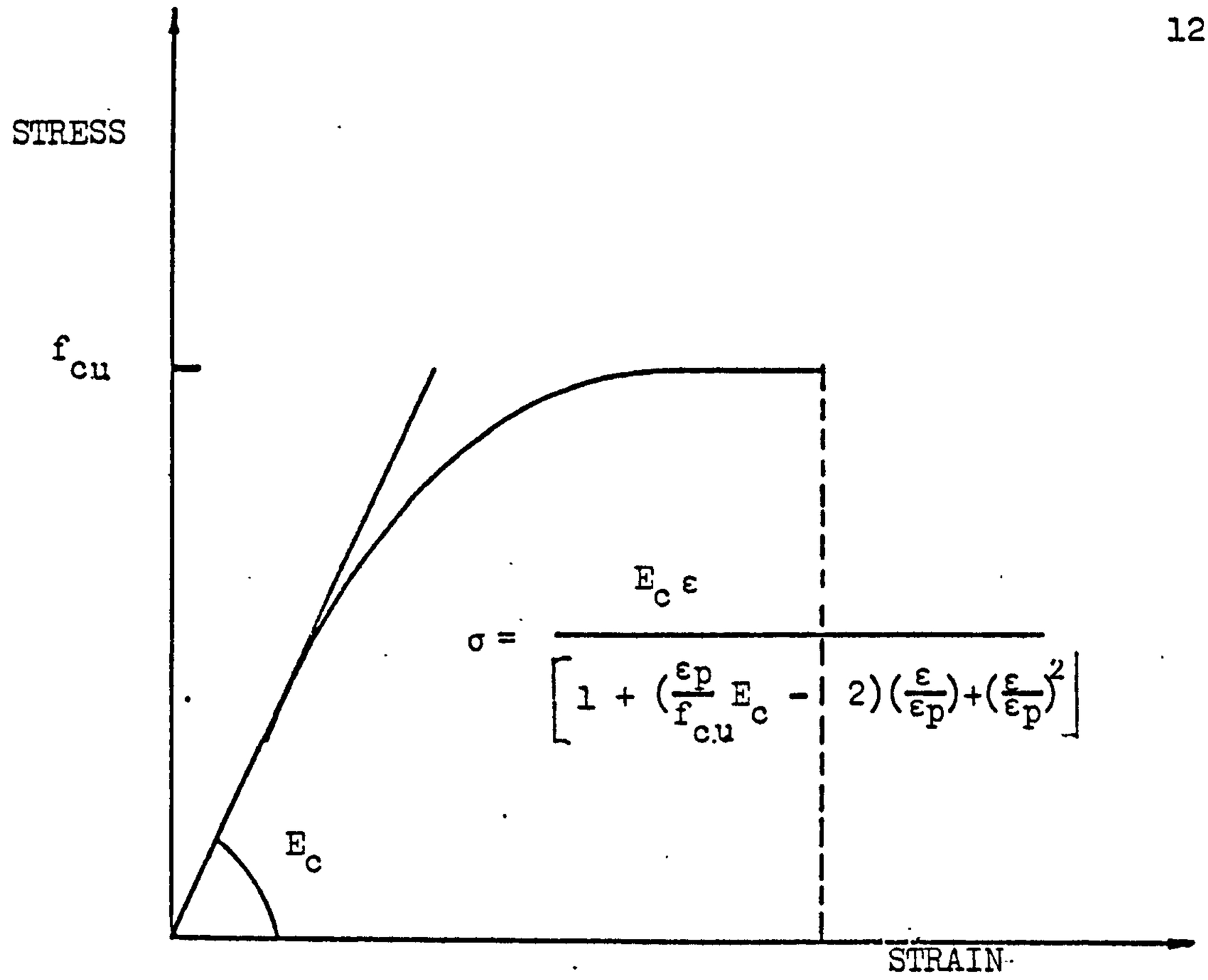

Figure (4.2) Stress-Strain relationship for concrete in compression

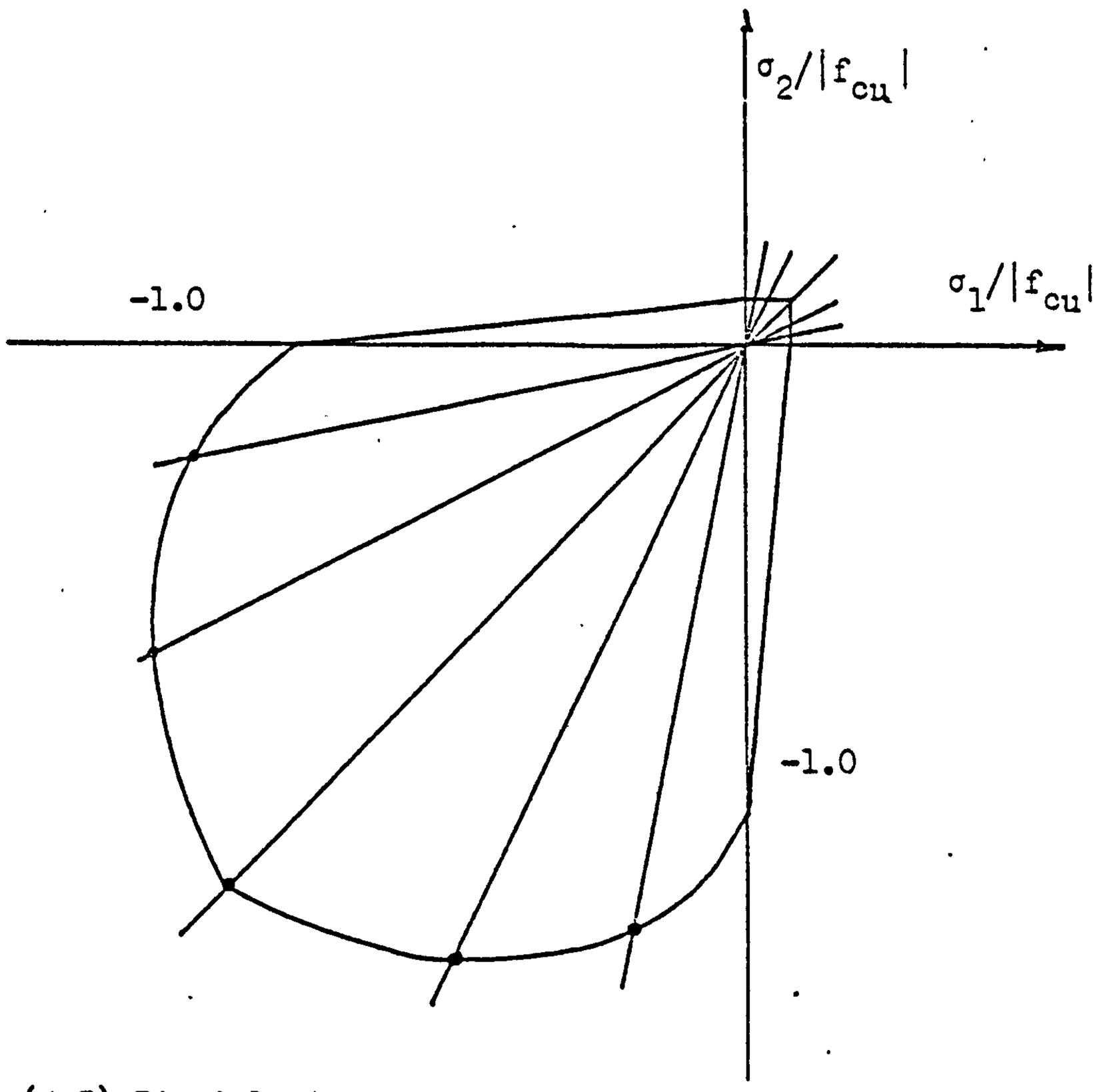

Figure (4.3) Biaxial strength of concrete

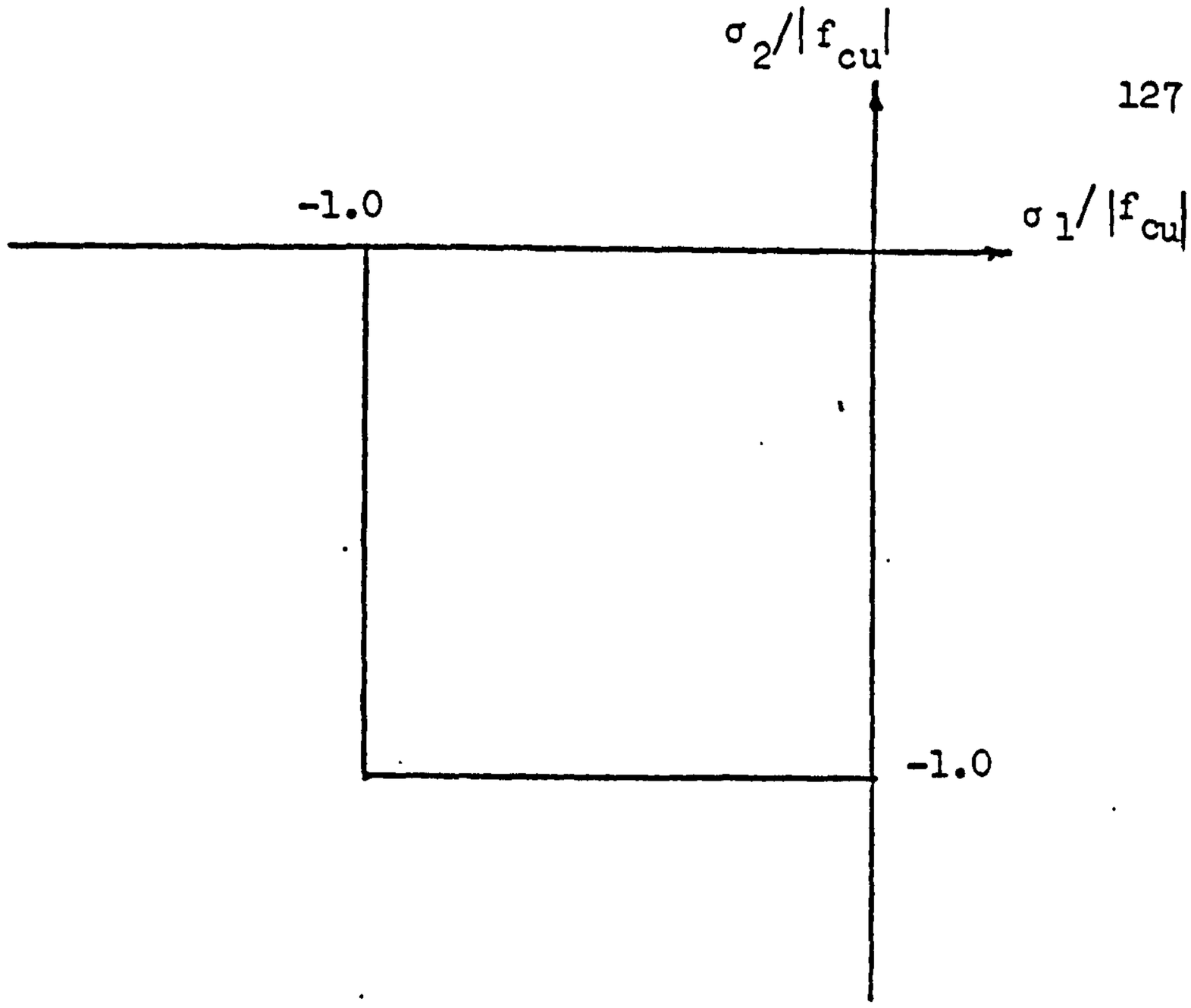

Figure (4.4) The square yield criterion for plain concrete

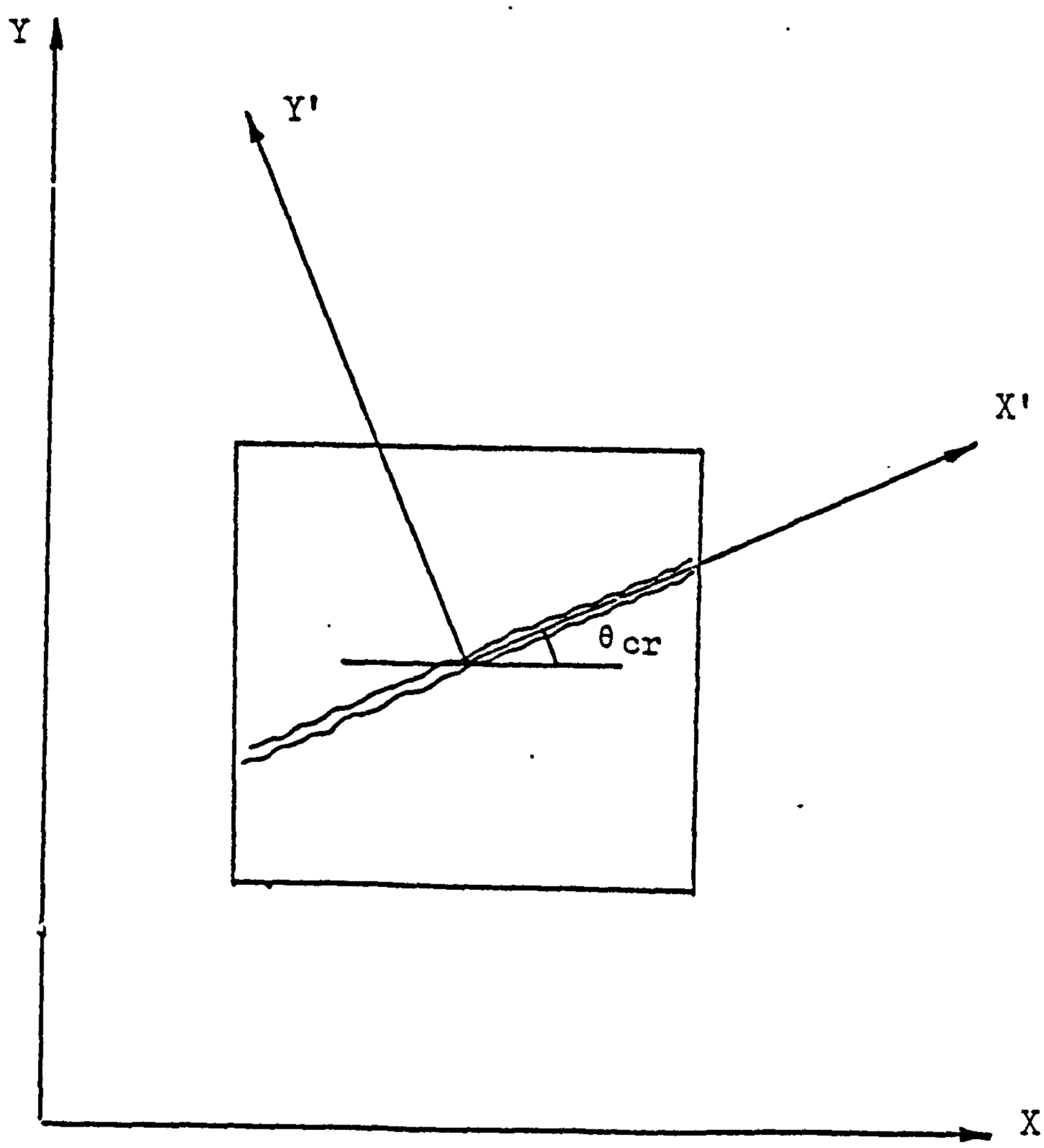

Figure (4.5) Transformation of cracked stiffness to global directions

For $\varepsilon < \varepsilon_{cr}$

$$\sigma = E_c \varepsilon$$

For $\varepsilon > \varepsilon_{cr}$

$$\sigma = f_t \left(c - \left(\frac{\varepsilon}{\varepsilon_{cr}}\right)\right)/(c-1)$$

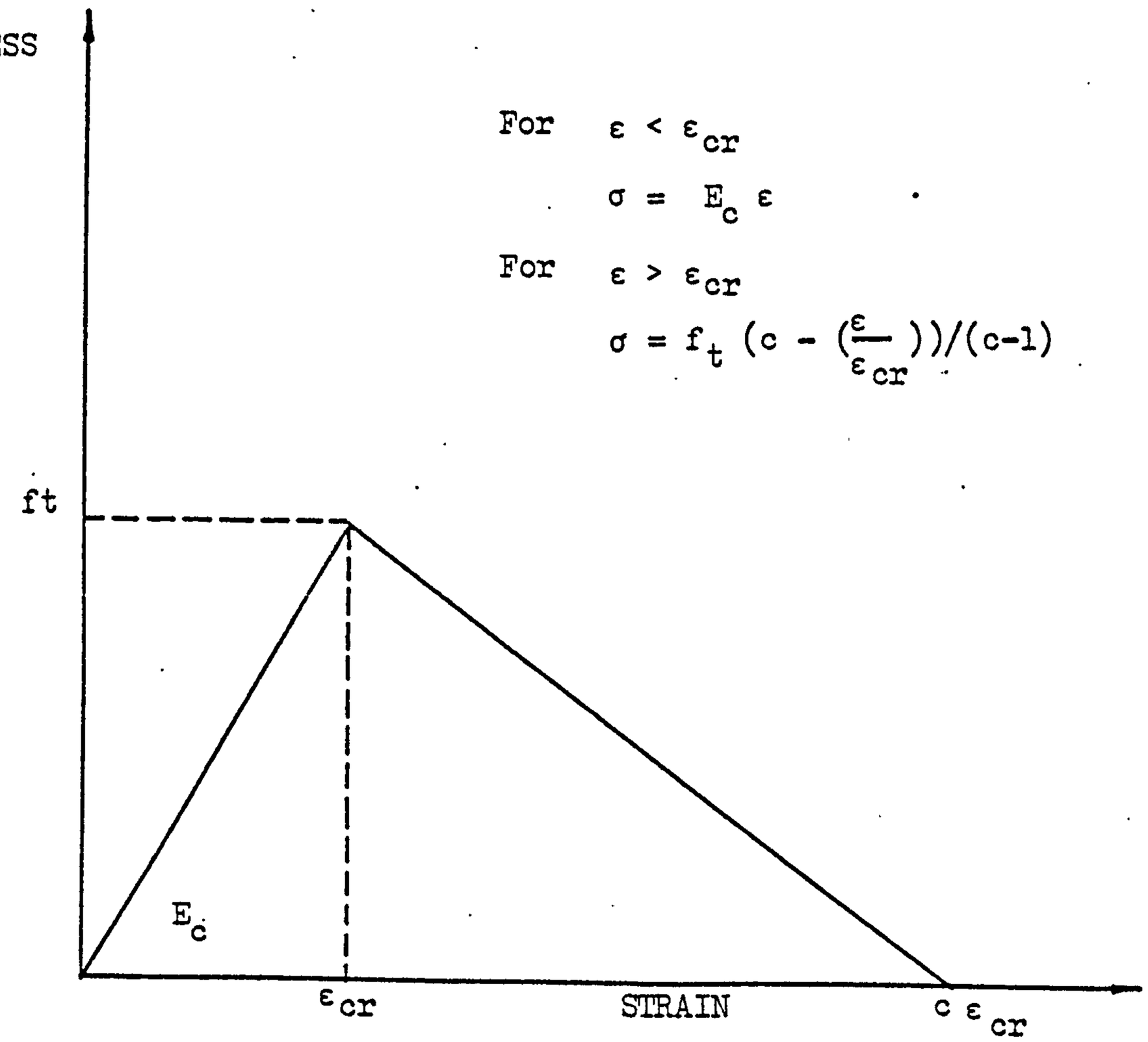

Figure (4.6) Tensile Stress-Strain curve for concrete

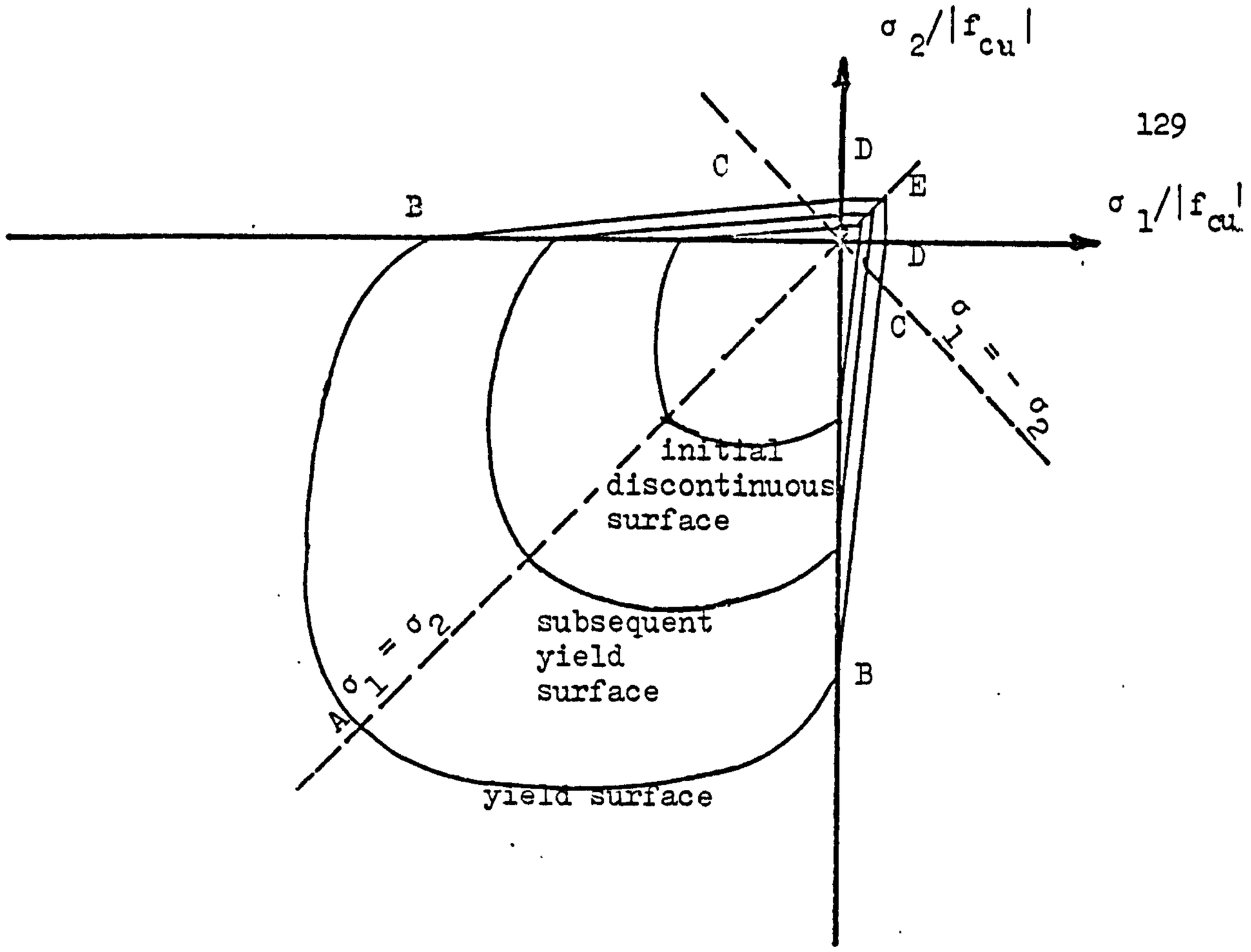

Figure (4.7) "Zoning" the yield surface - initial and subsequent loading surfaces

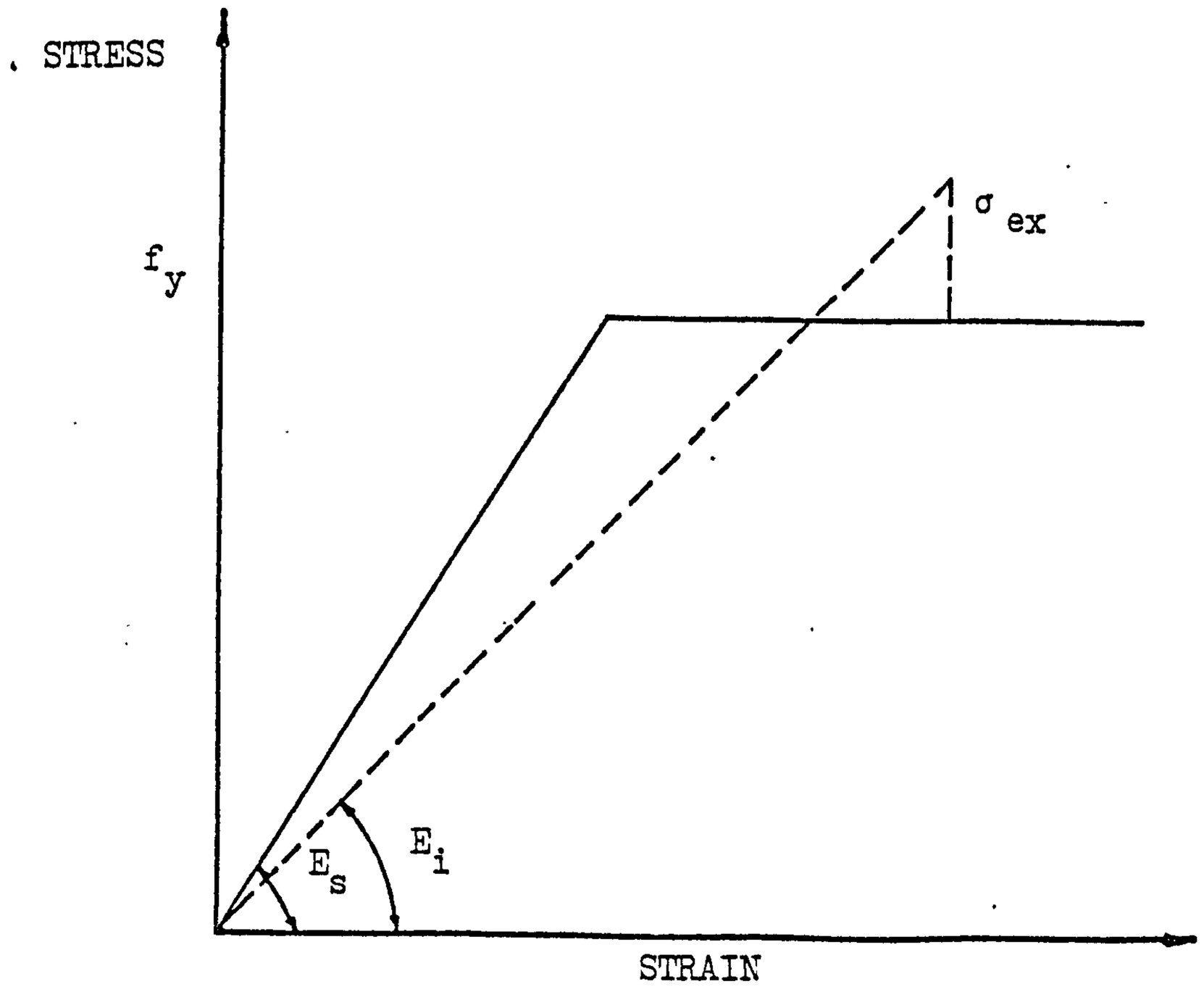

Figure (4.8) Stress-Strain curve for a steel layer

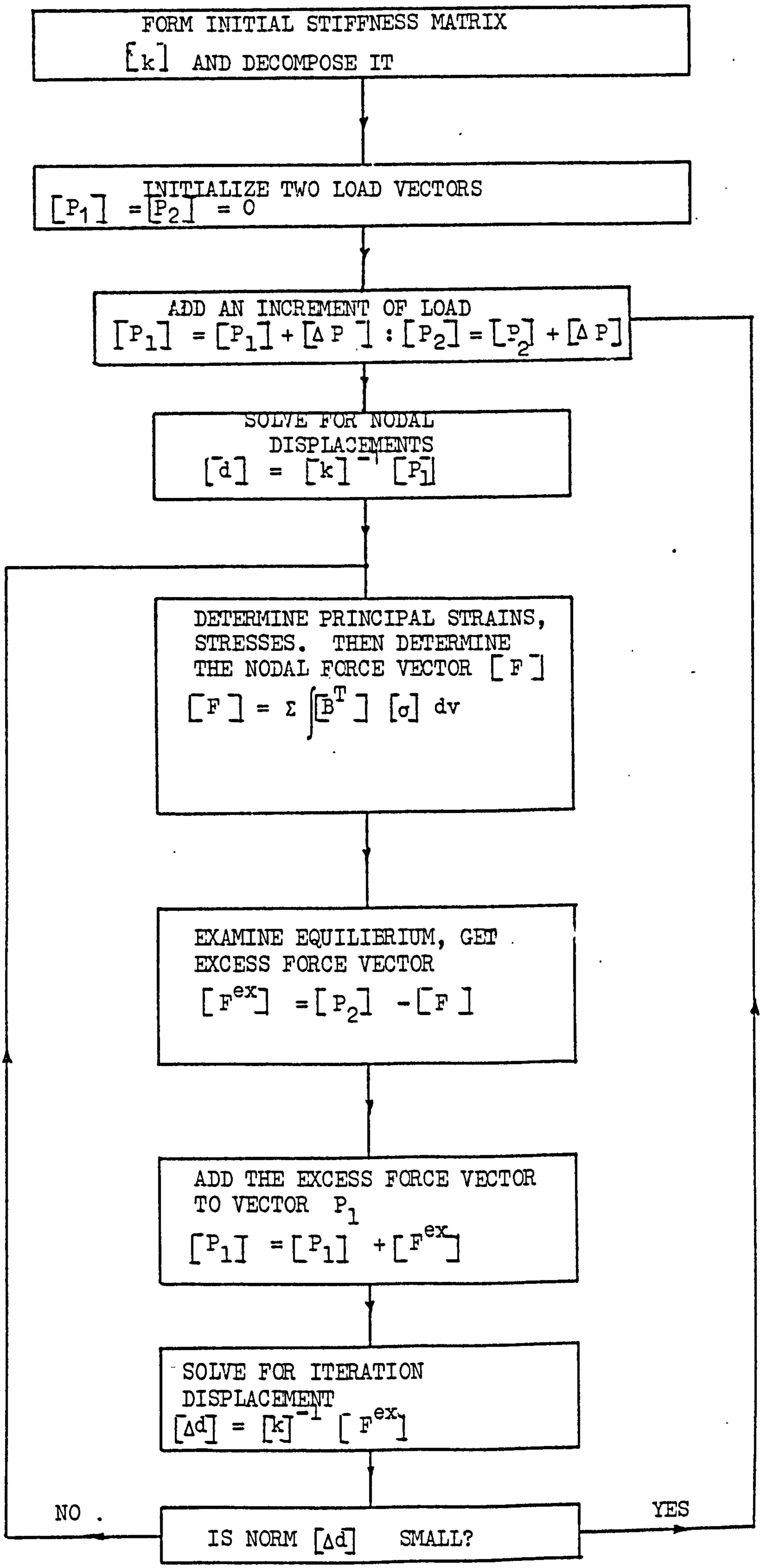

Figure (4.9) Details of the numerical procedure

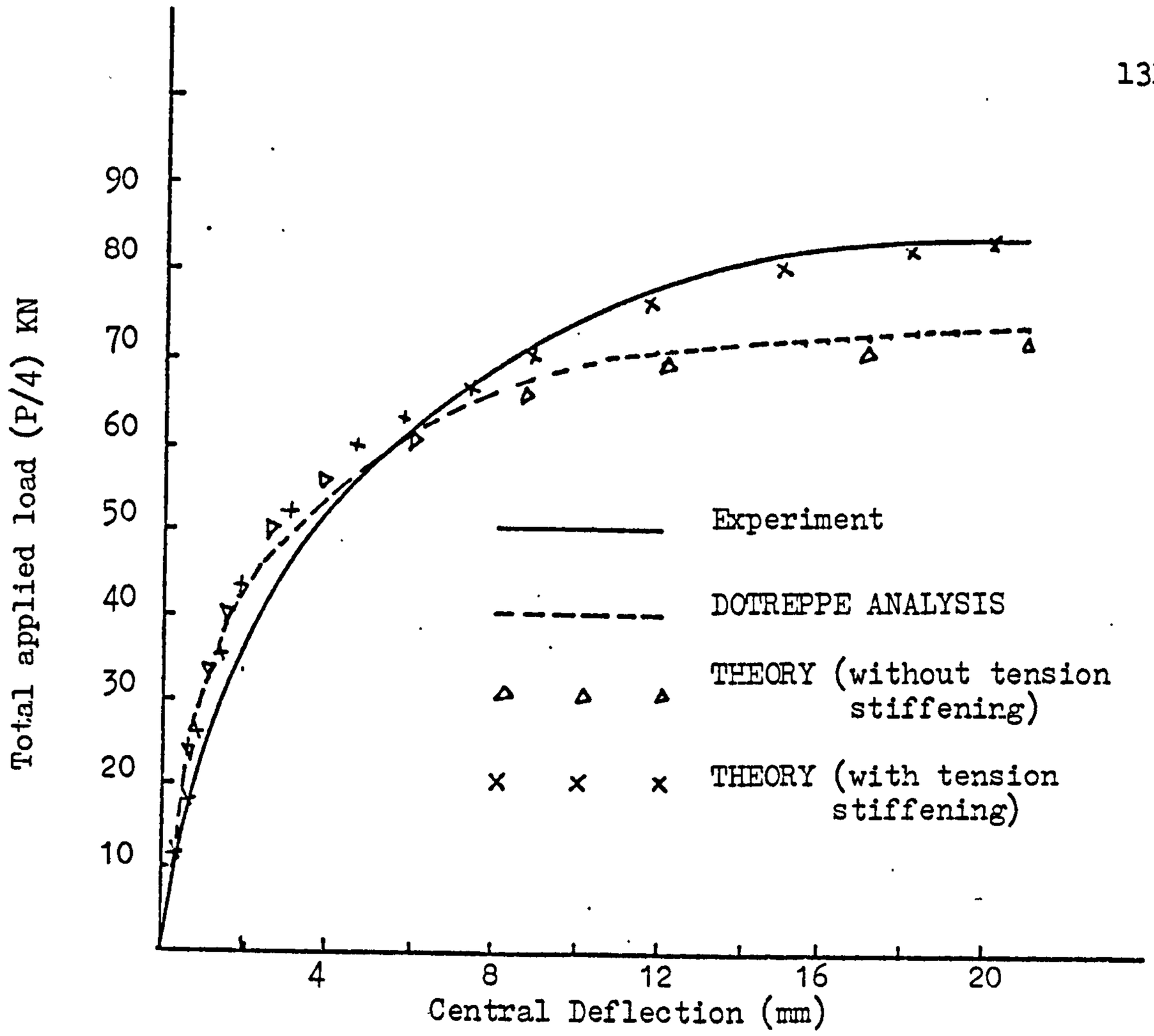

Figure (4.10.a) A square simply supported slab under a central point load

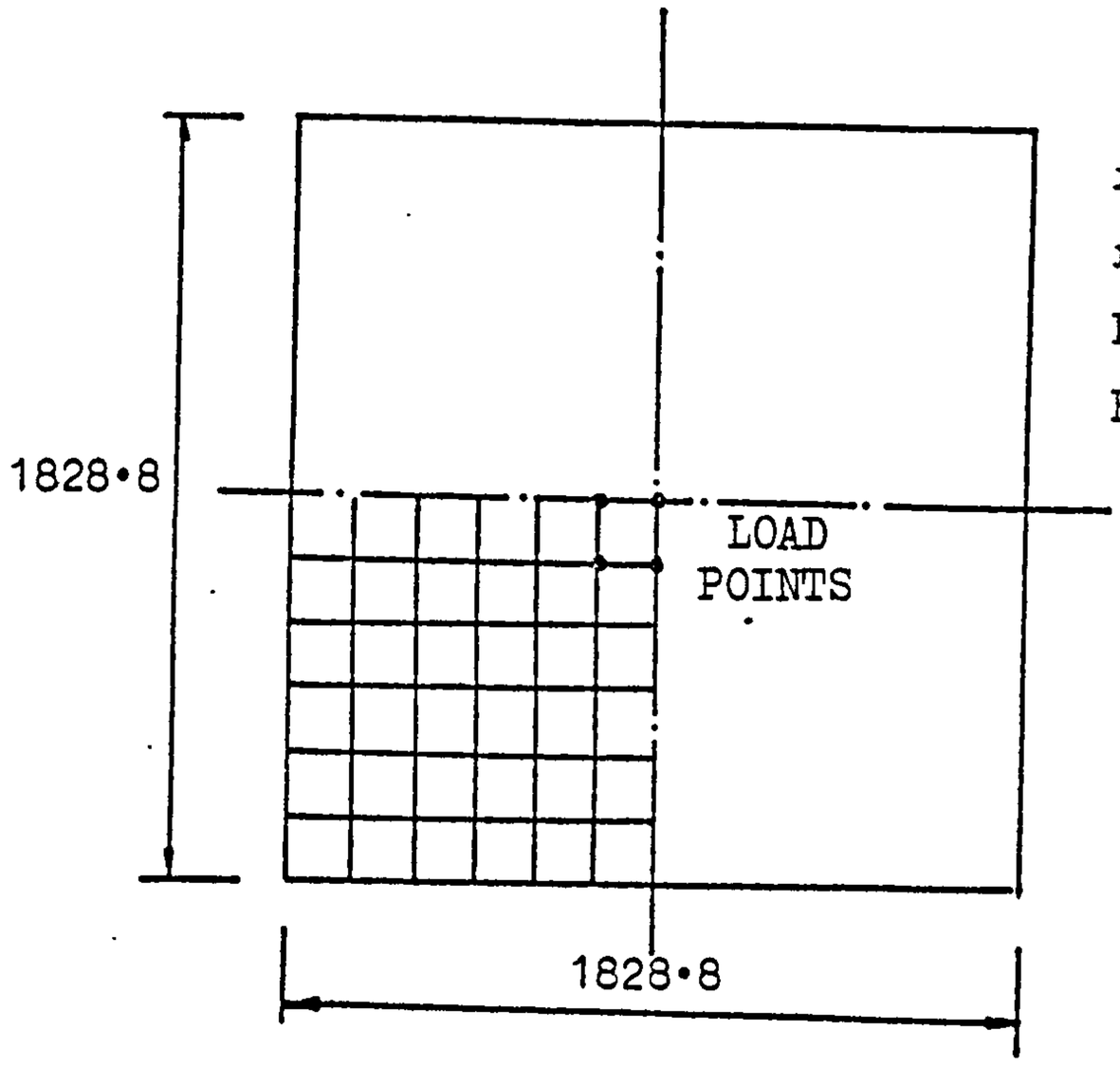

f_{cu} = 47·71 N/mm^2
f_y = 303·4 N/mm^2
E_c = 27580 N/mm^2
E_s = 206850 N/mm^2
h = 139.7 mm
d_1 = 114·3 mm
$\rho_x = \rho_y$ = 0·0099

Figure (4.10.b) Details of DOTREPPE slab

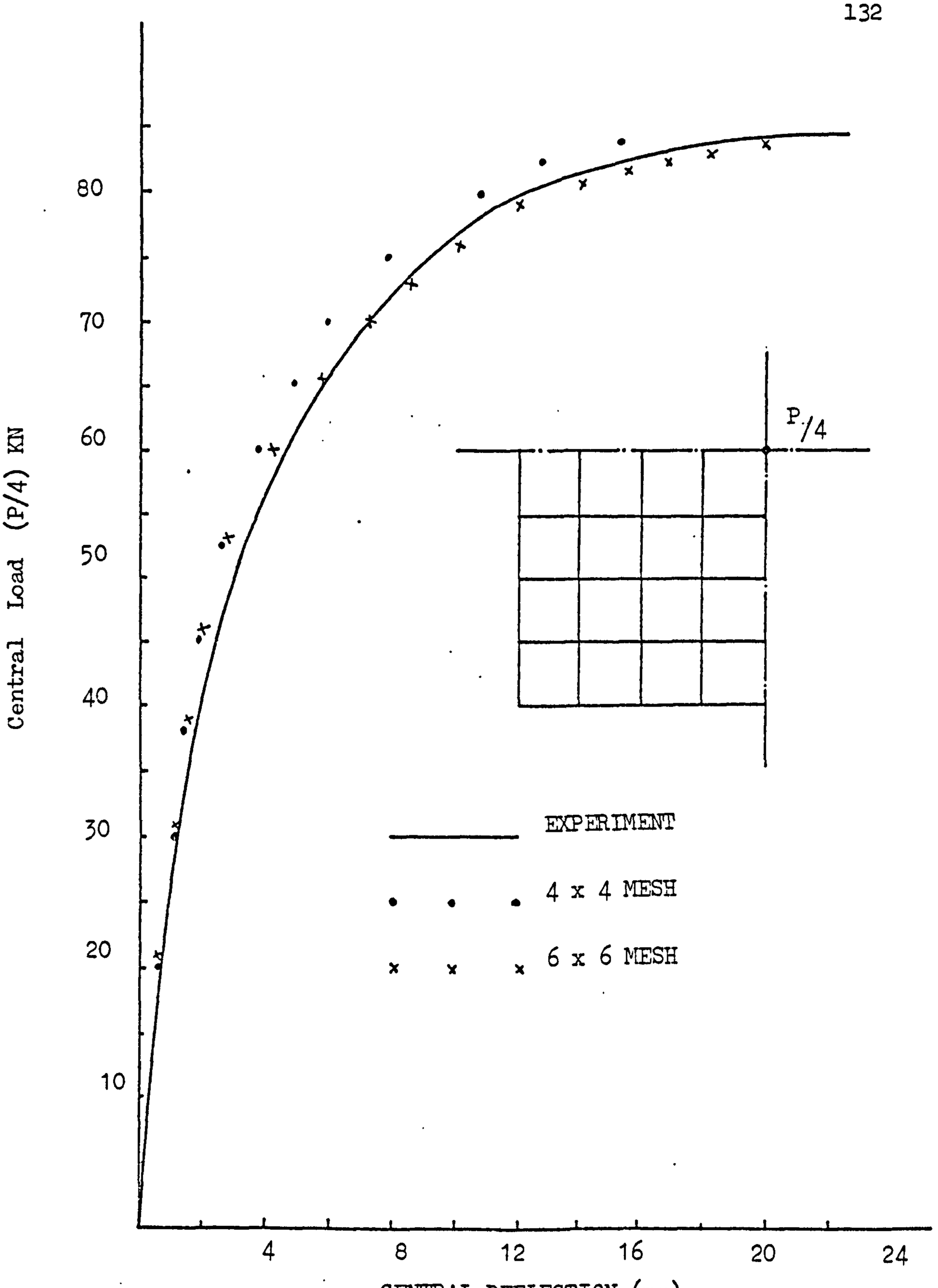

Figure (4.11) Comparison between the predictions made by different mesh subdivisions for the square simply supported slab under a central load

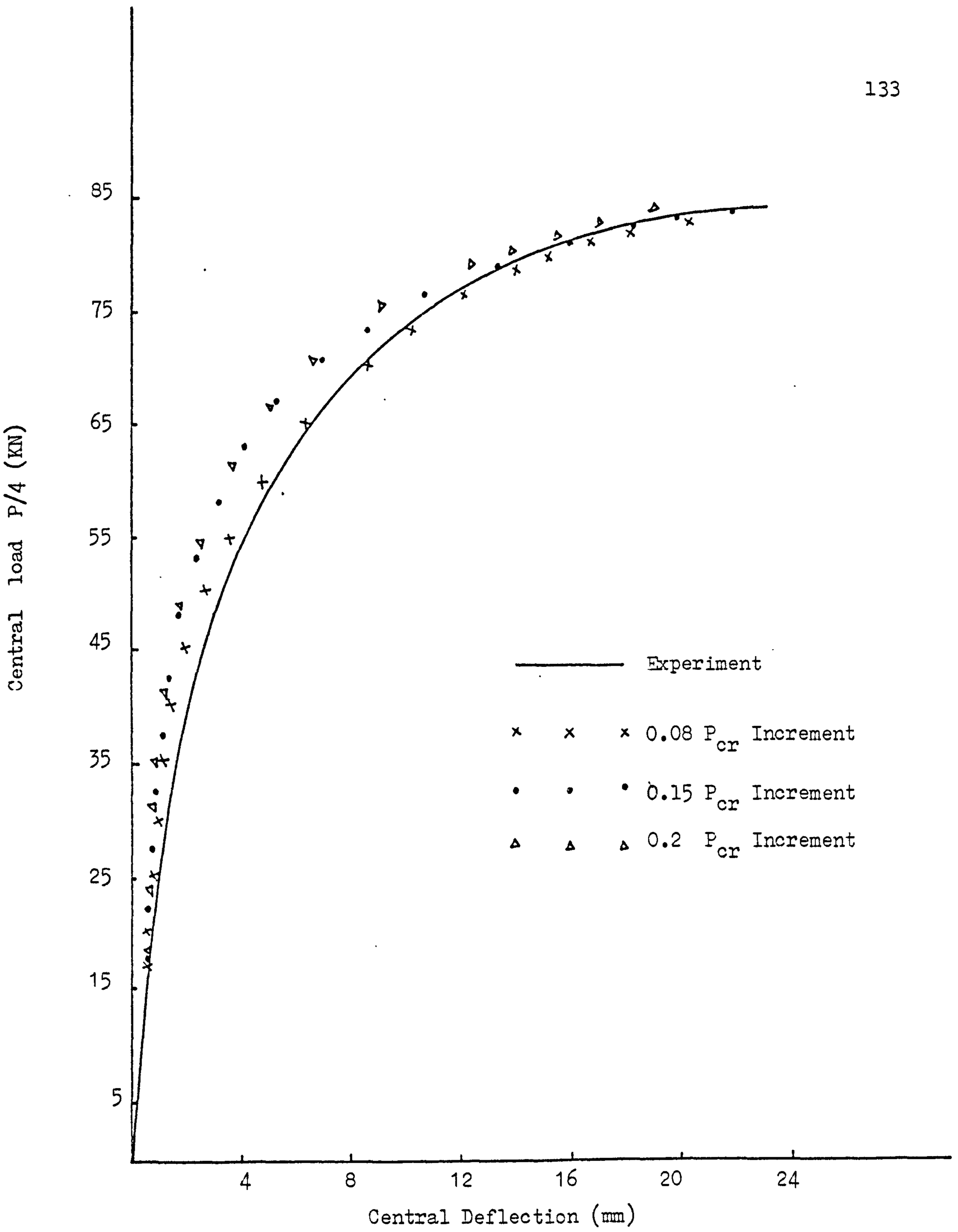

Figure (4.12) Effect of using various load increment sizes on the response of a simply supported slab.

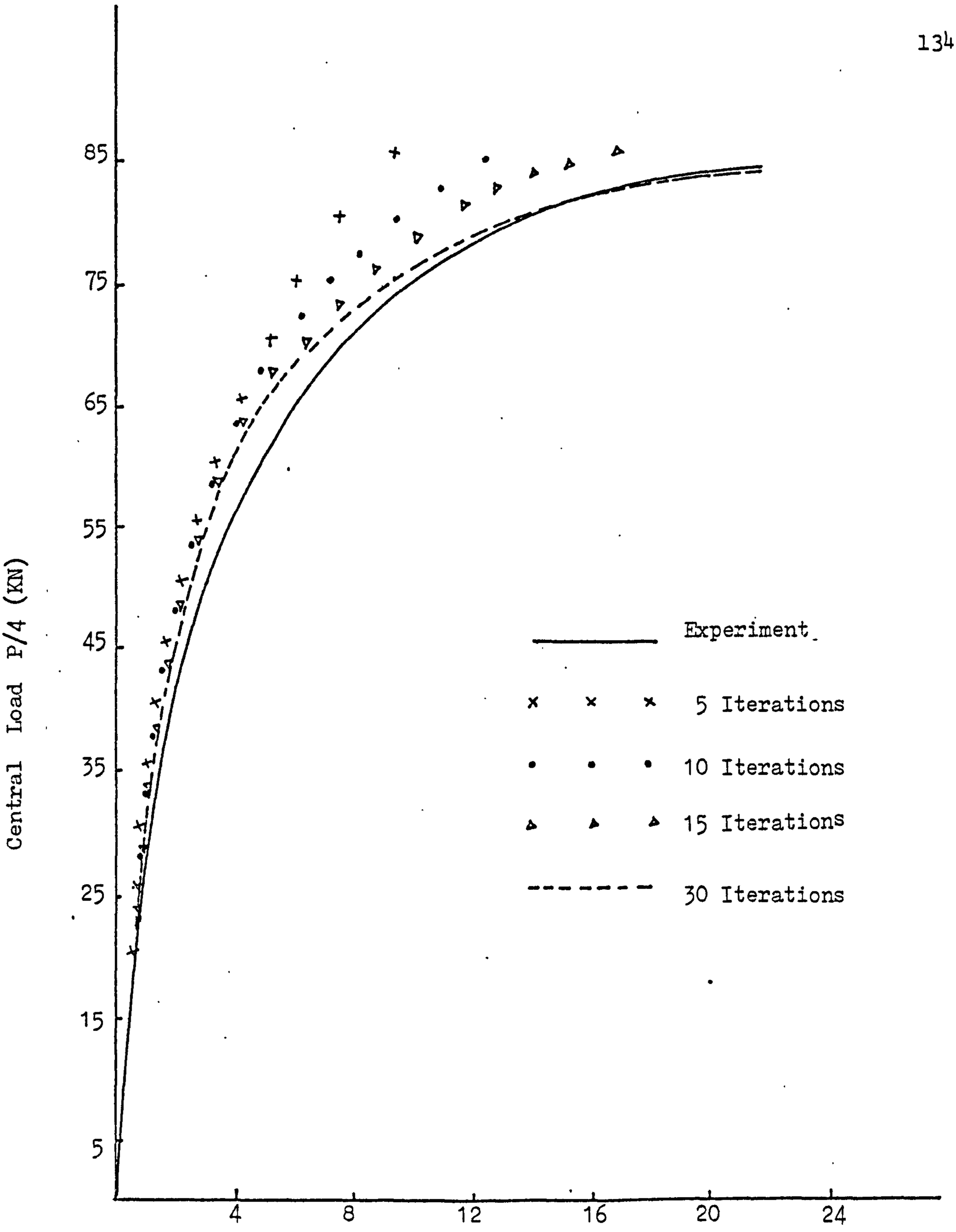

Figure (4.13) A simply supported slab under a central load. Effect of satisfying static equilibrium at each load level on the deflections.

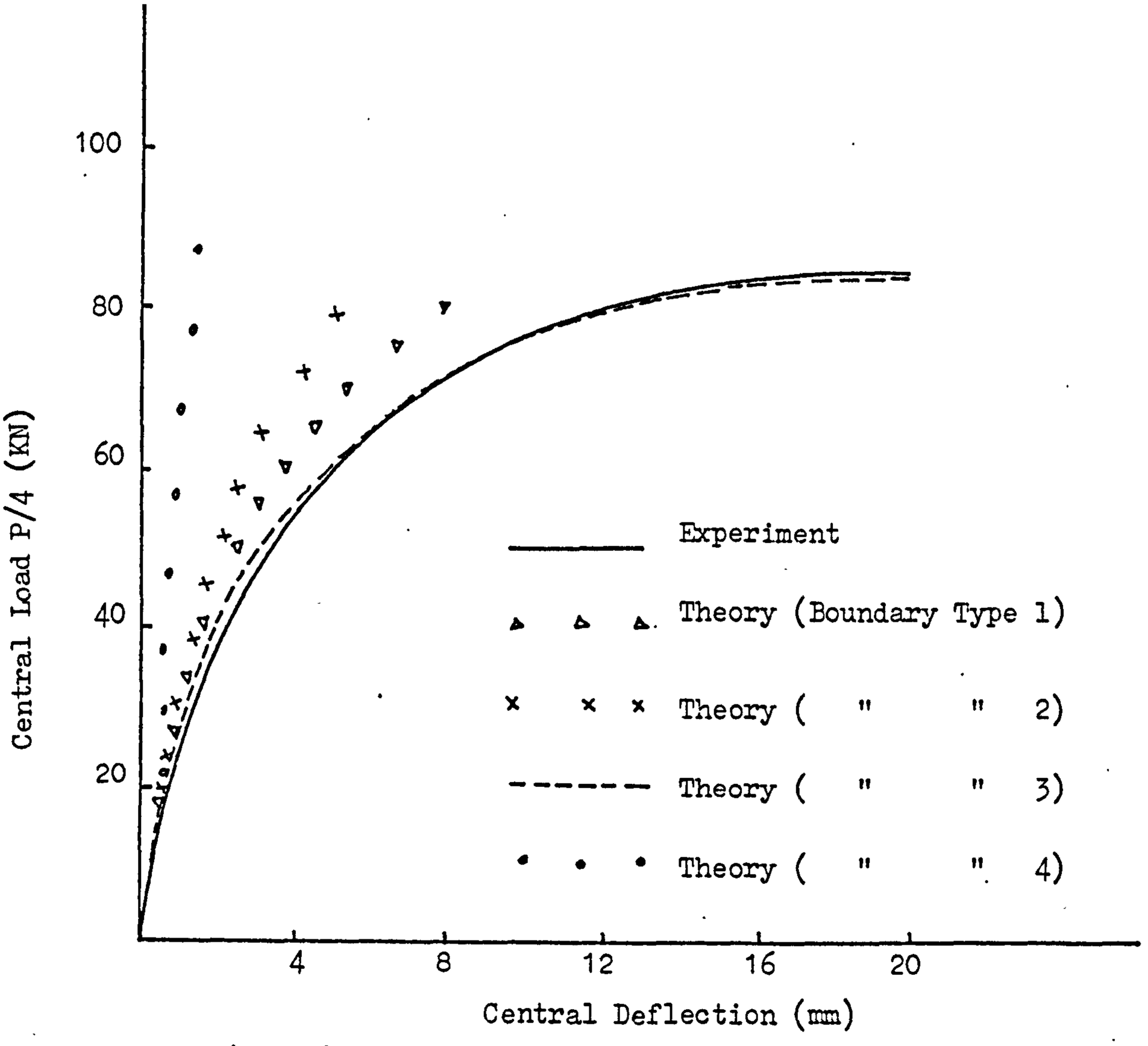

Figure (4.14a) Effect of various boundary conditions on the response

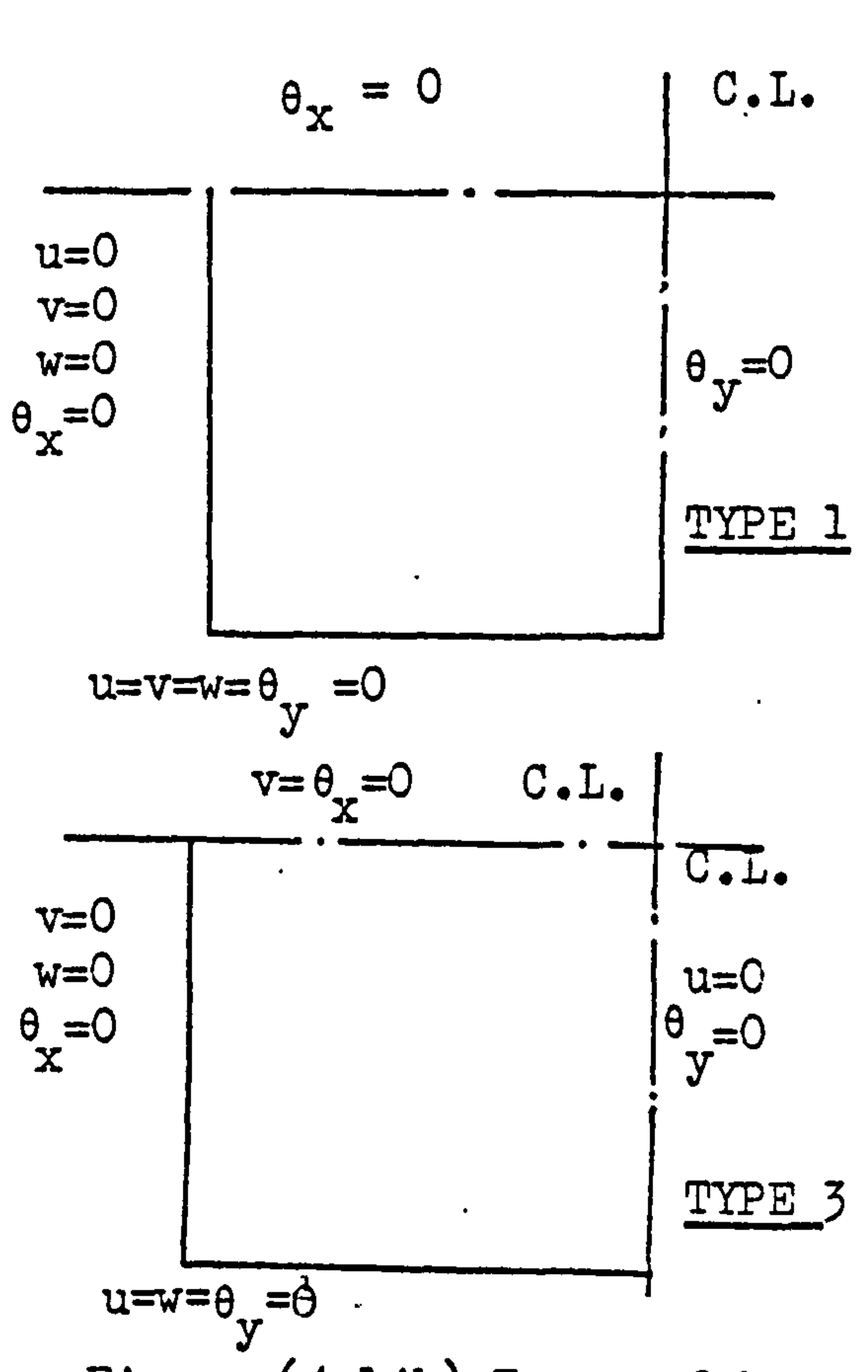

N.B. Type 4 = Type 2 + shifting the N.A. to the bottom of the slab.

Figure (4.14b) Types of boundary conditions for a simply supported slab

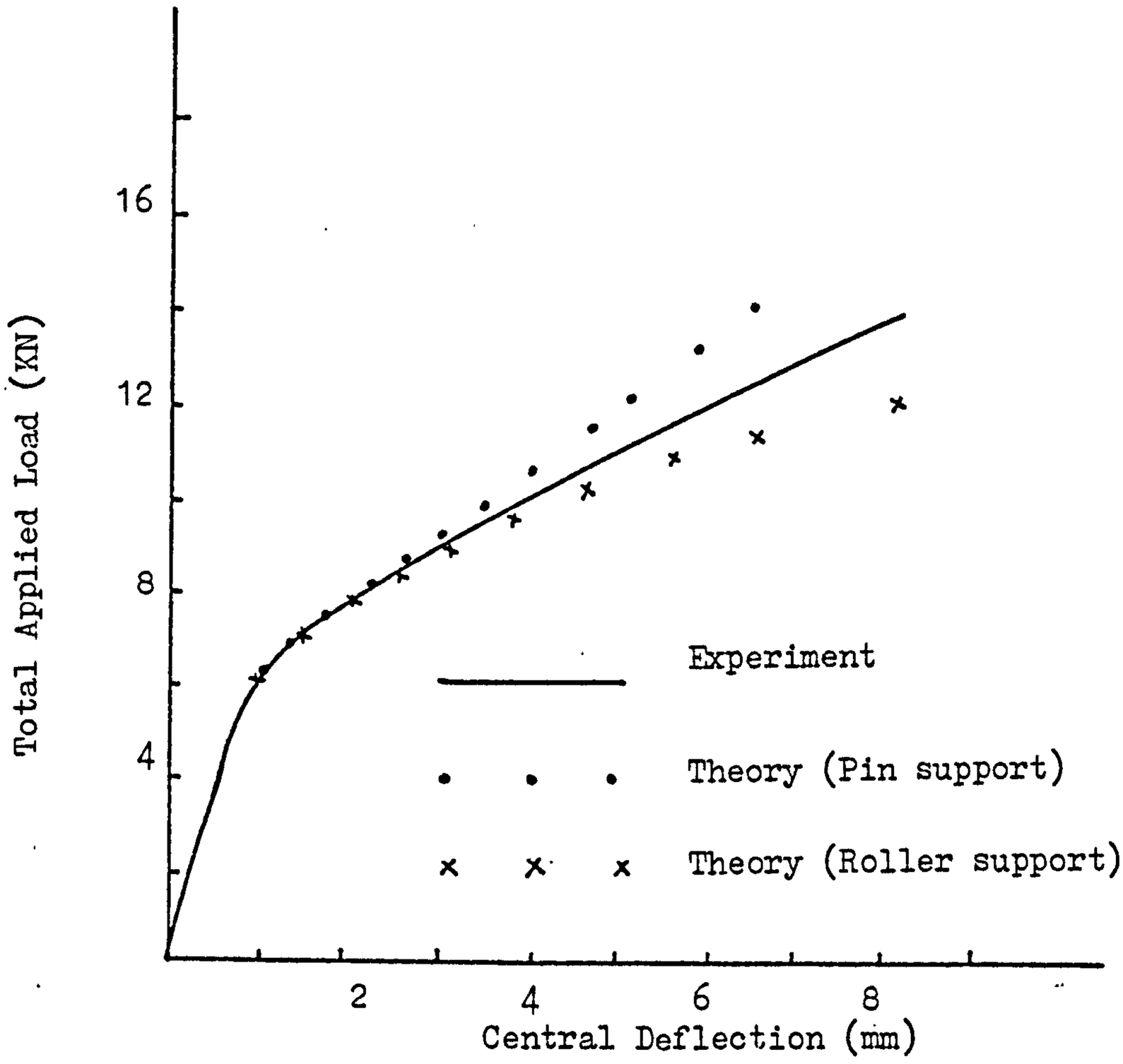

Figure (4.15) McNeice Corner supported slab.

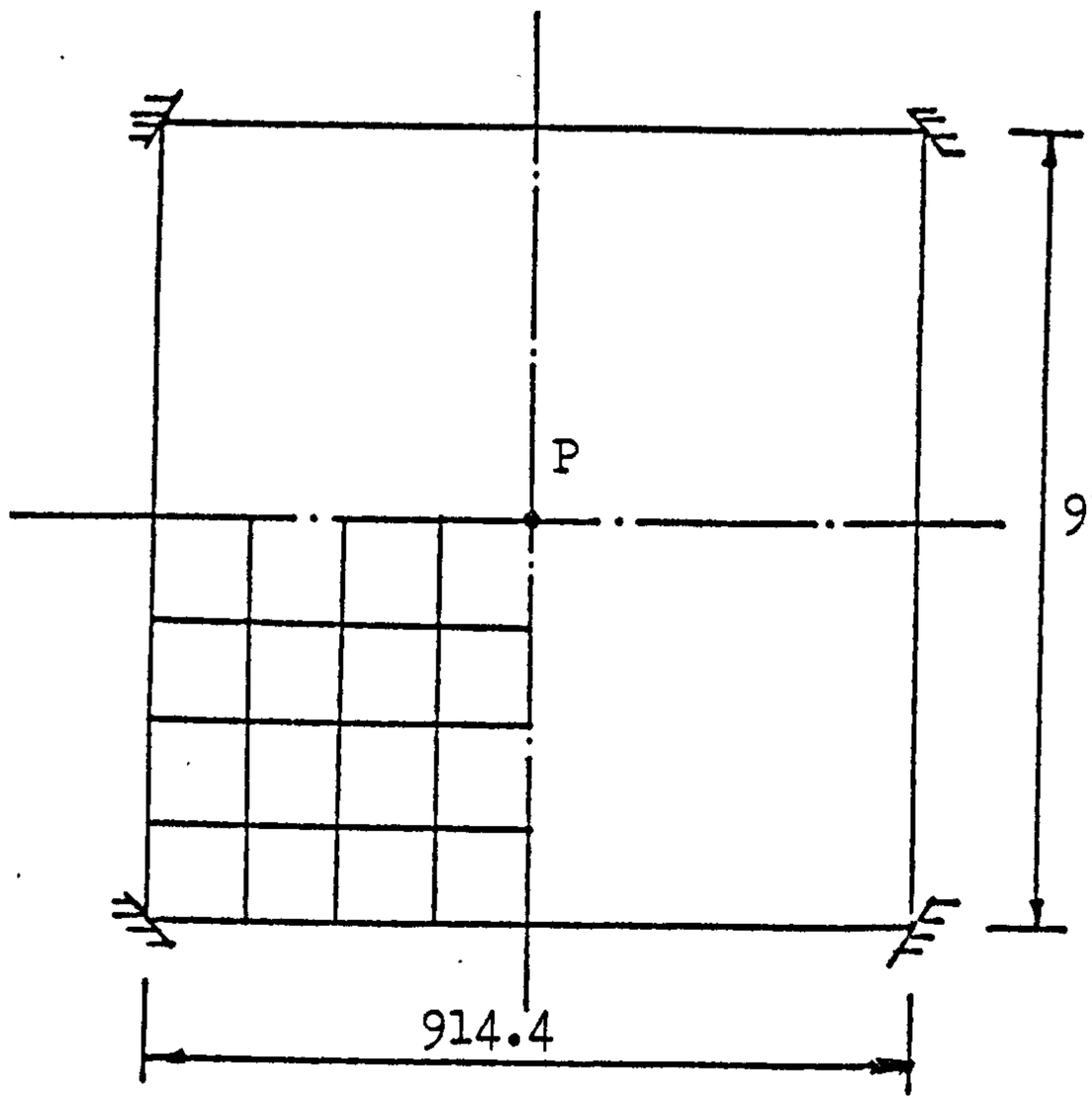

f_{cu} = 48.6 N/mm^2
f_y = 331 "
E_c = 28614 "
E_s = 200000 "
f_t = 2·413 "
h = 44·7 mm
d_1 = 33·3 "
$\rho_x = \rho_y$ = 0·0085

Figure (4.16) Details of McNeice Slab.

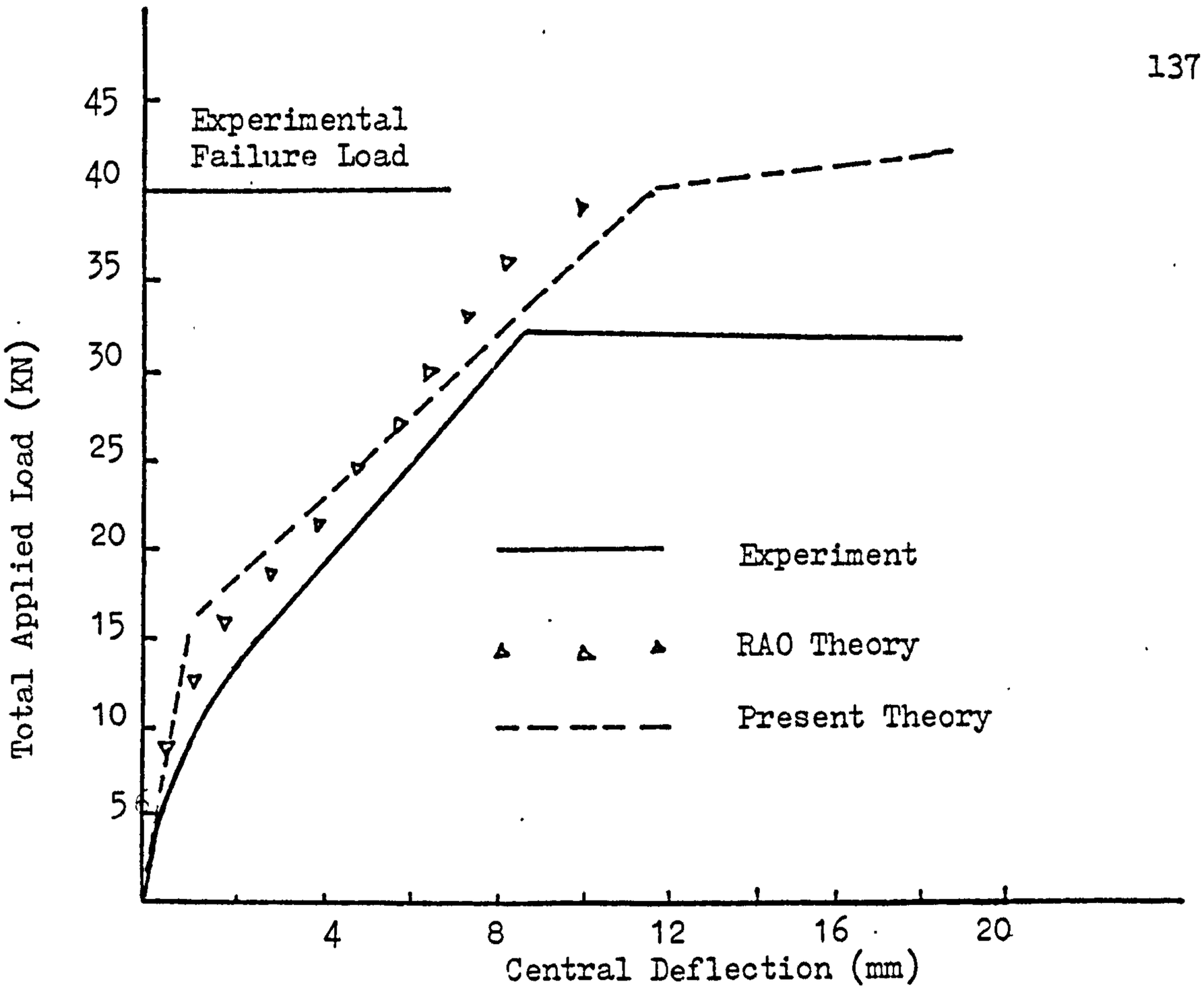

Figure (4.17) RAO TEE-BEAM B1

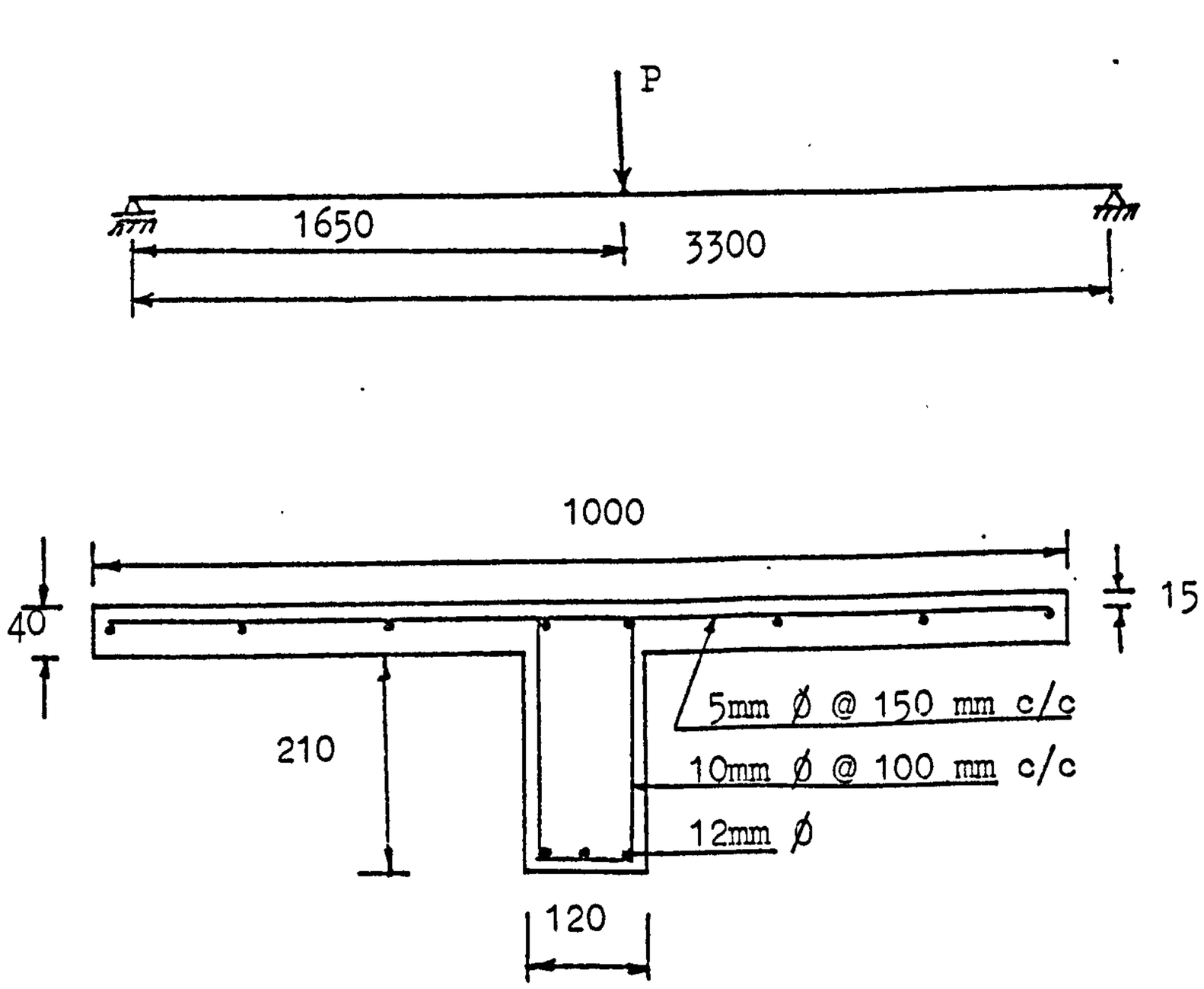

Figure (4.18) Details of RAO TEE-BEAM B1
(For materials properties see section 3.4.3)

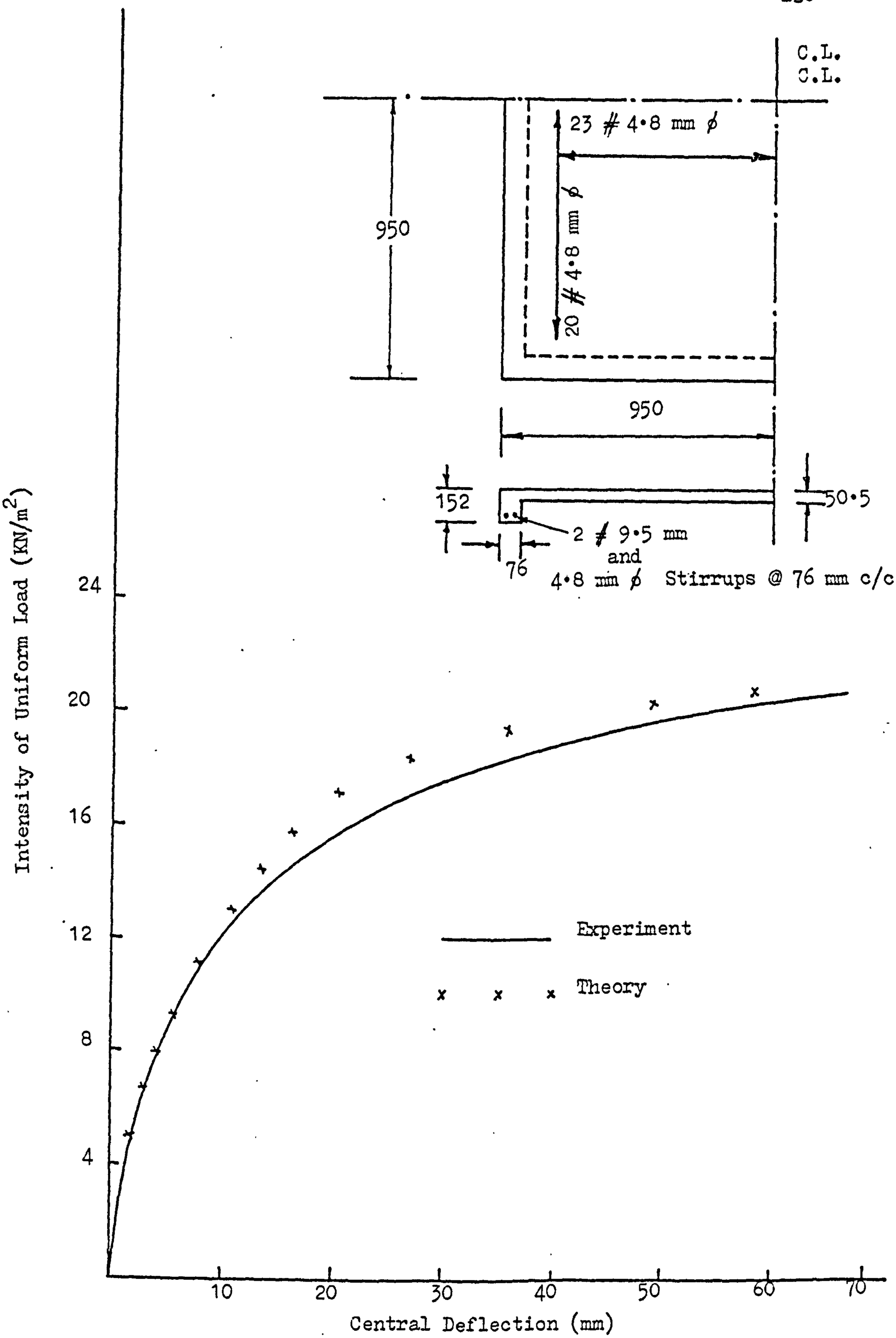

Figure (4.19) Details and load-displacement curve for Hayes' slab-beam system.

CHAPTER FIVE

THEORETICAL INVESTIGATION

5.1 INTRODUCTION

In the previous chapter a reliable finite element program was established. In this chapter, the proposed direct design procedure (Chapter 3) will be critically examined. The design procedure is dependant on the availability of a finite element program, and can be summarized as follows:

(1) The geometric details, materials properties and the design loads are used as the input data for the program. The program performs an elastic analysis on the slab, using the initial uncracked concrete section properties. The analysis establishes the stress distribution (N_x, N_y, N_{xy}, M_x, M_y, M_{xy}) at any point on the slab at the specified ultimate design load.

(2) Using the design equations of chapter (3), the required resisting moments are calculated at every point on the slab.

(3) Using the Limit State Theory (Appendix A), the steel areas required to provide the design resisting moments and membrane forces in step (2) are calculated for each element. The program then inserts the computed steel areas in the two orthogonal directions in their proper places in the layered finite element model.

(4) To check the service and ultimate behaviour of the slabs designed in this way, a full incremental nonlinear analysis is performed.

A wide range of problems has been investigated and their results will be presented in this chapter.

5.2 COMPARISON BETWEEN TORSIONAL AND TORSIONLESS ANALYSES:

5.2.1 General:

The provision of reinforcement to resist the three moment components M_x, M_y, M_{xy} in laterally loaded slabs can be regarded as an extension to the well known Hillerborg's strip method of slab design. In fact, the strip method provides reinforcement to resist the normal moment components M_x and M_y, while the torsional stress component M_{xy} is ignored. This is equivalent to assuming that the slab is designed as a series of parallel beams (in each direction) without torsional stiffness. Such an assumption is unsatisfactory in two ways. First, the method would produce unacceptable moment fields for cases in which torsional moments are dominant. Secondly, in pursuit of simple solutions, the designer may choose stress distributions which depart from the elastic distributions, which will jeopardize the service load behaviour.

In the slabs which are loaded uniformly the Code provisions for torsional moments may circumvent this, but in cases where slabs are subject to eccentric concentrated loads, or torsional loads, the Code provisions may not be applicable.

The proposed design method provides reinforcement to resist all three moment components, and is thus more general. A study to compare the two design procedures has been undertaken here. The object of the study is to compare the design moment fields in the two methods, and to show their relative merits in terms of economy by comparing the moment volumes. In both cases, the finite element program developed in Chapter (4) was used. For Hillerborg's strip method, the slab was assumed to possess zero torsional stiffness i.e. G = 0.0 in the finite element analysis. Such a numerical simulation would yield

a stress distribution in equilibrium with the applied loads, but with zero torsional moments everywhere. Accordingly, such an analysis will be called a "torsionless" analysis. On the other hand, for the present design procedure, isotropic properties for concrete slab were assumed, and the torsional modulus $G \neq 0.0$. This would also produce a stress distribution in equilibrium with the applied loads, but with $M_{xy} \neq 0$. As opposed to the torsionless analysis, solutions obtained with $G \neq 0.0$ are linked with the equations of Chapter (3), and will be termed as "torsional analysis".

5.2.2 Analyses and Results:

A series of slabs with various boundary conditions and differing sides ratios was investigated. The slabs were all analysed under a uniformly distributed lateral load. Table (5.1) summarizes the cases considered, and gives the results obtained. The results for the moment volumes have been plotted in Figure (5.1) and Figure (5.2). Comparisons for the moment fields for the two design procedures are presented in Figures (5.3) to (5.9) for the seven cases in Table (5.1) for square slabs. Results for rectangular slabs with sides ratios of 1.5 and 2.0 for the seven cases considered are given in Figures (D1) to (D56) in Appendix (D). In all figures, full lines _____ indicate the results of the proposed torsional analysis, while the broken lines -------- are those of the torsionless analysis. The numbers on the curves indicate the strip number as shown in the small diagrams near the curves in each figure. It should be mentioned that all slabs had been analysed using a regular mesh of 10 x 10 elements. Accordingly, the strip distance from the edge can easily be calculated in tenths of the span length.

Individual curves give the variation of the design moment along the strip. For general use, the results had been expressed in a

nondimensional form. The sign convention for the moments is that those causing tension on the underside of the slab are positive.

5.2.3 Discussion of Results:

From Figures (5.1) and (5.2), it is evident that the torsional analysis always gives higher moment volumes than that of no torsion. This is true for all cases considered. With slabs simply supported along all sides, the moment volumes corresponding to the bottom steel only are approximately the same in the two analyses, the maximum difference in this case is only 8% of the torsionless value (see Table 5.1). Accordingly, the apparent differences between the two analyses can be attributed to the torsional moments, which are concentrated near the discontinuous supported corners. In practice, torsional reinforcement is normally added at such corners, as a certain percentage of the midspan reinforcement. Following Cp 110[5], torsional steel moment volumes were calculated (see Appendix D1), and added to the torsionless analysis results. The resulting total moment volumes have been compared in Table (5.2), for the cases with discontinuous edges. The results of the final moment volumes indicate that, in case of slabs simply supported on all edges, the torsional analysis is at least 10% more economical than the torsionless analysis. For other types of slabs in Table (5.2), the torsional analysis gives moment volumes either very close to that of the torsionless analysis, or higher by up to 20%.

Large differences can also be seen in cases with free edges. The two methods produce moment volumes which differ considerably from each other, as can be seen from Figure (5.1). For the case of slabs with one free edge (case C), the difference is due to two reasons:

(a) The torsionless analysis underestimates the reinforcement normal to the free edge, as can be seen from Figures (5.5b), Figures (D18 and D22).

(b) The torsional reinforcement.

However nothing can be done about the reason in (a), but the torsional steel can be added according to CP110[5], over the two confined corners. This has the effect of reducing the difference in the moment volumes from an average of 48% (Table 5.1) to a maximum of 9.5% only (Table 5.2). This shows the importance of the torsional moments in this case. The slight (9.5%) difference is thus due to cause (a) above, and reduces in effect as the sides ratio tends to unity. But the effect of the torsional moments reduces with the reduction in the number of confined corners (between orthogonal discontinuous edges), which increases the effect of the normal moments in determining the total moment volume (cause (a) above). Take for example, the case of a slab simply supported along two orthogonal sides, and supported by a column at the opposite corner (case G). From Table (5.1), the difference in moment volumes in the two analyses ranges between 32.2% and 44.7%. Addition of torsional steel over the confined corner between the two simply supported edges reduces the difference to a maximum of 18.6%.

The difference in such cases is due to the large differences in the moment fields. A comparison between the moment fields produced by the two analysis for the seven cases in Table (5.1), is given in Figures (5.3) to (5.9) and in Appendix (D).

Considering the case of the simply supported slabs, the moment fields are given by Figures (5.3a, b, c, d) and Figures (D1 to D8).

While the torsional analysis gives a fairly gradual variation of design moments, the torsionless analysis produces a parabolic variation, with concentration of reinforcement in the central zone of the slab. The smooth variation of design moments in the torsional analysis provides a convenient way of placing the reinforcement in the strip. Unlike the torsionless analysis, the reinforcement design in the torsional analysis can thus be based on the maximum or the average value of the moment, without producing a significant difference. This is also an advantage over the designs based on the minimum weight principles[10], which requires continuously varying reinforcement pattern.

For clamped slabs (case B), results of the moment distributions are given in Figure (5.4) and Figures (D9 to D16). Although the torsionless analysis tends to give higher moment values, the two methods do not differ very much from each other. In the two analysis, the ratio between the support to central moment is about 2. The extension of the supports reinforcement in slabs with sides ratios greater than 1.0, agrees very well in the two cases. For edge strips, this steel extends the full strip length, and extends to about 0.2 L in the central strips.

For slabs with two adjacent edges simply supported and supported on a column on the opposite corner (case G) the two methods produce different distributions, as can be seen from Figures (5.9, D49 to D56). The torsionless analysis requires very strong bands of steel along the free edge strips, with little steel at the centre (the ratio of free edge to centre steel is about $2\frac{1}{4}$). On the other hand, the torsional analysis produces a more even distribution, even for this case.

Finally the present design approach, which is represented by the torsional analysis is compared with the yield line designs. The case

considered is the square simply supported slab of Table (5.1). It will be assumed in the yield line design that the slab is reinforced in a banded form, with the slab being divided into a central and two edge strips in each direction. The ultimate moments provided in the central strip of width 2x is m_2, that of edge strips is m_1. Differences in the lever arms will be neglected, so that the steel volume is proportional to the moment volume. By considering the two modes of failure in Figure (5.12), then the volume of steel is minimum when the ultimate loads of the two modes are the same. This will give $x = 0.375$ L where L is the span length, and

$$V = 0.0746\ q\ L^4$$
$$m_1 = 0.0241\ q\ L^2 \qquad (5.1)$$
$$m_2 = 0.0475\ q\ L^2$$

Now for the same slab, from Table (5.1) and Figure (5.3) we have:

$$V = 0.0744\ q\ L^4$$
$$m_1 = 0.0225\ q\ L^2 \qquad (5.2)$$
$$m_2 = 0.0475\ q\ L^2$$

The moment values in (5.2) are the central value and the value at the mid of strip 2 in Figure (5.3), which is at 0.15 L from the support. This distance is equivalent to $x = 0.35$ L as compared to 0.375 L in the yield line analysis.

Equations (5.1) and (5.2) show that the two methods yield the same results. The only difference is that while only three bands are used in each direction in the yield line analysis, the present design method assumes many more bands. Since the derivation in the yield line theory here had been based on an assumption of equal ultimate loads in two failure modes, it can be concluded that the use of banded

reinforcement will involve failure by simultaneous formation of many collapse mechanisms. In the limit when every point is designed according to the stress distribution, an infinite number of collapse modes will form at the design load, due to the yielding of all portions of the slab and not just along the yield lines.

5.2.4 Conclusions:

Based on what has been presented the following conclusions can be drawn:-

(1) The distribution of design moments in concrete slabs can conveniently be obtained by using the finite element method. Putting the shear modulus G = 0 in the analysis produces solutions without torsional moments, which is equivalent to the Fernando and Kemp's strip deflection method of slab design, and thus to Hillerborg's method (Torsionless Solutions).

(2) Using isotropic material properties with the shear modulus $G \neq 0.0$ in the finite element analysis, solutions were obtained which were linked with the design equations of Chapter (3) to produce distributions of design moments in concrete slabs. The procedure takes torsional moments as well as the normal moments in the calculation of the normal design moments (Torsional Solutions).

(3) The strip method represented here by the torsionless analysis produces moment volumes which compare within acceptable variance with those obtained from the proposed direct design method, provided the additional torsional steel is included.

(4) For slabs discontinuous on all edges (i.e. simply supported all around), the direct design method produces more economical solutions than the strip method. Using the torsional analysis suggested here a saving in steel can be obtained in this case of between 10 to 19% of that required by the strip method.

(5) The suggested torsional analysis provides a fairly smooth variation in the distribution of design moments. Accordingly, the designer can base the reinforcement design in the strip on either the maximum or the average value of the design moment in the strip, without departing far from the original distribution of moments in the strip.

(6) The proposed method provides both the required quantity of torsional steel at the corners, and the length over which such steel should extend. In normal practice, such a steel is only taken as a certain percentage of midspan steel, as prescribed by the Codes of Practice.

(7) The method also provides the amount and the distribution of transverse steel. In some cases, the simple strip method requires no steel in this direction, and the designer will provide such steel based on Code requirements.

(8) The method is found to compare accurately with designs based on the yield line theory involving failure under simultaneous collapse modes. The present direct design approach has the advantage of providing distributions of moments with a wider choice than that permitted by the yield line theory. The comparison lead to the conclusion that the proposed direct design approach which allows for yielding of all portions of the slab, permits failure with simultaneous collapse modes under the design ultimate load.

Case	Boundary Conditions	Sides Ratio L_x/L_y	MOMENT VOLUMES /q L_y^4								
			Bottom			Top		Total			
			$G \neq 0$	$G = 0$	$\frac{G \neq 0}{G = 0}$	$G \neq 0$	$G = 0$	$G \neq 0$	$G = 0$	$\frac{G \neq 0}{G = 0}$
A	Simply supported on all edges 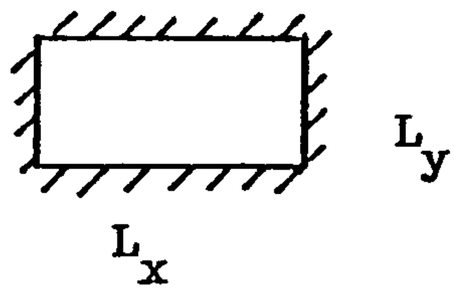	1.0	0.0744	0.0715	1.04	0.0138	0.0	0.0882	0.0715	1.234
		1.25	0.1019	0.0988	1.03	0.0181	0.0	0.1200	0.0988	1.215
		1.50	0.1372	0.1309	1.05	0.0228	0.0	0.1600	0.1309	1.222
		1.75	0.1719	0.1616	1.06	0.0266	0.0	0.1995	0.1616	1.235
		2.0	0.2066	0.1906	1.08	0.0291	0.0	0.2357	0.1906	1.237
B	Fixed on all edges 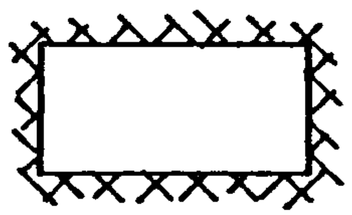	1.0	0.0154	0.0116	1.33	0.0154	0.0116	0.0309	0.0231	1.338
		1.25	0.0222	0.0169	1.31	0.0222	0.0169	0.0444	0.0338	1.314
		1.50	0.0287	0.0219	1.31	0.0287	0.0219	0.0574	0.0438	1.311
		1.75	0.0344	0.0266	1.29	0.0338	0.0266	0.0682	0.0533	1.282
		2.0	0.0397	0.0313	1.27	0.0391	0.0313	0.0788	0.0626	1.259

Table 5.1: Comparison between torsional and torsionless analyses

Case	Boundary Conditions	Sides Ratio L_x/L_y	MOMENT VOLUMES /q L_y^4							
			Bottom			Top		Total		
			G ≠ 0	G = 0	$\frac{G=0}{G=0}$	G ≠ 0	G = 0	G ≠ 0	G = 0	$\frac{G\neq 0}{G=0}$
C	Simply supported on 3 sides, free on the fourth 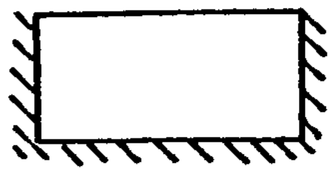	1.0	0.1000	0.0791	1.26	0.015	0.0	0.1156	0.0791	1.459
		1.25	0.1844	0.1444	1.28	0.0345	0.0	0.2189	0.1444	1.516
		1.50	0.2969	0.2375	1.25	0.0658	0.0	0.3627	0.2375	1.527
		1.75	0.4328	0.3656	1.18	0.1103	0.0	0.5431	0.3656	o.486
		2.0	0.5922	0.5359	1.11	0.1688	0.0	0.7609	0.5359	1.420
D	Fixed on 3 sides, simply supported on the fourth 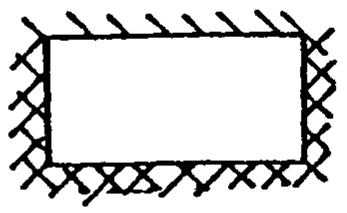	1.00	0.0211	0.0169	1.25	0.0155	0.0116	0.0366	0.0285	1.285
		1.25	0.0353	0.0285	1.24	0.0239	0.0175	0.0592	0.0459	1.290
		1.50	0.0497	0.0397	1.25	0.0316	0.0225	0.0813	0.0622	1.307
		1.75	0.0633	0.0505	1.25	0.0378	0.0272	0.1011	0.0773	1.308
		2.0	0.0756	0.0605	1.25	0.0430	0.0306	0.1186	0.0911	1.302

Table 5.1:continued

Case	Boundary Conditions	Sides Ratios L_x/L_y	MOMENT VOLUMES /q L_y^4							
			Bottom			Top		Total		
			G ≠ 0	G = 0	$\frac{G \neq 0}{G = 0}$	G ≠ 0	G = 0	G ≠ 0	G = 0	$\frac{G \neq 0}{G = 0}$
E	Fixed on 2// edges, simply supported on others 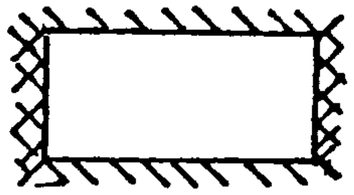	1.00	0.0277	0.0221	1.25	0.0154	0.0111	0.0431	0.0332	1.298
		1.25	0.0516	0.0428	1.21	0.0249	0.0169	0.0765	0.0677	1.299
		1.50	0.0806	0.0681	1.18	0.0338	0.0209	0.1144	0.0891	1.284
		1.75	0.1116	0.0950	1.17	0.0406	0.0231	0.1522	0.1181	1.289
		2.00	0.1428	0.1216	1.17	0.0453	0.0241	0.1881	0.1456	1.292
F	Fixed on 2 adjacent sides, simply supported on others 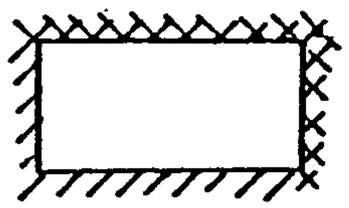	1.00	0.0364	0.0273	1.33	0.0156	0.0105	0.0520	0.0378	1.376
		1.25	0.0473	0.0402	1.18	0.0231	0.0155	0.0704	0.0557	1.264
		1.50	0.0616	0.0513	1.20	0.0294	0.0196	0.0910	0.0709	1.283
		1.75	0.0748	0.0613	1.22	0.0348	0.0234	0.1096	0.0847	1.294
		2.00	0.0867	0.0713	1.22	0.0395	0.0273	0.1262	0.0986	1.280

Table 5.1: continued

Case	Boundary Conditions	Sides Ratio L_x/L_y	MOMENT VOLUMES / $q\ L_y^4$							
			Bottom			Top		Total		
			$G \neq 0$	$G = 0$	$\frac{G \neq 0}{G = 0}$	$G \neq 0$	$G = 0$	$G \neq 0$	$G = 0$	$\frac{G \neq 0}{G = 0}$
G	Simply supported on 2 adjacent edges, propped at opposite corner 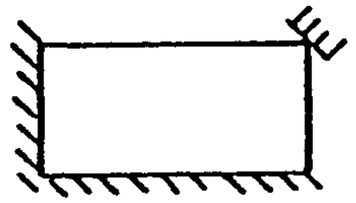	1.00	0.1383	0.1063	1.30	0.0155	0.0	0.1538	0.1063	1.447
		1.25	0.2234	0.1727	1.29	0.0271	0.0	0.2505	0.1727	1.45
		1.50	0.3367	0.2695	1.25	0.0498	0.0	0.3866	0.2695	1.435
		1.75	0.4727	0.4039	1.17	0.0868	0.0	0.5594	0.4039	1.385
		2.00	0.6326	0.5844	1.07	0.1398	0.0	0.7727	0.5844	1.322

Table 5.1: continued

Table (5.2): Comparison between moment volumes produced by Torsional and Torsionless analyses - Additional moment volume due to torsional reinforcement according to CP110 is added to the case of torsionless analyses.

N.B. All moment volumes are in terms of qL_y^4

Slab Type	$\frac{L_x}{L_y}$	$G \neq 0$	$G = 0$			TOTAL
		V_{total}	V_1	V_a	V_1+V_a	$\frac{V_{G \neq 0}}{V_{G=0}}$
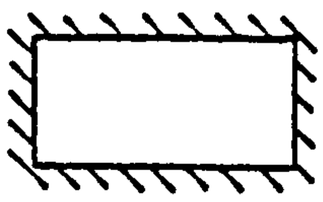	1.0	.0882	.0715	.037	.1085	.813
	1.25	.1200	.0988	.0487	.1475	.814
	1.50	.1600	.1309	.05952	.1904	.840
	1.75	.1995	.1616	.0655	.2271	.878
	2.0	.2357	.1906	.0691	.260	.907
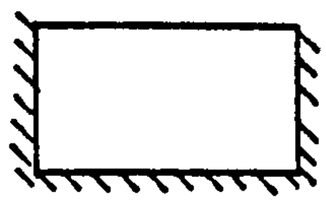	1.0	.1150	.0791	.0396	.1187	.970
	1.25	.2189	.1444	.0648	.2092	1.046
	1.50	.3627	.2385	.096	.334	1.086
	1.75	.5431	.3656	.1304	.496	1.095
	2.0	.7609	.5359	.1728	.7089	1.073
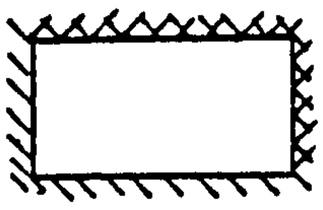	1.0	.0520	.0378	.0054	.0432	1.204
	1.25	.0704	.0557	.0071	.0628	1.12
	1.50	.0910	.0709	.0085	.0794	1.146
	1.75	.1096	.0847	.009	.0937	1.17
	2.0	.1262	.0986	.00912	.1077	1.172
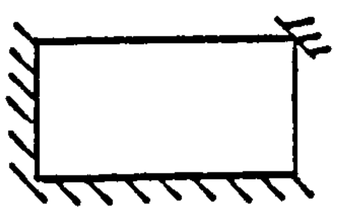	1.0	.1538	.1063	.0324	.1387	1.109
	1.25	.2505	.1727	.0438	.2164	1.157
	1.50	.3866	.2695	.0564	.3259	1.186
	1.75	.5594	.4039	.0704	.474	1.180
	2.0	.7727	.5844	.090	.6744	1.146

V_1 = moment volume without torsional steel

V_a = additional torsional steel moment volume

V = total moment volume = $V_1 + V_a$

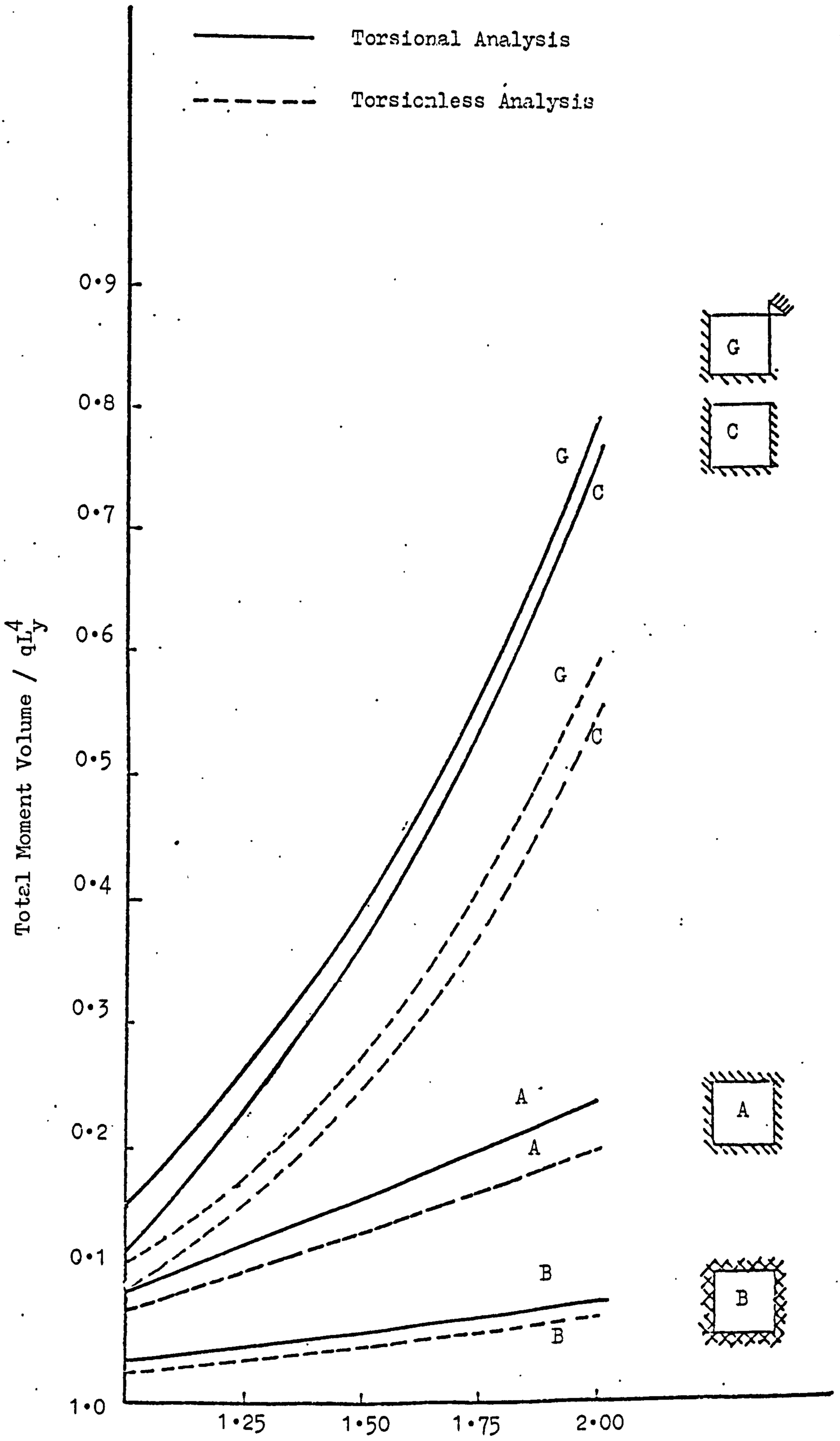

Figure (5·1) Comparison of moment volumes produced by torsional and torsionless analyses

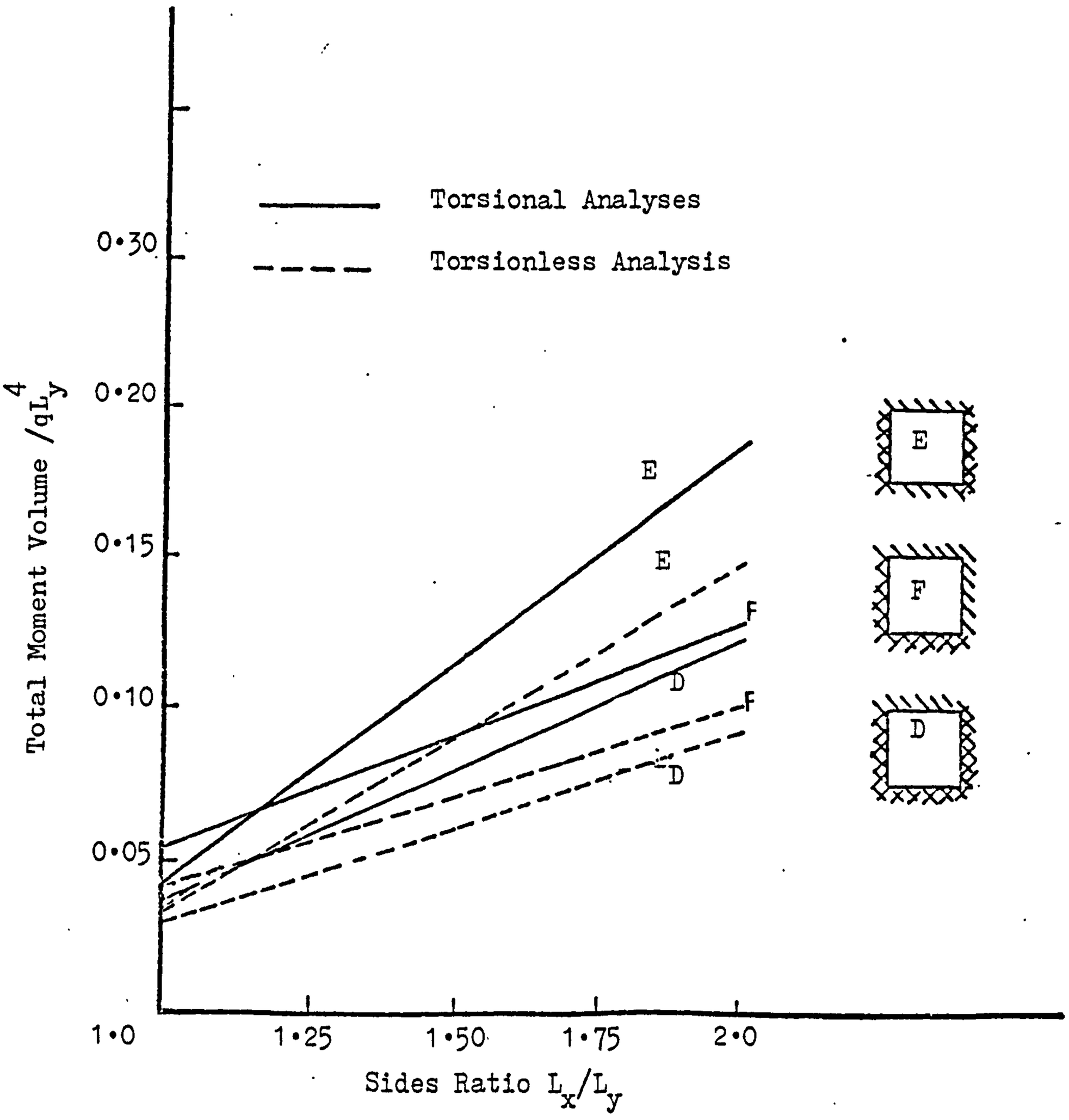

Figure (5•2) Comparison of moment volumes produced by torsional and torsionless analyses

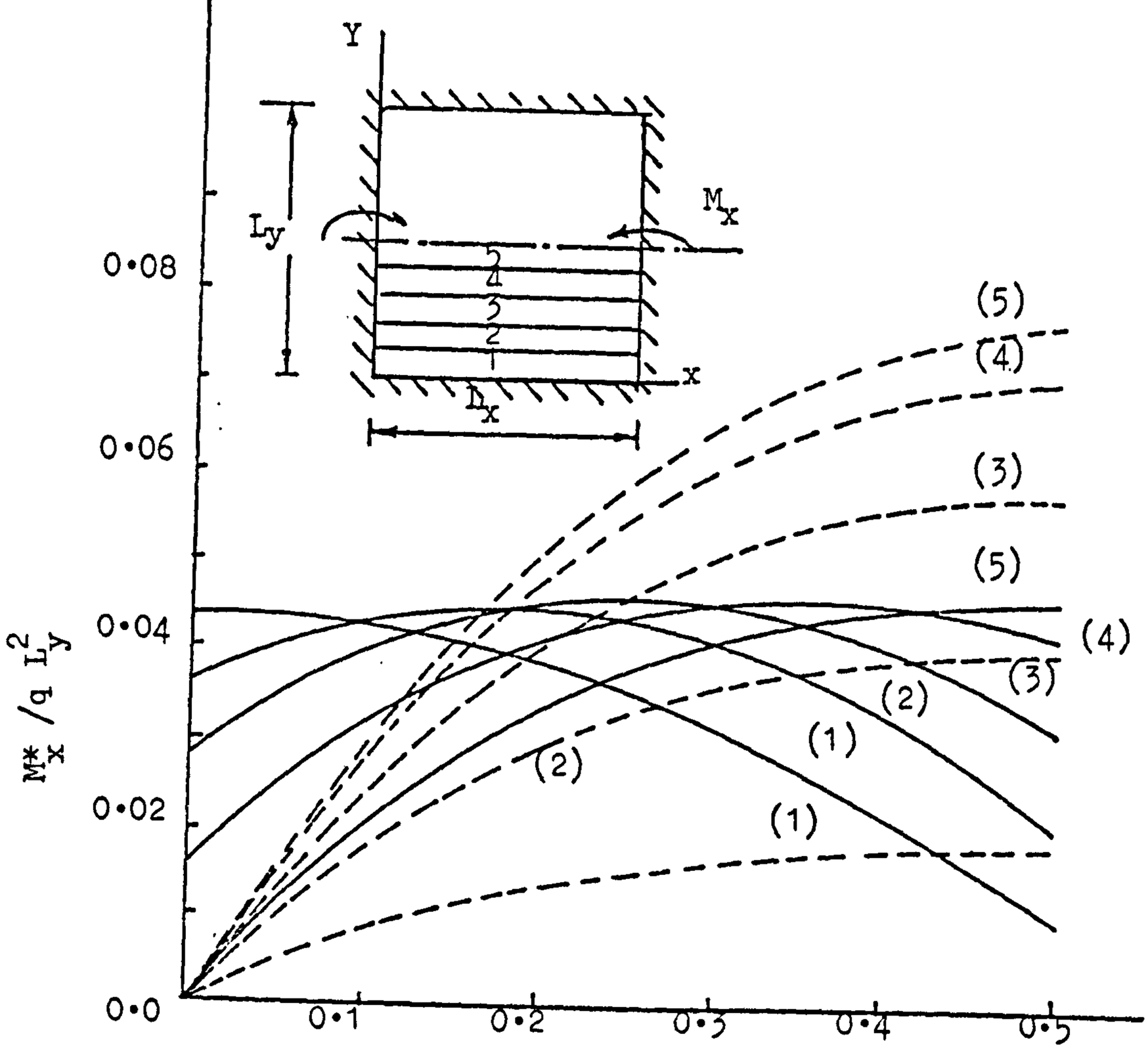

Figure (5.3a) Positive Moment M^*_x (L_x/L_y = 1·0)

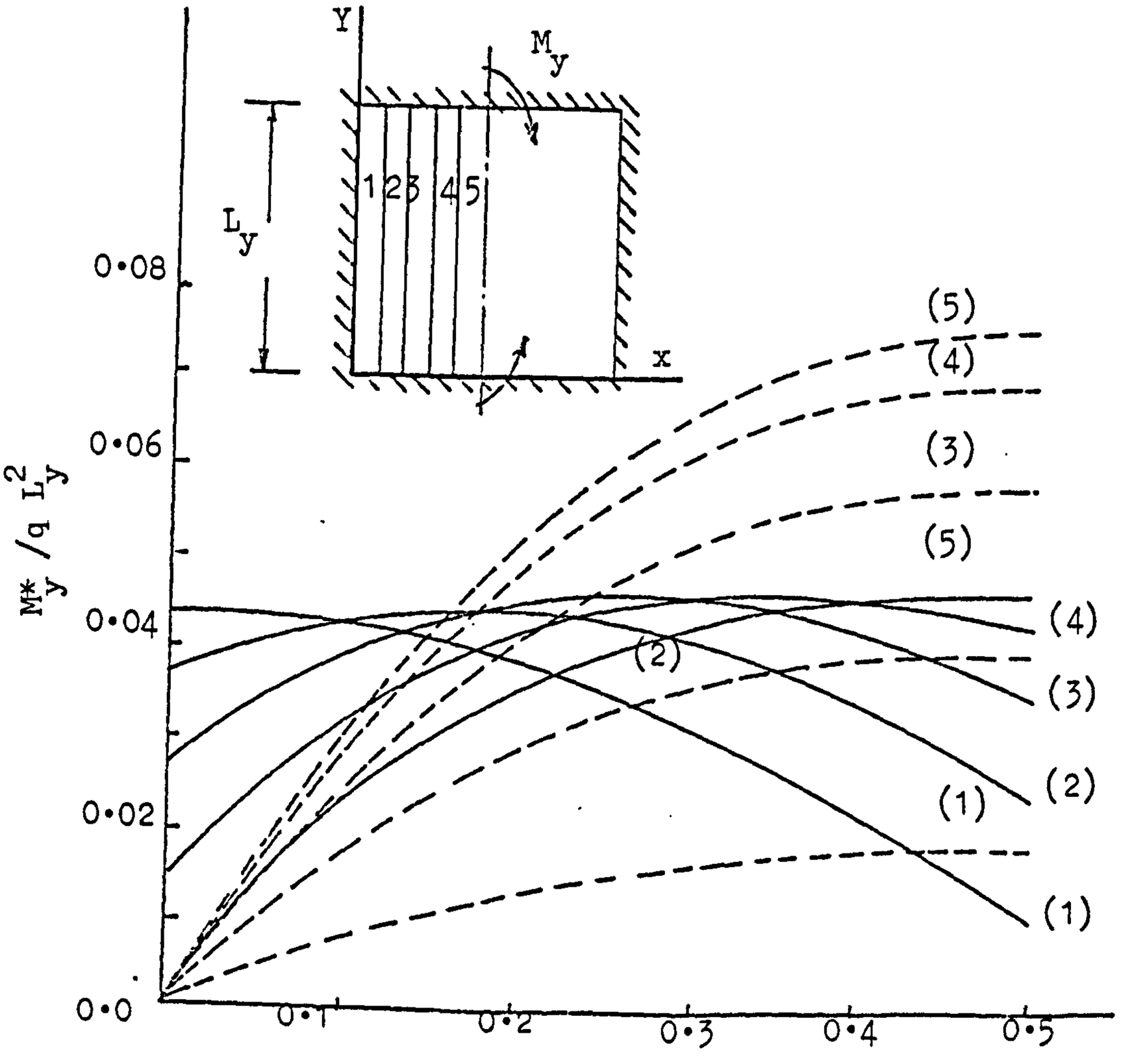

Figure (5.3b) Positive Moment M^*_y (L_x/L_y = 0)

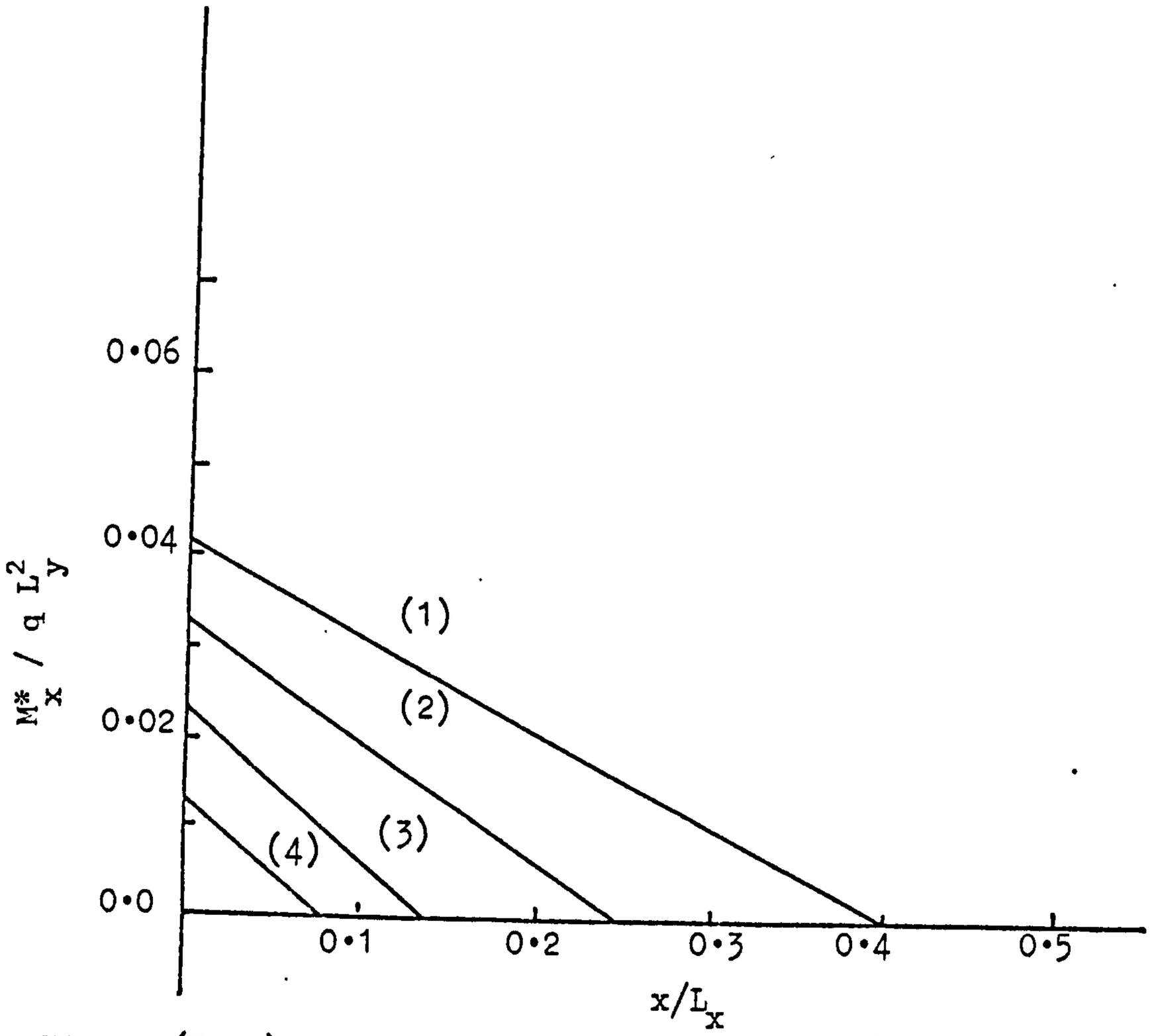

Figure (5.3c) Negative Moment M^*_x (L_x/L_y= 1•0)

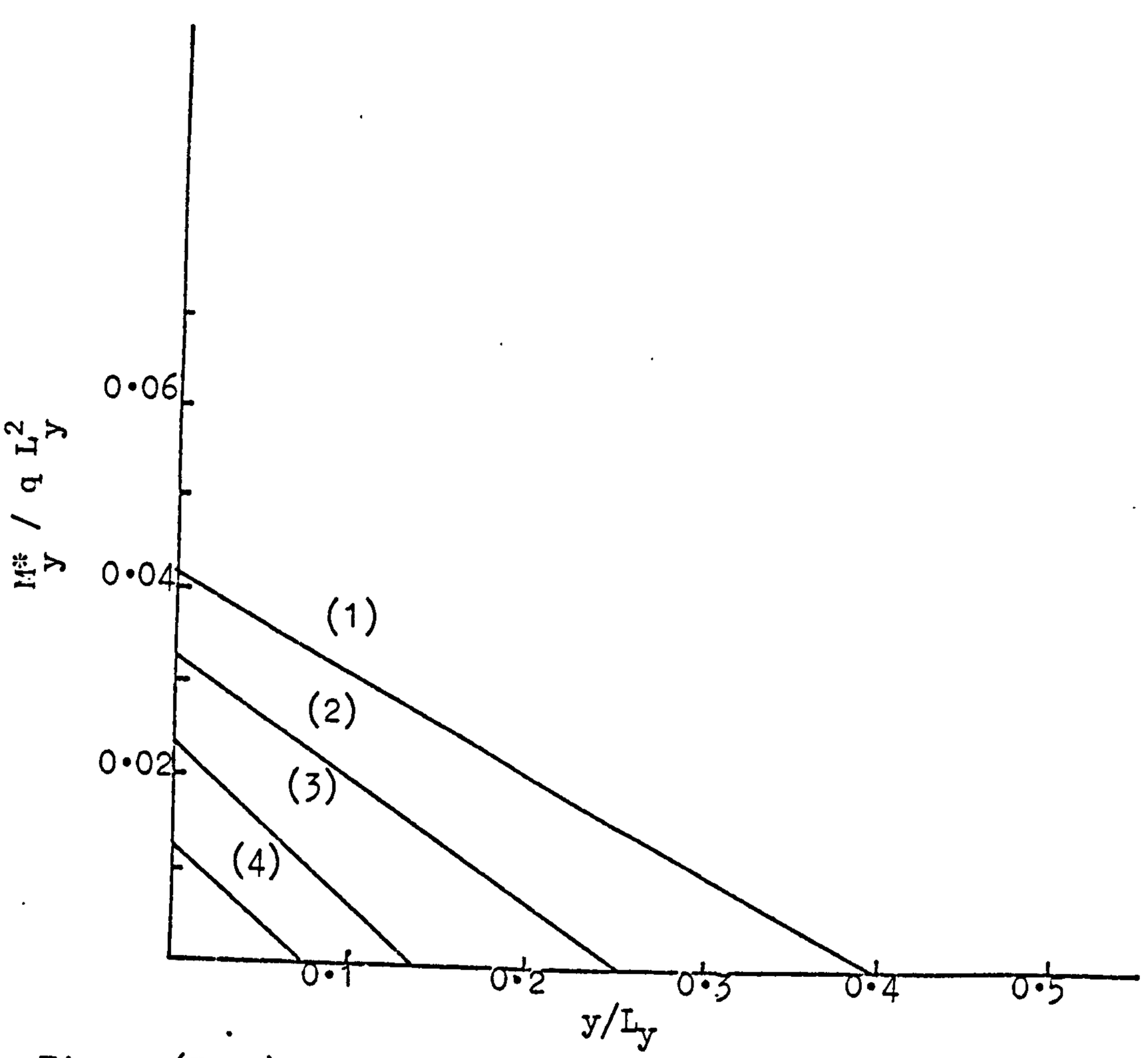

Figure (5.3d) Negative Moment M^*_y (L_x/L_y= 1•0)

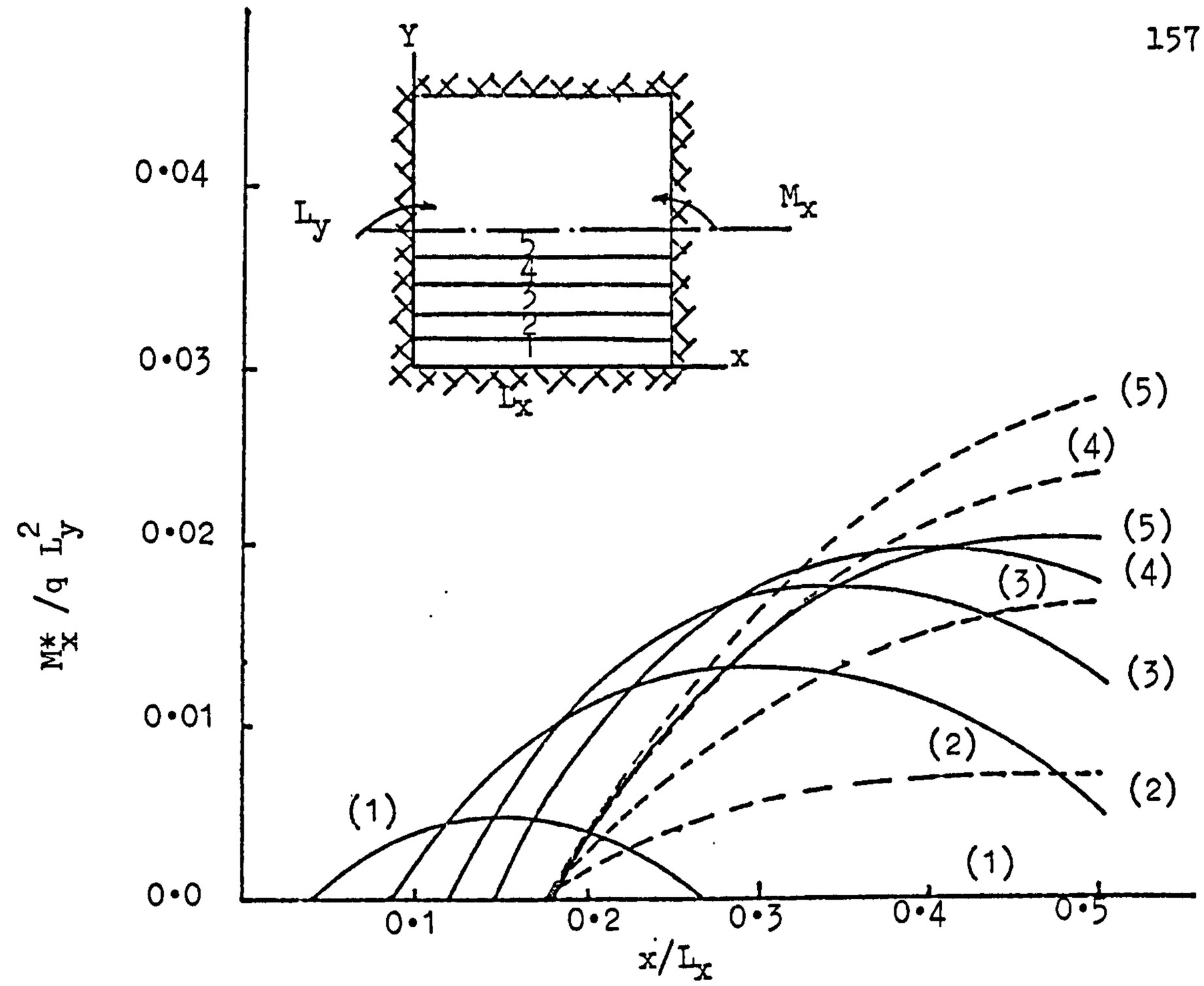

Figure (5.4a) Positive Moment M^*_x $(L_x/L_y = 1{\cdot}0)$

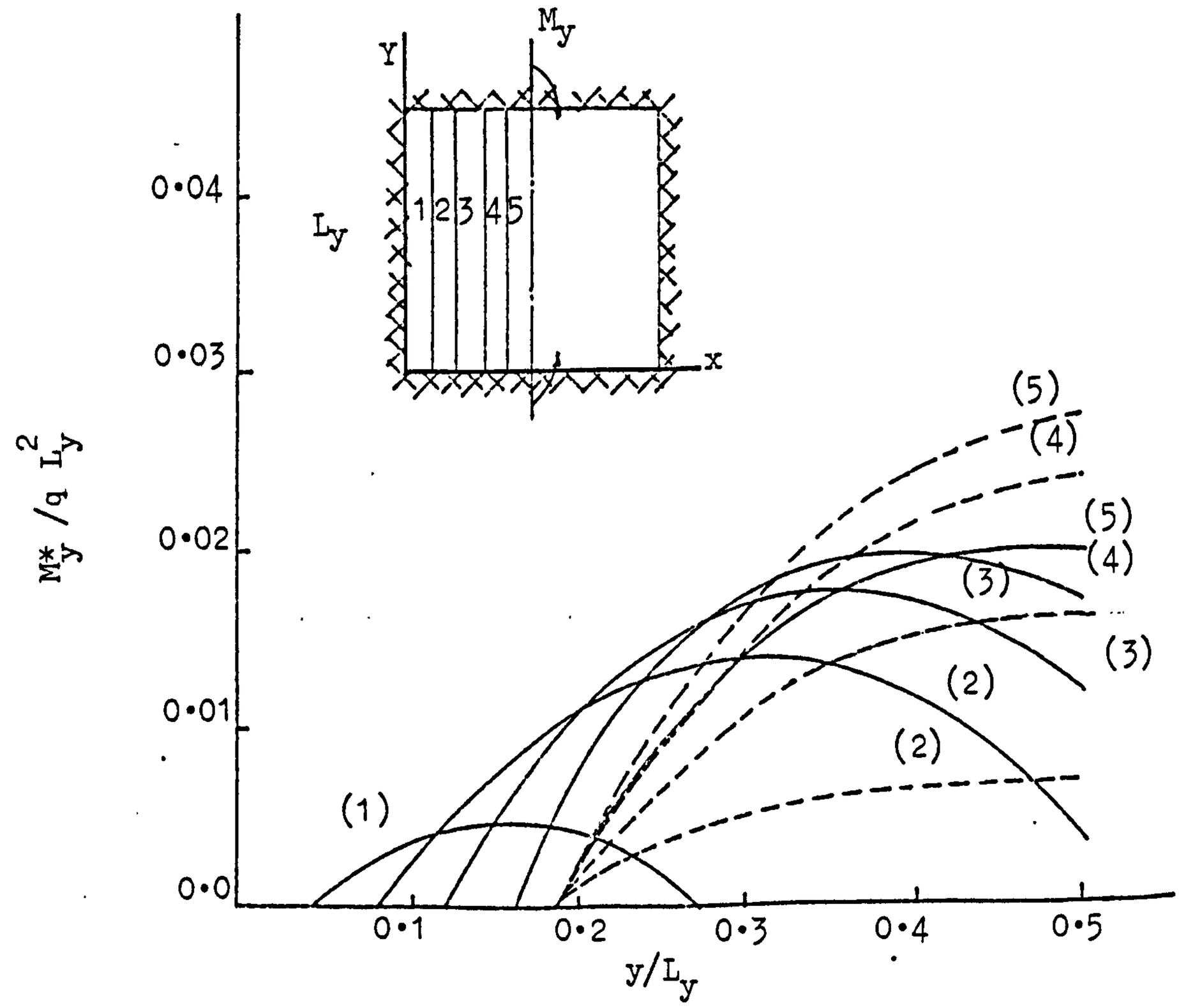

Figure (5.4b) Positive Moment M^*_y $(L_x/L_y = 1{\cdot}0)$

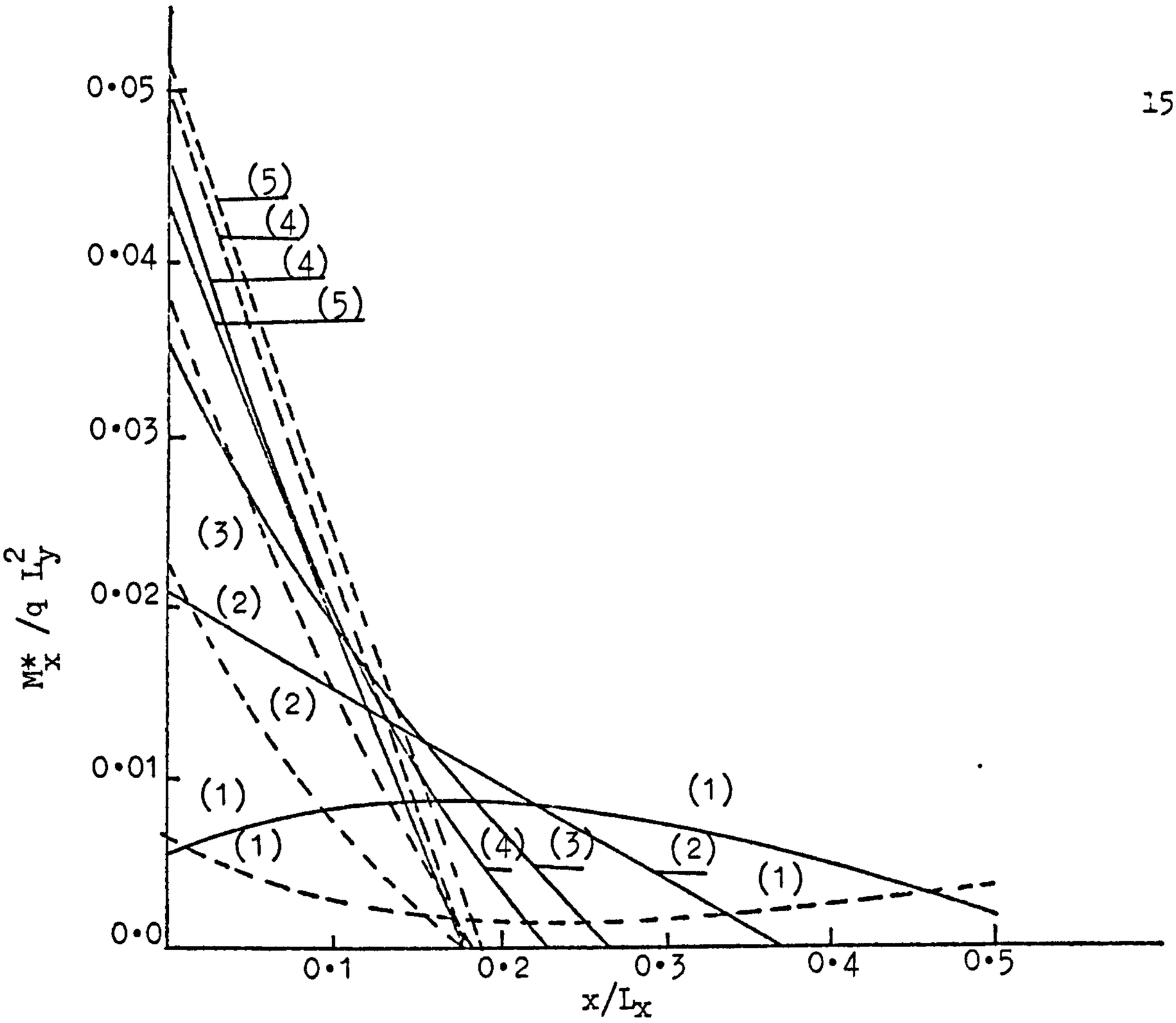

Figure (5.4c) Negative Moment M_x^* (L_x/L_y= 1·0)

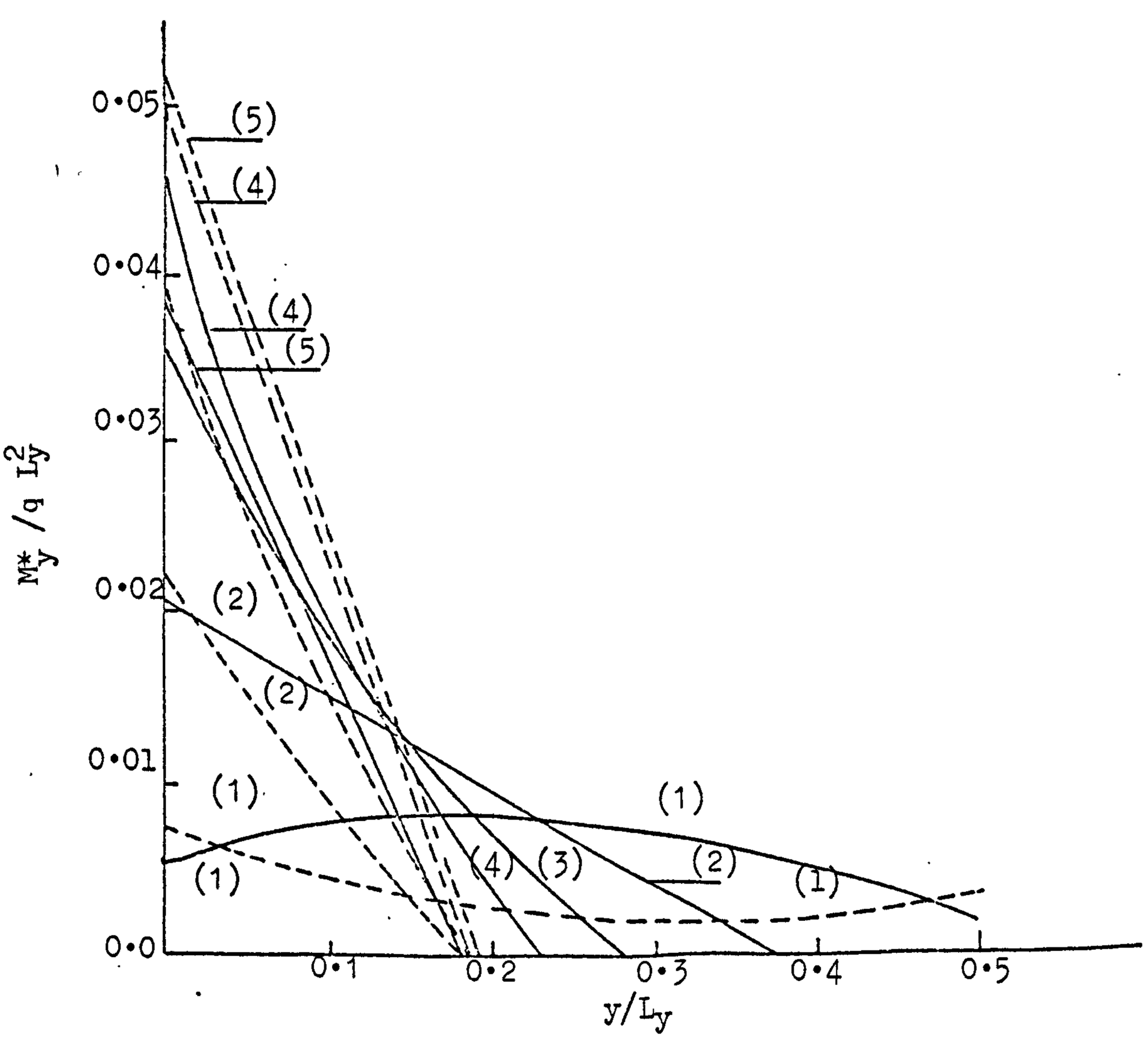

Figure (5.4d) Negative Moment M_y^* (L_x/L_y= 1·0)

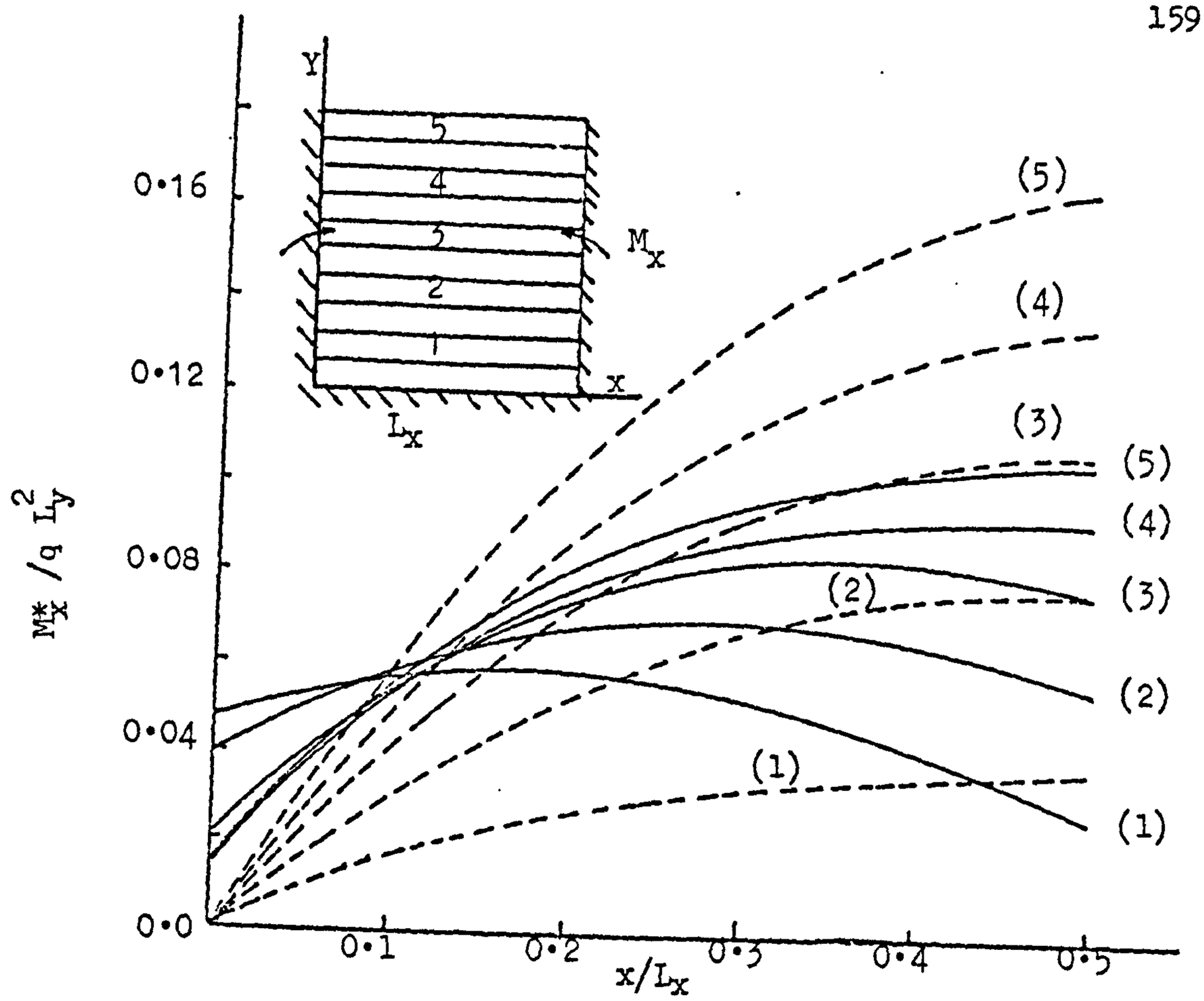

Figure (5.5a) Positive Moment M^*_x (L_x/L_y = 1·0)

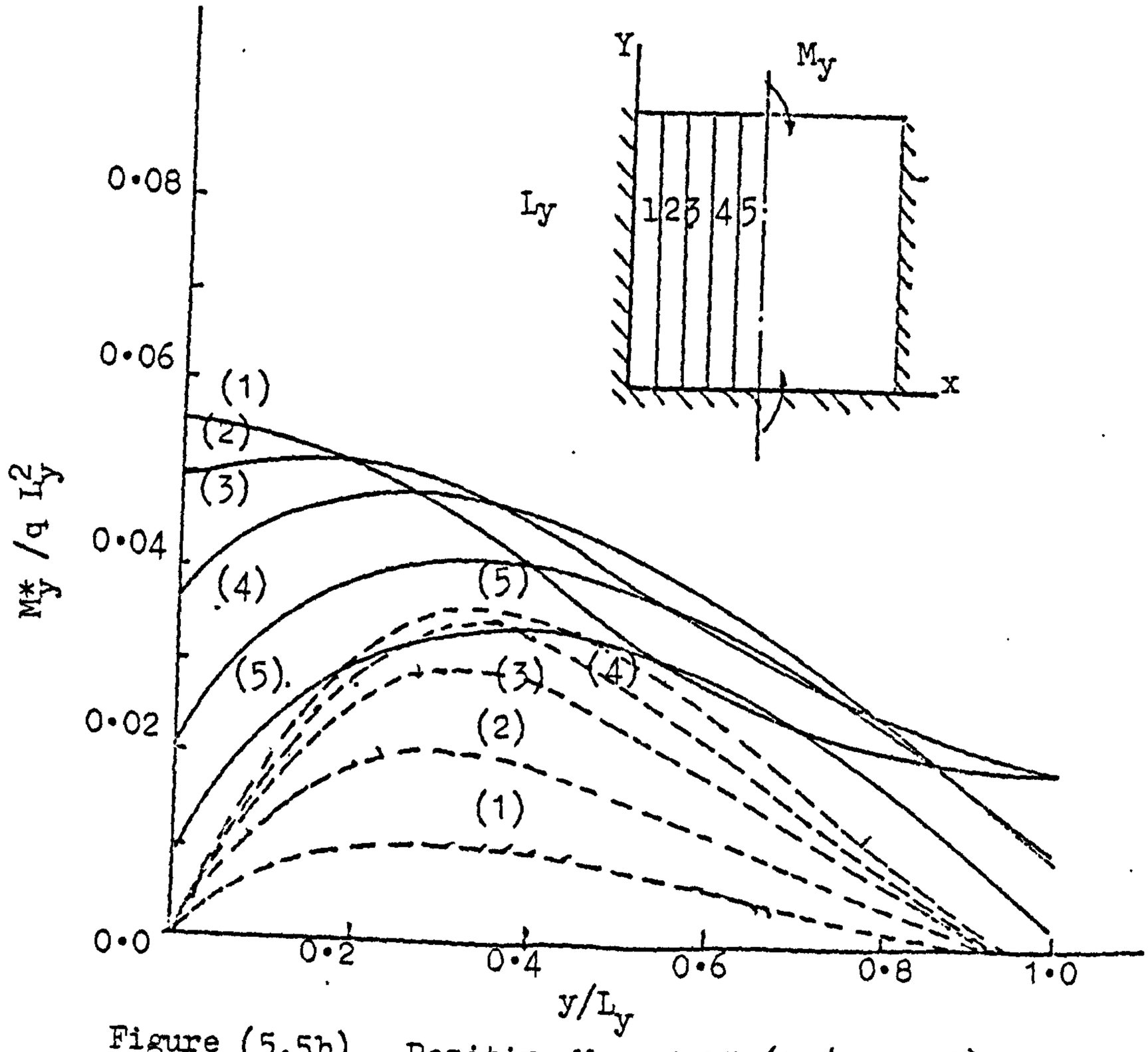

Figure (5.5b) Positive Moment M^*_y (L_x/L_y = 1·0)

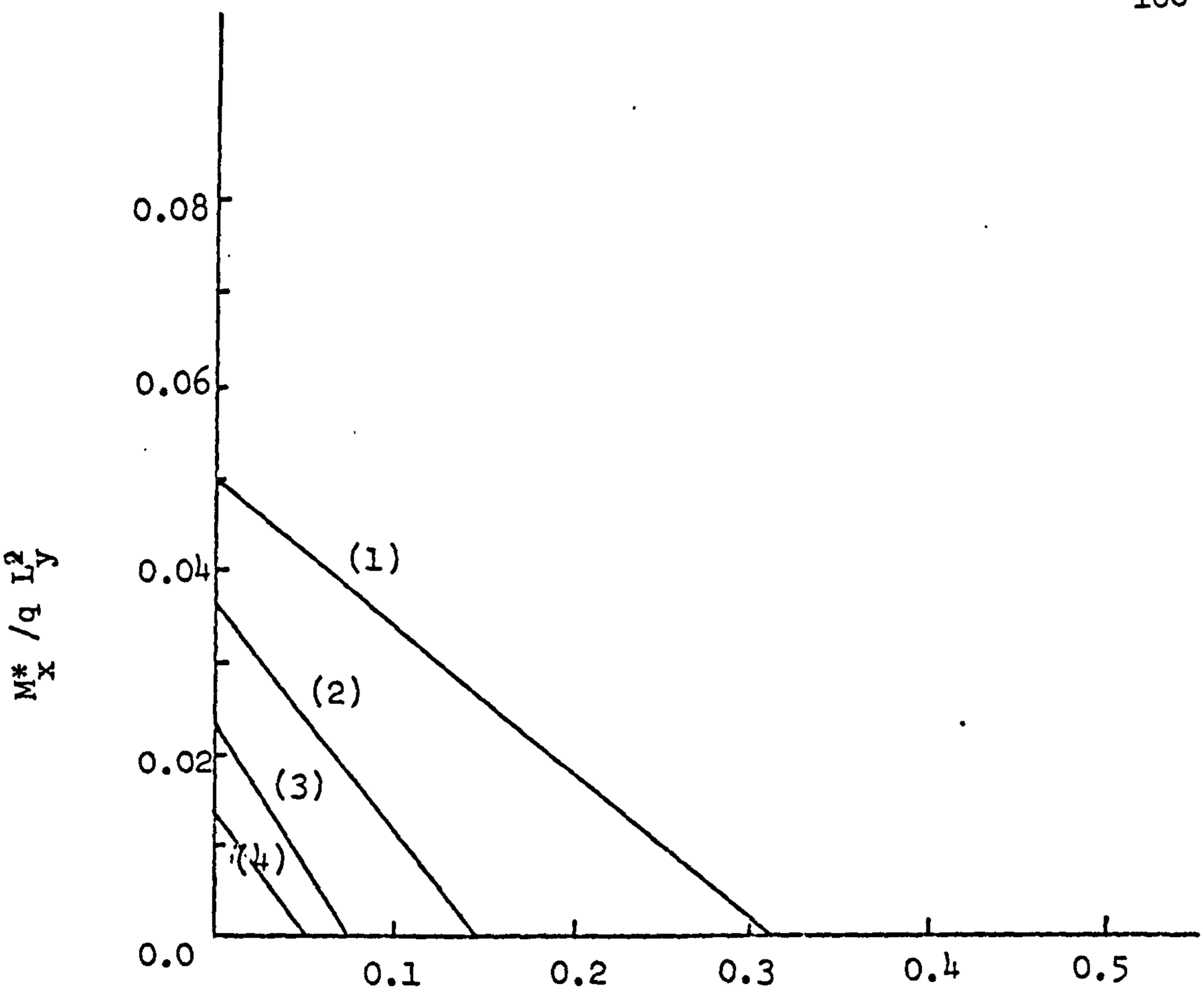

Figure (5.5c) Negative Moment M^*_x (L_x/L_y = 1.0)

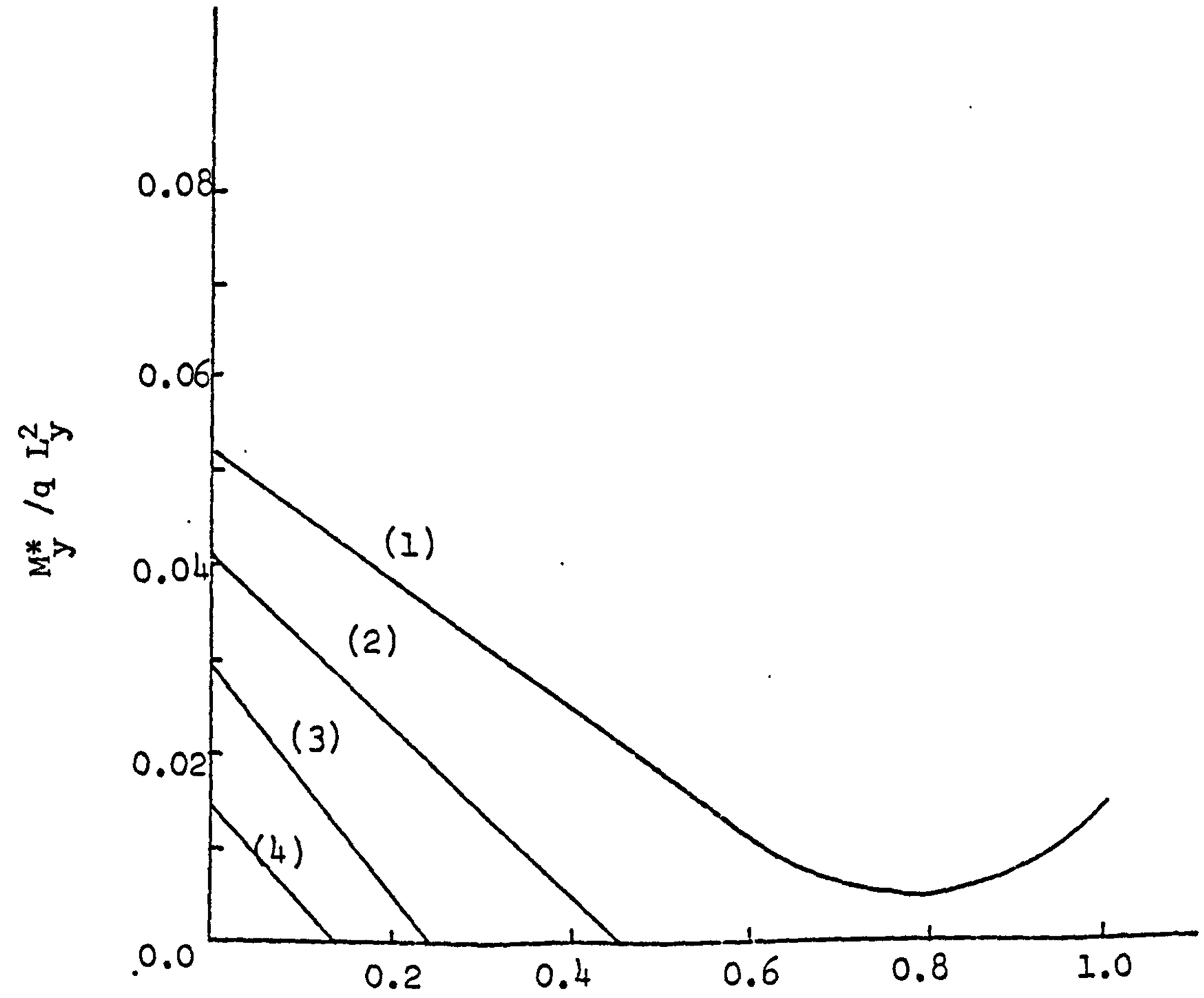

Figure (5.5d) Negative Moment M^*_x (L_x/L_y = 1.0)

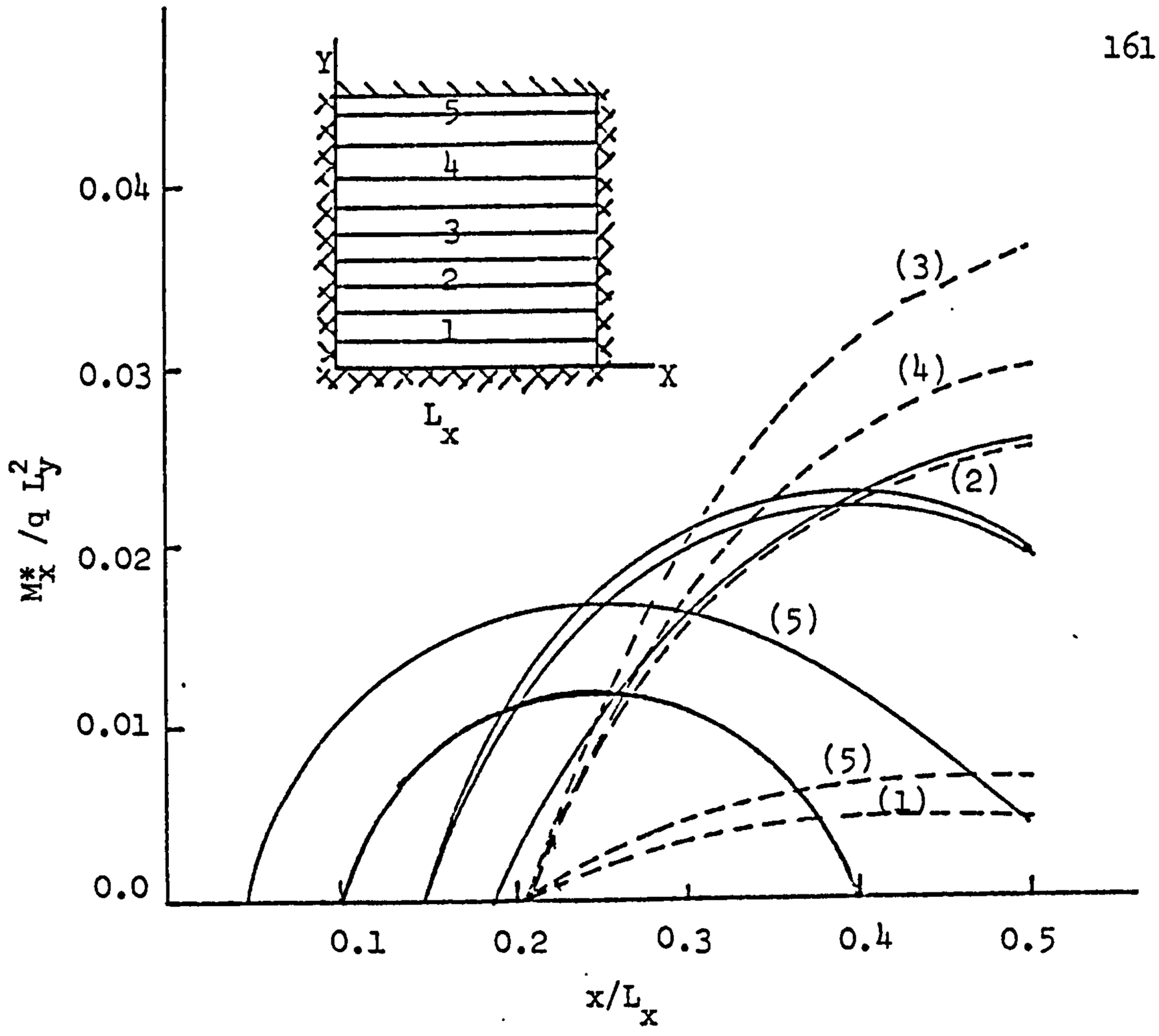

Figure (5.6a) Positive Moment M_x^* $(L_x/L_y = 1.0)$

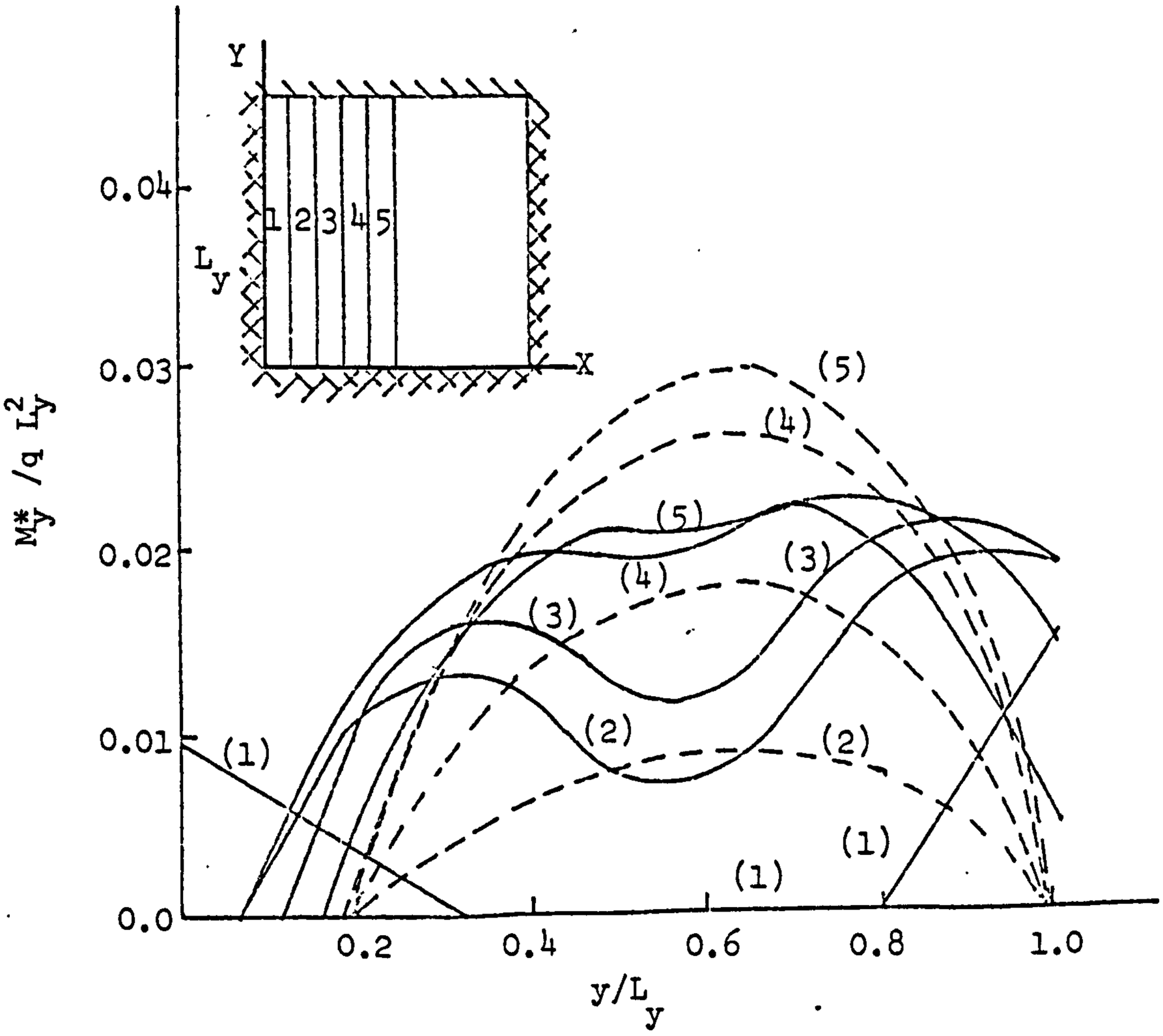

Figure (5.6b) Positive Moment M_y^* $(L_x/L_y = 1.0)$

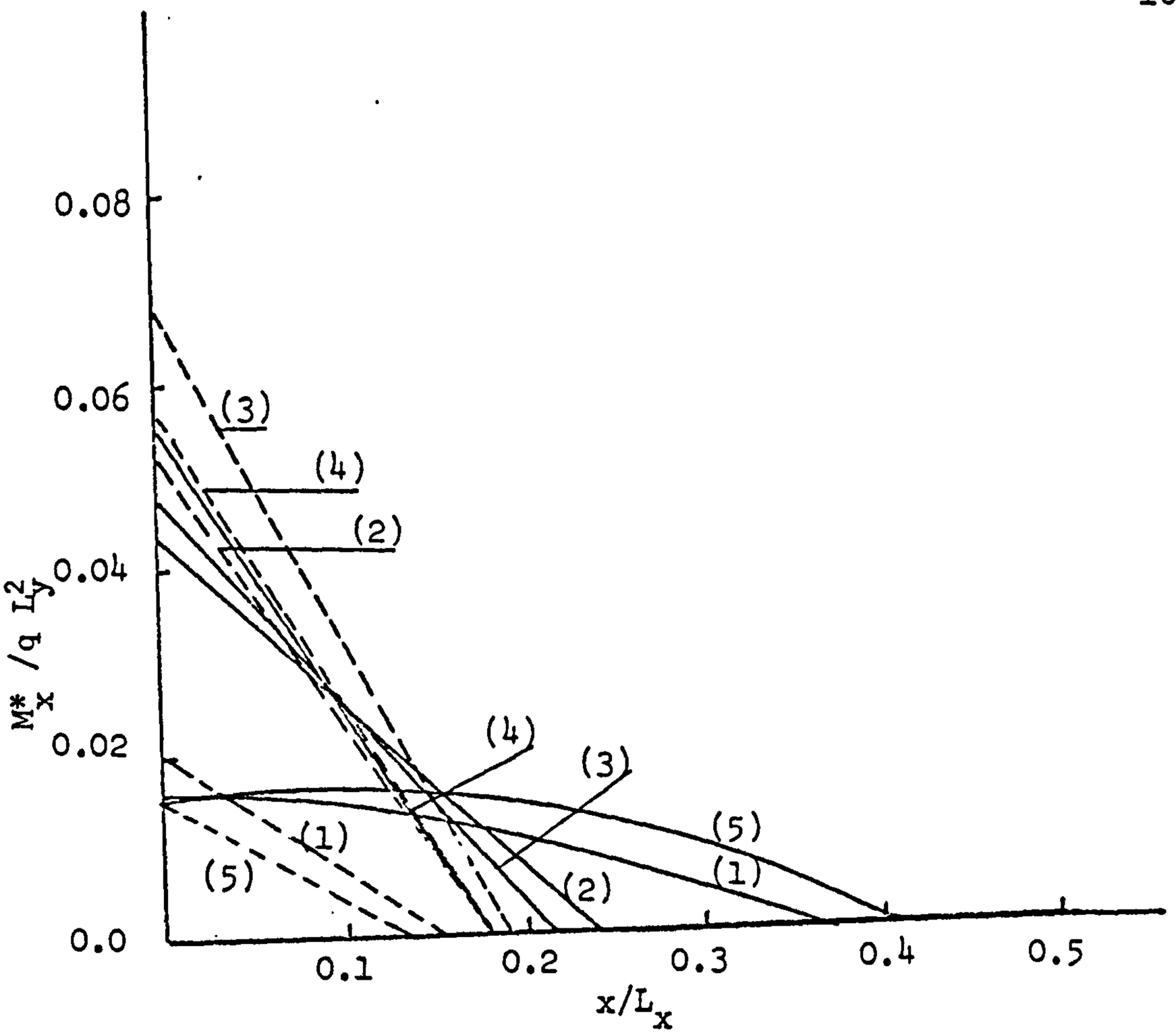

Figure (5.6c) Negative Moment M^*_x (L_x/L_y = 1.0)

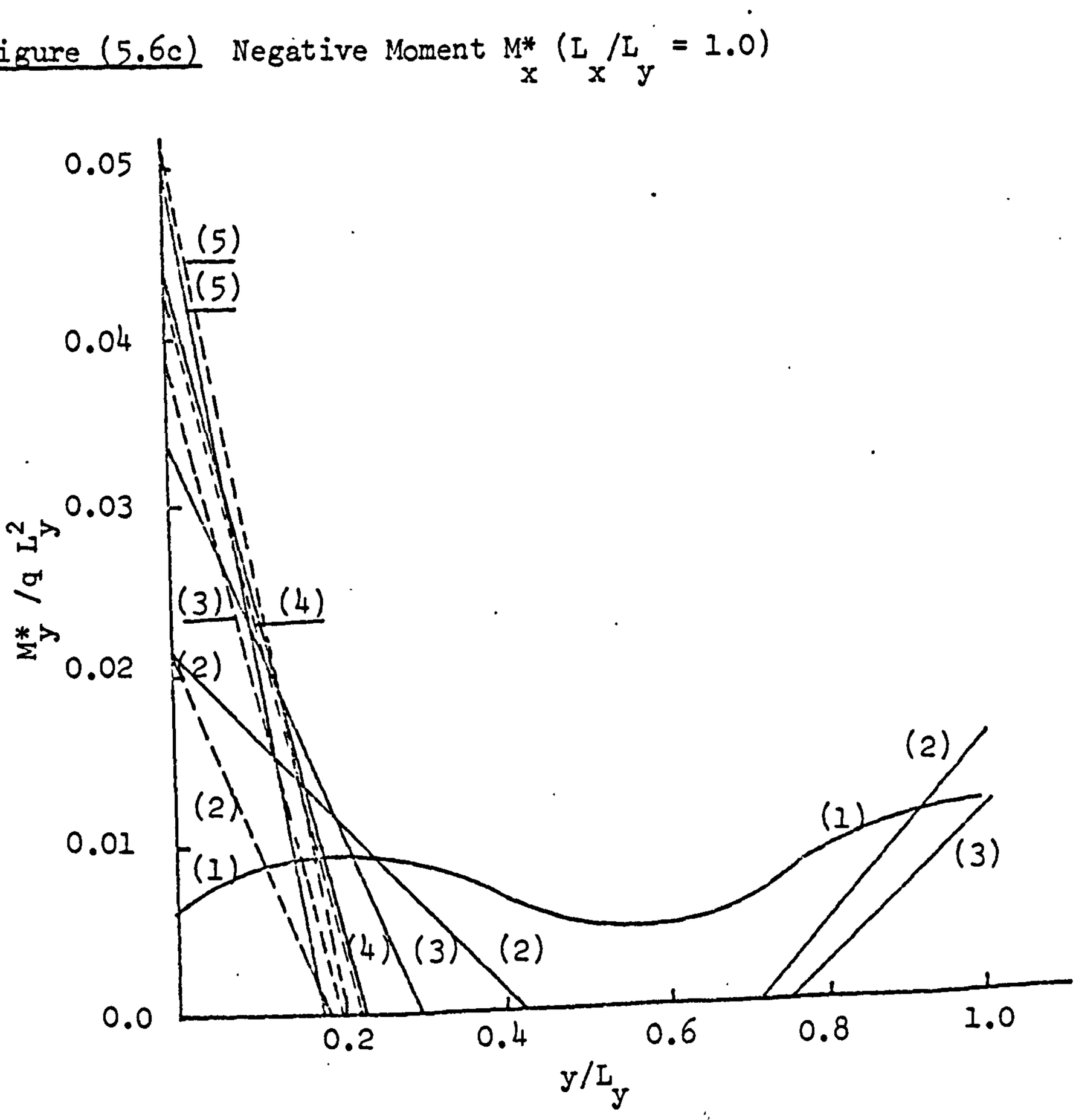

Figure (5.6d) Negative Moment M^*_y (L_x/L_y = 1.0)

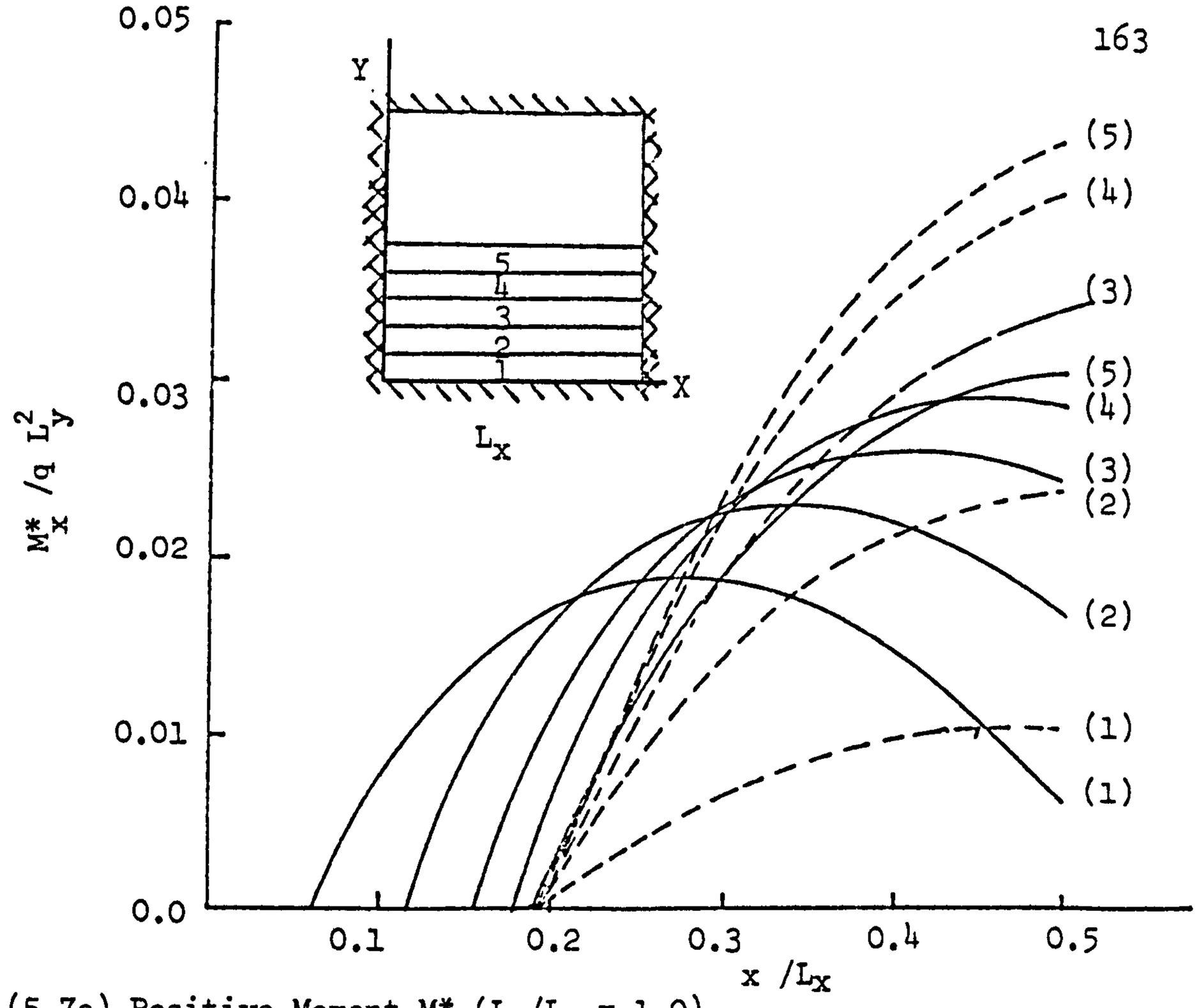

Figure (5.7a) Positive Moment M^*_x $(L_x/L_y = 1.0)$

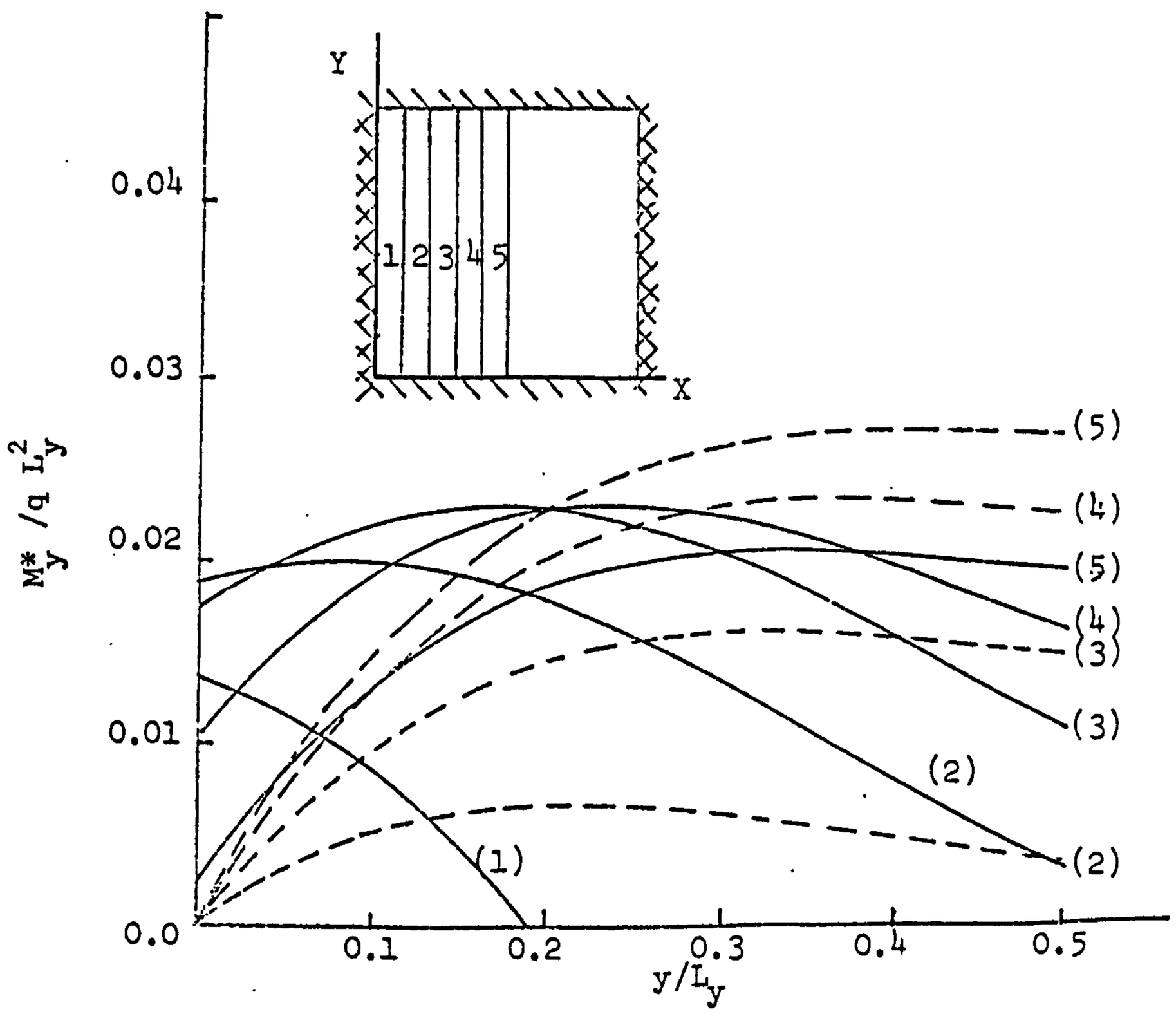

Figure (5.7b) Positive Moment M^*_y $(L_x/L_y = 1.0)$

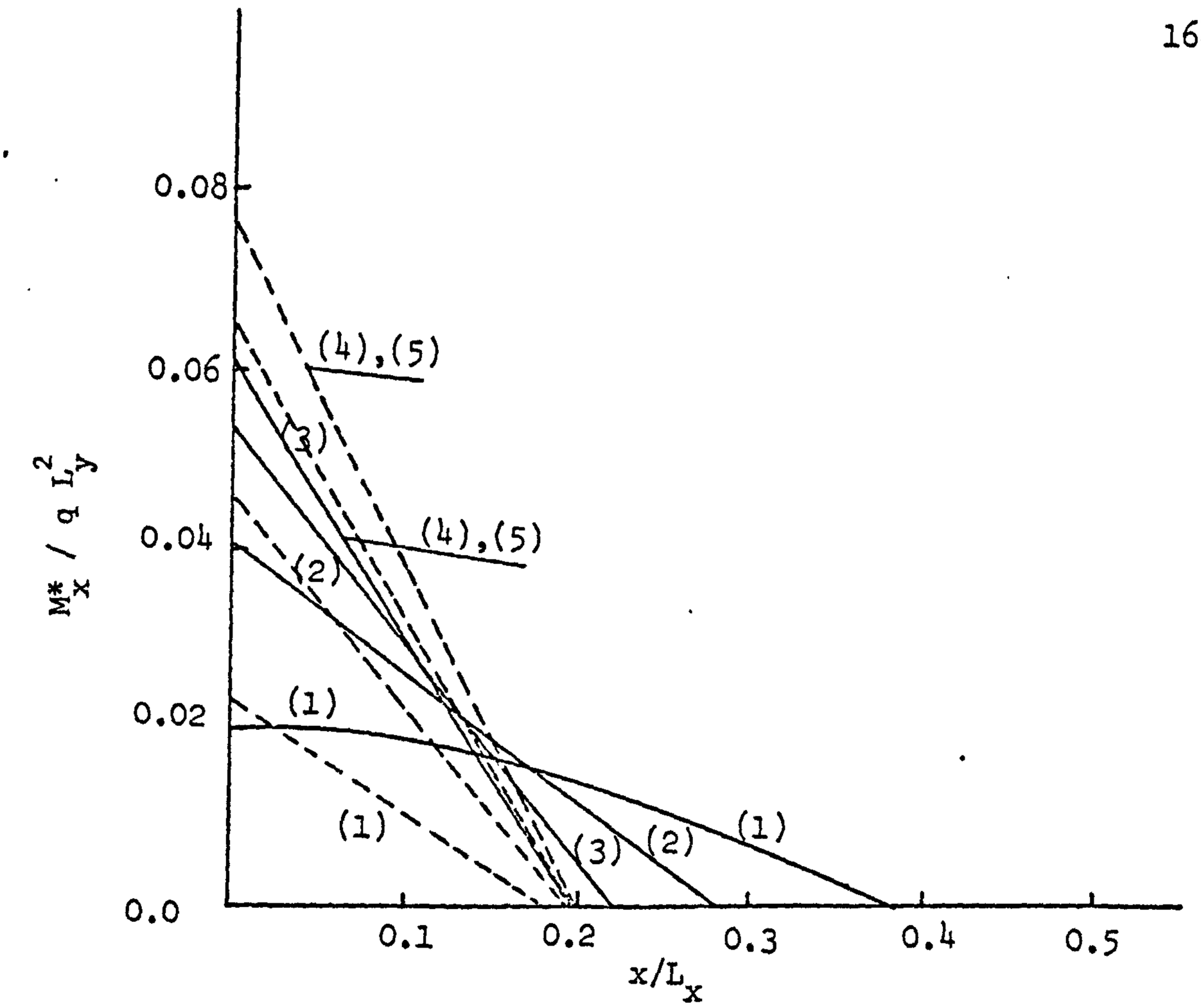

Figure (5.7c) Negative Moment M_x^* $(L_x/L_y = 1.0)$

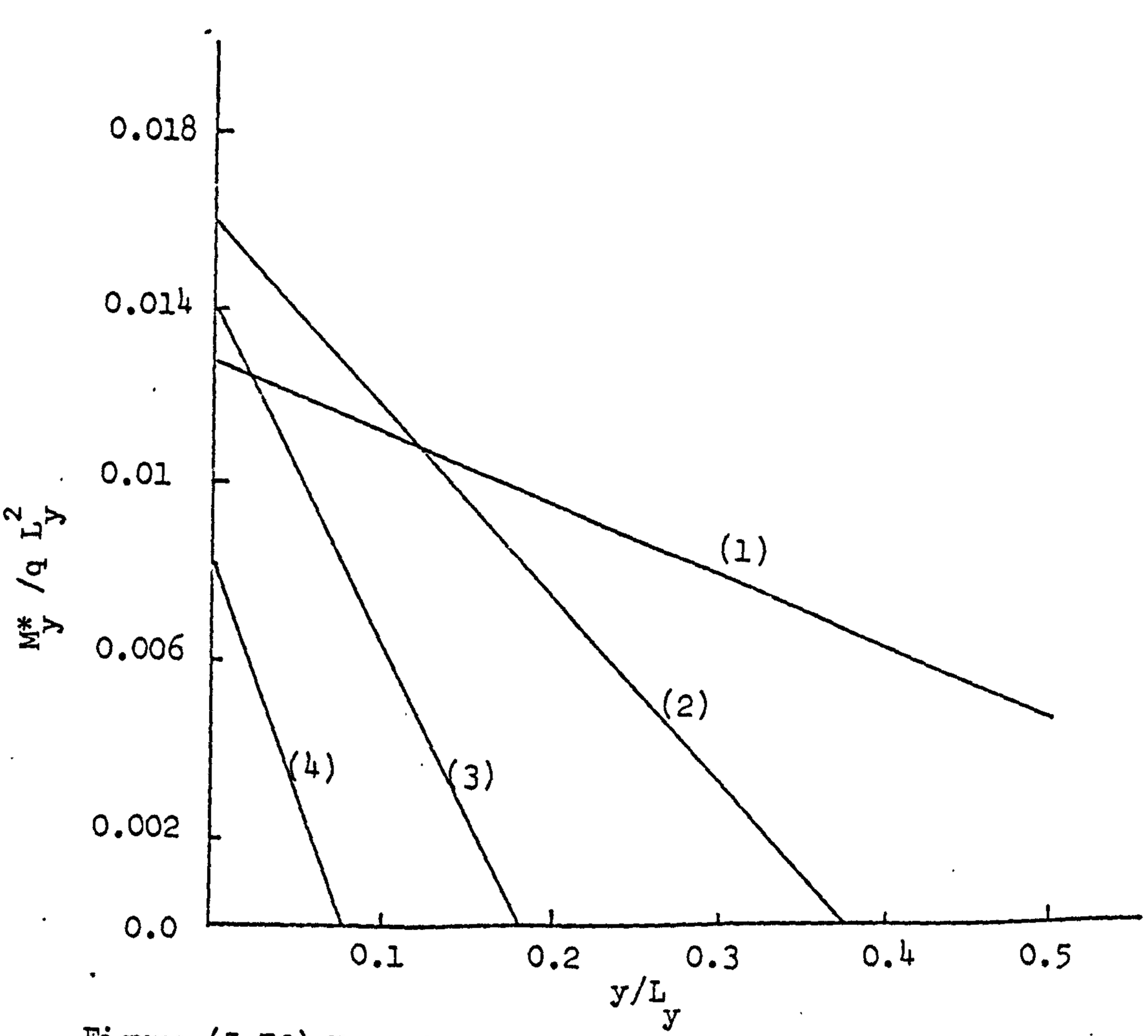

Figure (5.7d) Negative Moment M_y^* $(L_x/L_y = 1.0)$

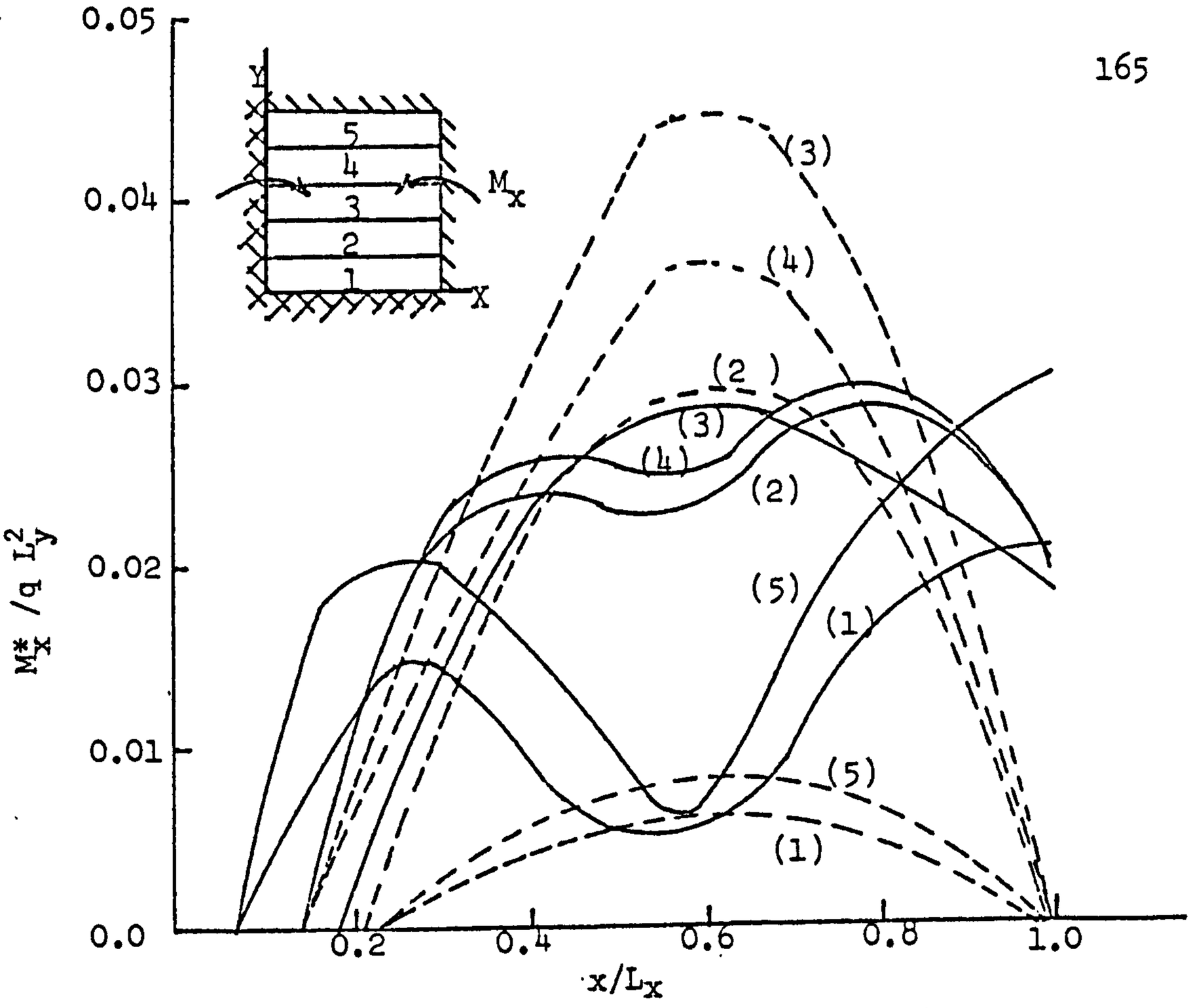

Figure (5.8a) Positive Moment M_x^* (L_x/L_y= 1.0)

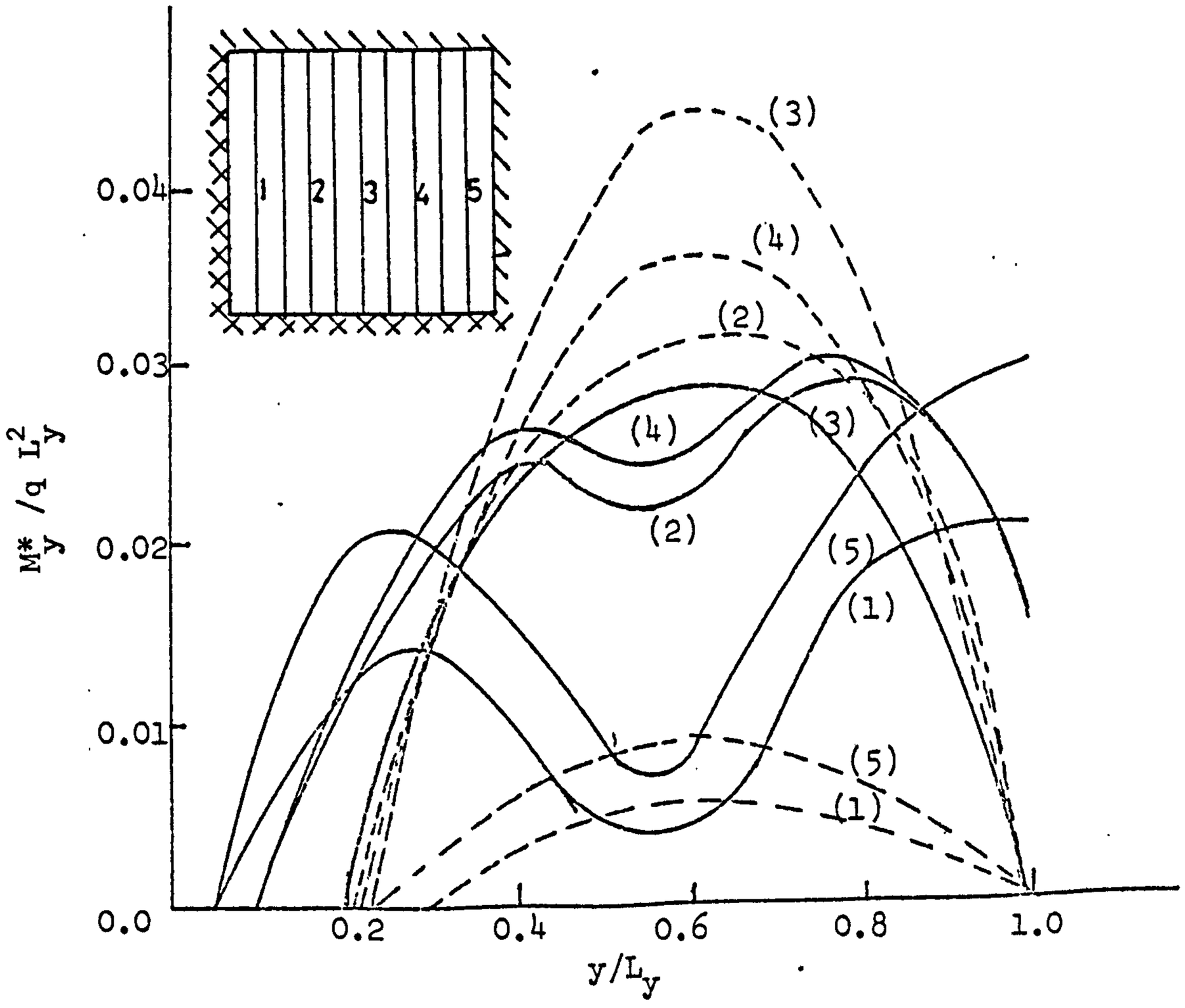

Figure (5.8b) Positive Moment M_y^* (L_x/L_y = 1.0)

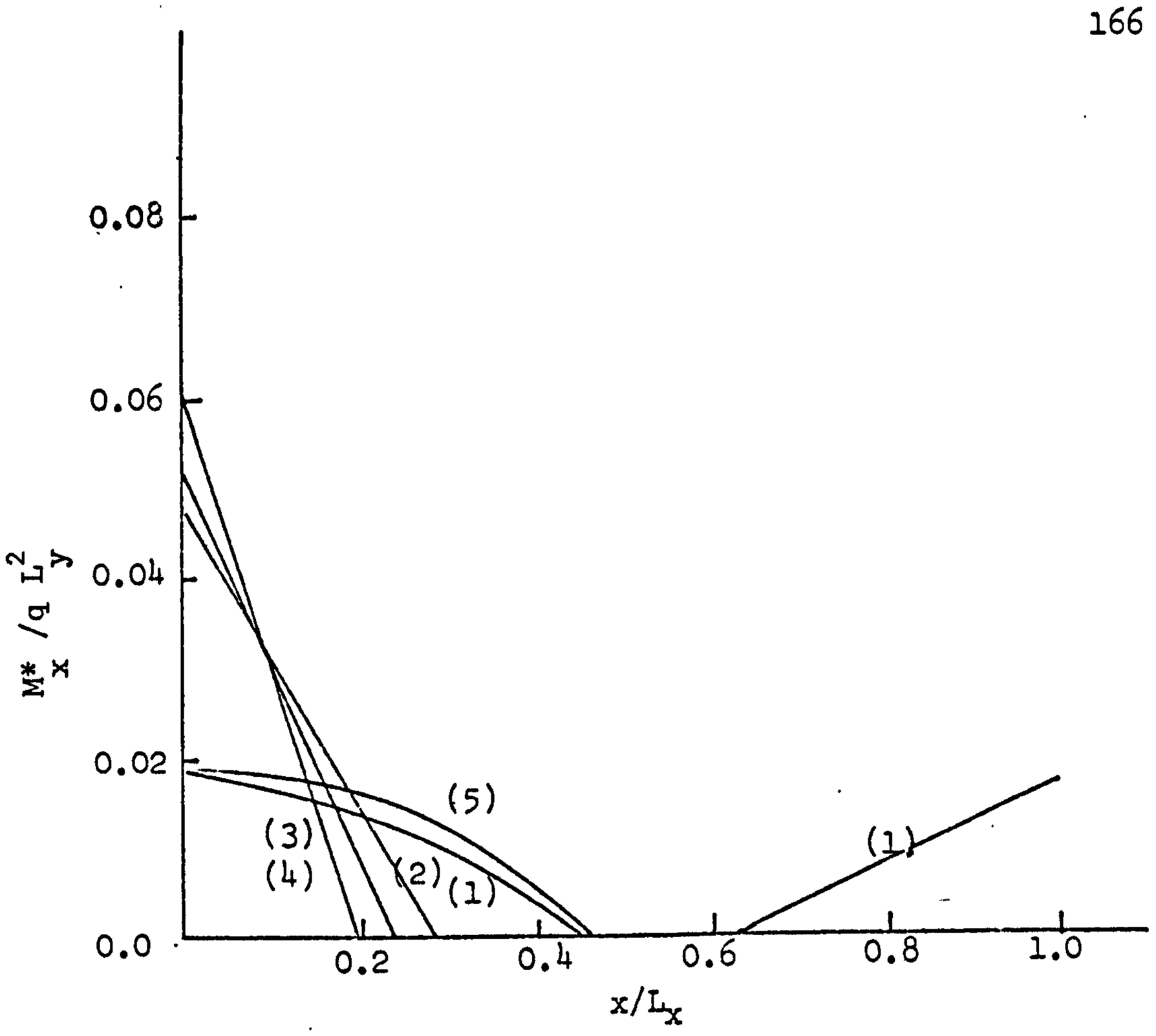

Figure (5.8c) Negative Moment M^*_x (L_x/L_y = 1.0)

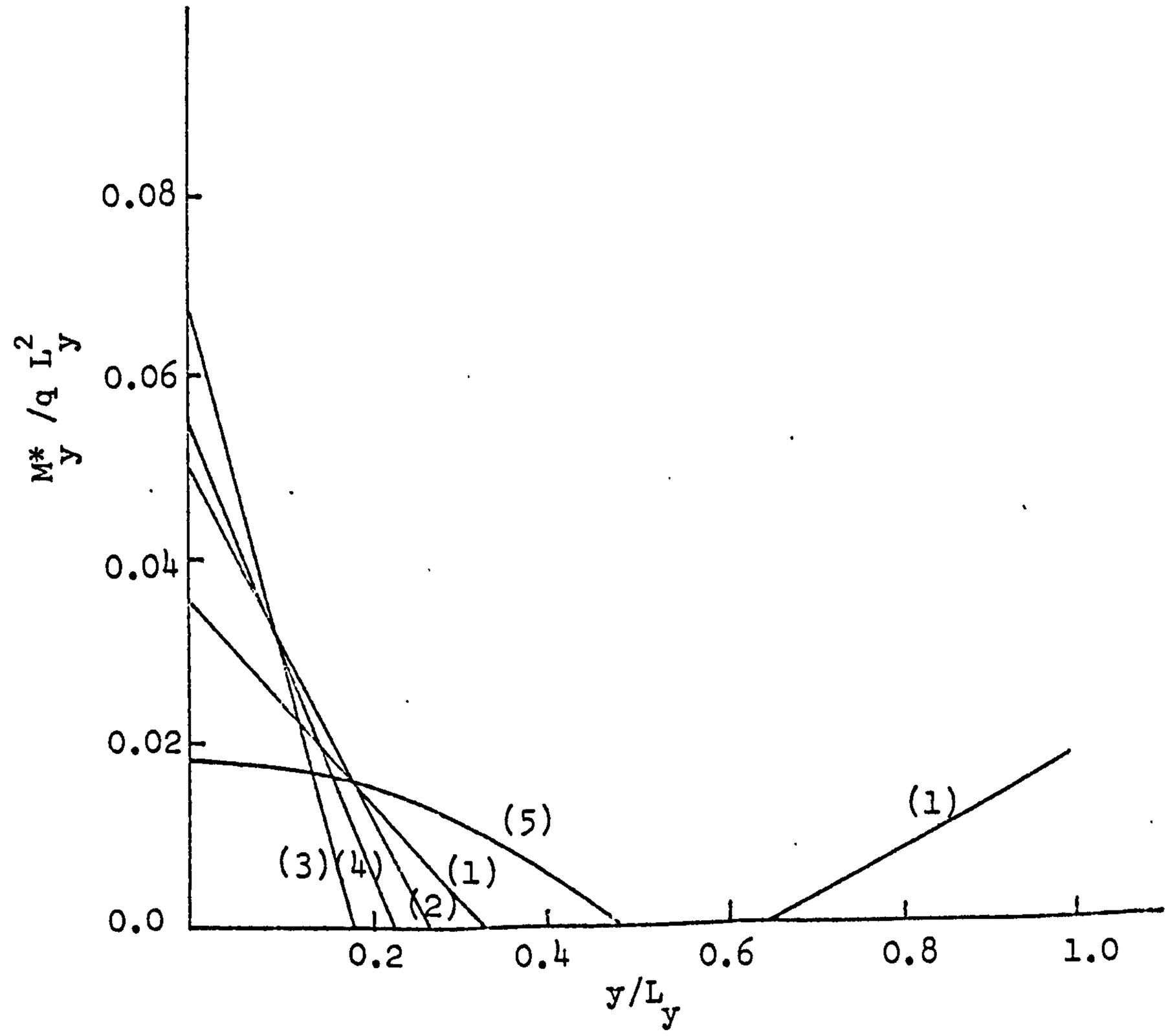

Figure (5.8d) Negative Moment M^*_y (L_x/L_y = 1.0)

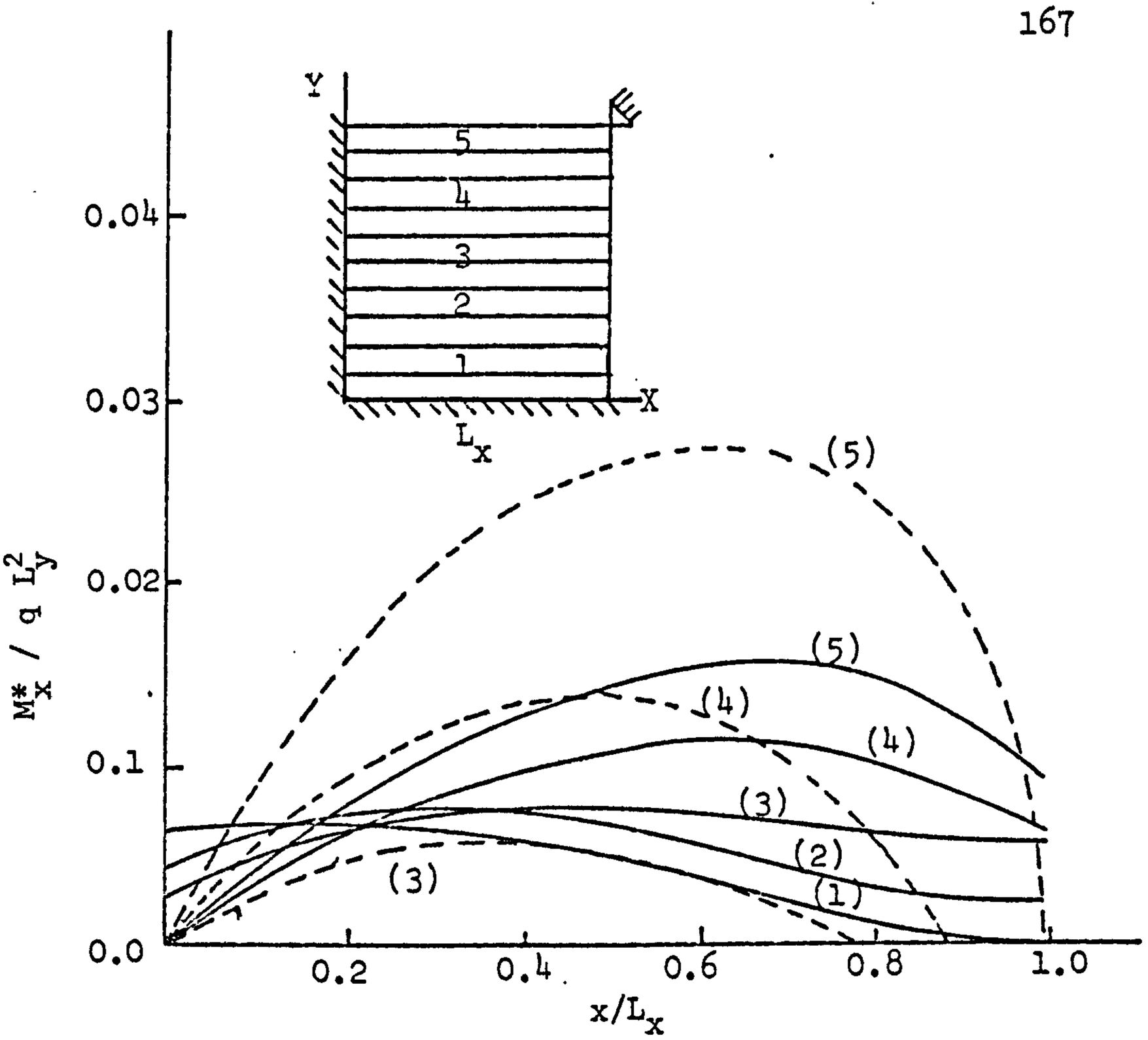

Figure (5.9a) Positive Moment M^*_x (L_x/L_y = 1.0)

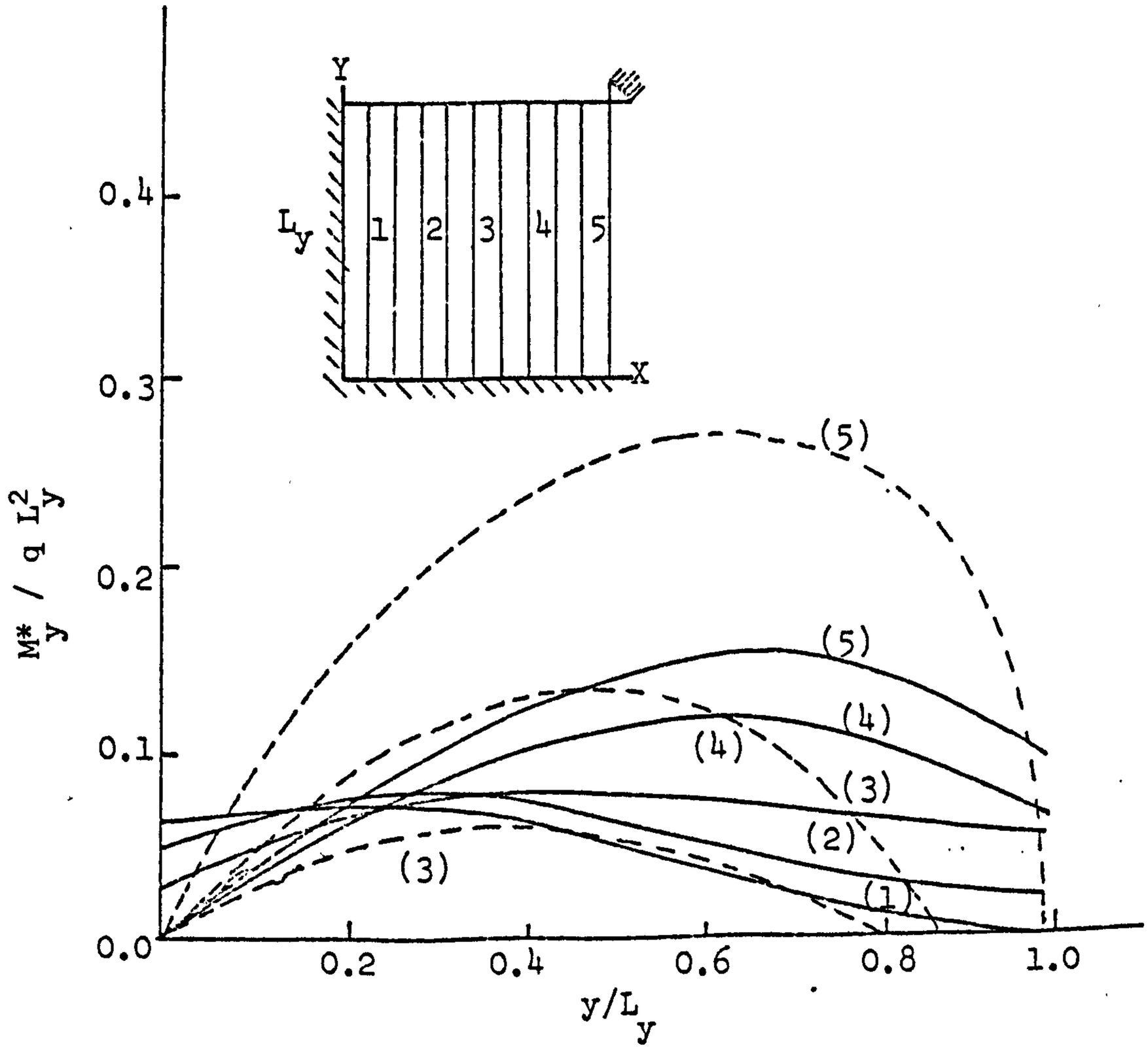

Figure (5.9b) Positive Moment M^*_y (L_x/L_y = 1.0)

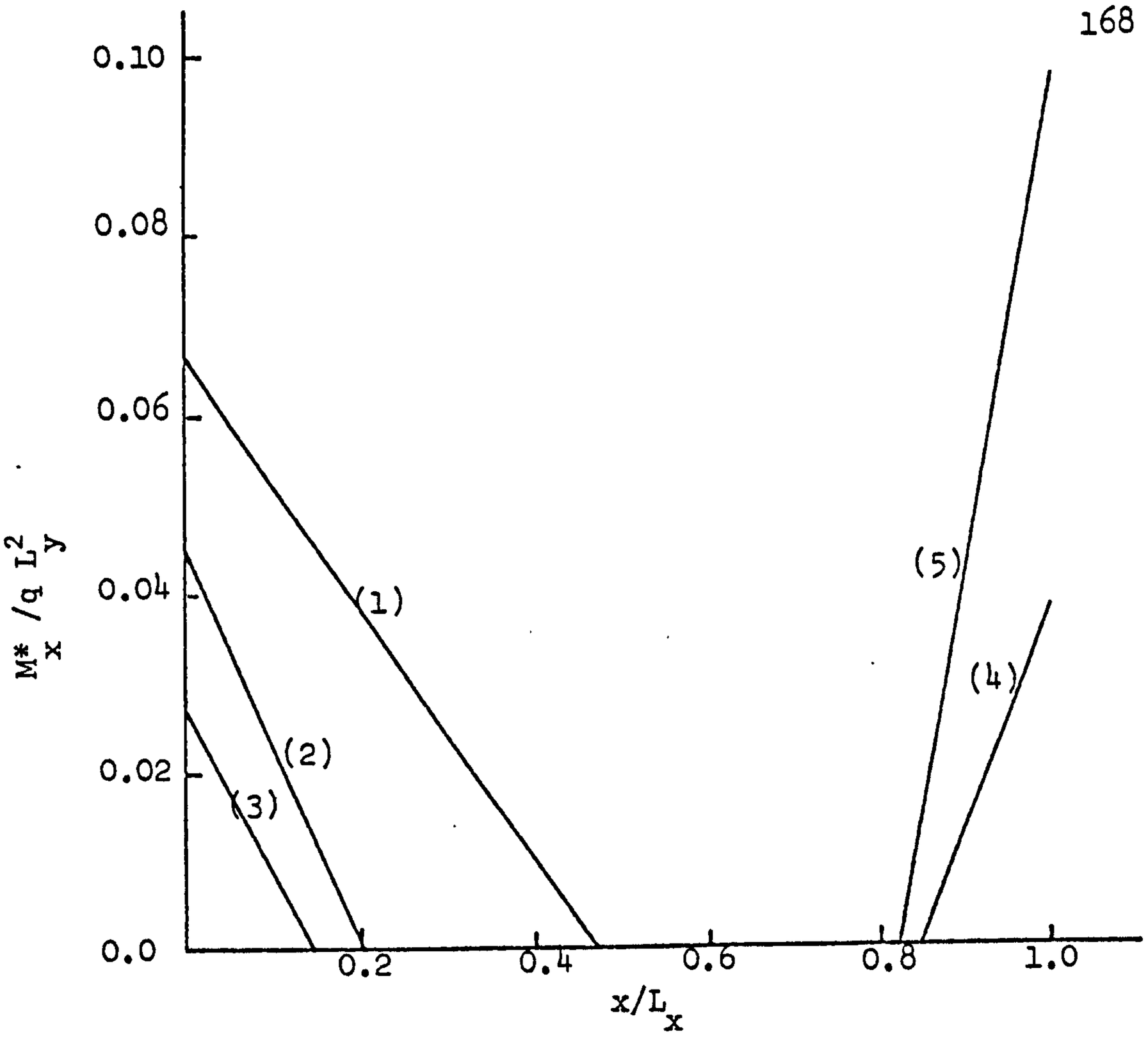

Figure (5.9c) Negative Moment M^*_x (L_x/L_y = 1.0)

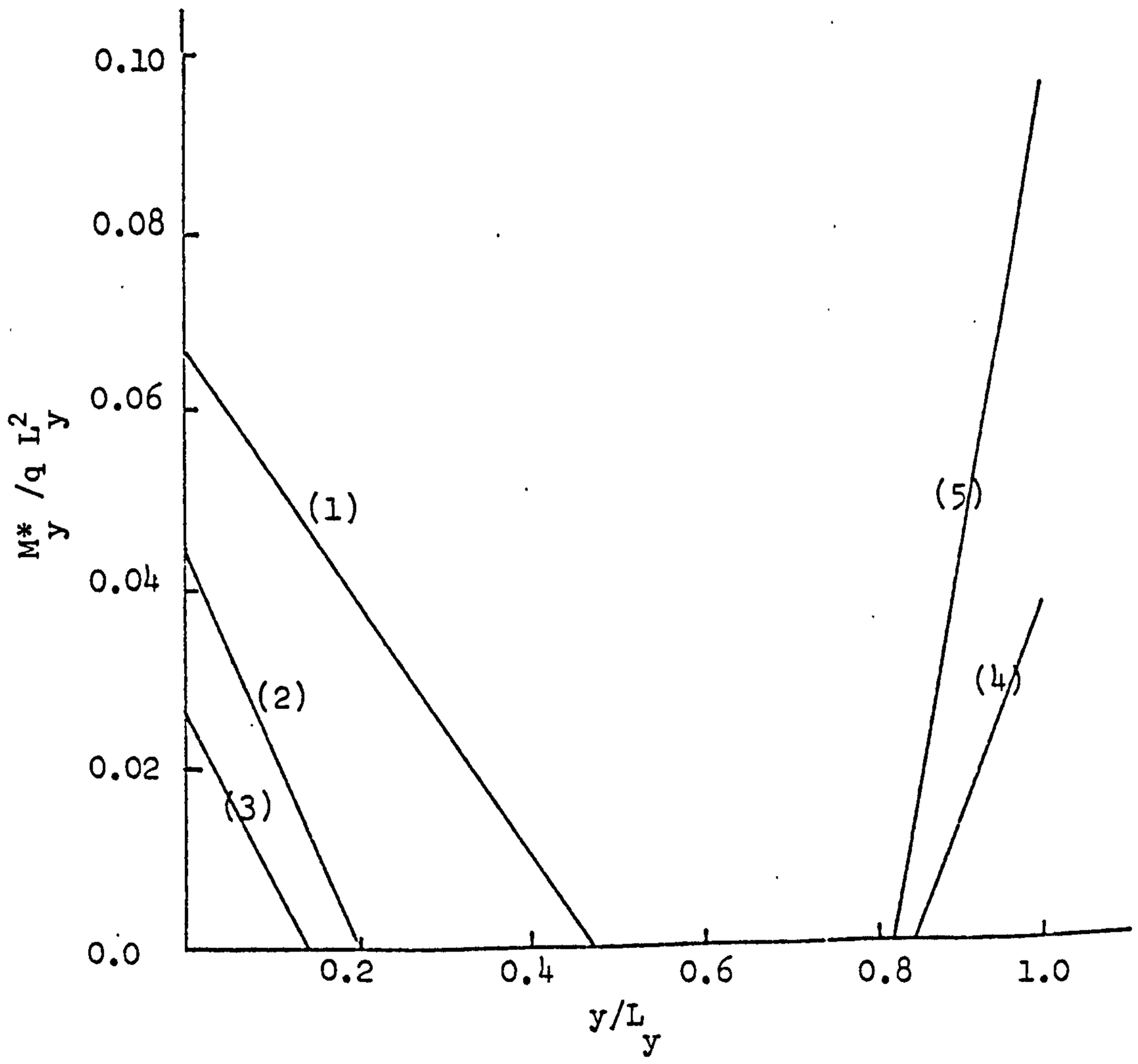

Figure (5.9d) Negative Moment M^*_y (L_x/L_y = 1.0)

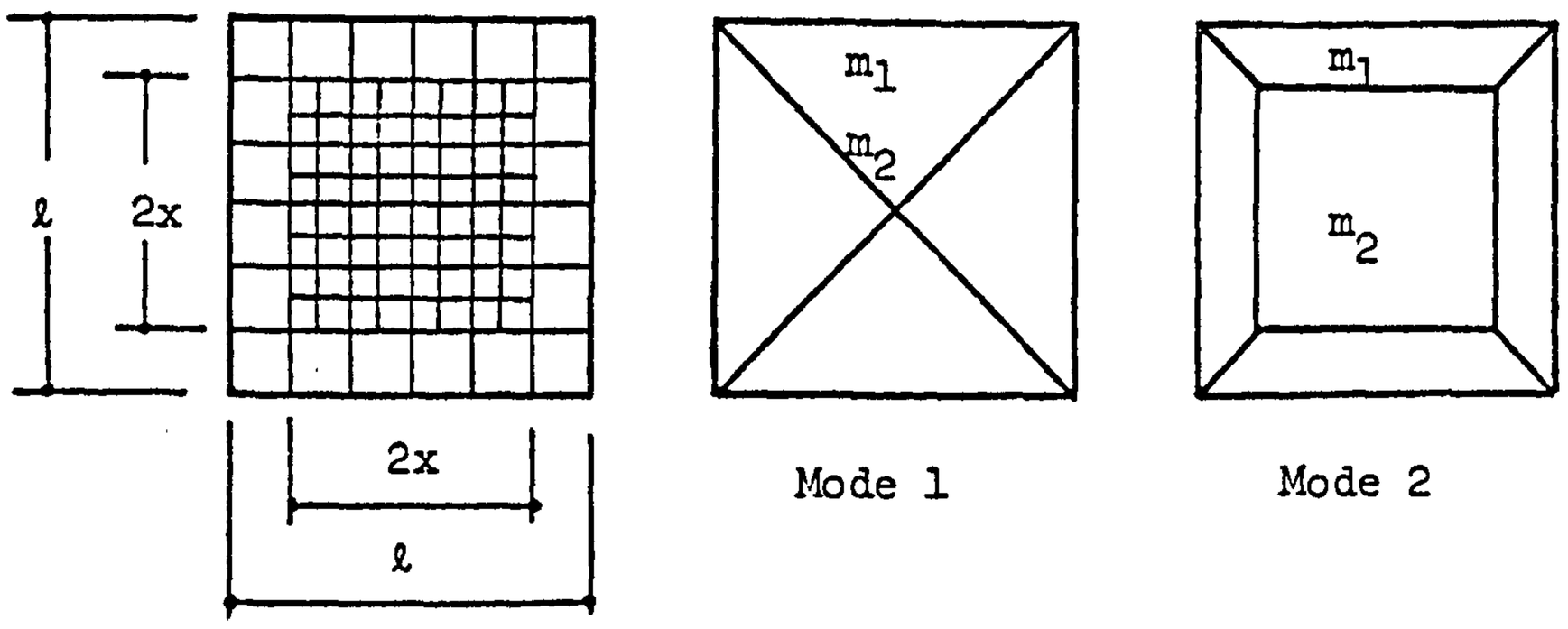

For unit deflection at the intersections of the yield lines.

$$\text{Mode 1}: \quad q\ell^2/3 = 4(m_1(\ell - 2x) + m_2\, 2x) \times \frac{2}{\ell}$$

$$\therefore \quad q = \frac{24}{\ell^2}\left[m_1\left(1 - \frac{2x}{\ell}\right) + 2m_2 x/\ell\ \right]$$

$$\text{Mode 2}: \quad q\left[(\ell - 2x)^2/3 + 4(\ell - 2x)\, x/2 + 4x^2\ \right]$$

$$= 4\, m_1 \frac{2\ell}{(\ell - 2x)}$$

$$\therefore \quad q = \frac{24 m_1}{\ell^2(1 - 8(x/\ell)^3)}$$

For a given x, the minimum moment volume is when the ultimate loads from the two modes are the same.

$$V = 2\ (m_1(\ell^2 - 4x^2) + m_2\ (2x)^2)$$

and for minimum volume

$$\frac{dv}{dx} = 0$$

This will give, $x = 0.375$ and,

$$V = 0.0746\ q\ \ell^4, m_1 = 0.0241\ q\ell^2, m_2 = 0.0475\ q\ell^2$$

Figure (5.12) Optimum Minimum Weight Solution for a Square Simply Supported Slab.

5.3 NUMERICAL EXPERIMENTS:

5.3.1 General.

A series of computer experiments, using the layered finite element program were conducted on a number of rectangular slabs. The slabs were all designed by the proposed direct design method, except two, which were intended for comparison with the direct design method. The object of these numerical experiments is to study the service and ultimate behaviour of the slabs designed by this method.

The proposed method uses the initial uncracked stiffnesses in the elastic analysis under the ultimate load. However, it is not likely that the resulting elastic stress distributions would actually occur in the slab under ultimate conditions, for the following two reasons:

(a) Owing to the progressive cracking as the load increases, the slab stiffnesses gradually deteriorate.

(b) The yield criterion adopted in the design is, after all an approximation to the exact yield criterion.

Accordingly, redistribution of stresses is bound to occur, though, it is anticipated here that this would be minimum. Although it is believed that the strength of under-reinforced sections is dependant on the steel provided, there is no guarantee that the behaviour under service loads will be satisfactory. The latter is more dependant on the stiffness of the cracked sections and the extent of cracking. Accordingly, such numerical experiments are justified.

The variables in the study are as follows:

(a) Boundary Conditions.

(b) Sides ratios.

(c) Materials properties.

The slabs in this study can be divided into five series as follows:

Test Series 1:- includes ten slabs simply supported on all sides.

Test Series 2:- includes five slabs simply supported on three sides, with one edge free.

Test Series 3:- includes five slabs simply supported along two adjacent edges, while the opposite corner is resting on a column.

Test Series 4:- includes three slabs supported by edge beams all around.

Test Series 5:- includes two slabs simply supported on three sides, free on the fourth. This test series is intended to provide a comparison between the proposed direct design approach and the simple strip method.

In each of the first three series, slabs with sides ratios between 1.0 and 2.0 were examined.

5.3.2 Designation of Slabs tested:

All test slabs were designed to carry uniform loads only. In each run, the slab was first designed for a specified ultimate load using the direct design approach. All safety factors on the design load and the materials were taken as unity, the slab was then analysed under an incremental load till failure. This would constitute a full computer experiment. The computer experiments were given the serial names NUMEX 1, NUMEX 2... etc., and Tables (5.3)to (5.7)

describe the type of each problem in each numerical experiment.

5.3.3 Proportioning and Loading.

In the slabs in Series 1 to 3, one dimension was chosen to be 2000 mm, while the other dimension, (always along the X-axis) was varied for each run. The slab depth in each case was taken as span/20. The definition of the term "span" used in calculating the depth depends on the boundary conditions of the problem. For slabs supported along four edges, the span length was taken as the length of the short side of the slab. For other cases involving free edges, the span length was taken as the length of the longer free edge.

An arbitrary design load was chosen, and an elastic analysis for the slab under the design load was obtained from the finite element program. The output from such an analysis would normally include the elastic deflections and the moment distribution under the chosen load. The design moments derived using the design equations of Chapter (3) in this research, were also obtained from the program. Since the initial uncracked stiffnesses were used in the analysis, these elastic deflections cannot be used directly as an indication of the deflections under service loads. Due to crack penetration through the depth of the slab, the flexural rigidity would be greatly reduced. In the present research, an effective moment of inertia was used to predict the deflections under the service load, using the Branson's[93] method. The assumptions and the derivation of the necessary equations are given in Appendix (E). Using the elastic deflections under the ultimate load, δ_e, the predicted maximum deflection under the service load is given by

$$\delta_p = \frac{\delta_e}{LF} \times \frac{I_g}{I_{eff}} \qquad (5.3)$$

where

δ_p = predicted maximum deflection under service load

δ_e = maximum elastic deflection under ultimate design load

LF = Load factor ($\doteq$ 1.5)

I_g = gross moment of inertia of the section

I_{eff} = Effective moment of inertia of the section.

In this study, the limiting service deflection δ_L was taken as the span/250. Accordingly, the predicted deflection was limited to that value, in choosing the suitable depth of the slab, or the design ultimate load.

5.3.4 Analysis:

For each experiment, the deformational behaviour resulting from various changes in slab material due to progressive cracking and yielding under increasing load, has been traced using the nonlinear finite element program, described in the previous chapter. For slabs having supports symmetry about their two orthogonal centre lines, only one quadrant was analysed using a 4 x 4 subdivisions. In cases with one axis of symmetry, half the slab was analysed using a mesh of 6 x 6 elements. The unsymmetrical cases in test series 3 were analysed using 8 x 8 elements over the whole slab. For the slab-beam systems in series 4, a mesh of 5 x 5 elements over a symmetric quadrant was used.

For all tested models, the slab thickness was divided into six concrete layers, plus two to four steel layers, as might be required by the reinforcement design according to the elastic analysis. The elastic analysis was done by using six concrete layers with no steel.

All experiments were assigned the following materials properties, except test series 4:-

Concrete compressive strength, f_{cu} = 20 N/mm^2

Concrete tensile strength, f_t = 1.5 N/mm^2

Young's modulus for concrete, E_c = 14000 N/mm^2

Poisson ratio for concrete, ν = 0.15

Yield strength of steel, f_{st} = 300 N/mm^2

Young's modulus for steel, E_s = 210000 N/mm^2

Experiments NUMEX 3,6 to 10 were designed to study the effect of varying materials properties on the behaviour of the slab. The slab tested in this series was simply supported with L_x/L_y = 1.50, and subject to a uniform load of 33.3 KN/mm^2 . The concrete strengths considered were 20, 25, 30, 35, 40 N/mm^2 with $f_t = 0.075\ f_{cu}$. NUMEX 10 was assigned f_{cu} = 20 N/mm^2, but f_{st} = 410 N/mm^2. In each test, a load increment size of 0.1 P_{cr} (the cracking load of the slab) was the maximum value used, for all slabs. 15 iterations were used in most cases (except in the slab-beam systems, where 30 were used), with 2 x 2 sampling points in each element. The displacement and force norms (see Section 4.3.5) used to limit the iterations were 1 x 10^{-4} and 0.01 respectively, (except the slab-beam systems, for which the force norm was taken as 0.05).

In every test, the following aspects of structural behaviour have been investigated:-

(1) Deflections: short term deflections under increasing load till failure. For simplicity, only the point of maximum deflection will be considered.

(2) Redistribution of internal stresses: The redistribution of bending moments in the reinforcement directions due to material nonlinearity will be considered.

(3) Cracking and yielding of steel: A quantitative measure of cracks is not feasible by the present model, since the model employs a smeared crack approach. But, since crack widths can be related to steel strains, the latter can be used as a measure of the crack widths, and accordingly will be investigated in this study.

(4) Failure loads: Although the use of the proposed design philosophy is expected to yield lower bounds on collapse loads, load enhancements due to strain hardening and membrane forces are also possible. The analysis will then try to study these effects.

5.4 RESULTS, DISCUSSIONS AND CONCLUSIONS:

5.4.1 Test Series 1.

This series includes tests on slabs which are simply supported along all edges, and can be divided into two subseries.

1. Subseries 1A: and includes the test runs NUMEX 1 to 5, and were aimed to study the behaviour of simply supported slabs with various sides ratios.
2. Subseries 1B: and includes the test runs NUMEX 3,6,7,8,9,10 which were made on a rectangular simply supported slab with sides ratio = 1.5, under a uniform load of 33.3 KN/m^2. The tests were aimed to study the effect of various materials properties on the response.

Results of both subseries are shown in Figures (5.13) to (5.18). For convenience, a summary of the results is given in Table (5.3) and Table (5.4), respectively.

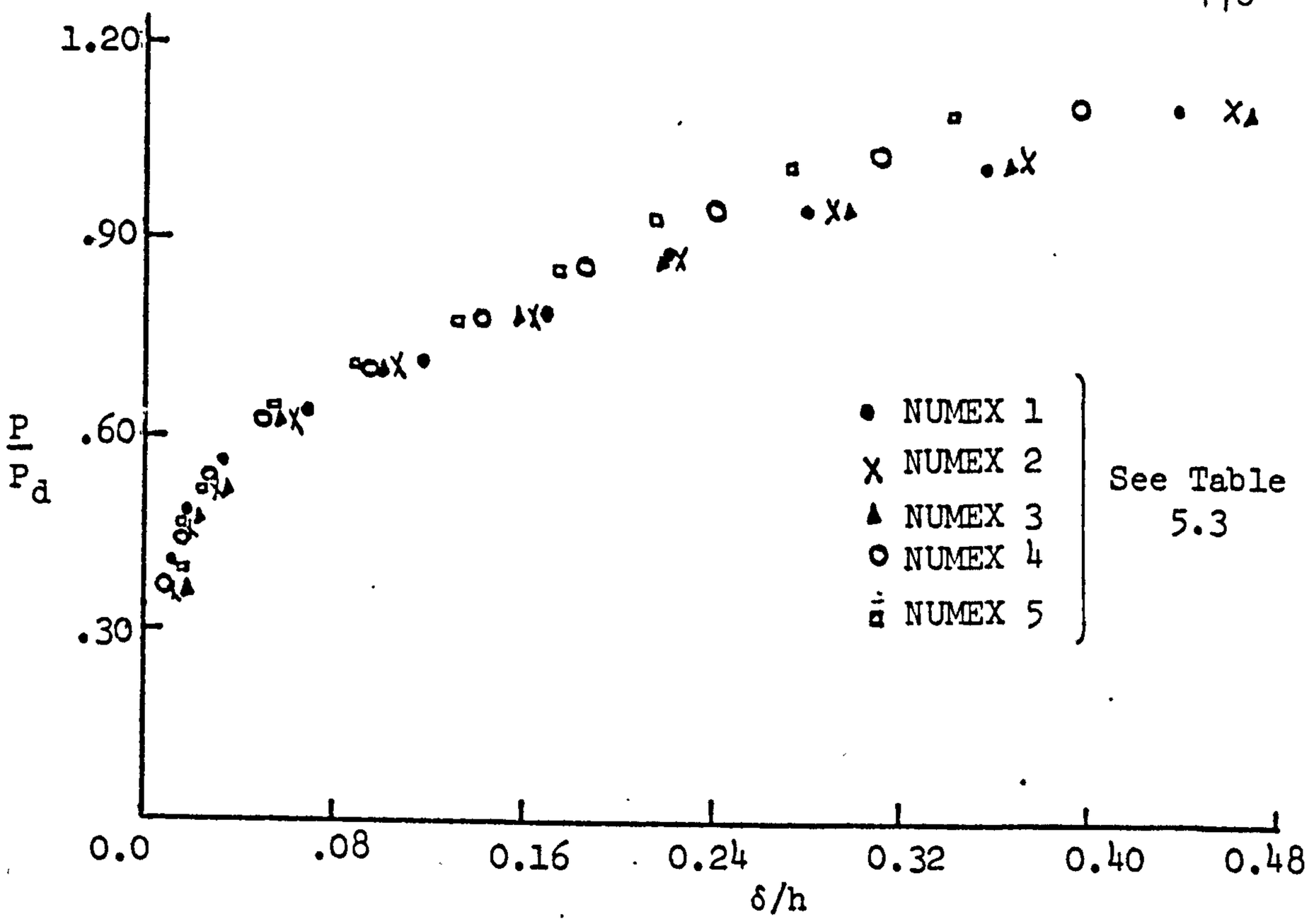

Figure (5.13) Load-Deflection Curves for the Slabs in Series 1A

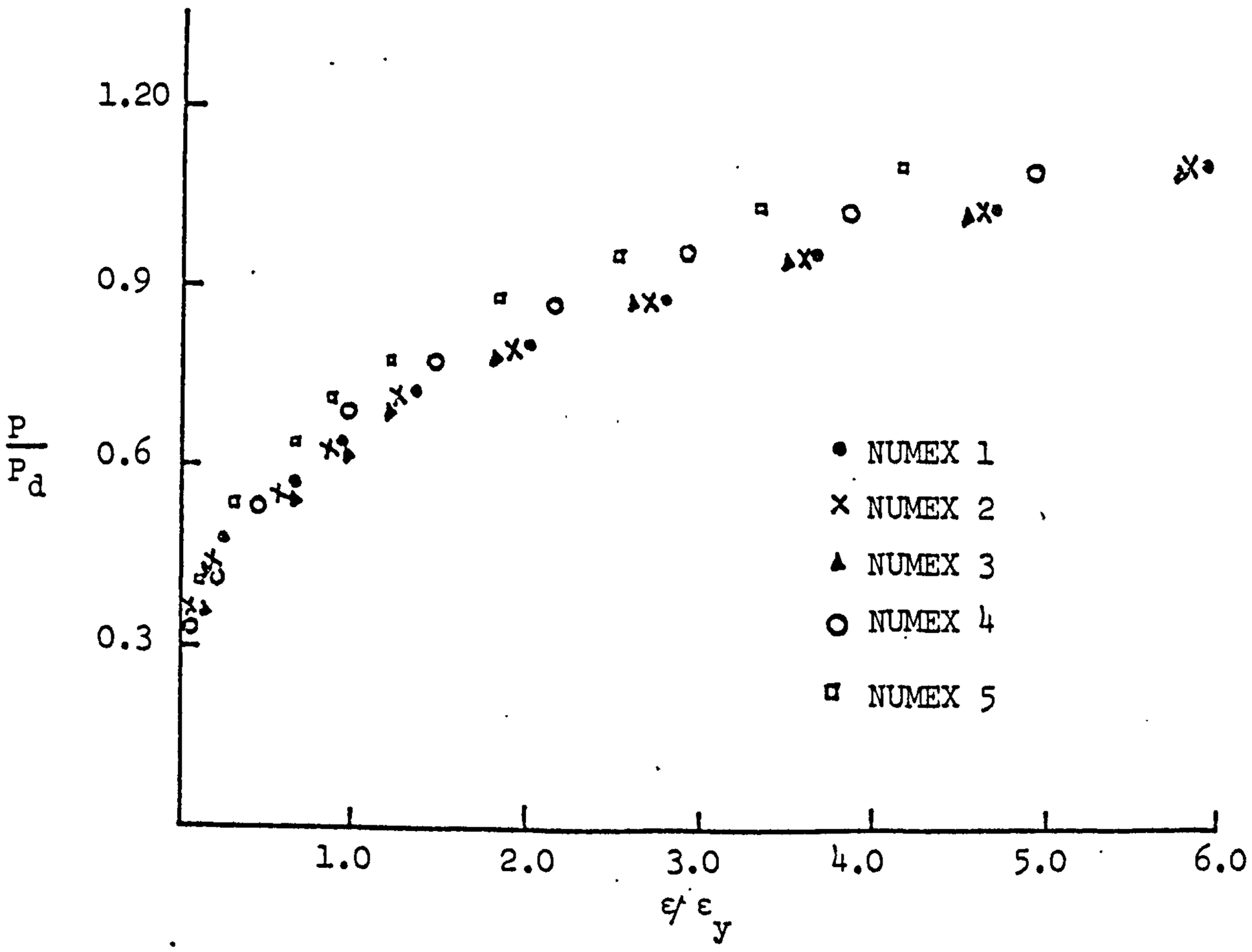

Figure (5.14) Load-Maximum Steel Strains in the Slabs in Series 1A

C.L.

.92	.76	.68	.68	
1.04	.8	.76	.68	C.L.
	.92	.8	.76	
		1.04	.92	

NUMEX 1

C.L.

.91	.73	.70	.65	
1.12	.83	.74	.70	C.L.
	.91	.82	.78	
		1.04	.99	

NUMEX 2

C.L.

.91	.78	.69	.65	
1.03	.82	.78	.69	
	0.91	.82	.78	C.L.
		1.04	1.04	

NUMEX 3

C.L.

.96	.78	.74	.74	
1.0	.83	.78	.74	
	.91	.87	.83	C.L
		1.129	1.129	

NUMEX 4

C.L.

.93	.78	.74	.74	
1.04	.83	.78	.78	C.L.
	0.91	0.87	.87	

NUMEX 5

P/P_d Causing Yield

Figure (5.15) Spread of Yield in the Slabs in Series 1A

NUMEX	Supports Type	L_x/L_y	f_{cu} N/mm^2	f_{st} N/mm^2	P_d KN/mm^2	$\frac{\delta p}{L_y}$	$\frac{P_{cr}}{P_d}$	$\frac{P_{\delta L}}{P_d}$	$\frac{P_y}{P_d}$	$\frac{P_u}{P_d}$	OBJECT
1	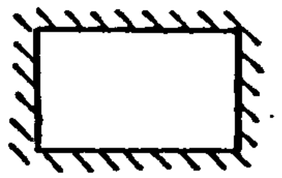	1·0	20	300	50	1/356	0·402	0·67	0·684	1·04	Sides Ratio
2	"	1·25	"	"	40	1/299	0·363	0·66	0·654	1·12	"
3	"	1·5	"	"	33.3	1/284	0·347	0·67	0·65	1·04	"
4	"	1·75	"	"	28	1/284	0·354	0·68	0·741	1·13	"
5	"	2·0	"	"	25	1/284	0·36	0·68	0·741	1·04	"

N.B.: L_y = 2000 mm, h = 100 mm, δ_p = Predicted service load deflection

Table (5·3): Results of the numerical experiments in subseries 1A.

5.4.2 CONCLUSIONS:

5.4.2.1 Subseries 1A.

1. The service behaviour of all the slabs in this series was satisfactory. The deflection limit of span/250 has been reached at an average of 67% of the design loads. This gives a high service load in terms of deflections. In terms of steel strains, first yield was observed at an average of 69·0% of the design load. All slabs showed an identical service behaviour.

2. Yield of steel was concentrated in the short span direction. Irrespective of the side ratio, 81% of the total steel in this direction has completely yielded when failure was reached. Yield in this direction reaches the boundaries of the slab at about 91 to 96% of the design load. On the other hand, only a small percentage of steel in the long span direction yields. This percentage reduces with the increase in sides ratio.

3. The distribution of normal moments at the design load is very close to that predicted by the elastic analysis, only in the short span direction. In the long span direction, the moments are much smaller than those predicted by the elastic analysis. The difference increases with the increase in sides ratio.

4. The slabs in this series did not record a significant increase in the ultimate load. Under the design load, many collapse mechanisms can combine from the extensive yielding on most of the slab portions.

5.4.2.2 Subseries B: (Variables: Concrete and Steel Strengths)

1. An improved service behaviour is obtained by increase in the compressive strength of concrete. This is represented by high cracking loads, low deflections and reduced steel strains.

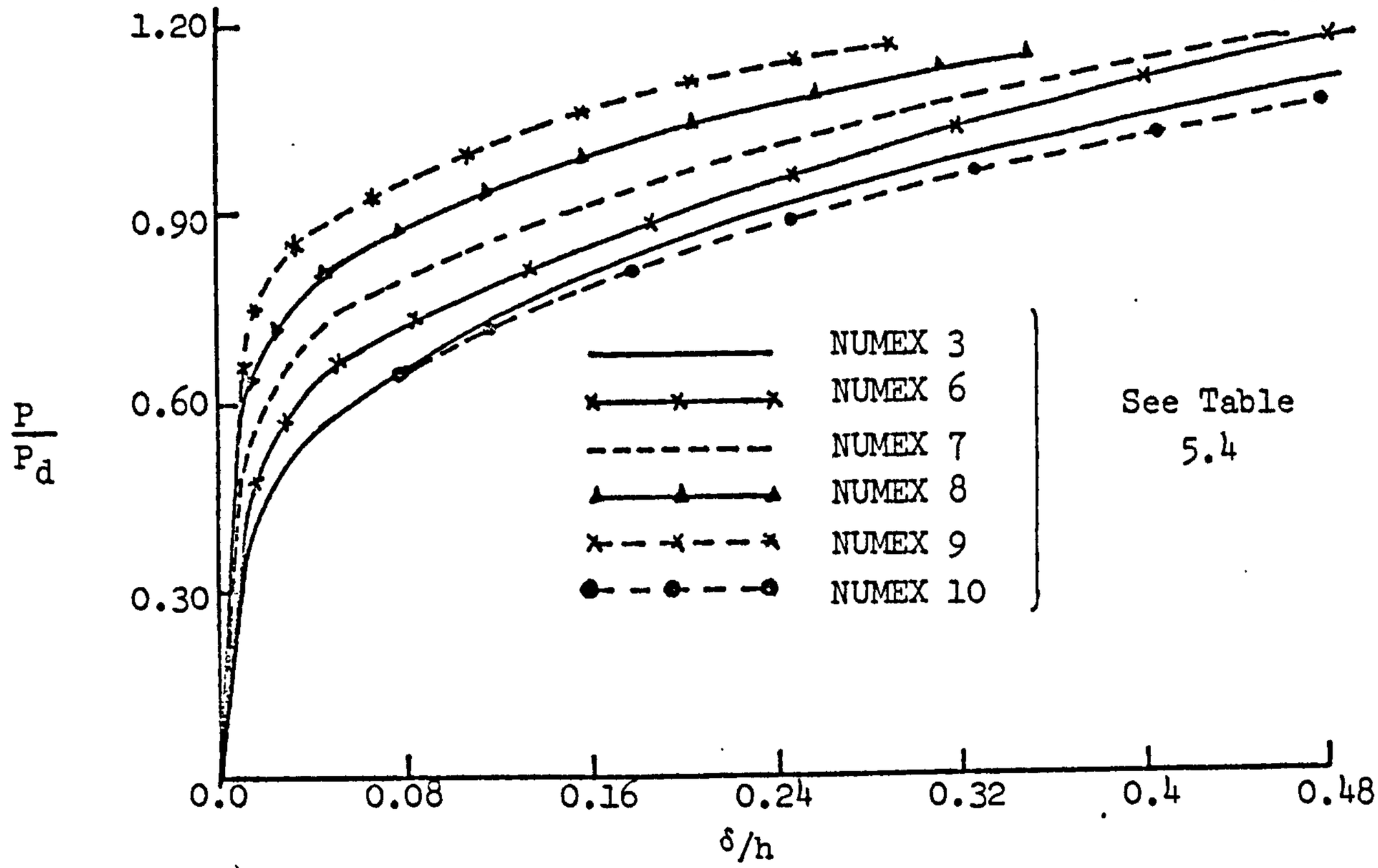

Figure (5.16) Load-Deflection Curves for the Slabs in Sub Series 1B

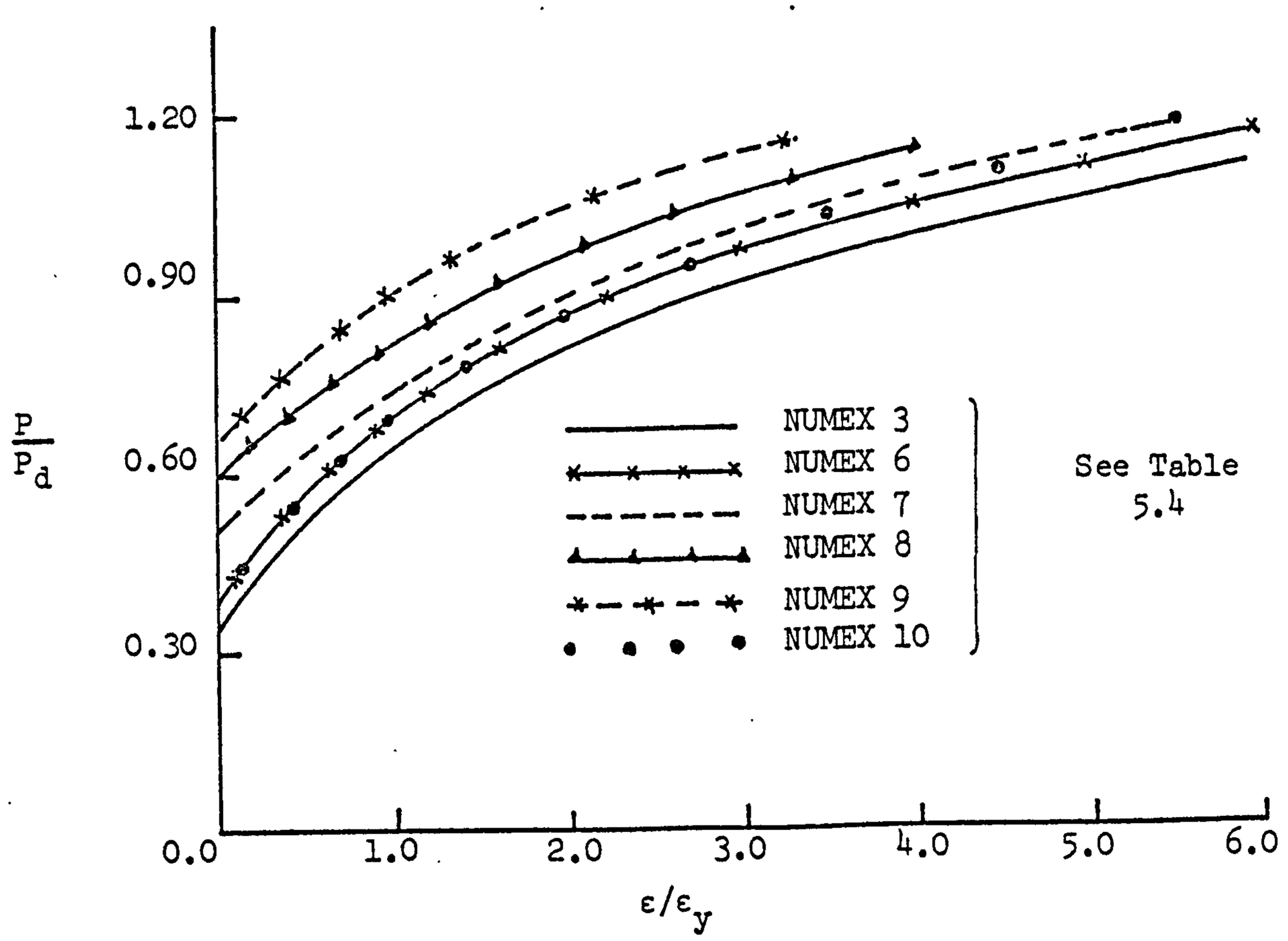

Figure (5.17) Load-Maximum Steel Strains in the Slabs in Sub Series 1B.

C.L.

0.91	0.78	0.69	0.65
1.04	0.82	0.74	0.69
	0.91	0.82	0.78
		1.04	1.04

C.L.

NUMEX 3

C.L.

1.0	0.81	0.73	0.73
1.04	0.85	0.77	0.77
	0.92	0.88	0.85
		1.15	1.15

C.L.

NUMEX 6

C.L.

1.04	0.87	0.80	0.77
1.06	0.90	0.84	0.8
	0.97	0.93	0.9
		1.197	1.197

C.L.

NUMEX 7

C.L.

1.11	0.92	0.86	0.86
1.11	0.95	0.89	0.89
	1.03	1.0	1.0

C.L.

NUMEX 8

C.L.

1.18	1.01	0.84	0.94
1.18	1.04	0.98	0.96
	1.11	1.08	1.06

C.L.

NUMEX 9

C.L.

0.99	0.78	0.73	0.73
1.08	0.82	0.76	0.73
	0.91	0.86	0.82
		1.12	1.12

C.L.

NUMEX 10

P/P_d Causing Yield

Figure (5.18): Yield Spread in the Slabs in Subseries 1B

NUMEX	Supports Type	L_x/L_y	f_{cu} N/mm²	f_{st} N/mm²	P_d KN/mm²	$\frac{\delta_p}{L_y}$	$\frac{P_{cr}}{P_d}$	$\frac{P_{\delta L}}{P_d}$	$\frac{P_y}{P_d}$	$\frac{P_u}{P_d}$	OBJECT
3	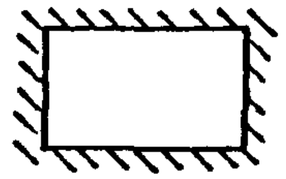	1·5	20	300	33·3	1/284	0·35	0·67	0·65	1·04	Concrete Strength
6	"	"	25	"	"	1/358	0·43	0·73	0·73	1·15	"
7	"	"	30	"	"	1/483	0·51	0·79	0·77	1·20	"
8	"	"	35	"	"	1/683	0·59	0·88	0·86	1·11	"
9	"	"	40	"	"	1/976	0·67	0·94	0·94	1·18	"
10	"	"	20	410	"	1/235	0·34	0·64	0·73	1·12	Steel Strength

N.B.: L_y = 2000 mm , h = 100 mm

Table (5.4): Results of the Numerical Experiments in Sub Series 1B.

2. The service behaviour of all slabs was satisfactory. The deflection limit of span/250 was reached at an average load of 0.78 Pd. With high compressive concrete strengths, deflection limits occur at loads close to the design loads, in this test series.

3. No yield of steel occurs within the service load range. In fact, for high grades of concrete, first yield loads were close to the 'design loads. An average value of 0.78 Pd was obtained for the first yield loads.

4. The use of high yield steel with low grades of concrete lead to a slightly flexible behaviour. But still the overall response was satisfactory.

5. Similar to the slabs in the previous series, the distribution of the normal moments in the short span direction was very close to that predicted by the elastic analysis, on most of the slab area. The distribution of the normal moment in the long span direction is different from that predicted by the elastic analysis.

6. For the same steel strength, the induced compressive membrane force at ultimate loads increased in magnitude with higher grades of concrete.

5.4.3 Test Series 2: (Slabs simply supported on 3 sides)

This series includes the test runs NUMEX 11 to NUMEX 15. The slabs in this series were all simply supported on three sides, and free on the fourth. The slabs were designed for a uniform load of 20 KN/m^2, and the analysis was intended to study the behaviour for

various sides ratios. In these slabs, the free edge has always been taken as one of the long edges, along the X-axis.

The distribution of the design moments for some of the slabs in this series can be found in Figures (5.5) and Figures (D17 to D24) in Appendix (D). The distribution of the support reactions is given in Figure (5.19). From these figures, it can be seen that most of the load is carried by bending of the strips parallel to the free edge. Figure (5.19) shows that for a square slab, 82% of the total load is carried by strips parallel to the free edge. This agrees quite well with the 45° load distribution recommended by CP110[5]. In this case, the 45° load distribution will give 75% of the total load to be carried by these strips. However, in both distributions, the proportion of the load carried by the strips parallel to the free edge reduces with the increase in sides ratios. For a slab with a side ratio of free to short edge of 2.0, the 45° distribution gives 50% of the total load, while the finite element gives 38% of it to be carried by the strips parallel to the free edge, which indicates that most of the load is carried by the short span strips.

Accordingly, if the span in the span/depth ratio was taken as the long free edge, the resulting behaviour would be satisfactory. In fact such an analysis was first undertaken, but it was found that this was too conservative, for slabs with sides ratio greater than 1.25. The results of such an analysis are not shown here, but it was found that, yield of steel started at an average load of 0.92 Pd, while the deflection limit was reached at 0.9 Pd.

The same slabs were redesigned with reduced depths. The assumed depths were chosen such that the predicted deflection did not exceed

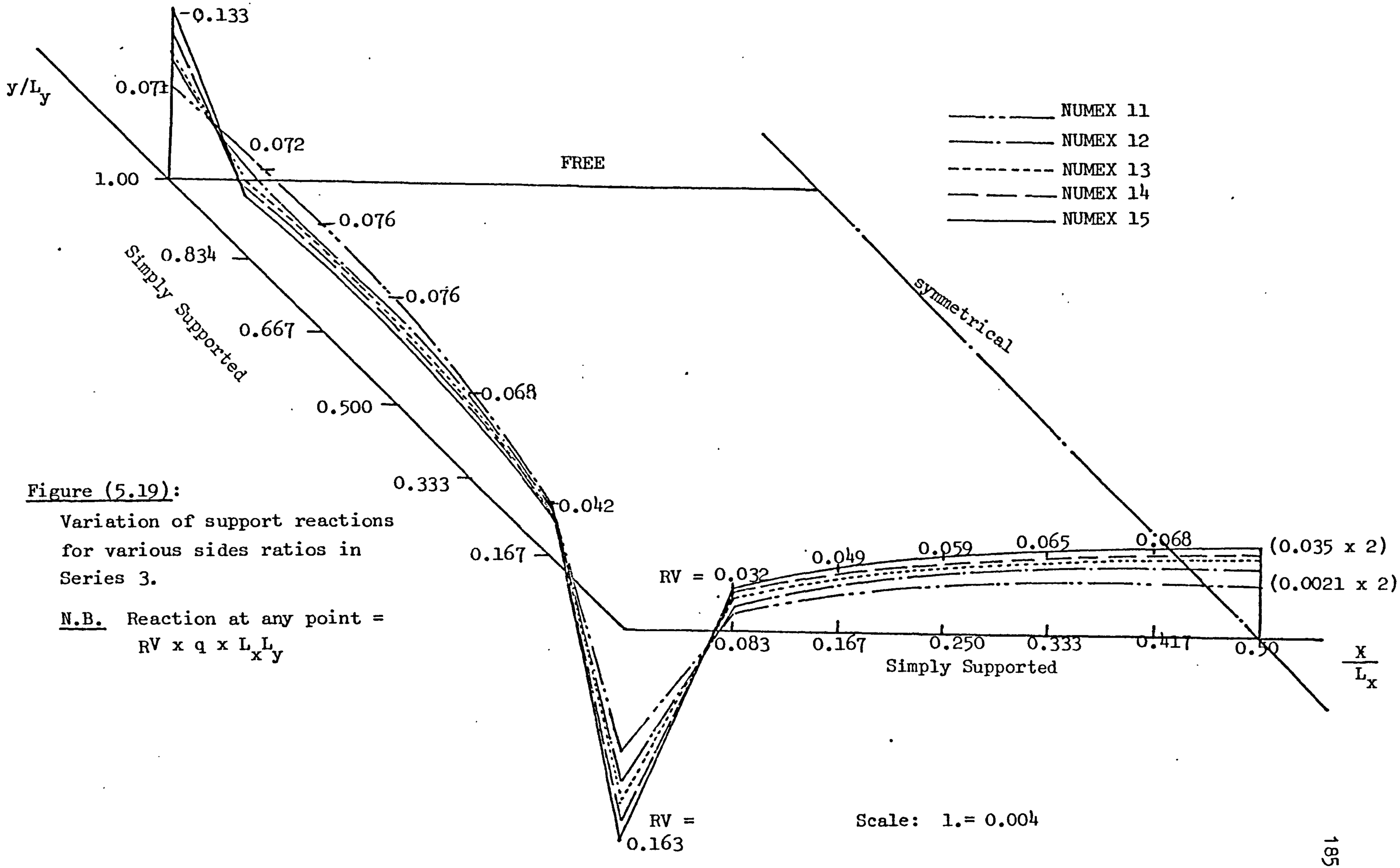

Figure (5.19):

Variation of support reactions for various sides ratios in Series 3.

N.B. Reaction at any point = $R^V \times q \times L_x L_y$

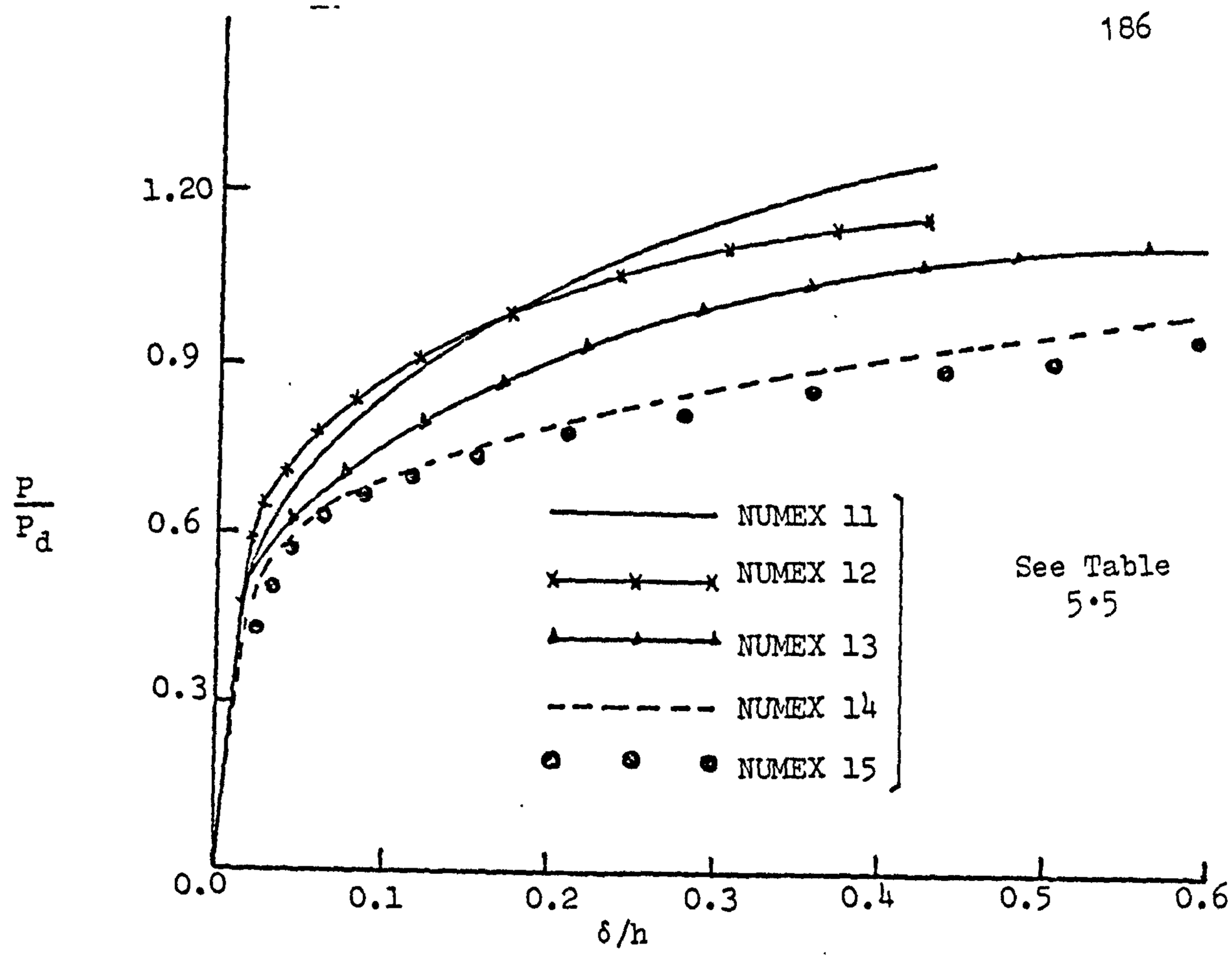

Figure (5.20): Load-deflection Curves for the Slabs in Series 2.

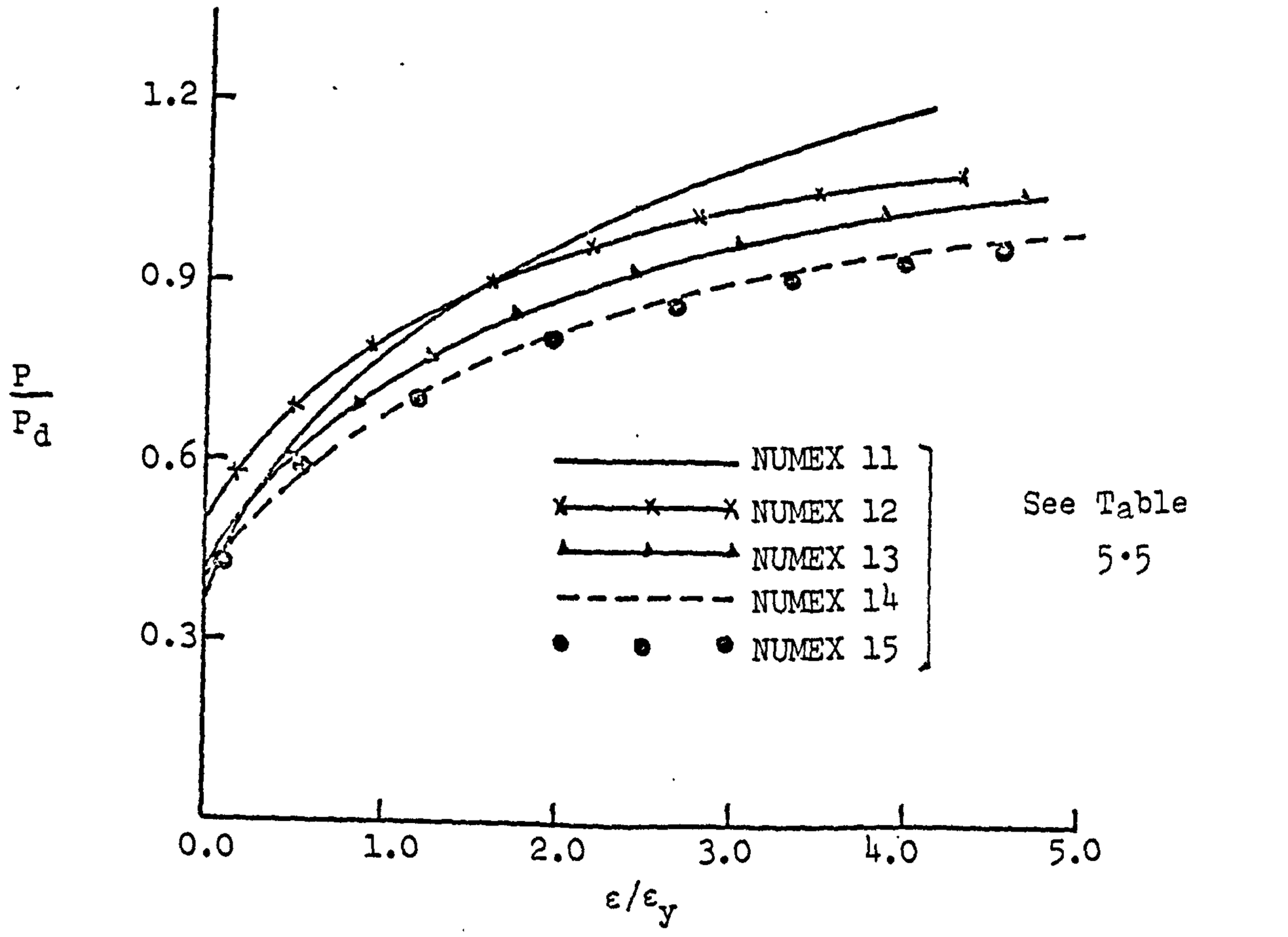

Figure (5.21): Load-Maximum Steel Strains in the Slabs in Series 2.

Free

simply supported	1.12	.96	.88	.85	.85
	1.12	.96	.88	.85	.81
	1.12	.96	.93	.85	.81
	1.1	.96	.93	.88	.85
	1.12	1.0	.96	.96	.93
			1.24	1.2	1.16

C.L.

simply supported

NUMEX 11

Free

simply supported	1.04	.91	.85	.85	.83
	1.04	.95	.89	.85	.83
	1.04	.95	.91	.87	.85
	1.05	1.0	.93	.91	.87
		1.05	1.02	.97	.97
					1.12

C.L.

simply supported

NUMEX 12

Free

simply supported	.97	.86	.75	.75	.71
	.97	.89	.82	.78	.75
	1.00	.93	.86	.82	.78
	1.04	.93	.89	.86	.82
		1.04	1.01	.97	.93

C.L.

simply supported

NUMEX 13

Free

simply supported	1.08	.93	.82	.71	.67	.67
		.93	.86	.78	.75	.71
		.97	.89	.82	.78	.75
		1.08	.93	.86	.82	.82
			1.04	.97	.93	.89
					1.08	1.12

C.L.

simply supported

NUMEX 14

Free

simply supported	1.12	.93	.81	.70	.70	.65
		.93	.81	.76	.73	.70
		.96	.88	.81	.76	.73
		1.12	.93	.88	.81	.81
				1.0	.93	.88
					1.12	1.12

C.L.

simply supported

NUMEX 15

Figure (5.22) P/P_d Causing Yield in Series 2.

NUMEX	Supports Type	L_x/L_y	h (mm)	f_{cu} N/mm^2	f_{st} N/mm^2	P_d KN/mm^2	$\frac{\delta_p}{L_x}$	$\frac{P_{cr}}{P_d}$	$\frac{P_{\delta L}}{P_d}$	$\frac{P_y}{P_d}$	$\frac{P_u}{P_d}$	Object
11	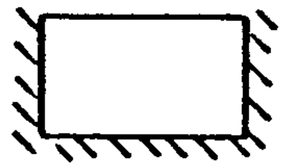	1.0	100	20	300	20	1/320	0.42	0.80	0.85	1.24	Sides Ratio
12	"	1.25	125	"	"	"	1/410	0.56	0.86	0.83	1.12	"
13	"	1.50	130	"	"	"	1/297	0.45	0.74	0.71	1.04	"
14	"	1.75	140	"	"	"	1/273	0.45	0.71	0.67	1.12	"
15	"	2.0	150	"	"	"	1/272	0.42	0.69	0.67	1.12	"

NB: L_y = 2000 mm

Table (5.5): Results of the Numerical Experiments in Series 2.

the limiting deflection of span/250. The results of the analysis of these slabs are given in Figures (5.20) to (5.22), and a summary is given in Table (5.5).

5.4.4 Conclusions:

(1) The service behaviour of all slabs in this series was satisfactory.

An average of 0.76 Pd was obtained for the service deflection load and 0.75 Pd for the first yield load.

(2) The response of the slabs in this series is sensitive to the early cracking of the elements on the free edges. As this method provides gradual distribution of steel, it is to be expected that the service behaviour will be governed by the conditions on the free edge. For better performance, it is suggested here that the steel on each strip to be provided according to the maximum moment in the strip, without curtailment. Adequate anchorage of the reinforcement on the free edges should be provided to ensure full transfer of load to the supports.

(3) An average enhancement in the ultimate load of about 12% is obtained for the slabs in this series. The enhancement is caused by the developed membrane action on the slabs.

5.4.5 Test Series 3

This includes the test runs NUMEX 16 to NUMEX 20. The slabs in this series were all simply supported on two adjacent edges and supported on a column on the opposite corner, while the other two edges were free. The slabs were designed for a uniform load of 20 KN/m^2, and the analysis was intended to study the behaviour for various sides ratios. In all slabs, the long free edge was always along the X-axis.

The distribution of the design moments for the slabs in this series are given in Figures (5.9) and Figures (D49-D56). Figure (5.28) gives the distribution of the support reactions, for the five cases considered. From these figures, it is found that the load dispersion is dependant upon the sides ratios of the slab. For a square slab, 37.5% of the total load goes to each of the supported edges. The column at the opposite corner always takes 25% of the total load, irrespective of the the sides ratio of the slab. As the sides ratio increases, more load is carried to the long side support. For a side ratio of 2, the load carried by the long support is 1.4 times that carried by the short side support. But in general, the bending moments in the long span strips are almost equal to those in the short span direction, and represent the maximum moments in the slab as a whole. It is also very interesting to note that, the variation of the design moments along each strip is very gradual, and is almost constant. The reaction at the end of the long free edge, Figure (5.28) indicates that a large proportion of the load dispersed in this direction is carried by the strips closer to the free edge.

Results of the nonlinear analysis of the slabs in this series are shown in Figures (5.23) to (5.27), and a summary is given in Table (5.6). In general, apart from the square slab, the maximum deflection in the slab occurs at a distance of $L_x/3$ from the column, along the long free edge. For the square slab the point of maximum deflection is at a distance of 0.53L from the column along the diagonal. The deflections plotted in Figure (5.23) refer to these points. Points of maximum strains are at 0.3 L_x from the column, on the free edge.

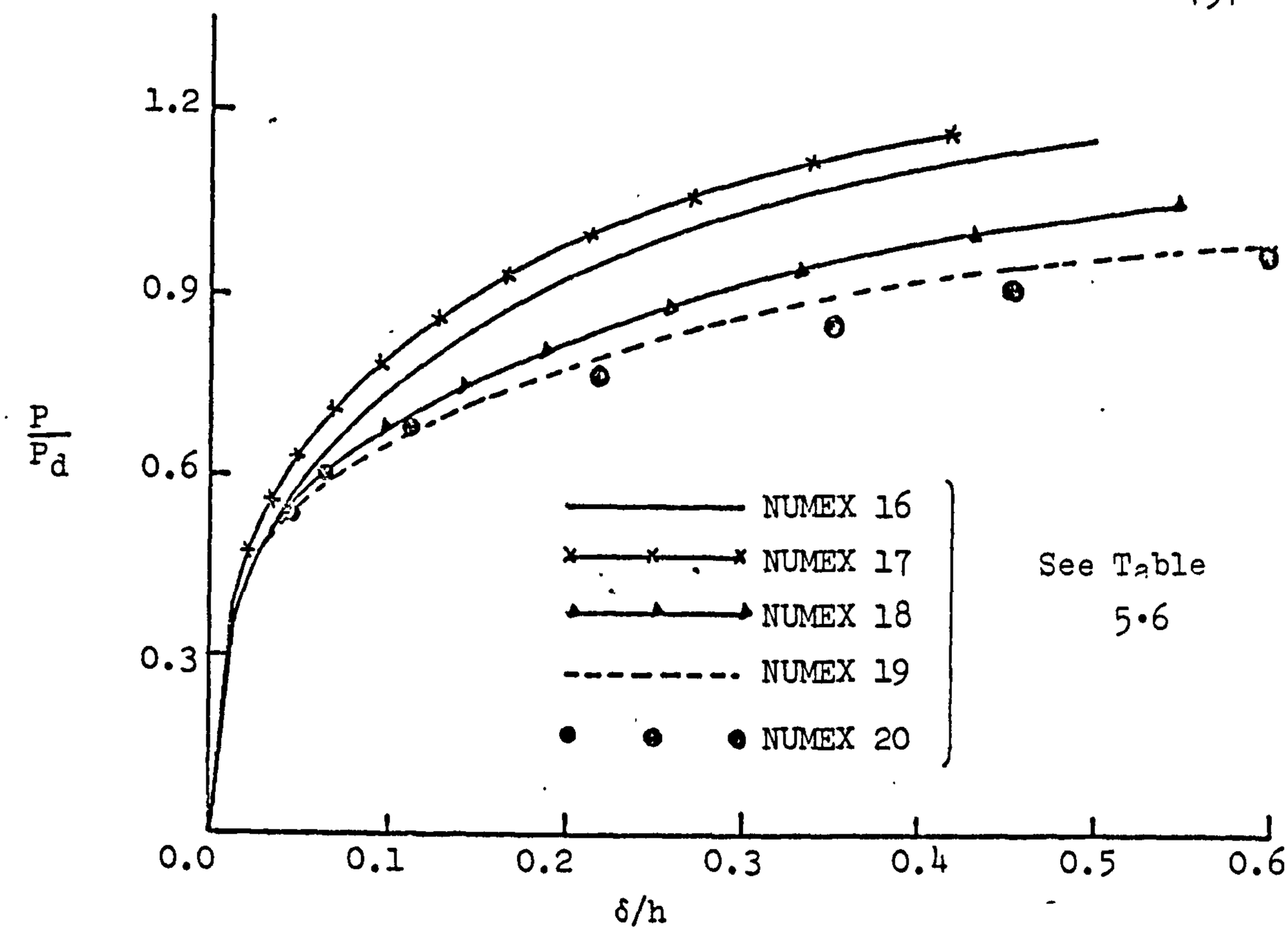

Figure (5.23): Load-deflection Curves for the Slabs in Series 3

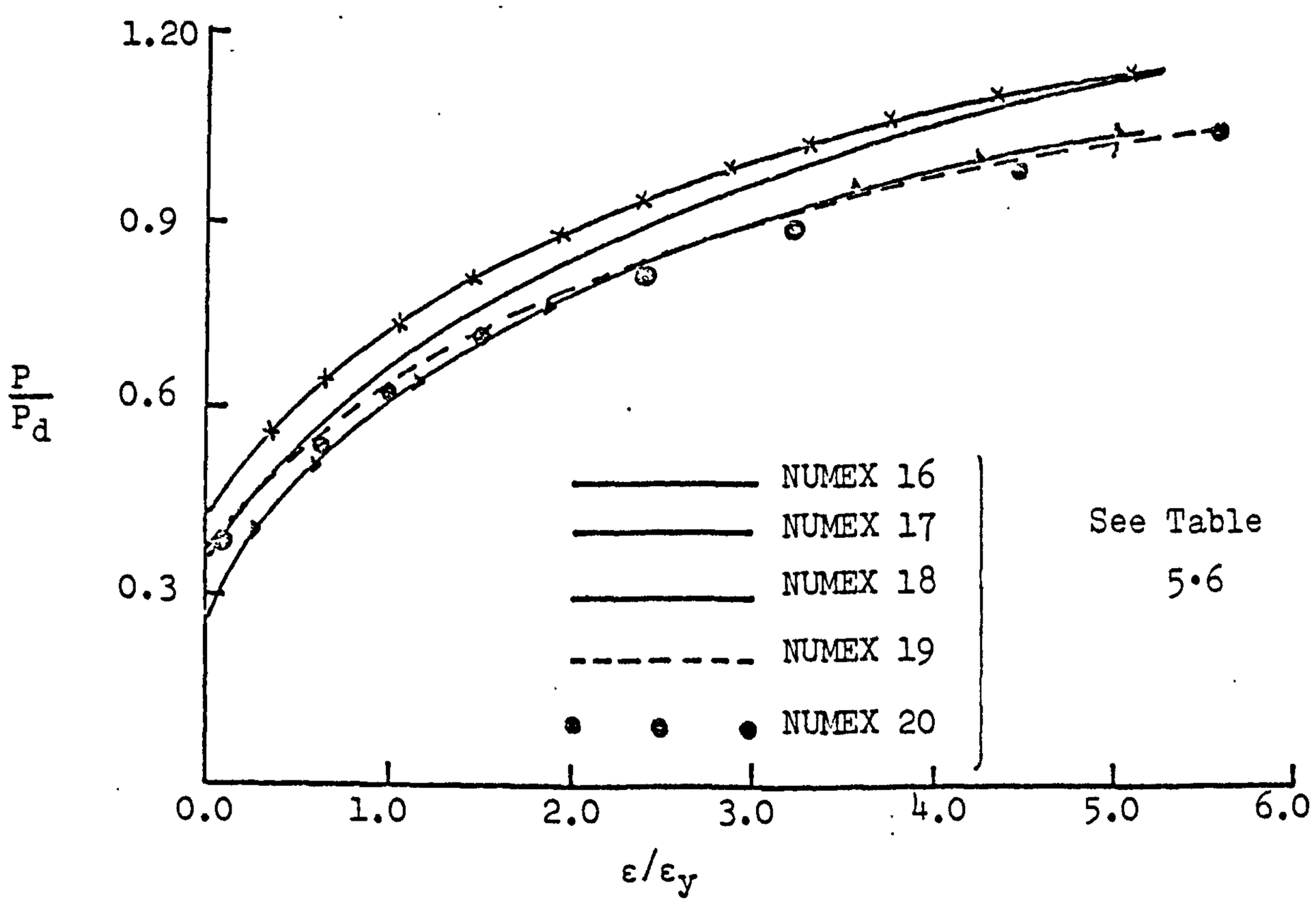

Figure (5.24): Load-maximum Steel Strains in the Slabs in Series 3.

Free

	.90	.80	.69	.69	.69	.74	.9
	.90	.80	.80	.80	.85	.95	.74
	.95	.80	.85	.90	1.0	.85	.69
	.95	.85	.90	1.0	.90	.80	.69
	1.06	.95	.95	.90	.85	.80	.69
	1.16	1.06	.95	.85	.80	.80	.80
		1.16	1.06	.95	.95	.90	.90

Simply supported

Free

Simply Supported

NUMEX 16

Free

	.91	.82	.77	.73	.73	.82	.96
	.96	.87	.77	.82	.82	.91	.87
	1.0	.87	.82	.87	.96	.91	.82
	1.0	.91	.87	.96	1.0	.87	.77
	1.05	.96	.96	1.05	.96	.87	.77
	1.14	1.05	1.05	1.10	1.00	.91	.82
					1.14	1.10	1.05

Simply Supported

Free

Simply supported

NUMEX 17

P/P_d Causing Yield

Figure (5.25) Yield Spread in the Slabs in Series 3

free

1.05	.84	.72	.68	.68	.64	.72	.84
1.05	.88	.76	.68	.72	.72	.80	.80
1.12	.88	.80	.72	.76	.84	.92	.76
	.92	.84	.76	.84	.92	.88	.76
	.97	.88	.84	.88	1.00	.84	.72
	1.05	.92	.92	1.00	1.00	.88	.76
			1.05	1.05	1.09	.97	.80

Simply supported — free

simply supported

NUMEX 18

free

1.04	.80	.68	.68	.68	.64	.72	.80
1.04	.84	.72	.68	.72	.72	.80	.80
	.88	.80	.72	.72	.80	.92	.80
	.92	.80	.76	.80	.88	.92	.76
	.96	.84	.80	.84	.96	.88	.76
	1.08	.92	.88	.92	1.12	.80	.76
		1.04	1.00	1.08		1.00	.84

Simply supported — free

simply supported

NUMEX 19

Figure (5.26) P/P_d Causing Yield in Series 3.

free

1.00	.83	.67	.67	.67	.63	.71	.92
1.04	.88	.71	.67	.67	.71	.80	.88
	.88	.80	.71	.71	.80	.92	.80
	.92	.83	.75	.75	.83	1.08	.75
		.88	.80	.83	.92	.96	.75
		.96	.88	.92	1.04	1.00	.80
		1.08	.96	1.00		1.12	.83

Simply Supported

free

Simply supported

NUMEX 20

Figure (5.27) P/P_d Causing Yield in Series 3.

Figure (5.28)

Variation of supports reactions for various sides ratios in Series 3.

N.B.: Reaction at any point = Rv x q x $L_x L_y$

NUMEX	Supports Type	L_x/L_y	h (mm)	f_{cu} N/mm²	f_y N/mm²	P_d KN/mm²	$\frac{\delta_p}{L_x}$	$\frac{P_{cr}}{P_d}$	$\frac{P_{\delta L}}{P_d}$	$\frac{P_y}{P_d}$	$\frac{P_u}{P_d}$	Object
16	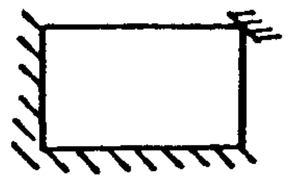	1.00	100	20	300	20	1/250	0.38	0.69	0.69	1.16	Sides Ratio
17	"	1.25	125	"	"	"	1/363	0.45	0.77	0.73	1.14	"
18	"	1.50	130	"	"	"	1/291	0.39	0.68	0.64	1.12	"
19	"	1.75	140	"	"	"	1/269	0.39	0.67	0.64	1.08	"
20	"	2.00	150	"	"	"	1/270	0.38	0.67	0.63	1.12	"

NB: L_y = 2000 mm

Table (5.6): REsults of the Numerical Experiments in Series 3

5.4.6 Conclusions:

(1) The service behaviour of all slabs in this series was satisfactory. The deflection limit of span/250 was reached at an average load of 0.70 Pd.

(2) Yield of steel started at an average load of 0.67 Pd. The spread of yield starts on the long free edge strips and progresses inward towards the centre.

(3) The distribution of the long span moments at the design load is very close to that predicted by the elastic analysis. With increase in sides ratio, the moment in the other direction at ultimate load is very much less than that predicted by the elastic analysis, except on the strips close to the short free edge.

(4) Similar to the slabs in the previous series, the behaviour is governed by the stress conditions on the free edges. Reinforcement in these edges can be provided based on the maximum on the strip without curtailment. Adequate anchorage has to be provided to transmit the load to the supports.

5.4.7 Test Series 4: (Slab-Beam Systems).

This series includes the test runs NUMEX 21, NUMEX 22 and NUMEX 23. The slabs were assumed to be monolithically cast with their supporting beams. All three slabs had the same dimensions, and had identical supporting beams, but differed in the amount and distribution of reinforcement. The dimensions of the slabs and the beams are given in Table (5.7).

The tests in this series were aimed at studying the behaviour of the slabs designed by the proposed direct design procedure, and

to compare the method with designs based on the yield line theory. Accordingly, NUMEX 21 and NUMEX 23 were designed for a uniformly distributed load of 20.8 KN/m^2 , which was the design load for NUMEX 22 by the yield line theory. NUMEX 22 was in fact designed and tested by Hayes and Taylor[84], by combining the composite rectangular mode and the diagonal mode of the slab, Figure (5.29). Accordingly, these slab-beam systems were designed to carry a uniform load of 20.8 KN/m^2.

In NUMEX 21, only flexural forces (M_x, M_y, M_{xy}) were considered, and the model was designed using the design equations of Section (3.4). However, NUMEX 23, which was also designed by the direct design approach, was designed for combined flexural and membrane forces. A sandwich model (Section 3.7) was used in this case, and the model was designed using the design equations of Section (3.6).

A comparison between the design moments and steel volumes in the two methods is given in Figures (5.31), and Table (5.8). At the middle of the slab, both the yield line theory and the present design procedure (for flexure only) give an ultimate moment of $\frac{q\ell^2}{24}$. In this particular case, both the upper and lower bound solutions coincide, when considering the diagonal collapse mode for the slab. On the other hand, if the compressive membrane force at the centre of the slab is taken into account, the corresponding moment of resistance required at the middle of the slab reduces by 15% of that required by the design for pure flexure (see Table 5.8). But the edge beams moments increase by about 18%, and is about 55% above that required by the yield line analysis. Thus, the reduction in the slab reinforcement is more than offset by an increase in the reinforcement of the supporting beams.

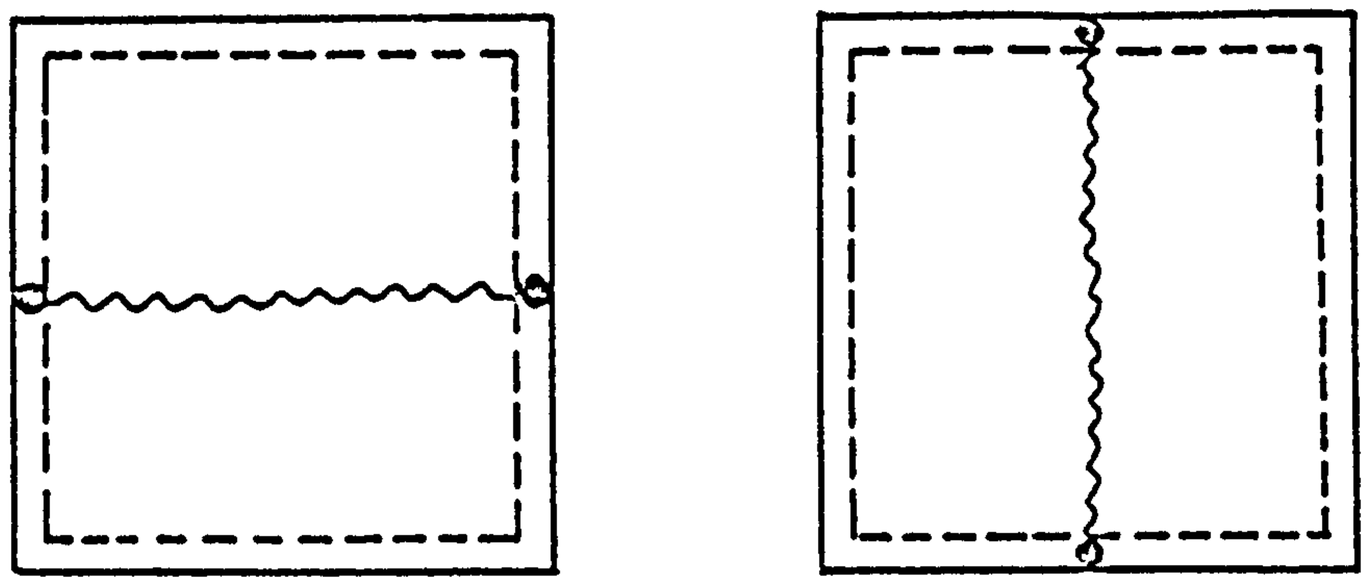

(Integral and Unintregal Systems)

Composite Rectangular Modes

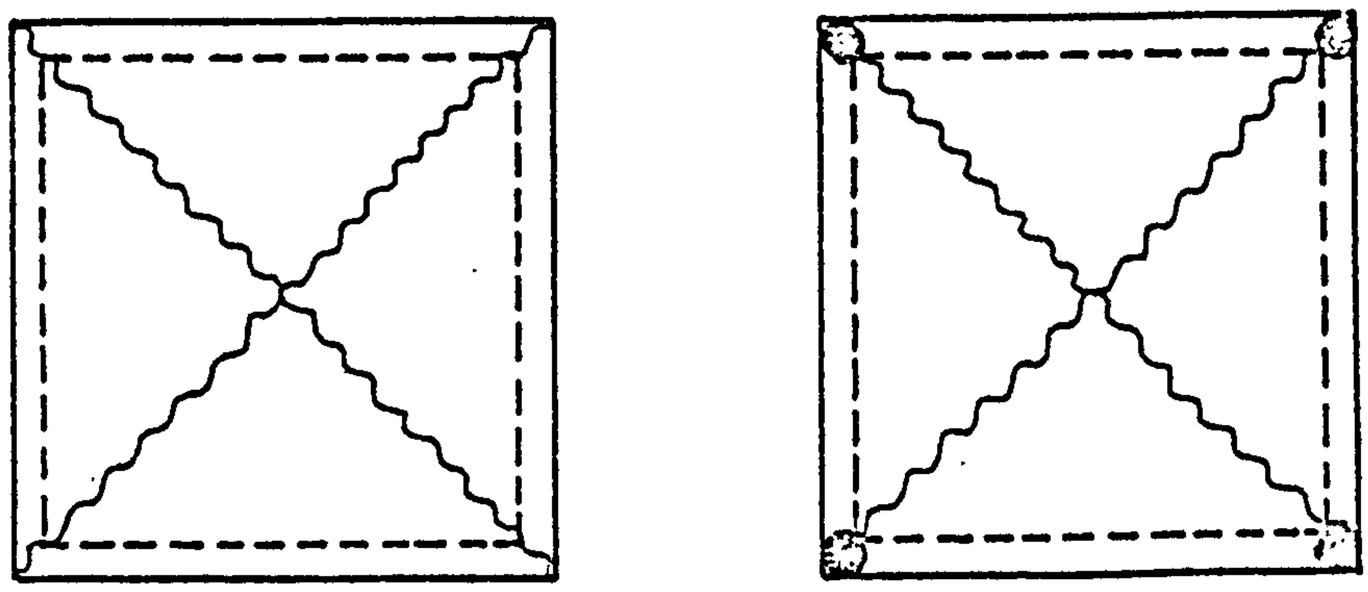

(Unintegral Systems)

Torsional Hinge Required
if Beams are connected
(Integral Systems)

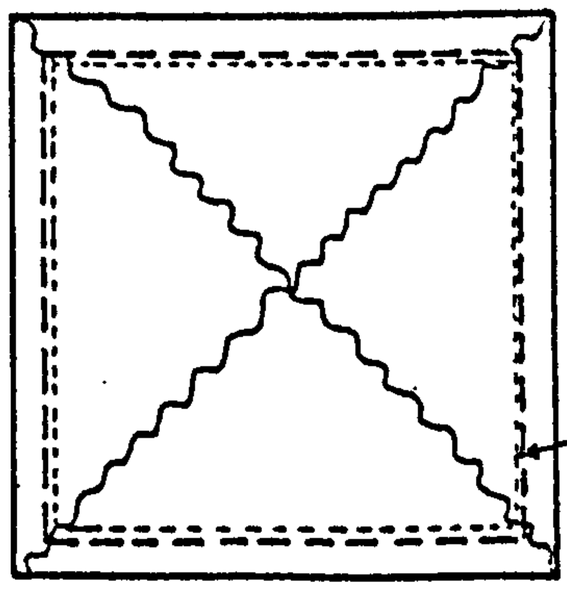

(Integral Systems)

Diagonal Collapse Modes

Figure (5.29): Possible Collapse Modes in Square Slab-Beams Systems

Although the unfilled sandwich model used here requires more steel than that required for flexure only, the increase in this particular case is only slight, and Table (5.8) gives a difference of only 7% between the two designs for the particular case at hand. But still both designs are more economical than the corresponding yield line design. A saving of up to 30% was achieved in this case.

The results of the nonlinear analysis for the slabs in this series are given in Figures (5.30) to (5.35), which are summarized in Table (5.7). From these results, the following conclusions can be drawn:

5.4.8 Conclusions.

1. All the slabs in this series had identical service behaviour.
   In all cases, both deflections and steel strains were within the acceptable limits in the working load range.
2. First yield of steel occurred at different loads in the slabs.
   In case of yield line design (NUMEX 22), first yield of steel started at the centre of the edge beams at 0.75 Pd, whereas in the systems designed by the present direct design approach (NUMEX 21, 23), yield of steel started at the corner at the junction between the two beams at about 0.67 Pd.
3. The initiation of yield at the corners of NUMEX 21 and NUMEX 23 was followed by yield spreading along the diagonals of the slab. The diagonal collapse mode formed in these slabs before the reinforcement in the beams started to yield.
4. The slight increase in reinforcement volume due to the consideration of membrane forces in the design of this system

produced slightly less deflections in the slab within the service load range, but did not affect the deflections after first yield in the slab.

5. Extending the midspan reinforcement in the beams of NUMEX 22 along the full length of the beam had the effect of enforcing a rectangular mode of failure. In such case, the diagonal mode did not form at all.

6. Under the present direct design approach, several simultaneous modes of collapse formed when the design load was reached.

7. No significant difference between the behaviour of the two slabs NUMEX 21 and NUMEX 23 was obtained. Accordingly, whether membrane forces were taken into account in the design or not, both systems designed by this method would behave satisfactorily.

5.4.9 Test Series 5:

Two slabs in this series were considered. The slabs were simply supported on three sides, free on the fourth long edge, with a side ratio of 2.0. Both slabs had the same dimensions and were designed for an ultimate load of 20 KN/m^2. The test slabs were designated NUMEX 15 and HILLERBORG, and were intended to study the behaviour of slabs designed according to the two design procedures, viz., the direct design (NUMEX 15), and the strip method (HILLERBORG). In HILLERBORG, the shear modulus G = 0 in the elastic analysis (Torsionless analysis), while the nonlinear analysis was performed on the slab with G ≠ 0, in the normal way.

A comparison of the design moment fields in the two slabs is given in Figures (D21, D22, D23, D24) in Appendix (D). And as has

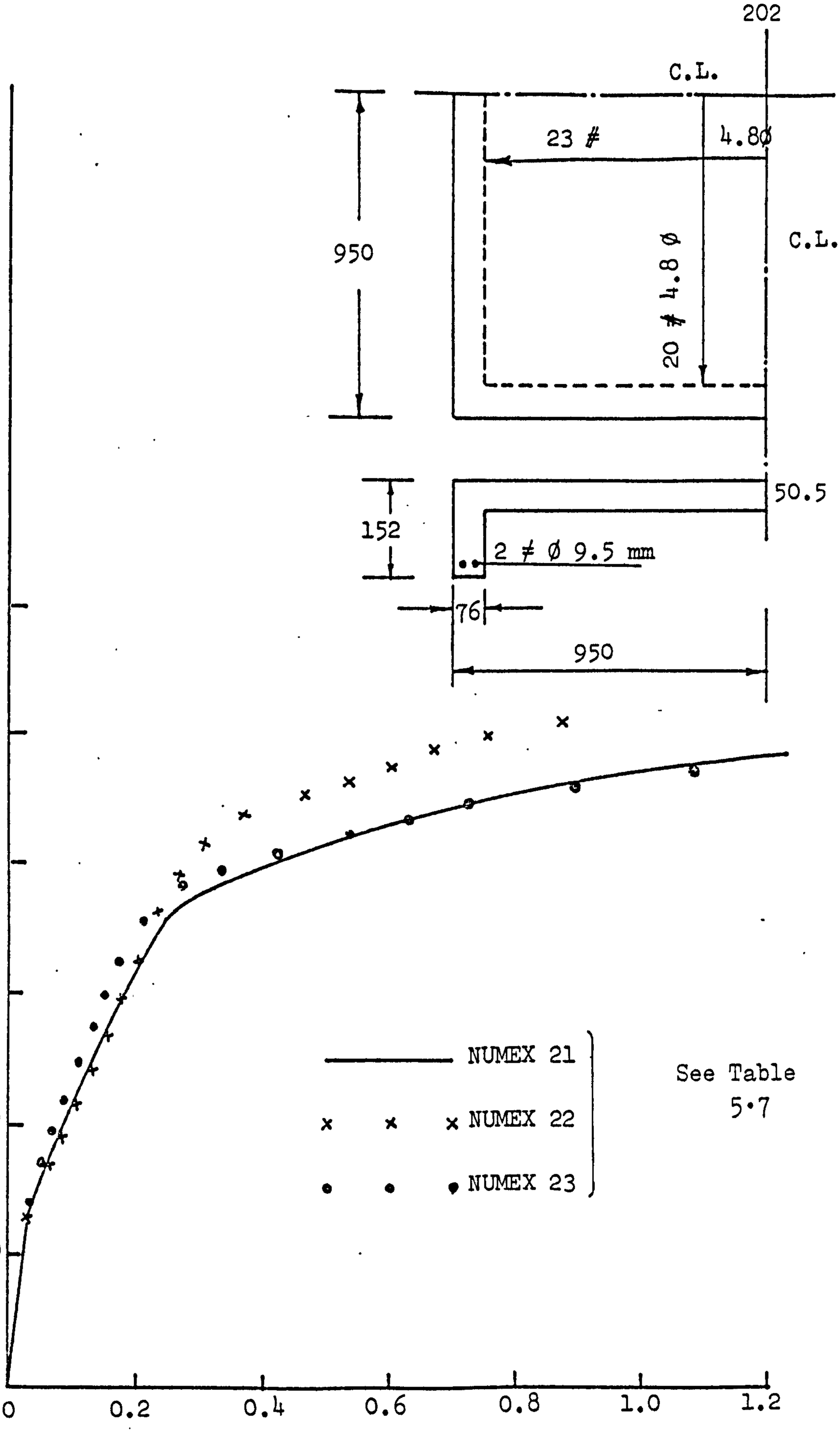

Deflection at the Centre of the Slab

Figure (5.30): Load-Deflection Curves for the Slabs in Series 4.

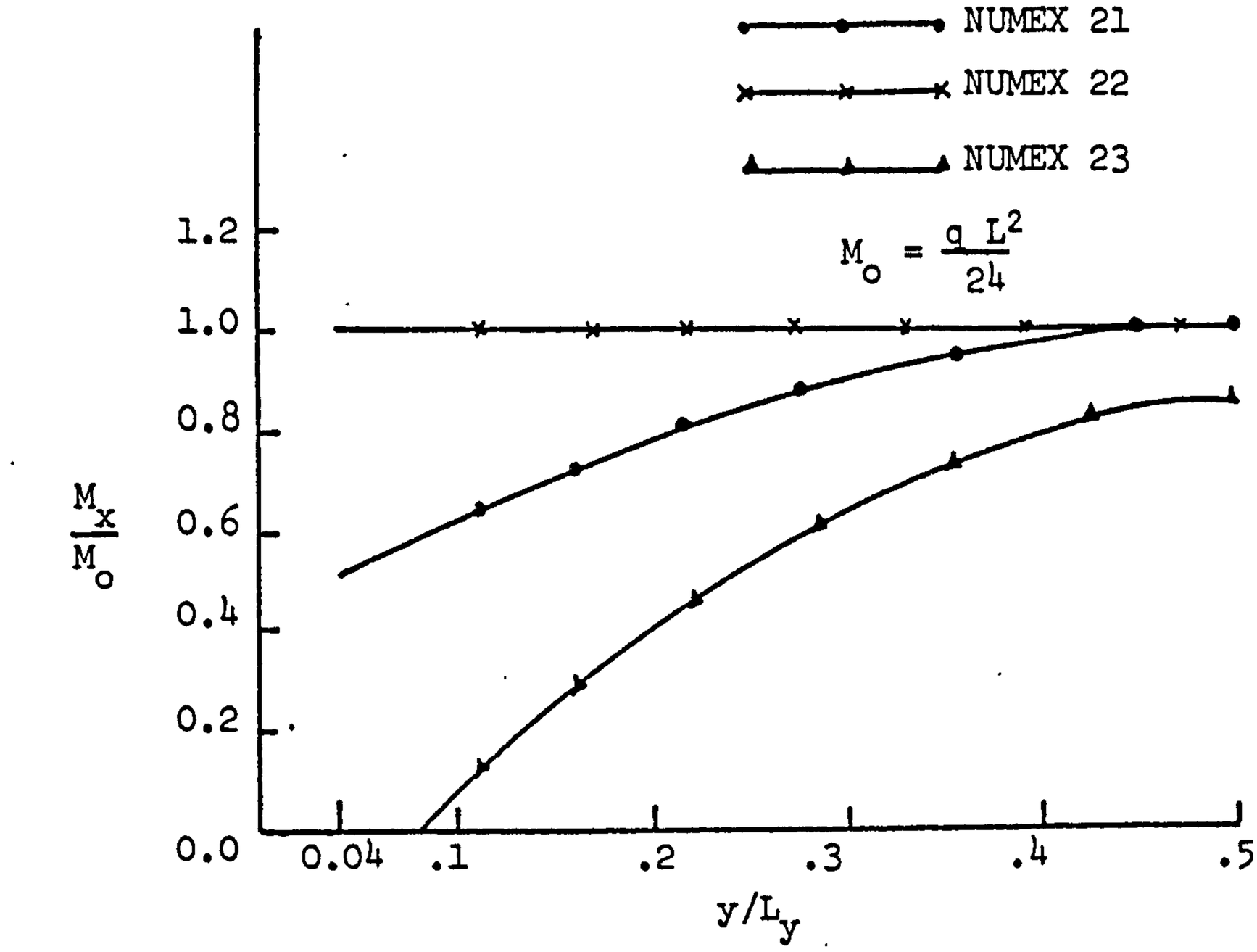

Design Moments in the Slab

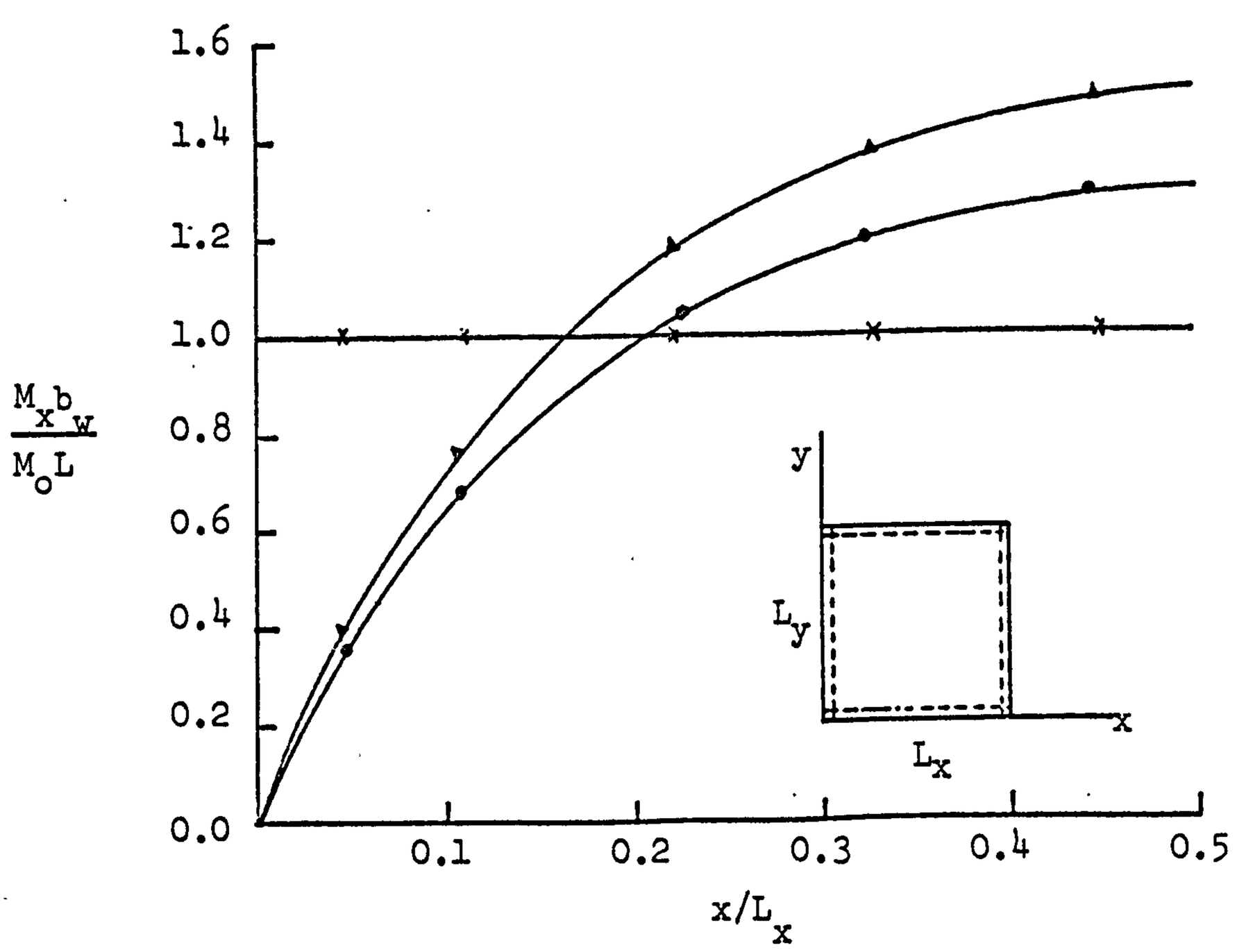

Design Moments in the Beams

Figure (5.31) Design Moments in the Slabs in Series 4.

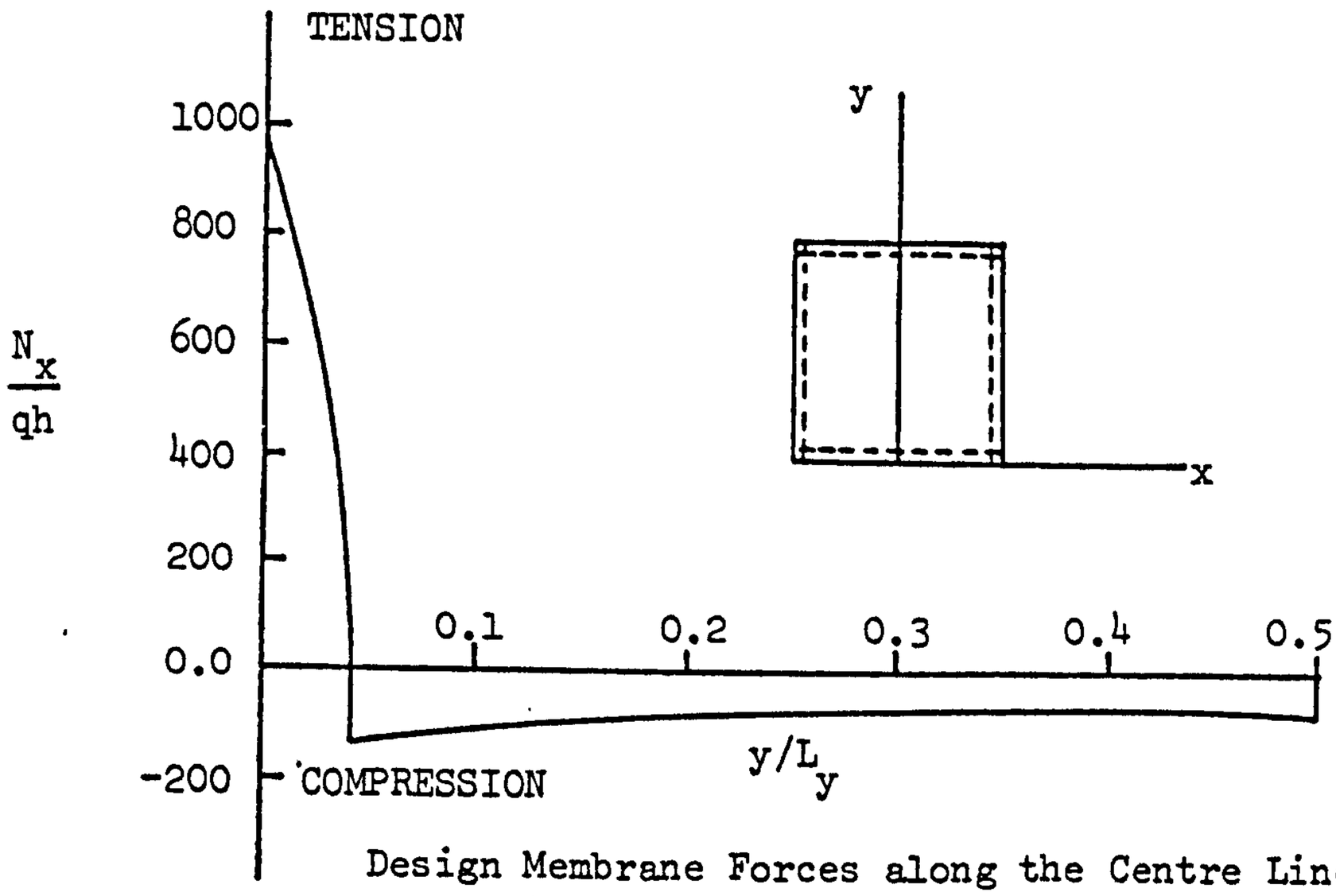

Design Membrane Forces along the Centre Line of the Slab

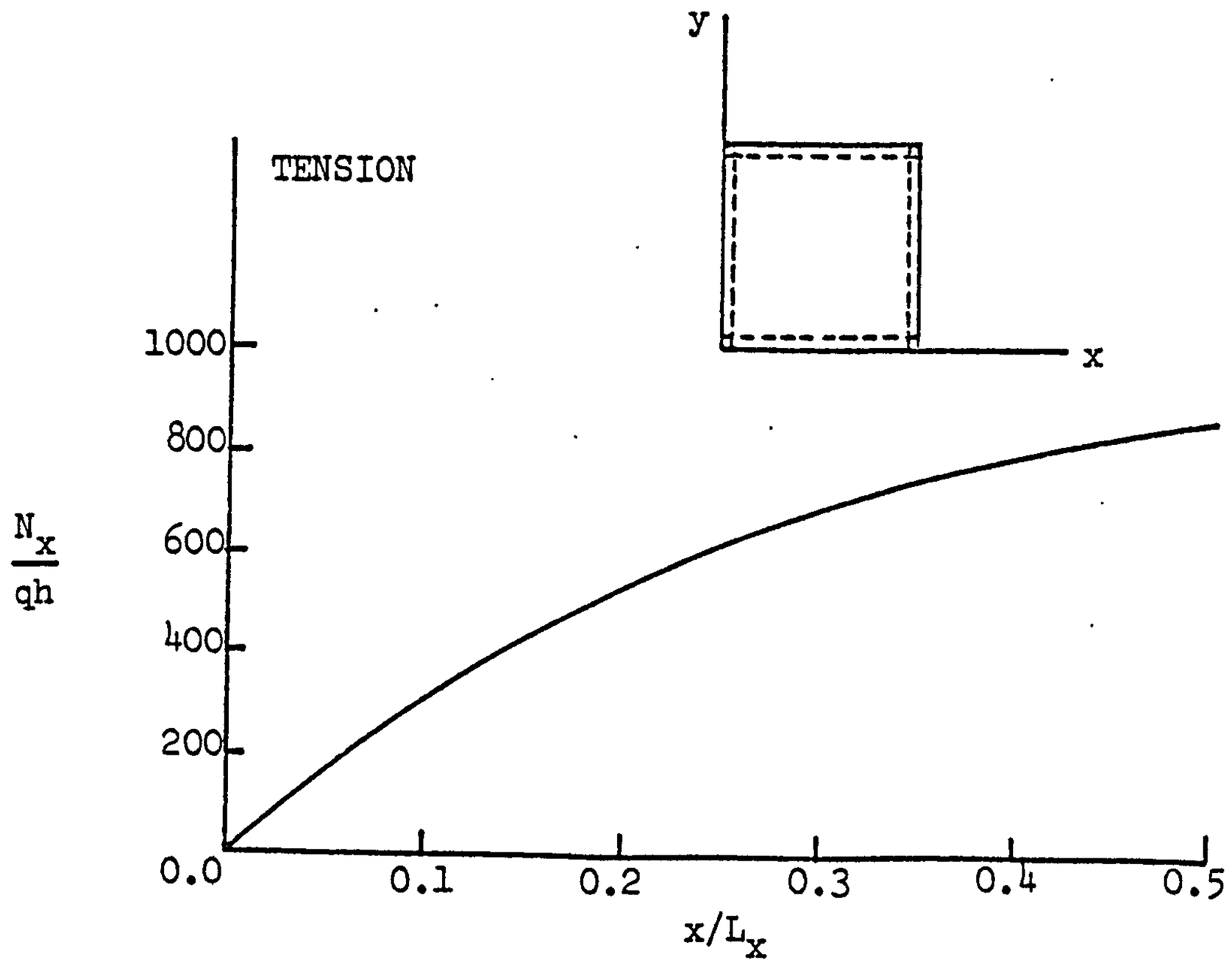

Membrane Forces along the Edge Beam

Figure (5.32) Membrane Forces in the Slabs in Series 4.

C.L.

.96	.98	.81	.78	.76	
.93	.83	.78	.78	.78	C.L.
.91	.78	.78	.78	.81	
.66	.76	.78	.83	.98	
.66	.66	.91	.93	.96	

NUMEX 21

C.L.

.75	.91	.91	.91	.89	C.L.
.77		.96	.94	.89	
.84			.99	.89	
.91				.89	
	.91	.84	.75	.75	

NUMEX 22

C.L.

.99	.99	.83	.78	.75	C.L.
.91	.86	.81	.78	.78	
.81	.78	.81	.81	.83	
.73	.78	.78	.86	.99	
.68	.73	.81	.91	.99	

NUMEX 23

Figure (5.33) P/P_d Causing Yield in Series 4.

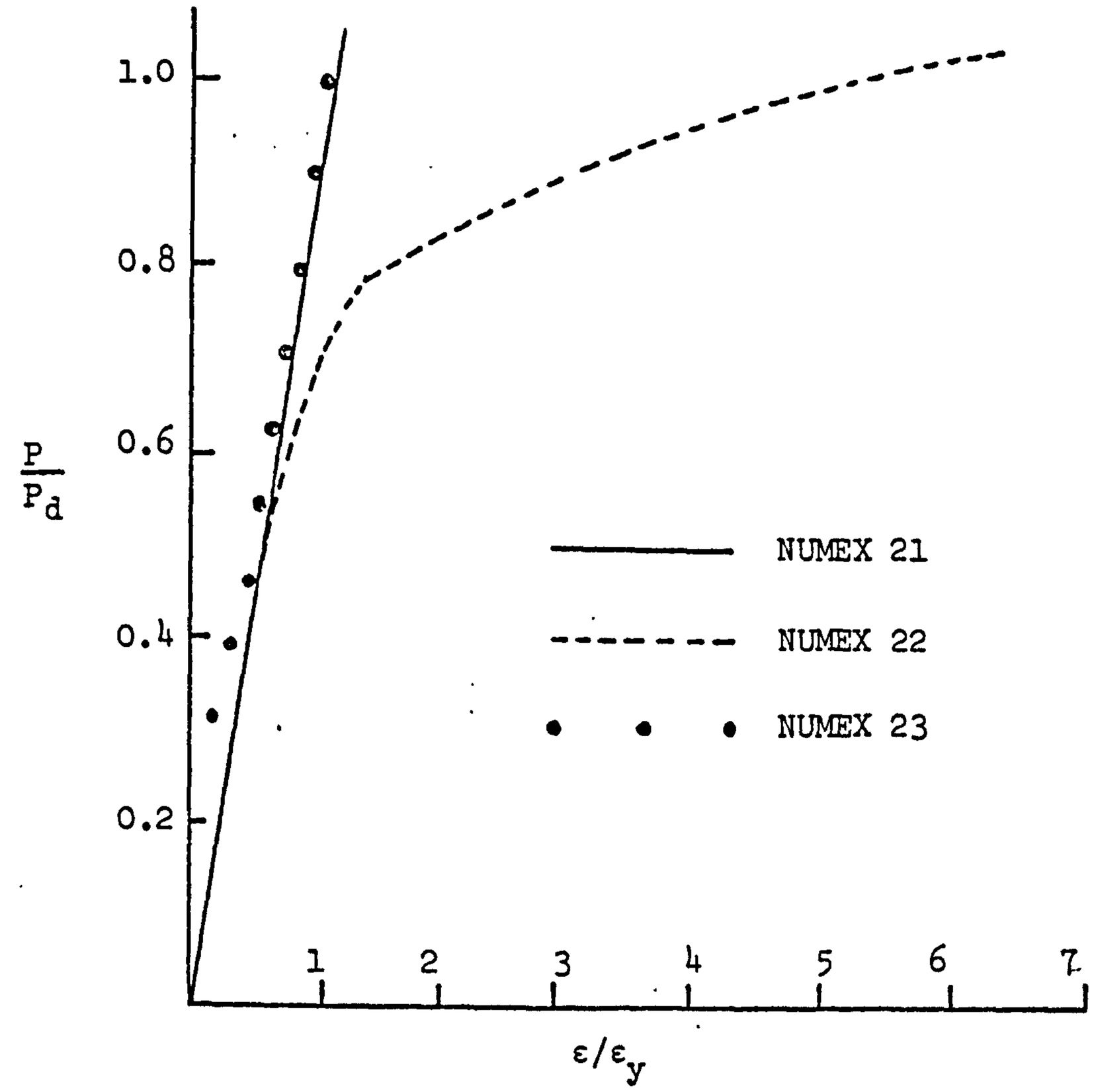

Figure (5.34) Load-steel strains in the supporting beam (mid span section)

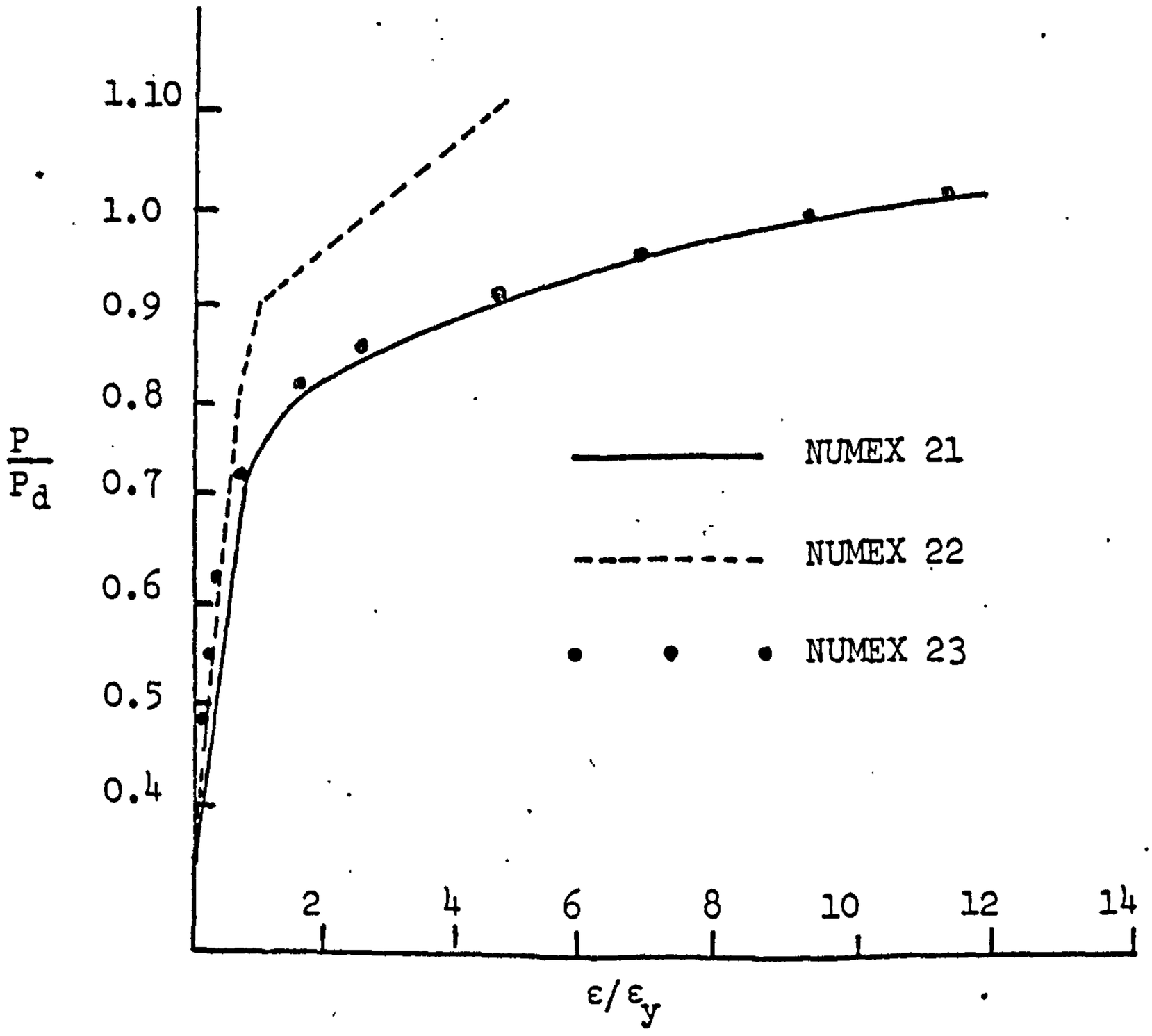

Figure (5.35) Load-maximum steel strains in the slabs in Series 4.

Series	NUMEX	Supports Type	L_x / L_y	L_y (mm)	h (mm)	f_{cu} N/mm^2	f_y N/mm^2	P_d KN/mm^2	$\frac{P_{cr}}{P_d}$	$\frac{P_{\delta L}}{P_d}$	$\frac{P_y}{P_d}$	$\frac{P_u}{P_d}$	Object
4	21	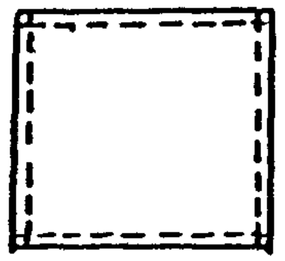	1.0	1900	50.5	35.3	300	20.8	0.26	.53	.66	1.0	Comparison between direct design and yield line theory
	22	"	1.0	1900	50.5	35.3	300	20.8	0.24	.55	.75	1.0	
	23	"	1.0	1900	50.5	35.3	300	20.8	0.26	.60	.68	1.0	
5	15 Hillerborg	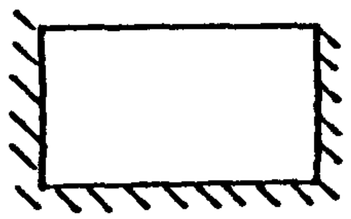	2.0	2000	150	20	300	20	.42	.69	.70	1.12	Comparison between direct design and Hillerborg Method
		"	2.0	2000	150	20	300	20	.47	.73	.86	1.22	

Table (5.7): Results of the Numerical Experiments in Series 4 and 5.

Table (5.8): Comparison of Steel Quantities in the Slab-Beam Systems in Series 4.

	NUMEX 21	NUMEX 22	NUMEX 23
Design Load (KN/m^2)	20.8	20.8	20.8
Method of Design	Direct design for flexure	Yield line * Theory	Direct design for combined flexure and membrane forces (unfilled sandwich model)
Maximum Slab Moment M_s (Nmm/mm)	2800	2880	2344
Maximum edge beam moment M_b (Nmm/mm)	87000	69000	103000
Steel volume in beams (mm^3)	2.606×10^5	2.7×10^5	3.119×10^5
Steel volume in slabs (mm^3)	2.034×10^5	3.392×10^5	1.851×10^5
Total steel volume (mm^3)	4.644×10^5	6.092×10^5	4.97×10^5

* For reinforcement layout in NUMEX 22 see Figure (5.30)

been shown in Section(5.2.3), the design moments in the two cases are quite different.

Results of the nonlinear analysis of the two slabs are given in Figure (5.36), to Figure (5.38), and a summary is given in Table (5.7).

5.4.10 Conclusions

1. The increased amount of steel in the outer strips of(HILLERBORG) had the effect of raising the cracking load of the slab.
2. The service behaviour of both slabs was satisfactory. A deflection limit of span/250 was first reached in NUMEX 15 at 0.69 Pd.
3. In the post yield behaviour, the slab designed by the direct design method (NUMEX 15) behaved in a more flexible way than the one designed by the strip method. Both deflections and steel strains were very much greater in NUMEX 15 than in HILLERBORG. The spread of yield in the two cases was quite different. Yield in HILLERBORG started at loads closer to the design load, and was concentrated on the strips near the free edge. Yield in the inner strips occurred either at or after the design load. In the case of NUMEX 15, yield started on the free edge at 0.65 Pd. Subsequent spread of yield covers most of the slab area, and does not follow a regular pattern.
4. The distribution of the long span moments under the design load is identical to that predicted by the elastic analysis, in the two cases. The other normal moment is quite different in both cases at the design load.

5. Both slabs supported loads in excess of their design load. While NUMEX 15 recorded 12% above the design load, HILLERBORG recorded 22% enhancement at failure.

6. Enhancement in the ultimate loads is caused by the induced compressive membrane force, which was higher in HILLERBORG than in NUMEX 15.

7. In the examples given here, although the proposed direct design procedure requires about 35% more steel than the simple strip method, the slab designed by the strip method behaved in a better way than that designed by the direct design method. The effect is caused by concentrating the reinforcement in the free edge strips in the strip method.

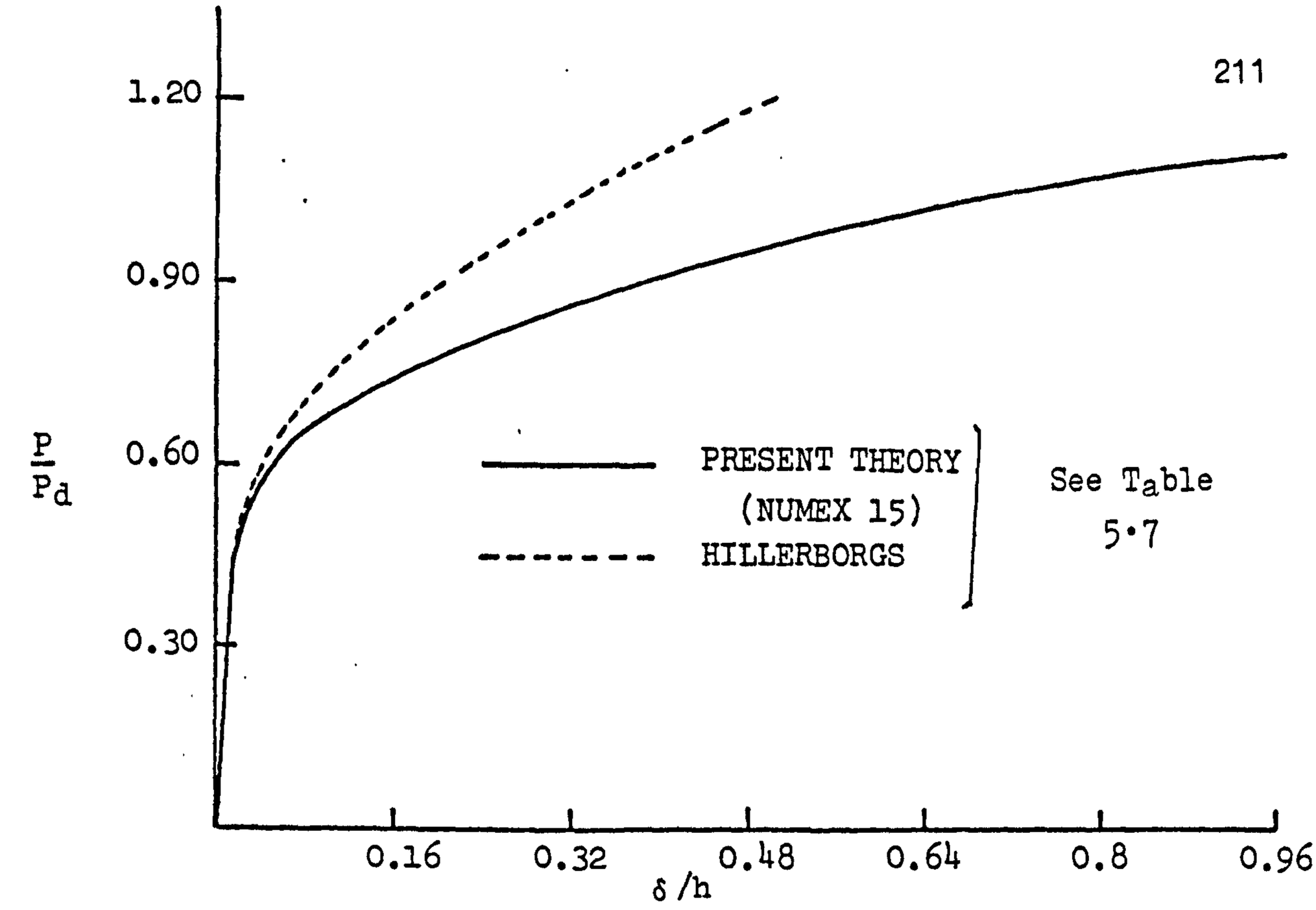

Figure (5.36): Load-Deflection Curves for NUMEX 15 and HILLERBORGS

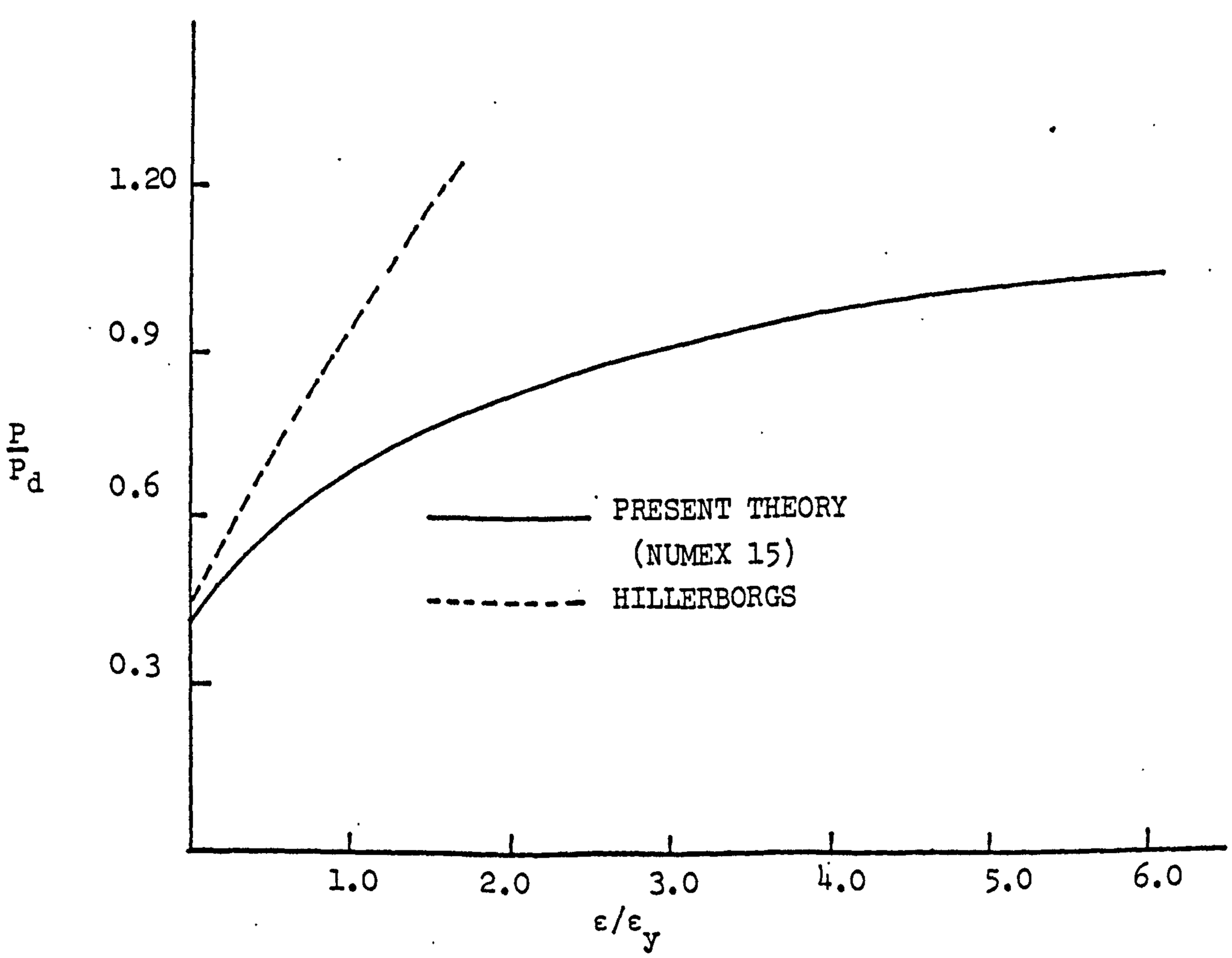

Figure (5.37): Load-Maximum Steel Strain for NUMEX 15 and HILLERBORGS

Free

1.12	.93	.81	.70	.70	.65
	.93	.81	.76	.73	.70
	.96	.88	.81	.76	.73
	1.12	.93	.88	.81	.81
			1.0	.93	.88
				1.12	1.12

Simply Supported — Centre Line

P/P_d Causing Yield in NUMEX 15

Free

0.96	0.90	0.90	0.86	0.90	0.93
0.96	0.93	0.93	0.96	0.93	0.93
1.11	1.11	0.96	1.0	1.0	1.0
			0.93	1.08	1.08
		1.22	1.18	1.18	1.22
1.0	0.96	1.18			

Simply Supported — Centre Line

Simply Supported

P/P_d Causing Yield in HILLERBORGS

Figure (5.38) Yield Spread in NUMEX 15 and HILLERBORGS

CHAPTER SIX

EXPERIMENTAL INVESTIGATION

6.1 INTRODUCTION

The theory given in Chapter Three has been used in the design of the experimental slabs. The work is intended to provide information on the practical problems involved in implementing the proposed design method, and give a clear insight into the behaviour of the models designed accordingly. In this chapter, full account of the experimental work is given.

6.2 PARAMETERS OF STUDY:

Only rectangular slabs have been considered. Large scale models with a minimum dimension of 2000 mm were tested. Since the design procedure would yield a continuously varying reinforcement pattern, the use of such large dimensions is obligatory,in order that the variation in steel can be properly represented. The thickness of all designed slabs was chosen to comply with the limiting span/depth ratios specified by Section (3.3.8) of CP110[5]. A fixed span length of about 2000 mm is used in all the slabs tested, and accordingly, the depth was fixed at 100 mm. The other length of the models was varied from 2000 mm to 3000 mm, covering three sides ratios of 1.0, 1.30 and 1.5.

The support conditions considered included the simple support, point support, and integral slab-beam systems. For each test, the following were recorded:

1. Lateral deflections
2. Steel and concrete strains
3. Crack widths and development of cracks
4. Failure loads.

6.3 SLABS DESIGNATION:

In all, six slabs were tested. Table (6.1) gives the details of boundary conditions and the dimensions of each slab.

Table (6.1) Tested Slabs-designation and dimensions

Test	Designation	Support conditions	Dimensions
1	Model 1	simply supported on all sides	3100 x 2140 x 100
2	Model 2	"	2600 x 2140 x 100
3	Model 3	"	2100 x 2140 x 100
4	Model 4	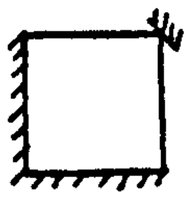	2040 x 2000 x 100
5	Model 5	simply supported on all sides	3100 x 2140 x 100
6	Model 6	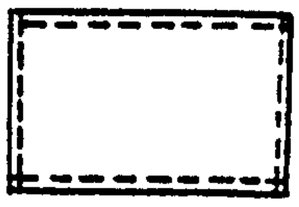 slab-beam system	3120 x 2180 x 100 All beams are 200 x 300 mm monolithic cast.

6.4 DESIGN OF THE MODELS

For a given load, the design moments are obtained by performing an elastic analysis on the slab using the finite element program, and the design equations of Chapter Three. For a given calculated design moments (M^*_x , M^*_y) the reinforcement at any point on the slab is designed according to the limit state theory, with all safety factors on both loads and materials taken as unity, and the design is made according to the assumed stress block shown in Appendix A. This results in a variable reinforcement pattern like the one given in Figure (6.1). The amounts of steel given at any point are per unit

length. Two methods can be used to replace the distributed steel areas by reinforcing bars:

(a) Since the variation of the distributed steel areas is not severe from point to point, these areas can be averaged over a certain width. The total steel area is then obtained by multiplying the average value, by the corresponding width, and hence can be replaced by one bar of an equivalent sectional area.

(b) Over a certain width, the design can be based on the maximum value of the distributed steel areas. Total steel area needed over such a width can thus be obtained by multiplying by the corresponding width.

For the range of problems tested here, the reinforcement in each element was approximately constant, and accordingly, the design was based on averaging the distributed steel areas within each element. This reduces the problem to one of providing reinforcing bars in parallel strips, each having a width equal to the width of one element. The procedure can best be illustrated by the aid of Figures (6.2), (6.3).

Along the strips, the averaging process was done only when the distributed steel areas do not differ by more than 25% of the larger. Normally the variation of steel from element to element along one strip is smooth, as can be seen from Figure (6.2), and accordingly, an average value or a maximum value can be used until the difference exceeds the 25% value of the maximum. In cases where there is a high stress gradient within a strip, as is usually seen in those containing concentrated loads, an average value is used throughout the strip length, and the extra steel needed over the average provided is added locally across the elements containing the load. The average reinforcement in this area is usually carried right to the supports to ensure

adequate transmission of load to the edges.

In cases where no steel is needed over an element, it might still happen that a bar has to be carried on to the supports. This is done in order to comply with code requirements. Such areas are normally found near the supports, where shear stresses might be high, and thus extending some bars in this region is justified as providing increased shear resistance. Since the program does not take shear stresses into account, a check has to be made to ensure that the slab will not have a premature shear failure. Accordingly, the shear requirements of Section (3.3.6) in CP110[5] were followed. In one case, shear reinforcements had to be provided over the concentrated corner support of model 4.

Torsional reinforcement was also needed for the supporting beams in model 6. The flexural reinforcement in the beam was provided by the finite element program, but the additional torsional steel had to be provided in accordance with Section (3.3.7) of CP110[5]. Shear reinforcement in the form of stirrups was only provided in the supporting beams of model 6, according to CP110.

One important factor in choosing the reinforcing bars is the bond stress. The designer may have to change the layout of the bars more than one time, until he is sure that the permissible bond stress is nowhere exceeded. In this work, each bar was hooked at both ends, and was adequately secured so that the bars formed a strong mesh, and the bond requirements of Section (3.11.6) of CP110[5] were strictly followed.

In trying to achieve a reinforcement distribution close to that required by the elastic analysis, and at the same time to comply with the code regulations, the total steel volume provided is in general

much more than what is required. Table (6.2) gives a comparison between the theoretical steel needed and that provided for the six models tested in this investigation. Figures (6.4) to (6.9) give the reinforcement provided in each model.

6.5 MATERIALS

Cement: Ordinary Portland Cement was used in all tests.

Aggregates: Hynford sand and gravel were used for all mixes. The maximum size of the uncrushed gravel used was 10 mm, and the sand grading was Zone 2.

Concrete mixes: The concrete mixes were designed to give an average cube strength of 40 N/mm^2 at 28 days. Two mixes with the same strength but different workabilities were used. A medium workability mix was used for the models for which the mix was produced in the laboratory, and a high workability was used for ready made mixes, supplied by a ready mix Company, and was used to cast models Nos.1, 5 and 6. These models had very large sizes, and therefore it was convenient to use ready made mixes rather than make the concrete in the laboratory. For the other models, the mix is produced in 14 to 18 batches of 70 kg each.

For each model, the control specimens were eight 100 mm cubes and eight 150 mm diameter cylinders. Half the control specimens was cured in water, the other half was kept near the model under a polythene cover.

All control specimens were tested on the same day as their respective models.

Standard tests to determine the cube compressive strength, cylinder splitting tests, and the static modulus of concrete were

conducted according to the British Standards[61], No. BS.1881:1970. The concrete tensile strength obtained from the cylinder splitting test as

$$f_t = \frac{2P}{\pi DL}$$

as shown in Figure (6.10). Average values for the materials properties for each model were calculated and are given in Table (6.3).

Reinforcement: High yield deformed bars were used in all models, except model 6. Because a considerable amount of reinforcement involving different bar sizes have been used, only certain random samples were cut off from the batches of the steel bars for different sizes, and were tested in an Oslen testing machine, fitted with an S-type electronic extensometer. The testing procedure followed the manufacturer's instruction manual. The yield point for the high yield steels used was taken as the proof stress corresponding to 0.2% strain. Figure (6.11) gives the stress-strain curve for the type of steel used. Tests on several bars gave an average yield point of 473 N/mm^2, and an initial modulus of 214 KN/mm^2 .

For model No.6, the amounts of reinforcement in the slab was very small, due to the effect of surrounding beams. Since the smallest available bar diameter was 8 mm for high yield steel, it was discarded, and mild steel was used instead. The stress-strain curves for the type of steel used is given in Figure (6.12). Average values obtained were 300 N/mm^2 for the yield point, and 214 KN/mm^2 for Young's modulus.

6.6 STRAIN GAUGES:

Prior to casting each model, strain gauges were attached to the reinforcing bars. The strain gauges used were electrical resistance

gauges of the type EA-06-250BG-120 with 120.0 Ω ± 0.15% resistance and 2.095 ± 0.5% gauge factor at 75°F. The gauges are made of a thin foil of Constantan in combination with a tough, flexible, polyimide backing. The constantan alloy is made in self temperature-compensated form. The strain gauges were attached to the reinforcing bar after filing off the ribs of the bar, and were bonded using an M-bond 200 adhesive following the manufacturer's instructions. The connection wires are then soldered to the strain gauges and were protected against humidity and temperature by an air drying acrylic M-coat-D after the connections have been thoroughly checked. To protect the gauges against mechanical damage during the casting process, the gauges were coated with Araldite rapid hardening epoxy adhesive. The strain gauges were then connected to a data logger.

6.7 CASTING AND CURING:

After fixing the strain gauges on the steel, the reinforcing mesh was assembled on the form after the proper positions of the bars have been marked by a marking pen. Each model was then cast in several batches of concrete, and was properly compacted using an immersion type vibrator. When casting and compacting was complete, the model was left for about 5 hours to dry in the open air. The position of the holes on the model were checked by measuring the positions of the bolts provided for that purpose. These bolts would later be used to lift the model from the framework to the loading rig, and the holes which they leave on the model were later used for loading the slab.

After the concrete has set, the whole of the model together with the control specimens were then covered with a polythene cover, to

control the humidity. The cover is then removed after three days from the day of casting, and left to dry in the natural conditions of the laboratory. The model was lifted off the forms after a further five days using the electric crane in the laboratory, and was placed over the load supports.

6.8 SUPPORTS

The simple support system used for the first five models consisted of two steel flats 12 mm thick separated by a round 25 mm diameter black invar bar as a roller, Figure (6.13a). This supports system extends over the whole length of the model, except at the corners. Proper seating of the slab on the supports was effected by applying a thin layer of gypsum plaster between the flats and the slab.

For a slab supported all around and transversely loaded, the corners are liable to lift up, and might thus reduce the ultimate capacity of the slab. To prevent this, all corners were held down using a separate "corner supports". This supports system, shown in Figure (6.13b) consisted of a system of orthogonal flats-rollers to provide free rotation in all directions just like a ball seat, and a high tension steel bar 5 mm in diameter passing through the orthogonal flats-rollers system at their midpoint. The steel bar had an ultimate strength of 1750 N/mm^2, and was made to pass through a hole in the slab corner provided at the time of casting, then through the orthogonal flats-rollers system, and was anchored to the loading rig. Figure (6.14) shows the corner arrangement in one of the models. Spreader plates were used on the top surface of the slab corner to prevent high shear stresses resulting from the corner pulls. To keep the corner arrangement intact, the steel bar in the arrangement

was slightly pretensioned before the start of the test.

Each slab allowed 100 mm overhang beyond the centreline of the support. The slabs dimensions given in Table (6.1) are gross values. The effective dimensions are obtained from these by subtracting the overhang over each support.

For Model 6, the beams which were monolithically cast with the model, were supported by sets of orthogonal Vees-rollers and orthogonal flat-rollers at alternate corners. The system is so arranged that each beam will act as if it were pinned at one end and freely supported at the other, Figure (6.15).

6.9 LOADING RIG AND LOADING SYSTEMS:

All models were tested on the loading rig shown in Figure (6.16). The rig was designed for testing slabs subjected to lateral loads only. It was designed to support slabs with various sides ratio including 1.0, 1.25, 1.50, 1.75 and 2.0. The longer span can vary from 1 m up to 3.0 metres. The rig was made of universal steel beams and stanchions, and was designed to support loads up to 600 KN, with a safety factor of 1.5. A height of 1.5 m under the slab bottom surface is provided by the rig, to facilitate studying the bottom surface of the tested models.

Loads were applied as concentrated loads. This was done by using loading cables passing through holes provided in the slab at the time of casting, and corresponding holes in the floor of the laboratory. The loading cables were high yield prestressing 7-wires tendons, having an ultimate strength of 150 KN. According to the total load applied on each model, the methods of load application can be divided in the following manner:

(1) Two points system:

This was used for model 4 and consisted of one loading cable passing through a hole at the centre of the model. The cable transmits its load to the slab at two points 500 mm apart, using a short simply supported spreader beam.

(2) Four points system:

This was used for model 3 only. In this case, four loading cables, symmetrically arranged about the model centre lines, were passed through four holes in the slab. The cables were then anchored on the top surface of the model, and a spreader flat 200 mm x 200 mm x 10 mm was used to distribute the load at each point.

(3) Eight points system:

This system is a combination of the previous two systems. Each of the four loading cables transmits its load at two points by a spreader beam. Accordingly, the load on the slab is applied at eight points, using only four cables. This system of loading was used for the rest of the models. The loading systems are shown in Figure (6.17).

Each loading cable is tensioned by a 20 ton-hydraulic jack resting against the bottom surface of the floor of the laboratory. Each jack was connected via hoses to a regulating electric pump, capable of sustaining up to 10000 psi of oil pressure. The four hoses were connected to the pump at one connection point, using a distributor. This arrangement was made to ensure equal pressure distribution in the four jacks, and would thus eliminate unequal frictional effects on the separate jacks.

Loads on the top surface of the slabs were measured using 50 tons

electrical load cells.

Prior to tests the load cells were calibrated. Each loading cable was passed through a load cell and, was anchored on its top using a flat spreader. Figure (6.18) shows the details of the loading arrangement.

Corner reactions were also measured using small electrical load cells of 5 tons capacity each. All the load cells are then connected to a load amplifier, and further to a data logger.

6.10 FURTHER INSTRUMENTATION:

Deflections were measured by electrical transducers, which were linear displacement potentiometers manufactured by Nouatech of Surrey. The transducers were mounted on an independently supported measuring frame. Transducers capable of measuring up to 50 mm were used. Each transducer was then given an identification number and was then connected to the data logger for data processing. A cross check for the transducers is provided by a dial gauge located under the slab bottom at the centre. The dial gauge used was capable of measuring up to 50 mm, reading up to 0.01 mm.

The data logger was used to measure the loads, the strains and deflections. This was an IBM 5000 type which has an MB-Metals 200 channels data logger controlled by a PDP8 computer using the language FOCAL. Programs were written to process the results of each test. The output at each loading step consists of the load values read on the load cells in DVM (Digital Voltmeter) units, deflections in (mm) measured by the transducers, and then the strains in micro mm/mm. The DVM units are later converted to loads using the calibration curves for each load cell.

The underside of each test model was illuminated using four powerful light sources. Cracks on the bottom surface of the slab were monitored with the aid of a magnifying glass. Crack widths were measured under the load points,using a crack measuring microscope, reading up to 0.01 mm.

6.11 TEST PROCEDURE:

All electrical connections were first checked by the computer. Deflection transducers were then checked to ensure that they were truly vertical, and they would operate properly under test. The strain gauges were also checked and defective ones were immediately disconnected. The load cells were also checked by applying a small load to the slab, and then unloading. Leaks on the hoses and the jacks also appear during the initial test loading and unloading, and if detected, they were soon remedied. When all primary checks have been made, the test was started by applying the load in increments of 5 KN per load cell. An amplifier read the loads on the load cells, and when the desired load level was reached, the computer was started for a complete scan. Results for this load increment were then printed. The loading was maintained for about 10 minutes, while the underside of the slab was studied for cracks. The dial reading was also taken at this stage. The pump was started, a new load increment was applied, and the whole procedure was repeated until the ultimate load was reached.

Slab Designation	Theoretical Steel Volumes (M^3)			Volumes of Steel Provided (M^3)		
	Top	Bottom	Total	Top	Bottom	Total
Model 1	0.00101	0.00567	0.00668	0.00152	0.0068	0.00832
Model 2	0.00045	0.00228	0.00273	0.00143	0.00353	0.00496
Model 3	0.00034	0.00174	0.00208	0.00089	0.00278	0.00367
Model 4	0.00019	0.00173	0.00192	0.0010	0.0030	0.0040
Model 5	0.00055	0.00277	0.00332	0.00083	0.00454	0.00537
Model 6	0.000424	0008	0.00843	0.0028	0.0113	0.0141*

*This includes additional torsional steel in the supporting beams

Table (6.2) Comparison between the theoretical steel and that actually provided in the test slabs.

Slab Designation	Design Load KN	f_{cu} N/mm^2	f_t N/mm^2	E_c KN/mm^2	f_y N/mm^2	E_s KN/mm^2	Slab Dimensions (mm)
Model 1	417.5	55.6	3.41	25.6	473	214	3100 x 2140 x 100
Model 2	216.0	43.0	3.68	21.5	473	214	2600 x 2140 x1100
Model 3	213.3	46.1	3.40	21.5	473	214	2100 x 2140 x 100
Model 4	90.0	37.3	2.97	20.4	473	214	2040 x 2000 x 100
Model 5	217.5	43.7	2.83	19.2	473	214	3100 x 2140 x 100
Model 6	188.6	48.3	3.15	21.6	300	214	3120 x 2180 x 100 + Beam Ribs 200 x 200

Table (6.3) Dimensions and materials properties of test slabs

	355	255	255	250	250	185
145	.089 .152	.186 .343	.342 .506	.429 .652	.477 .739	.512 .772
145	.182 .252	.257 .440	.388 .595	.492 .763	.489 .809	.519 .837
145	.273 .345	.332 .542	.466 .742	.549 .924	.489 .921	.524 .973
178.3	.365 .431	.417 .607	.560 .809	.502 .836	.496 .888	.410 .809
178.3	.444 .488	.479 .596	.424 .650	.452 .620	.379 .581	.287 .482
278.3	.481 .496	.482 .519	.451 .490	.360 .410	.245 .305	.134 .192

C.L.

C.L.

LEGEND

Top figures represent x steel while bottom figures represent y steel

e.g.
0.481 = x steel
0.496 = y steel

Figure (6.1) Distributed Steel in Model 1

(N.B. Quoted are elemental values averaged from 4 Gauss points in each element)

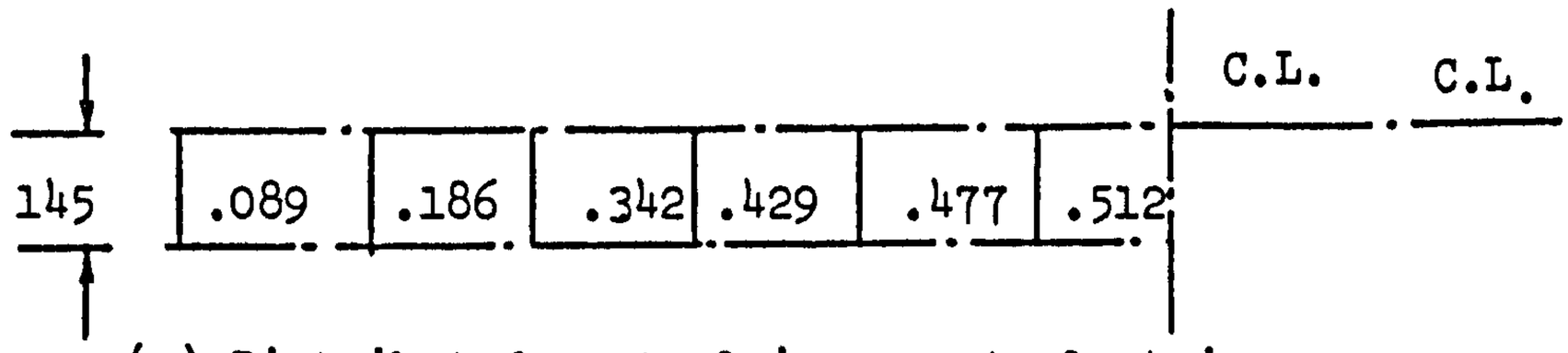

(a) Distributed x steel in a central strip.

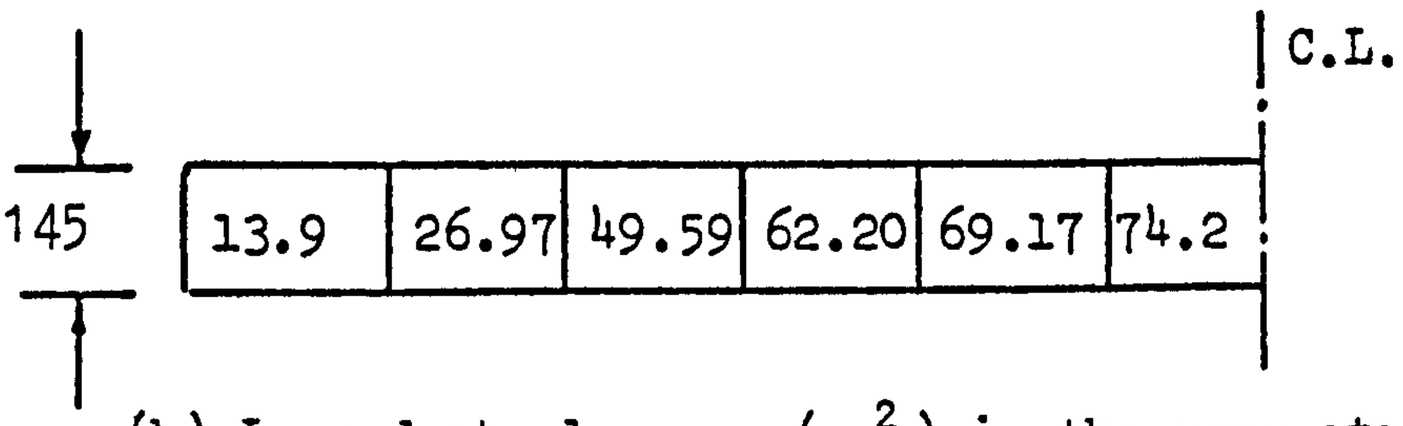

(b) Lumped steel areas (mm^2) in the same strip.

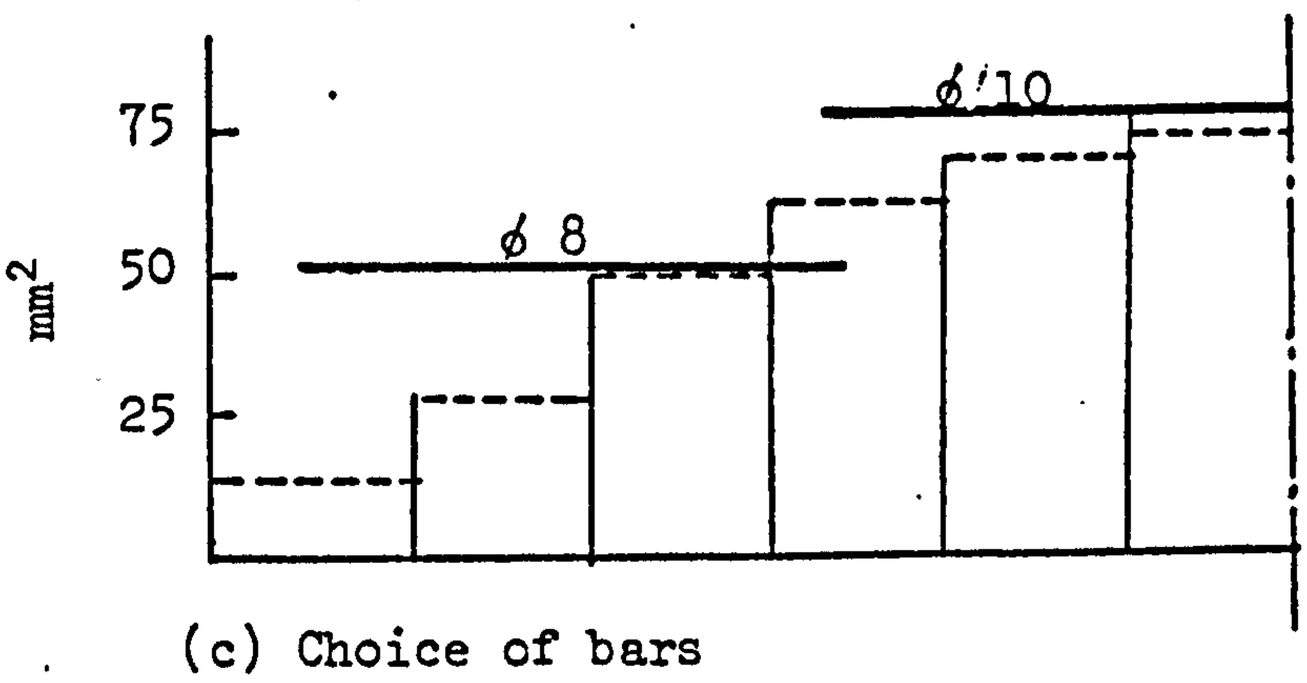

(c) Choice of bars

Figure (6.2) Design of x steel in a central strip

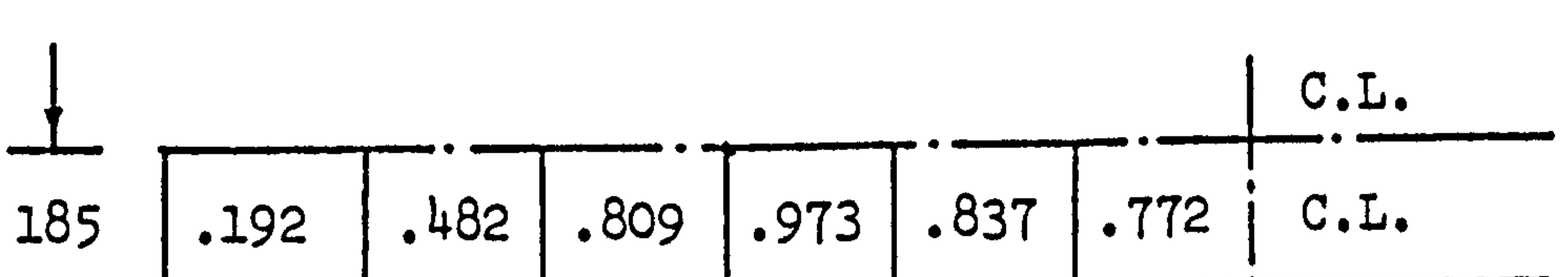

(a) Distributed y steel in a central strip

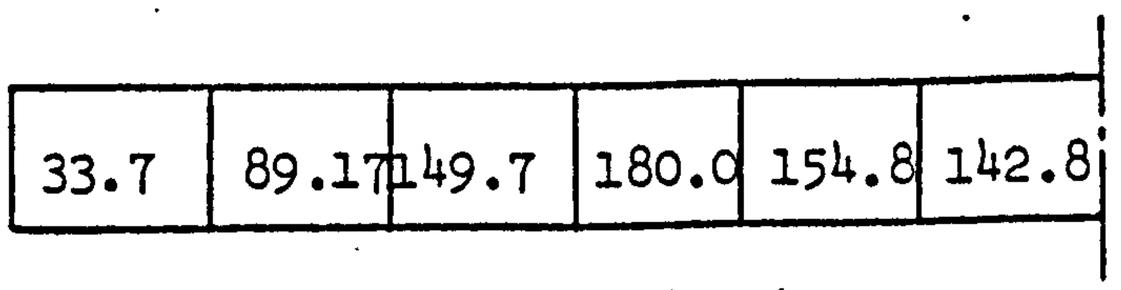

(b) Lumped steel areas (mm^2) in the same strip

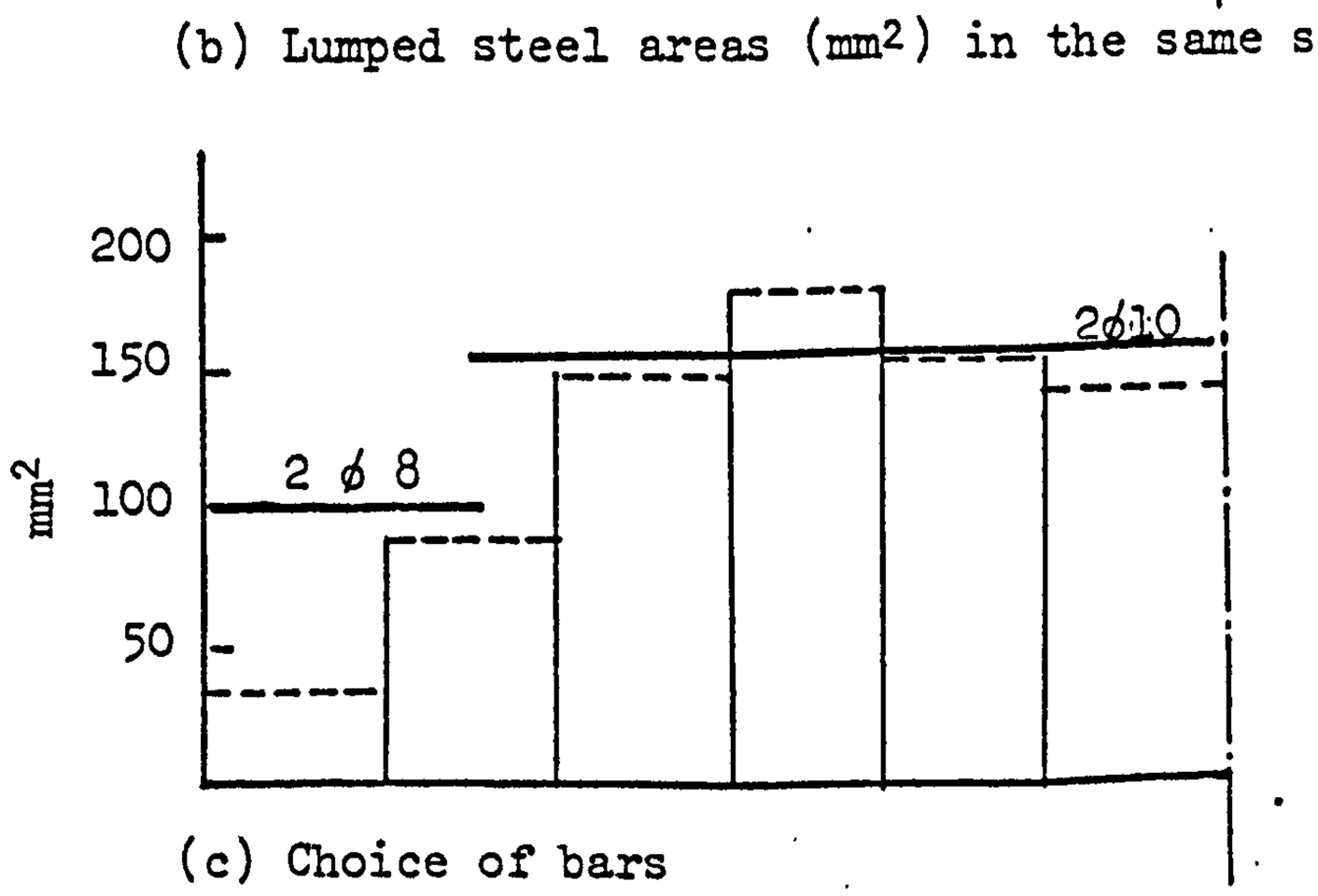

(c) Choice of bars

Figure (6.3) Design of y steel in a central strip

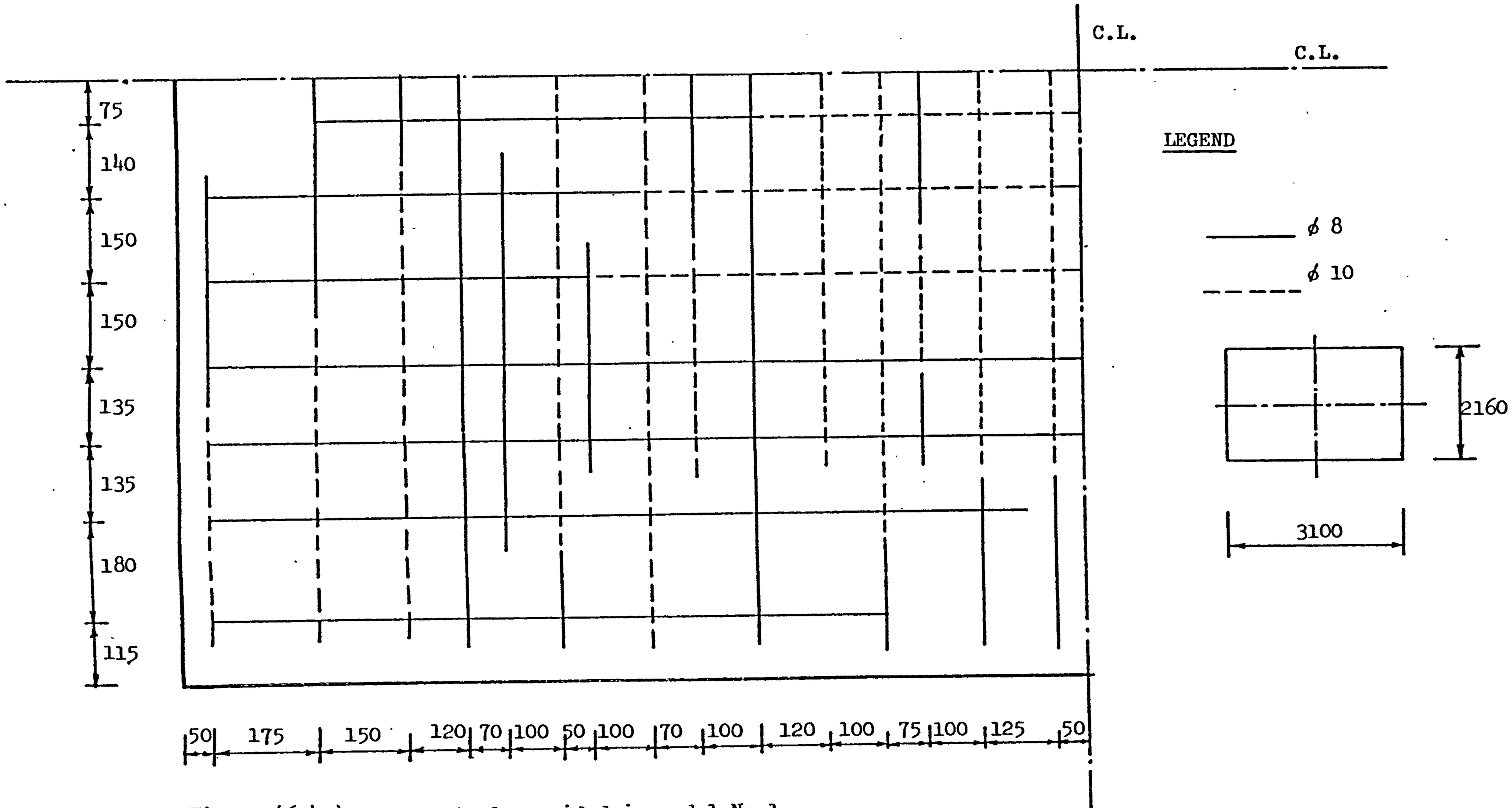

Figure (6.4a) Bottom steel provided in model No.1

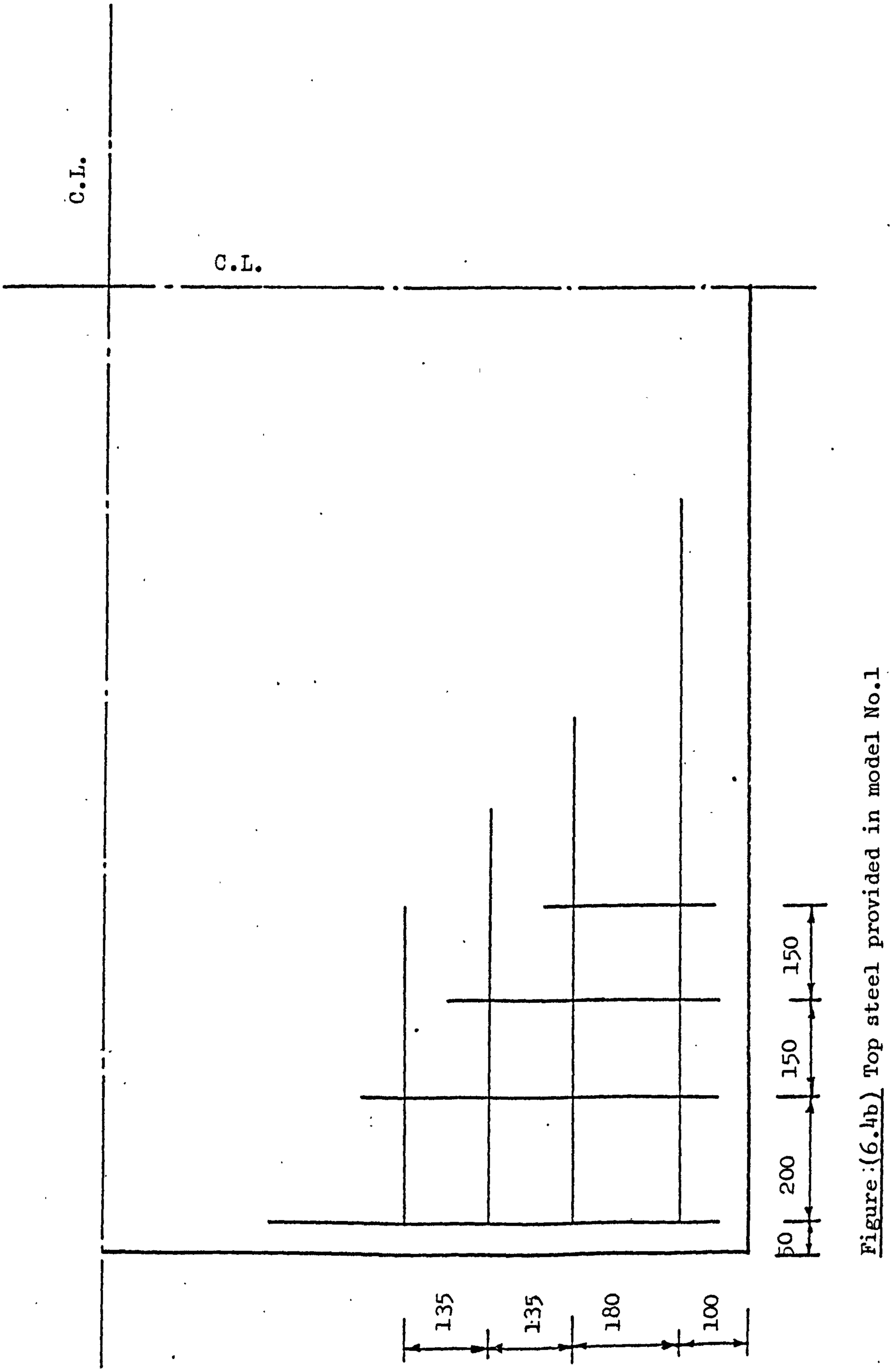

Figure:(6.4b) Top steel provided in model No.1

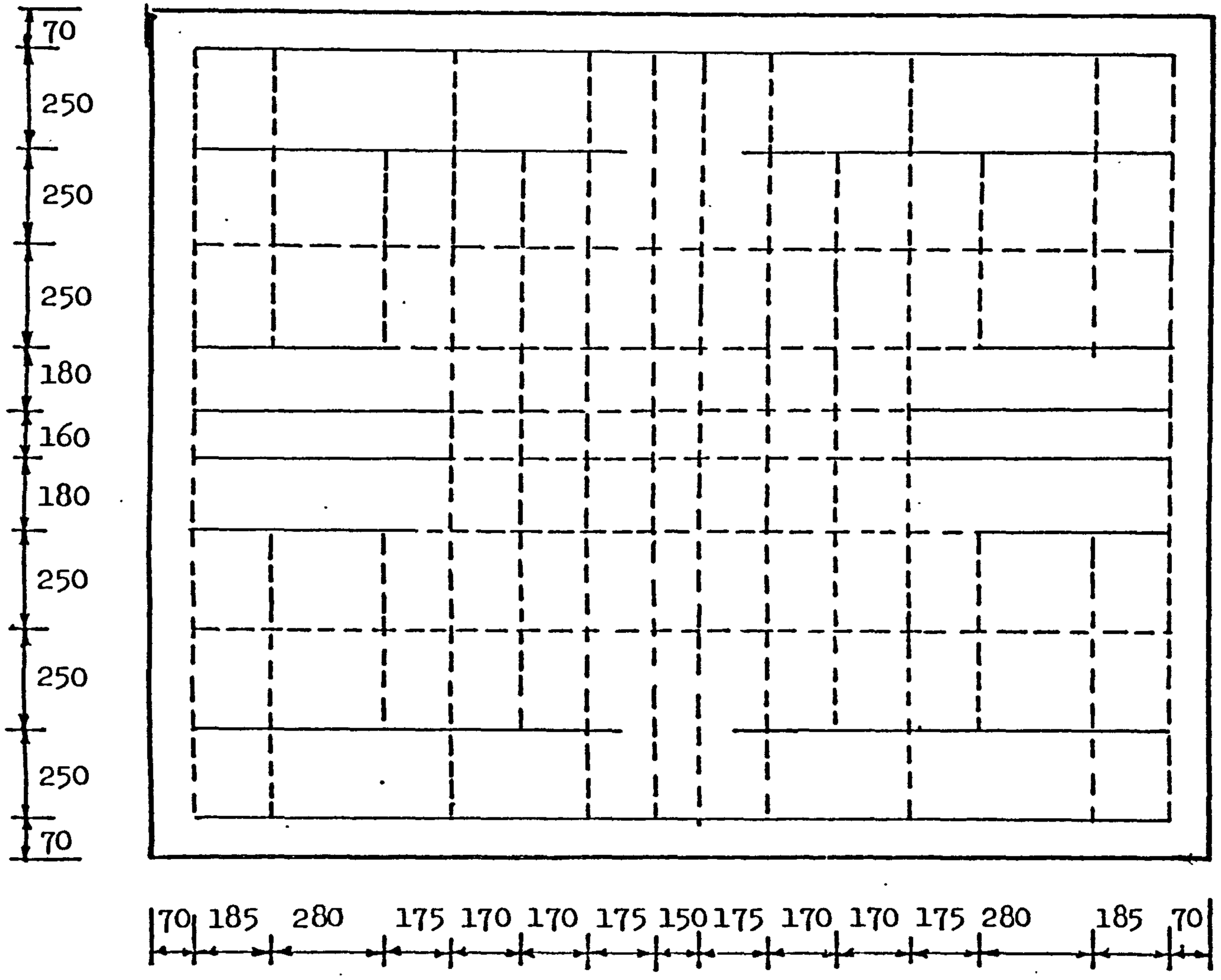

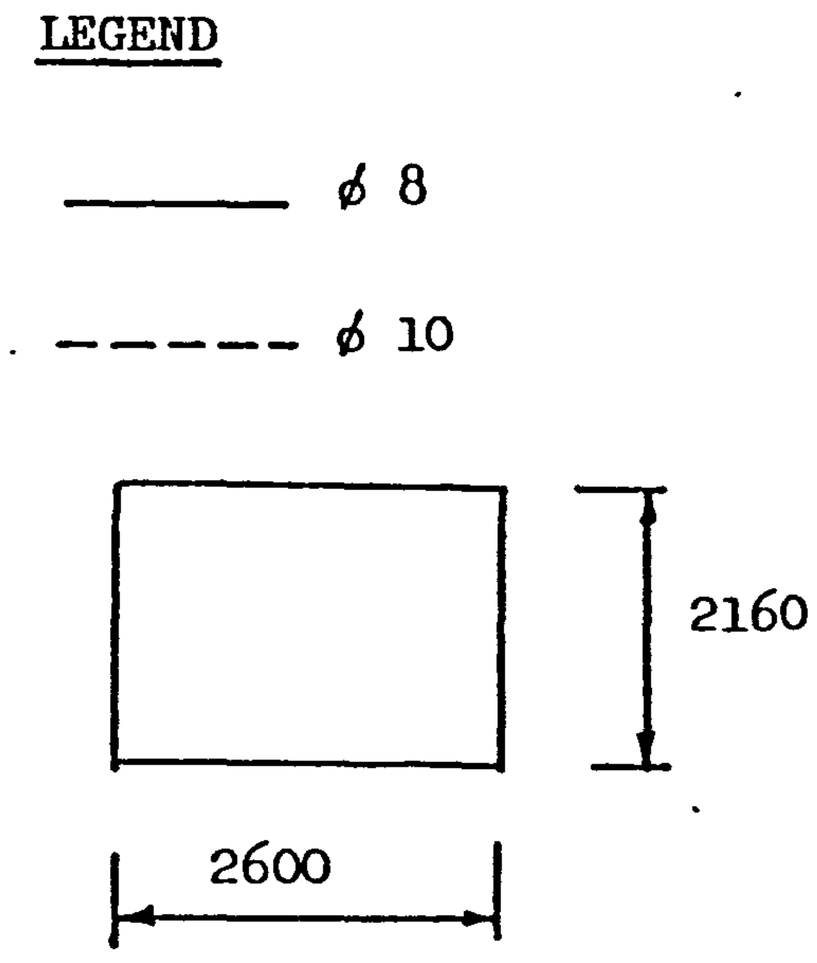

Figure (6.5a) Bottom Steel in Model No.2

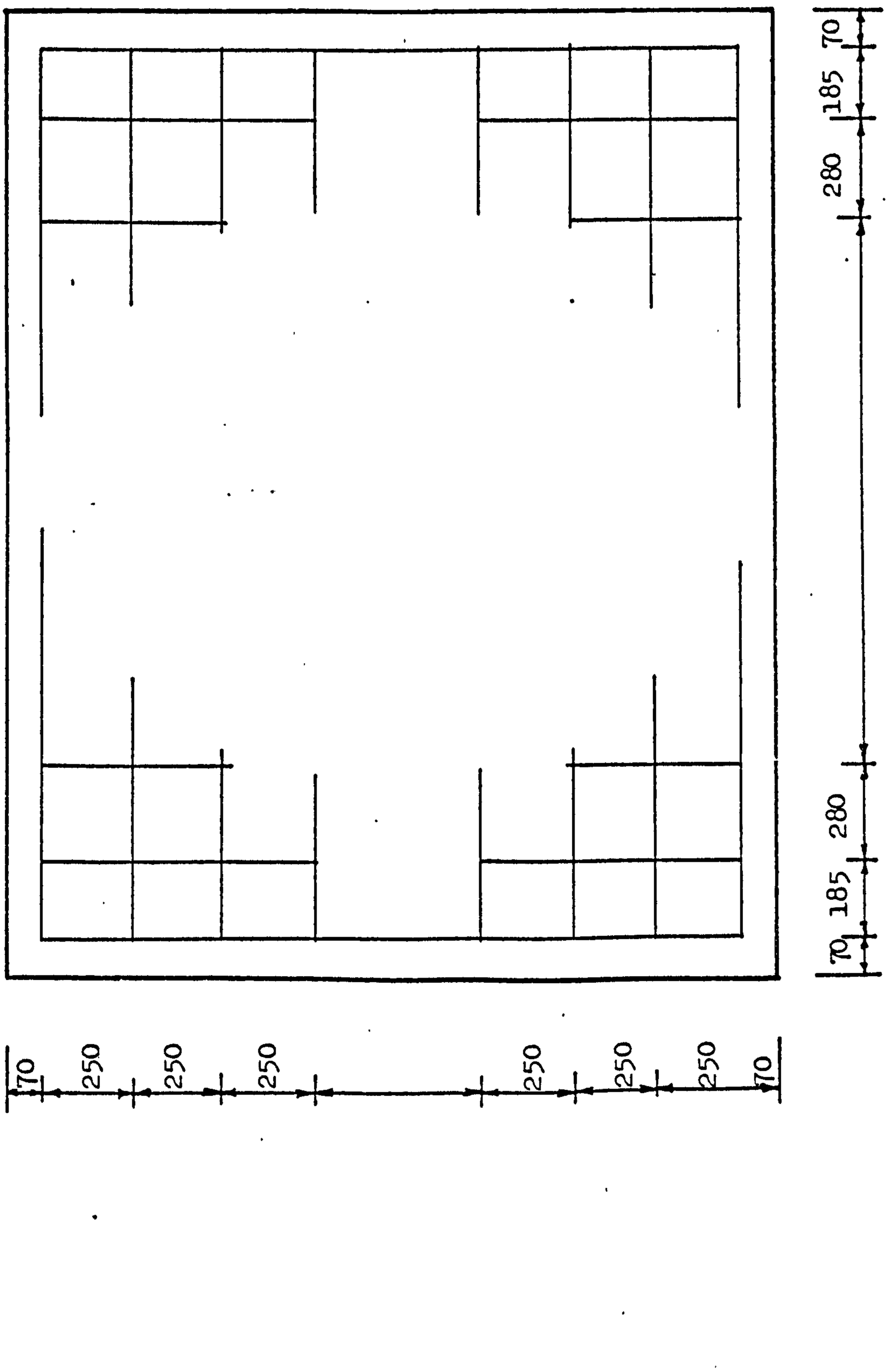

Figure (6.5b) Top Steel in Model No.2

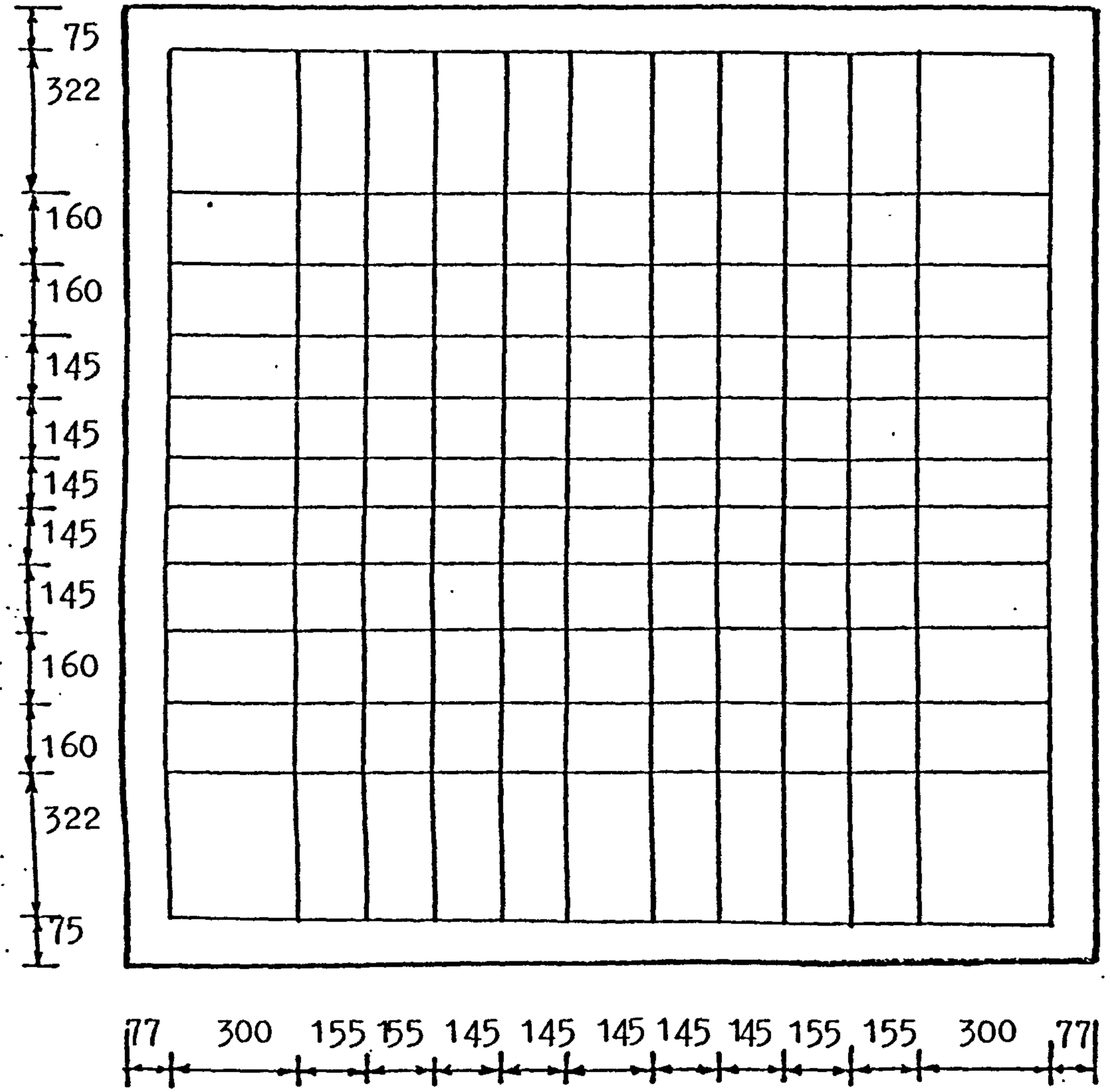

Figure (6.6a) Bottom Steel in Model No.3

LEGEND

All Bars are ∅ 8

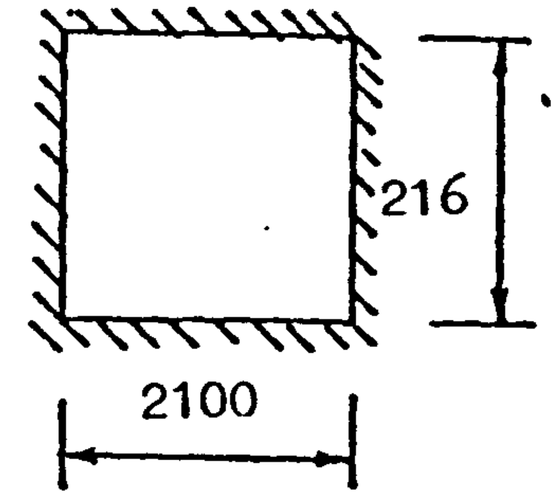

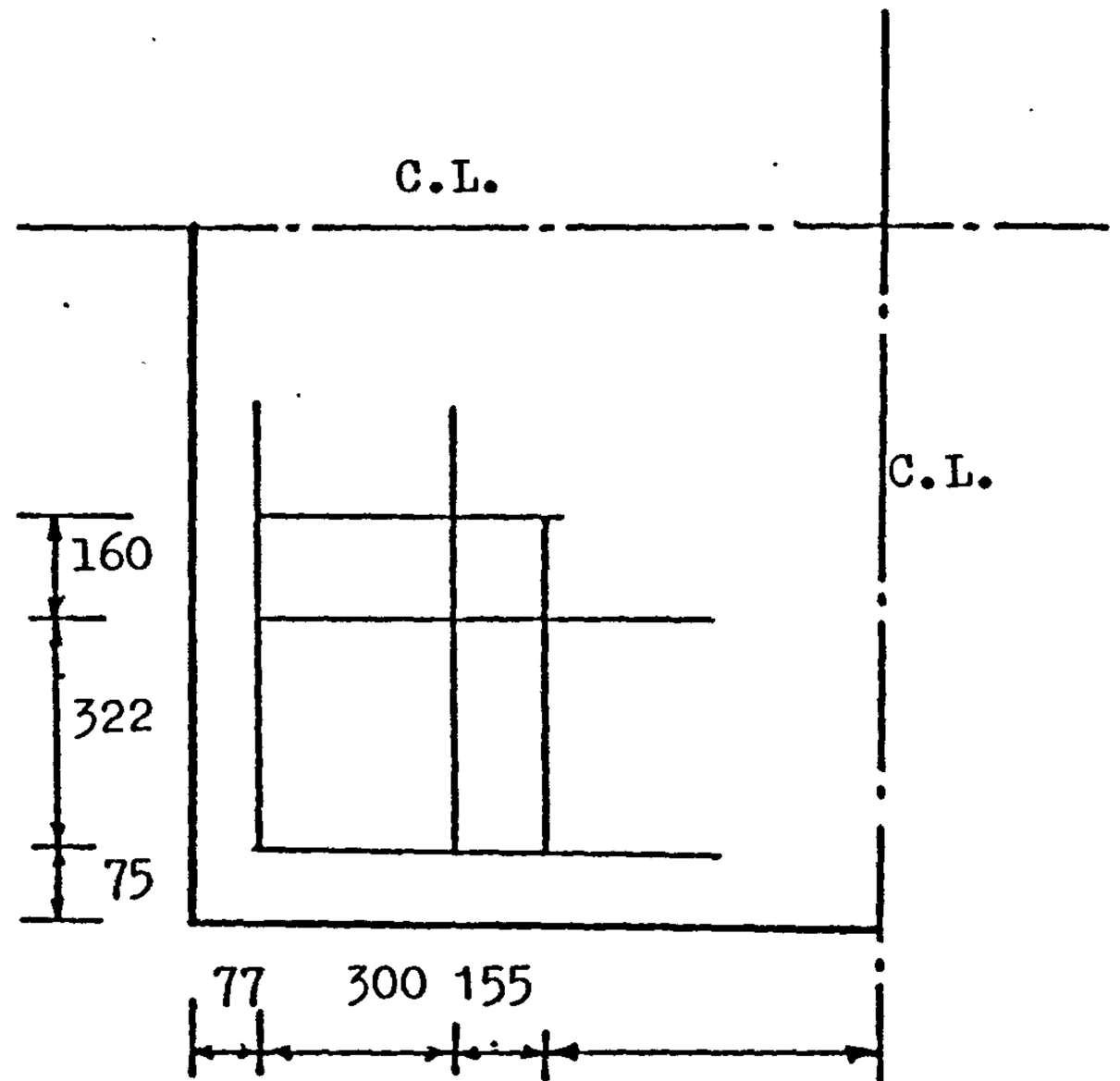

Figure (6.6b) Top Steel in Model No.3

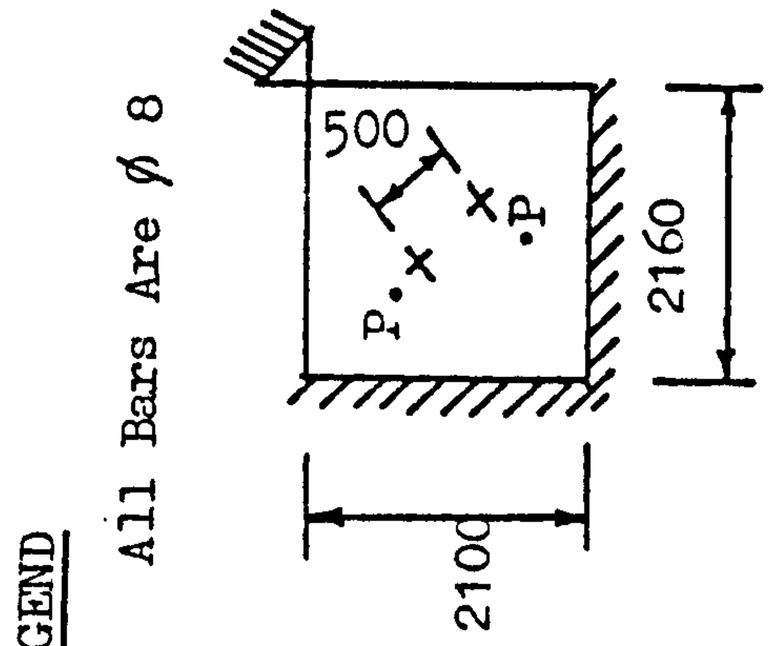

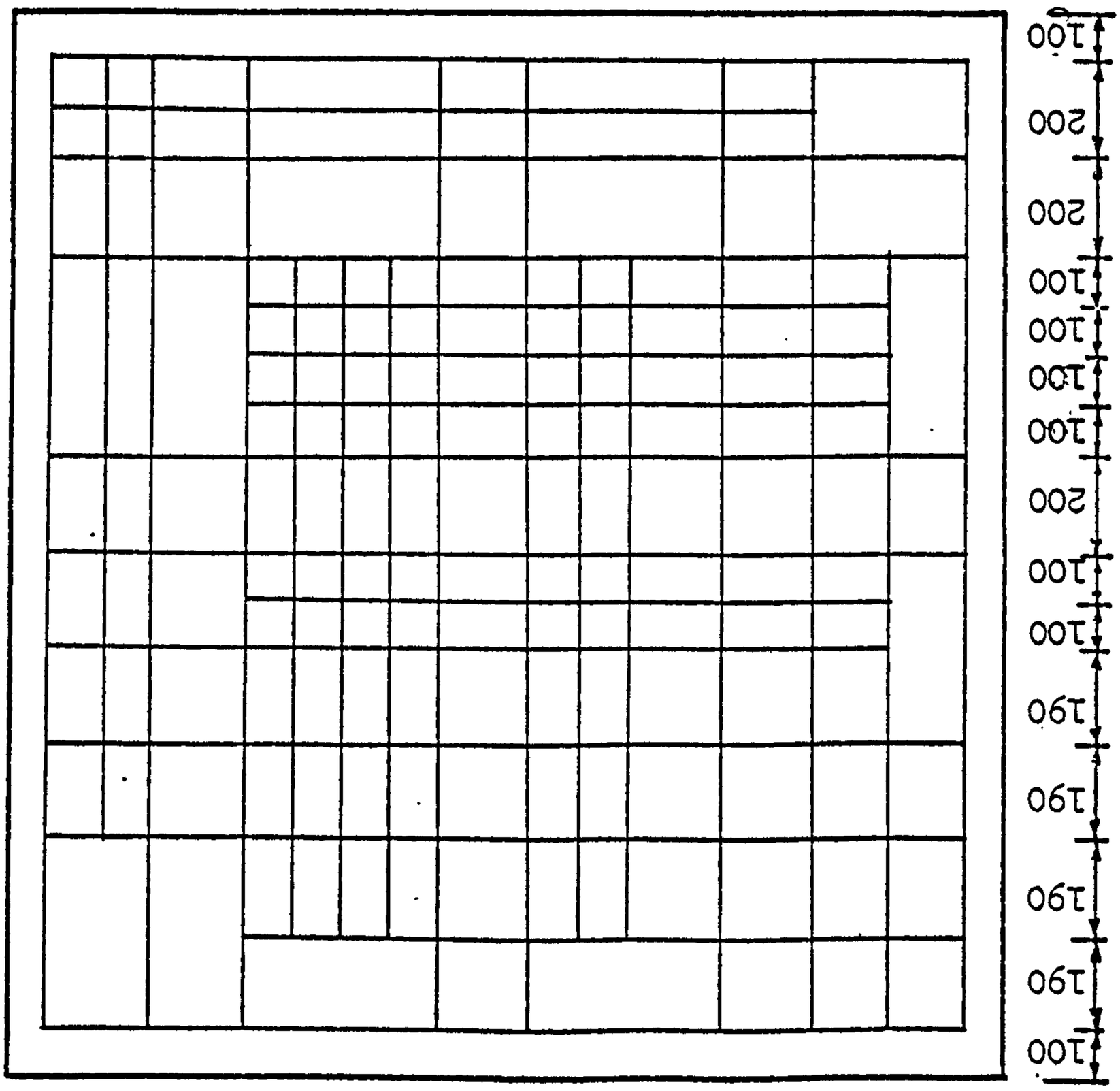

Figure (6.7a) Bottom Steel in Model 4

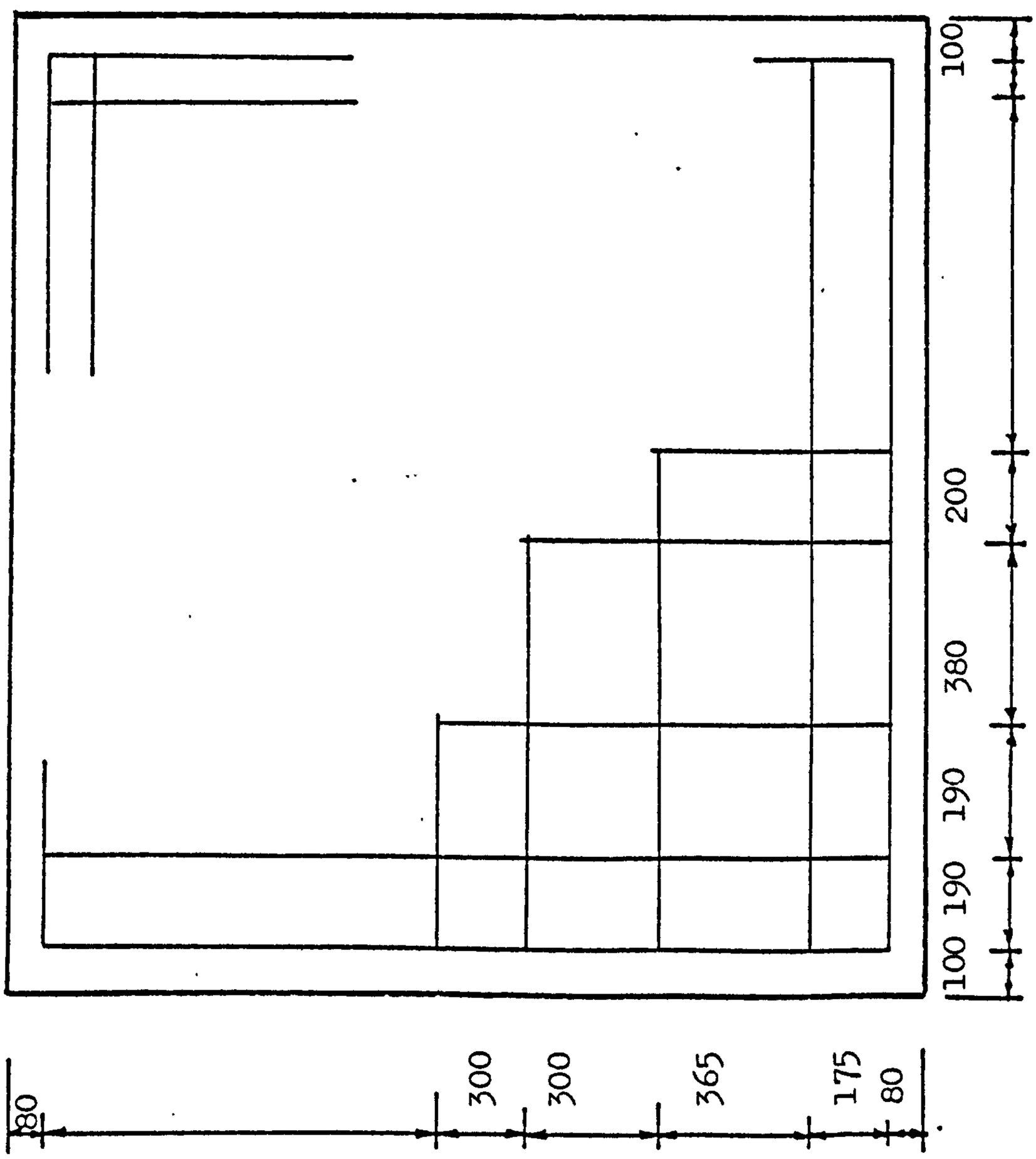

Figure (6.7b) Top Steel in Model No.4

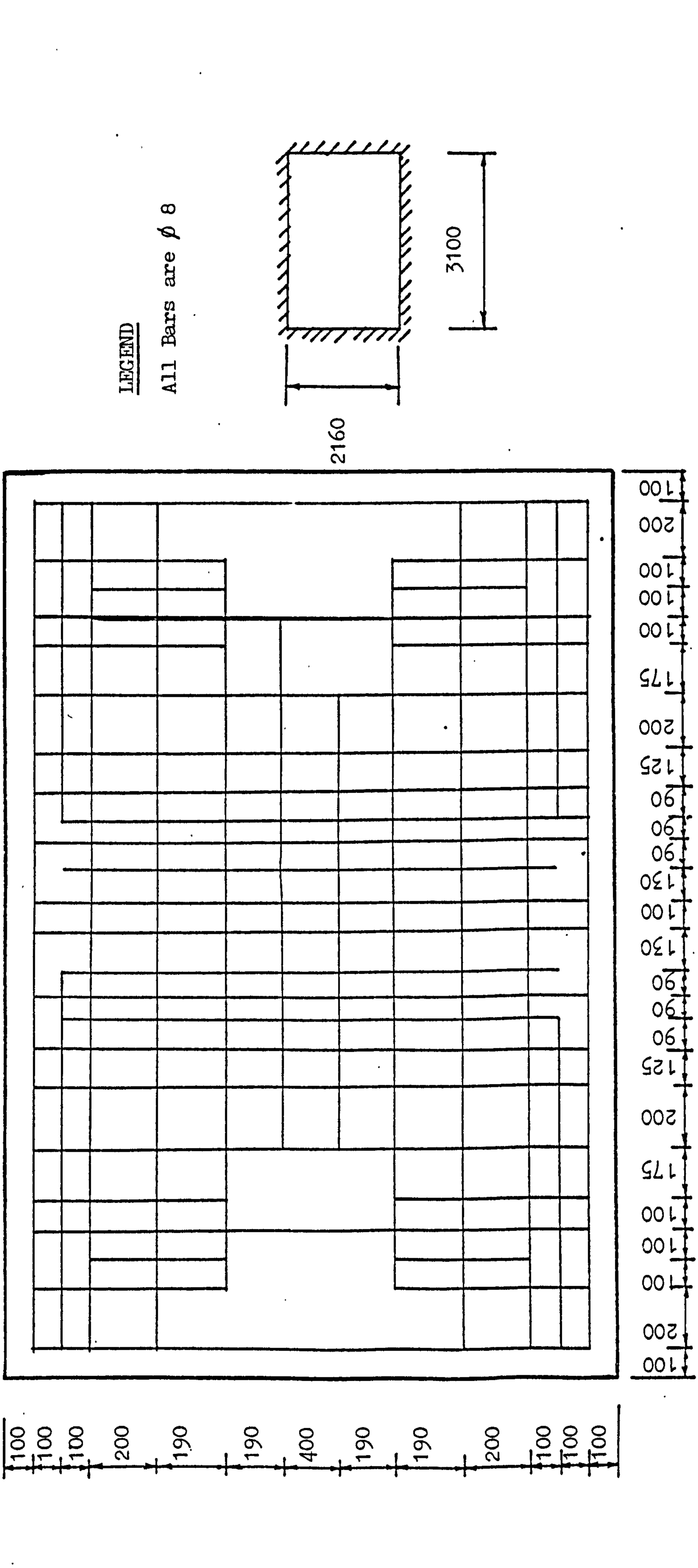

Figure (6.8a) Bottom Steel in Model No.5

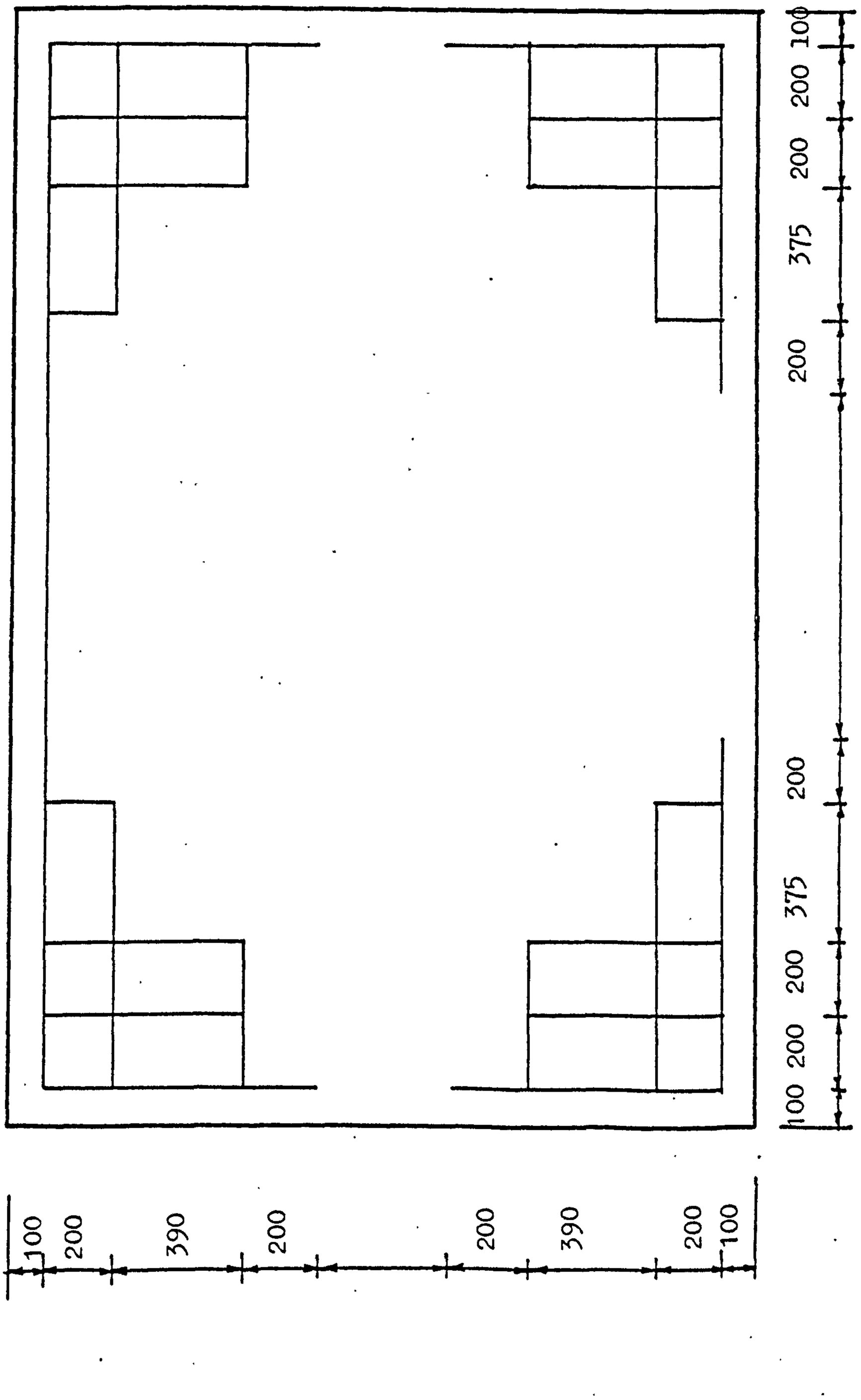

Figure (6.8b) Top Steel in Model No.5

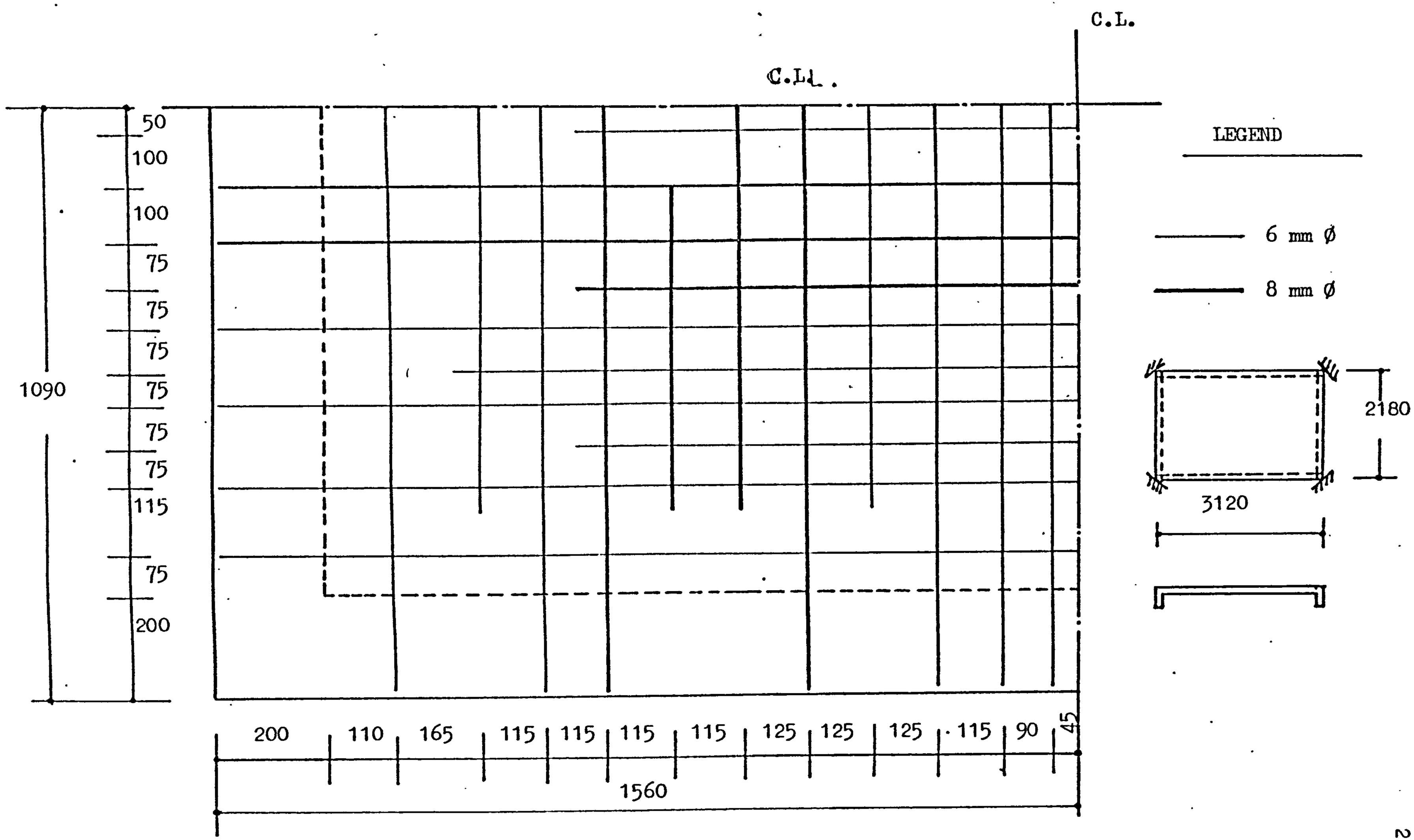

Figure (6.9a) Bottom steel in the slab of Model 6

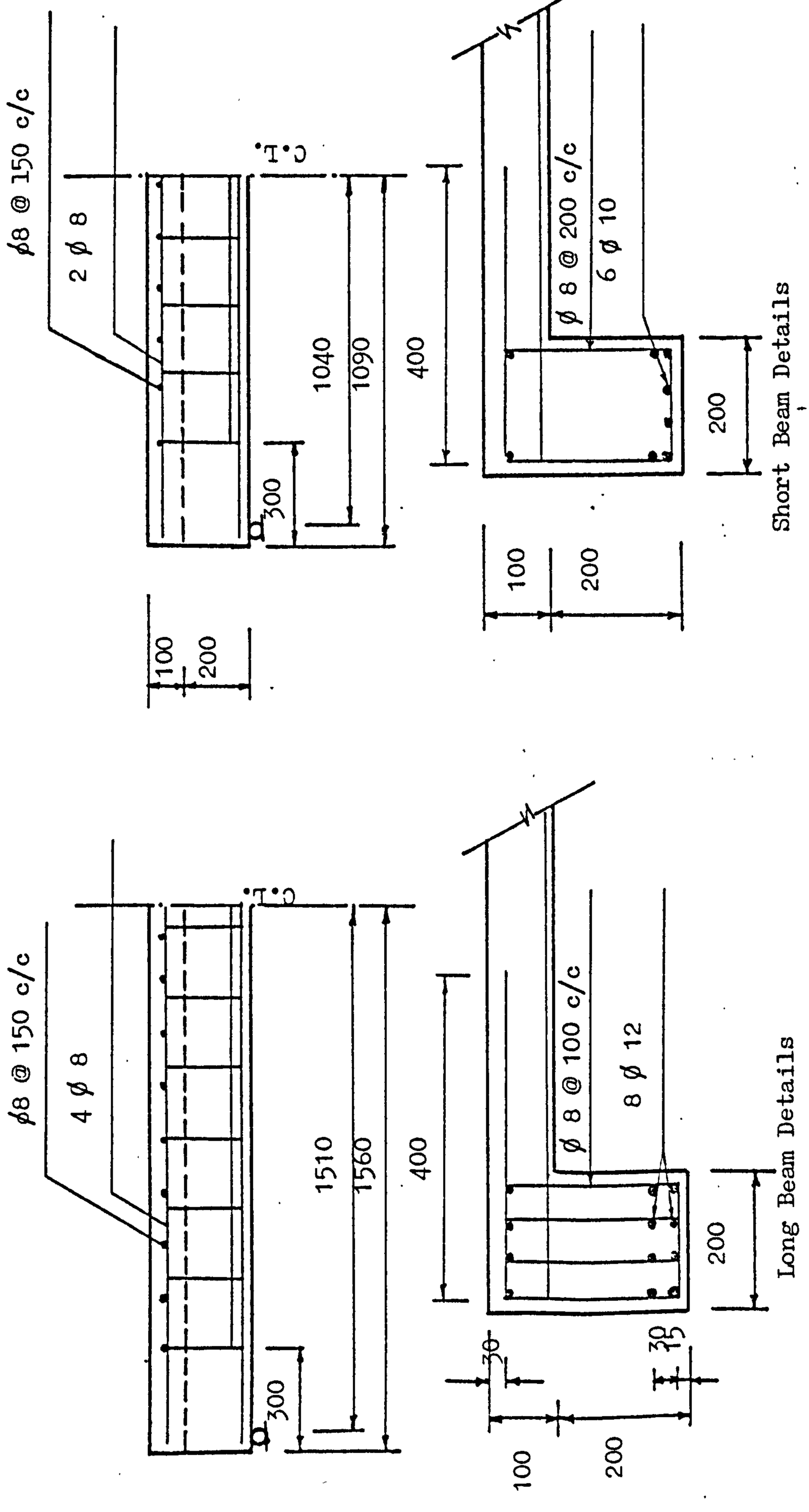

Figure (6.9b) Supporting Beams Details in Model 6.

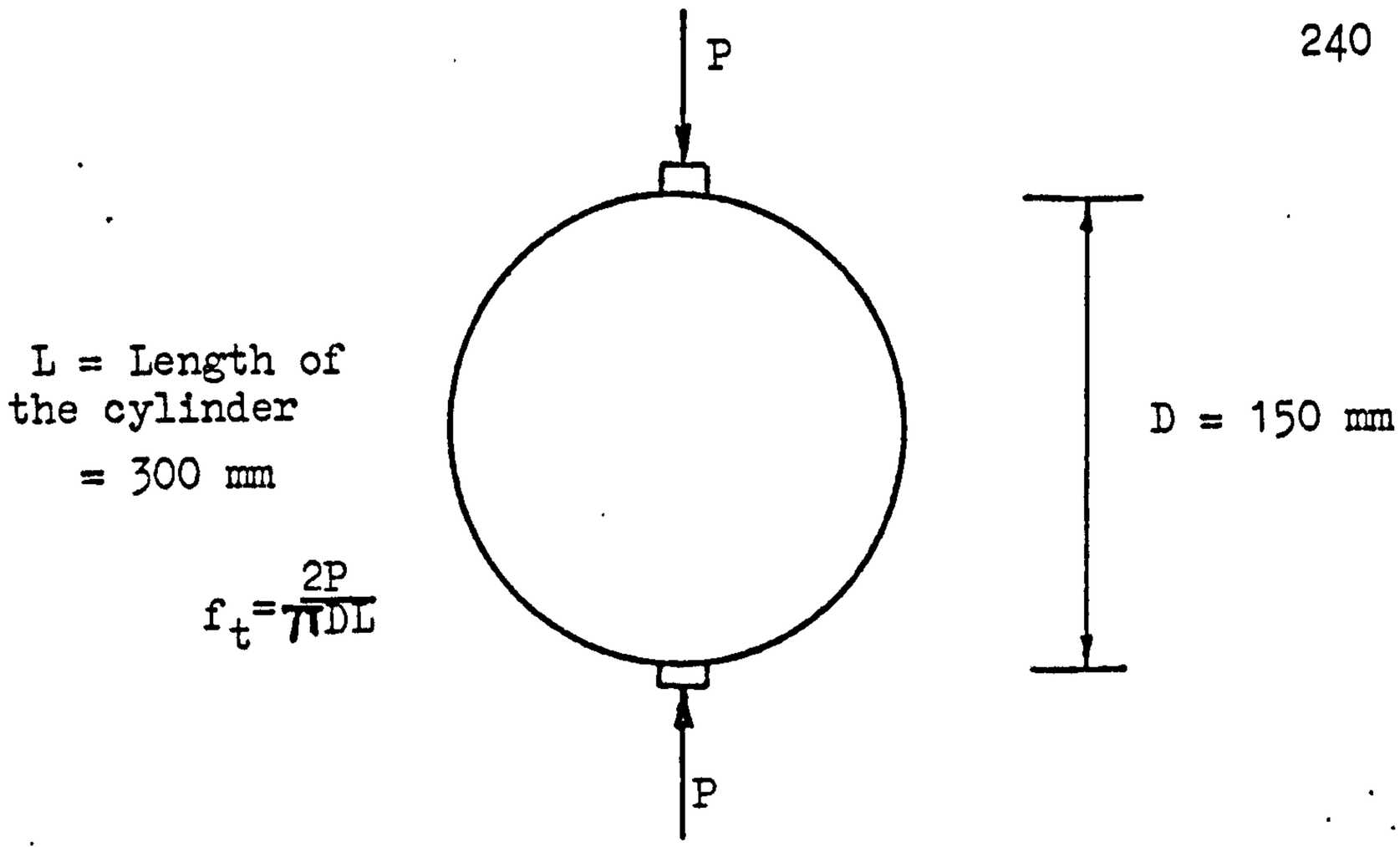

L = Length of the cylinder = 300 mm

$$f_t = \frac{2P}{\pi DL}$$

Figure (6.10) Cylinder Splitting Test for Concrete

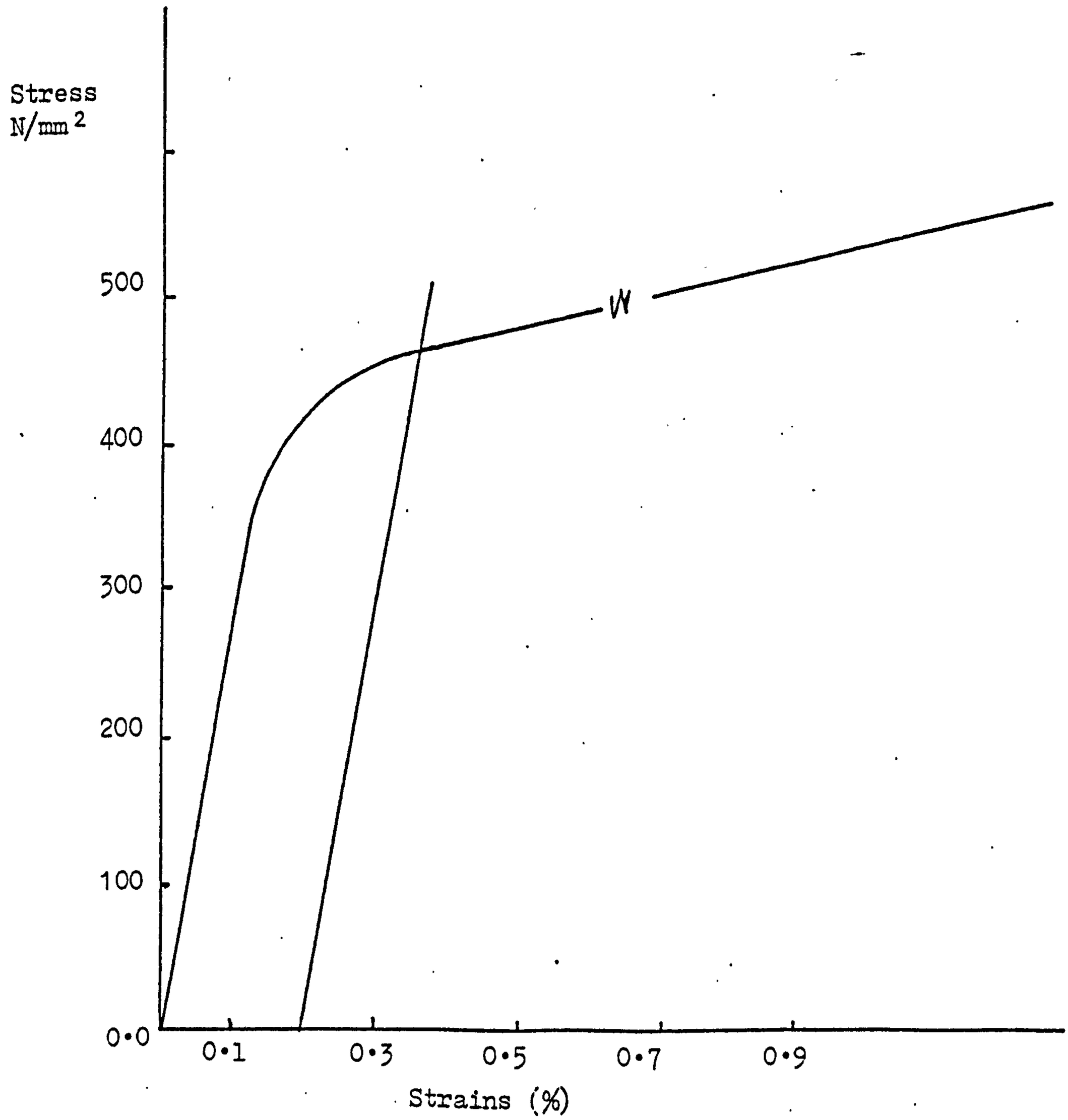

Figure (6.11) Stress-Strain Curve for the High Yield Steel Used.

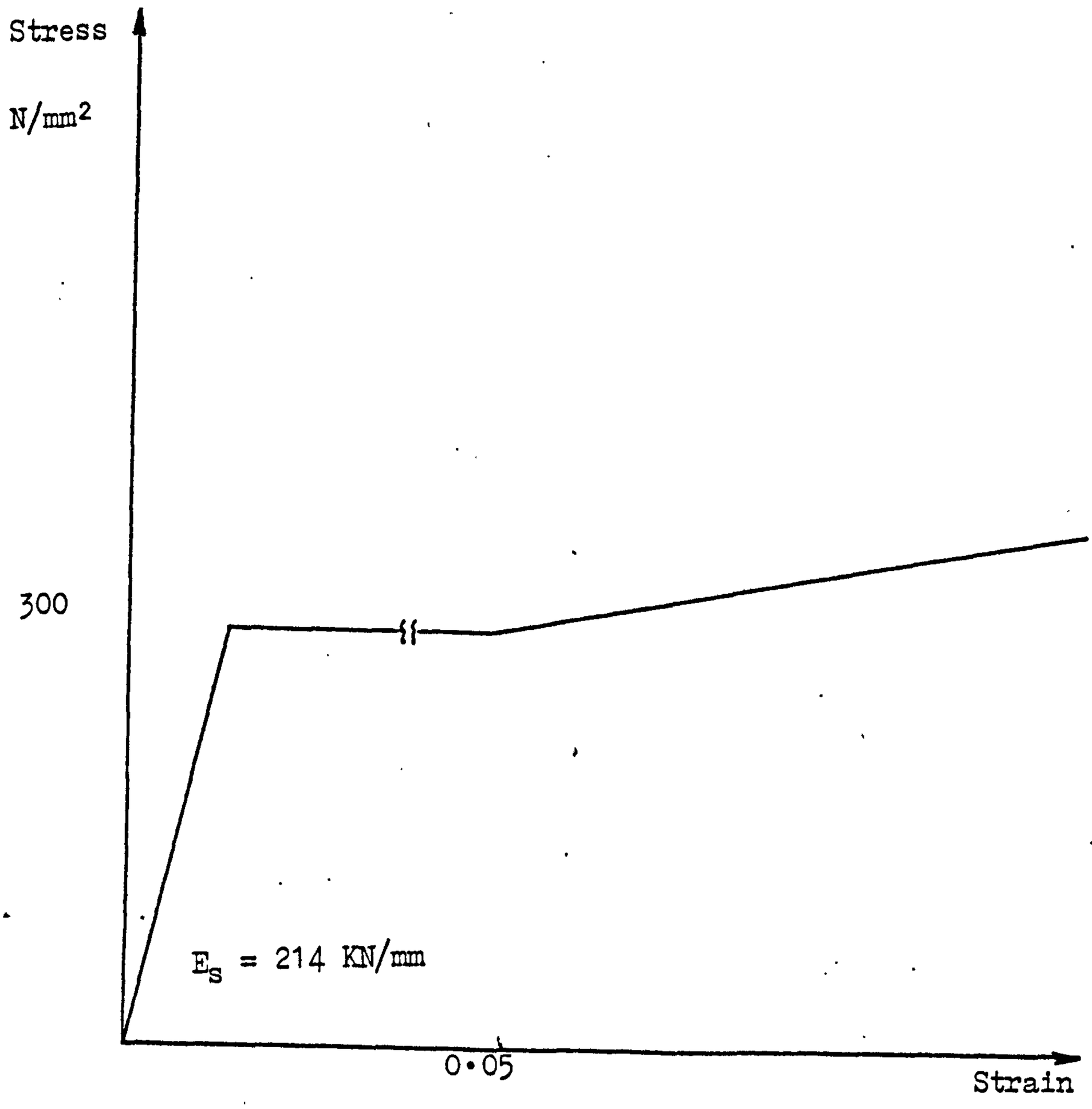

Figure (6.12) Stress-Strain Curve for the mild steel used.

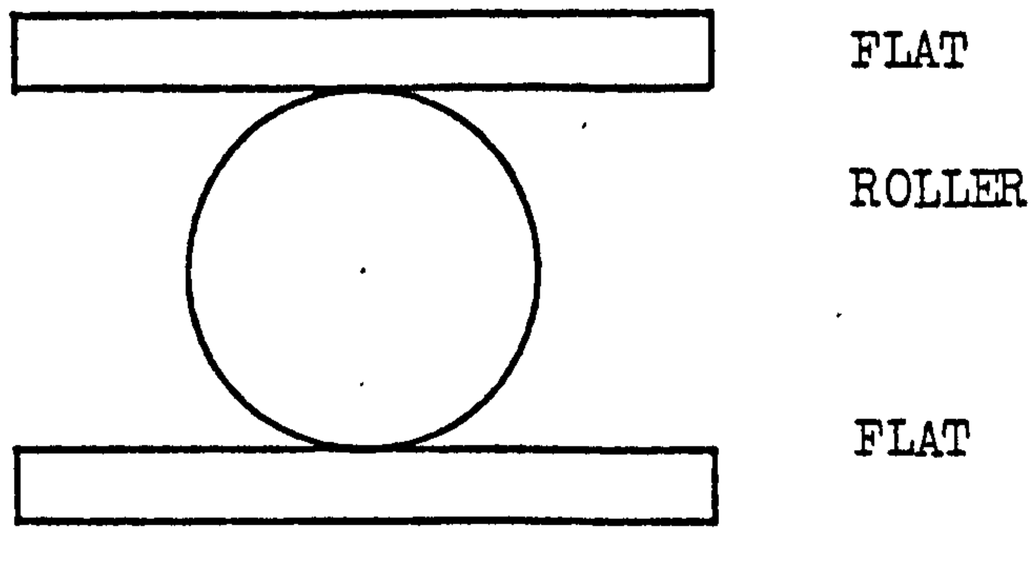

(a) Flats-Roller System

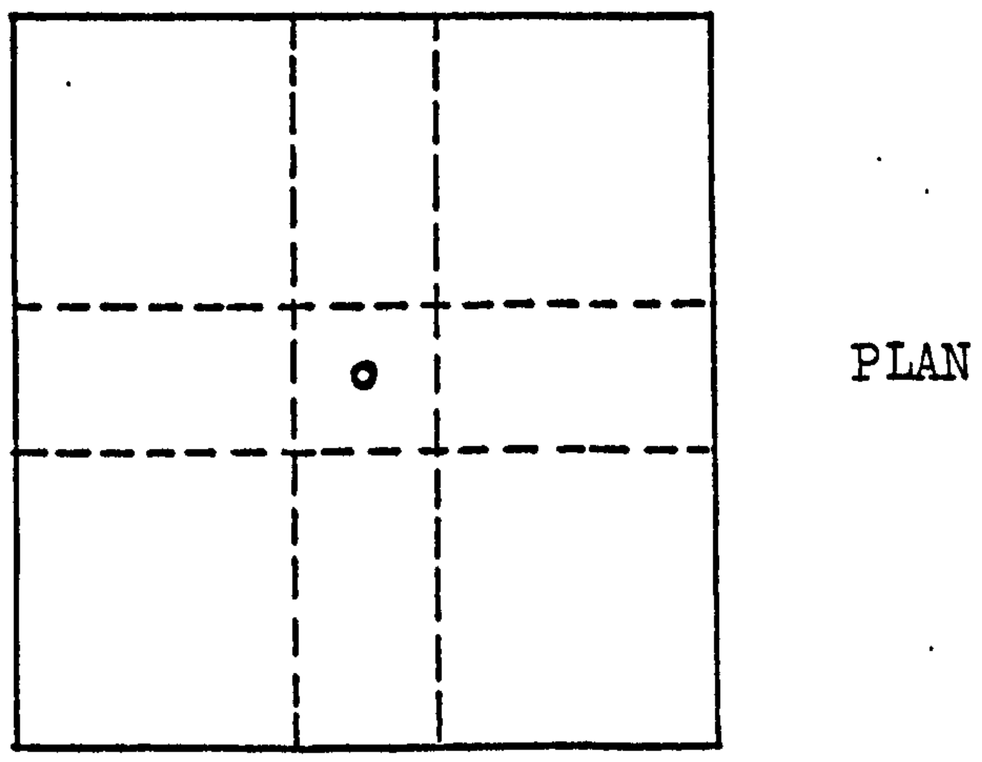

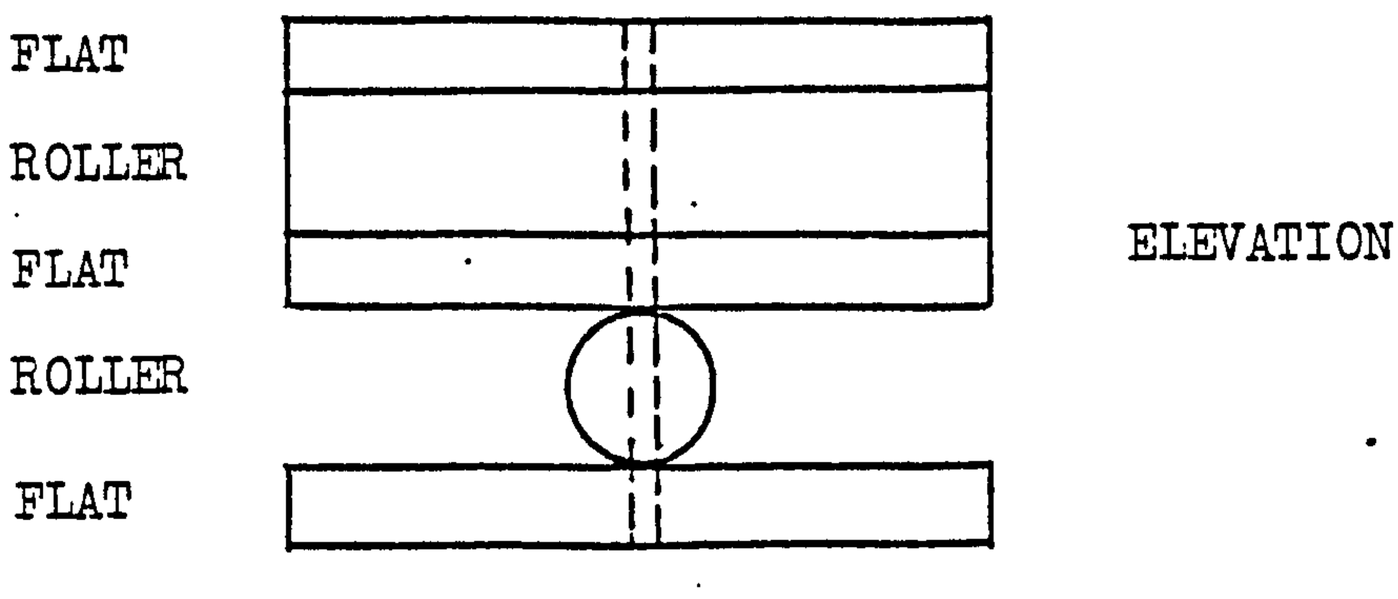

(b) Corner Support System

Figure (6.13) The Support Systems

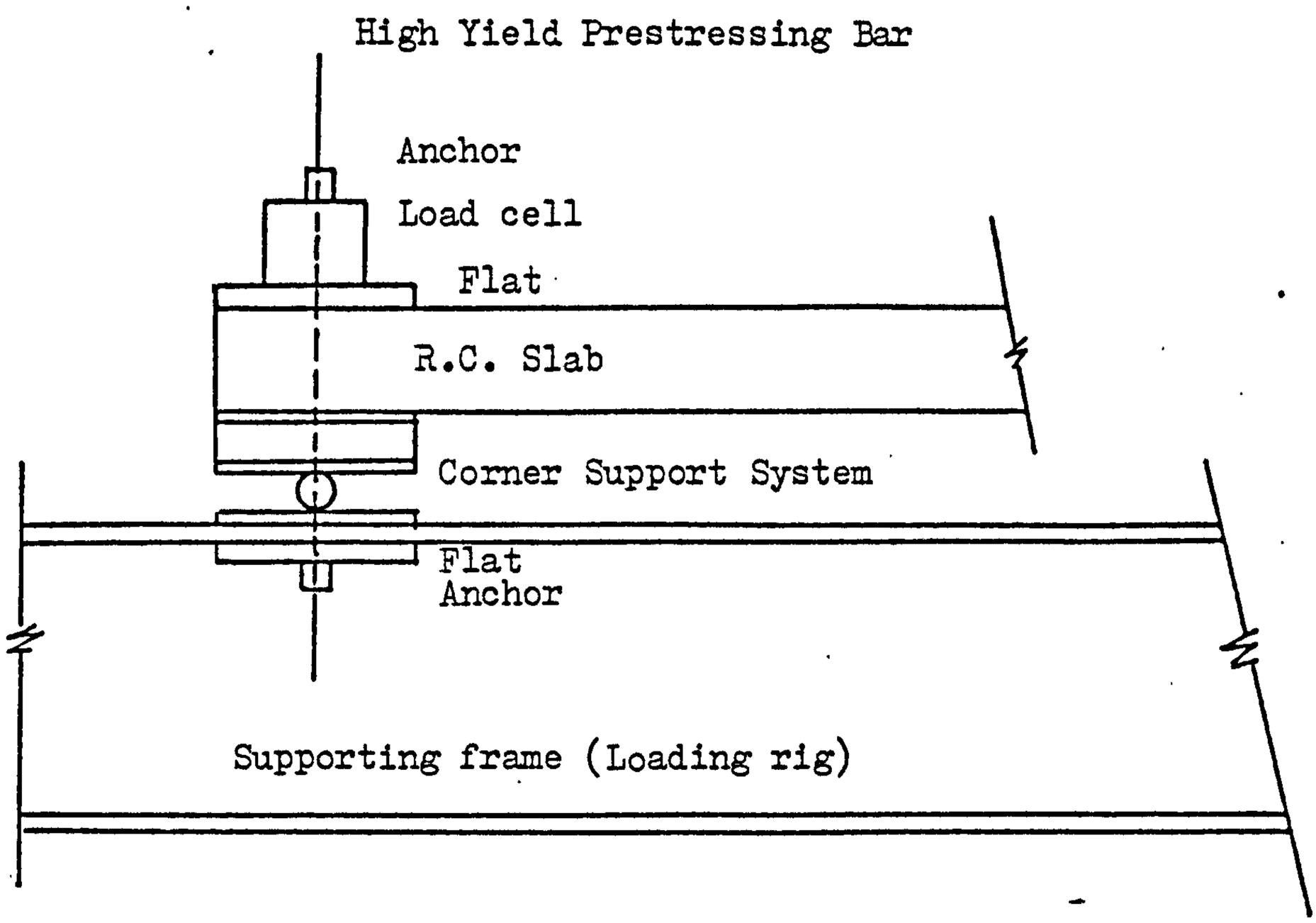

Figure (6.14) Holding the Corners using "Corner Holders".

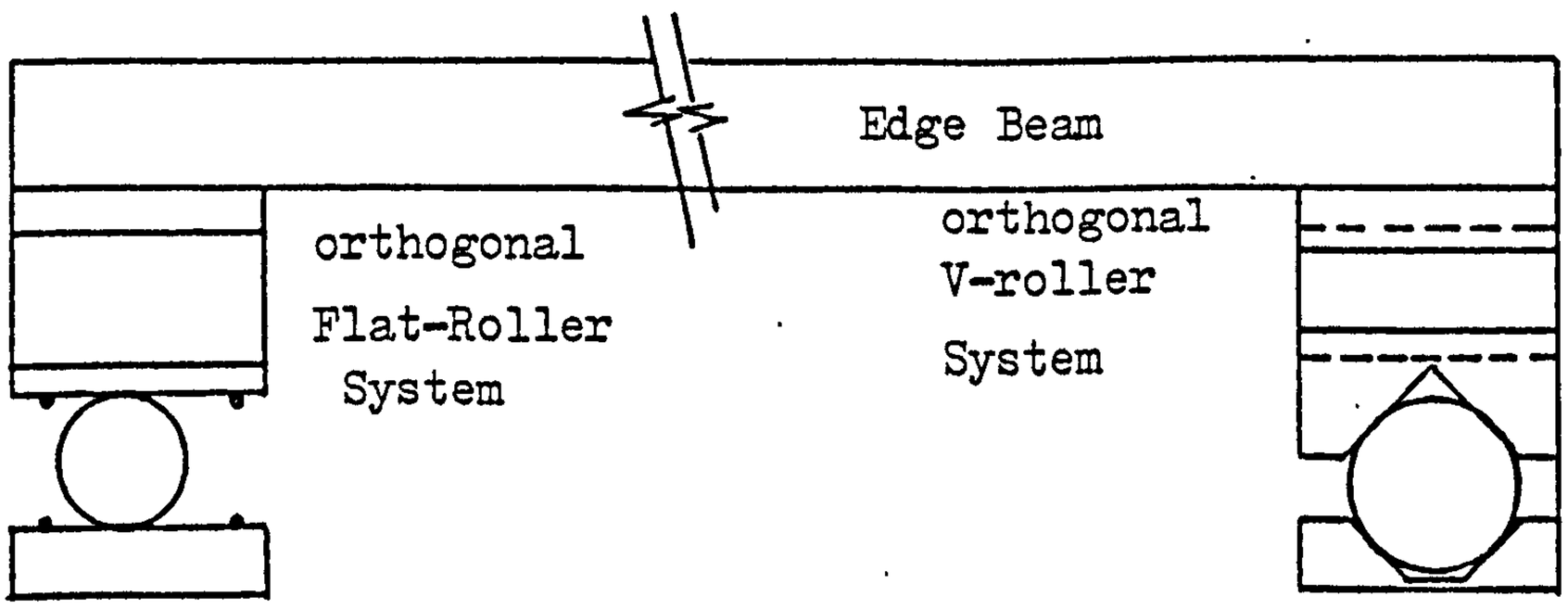

Figure (6.15) Support Systems used in Model 6

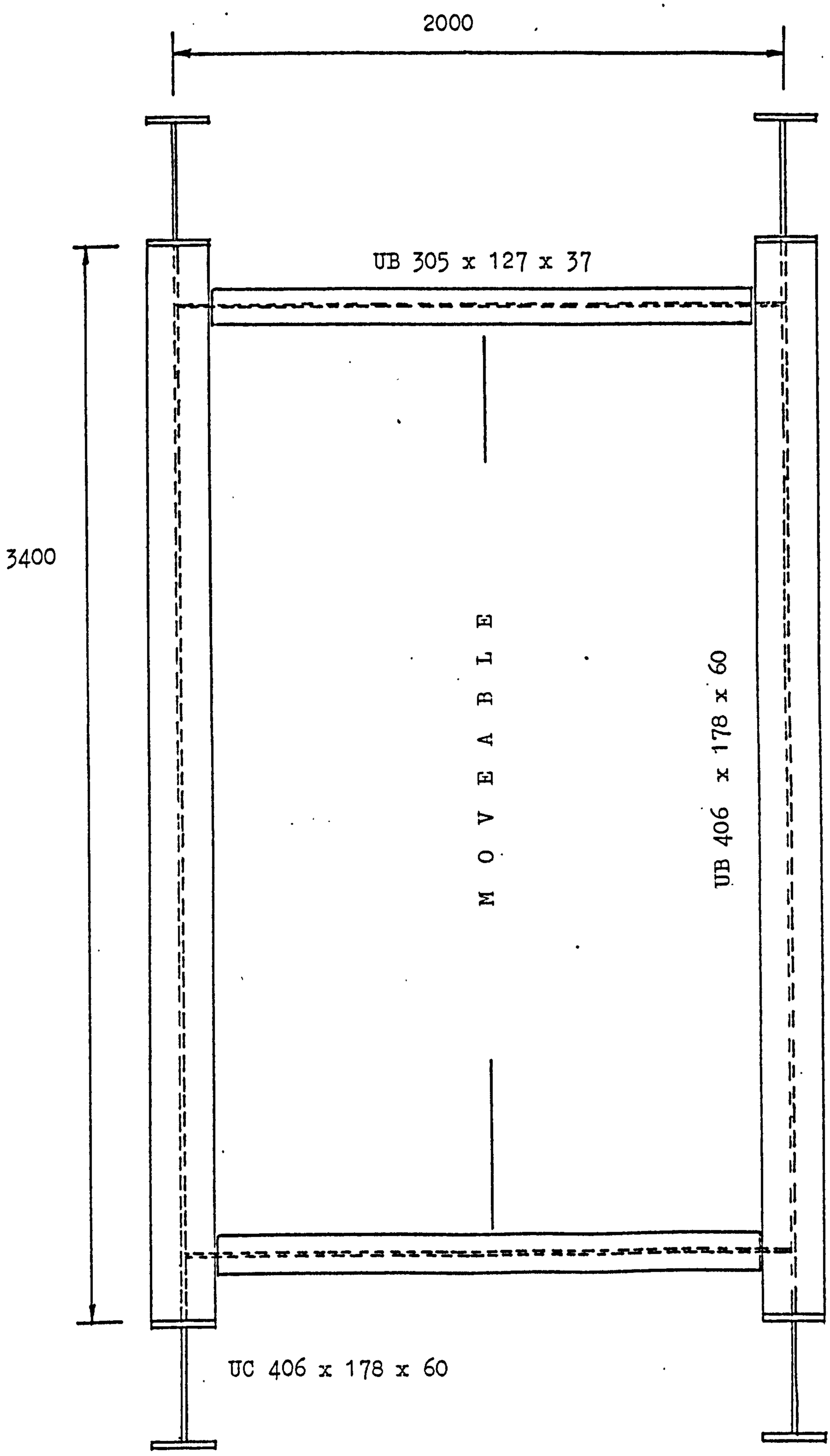

Figure (6.16) The Loading Frame

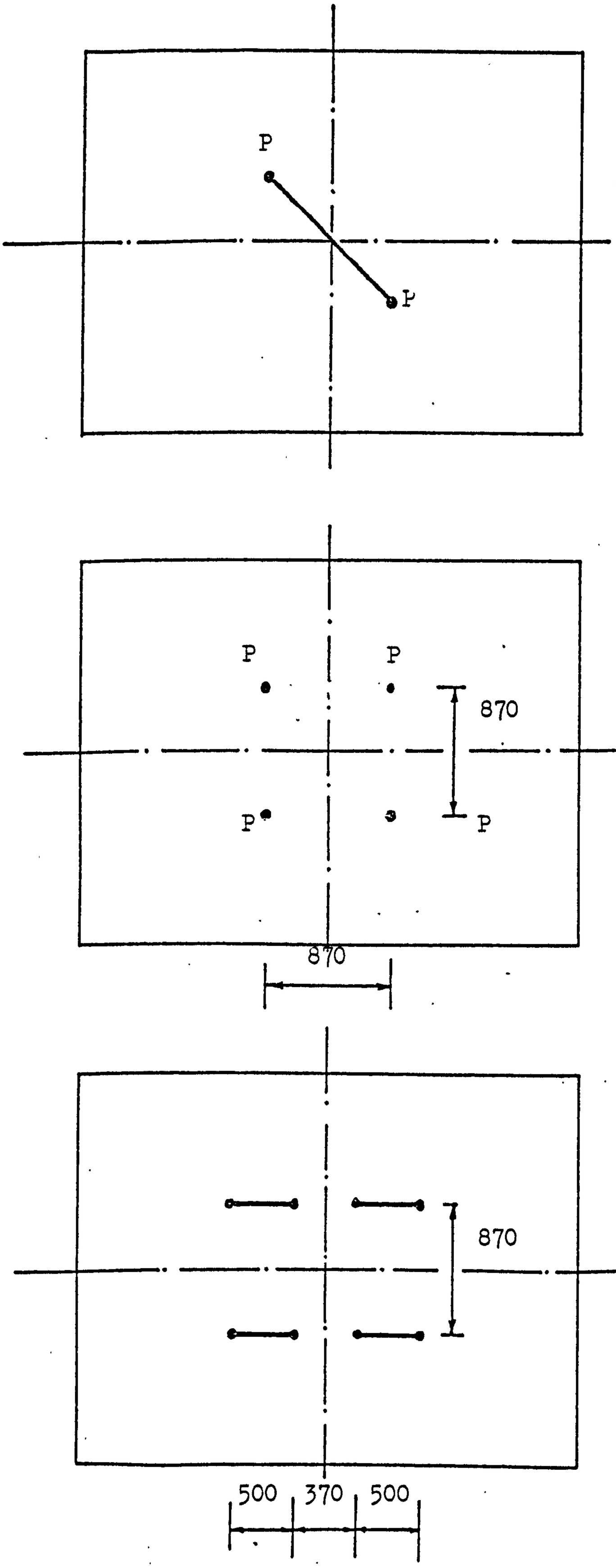

(a) Two points Loading System

(b) Four points Loading System

(c) Eight points Loading System

Figure (6.17) The Loading Systems

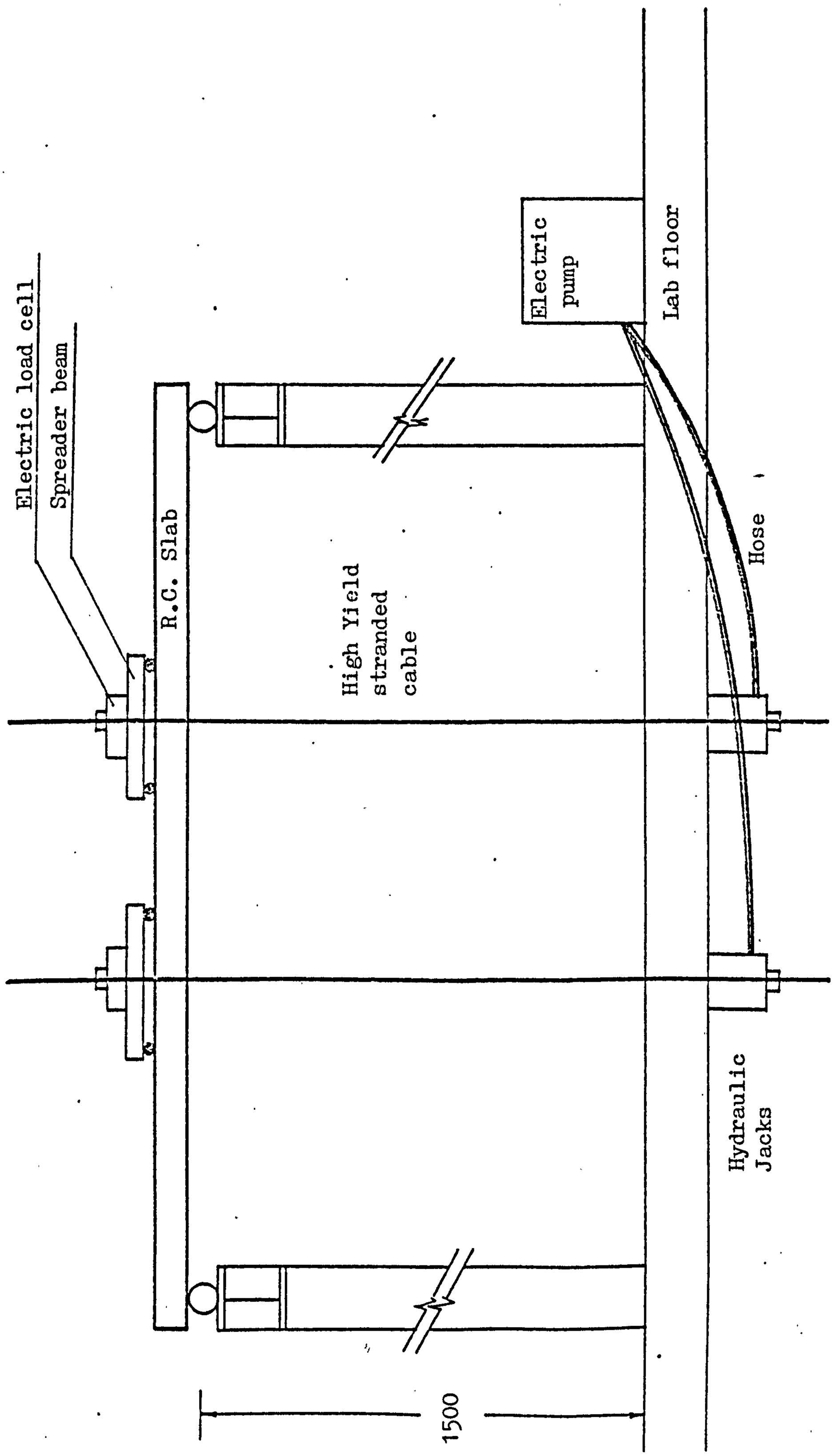

Figure (6.18) Details of the loading apparatus

CHAPTER SEVEN

EXPERIMENTAL RESULTS

COMPARISONS, DISCUSSIONS AND CONCLUSIONS

7.1 INTRODUCTION

In this chapter the results of tests on the large "models" described in chapter 6, are presented. The behaviour of the slabs under increasing load is examined. The tests were designed to:

(a) Check the validity of the proposed design procedure, with respect to service and ultimate behaviour.

(b) Provide information on the detailing problems associated with this method, and the resulting effects on the slab behaviour.

(c) Carry out a detailed numerical analysis on these slabs to gain a proper understanding of the redistribution of forces at high levels of loading.

All the slabs were tested under the action of concentrated loads. Details of the test slabs, material properties and method of testing have been given in the previous chapter.

7.2 GENERAL DESCRIPTION OF THE BEHAVIOUR OF THE MODELS

7.2.1 Model 1 (L_x/L_y = 1.5, simply supported):

This was a rectangular simply supported slab with an aspect ratio (L_x/L_y) of 1.5. The slab was designed for a total load of 416 KN. This design load was chosen in order to obtain reasonable percentages of steel in the structure. The steel bars were curtailed exactly at the points where they were no longer needed. The curtailment of steel was done using the design bending moments in each strip of

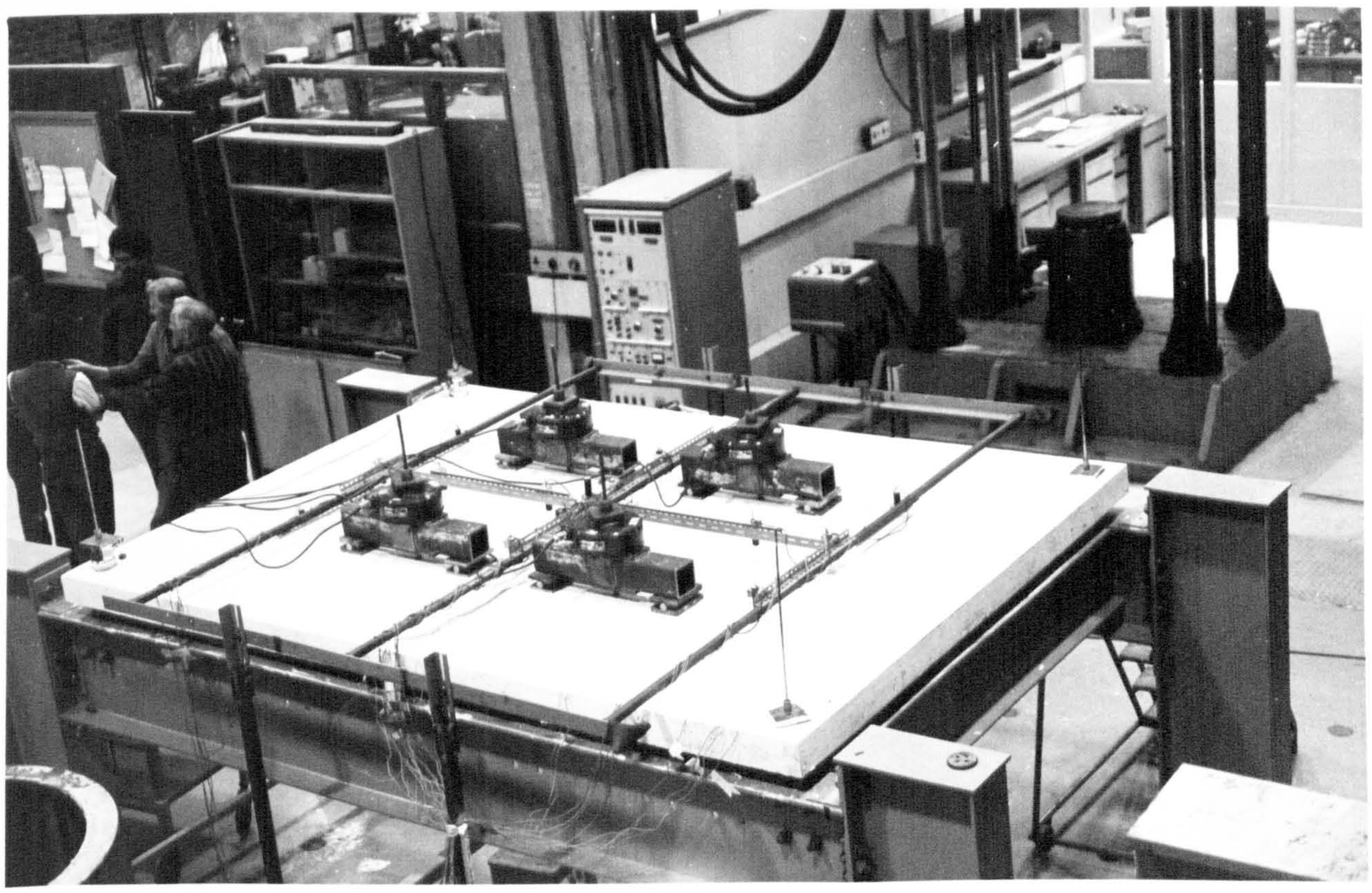

Figure (7·1) A Slab Model Under Test

elements, according to the method described in section (6.4). Welding was used to connect bars of different diameters, and was carried out according to CP110 rules[5]. The total volume of steel provided in this model, including hooks etc., is given in Table (6.2).

The load-central deflection curve for this model is given in Figure (7.2). First visible cracking started at about 0.29 P_d, but a slight nonlinearity in the curve is visible at a load of 0.18 P_d. This is caused by the early microcracks, which probably formed during the loading and unloading prior to test.

The first cracks were observed under the load points and were a maximum width of 0.13 mm at 0.29 P_d. With increasing loads, the cracks tended to spread from the load points and to cover the central zone bounded by the load points. Subsequently, they spread along the diagonals towards the corners. There was a general tendency to form new cracks rather than widening of the existing cracks. Deflections continued to increase at a higher rate, and at 0.4 P_d, the central deflection was 8 mm. This represents the permissible service deflection according to CP110[5]. At this load, the cracks covered the entire central zone. The maximum crack width reached 0.3 mm at a load of 0.45 P_d, directly under the points of application of the load.

Yield of steel was first observed at 0.69 P_d. This occurred in the short span direction at the centre of the slab. At this load, tiny visible cracks in a narrow band along the diagonals reached the corners of the slab. Up to this stage, no major crack had formed, and the cracks were evenly distributed over the bottom surface of the slab.

At about 0.63 P_d, a few cracks appeared on the top surface of the slab at the four corners near the corner holders. By a load of 0.73 P_d,

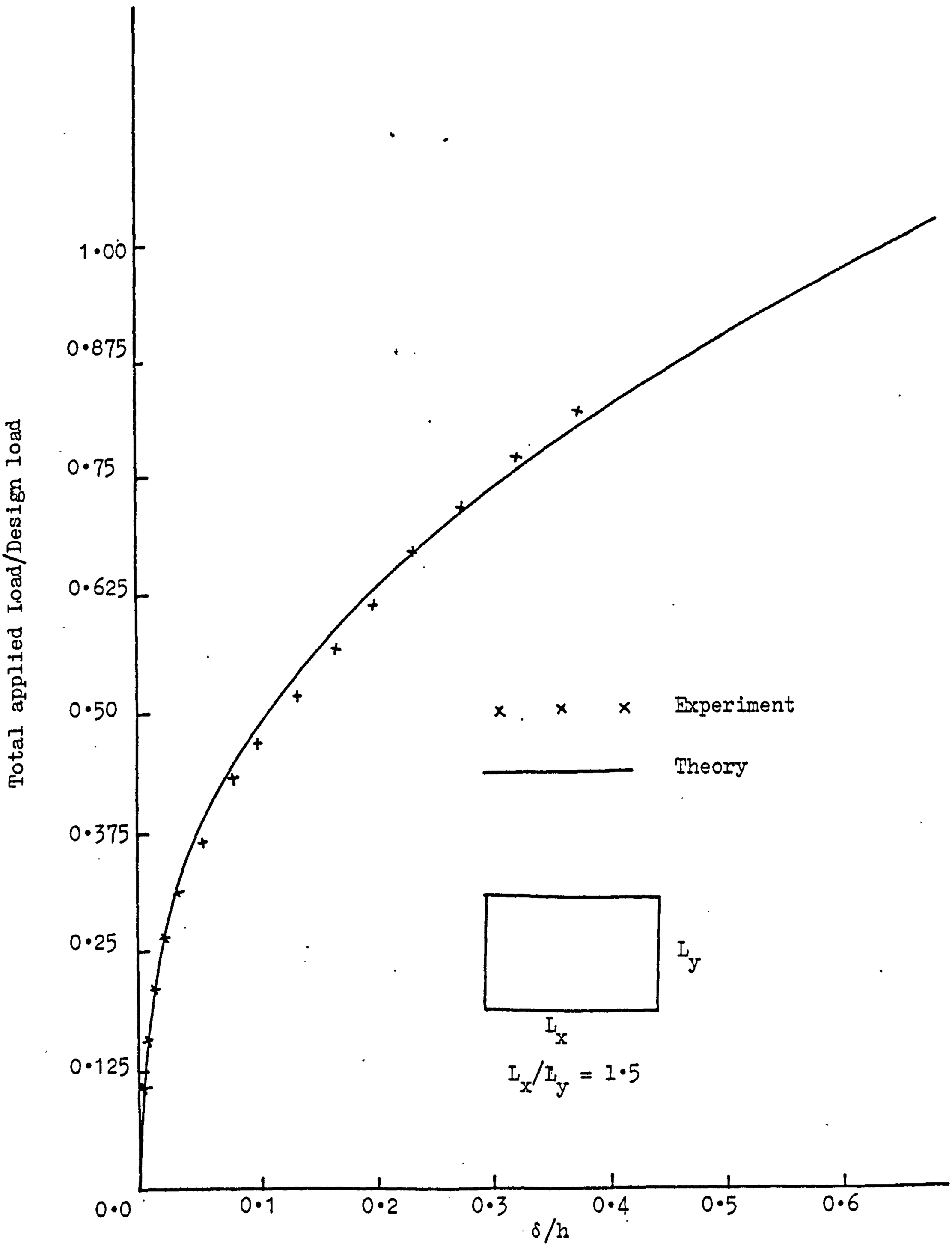

Figure (7·2) Load Central Deflection Curve for Model 1

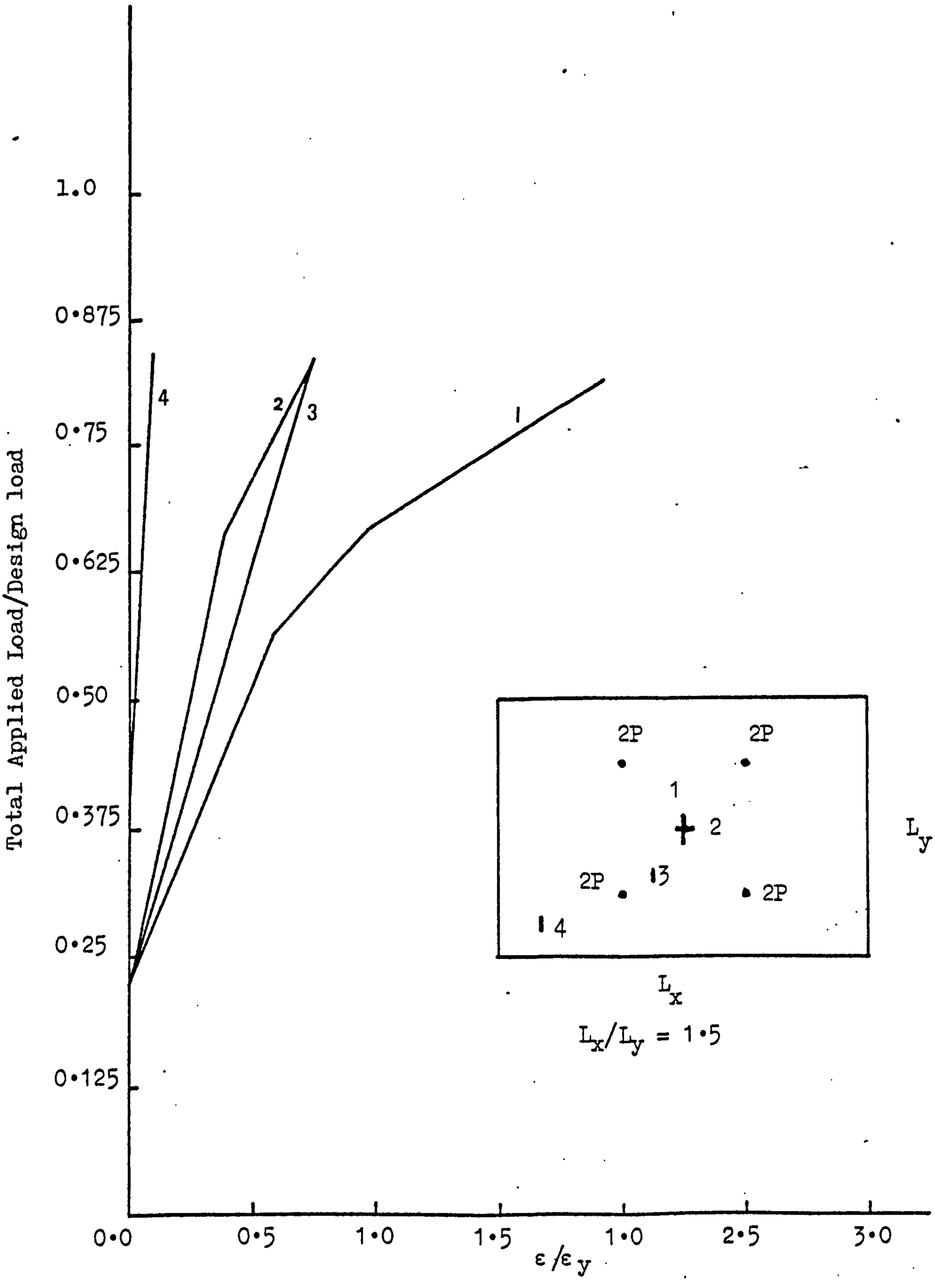

Figure (7•3) Load-Steel Strains in Model 1

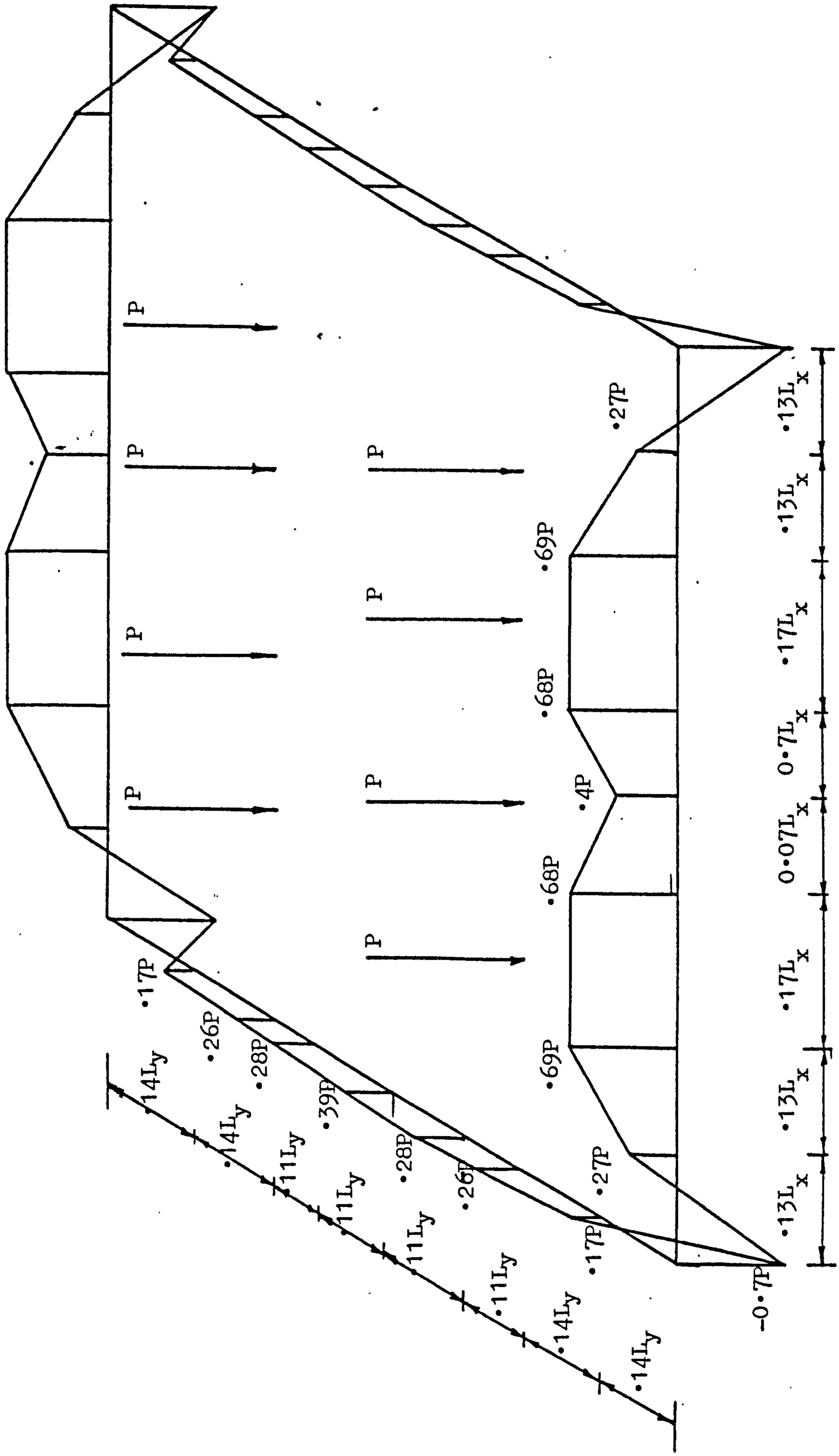

Figure (7.4) Loads and Supports Reactions on Model 1 1

a well defined yield line pattern was developing. The strains in the reinforcing steel were also small (see Figure 7.3), and only the steel at the centre was yielding. At 0.8 P_d, when the deflection was about 0.38 h, a sudden shear failure occurred. This was a deep long crack running near and parallel to the long supported edges. The concrete cover on the bottom surface of the slab spalled off along the shear crack. Due to the sudden shear failure, the whole of the central zone dropped down significantly relative to the supports with a clinking sound. This was a bit unfortunate. However a check on the shear strength using CP110[5] revealed that the slab was in fact weak in shear.

7.2.2 Model 2 (L_x/L_y = 1.3, simply supported):

This is a rectangular simply supported slab with an aspect ratio (L_x/L_y) of 1.3. The slab was designed for a load of 213 KN. A photograph of the crack pattern on the underside is given in Figure (7.5). As in the previous model, the load was applied in increments of 5 KN per load cell.

The load-central deflection curve for this model is shown in Figure (7.6), and a summary of the behaviour is given in Table (7.1). Similar to the previous model, first visible cracking was observed at a load of 0.56 P_d. Also these first cracks appeared under the load points, and were in the direction of the diagonals.

The maximum width of these cracks under the cracking load was 0.12 mm. Between a load of .56 P_d and 0.8 P_d, cracks spread all over the central zone bounded by the load points, while the deflections increased to twice their values before the cracking load. The spread of cracks in the central zone tended to be along the diagonals. During

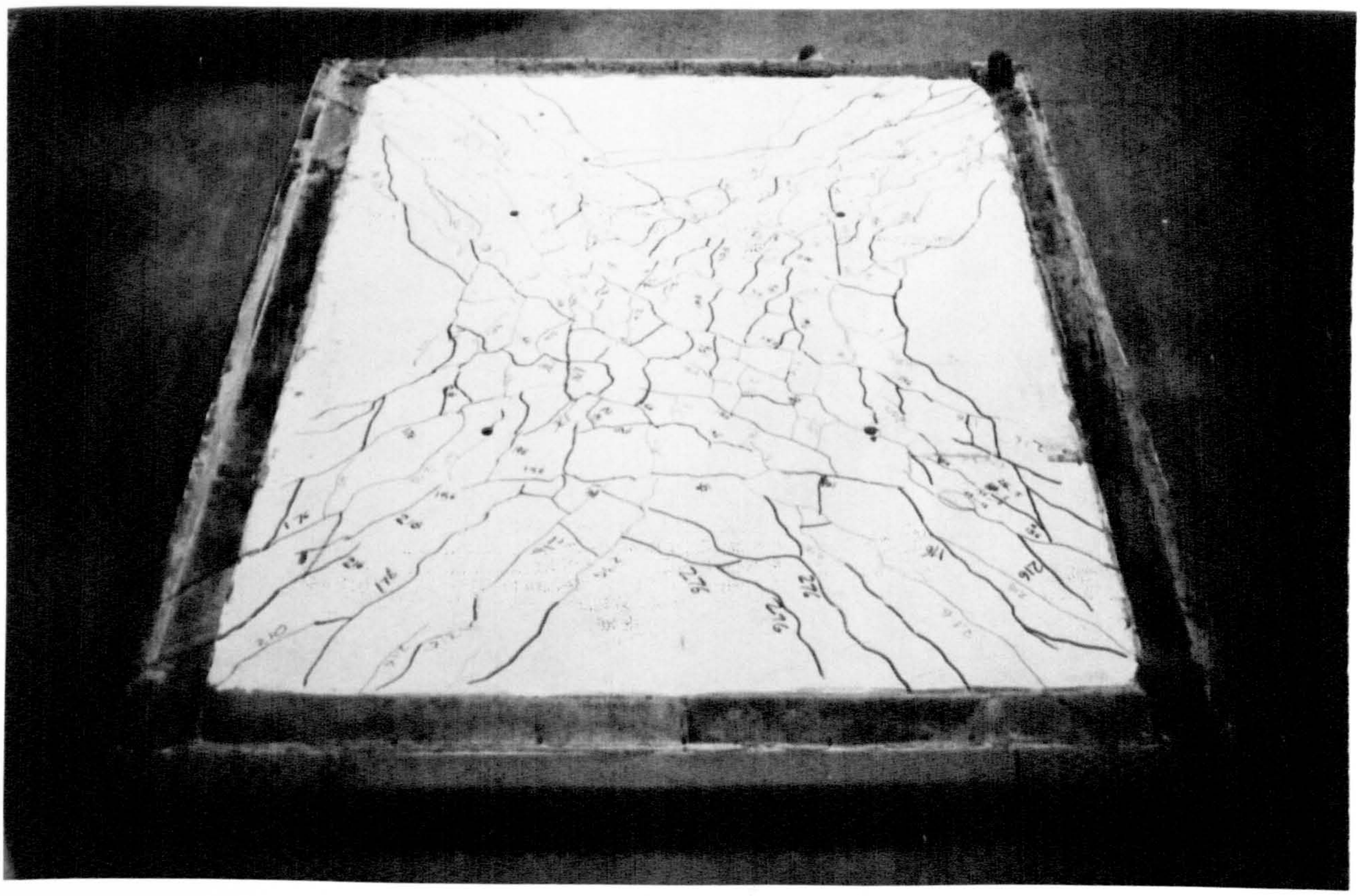

Figure (7·5) Crack Pattern on the Underside of Model 2

the next load increment, which corresponds to a total load of 0.9 P_d, new surface cracks spread further covering most of the central zone between the loads, and very near the corners of the slab. But only at P_d did they reach the slab boundaries. Thus a well defined yield line pattern formed under this load.

The deflection limit of span/250 was reached at 0.75 P_d, and a crack width limit of 0.3mm at 0.85 P_d. This definitely represents a very high service load. In addition, the strain measurements showed that steel did not yield at all at this high service load. First yield of reinforcement was detected in the short span steel around the slab centre. This first yield occurred at 0.94 P_d. However, a rapid increase in steel strains was observed after the first yield load, as can be seen from Figure (7.7). After a load of 0.98 P_d, cracks tended to intensify and increase in width. The sound of concrete cracking could clearly be heard at this stage.

At 1.13 P_d, most of the strain gauges on the steel bars indicated strains higher than yield strain for steel. At this load level top surface cracks started to appear. At 1.31 P_d, the dial gauge at the centre of the slab was rotating freely and the load on the load cells started to drop. It was very difficult to maintain the load at that level.

The load of 1.31 P_d was then taken as the failure load for this slab. An ultimate deflection of 50 mm at the centre of the slab was the value taken just before the dial was removed.

A clear well defined yield lines pattern has already developed when the slab failed. Each corner reaction measured only 7% of the failure load at collapse.

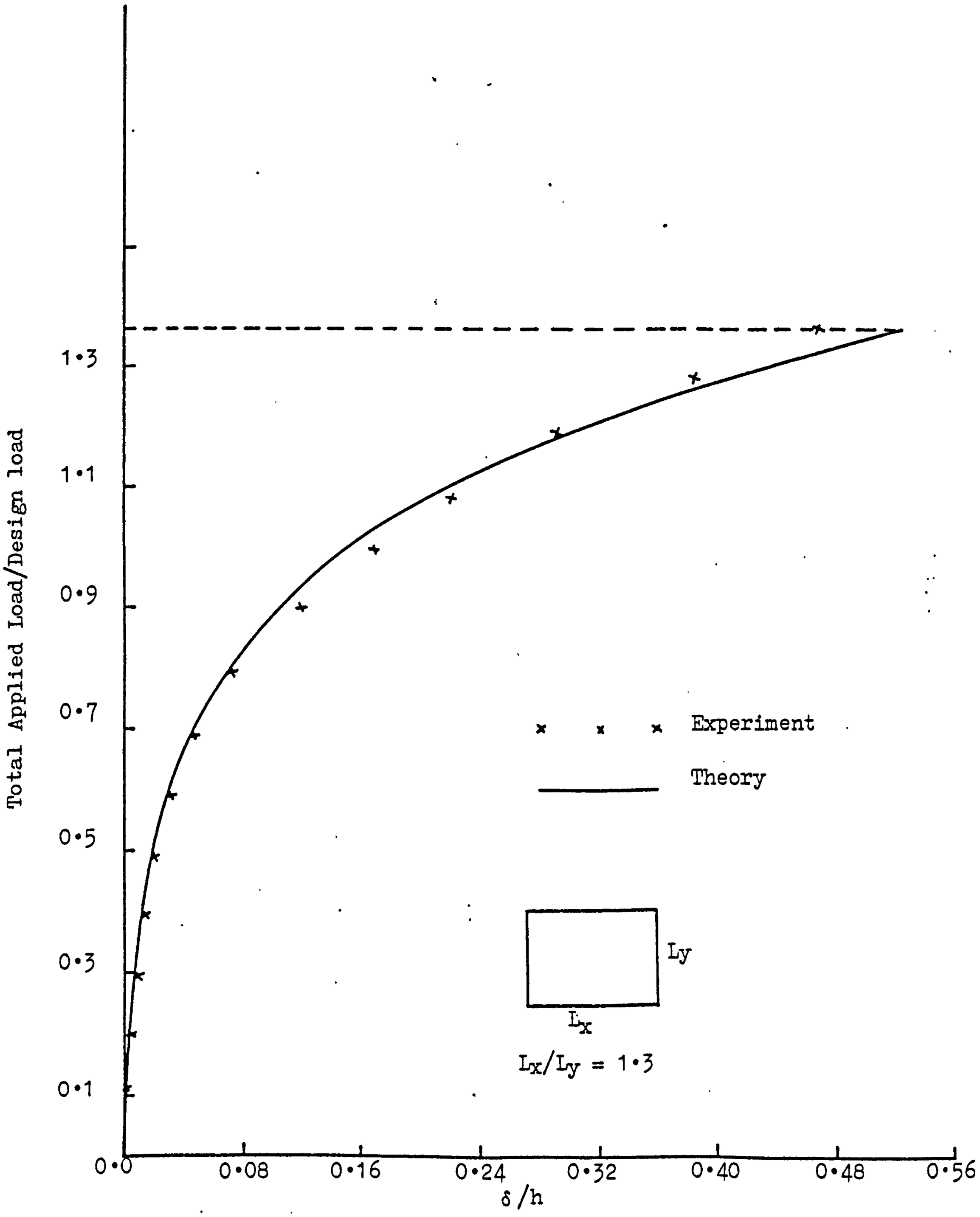

Figure (7·6) Load-Deflection Curve for Model 2

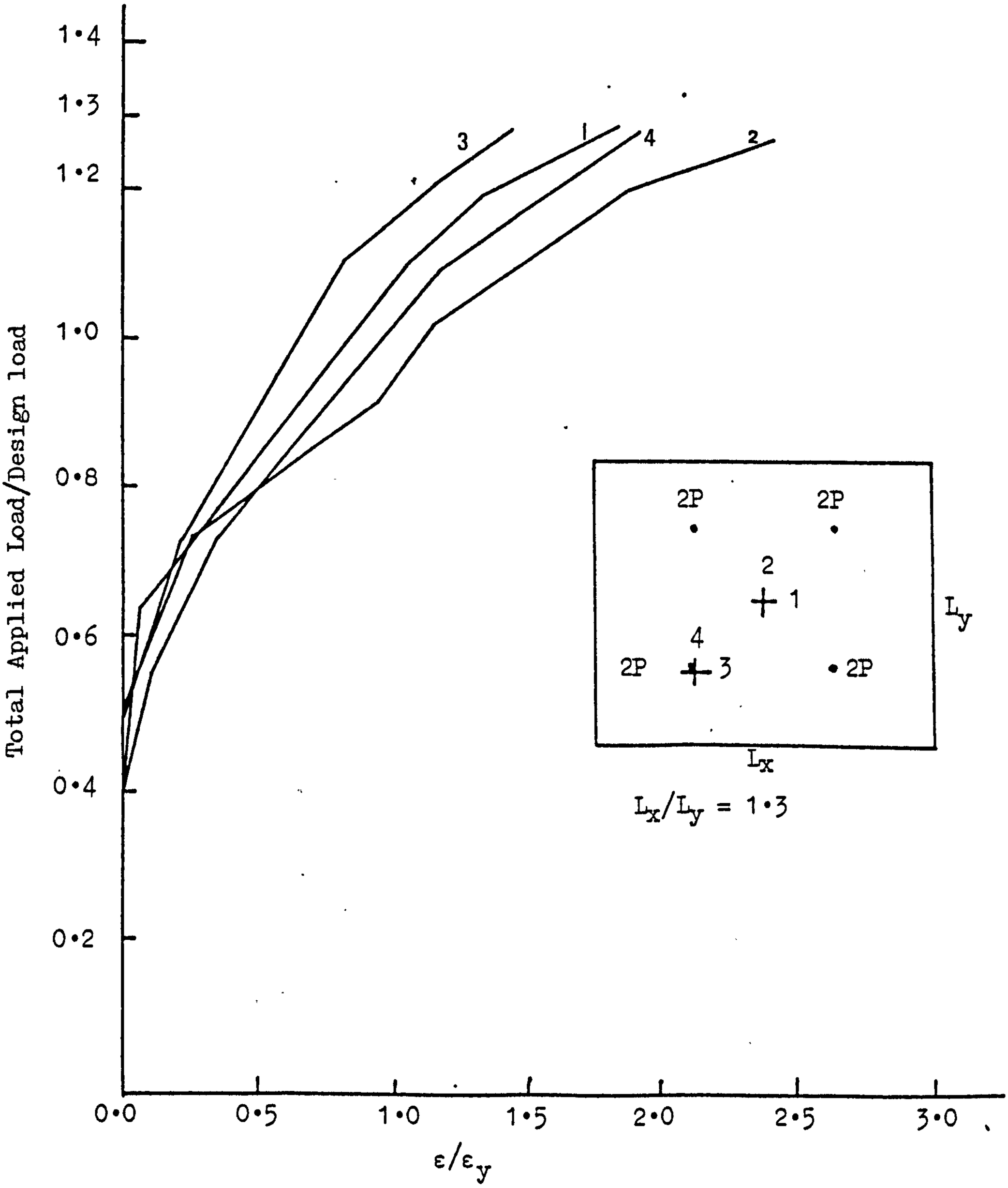

Figure (7·7) Load-Steel Strains in Model 2

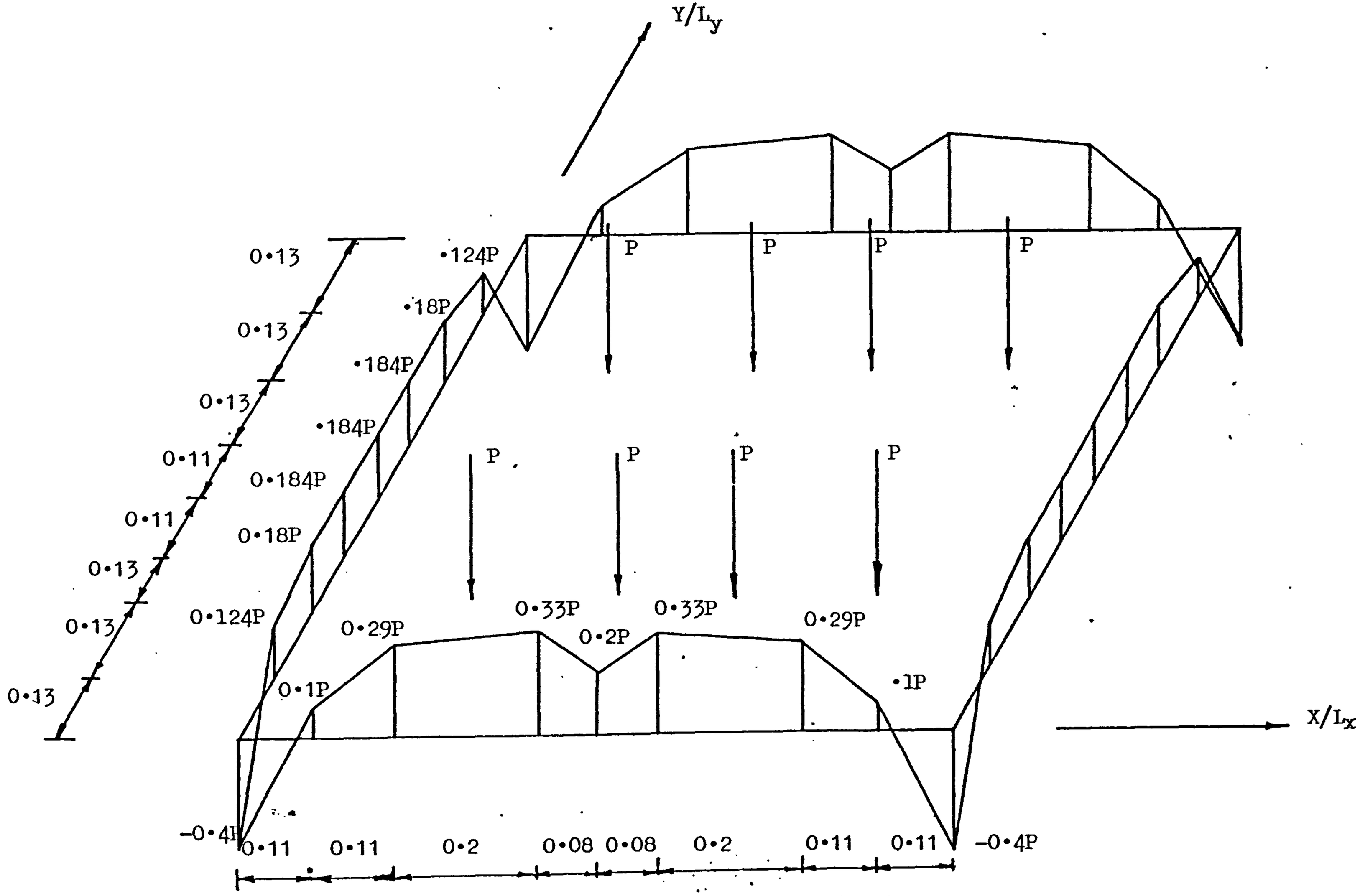

Figure (7•8) Loads and Supports Reactions on Model 2

7.2.3 Model 3 ($L_x/L_y \doteq 1.0$, simply supported):

This is a square simply supported slab which was designed for a total load of 210 KN. The load was applied as a four-points-load system, as can be seen from Figure (7.13). The model was loaded in increments of 5 KN per load cell.

The load-deflection curve for this slab is given in Figure (7.11). First visible cracking was observed directly under the four load points at about 0.38 P_d and measured a maximum of 0.04mm. Under the cracking load, no cracks appeared in the central zone of the slab. The first of these cracks in this zone was observed at about 0.48 P_d, and were along the slab diagonals. The spread of surface cracks in this model was faster than in the previous two models. Under the load of 0.48 P_d, the surface cracks continued to extend towards the boundaries - (see Figure 7.9).

The limiting deflection of span/250 was attained at about 0.72 P_d, while the crack limit width of 0.3mm was reached at 0.67 P_d. At 0.76 P_d the diagonal cracks were running right through to the corners, although some new cracks continued to form outside the central square bounded by the loading points.

Intensive cracking represented by fast development of new cracks and further widening of the diagonal cracks occurred after a load of 0.86 P_d. The newly developed cracks formed outside the central zone on the slab, formed by the four load points (Figure (7.13)). Top surface cracks also appeared near the corners of the slab at this load level (Figure (7.10)). At 0.95 P_d more corner cracks were forming. Beyond this load, the deflections increased rapidly.

A flexural failure, similar to that obtained with model 2, occurred at about 1.16 P_d.

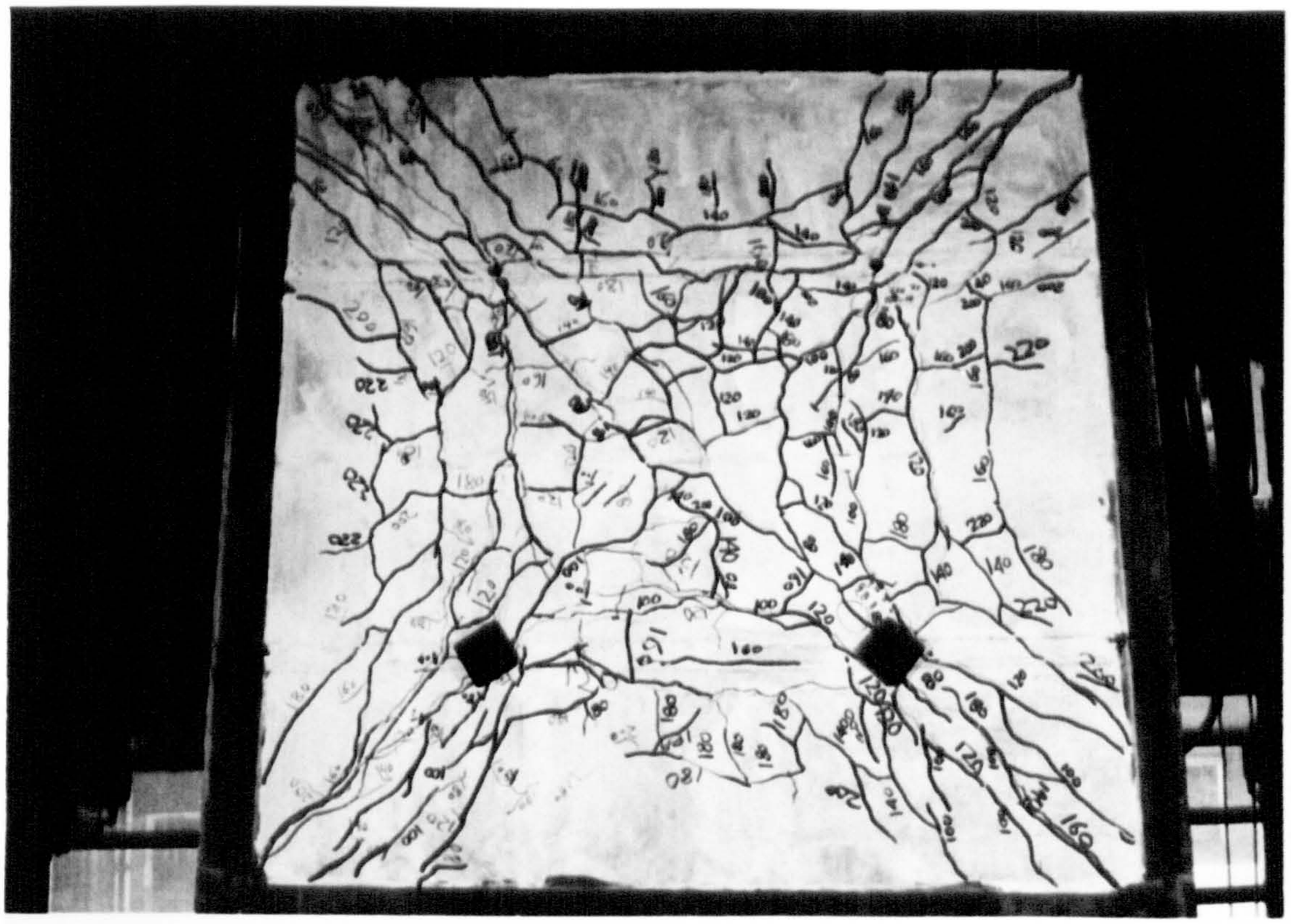

Figure (7·9) Crack pattern on the underside of Model 3

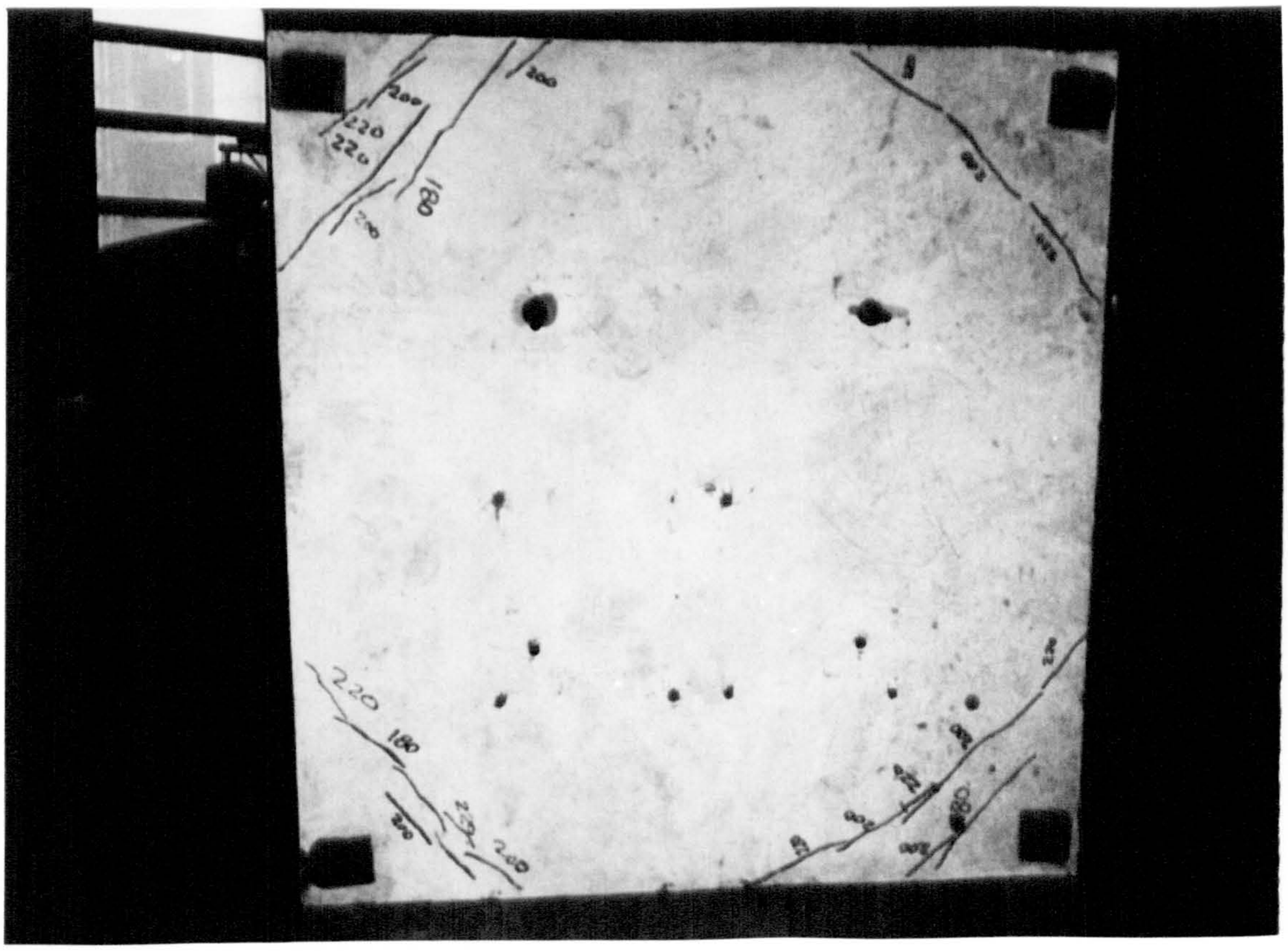

Figure (7.10) Crack pattern on the top face of Model 3

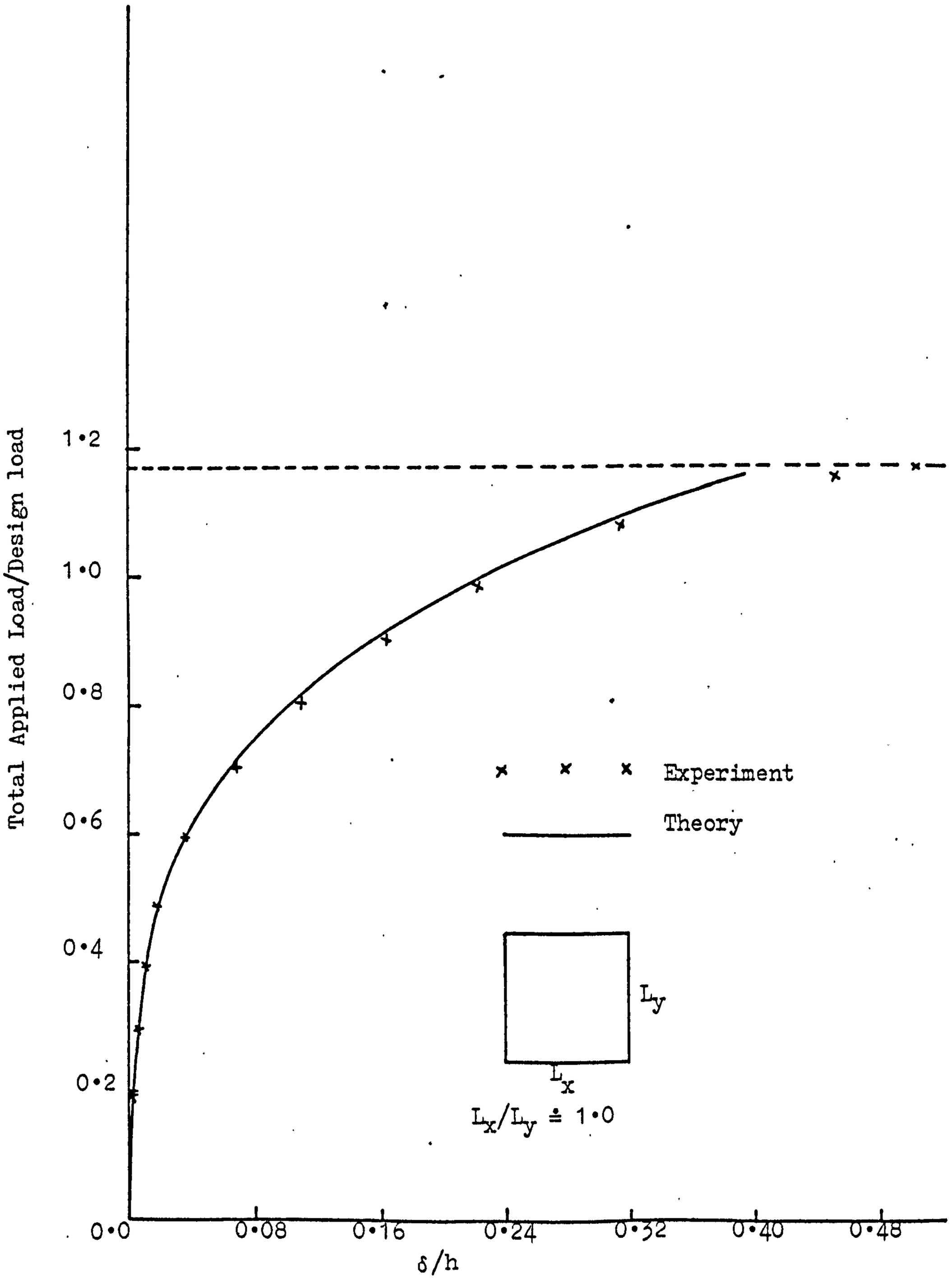

Figure (7.11) Load-Deflection Curve for Model 3

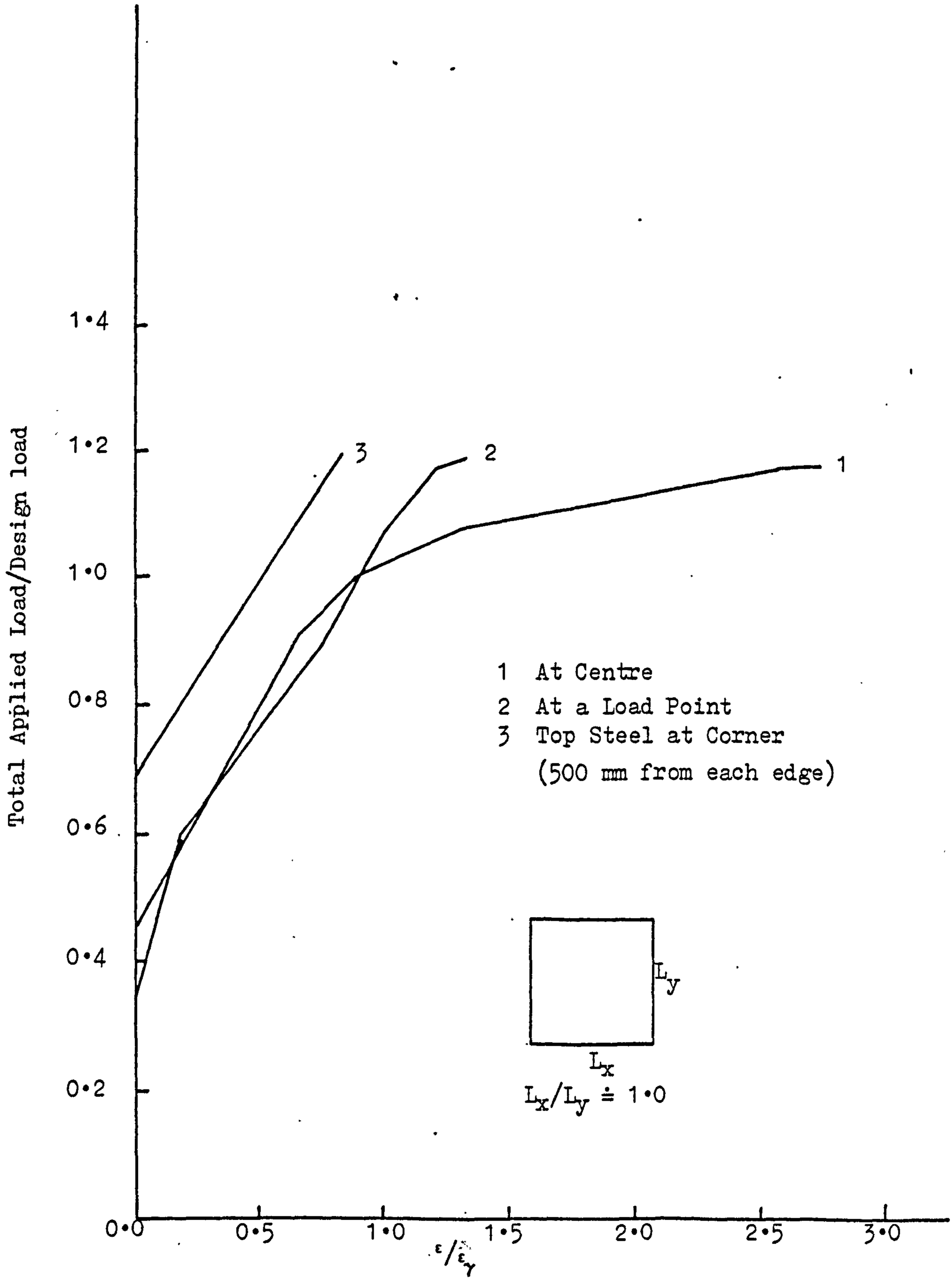

Figure (7·12) Load-Steel Strains in Model 3

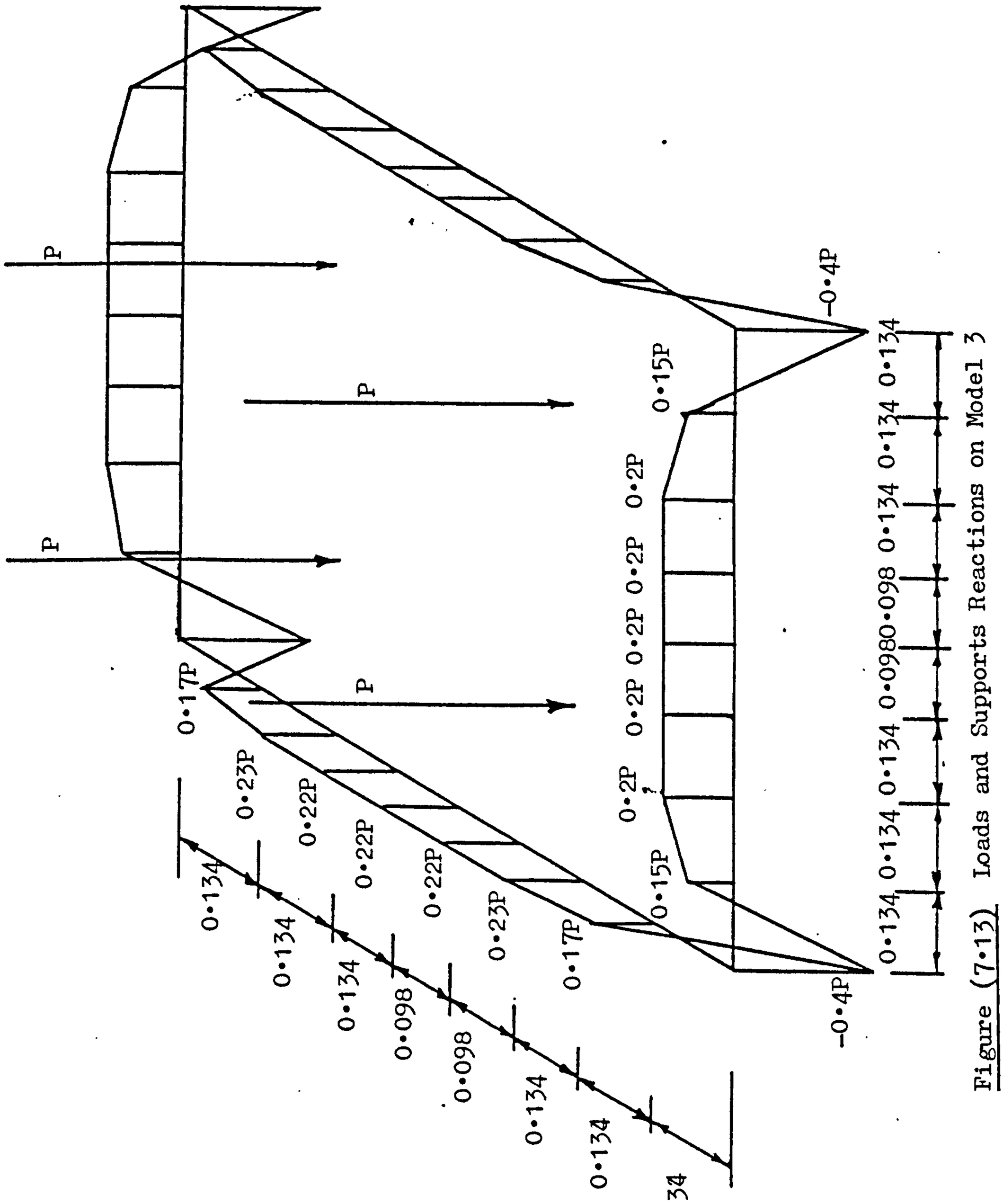

Figure (7·13) Loads and Supports Reactions on Model 3

7.2.4 Model 4 (L_x/L_y = 1.02 , 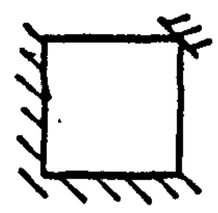)

This is a square slab (L_x/L_y= 1.02) simply supported along two adjacent sides only, pinned at opposite corner. The slab was designed for a total load of 90 KN, and was applied as two point loads. Details of loading and the resulting support reactions are given in Figure (7.19).

For deflections, the critical points on the slab are point d (see Figure (7.16)), and the point at the middle of the free edge, Figure (7.17). Accordingly, the load-displacement curves for these points are given in Figure (7.16) and Figure (7.17).

First visible cracks were observed on the underside of the slab at three points: under the two load points, and around the middle of the free edges. These occurred at a load of 0.39 P_d and were 0.04, 0.05 and 0.06 mm in width respectively. With increasing loads, the cracks tended to spread from the centre of the slab towards the free edges, running almost parallel to the slab diagonal joining the ends of the orthogonal supporting system (see Figure (7.14)). Cracks developed over a wide band covering the zone between the load points and the propped corner. Cracks reached the confined corner at a load of 0.60 P_d. A deflection of span/250 was reached at 0.64 P_d, and the maximum crack width measured was 0.3 mm, under one of the point loads. At the centre of the free edge, the maximum crack width measured at this load level was only 0.18 mm, and the deflection near the same point was only 6 mm. By a load of 0.67 P_d, a definite Tee-shaped crack pattern had developed, but still new cracks were developing near the corner prop (see Figure (7.14)). Strain measurements indicated that yielding of steel first started at the centre between the two load points, at a load equal to

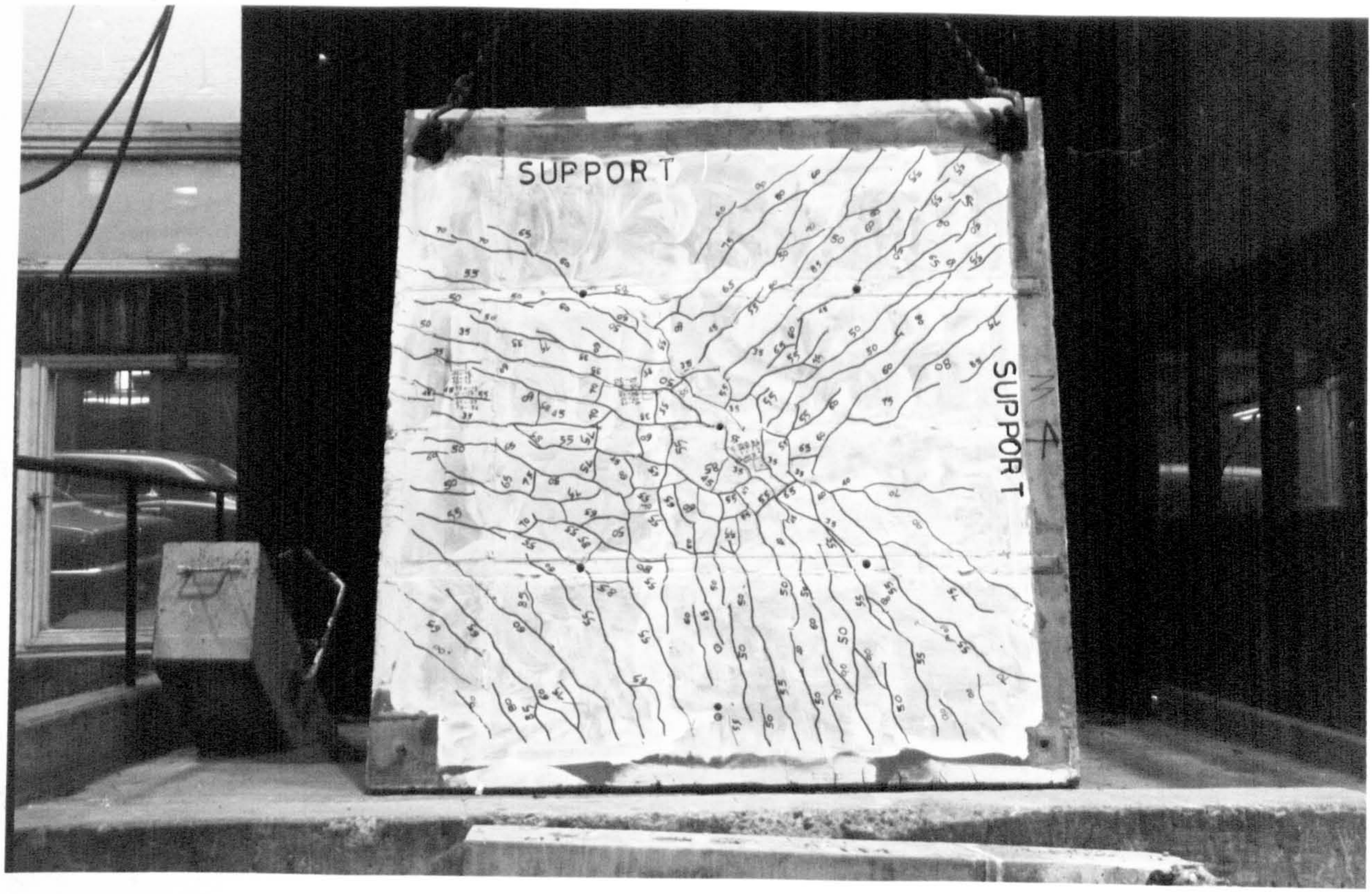

Figure (7·14) Crack Pattern on the Underside of Model 4

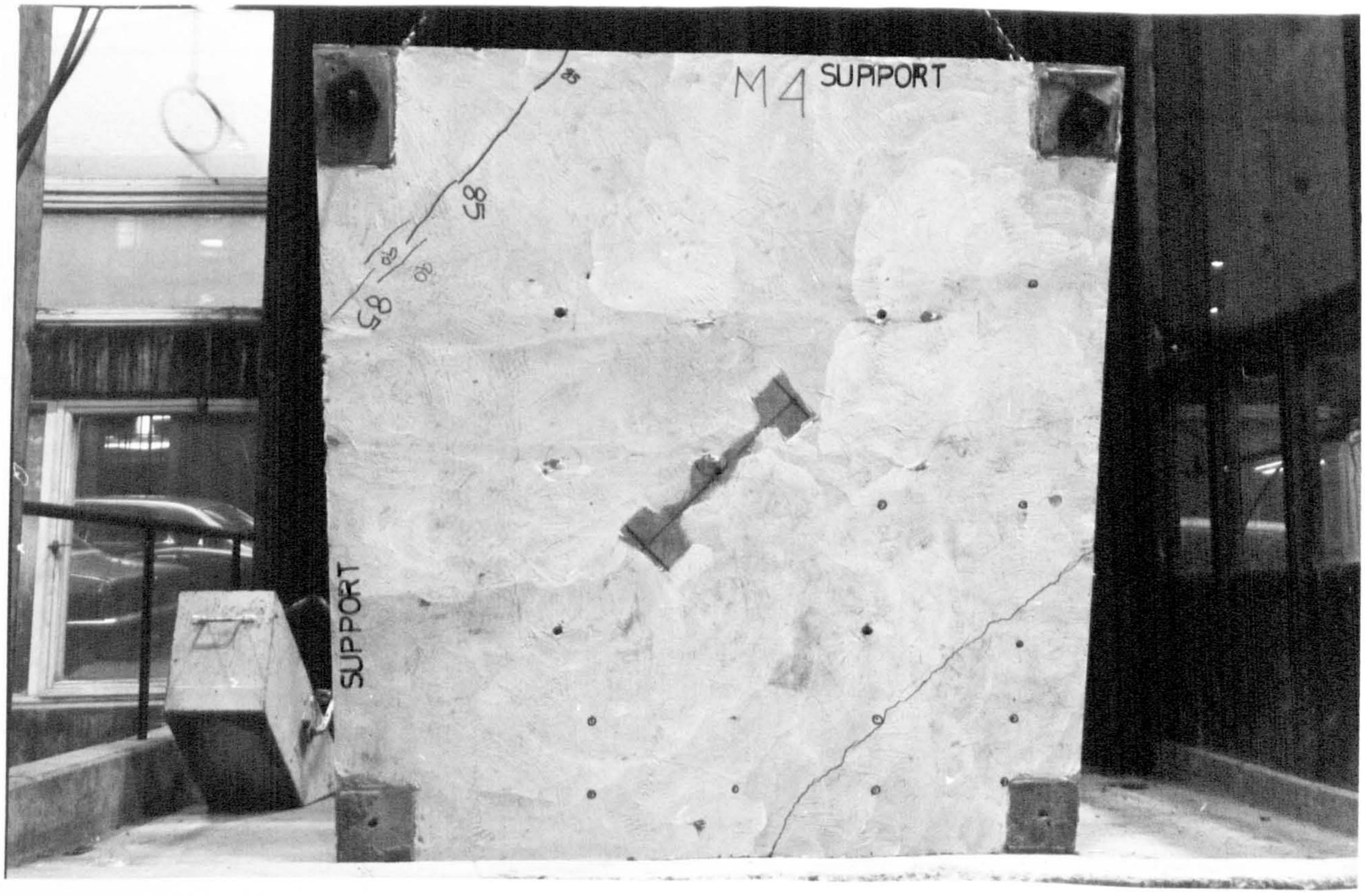

Figure (7·15) Crack Pattern on the Top Face of Model 4

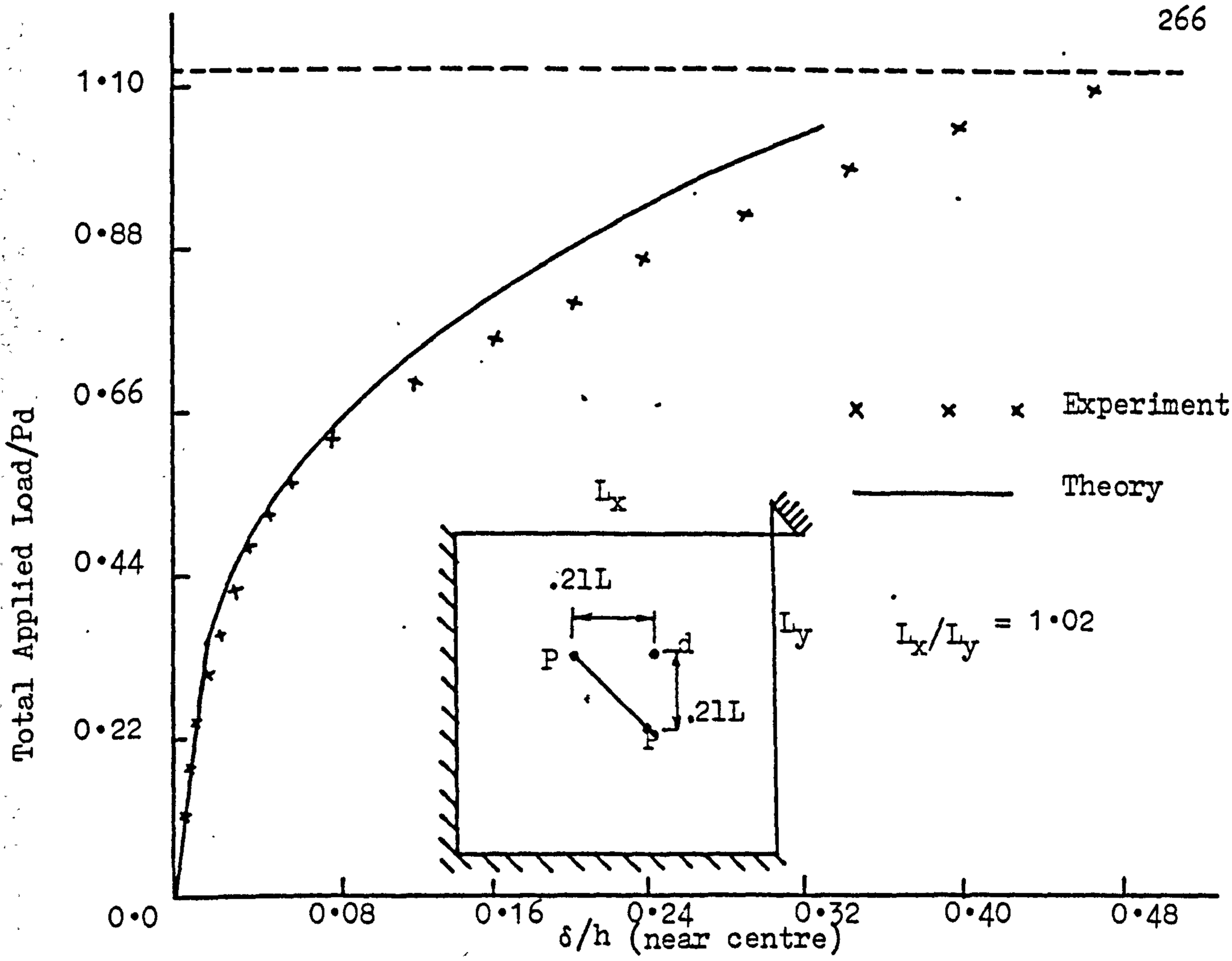

Figure (7•16) Load-Deflection Curve for Model 4

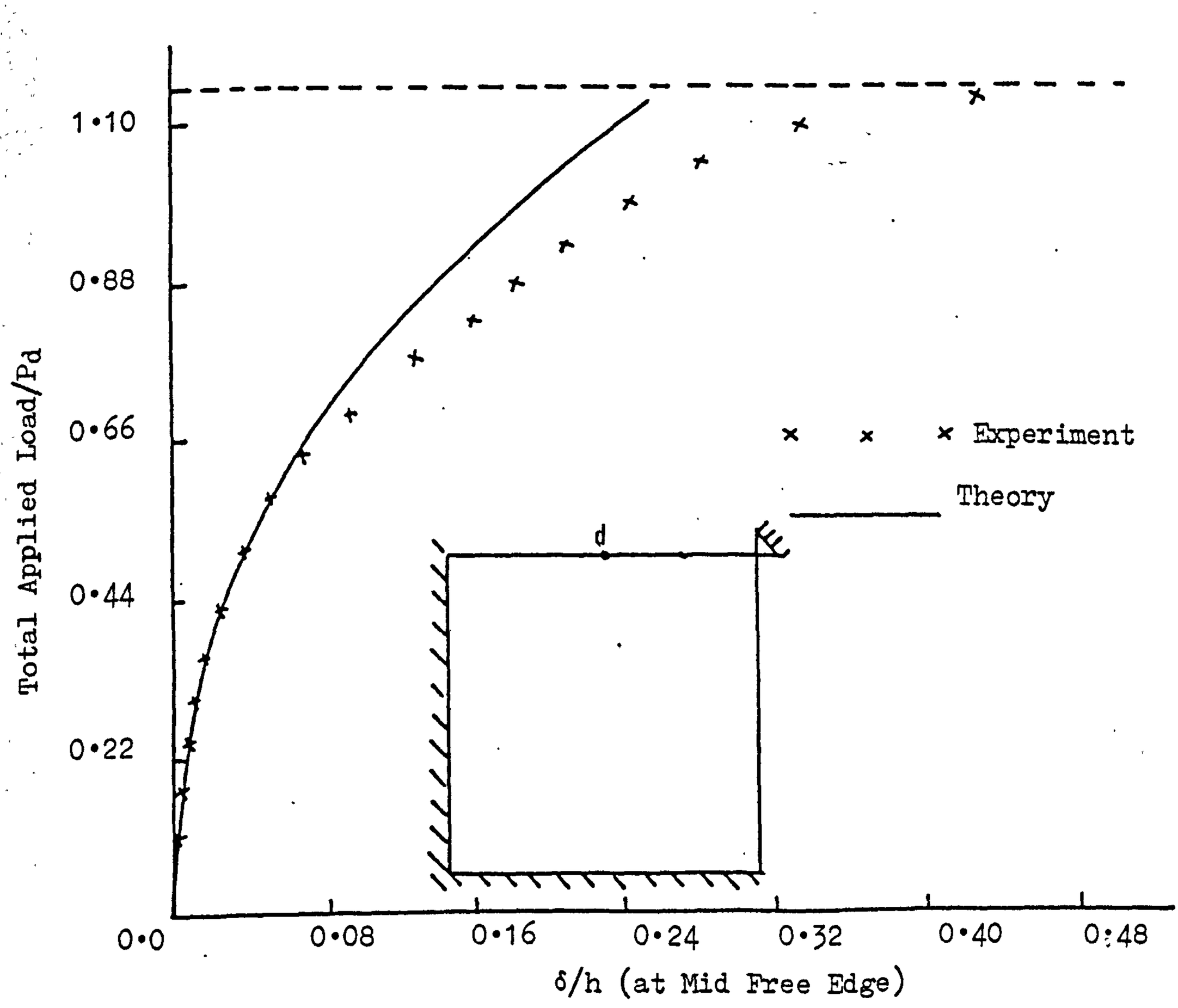

Figure (7•17) Load-Deflection Curve for Model 4

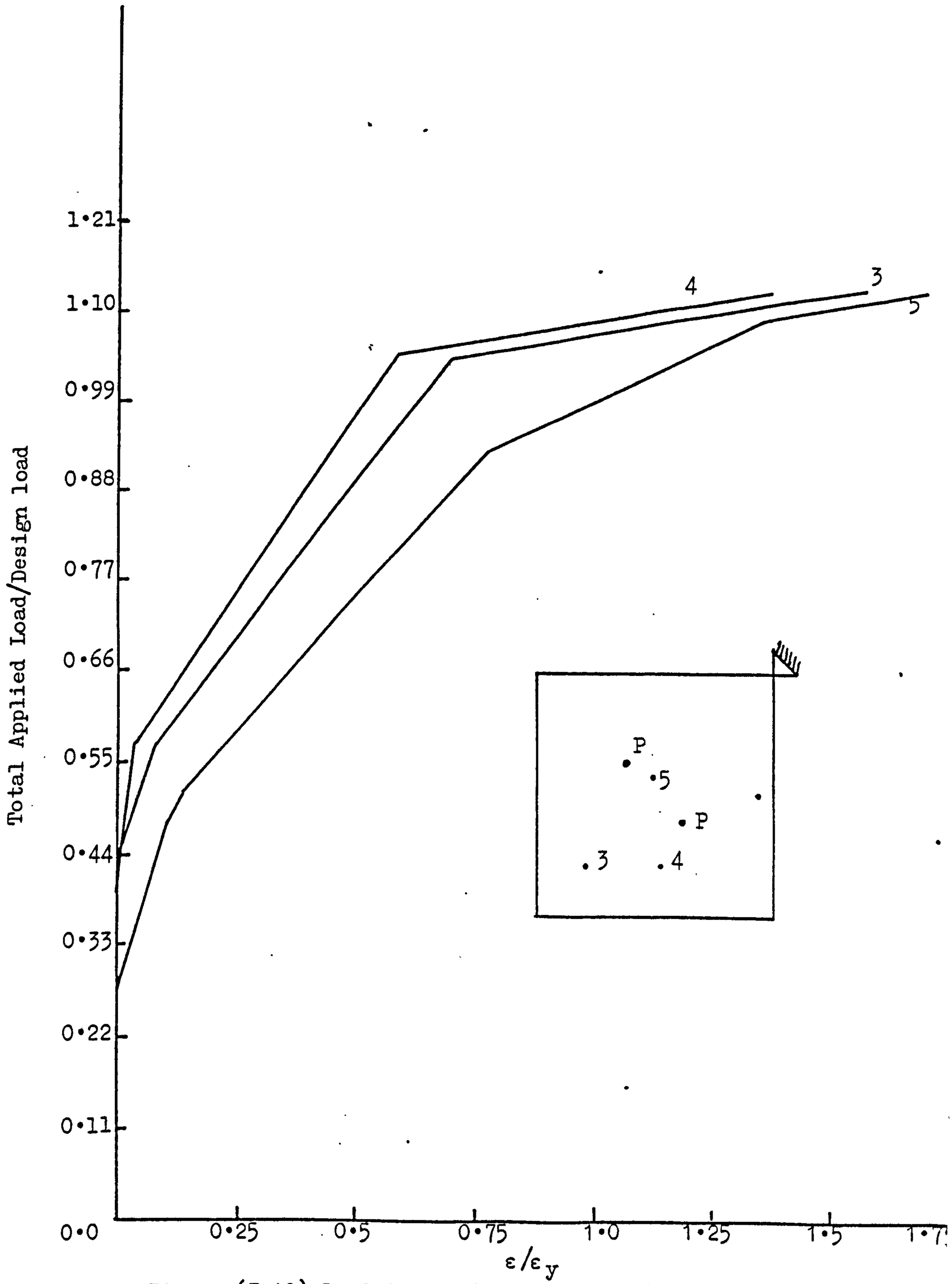

Figure (7•18) Load-Steel Strains in Model 4

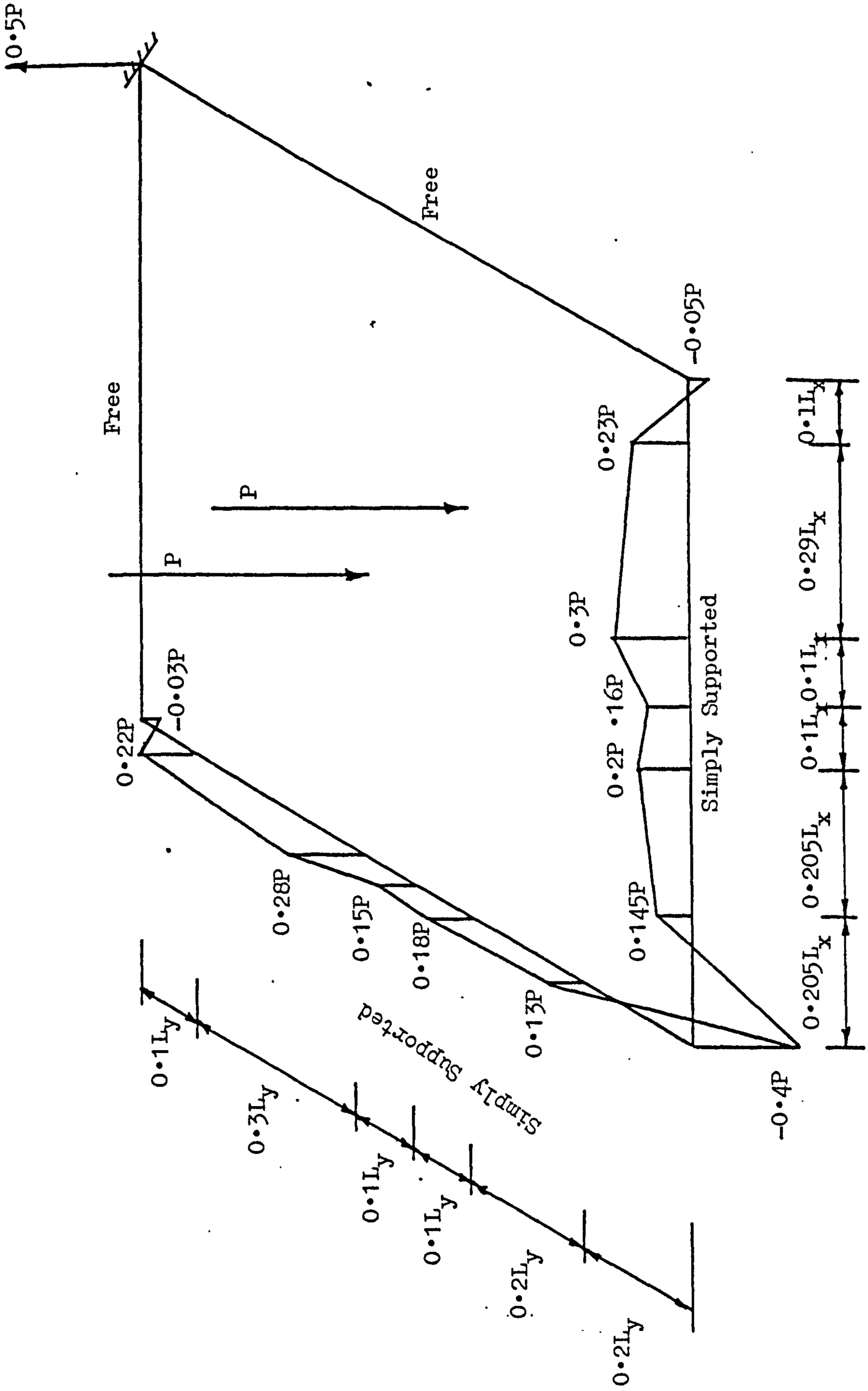

Figure (7·19) Loads and Supports Reactions in Model 4

the design load, and then at the centres of the free edges at 1.1 P_d. The model failed by excessive deflection near the centre, at a load of 1.12 P_d. The load cell at the corner diagonally opposite to the propped corner measured a holding reaction of 15% of the failure load at collapse.

The top surface cracks near the held down corner between the two supported sides were first formed at a load of 0.94 P_d.

7.2.5 Model 5 (Simply Supported, $L_x/L_y = 1.5$):

This model had the same dimensions as model 1, but was designed for a lower load of 216 KN. The model was reinforced according to the average moment in the strips, and steel was curtailed at points where it was not needed. Details of the loading arrangement together with the resulting supports reactions are given in Figure (7.24). Design loads and a summary of the slab behaviour are given in Table (7.1).

The load-central deflection curve for this model is given in Figure (7.22). Unlike model 1, cracking in this slab started earlier, and was observed at about 0.46 P_d. This early cracking had the effect of producing flexible behaviour over the slab loading history. This could be due to the use of a lower grade of concrete, than in the case of model 1, which was 25% higher than model 5.

The first visible cracks were observed under the load points. Similar to previous models, cracks spread in a fine evenly distributed pattern, particularly in the central square defined by the loading holes. At the cracking load, maximum crack widths measured 0.15 mm and 0.18 mm near one load point near the centre, and at the mid point of the slab. Cracks reached the corners of the slab at a load of 0.69 P_d. Both the

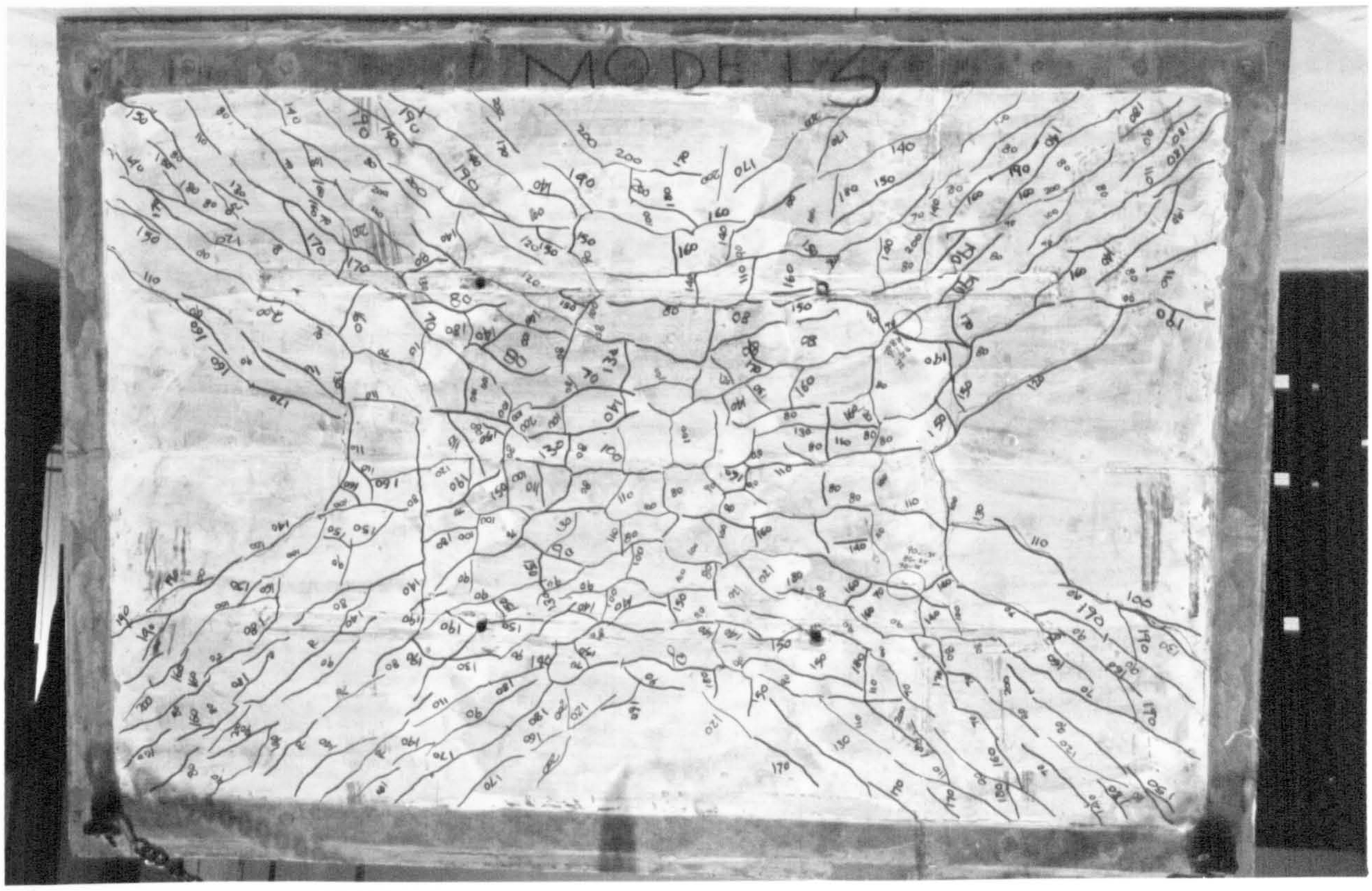

Figure (7·20) Crack Pattern on the Underside of Model 5

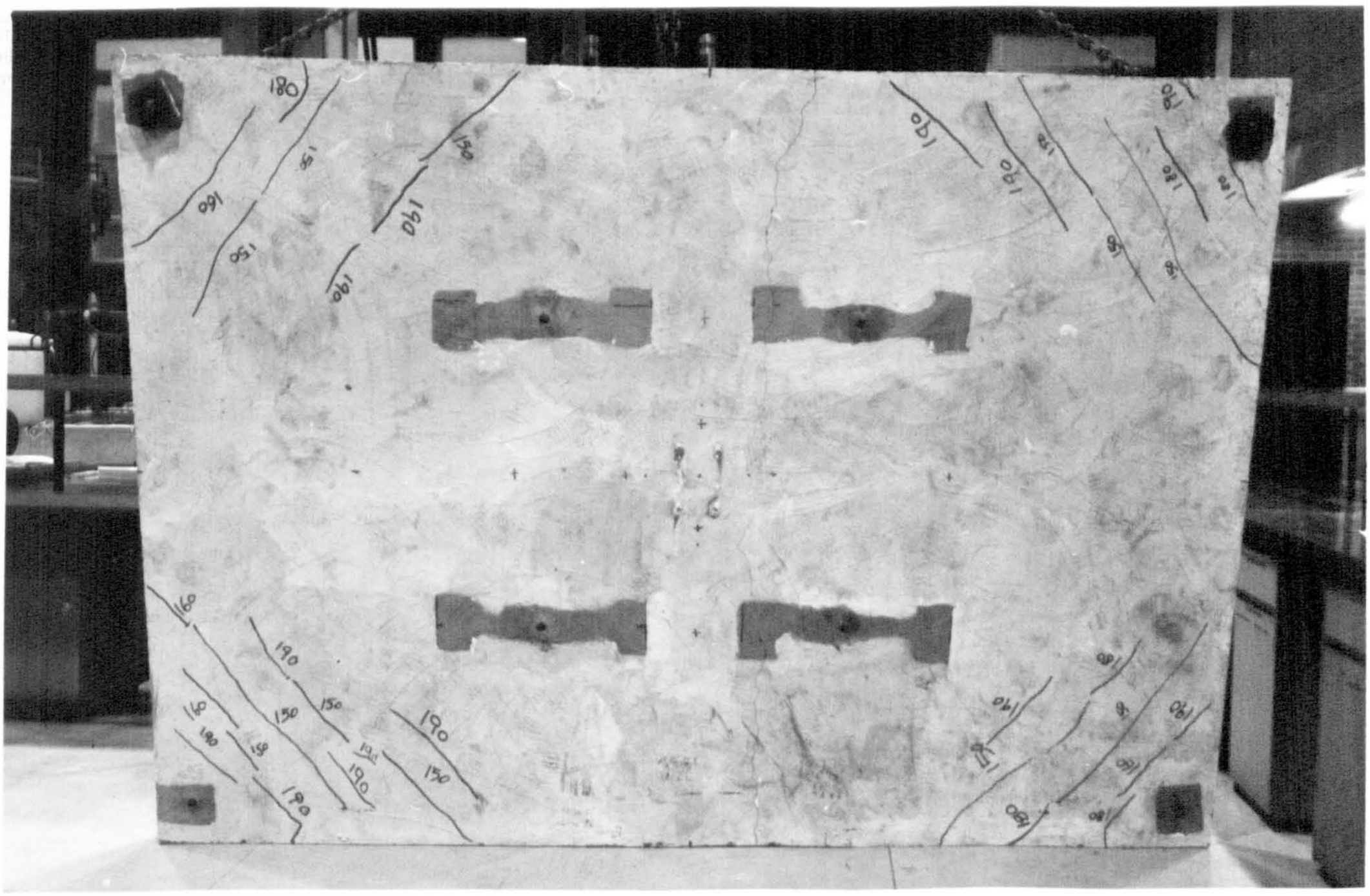

Figure (7·21) Crack Pattern on the Top Face of Model 5

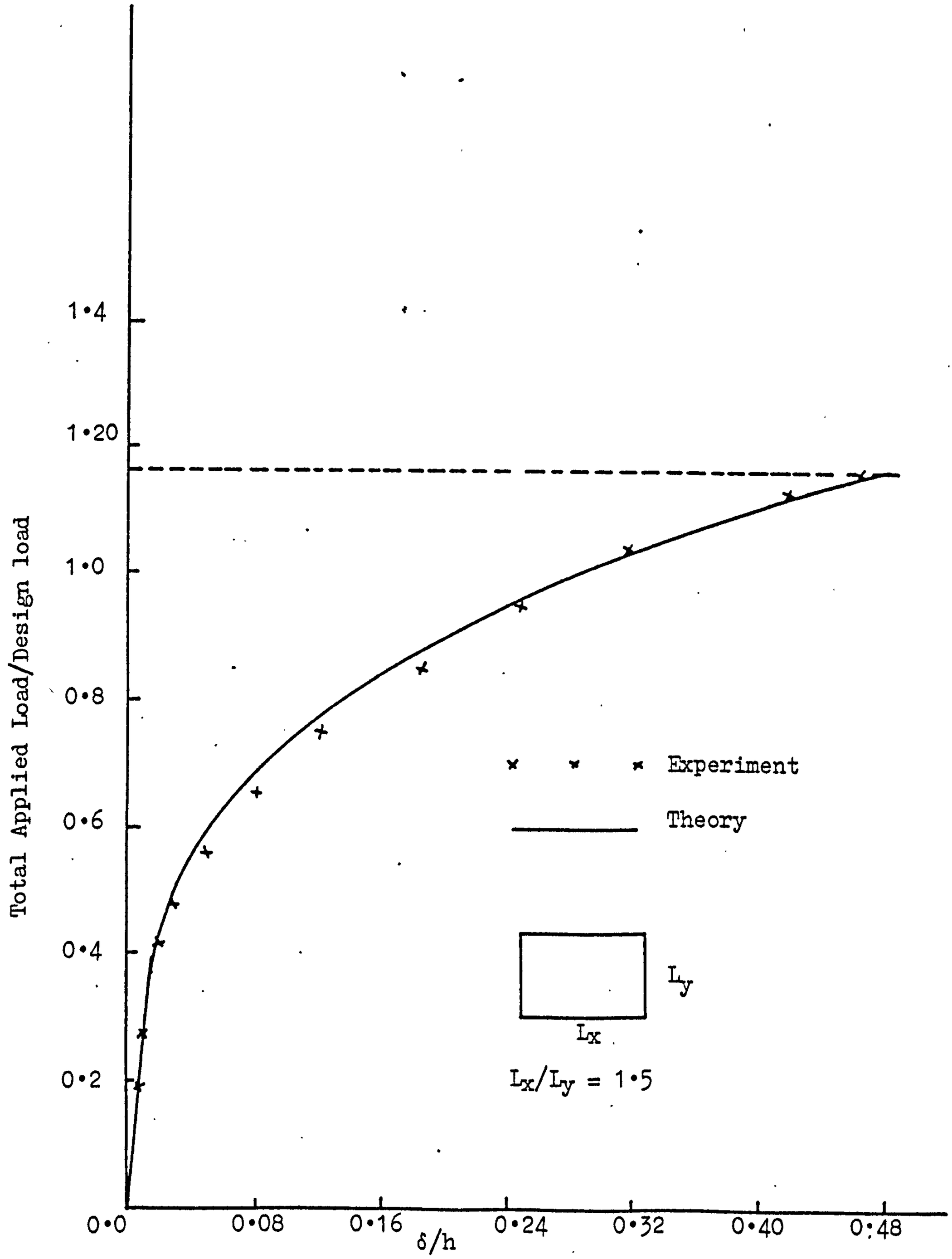

Figure (7•22) Load-Deflection Curve for Model 5

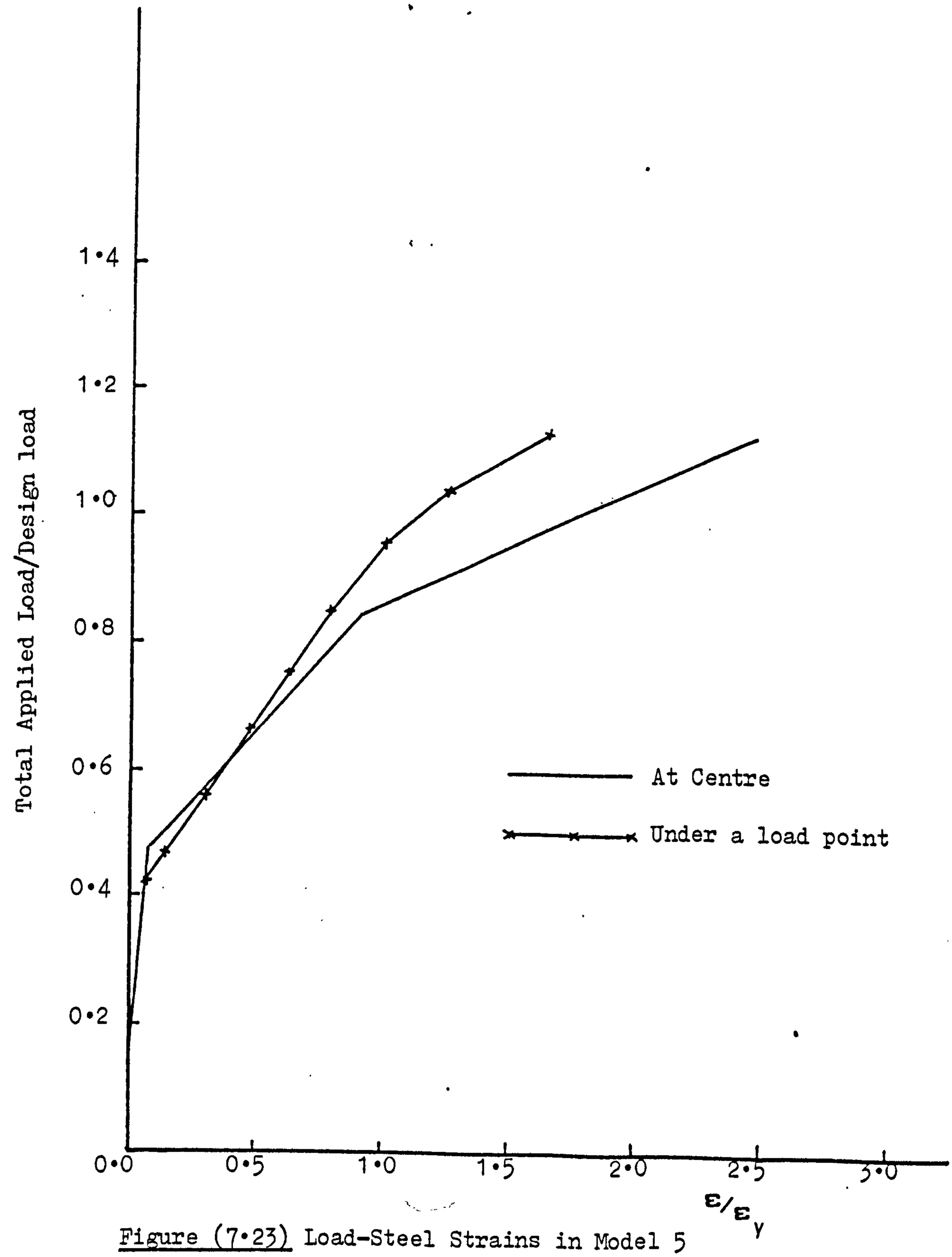

Figure (7•23) Load-Steel Strains in Model 5

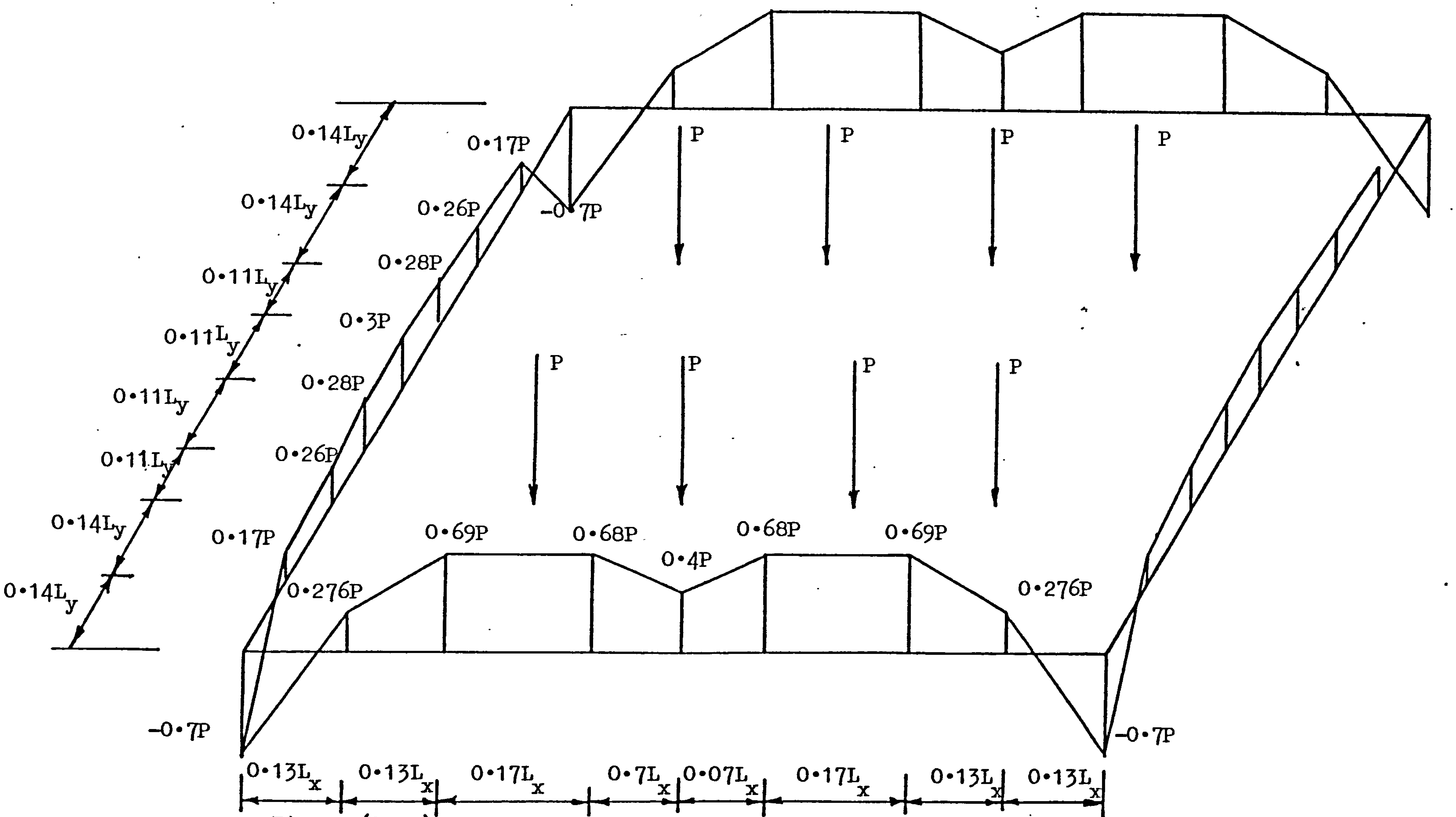

<u>Figure (7·24)</u> Loads and Supports. Reactions in Model 5

deflection limit of span/250 and the crack width limit of 0.3 mm were reached simultaneously at a load of 0.63 P_d.

First cracks at the top surface were observed at 0.69 P_d. With increasing loads new top surface cracks tended to form rather than widening the existing cracks, which indicates that a large redistribution of forces is not taking place. A well developed yield line pattern on the top and bottom of the slab was clearly formed when the design load was reached. The slab failed in a flexure mode similar to previous models at a load of 1.07 P_d.

7.2.6 Model 6 (A slab-beam system, $L_x/L_y = 1.5$):

This was a rectangular slab supported by monolithic edge beams on the four sides. The beams had the same cross-sectional dimensions all around. The dimensions, materials properties and design loads for this model are given in Table (7.1).

The elastic analysis of this model by the layered finite element model predicts the stress resultants (N_x, N_y, N_{xy}, M_x, M_y, M_{xy}), due to the shift of the middle plane of the beams, to the level of that of the slab. However, in the design of reinforcement for this model, the membrane components of the stress resultants were neglected, and the system was designed for flexural components only. In addition, due to the fact that the present layered finite element model underestimates the torsional forces in the beams (see Section 4.4.4), additional torsional reinforcement in the supporting beams was added, according to CP 110[5]. The torsional reinforcement was provided in the form of longitudinal bars and links. Also because of the underestimated torsional forces on the beams, tensile reinforcement on the top surface

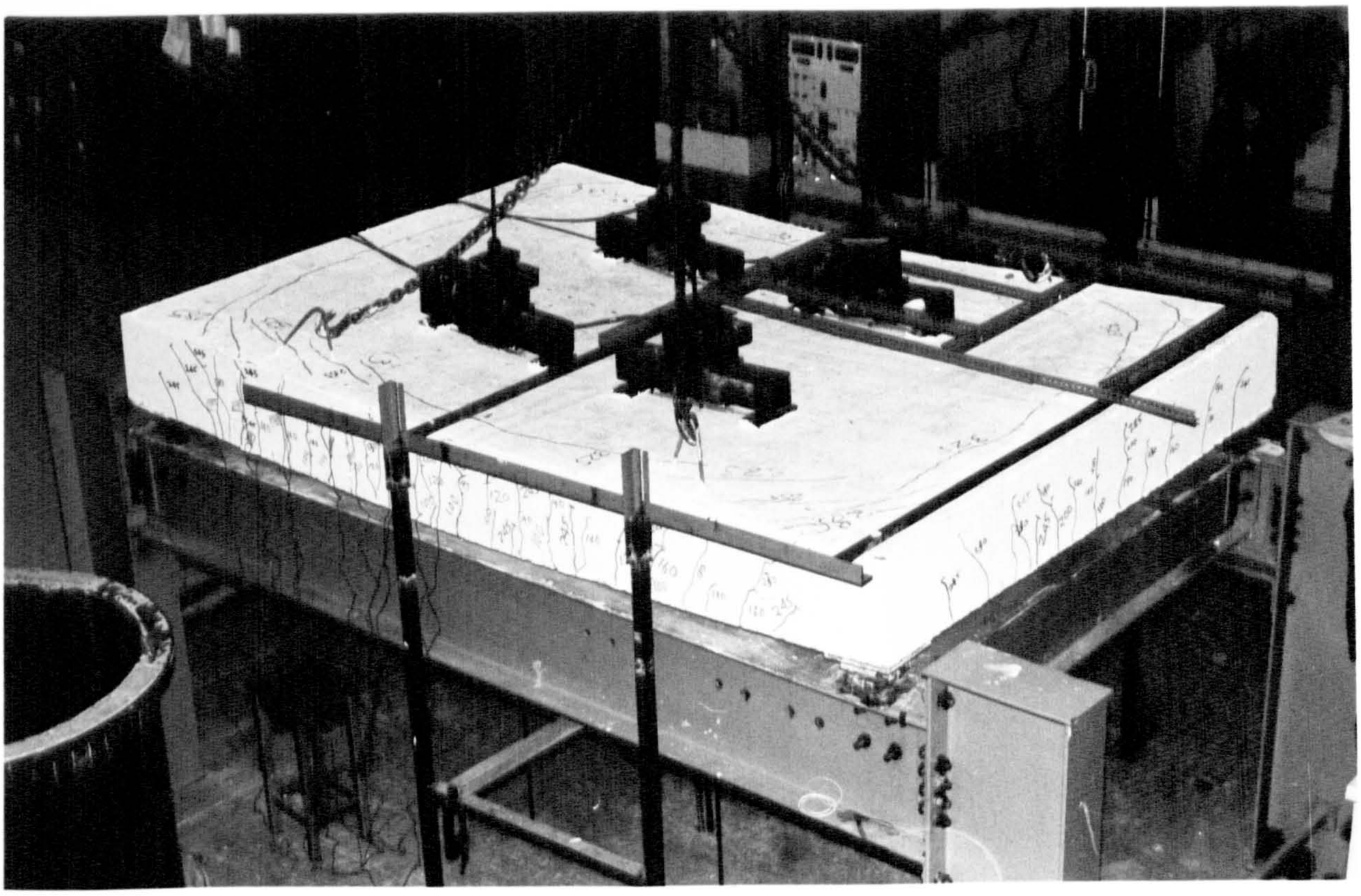

Figure (7·25) Model 6 Under Test

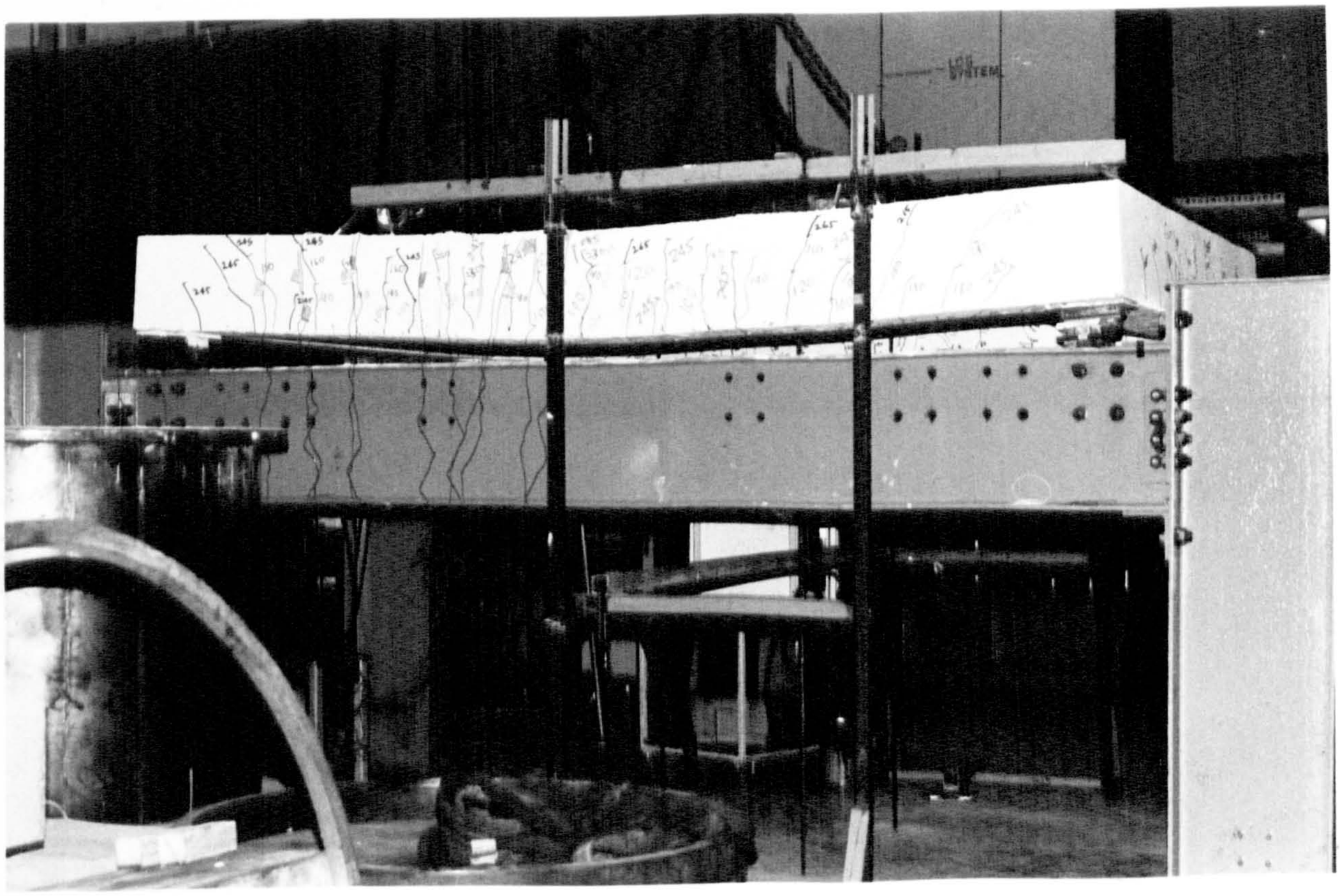

Figure (7·26) Cracks on the long beam of Model 6

between the slab and beams was very small. Accordingly, this reinforcement was also provided according to CP110[5].

The total design load for this model was 240 KN. Resulting reinforcement distribution in the slab is shown in Figure (6.9a), and for the beams in Figure (6.9b). The model was tested to failure by applying the load in increments of 5 KN per load cell. Figure (7.25) gives a photograph for this model under test.

As far as deflections are concerned, the critical points are those at the middle of the slab, and at the mid point of each beam. Accordingly, the load-displacement curves at these three points are given in Figures (7.29), (7.30) and (7.31). The behaviour of the model is generally linear up to a load of 0.38 P_d, when the first visible cracks were observed on the inner side of the ribs of the long beams, around points in line with the loading holes marked in Figure (7.33).

By examining the load-deflection curves in Figure (7.29) to (7.31), it can be seen that the slab is not very much affected by cracking at this load level and was probably behaving in an elastic manner. However, nonlinearity in the deflections of the long beams starts earlier than this, and can be attributed to invisible microcracking in the edge beams. At a total load of 0.46 P_d, cracks were spreading in the middle third of the inner side of the rib, but did not reach the outer face of the long beams. This cracking at the middle third of the beam caused tiny cracks to form at the middle of the slab at a load of 0.533 P_d. These tiny cracks were running parallel to the short edge beams, and had a maximum width of 0.03 mm at 0.533 P_d. At this load, the cracks on the long beams were extending to the bottom face of the rib, and reached the outer faces of the beams. The depth of these cracks on

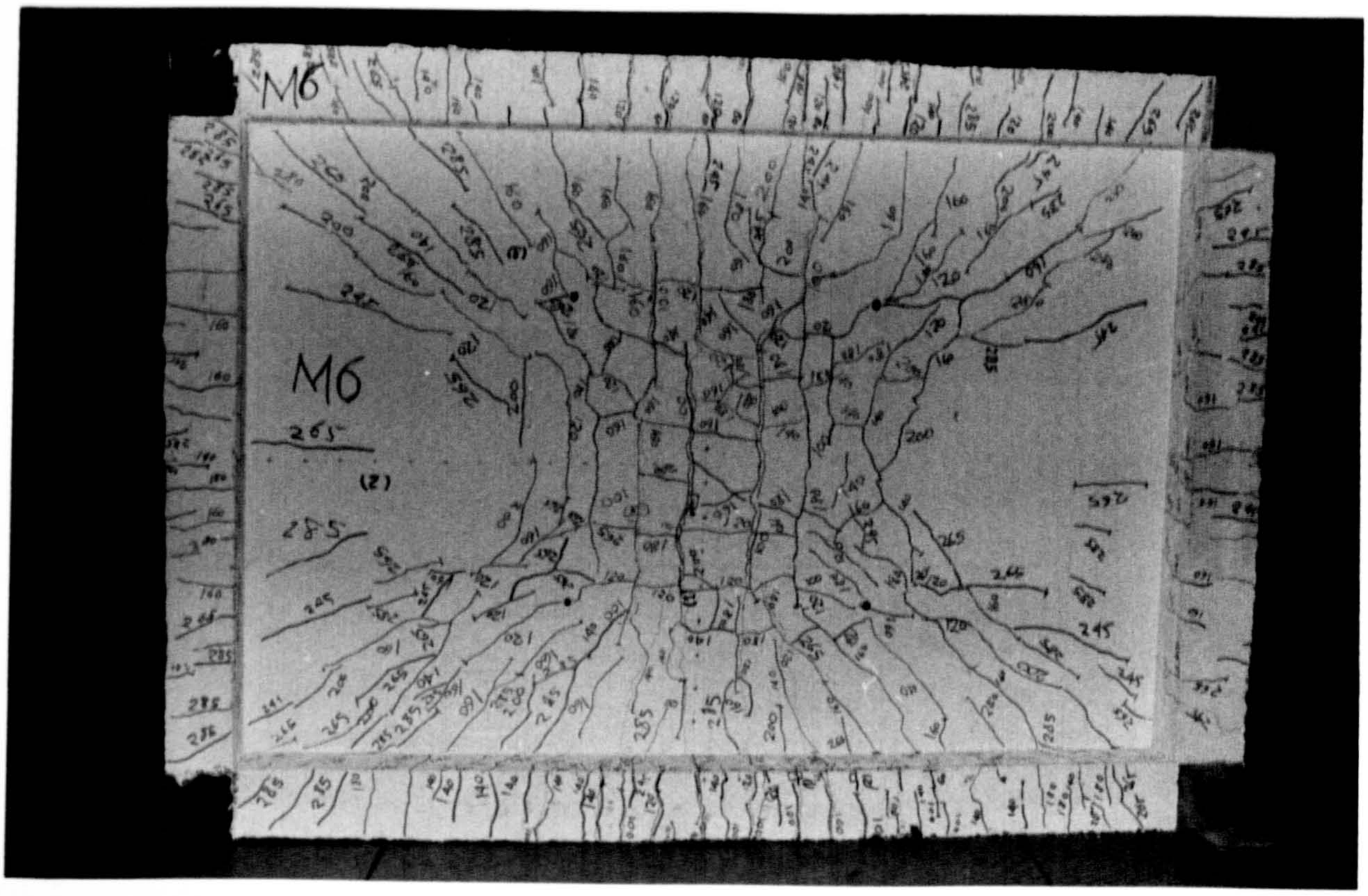

Figure (7·27) Crack Pattern on the Underside of Model 6

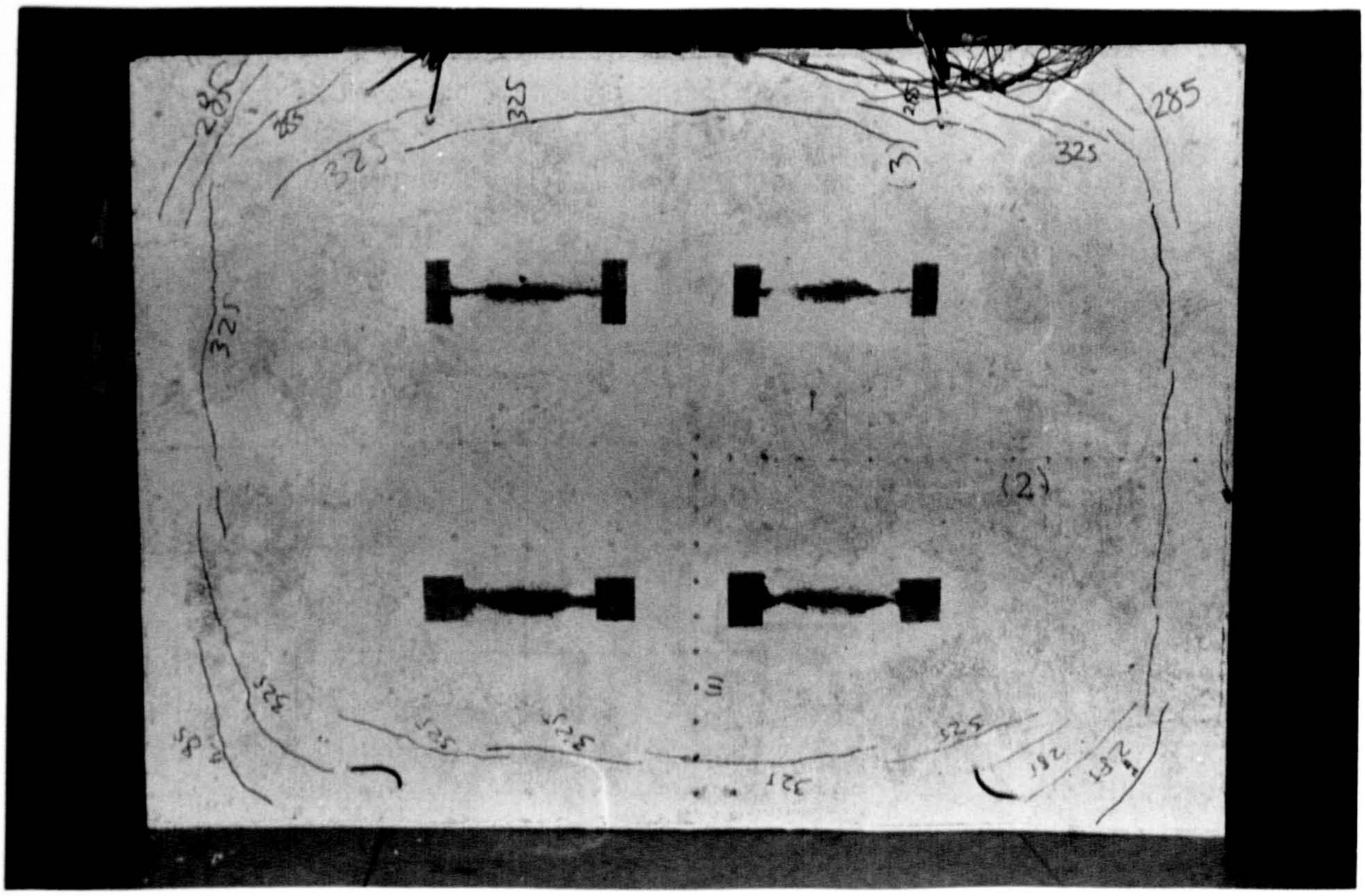

Figure (7·28) Crack Pattern on the Top Face of Model 6

the inner side of the ribs of the long beams did not reach the mid depth of the rib at this load. A general trend to form new surface cracks rather than to open up the existing cracks was observed. The maximum crack width in the middle third of the ribs of the long beams was 0.10 mm at a load of 0.533 P_d.

At a load of 0.625 P_d, more new cracks formed in the middle third of the long beams. However, the first cracks on the long beams at points in line with the loading holes (Figure (7.33)), reached the midheight of the ribs at a load of 0.625 P_d. Although this load may be taken as the service load for this model, cracks were generally still very narrow. The maximum crack width at this load was only 0.13 mm near the inner edge of the ribs of the long beams, at points in line with the loading holes. At this load, first cracks were observed on the outer face of the short edge beams. These cracks were much smaller in width than the cracks in the slab, and thus were not measured. Also at this load, the cracks at the centre of the slab were spreading outwards towards the long supporting beams, with a general inclination of about 35° to the edge beams. Some of these cracks reached the loading holes at a load of 0.625 P_d.

At a load of 0.72 P_d, most of the first cracks in the middle third of the long beams covered the full height of the rib from inside, and reached the junction between the slab and the rib. The maximum width of the largest crack measured 0.2 mm, just under the loading holes on the inner side of the ribs of the long beams. On the outer face of the ribs, most of the cracks extended to about half the total depth of the beams. Cracks on the outside of the short beams also reached their mid depth, but still no cracks appeared on the inner face

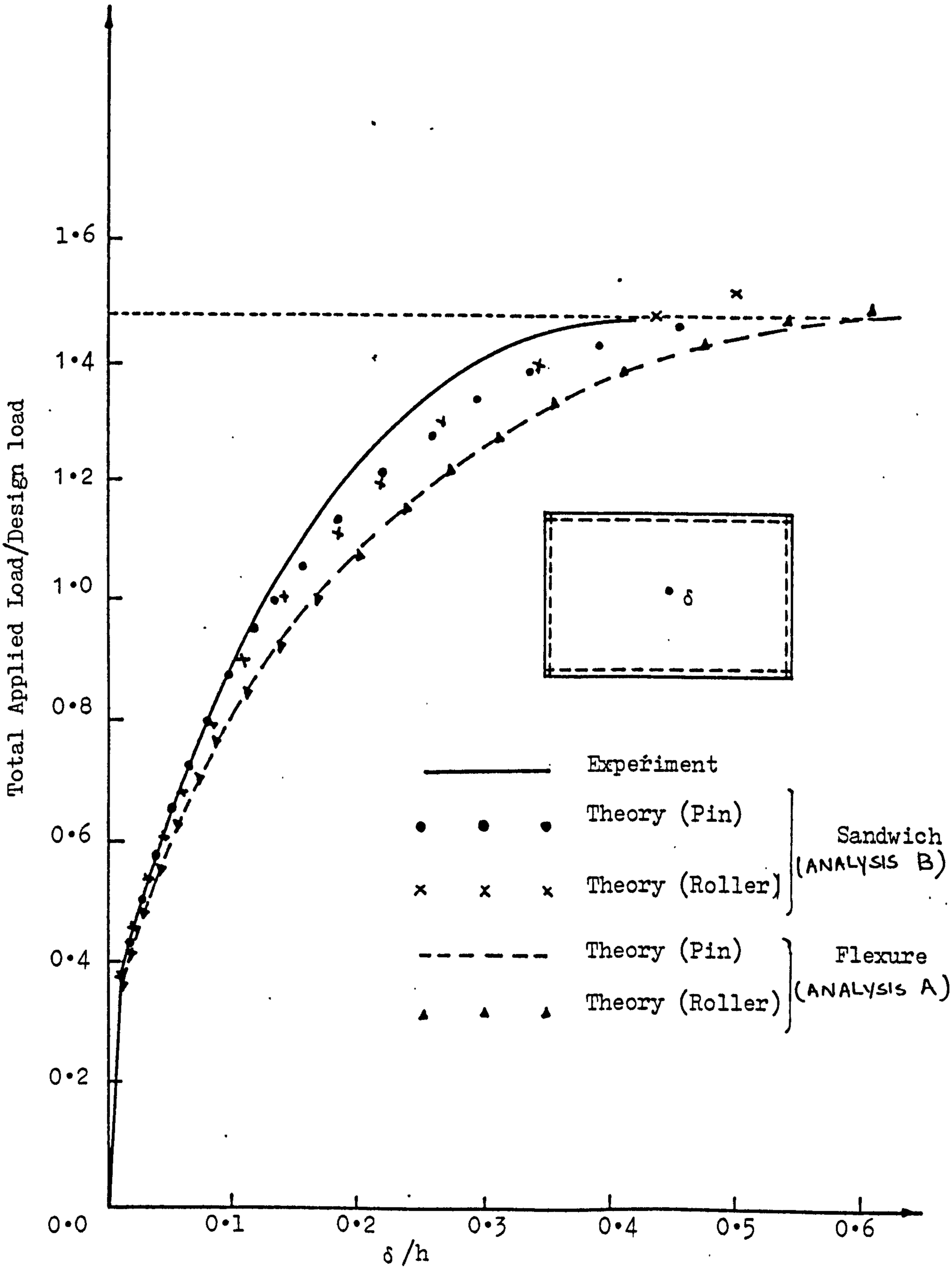

Figure (7·29) Load-Central Deflection in Model 6

of their ribs. On the bottom of the slab, the first cracks to form were observed to reach the supporting long beams, indicating the first step towards the formation of one collapse mechanism. Crack widths on the underside of the slab measured a maximum of 0.08mm only under this load.

At a load of 0.8 P_d, the maximum total deflection at the slab centre was only 8 mm. This represents the limiting service deflection for this model according to CP110[5]. At this load, the first inclined cracks on the long beams were formed on the inner side of the rib near the supported corner, and were extending to one third the depth of the rib, but did not form on the outer face of the rib. These cracks were generally inclined at about 150° with the centreline of the long beams, measured from the corner side. The first cracks on the inner side of the short beams were also observed at this load and were rapidly covering its middle third zone. The maximum extension of these cracks did not exceed one third the rib depth, and did not extend beyond the middle of the rib breadth from the bottom face. On the under side of the slab, the major cracks at the centre of the slab had reached the long beams, and joined with the main crack at the middle of the beams.

At 0.9 P_d more inclined cracks on the long beams appeared near the corners. This time this cracking also occurred on the outer face of the beam ribs and were running in a direction normal to those formed on the inside of the ribs. These cracks may be due to the interaction between shear and torsional effects. In the previous load increment, this interaction was seen to cancel the simultaneous appearance of the torsional cracks on the outer face of the long beams. At this load level, the earliest cracks were noticed to widen. The maximum crack

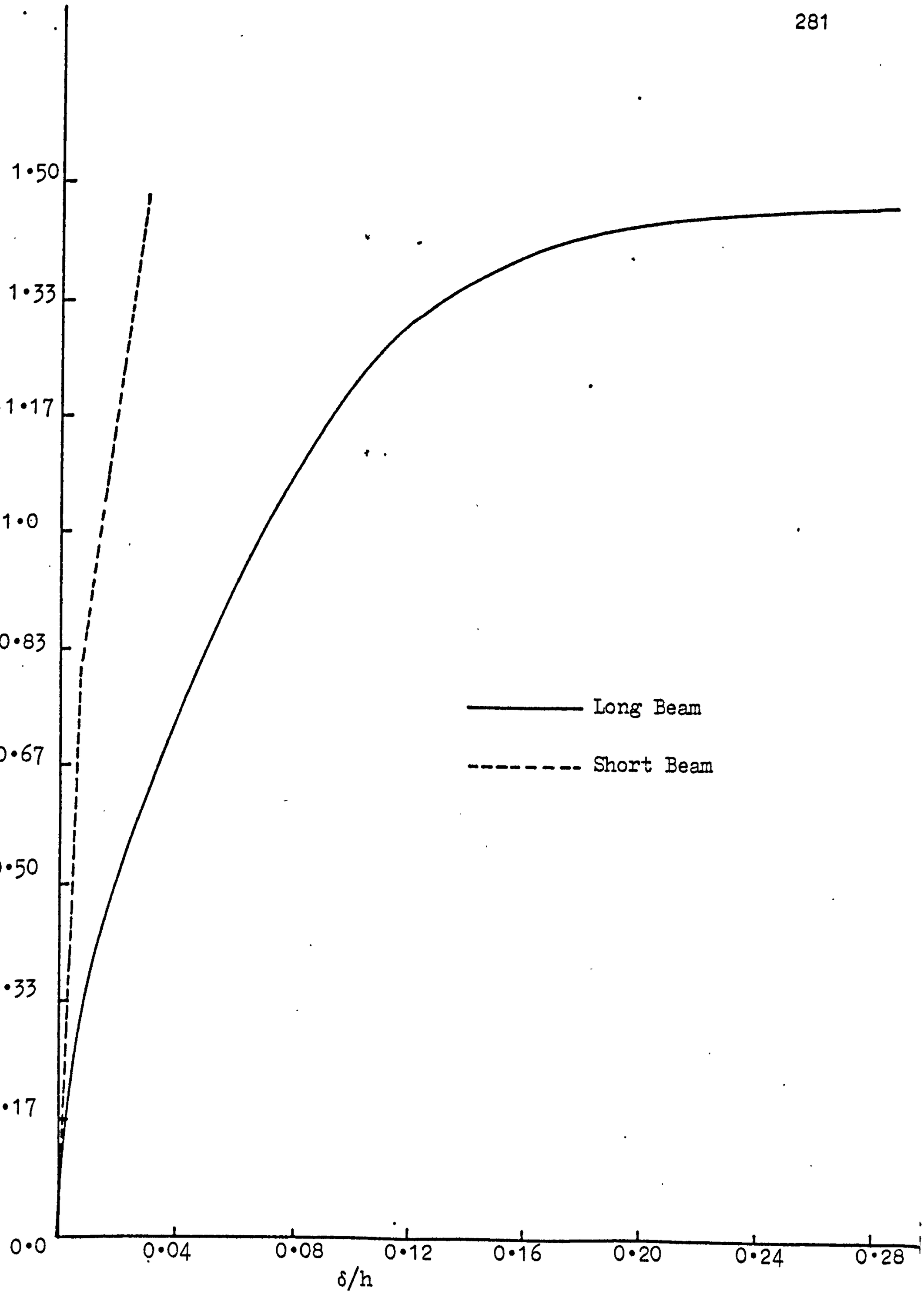

Figure (7•30) Load-Mid Beams Deflections in Model 6

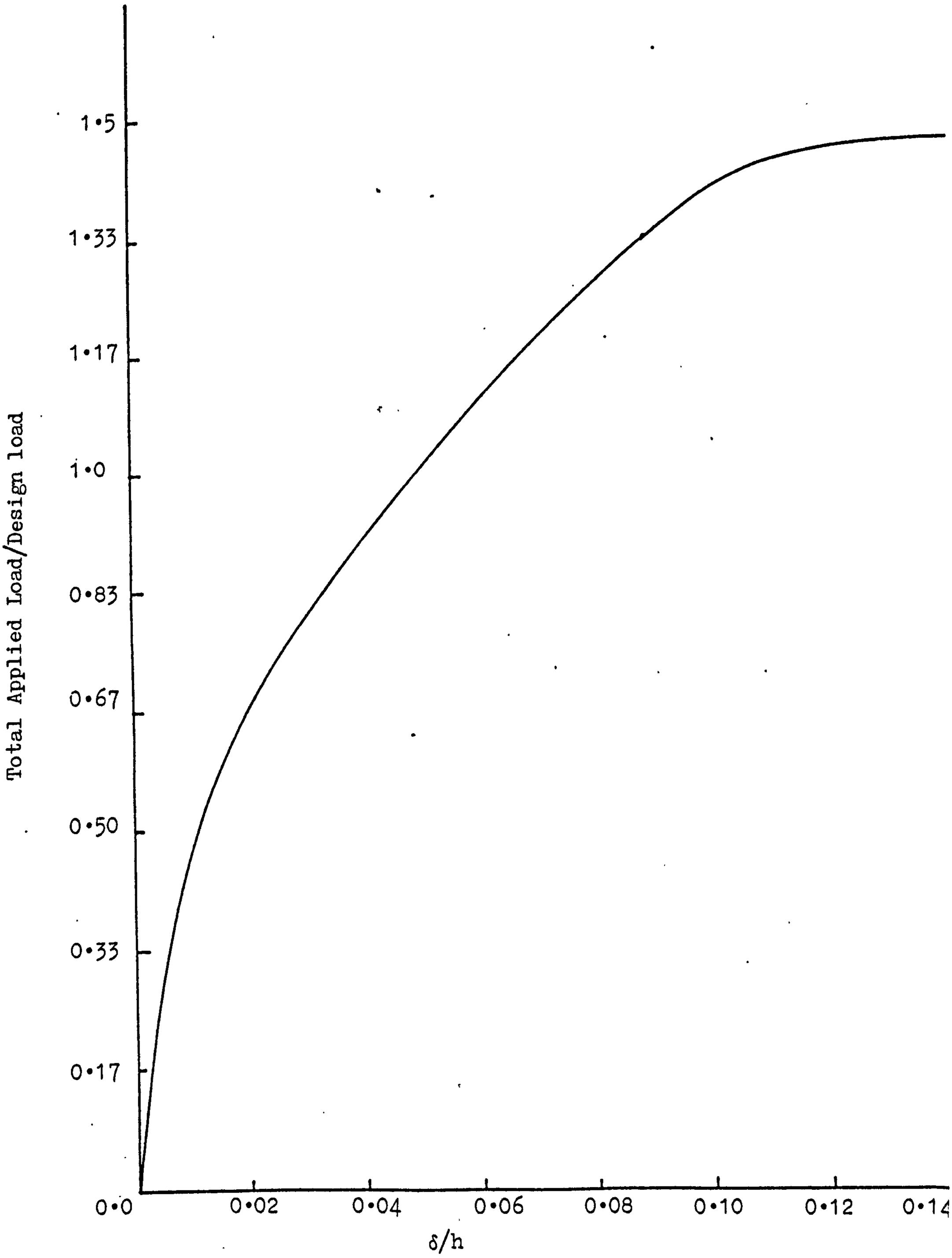

Figure (7•31) Load-Relative Deflection between Slab and Long Beams in Model 6

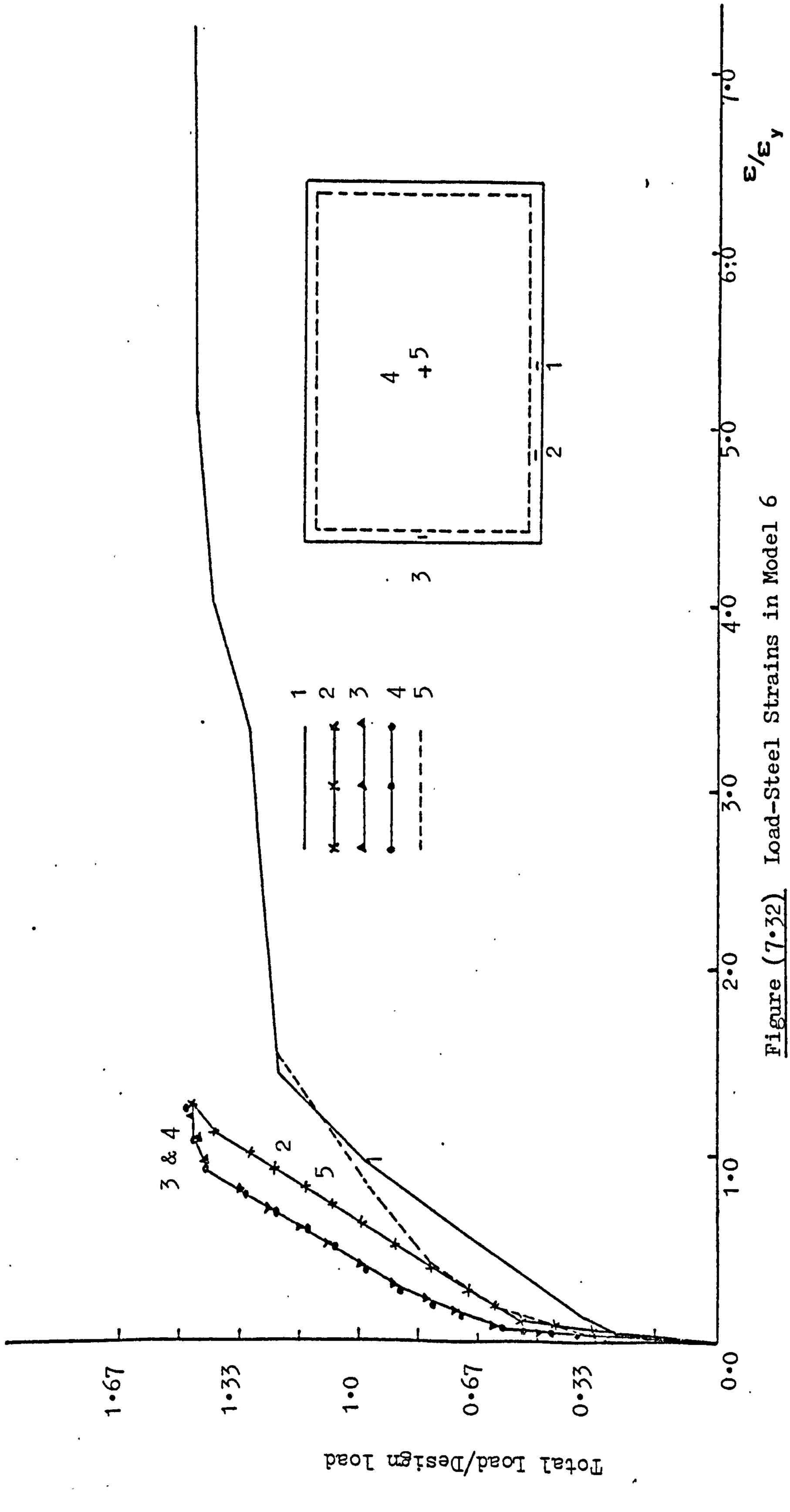
1
2
3
4
5
+5
1·0
2·0
3·0
4·0
5·0
6·0
ε/εy
Load-Steel Strains in Model 6
Total Load/Design load
1·67
1·33
1·0
0·67
0·33
0·0
3 & 4
2
5
1

Figure (7·32)

N.B. Loading Holes Marked +

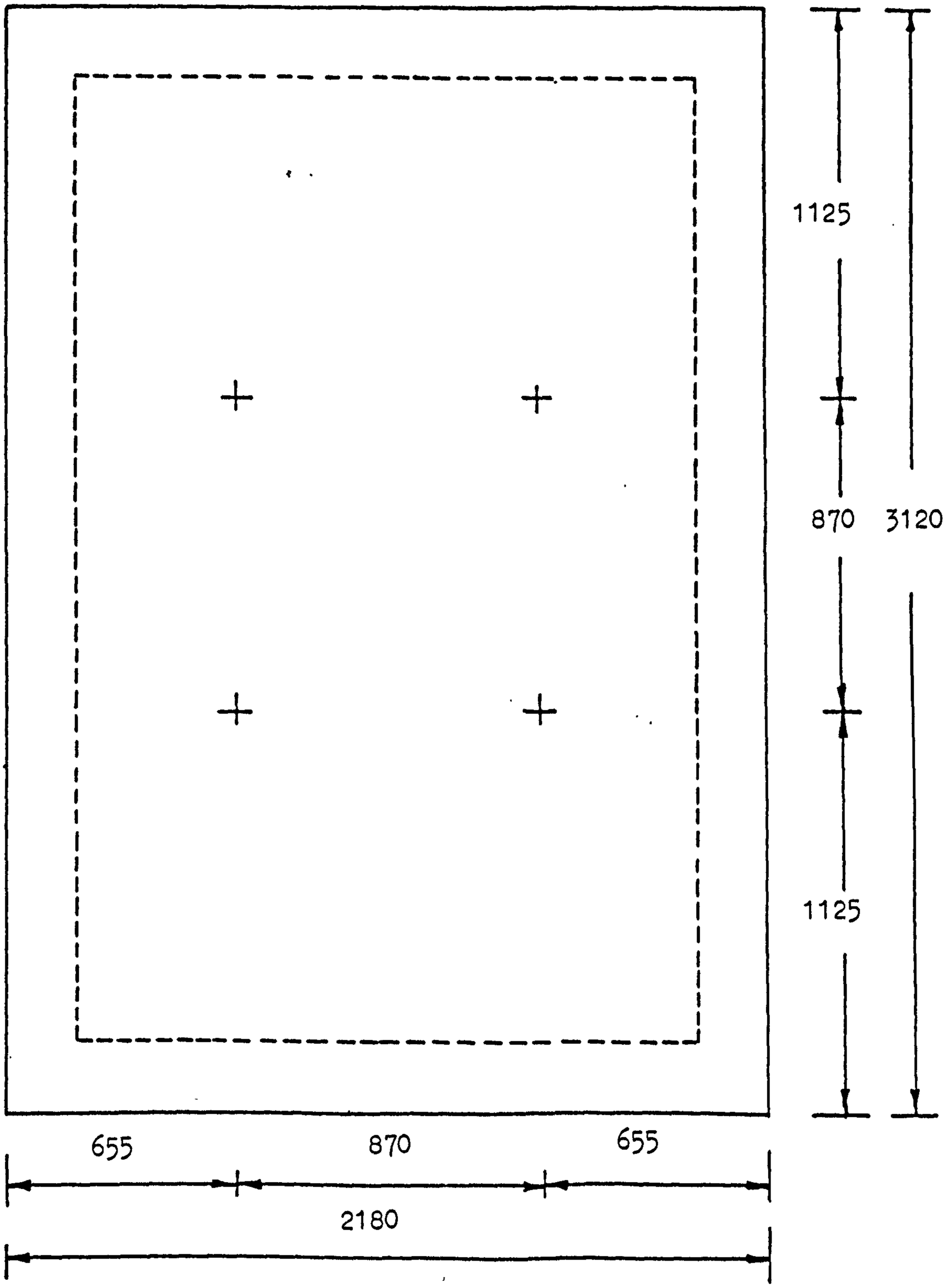

Figure (7·33) Dimensions and Loading Positions on Model 6

width was 0.3 mm near the loading holes on the ribs of the long beams. The change in stiffness of the short beams due to extensive cracking at this load can clearly be seen from Figure (7.30).

On subsequent load increments, very few new cracks formed, and these were confined to the extensions of old cracks near the corners of the slab. A major crack through the corner junction between the two beams was formed at about a load of 1.19 P_d, indicating the disruption of the corner connection. Top surface cracks were observed around this load near the corners, along the junction between the beams and the slab. On the bottom face of the slab, the major crack at the centre was widening, and was continuous with that at the middle of the long beams. Deflections rapidly increased by a load of 1.48 P_d, the dial gauge under the centre of the slab was rotating freely, and it was very difficult to maintain the load at a certain value. The test was then stopped, due to excessive deflection, and the load of 1.48 P_d was taken as the ultimate load.

7.3 DISCUSSION OF TEST RESULTS:

7.3.1 Serviceability Limit States.

Table (7.1) summarizes all the test results. The service load is taken as the minimum of two values: one based on a deflection limit of span/250, the other on a maximum crack width of 0.3 mm[5]. Accordingly, the general conclusion to be drawn from the table is that the service behaviour of all slabs tested is satisfactory, except model 1. This model actually failed in shear, due to an error in its design.

In the adoption of the present design procedure, use had been made of the elastic stress distribution under the design load by the

Model No.	Live Load (KN)	Dead Load (KN)	Design Load Pd(KN)	P_{cr}/P_d	P_{sl}/P_d	P_{scr}/P_d	P_y/P_d	P_u/P_d	Remarks
1	400	16	416	0·33	0·40	0·45	0·69	-	Shear Failure
2	200	13	213	0·62	0·75	0·85	0·94	1·31	Flexural Failure
3	200	10	210	0·52	0·70	0·67	0·97	1·16	"
4	80	10	90	0·39	0·63	0·63	0·99	1·12	"
5	200	16	216	0·47	0·63	0·63	0·80	1·07	"
6	210	30	240	0·36	0·82	0·90	0·99	1·48	"

P_{cr} = Cracking load, P_{sl} = Limit service load of deflection, P_{scr} = Limit service load of cracking,

P_y = First yield load, P_u = Ultimate load.

Table (7·1): Service and Ultimate Behaviour of the Tested Slabs.

finite element method. However, such an analysis normally predicts "elastic" deflections under the design load. Since elastic uncracked stiffnesses have been used in the analysis, such elastic deflections would be a serious underestimation of the true deflections under service loads, as has been shown in Chapter (5). However, a valid design to Limit Theory should satisfy serviceability criteria, and the normal practice is to design for the ultimate limit state, and then check for serviceability. Accordingly, in the present design procedure, since the elastic deflections cannot directly be used to check for serviceability, they can be useful if an effective partially cracked section properties had been used. In this study, the elastic deflections have been used with the Branson's method (Section 2.3.1.1), to predict the deflections under the service loads. So if δ_e is the elastic deflection under the design ultimate load, the service deflection will be

$$\delta_p = \delta_e \times I_g/(LF \times I_{eff})$$

where

δ_p = Predicted deflection

δ_e = elastic deflection,

I_g = gross moment of inertia

I_{eff} = effective moment of inertia of the section

LF = Load Factor

The method is fully described in Appendix (E).

A summary of the predicted behaviour of all test models is given in Table (7.2). Deflections have been predicted, using the simplifying assumptions for cracked sections (Appendix E). Due to the fact that in most tested slabs the live load is about 10 times the dead load, the service load is taken as $P_d/1.6$ (i.e. $0.625\ P_d$).

Model No.	ft N/mm^2	$m = E_s/E_c$	Total Depth h(mm)	Effective Depth d(mm)	Service Moment M_s Nmm/mm	Cracking Moment Nmm/mm	Area of Steel As mm^2/mm	Elastic deflection δ_e(mm)	Predicted deflection δ_p(mm)	δ_p / δ_m
1	3·68	8·3	100	85	20000	6655	0·792	6·12	12·0	0·57
2	3·68	9·95	"	"	8237	6397	0·327	3·04	3·55	1·02
3	3·40	9·95	"	"	10933	5994	0·439	2·25	4·14	1·04
4	2·97	10·5	"	"	8070	5163	0·308	4·03	6·72	0·67
5	3·0	9·70	"	"	10000	5249	0·389	3·56	7·28	1·02
6	3·15	9·91	"	"	7100	5544	0·428	4·97	5·55	1·10

ft = Tensile strength of concrete, δ_m = measured maximum deflection in the slab

Table (7·2): Predicted and Experimental Service Deflections of the Test Slabs

As can be seen from Table (7.2) except for model 1, that the adopted procedure yields excellent predictions. Accordingly, the adoption of elastic deflections modified by the cracked transformed section properties, will yield acceptable checks on the serviceability of the slab. The large deviation in the case of model 1 is due to the fact that this model has got a low ratio of P_{cr}/P_d.

The maximum crack width in each test slab is shown in Figure (7.34), as a function of the total load on the slab. The crack having the maximum width had always been one of the first cracks to appear on the underside of the model. This crack had always been under the load points, except in model 6, where the crack having the maximum width occurred on the soffit of the long supporting beams, in line with the points of application of the loads.

The rate of increase in the maximum crack width is smooth and uniform, as can be seen from the figures. No sharp increase or rapid rate occurs, which is a natural result of even spread of cracks on the surface of the slabs. In cases where the distribution of the reinforcement departs from the elastic analysis of the stresses, sharp and rapid increase in crack widths is liable to occur. Opposed to this, in all the models tested here, new cracks were always forming, and the behaviour was not governed by few major cracks, until the design load is exceeded.

In terms of service behaviour, all tested models behaved in a satisfactory manner (except Model 1). Both serviceability limits were reached either simultaneously or at loads close to each other (Table 7.1). Accordingly, if a limit deflection of span/250 is taken as a criterion, then service loads are defined by deflections rather than by crack widths. An average limit state of deflection load of 0.735 P_d is obtained for the last five models.

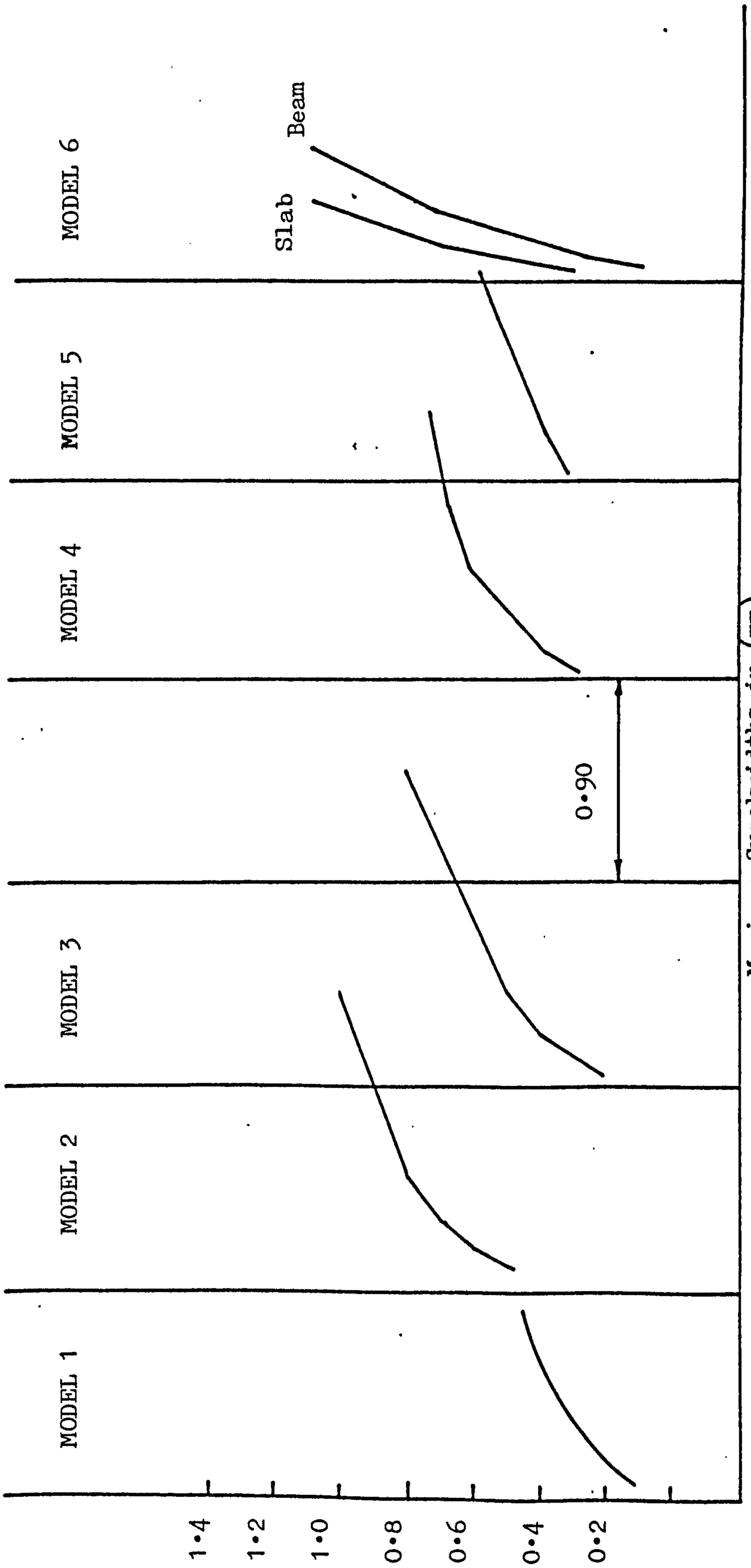

Figure (7·34) Load-Maximum Crack Widths in Tested Models

The slab in model 6 showed an excellent service behaviour. Both serviceability limits were reached at loads close to the design load. It should be mentioned here that the deflection values referred to in table (7.1) actually refer to the total values at the centre of the slab. If the deflections relative to the edge beams were considered, the deflection limit on the slab was reached at a load of 1.29 P_d (Figure 7.31). Furthermore, the Limiting crack width was reached at 1.2 P_d.

7.3.2 Ultimate Limit State:

Table (7.1) summarizes the results obtained concerning the ultimate behaviour of the tested models. The behaviour will be considered from two criteria, viz. the first yield, and the failure loads.

As far as first yield loads are concerned, no yield of steel took place within the service load range in all models. Even the slab in model 1, although its steel was highly stressed due to early cracking, the reinforcement did not yield within the service load. An average value for the first load in all models was equal to 0.88 P_d.

The measured failure loads were all in excess of the design loads for all models, except model 1. The shear failure of this model truncated the "flexural" ultimate behaviour of the slab. For the rest four models without edge beams, an average enhancement of 16% in the design load is observed. This possibly indicates that very little redistribution had actually taken place before the slab became a mechanism.

The slab-beam system in model 6 recorded a higher load enhancement. In fact, both the service and ultimate behaviour of this model are

affected by the presence of the strong supporting beams. The effect of having strong supporting beams is to restrain the lateral inplane movements in the slab. This results in the development of compressive membrane forces at the centre of the slab, which will considerably enhance its load carrying capacity. This compressive membrane action in the slab is different from the tensile membrane action which develops at high loads. The latter would occur only when the slab undergoes very large deflections, and in most cases, the crack at the centre of the slab runs right through the slab depth. This of course will depend on the amount of strain in the reinforcement, because at very large strains the reinforcing bars may rupture altogether. This will then prevent the development of the tensile membrane action.

In the models tested here, it was not possible to reach this stage. Although at failure, the slabs were undergoing very large deflections, no increase in the loads was observed. The central deflections of the slabs were rapidly increasing, which made it extremely difficult to maintain the loads. In case of model 6, perhaps the failure of the corner connection, and the top connection between the slab and the supporting beams (Figure (7.28)), prevented the development of the tensile membrane action. In any case, this model recorded an enhancement of 48% in its design load. The factors contributing to this enhancement in the ultimate loads will be discussed in the following section.

7.3.3 Possible Reasons for the Differences Between the Assumed (Elastic Fields) and True Ultimate Behaviour of the Models.

To explain some of the phenomena encountered during the experiments on the models, the following factors contributed to the deviations

between the assumed (elastic) and real distribution of forces at ultimate loads.

(1) Concrete Strength

This factor does not affect the design procedure. The effect of concrete strength on the amounts of steel needed is almost insignificant as has been shown in Chapter 5. Clark [80] and Morley[71] showed that the yield criterion used (equation 3.14) is exact only for concrete with infinite strength. For concrete with finite strength, the yield criterion is not as exact, but the inaccuracy was shown to be insignificant[80].

But the variation in concrete strength has significant effects on the stiffness of the slab, particularly in the post cracking range. The concrete strength relates to Young's modulus and the tensile strength both of which control the slab deflections, and the cracking load of the slab. As the slab stiffness within the working load is affected by crack initiation and propagation, which are in turn governed by the concrete strength, the higher the strength the higher will be the stiffness. This factor contributed to the good service behaviour of the slab-beam system in model 6.

(2) Increased amounts of steel

Affects both the service and the ultimate behaviour of the slab. In the former case, by providing extra stiffness to the slab (although not affecting the cracking load significantly) leads to improved deflection characteristics. Crack spread over the slab surface will not be affected, but the factor has the desirable influence of restricting crack depths. Consequently, less crack widths, and hence slow stiffness degradation. The total effect is an overall improvement in the service behaviour.

Increasing the amount of steel provided delays the initiation of yield. In the experiments, both model 2 and model 6 were provided with extra steel, as can be seen from Table (6.2). In case of model 2, the extra steel was not an additional steel, but rather resulted from not curtailing the reinforcing bars near the supports to avoid shear failures. In case of model 6, the model had been designed for flexure only, and additional steel was added to resist the excess torsional stresses over those predicted by the layered model (see Section 4.4.4). And definitely some of this additional steel has contributed to the improved behaviour of the model. This effect will be discussed in detail in Section (7.4).

(3) Strain hardening of steel

Table (7.3) lists the properties of the steel used in the experiments. Typical stress-strain curves are given in Figures (6.11) and (6.12). As can be seen from Table (7.3), the type of steel used had a good reserve of strength after the yield, both in the case of high yield and ordinary mild steel. This factor definitely does not affect the service behaviour, but generally contributes to the ultimate strength of the slab (as will be shown in Section 7.4).

(4) Membrane forces

Inplane forces resulting from edge restraints in laterally loaded slabs can be classified in two groups:-

(a) Compressive membrane action developing at low deflections, which contributes to the increase in ultimate loads. Although every effort was made to eliminate edge restraints in the experiments, still some frictional resistance between the rollers and the flats (see Figure 6.13) is bound to occur. In any case, the effect of this factor

Bar Diameter (mm)	Type	E_s KN/mm^2	f_y N/mm^2	ε_y %	f_u N/mm^2
8	High yield	219·1	467·0	0·413	557·0
10	"	214·1	481·6	0·425	572·3
6	Mild steel	186·4	298·2	0·160	495·0
8	"	188·5	377·0	0·200	621·0
10	"	198·4	277·8	0·140	450·0
12	"	223·9	356·0	0·159	488.0

Table (7·3): Properties of the steel used in the experiments

is probably not significant in the first five models, as can be seen from the low enhancement obtained in the ultimate load. But in model 6, the strong edge beams provided a strong restraint to the outward movement of the slab bottom surface. Such a restraint is represented by the observed inward bowing of the long beams and the outward bowing of the short beams. Accordingly, an induced compressive membrane force sets up in the slab, which contributed to the enhancement in the ultimate load of this model. Fortunately, the layered finite element model can deal with this problem, as will be shown in the next section.

(b) Tensile membrane action developing at large deflection, and happens at high loads. At this stage, bottom surface cracks would run through the whole of the slab thickness, and the load will be carried by the tension bars with slab acting as a catenary. Literature [99] reveals that this action occurs when the deflection is approximately equal to the slab thickness.

This situation could not be achieved in all the models tested, due to the limitation of the loading apparatus. Unfortunately, the present finite element model cannot treat this problem, since it ignores large displacement effects.

7.4 NONLINEAR ANALYSIS OF THE TEST MODELS:

Using the nonlinear finite element program developed in this study, an incremental analysis of the test models was performed. Details of the materials properties, mesh size, load increment size and the number of iterations used in the analysis of each model are given in Table (7.5). The materials properties used are those

Table (7·4): Results of the nonlinear analysis of the experimental models

Model No.	P_{cr1}/P_{cr2}	Service Load		Design Load		P_{u1}/P_{u2}
		δ_1/δ_2	$\varepsilon_{s_1}/\varepsilon_{s2}$	δ_{d_1}/δ_{d2}	$\varepsilon_{d1}/\varepsilon_{d2}$	
1	0·75	1·09	1·15	-	-	-
2	0·90	0·68	0·82	1·0	0·73	0·98
3	0·83	0·98	0·72	0·98	1·15	0·97
4	0·93	1·0	0·83	0·81	0·54	0·97
5	0·87	0·86	0·78	1·00	0·85	1·00
6	1·00	1·00	1·12	1·12	1·04	1·00

P_{cr} = The Cracking Load

δ = Maximum deflection under service load (0·625 P_d)

ε_s = Maximum steel strain under service load

δ_d = Maximum deflection under design load (P_d)

P_u = Ultimate load of the slab

Suffix 1 for theoretical results

Suffix 2 for experimental results

Model No.	f_{cu} N/mm²	f_t N/mm²	E_c KN/mm²	f_y N/mm²	E_s KN/mm²	Hardening parameter KN/mm²	Mesh	Increment size	Iterations
1	55•5	3•68	25•6	476	210	6•43	4 x 4	0•15	15
2	40•3	3•68	21•5	460	210	6•43	6 x 6	0•10	15
3	44•2	3•4	21•5	460	214	6•43	6 x 6	0•10	15
4	37•3	2•97	20•4	473	214	0	8 x 8	0•10	15
5	43•0	3.0	22.0	473	214	6•43	4 x 4	0•10	15
6	48•3	3•15	21•6	300	214	0	7 x 7	0•10	20

Table (7•5): Description of models materials and the numerical data used in the finite element analysis of the test models.

measured in the laboratory on the same day the model was tested. For models 1 to 5, the idealized stress-strain curves given in Figure (7.35) has been used. This idealization takes into account the strain hardening in the reinforcement after the bars attain their yield strength. In the case of model 6, no strain hardening was assumed. The reason for this can be seen from Figure (6.12) for the actual stress-strain curve for the type of mild steel used. Strain hardening in such a type of steel starts after a long horizontal plateau.

All models analysed were designed for flexure only. Due to the edge restraints produced by the eccentric supporting beams in model 6, significant membrane forces are predicted by the elastic enalysis. Typical variations of the normal moments and membrane forces along the long and the short centre line of model 6 are shown in Figure (7.49) and (7.51) respectively. The effect of such distributions is that, the predicted compressive membrane forces in the slabs are balanced by tensile membrane forces in the supporting beams. However, two types of analysis had been undertaken here for this model. In the first, the model was designed for flexure only, and the membrane forces were completely ignored. The design for this case was done using the equations for flexure in section (3.4). In the second analysis, the model was designed for combined flexure and membrane forces, using the open sandwich model, as has been described in section (3.7). In this sandwich model, the core (filling) contribution in resisting the forces is completely ignored.

The results of all analyses are given in Figures (7.2) to (7.51), and are summarized in Table (7.4). In general, a very good agreement between theory and experiment can be seen from these results. In the case of model 4, it can be seen that the response up to the service load

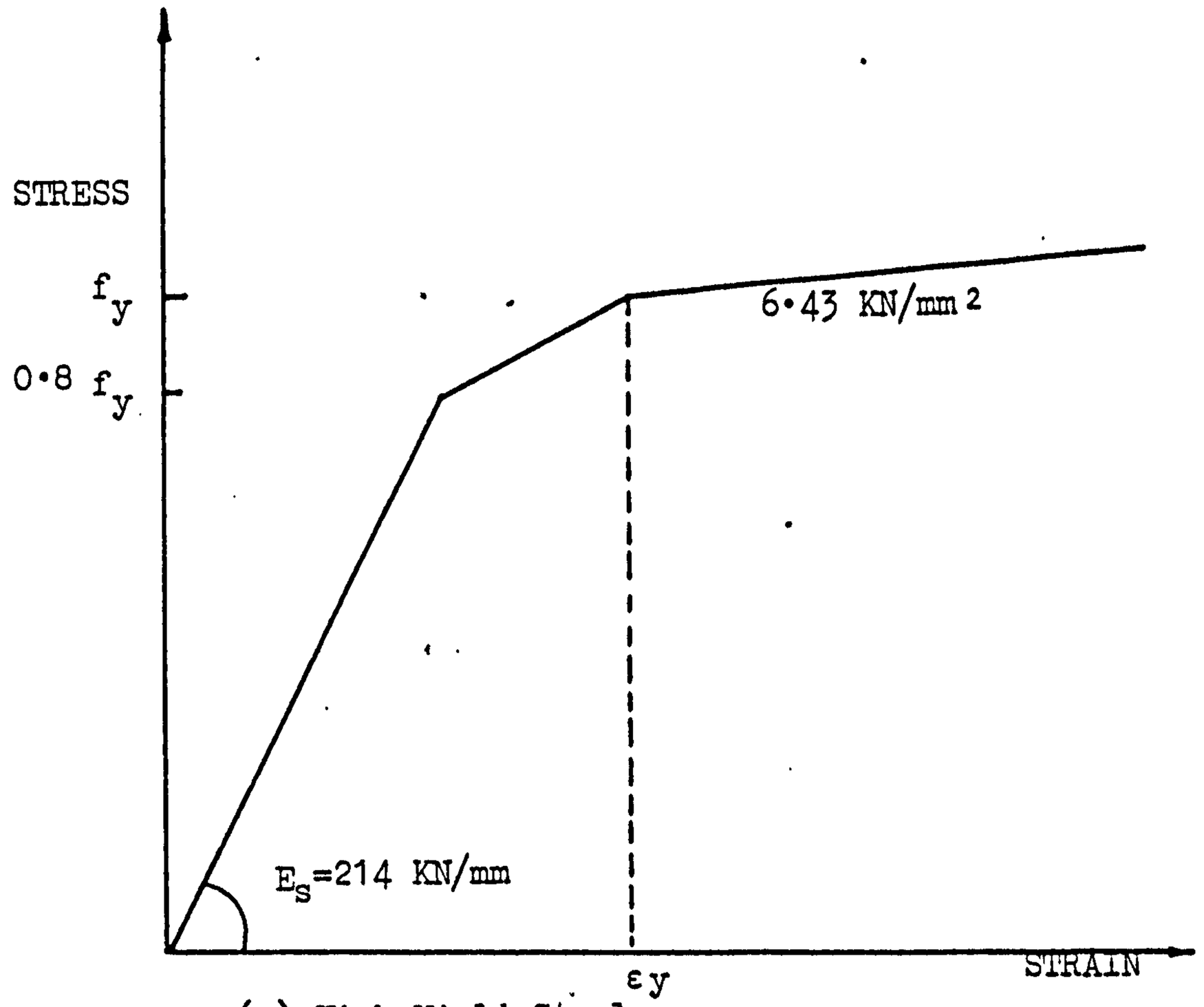

(a) High Yield Steel

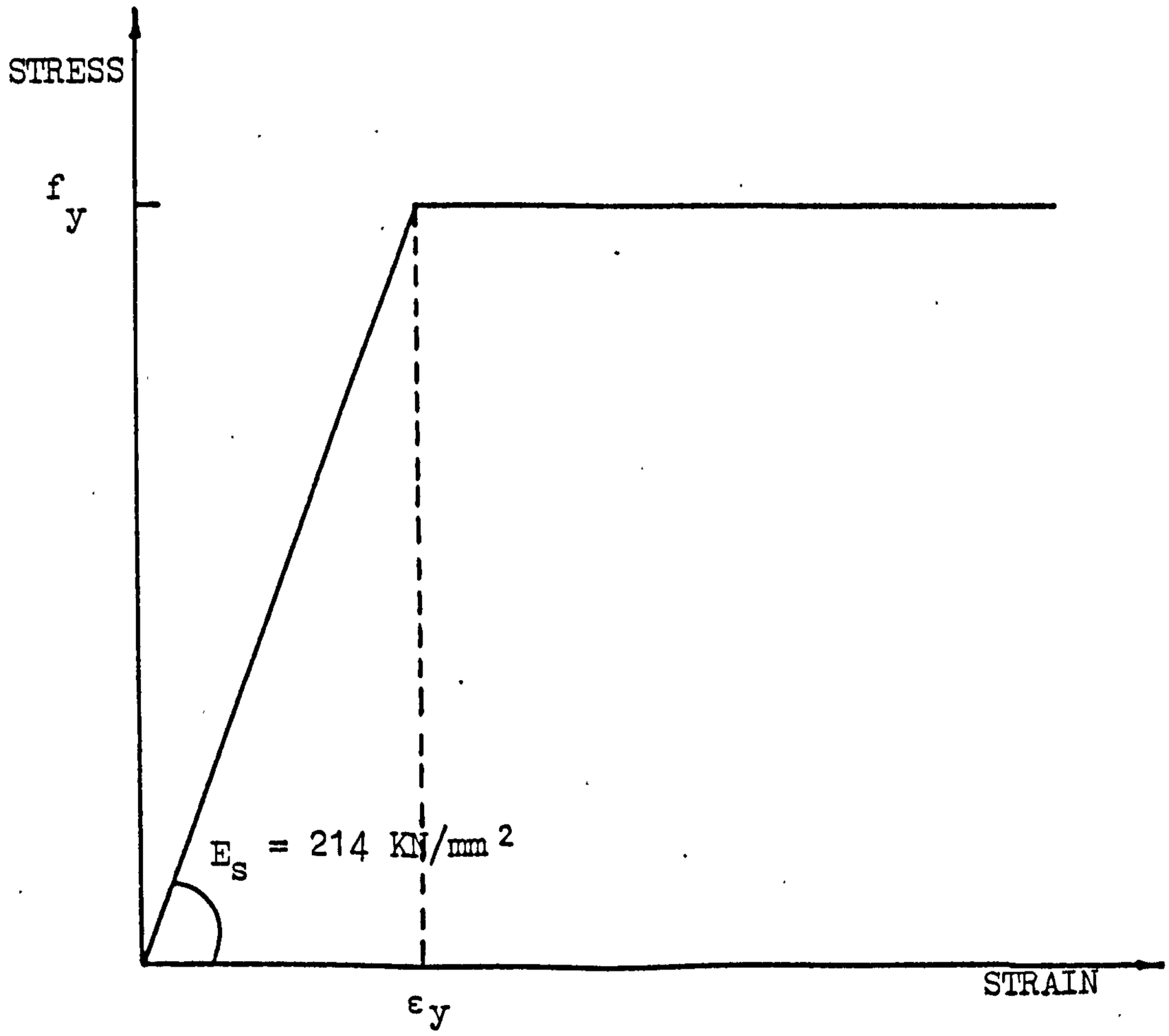

(b) Mild Steel

Figure (7·35) Idealized Stress-Strain Curves for Steel used in the experiments

is very well predicted by the finite element model. But at high loads, the theoretical model shows a stiffer response than the experiment. This stiffening effect can be seen from Figures (7.16, 7.17 and 7.42) beyond the service load range. The effect is a numerical one, and is caused by poor rate of convergence after the first yield in the slab. To eliminate this, a larger number of iterations could be used, and probably with a smaller size of load increment. However, this would lead to an expensive analysis, but would definitely yield the desired result. As the analysis conducted here was successful up to 80% of the ultimate load, there does not seem any need to refine the analysis after that. And thus the results are considered satisfactory.

The analysis of the first five models indicated that the enhancement in the ultimate loads can be attributed to membrane forces, strain hardening, and increase in the amounts of steel. To quantify the effects of individual parameters on the response, Figure (7.36) has been computed. The problem considered was model 2. As can be seen from the figure, the concrete strength influences the service behaviour of the slab under working loads, but does not contribute much to the ultimate strength of the section. On the other hand, the strain hardening does not affect the service response, but contributes very slightly to the ultimate behaviour of the slab. The biggest influence on ultimate behaviour are those due to the increased amount of steel, and the membrane forces. The effect of increasing the amount of steel on the section is to increase the ultimate moment at the section. Similarly, the existence of compressive membrane action on the section will considerably enhance its ultimate moment capacity, as has been shown by Wood[4]. Figures (7.40) to (7.48) also show this fact.

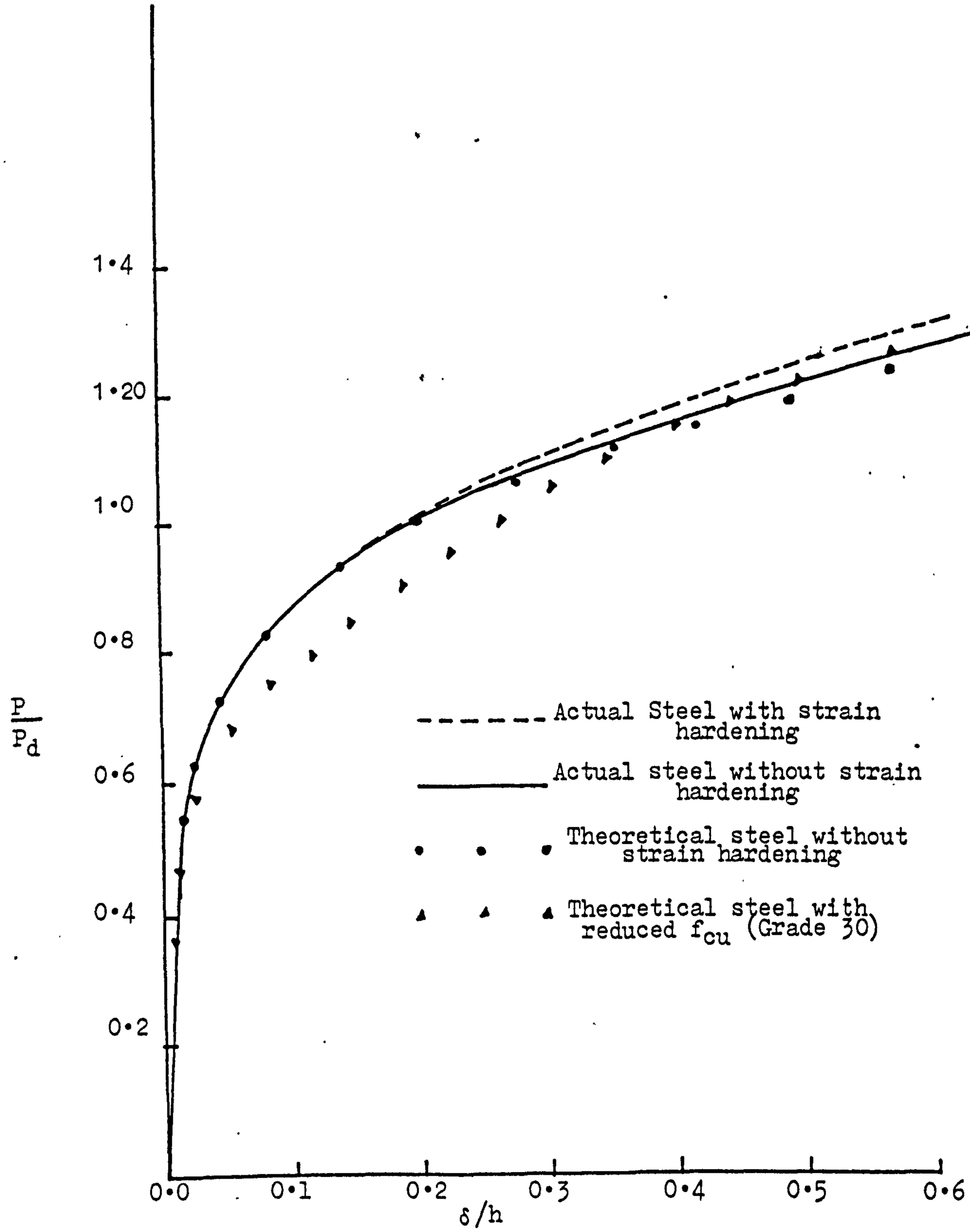

Figure (7·36) Effect of Various parameters on the response of Model 2

The moments capacity at the critical sections in the test models increased due to the induced compressive membrane forces at high load levels. The analytical results of the analysis of model 6 (designated Analysis A in Fig.(7.29)) were slightly more flexible than the experimental curve at high load levels. This is mainly caused by the torsional stiffness of the supporting beams, being underestimated in the analysis.

Since in the design of model 6, the membrane forces were completely ignored, it was thought worthwhile to investigate the effect of including membrane forces in the design. In order to do this, an analysis (designated Analysis B in Fig.(7.29)) was done on a hypothetical model (no experimental equivalent) with identical dimensions, design loads and materials strengths to those of model 6. The main difference was that, in this analysis, both membrane forces and flexural forces were considered in the design, using the open sandwich model (Section 3.7). It was found that the reinforcement in the slab was generally less than that needed for flexure only (Analysis A). But as a result of the tensile forces in the edge beams, the reinforcement in them was higher than that required for flexure only (Analysis A). However, an increase of 25% in the total reinforcement over that needed by disregarding membrane forces is required. This additional strength to the supporting beams which justifies the improved service response of this model. The analysis of the model whether for flexure or combined flexure and membrane forces show that in both cases the designed system will behave satisfactorily under service loads, although, designs for combined flexural and membrane forces would behave better.

7.5 CONCLUSIONS

The general conclusions to be drawn from these tests can be summarized as follows:-

1. The proposed method of design provides a practical layout of steel. Although the theoretical elastic moment fields are of continuously varying nature, when linked with the yield criterion (Equation 3.14) results in a gradual variation of steel pattern. This statement is strictly true within a reasonable strip width, and does not necessarily cover very wide strips. The maximum width of a strip considered here was L/8, where L is the span length in any direction.

2. Tests results indicated that the behaviour of the slabs designed by the proposed method was satisfactory. Both deflections and crack widths in the working load range were within acceptable limits, as defined by CP110[5], deflections not greater than span/250 and crack widths < 0.3 mm.

3. No yield of steel occurred in all tests within the service load range. First yield loads were very close to the design loads, and an average of 90% of the design load was obtained.

4. Whether the design of the steel is based on the maximum or the average design moment in the strips, the resulting service behaviour will be satisfactory. Two examples in this case were given by model 2 and model 5. If the maximum moment in the strips or the exactly curtailed pattern is used, both the service and ultimate load behaviours will be greatly improved.

5. The ultimate behaviour of all models was satisfactory, with the reinforcement yielding at loads very close to the design loads.

Failure loads in all models were in excess of the design loads. An average load enhancement in the ultimate loads of 16% were mainly caused by the induced compressive action and the strain hardening of the reinforcement.

6. In the case of slab-beam systems, no saving in steel can be achieved by considering membrane action. In fact the proposed design method required 25% more steel when membrane forces were considered than when neglected. A reduction in the slab reinforcement is overbalanced by a larger increase in the beam reinforcement.

7. In slab-beam systems, whether membrane forces are considered in the design of the system or not, the system designed by the proposed method will behave satisfactorily in the two cases. Consideration of membrane forces in the design (Sandwich Models) produces improvements on the behaviour of the system than when neglected.

8. Both the experiments and theoretical analysis by the finite elements on slab-beams systems, indicated the importance of the corner connection. Initiation of failure at the corner junction between the two beams expedites the collapse of the system, due to the fact that the torsional fixity of the beams is considerably reduced.

9. Prediction of the service behaviour can be made using any of the methods described in Chapter 2. If the assumptions in Appendix (E) are adopted, the use of an effective moment of inertia using a cracked transformed section can very well predict the service behaviour of the slabs designed by the present method. The

accuracy and reliability of the method of calculation depends on the cracking load of the slab. With cracking loads in excess of 40% of the design load, this method predicts the service behaviour of the slabs designed by the proposed direct design procedure, with acceptable accuracy.

10. The nonlinear, layered finite element model developed in this study proved to be a powerful tool for the analysis of reinforced concrete slabs and slab-beams systems. Excellent agreement between the theoretical predictions made by the finite element method and the actual slab behaviour has been obtained.

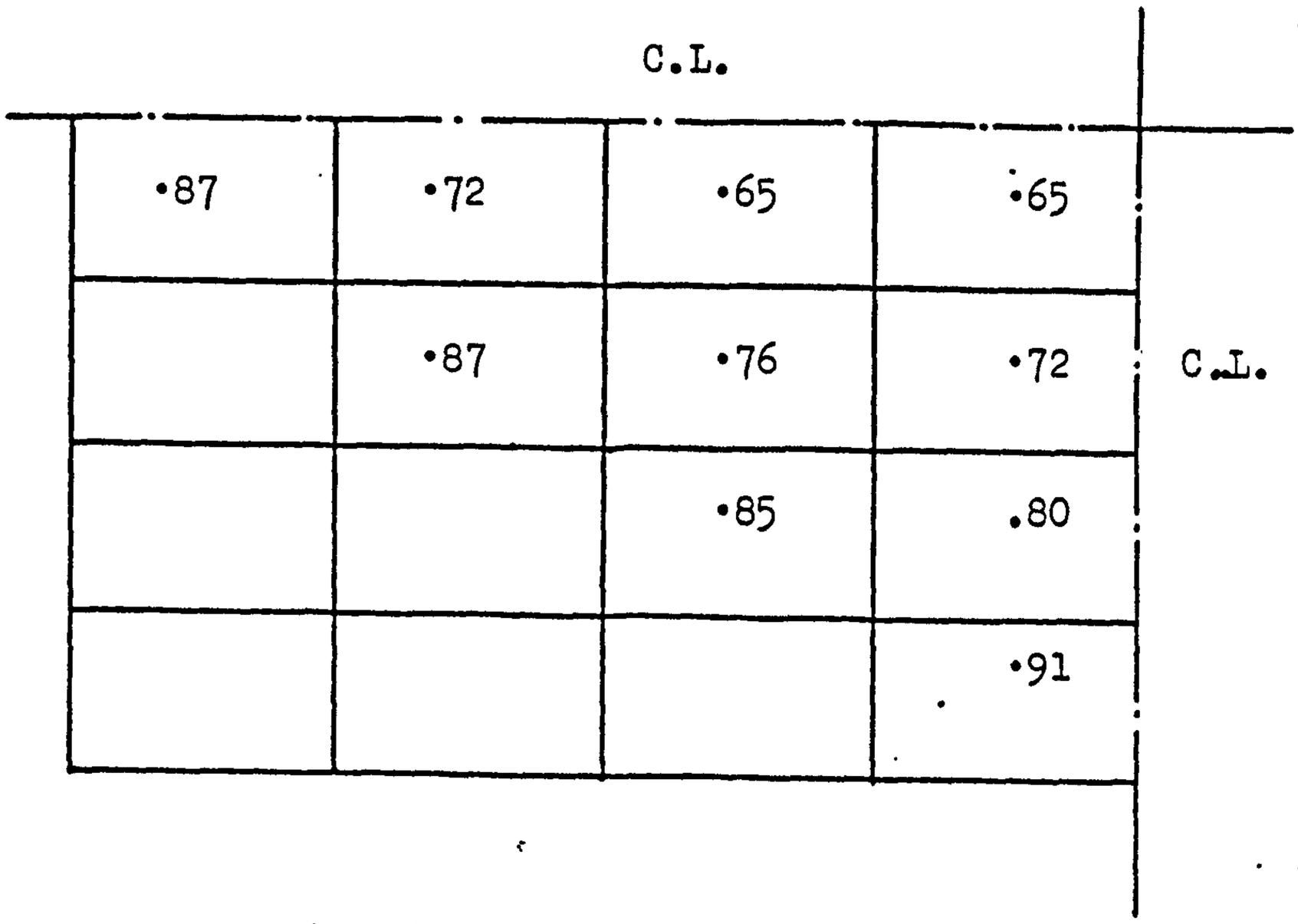

Figure (7·37) P/P_d causing yield in Model 1

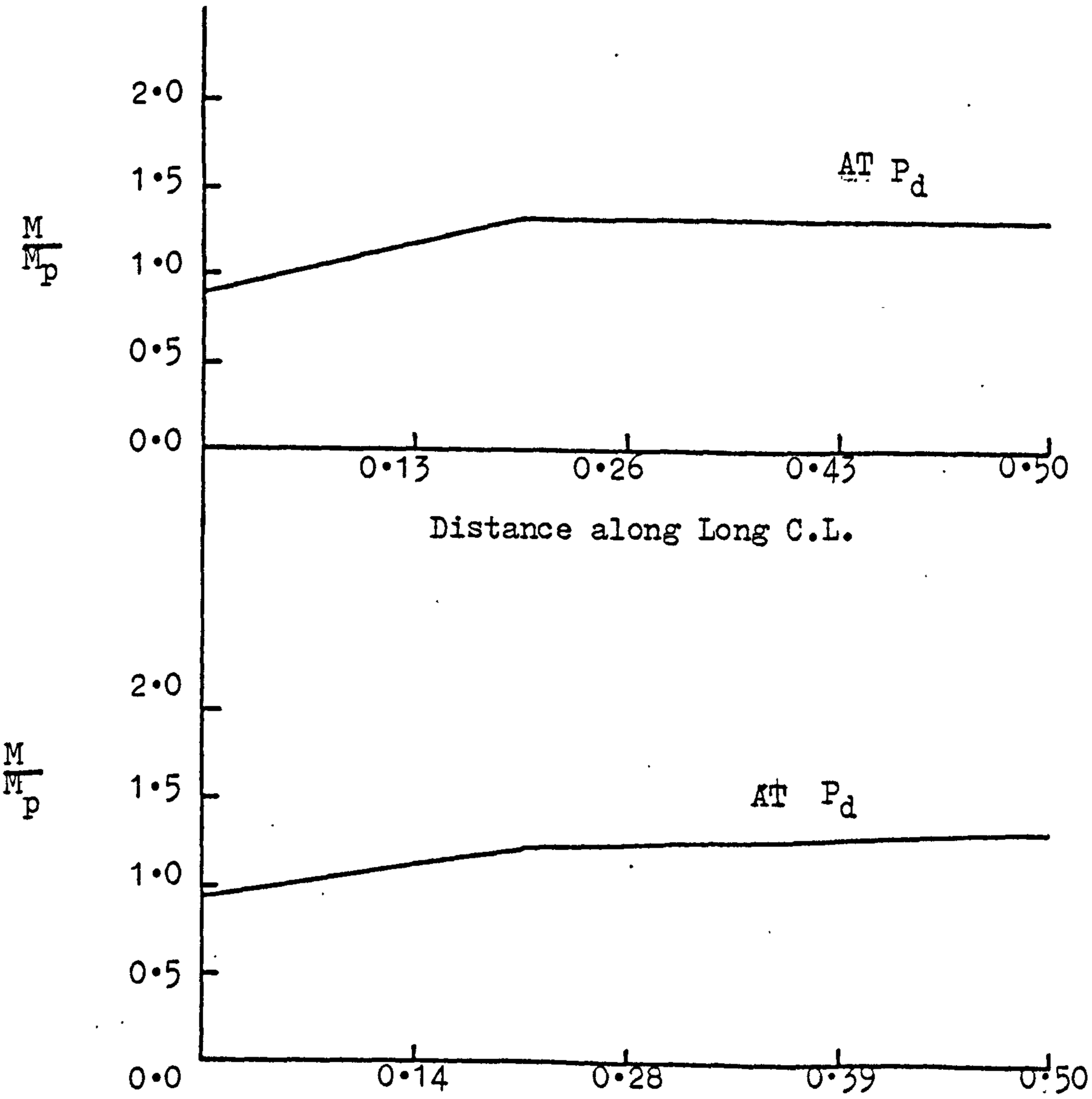

Figure (7·38) Ultimate behaviour of Model 1

C.L.

	1•11	1•0	•91	•81	•81
	1•11	•96	•85	•81	•81
	1•06	•96	•90	•85	•81
	1•21	1•11	1•06	1•06	1•06
			1•06	1•06	1•15

C.L.

Figure (7.39) P/P_d causing yield in Model 2

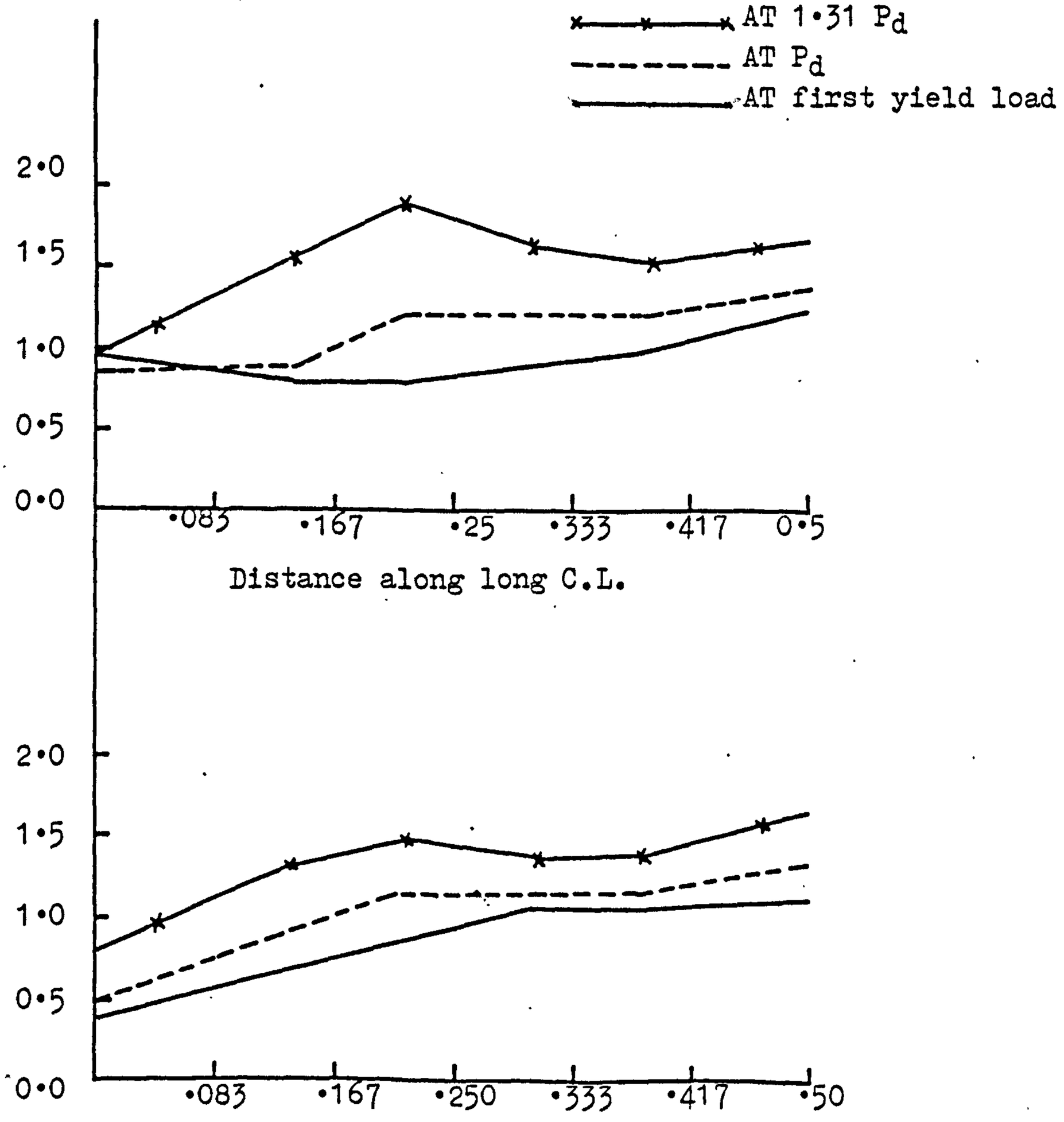

Figure (7.40) Ultimate Behaviour of Model 2

C.L.

1·0	0·80	·77	·77
0·96	0·8	·77	·77
	0·8	·80	·80
		·98	·98

C.L.

P/P_d causing yield in Model 3

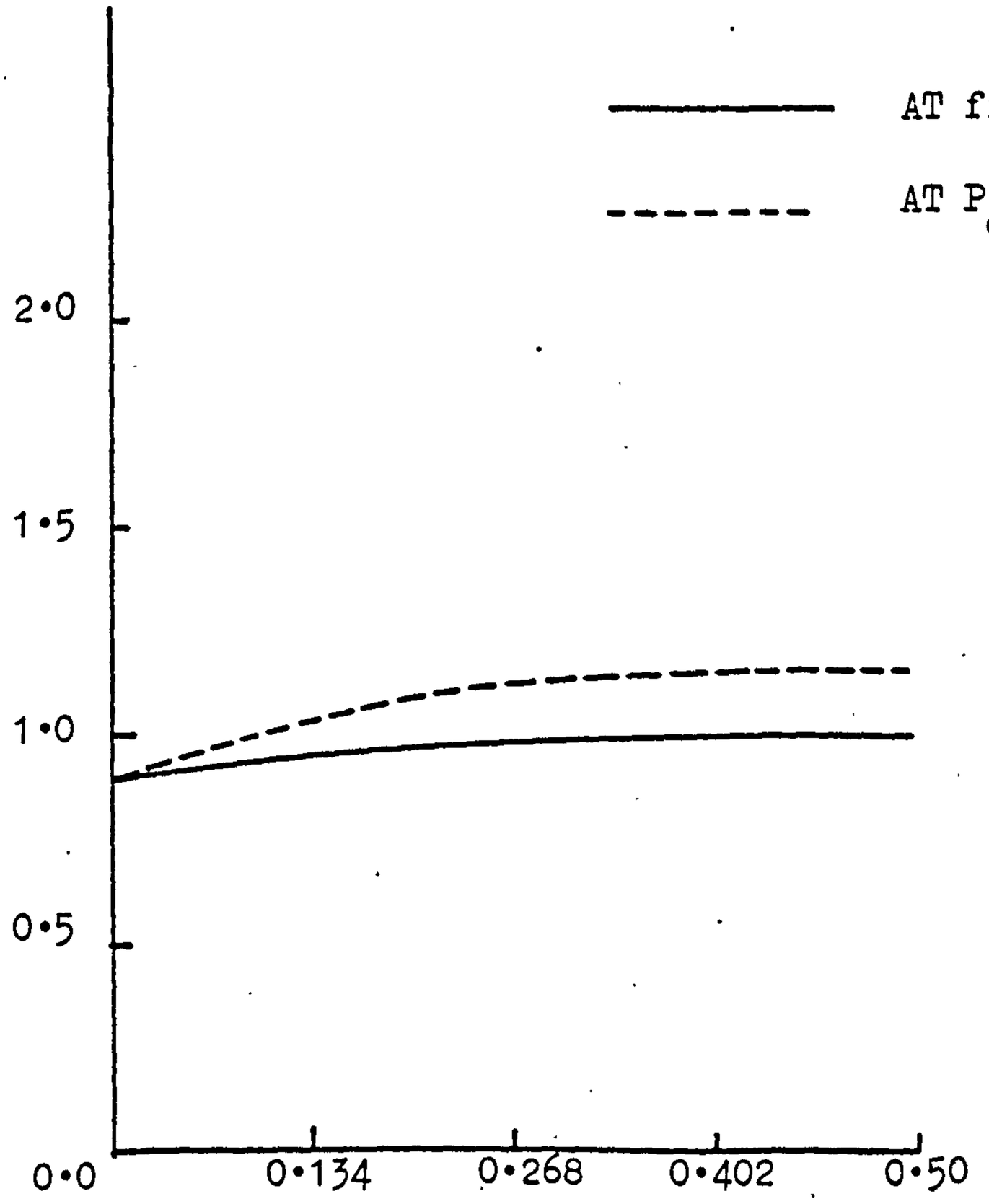

Figure (7·41) Ultimate behaviour of Model 3

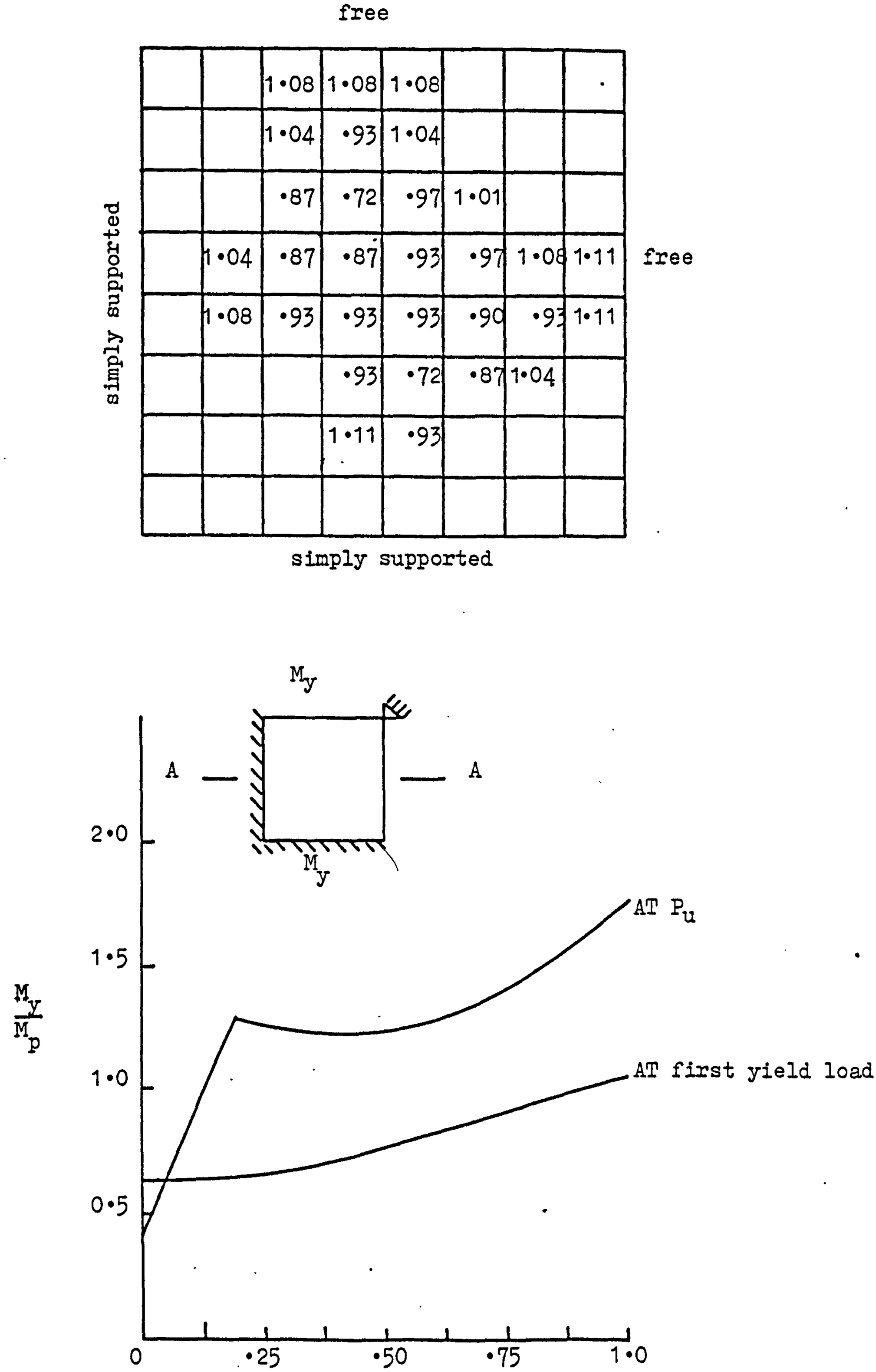

Figure (7•42) Ultimate behaviour of Model 4

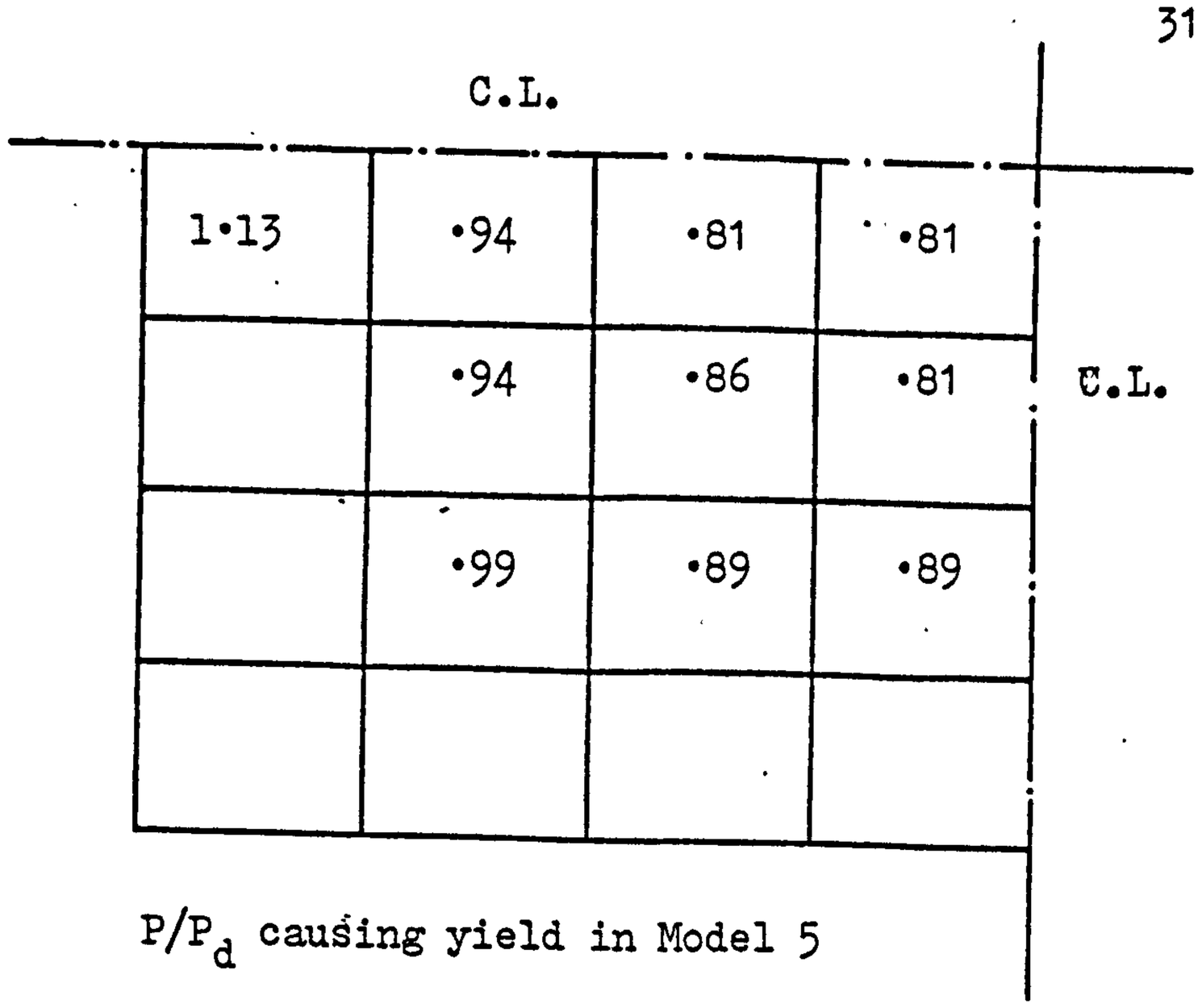

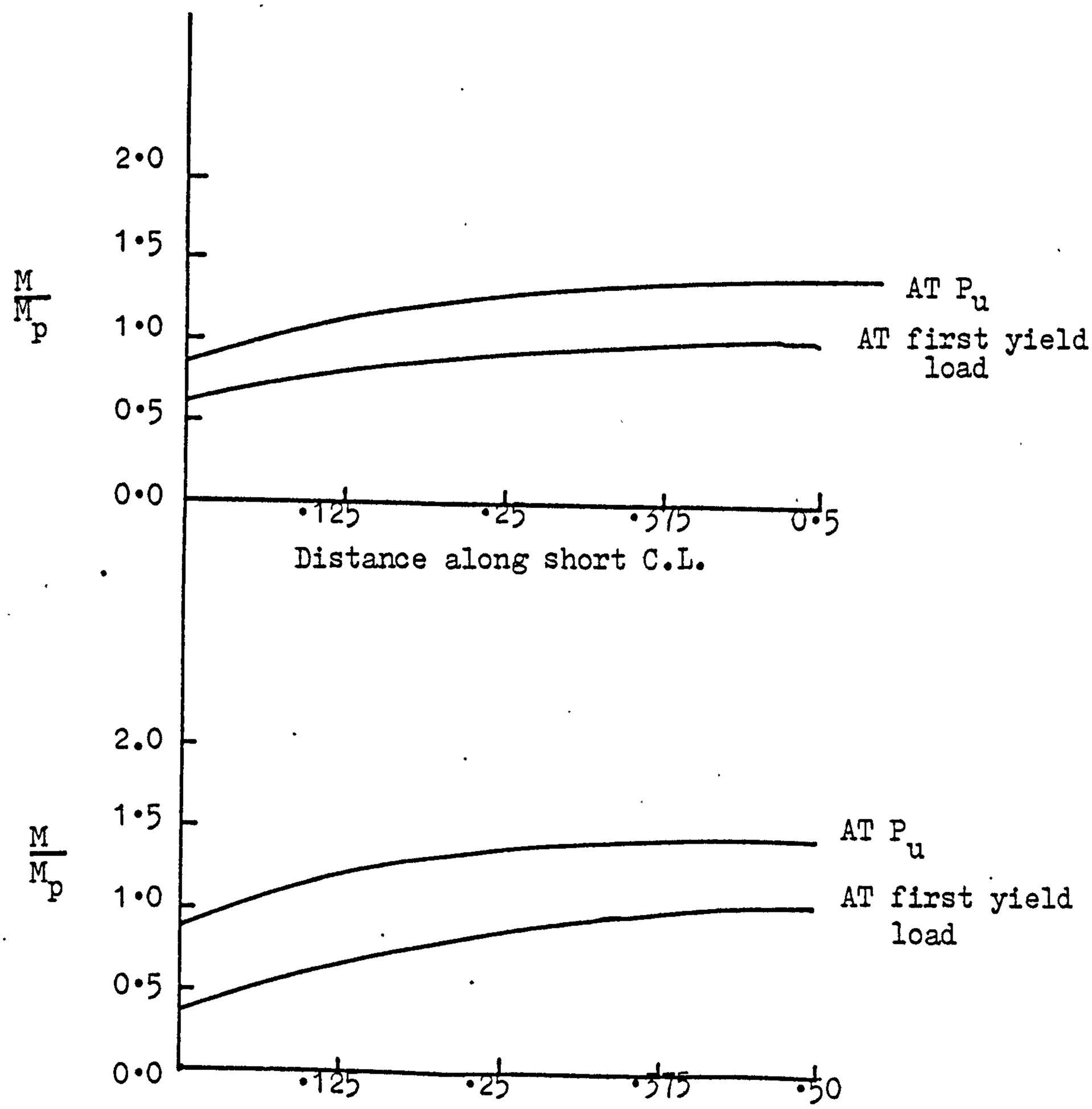

Figure (7.43) Ultimate behaviour of Model 5

C.L.

•92	1•39	1•39	1•33	1•18	1•07	1•07
•92	1•39	1•39	1•33	1•07	1•07	1•07
•97	1•54	1•39	1•13	1•07	1•07	1•07
•97	1•59	1•23	1•07	1•07	1•23	1•28
1•02	1•33	1•18	1•18	1•33	1•39	1•39
•97	1•18	1•18	1•49	1•49	1•44	1•39
1•02	•97	•97	•87	•87	•87	•87

C.L.

Flexural Design

C.L.

•93	-	1•41	1•35	1•20	1•09	1•09
•99	-	1•56	1•35	1•09	1•09	1•04
•99	-	1•51	1•14	1•09	1•14	1•14
•99	-	1•30	1•14	1•20	1•35	1•51
1•04	1•41	1•30	1•35	-	-	-
1•04	1•25	1•30	1•62	-	-	-
1•04	1•04	1•04	1•04	1•04	•99	•93

C.L.

Combined Flexure and Membrane Forces

Figure (7•44) P/P_d causing yield in Model 6

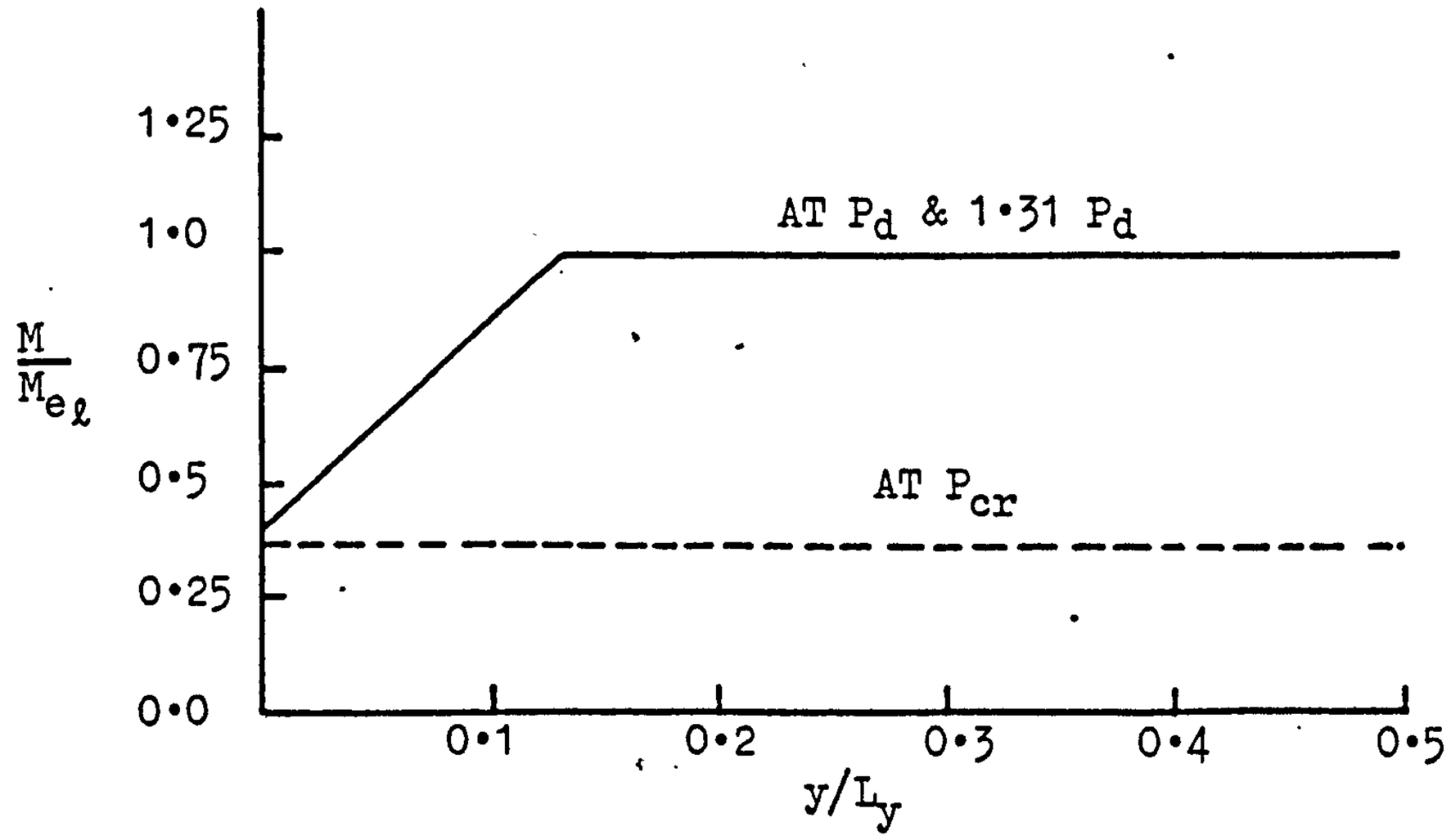

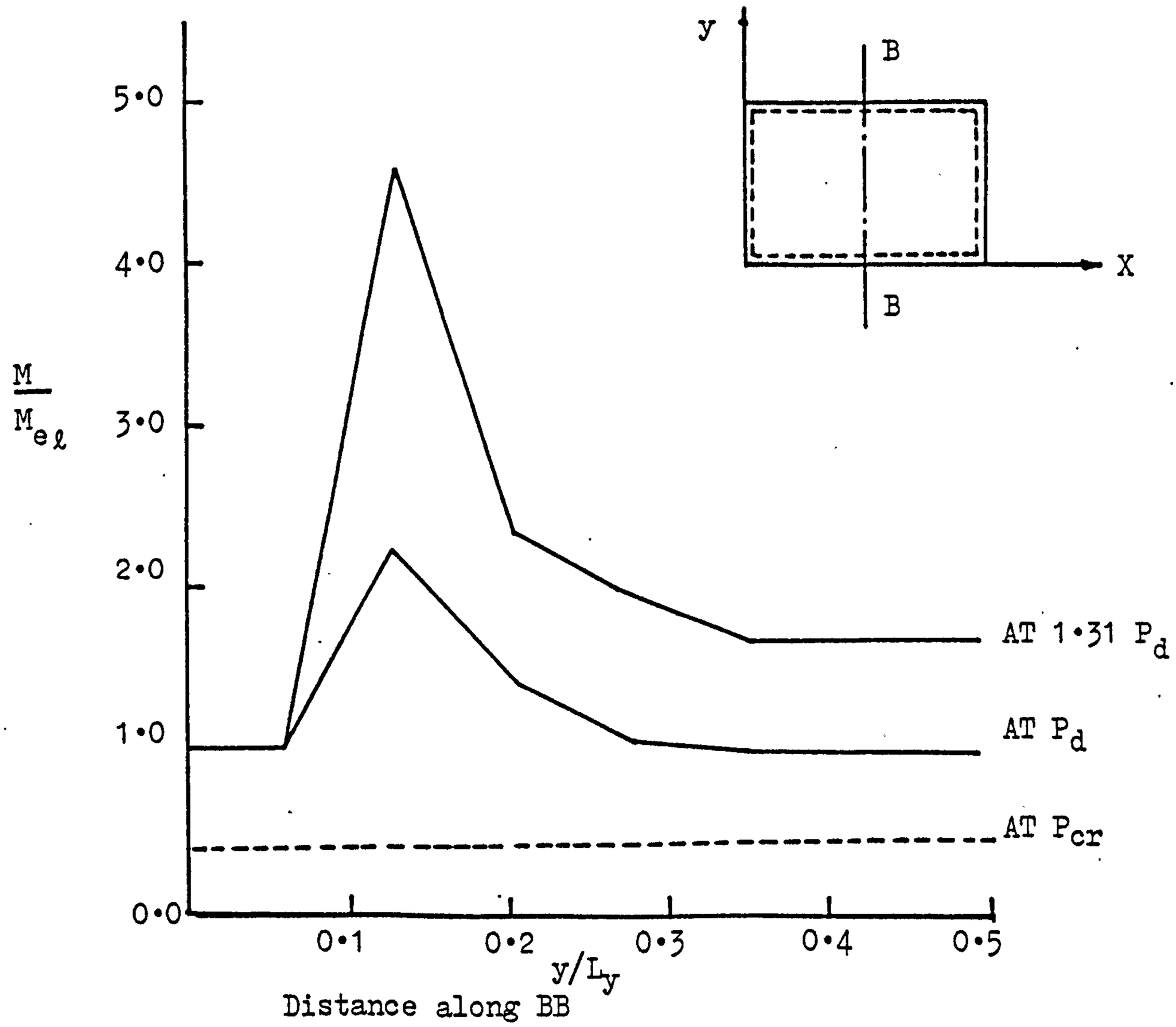

Figure (7·45) Moments Redistribution in Model 6

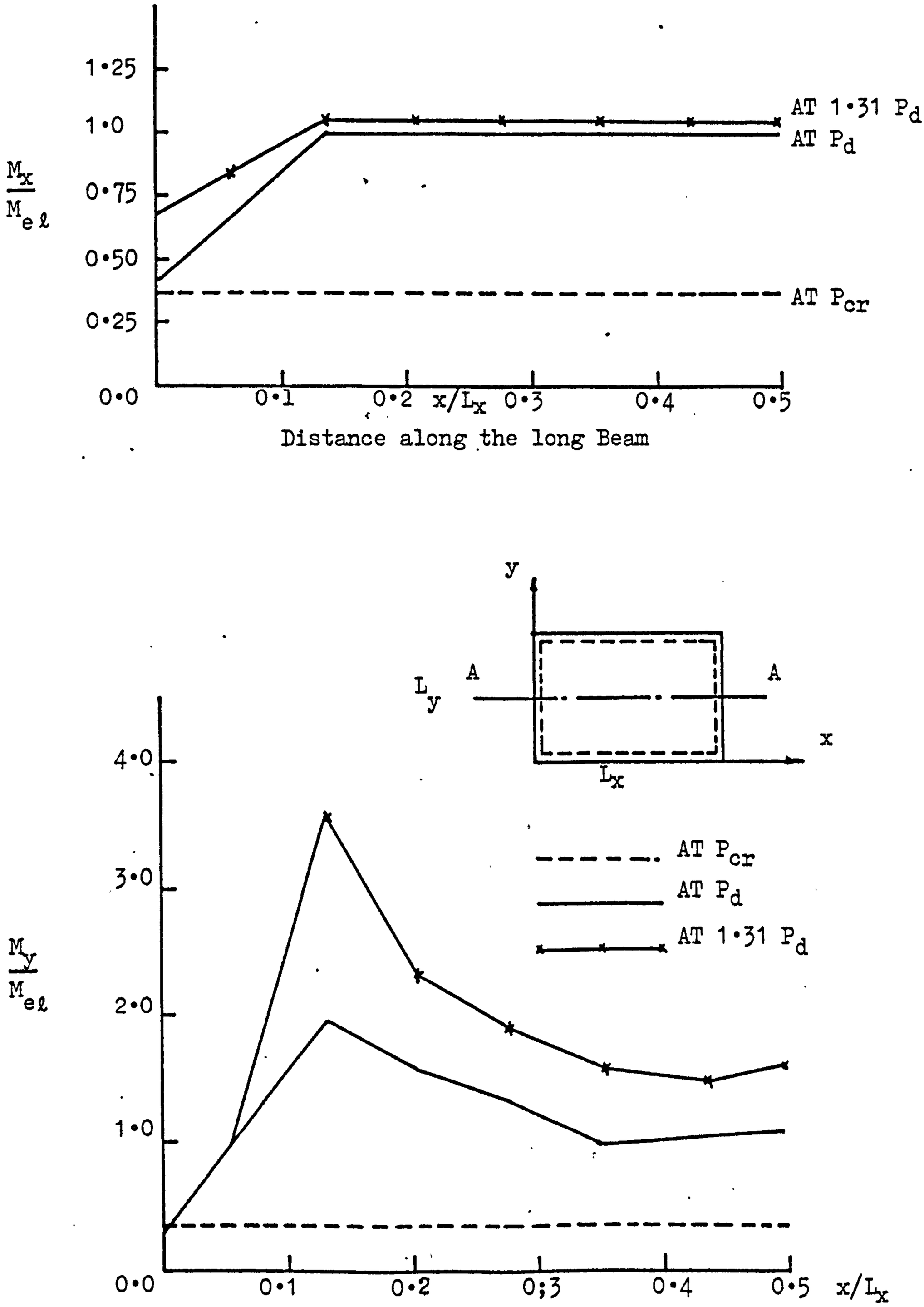

Figure (7•46) Moments Redistribution in Model 6

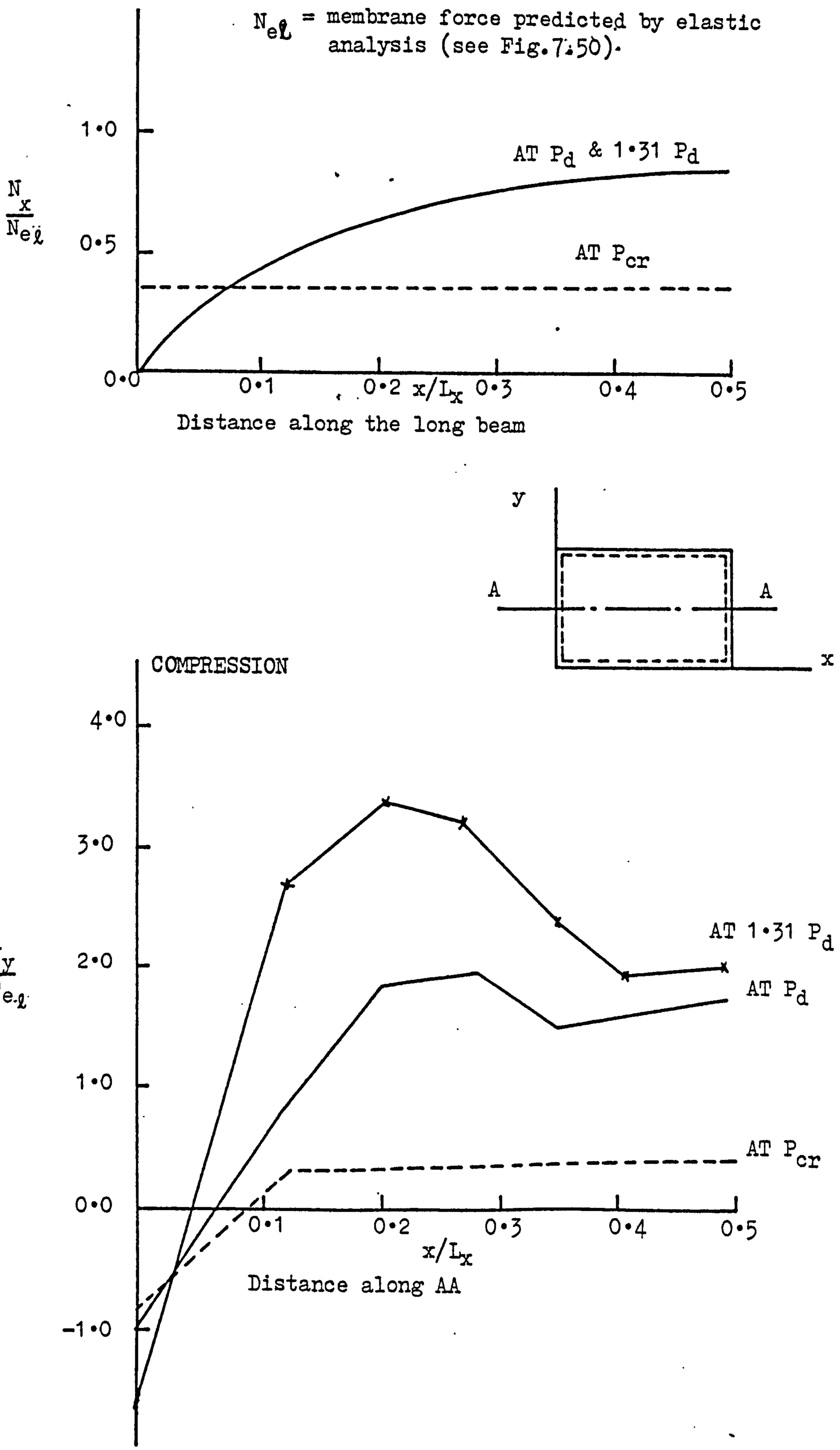

Figure (7·47) Redistribution of Membrane forces in Model 6

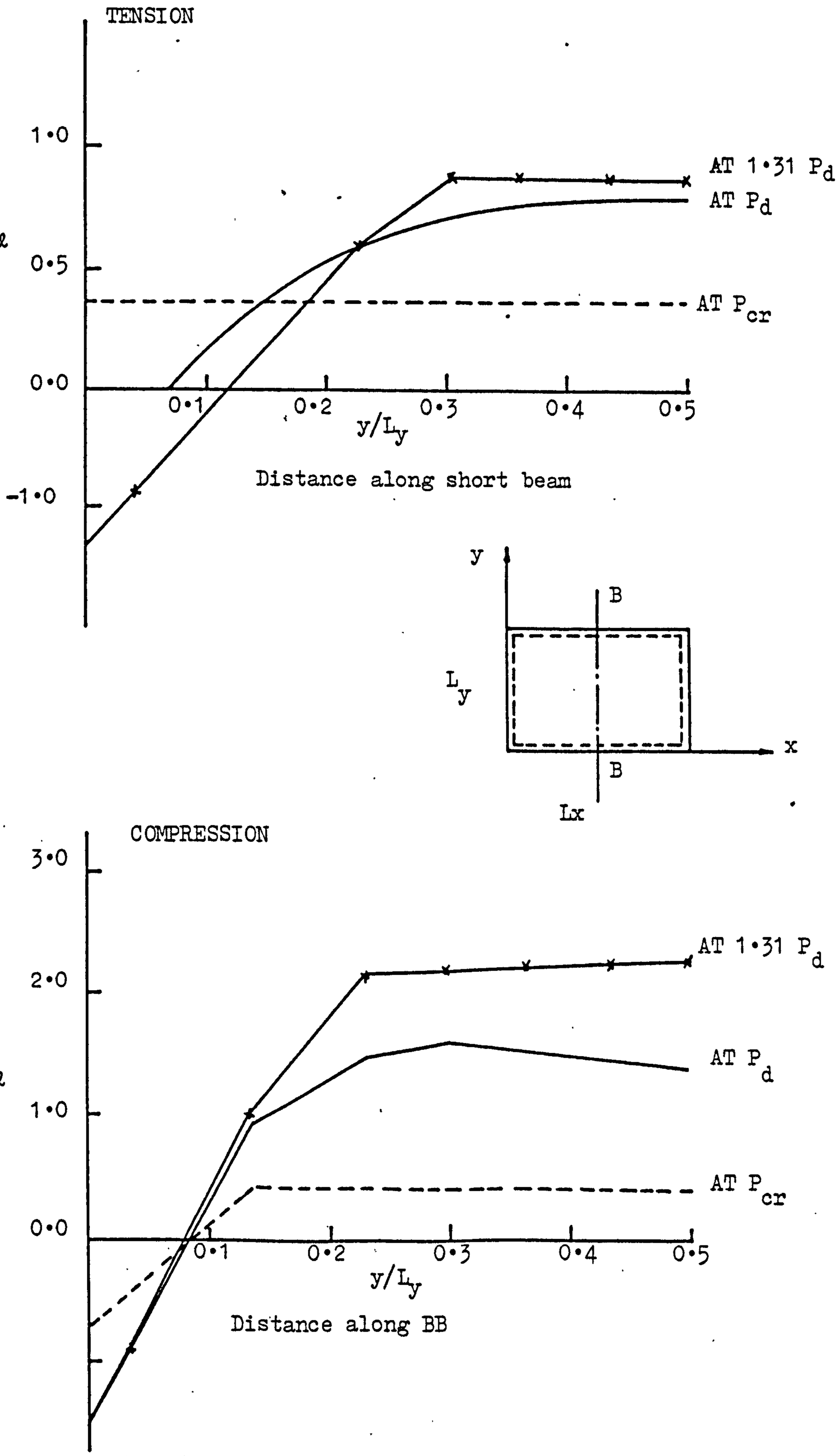

Figure (7·48) Redistribution of Membrane Forces in Model 6

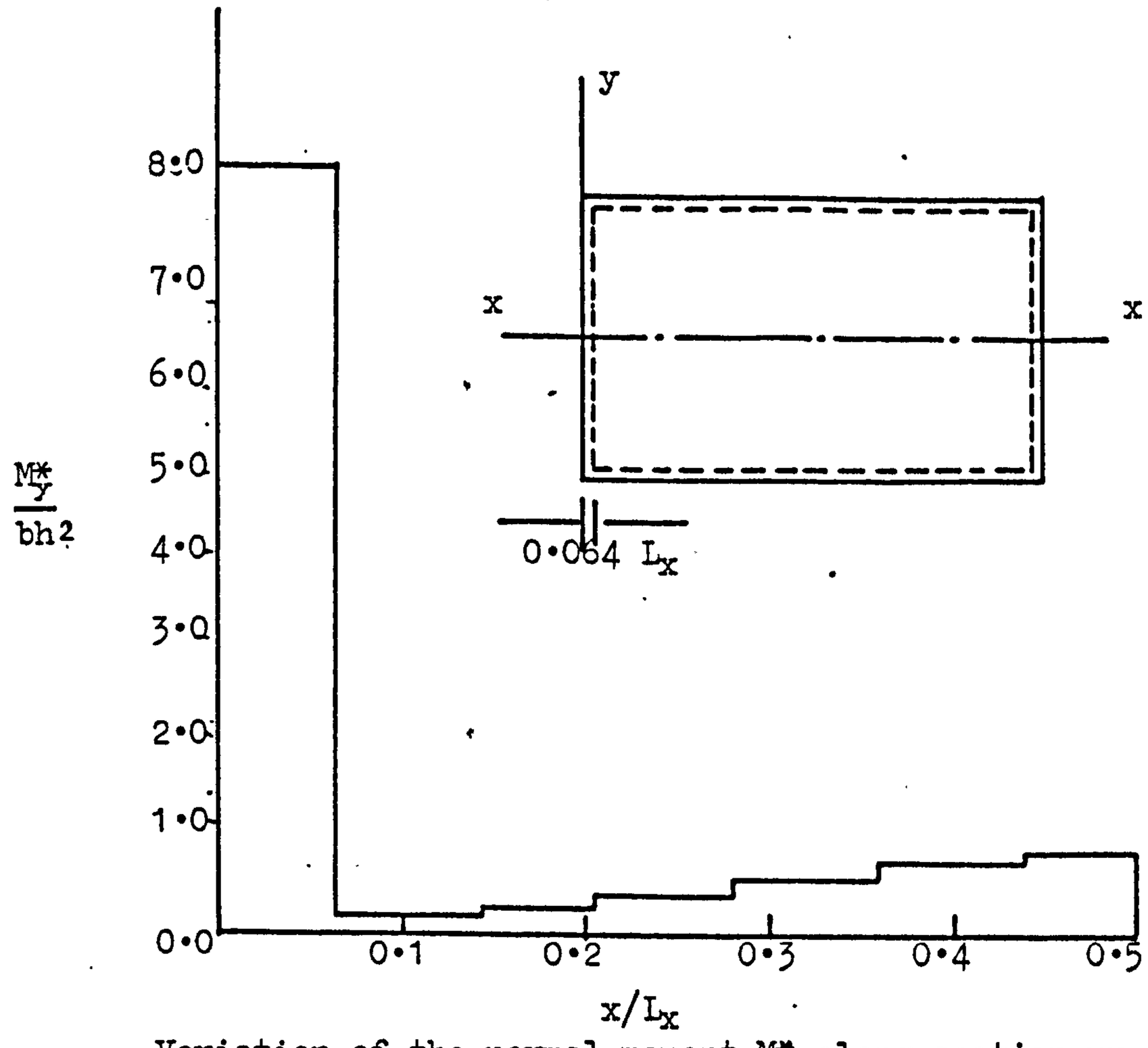

Variation of the normal moment M_y^* along section xx (Elastic Analysis)

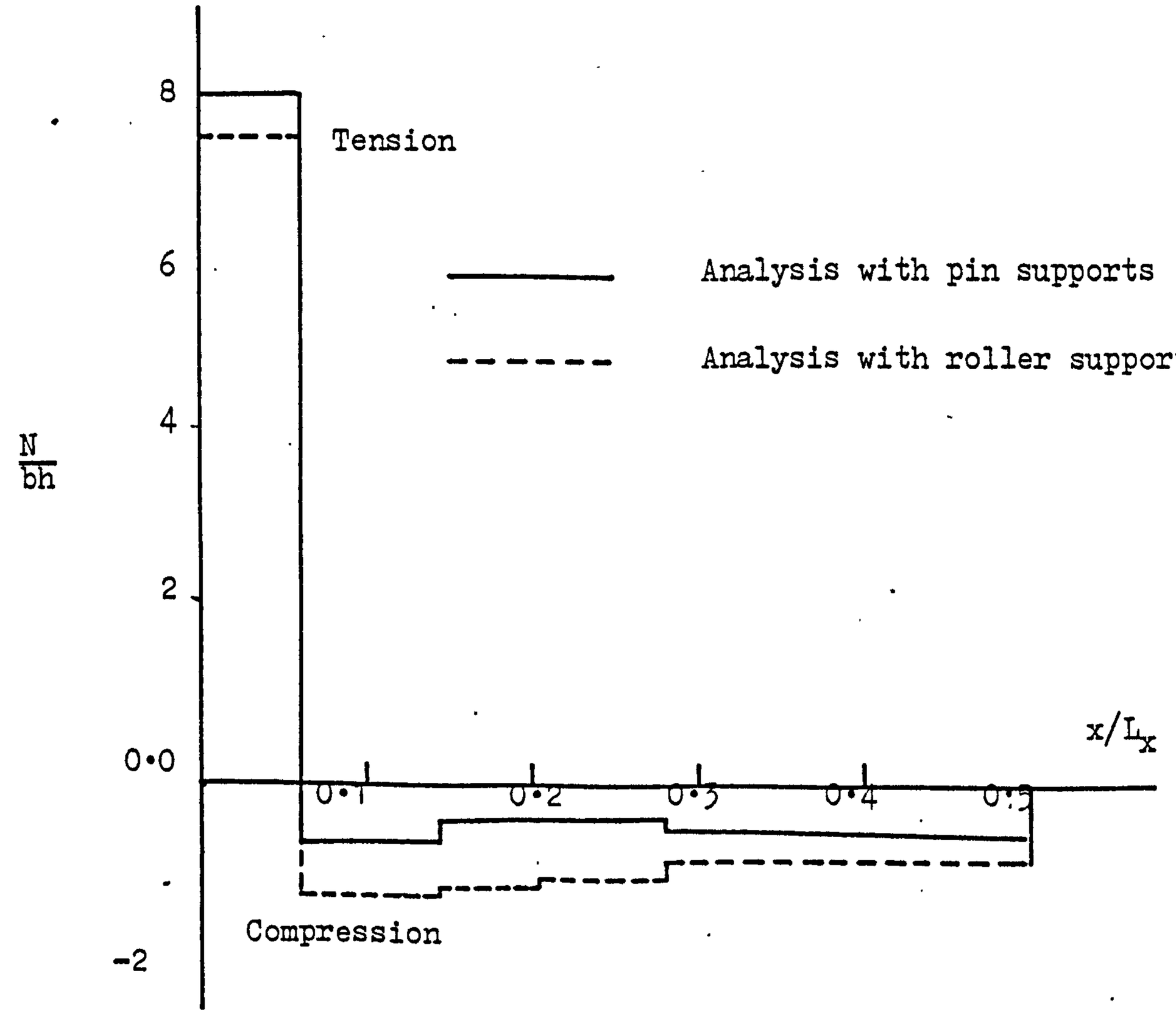

Figure (7.49) Variation of Membrane force N_y along xx (Model 6)

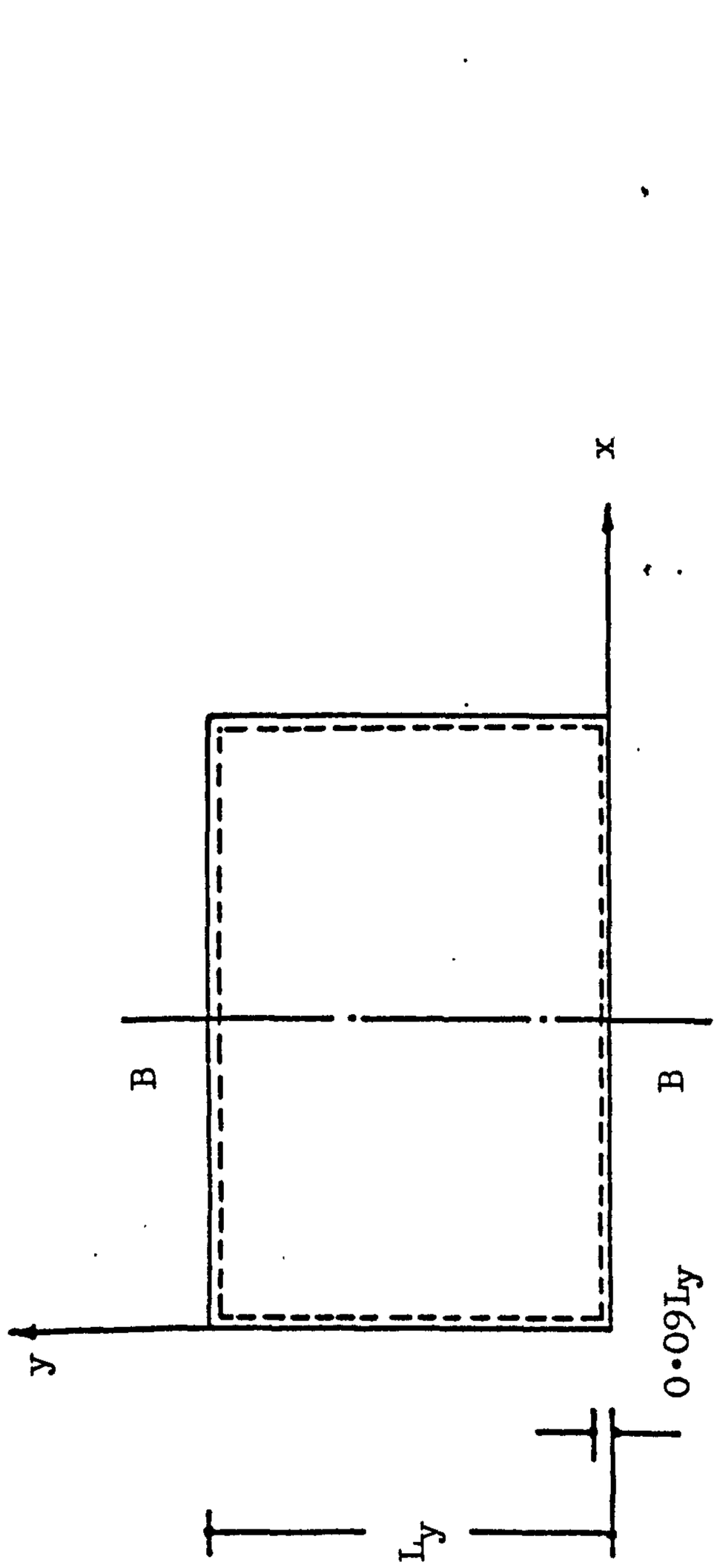
x
y
B
B
L_y
$0{\cdot}09L_y$

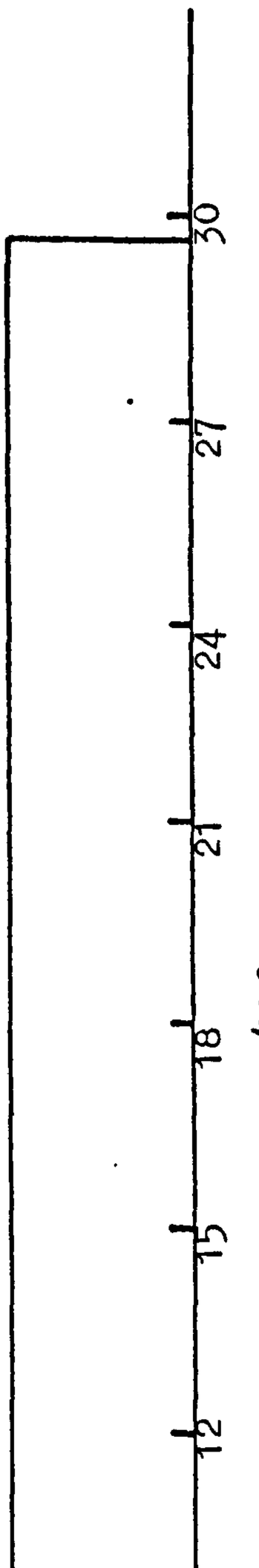
30
27
24
21
18
15
12
9
6
3
Normal Moment M_{el}/bh^2
Along Section BB (Model 6) - Elastic Analysis
Variation of Normal Moment M_x^*

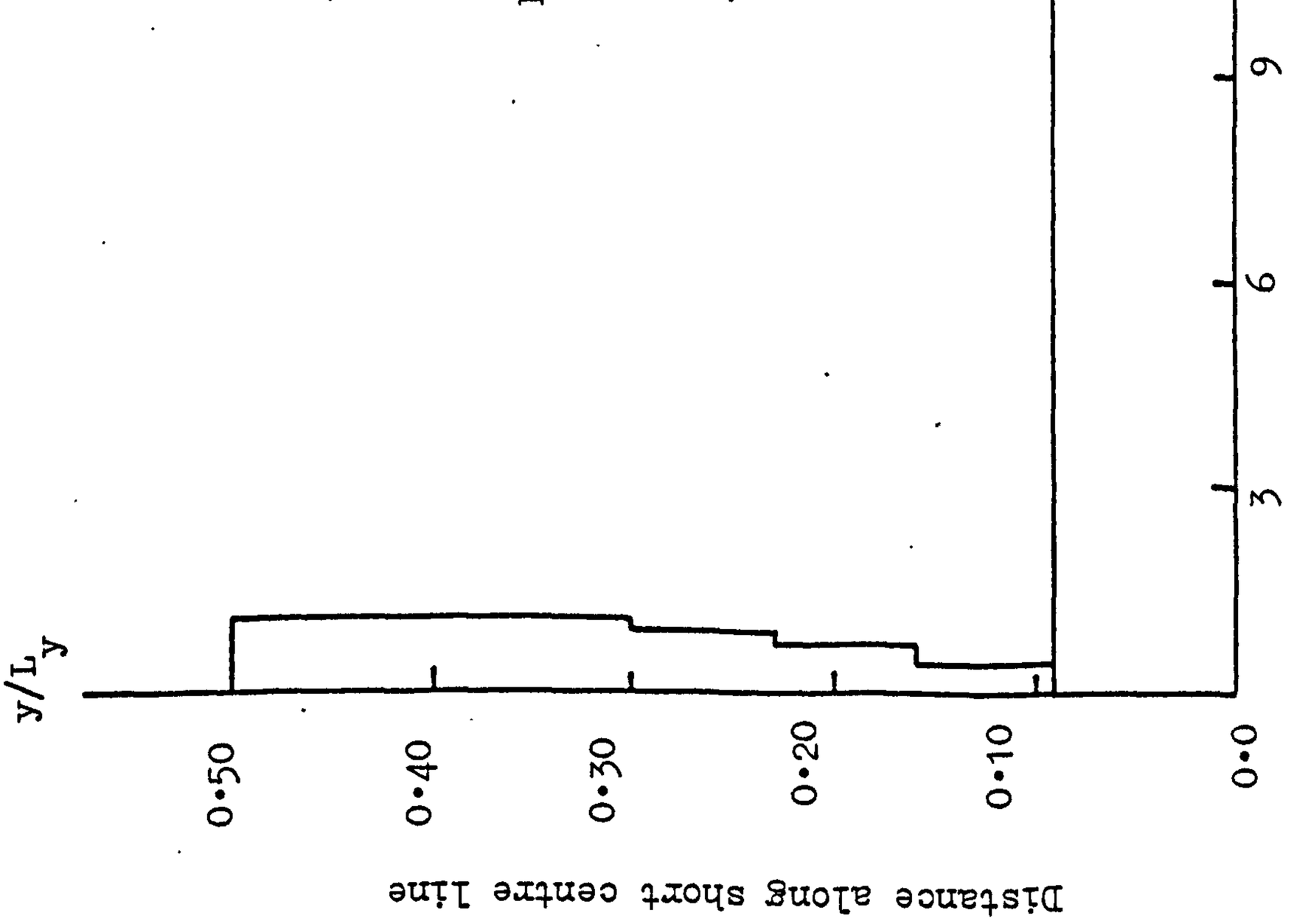
y/L_y
0·50
0·40
0·30
0·20
0·10
0·0
Distance along short centre line

Figure (7·50)

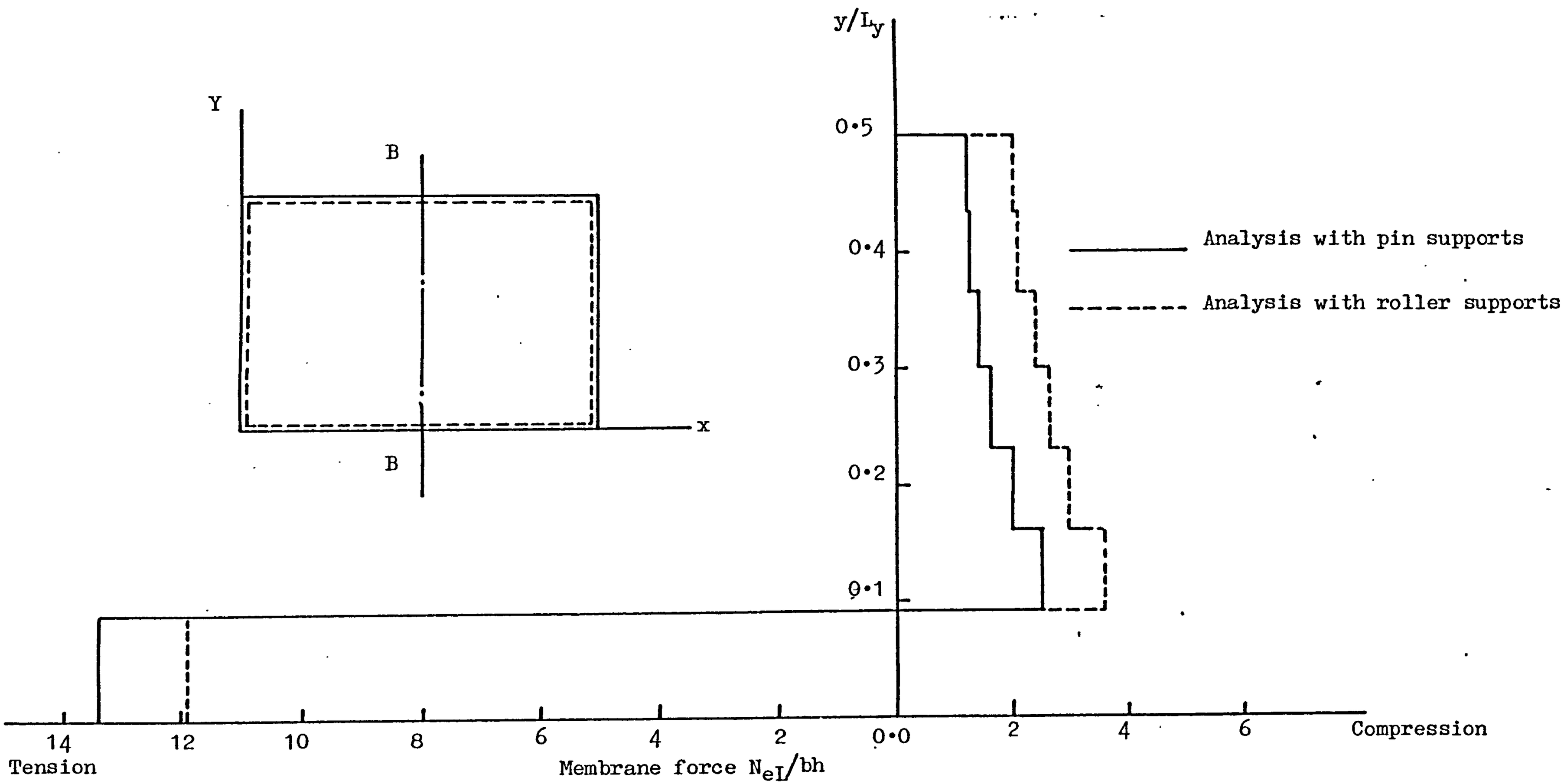

Figure (7•51) Variation of Membrane Forces along Section BB (Model 6) Elastic Analysis

CHAPTER EIGHT

CONCLUSIONS AND SUGGESTIONS FOR FUTURE WORK

Although each chapter has been provided with a set of conclusions at its end, for clarity the most important of these will be summarized below:-

8.1 Conclusions:

(1) In the finite element analysis, a mesh division which is satisfactory for the elastic analysis is also adequate for nonlinear analysis of reinforced concrete planar structures. A numerical integration order of 2 x 2 is quite sufficient to produce acceptable results for laterally loaded slabs and slab-beam systems.

(2) Using the formulation of the layered finite element suggested in this study, accurate predictions for the response of concrete slabs can be obtained by demanding equilibrium at each load level. Acceptable predictions can also be obtained with reasonable norms prior to yield, and by reducing the size of the load increment and allowing a limit iterations number to be reached. In this study, it was found that an average of 10 iterations per load increment is quite adequate to produce acceptable predictions for the response of concrete slabs, provided that, the increment is about 0.10 of the cracking load. In the case of slab-beam systems, an average number of 30 iterations may be needed.

(3) In the analysis of slab-beam systems by the method proposed here, accurate predictions of the flexural response can be obtained in any case using the limitations on the load increment and number of iterations described above. One disadvantage of this method is that it underestimates the torsional stresses and stiffness of the supporting beams, due to the neglect of the vertical shear component (see Chapter 4). Accordingly, if the direct design procedure is used, a check on the torsional strength of the beams has to be made. In this research, it was assumed that the torsional moments on the edge beams predicted by the finite element model used here, represent only half the actual torsional moments. An element that includes the vertical shear component in its formulation is strongly recommended.

(4) A comparison between the direct design and the Hillerborg's (Torsionless) methods showed that the two methods produce stress distributions, which are generally different. By considering additional "torsional steel" at the corners as suggested in CP 110[5] in the Hillerborg's method, the two methods produce moment volumes close to each other.

(5) Unlike the torsionless analysis, the direct design procedure produces in most cases a smooth variation of the design moments in the slab. The design can then be based on either the maximum or the average moment in the strip, without departing far from the original distribution.

(6) In the case of slab-beam system under uniform load considered in Chapter (5), the yield line solution requires 30% more steel over that needed by the direct design method. In the system designed by the direct design procedure, yield starts near the corners, and this type of yield would eventually cause the disruption of the corner connection, which reduces the torsional strength of the system by reducing the rotational restraints. By appreciating the fact that this zone is subjected to a very complex stress system, it may be advisable to add more steel in the beams near the corners. Following CP110[5], 50% of the steel at midspan section can be carried on to the end of the beam, and properly anchored.

(7) In the slab-beam systems, consideration of membrane forces in the design of the reinforcement, although reduces the reinforcement in the slab, requires more steel in the supporting beams. Designs including membrane forces require about 7% more steel than those for flexure only, for the case of uniform lateral loads. For concentrated loads, the difference in the total steel volume could be as high as 25% and sometimes even more.

(8) Whether membrane forces are considered in the design of slab-beam systems, or not, the system designed by the proposed direct design procedure will behave satisfactorily. Inclusion of membrane forces in the design produces improvements in the service behaviour of the system.

(9) All the slabs considered in this study which were designed by the direct design method behaved satisfactorily under working loads. Results indicated that both the deflections and crack widths were within acceptable limits in the working load range. No yield of steel occurred in all tests within the working load range (Chapter 7). In fact, first yield loads were very close to the design loads, with an average of 90% of the design load.

(10) Crack spread in a fine evenly distributed pattern. At all stages of loading, there was a tendency to form new cracks rather than to open the already formed cracks. Accordingly, the behaviour at any stage was not governed by a few wide cracks. This process was observed even after the attainment of the design loads.

(11) All the slabs designed by the direct design approach recorded failure loads very close to their design loads. In most cases, an average enhancement of 16% in the ultimate load was obtained, which is attributed mainly to membrane action, and strain hardening of the reinforcing bars.

(12) The nonlinear layered finite element developed here proved to be a powerful tool for the analysis of reinforced concrete slabs and slab-beams systems. Excellent agreement between the theoretical predictions and actual slab behaviour has been obtained, in most cases.

8.2 SUGGESTIONS FOR FUTURE WORK

The procedure suggested here can be extended to include experimental and theoretical studies on skew slabs with various sides ratios and support conditions. The most effective steel orientation can thus be found by systematic study of the various parameters involved. The layered finite element using isoparametric formulation provides an effective means of treating this problem.

The study can also be extended to include built-in panels of various sides ratios to check if any significant redistribution will occur. In the finite element method, use can be made of the progressive relaxation of edge rotation technique developed by Johnarry[43]. A detailed finite element study will be involved in applying the technique to the element developed here, before it can be used for checking the direct design procedure.

More experimental work is needed on slab-beams systems. In the present research, the membrane forces were not considered in the design of the experimental model. It is suggested that such forces to be taken into consideration. A comparison between designs based on open and filled sandwich models can also be undertaken by experiments. The design of slab-beams systems in this study tended to overestimate the ultimate loads by nearly 50%. A more detailed study of the phenomena is needed before a more economical design can be recommended.

A P P E N D I C E S

APPENDIX (A)

Calculation of the steel required for a certain design moment M* per unit width.

Using the ultimate limit state theory, it can be assumed that the stress distribution in the section will have the form shown in the Figure below:

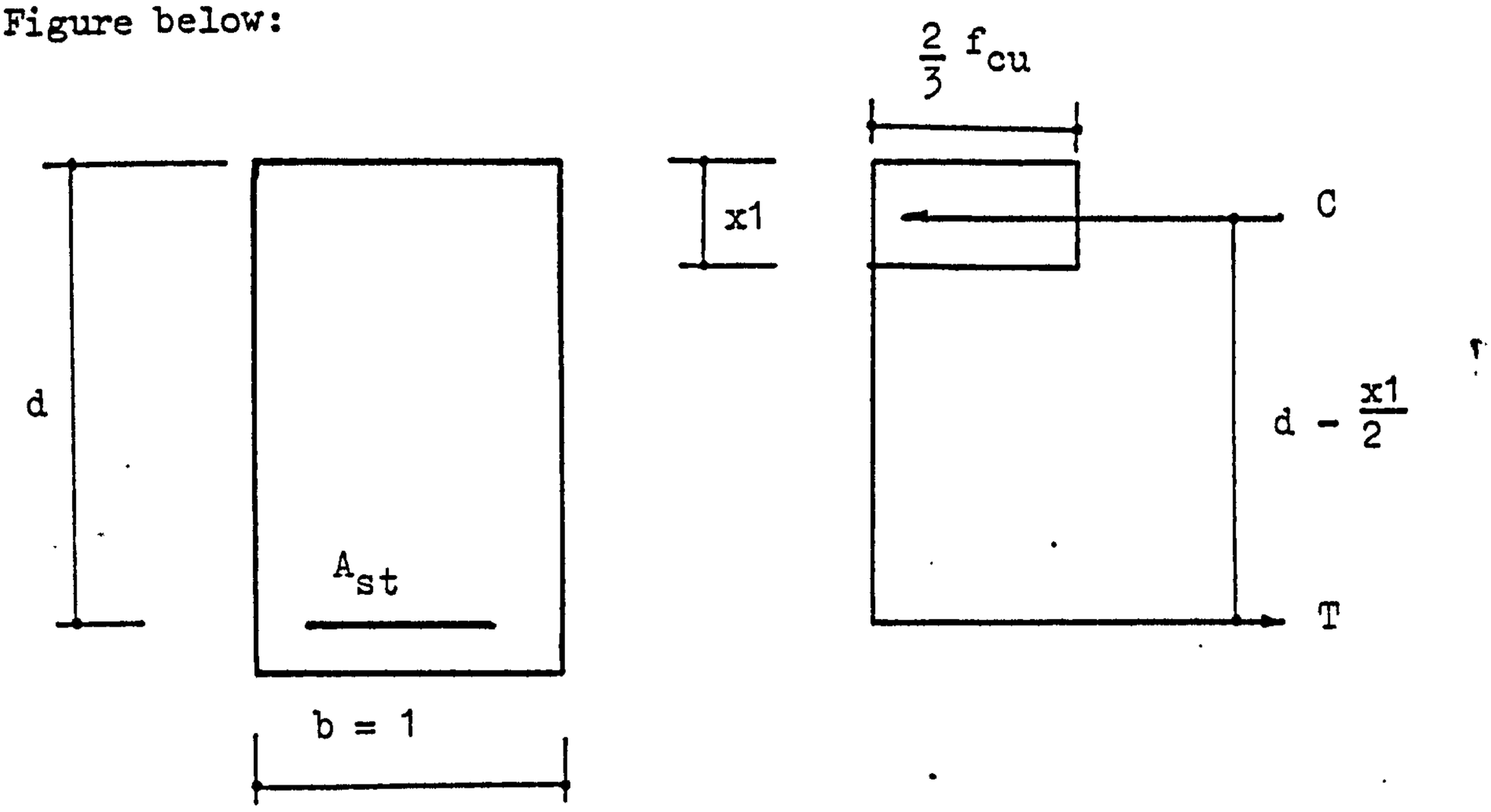

Taking the partial safety factors on both concrete and steel equal to unity, and by considering the horizontal equilibrium of the section for no net force:

then $$c = T \qquad (1)$$

Using the stress distribution at ultimate

$$\therefore \frac{2}{3} f_{cu}\, x1 = A_{st} f_y \qquad (2)$$

$$\therefore x1 = 1.5\, A_{st} \frac{f_y}{f_{cu}} = 1.5 d\rho\, f_y/f_{cu} \qquad (3)$$

where $\rho = A_{st}/d$ = reinforcement ratio.

Taking moments about the compression force and equating external and internal moments, then

$$M^* = T.\ (d - \frac{x'}{2})$$

$$= A_{st}\ f_y.(d - 1.5\ \rho d\ f_y/2\ f_{cu})$$

$$= \rho d^2\ f_y\ (1 - 1.5\ \rho\ f_y/2\ f_{cu})$$

$$= \rho\, d^2 f_y - .75\ \rho^2 d^2 f_y^{\,2}/f_{cu} \qquad (4)$$

arranging we get the quadratic in ρ:

$$(.75\ \frac{f_y}{f_{cu}})\ \rho^2 - \rho + \frac{M^*}{d^2\ f_y} = 0 \qquad (5)$$

Solving and substituting $\rho = A_{st}/d$

$$\therefore \quad A_{st} = \frac{f_{cu}\ d}{1.5\ f_y}\left[1 - \sqrt{(1 - \frac{3\ M^*}{d^2\ f_{cu}})}\right] \qquad (6)$$

Equation (6) is used for both top and bottom steel.

APPENDIX B

PROGRAM DESCRIPTION AND IMPLEMENTATION

This part is intended to give a brief description of the main features of the computer program used in this study. The program stems from an existing program developed by Johnarry[43] in Strathclyde University. Extensive modifications were introduced and these included: element reformulation, cracking and plastification of concrete, yielding of steel, details of which was given in Chapter 4 of this study. Modôfications also included the introduction of design routines and omission of some routines in the previous program.

One basic feature of this new program is the omission of back store facilities. Accordingly, the program running time is greatly reduced.

The program is built up of twelve subroutines which are listed in the following

1. Program FEM
2. Subroutine INTEGRATION
3. Subroutine LSTIF
4. Subroutine BMATX
5. Subroutine MAKERNA
6. Subroutine RMMULT
7. Subroutine LNSRKM
8. Subroutine BOUNDARY
9. Subroutine NORSOL
10. Subroutine REACTIONS
11. Subroutine DESIGN
12. Subroutine LNPLANED

in addition, the standard master library routine FOLAAF is used to

invert a matrix, in obtaining the coefficients matrix of the displacements polynomials (section 4.2.1), which is needed in both the stiffness and uniform load vector formulations.

The following sections will describe in brief the functions of the various subroutines, and the structure and organization of the main program.

1. Program FEM:

This is the monitoring module in which all other routines are called in appropriate places. All input data is first read in this module, and control data pertaining to mesh generation, arrangement of nodal parameters are all computed at the beginning of the program. The flow operation in this module is well explained as follows:

a. Major data is read, and control data is computed.

b. Stiffness matrix is formed and assembled in a banded form.

c. The load vector made up of uniform load, concentrated loads or membrane force contributions, is assembled.

d. The stiffness matrix is decomposed using the Gaussian elimination[31] procedure, and the equations are solved for the nodal displacements.

e. Middle plane strains and curvatures are computed, and strains and stresses at the Gauss points are computed.

f. Results are then scaled up or down to these corresponding to the load causing the first cracks in the most highly stressed point, and step c to e are repeated. Subsequent load increments are later given in terms of this cracking load P_{cr}.

g. The state of stress at a Gauss point is checked and a set of pseudoforces is found.

h. The structure is reanalysed under the effect of these pseudoforces, until equilibrium is maintained.

i. Results output.

2. Subroutine INTEGRATION:

This routine is called only once at the beginning of the FEM module. The routine sets the Gauss points coordinates and weighting factors, according to the order of integration specified in the data.

3. Subroutine LSTIF:

This routine calculates the equivalent D matrix for a layered element from the layers contributions, using equation (4.17). The routine is called everytime the stiffness of a layer is needed.

4. Subroutine BMATX:

This routine performs two functions:

a. Calculates the coefficient matrix (matrix C in equation 4.5) using the displacement polynomial functions defining the elements, equations (4.1) to (4.3), and the corner coordinates of the element.

b. Calculates the strain matrix B using the strain-displacement relationships, given by equation (4.10).

Both the interpolation and the strain matrices are dependant on the element dimensions only and are independent of the layering system. The routine is called whenever a different element type defined by its sides lengths is encountered. The routine is called during the stiffness formation phase, and the coefficient matrix is needed only in the calculation of the consistent load vector from uniform loads. Different elements strain matrices are stored and used in the stiffness phase, middle plane strains phase, and later used when integrating the

stress resultants to get the internal nodal force vector.

5. Subroutine MAKERNA:

The element load vector (nodal forces) computed for a given intensity of uniform lateral load is calculated in this routine. These nodal forces are obtained from[68]:

$$F = \{ - [C]^{-1} \}^{T} \int\!\!\int [P]^{T} \; q \; dx \; dy$$

where matrix C is the coefficient matrix obtained from the previous routine. P is the polynomial function given in equation (4.3), and q is the intensity of the uniform load. The integration is carried explicitly and formulated in the routine. The integrand depends on the element dimensions, and accordingly, the routine is called whenever a different type of element is encountered.

6. Subroutine RMMULT:

This routine multiplies two matrices to produce a third. Accordingly it is used in more than one position in the program.

7. Subroutine INSRKM:

This routine inserts elements stiffness matrices in their proper places in the global stiffness matrix. Since the program employs a constant stiffness method, this routine is called once only for each element in the stiffness formation phase.

8. Subroutine BOUNDARY:

This routine identifies the restrained boundary degrees of freedom. A restrained displacement is given a code of 1. Later in the solution phase, such degrees of freedom are removed from the stiffness matrix. Prescribed displacements at the nodes are not treated as restraints on the nodes. This routine need be called only once in the program.

9. Subroutine NORSOL:

In this routine, the banded stiffness matrix is first decomposed into a triangular form using the Gaussian elimination method[31]. The stiffness matrix is decomposed only on first entry to the routine. In subsequent entries, only the load vector is decomposed, and the nodal displacements are obtained by back substitution into the decomposed matrix.

This is the most extensively used routine. It is called at the beginning of each load increment, and once during each iteration.

10. Subroutine REACTIONS:

This subroutine computes the nodal reactions on the boundary nodes. The routine is called only once, and reactions are obtained only for the first load increment, and during the design phase.

11. Subroutine DESIGN:

This routine is called only when a design for the flexural reinforcement is needed. The design is done according to the equations of section (3.4). This is an optional routine, and need be entered only once.

12. Subroutine INPLANED:

This routine is called only when a design for membrane reinforcement is needed. The design is done according to the equations of section (3.6). This is an optional routine, and need be entered only once.

User Instructions Manual to the Program FEM

Card No.	Format	Description
1	20 A4	TITLE: Any sentence defining the problem.
2	I5,4F10	Nonelastic, Elastic, UDULTIMATE, DPB, TBEAM If nonlinear analysis needed, NONELASTIC = 1, and zero otherwise. To design flexural steel use Elastic = 1.0. UDULTIMATE is the design uniform load in N/mm^2. DPB = 1.0 Deep beams with elastic design for the reinforcement. DPB = 2.0 for Deep beams with a given reinforcement. For slabs put DPB = 0.0 TBEAM = depth of slab and supporting beams.
3	20I5	IOUTPUT = nodes numbers for which displacements output is required.
4	20I5	IOUTPUT = Elements numbers for which stresses and strains are requested in output.
5	14I5	NREF1, NREF2, NREF3, NREF4, NREF5, NG, NPNODES, NDIFEL, NPOINT LOADS, NBCS, NLC, INPLAY, MOMEL, NSTIF. Control data : NREF1 = 1- for unbounded plasticity . NREF2 = 1 for bounded. Only one of these should be $\neq 0$. NREF3 = node number for relaxation analysis ($\neq 0$ only when NREF4 $\neq 0$). NREF4 = 1 For fixed slabs only, otherwise = 0. NREF5 = 1 For nontorsional analysis, otherwise = 0. NG = No. of Gauss points in the element (4 or 9) NPODES = No. of Inplane point loads. NDIFEL = No. of different elements types. NPOINTLOADS = No. of point loads. NBCS = No. of boundary conditions. NLC = Total No. of load increments. INPLAY = 1 for additional steel to any element. MOMEL = Element No. for which a summary will be given at the end of the analysis. NSTIF = No. of additional stiffnesses.
6	8F8	SLX, SLY, DIVX, DIVY, REGULAR, SPANX, SPANY, GMOD.

Card No.	Format	Description
		SLX & SLY are lengths of the slab (or beam)
		DIVX, DIVY divisions in the X and Y directions
		REGULAR = 1.0 for equal subdivisions in the two directions, otherwise = 0.
		SPANX & SPANY are total spans in the two directions
		GMOD need be specified only when Nref5 in card 5 is $\neq$ 0. GMOD is the shear modulus of concrete.
7	I5,5F10	ITERTOT, SCALE LOAD, DISNORM, FNORM, ACCELERATOR, TTN
		ITERTOT = Max. No. of iterations in a load increment
		SCALELOAD = size of the load increment as a ratio of the cracking load. Use around 0.1
		DISNORM = convergence limit for displacement norm. Use 0.00001
		FNORM = convergence limit for force norm. Use 0.01 to 0.1
		ACCELERATOR = 1.0
		TTN = Tension stiffening factor c in Figure (4.6) use between 1.0 and 10.
8	8 F10	FCU, FST, FTC, EC, ES, P, HARD1, HARD2
		FCU = concrete compressive strength in N/mm^2
		FST = steel yield point in N/mm^2
		FTC = concrete tensile strength in N/mm^2
		EC = concrete modulus in N/mm^2
		ES = steel modulus in N/mm^2
		P = Poisson's ratio for concrete
		HARD1 = hardening modulus 1
		HARD2 = hardening modulus 2.
9	6 F10	SKEW, STEELANG1, STEELANG2, T, ASTX, ASTY,
	4 F5	LS1, LS2, LS3, LS4
		SKEW = angle of skew in degrees (90° for orthogonal)
		STEELANG1 = the angle the steel in the first direction makes with the x axis (ϕ° for orthogonal)
		STEELANG2 = the angle the steel in the second direction makes with the x axis (90° for orthogonal)

Card No.	Format	Description
		T = slab or beam thickness (mm)
		ASTX = 1 for main steel in X
		ASTY = u < 1 proportion of steel in Y direction
		LS1, LS3 = Y steel layers numbers
		LS2, LS4 = X steel layers numbers
10	3 F12	UD, PRX, PRY
		UD = intensity of uniformly distributed load in N/mm^2
		PRX = X prestress in N/mm^2
		PRY = Y prestress in N/mm^2
11	8 F10	XSIDE(I) = lengths of X divisions. Total No. of such divisions should be equal to DIVX, and more cards can be used if > 8 divisions. IF REGULAR = 1.0 in card No.6, this card is not needed.
12	8 F10	YSIDE(I) = length of Y divisions. Total No. of such divisions should be equal to DIVY, and more cards can be used if > 8 divisions. IF REGULAR = 1.0 in card No.6, this card is not needed.
13	12 F6	TT12(I) = layers %age thicknesses. Up to 12 layers can be used.
14	12 F6	BEAML(I) = layers %age thicknesses for T beam elements. Up to 12 layers can be used.
15	2 F6	DN, DNBEAM DN = depth of middle plane of the slab. If unspecified, the default value of T/2 will be used. DNBEAM = depth of reference plane in Tbeam problems, which may be different from its middle plane.
16	2 I7, 5 F10	(NBOUND(I), (NFIX(I,J), J=1,5), PRESC (I,J), J=1,5), I = 1,NBCS. NBOUND(I) = boundary nodes where restraints are to to be applied. NFIX (I,J) = Fixity code for the five degrees of freedom in the order u, v, w, $\frac{\partial w}{\partial y}$; $\frac{\partial w}{\partial x}$. If a certain degree of freedom in a node is restrained,

Card No.	Format	Description
		it is code 1 otherwise ∅.
		PRESC(I,J) = the prescribed displacement in the direction of any of the degrees of freedom of the boundary nodes.
17	13 I2	((IL,LMOD(I,J), J=1,12), I = 1,NDIFEL)
		IL = sequential order of the different elements with different layers arrangements.
		LMOD(I,J) = Type of layers for each type of element.. The following codes are used
		LMOD = 1 for concrete layers
		LMOD = 2 for steel layers
		LMOD = 0 for zero layers
18	20 I4	NEWEL(I), LDIF(I), I = 1, NDIFEL
		NEWEL = elements numbers with different layering systems.
		LDIF = layering system number corresponding to IL in previous cards.
		If all elements have the same layering system then this card may be left blank.
19	40 I2	IELC(LE), LE = 1, NEL, NEL = Total no. of elements.
		IELC = element type no. as it appears on the mesh. According to their sides lengths and layering system, elements can have different element type numbers IELC.
20	I5, 2F10	NPRES(I). FNPX(I), FNPY(I)
		NPRES(I) = boundary node numbers where inplane force in X direction FNPX(I) or in the Y direction FNPY(I) are applied, and the magnitude and direction of these forces. These forces are positive if they act in the positive directions of the global axes. The number of such cards will be equal to NPNODES in card No.5
21	I5,5 F10	NREST(I), FIXITY(I,J), J = 1,5
		NREST(I) = node no. at which support stiffnesses

Card No.	Format	Description
		FIXITY(I,J) in any direction of the five degrees of freedom can be assigned. The number of such cards will be equal to NSTIF in card 5.
22	I3, F10	LOADPOINTS(I), POINTLOADS(I), PMOM(I,J),J=1,2 LOADPOINTS(I) = Node nos. at which lateral concentrated loads. POINTLOADS(I) and concentrated moment in X and Y directions PMOM(I,J) are applied. Total no. of cards will be equal to NPOINTLOADS in Card 5. If an elastic design is required (with ELASTIC = 1.0 in card 2) this set of cards should represent the design point loads and accordingly, another set with small loads (of 1/15th the first design loads) are also to be added. This last set of point loads is needed to start the incremental analysis.
23	2I3, F10	NDNODE, LDIR, DLOAD NDNODE = node no. at which incremental membrane force in direction LDIR is to be applied. If force DLOAD is in the X direction use LDIR = 1, and if in Y direction, LDIR = 2. The number of such card will be equal to NPNODES in card No.5.

Program Flow Chart

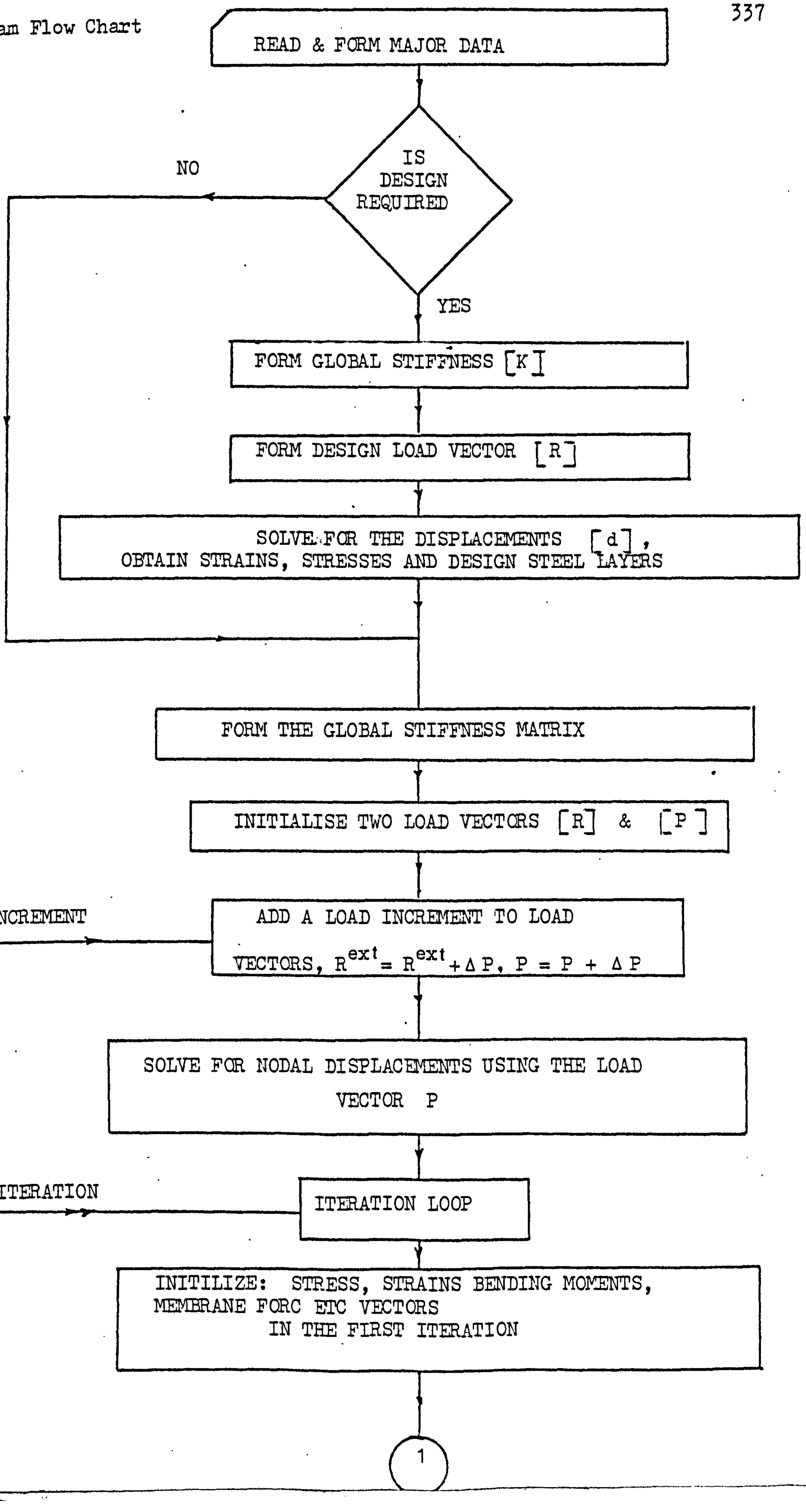

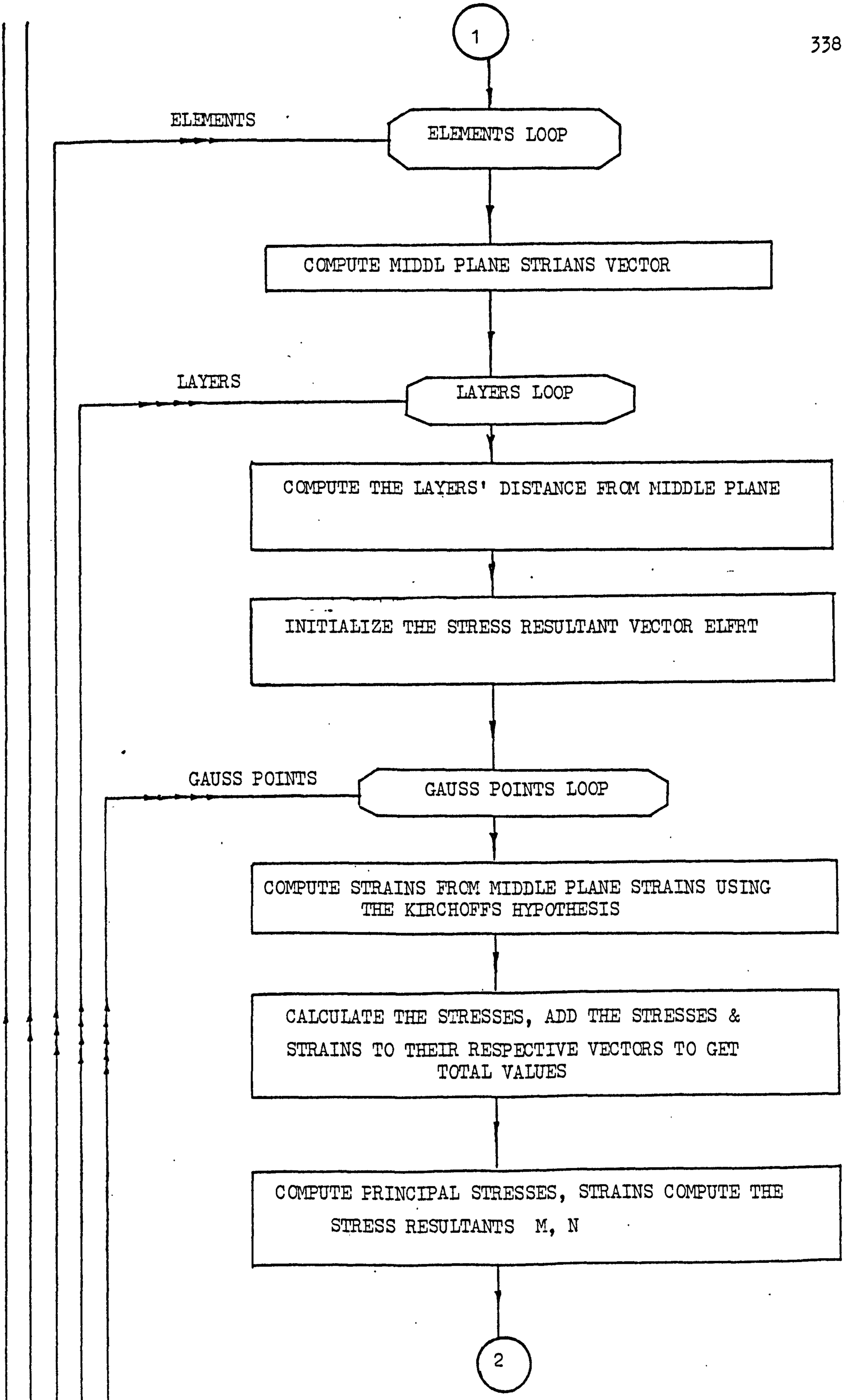
1
ELEMENTS
ELEMENTS LOOP
COMPUTE MIDDL PLANE STRIANS VECTOR
LAYERS
LAYERS LOOP
COMPUTE THE LAYERS' DISTANCE FROM MIDDLE PLANE
INITIALIZE THE STRESS RESULTANT VECTOR ELFRT
GAUSS POINTS
GAUSS POINTS LOOP
COMPUTE STRAINS FROM MIDDLE PLANE STRAINS USING THE KIRCHOFFS HYPOTHESIS
CALCULATE THE STRESSES, ADD THE STRESSES & STRAINS TO THEIR RESPECTIVE VECTORS TO GET TOTAL VALUES
COMPUTE PRINCIPAL STRESSES, STRAINS COMPUTE THE STRESS RESULTANTS M, N
2

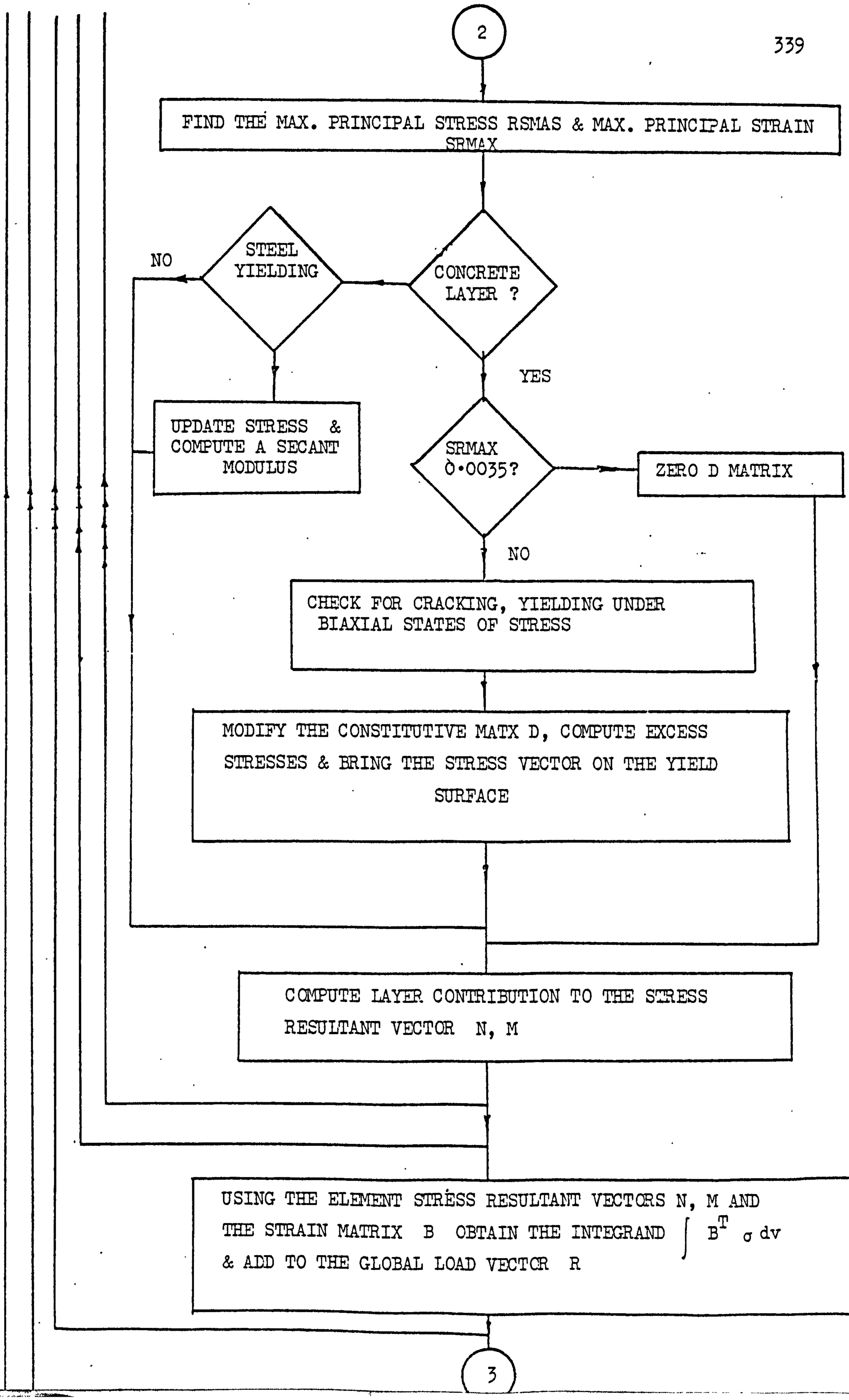
2
FIND THE MAX. PRINCIPAL STRESS RSMAS & MAX. PRINCIPAL STRAIN SRMAX
CONCRETE LAYER ?
STEEL YIELDING
NO
YES
UPDATE STRESS & COMPUTE A SECANT MODULUS
SRMAX ⩾0.0035?
ZERO D MATRIX
NO
CHECK FOR CRACKING, YIELDING UNDER BIAXIAL STATES OF STRESS
MODIFY THE CONSTITUTIVE MATX D, COMPUTE EXCESS STRESSES & BRING THE STRESS VECTOR ON THE YIELD SURFACE
COMPUTE LAYER CONTRIBUTION TO THE STRESS RESULTANT VECTOR N, M
USING THE ELEMENT STRESS RESULTANT VECTORS N, M AND THE STRAIN MATRIX B OBTAIN THE INTEGRAND $\int B^T \sigma \, dv$ & ADD TO THE GLOBAL LOAD VECTOR R
3

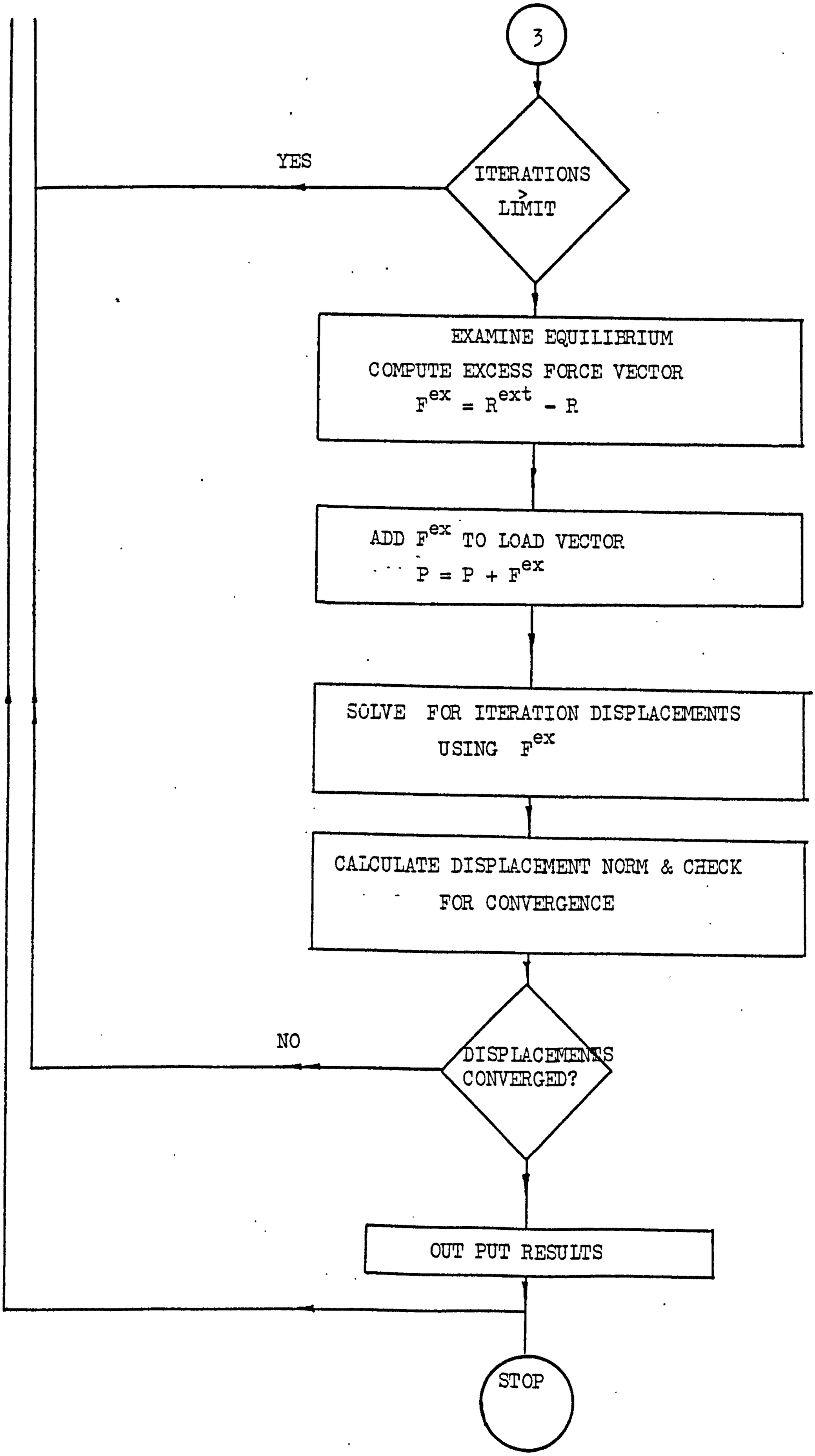
3
ITERATIONS > LIMIT
YES
EXAMINE EQUILIBRIUM
COMPUTE EXCESS FORCE VECTOR
$F^{ex} = R^{ext} - R$
ADD F^{ex} TO LOAD VECTOR
$P = P + F^{ex}$
SOLVE FOR ITERATION DISPLACEMENTS USING F^{ex}
CALCULATE DISPLACEMENT NORM & CHECK FOR CONVERGENCE
DISPLACEMENTS CONVERGED?
NO
OUT PUT RESULTS
STOP

APPENDIX C

DERIVATION OF THE BOUNDED PLASTIC LOADS

Using the principle of uniform deformation, the plastic load increment f_p may be obtained from the current plastic load R_p as

$$\Delta f_p = \lambda R_p \qquad (1)$$

where

$$R_p = \Sigma (R - \Sigma B^T \int_a \sigma \, dV) \qquad (2)$$

in which, R_p = total force imbalance vector

and Δf_p = increment of plastic load vector

R = load vector

Assuming the load-displacement curve can be fitted by a second degree curve

$$y = a_o + a_1 x + a_2 x^2$$

the nonlinearity at any stage is

$$R_p = a_1 x - y$$

$$= - a_o - a_2 x^2$$

and $$dR_p = - 2a_2 x \, dx$$

for $a_o = 0$

$$dR_p / R_p = 2dx/x$$

or $$\Delta R_p = \Delta f_p = 2R_p \, \Delta d/d.$$

If the degree of nonlinearity is mild,

$$\Delta d/d \simeq \Delta R/R$$

where d and Δd are deformation vectors.

Hence the increment of plastic load must be

$$\Delta f_p = 2R_p \, \Delta R/R$$

and $$f_p = f_p + \Delta f_p$$

so that $$k_o d = R + f_p$$

where k_o is the initial stiffness matrix, and R is the total load vector. The analysis then continues along the same lines as before, but with the incremental plastic loads bounded.

APPENDIX (D)

Comparison Between Moment Fields Produced by Torsional and Torsionless Analyses, for Slabs with Sides Ratios of 1·5 and 2·0.

N.B.

The Strip numbering system in the following figures is the same as that in Figures (5·3) to (5·9) in Chapter 5.

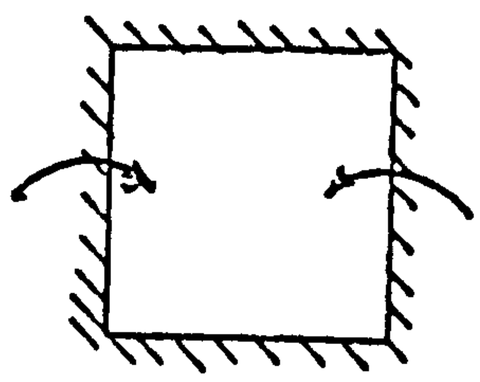

Figure (D1) Positive Moment M^*_x (L_x/L_y = 1.5)

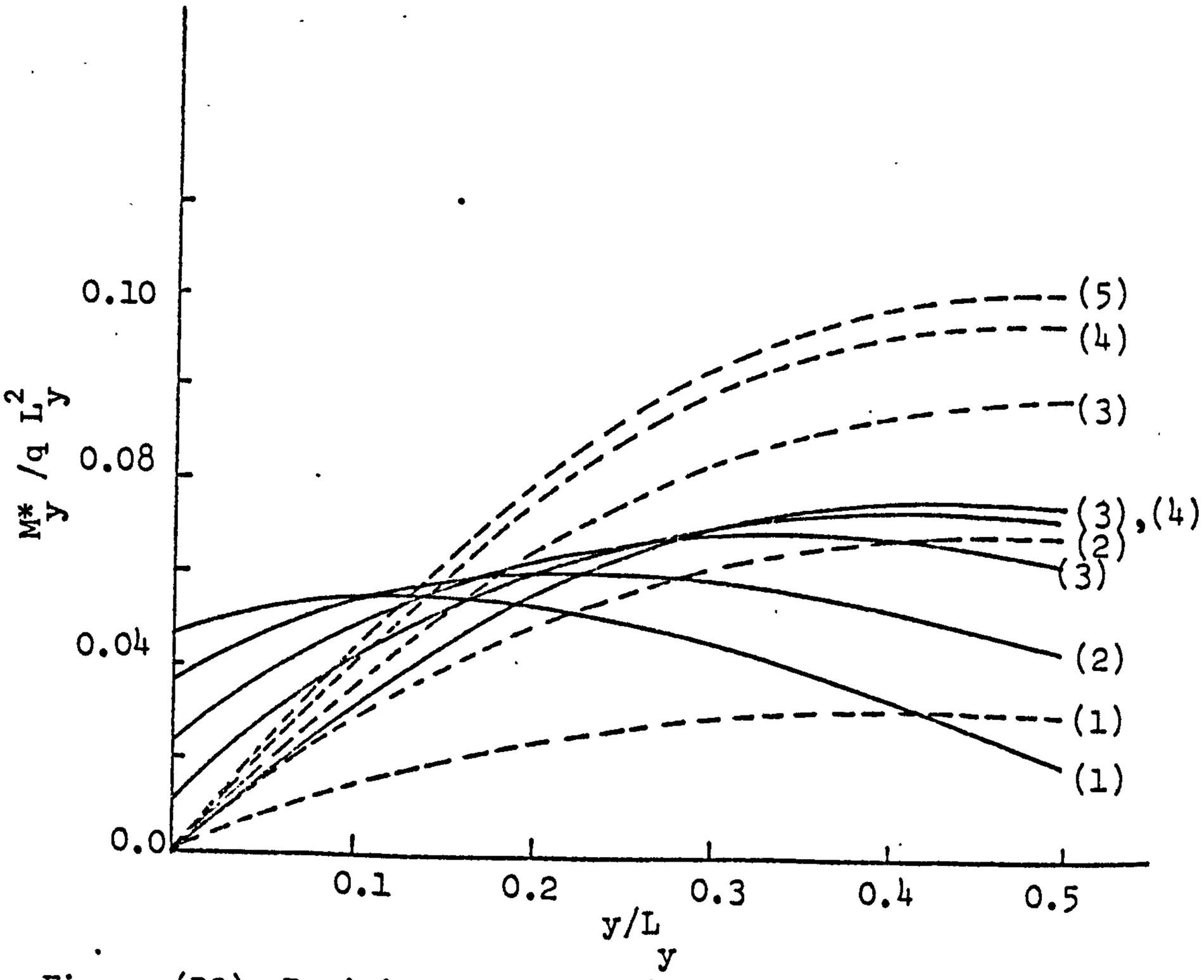

Figure (D2) Positive Moment M^*_y (L_x/L_y = 1.5)

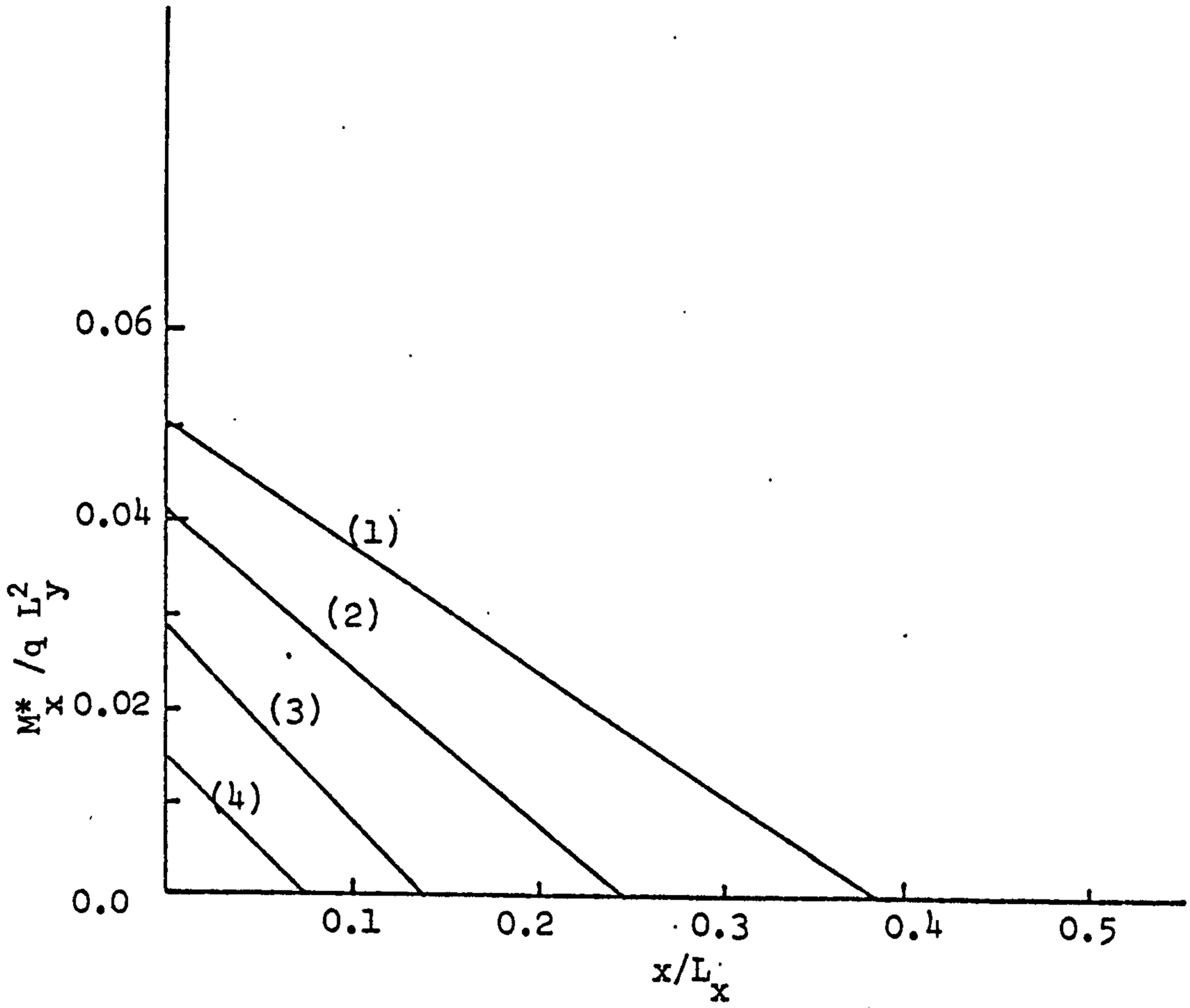

Figure (D3) Negative Moment M^*_x ($L_x/L_y = 1.5$)

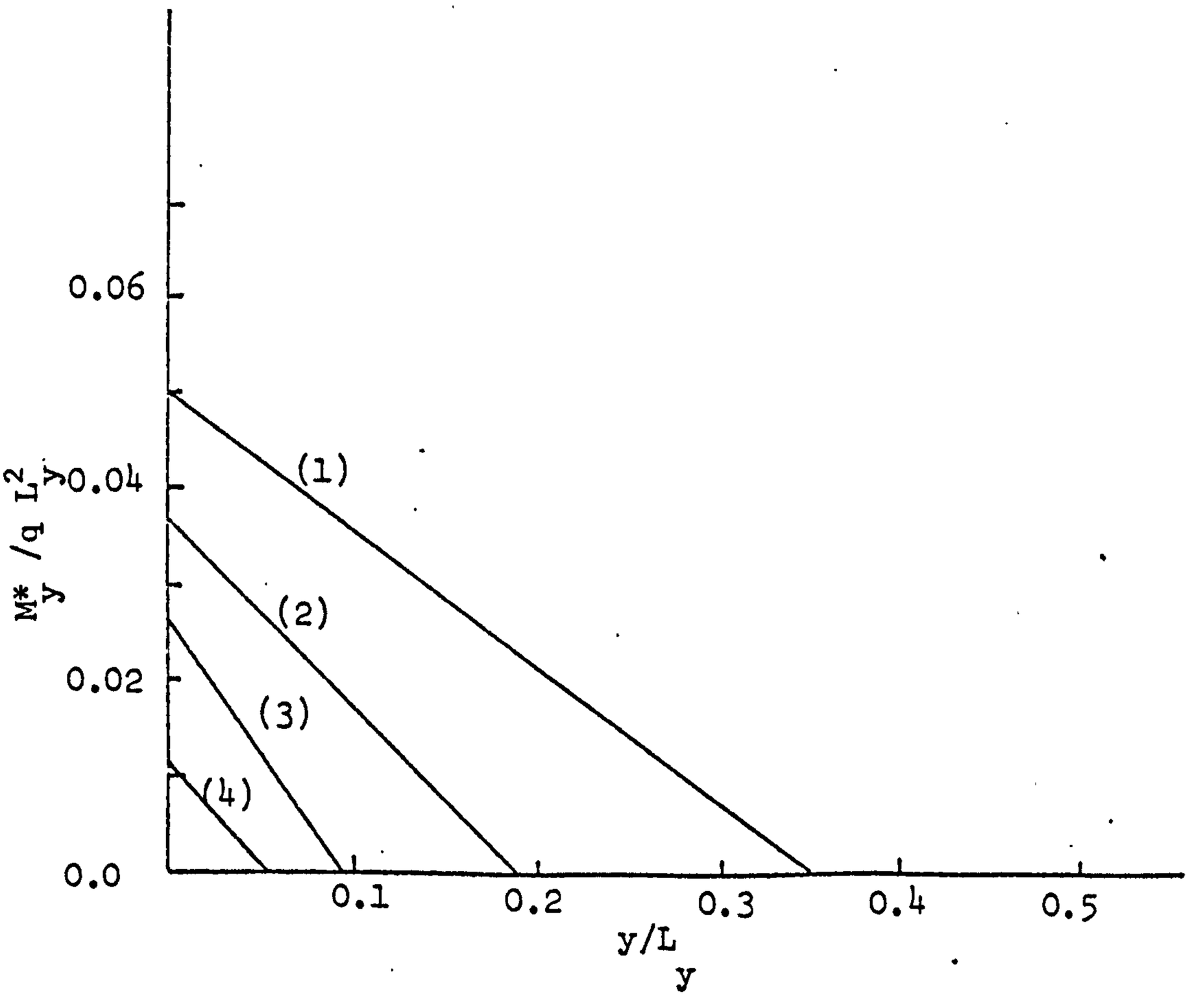

Figure (D4) Negative Moment M^*_y ($L_x/L_y = 1.5$)

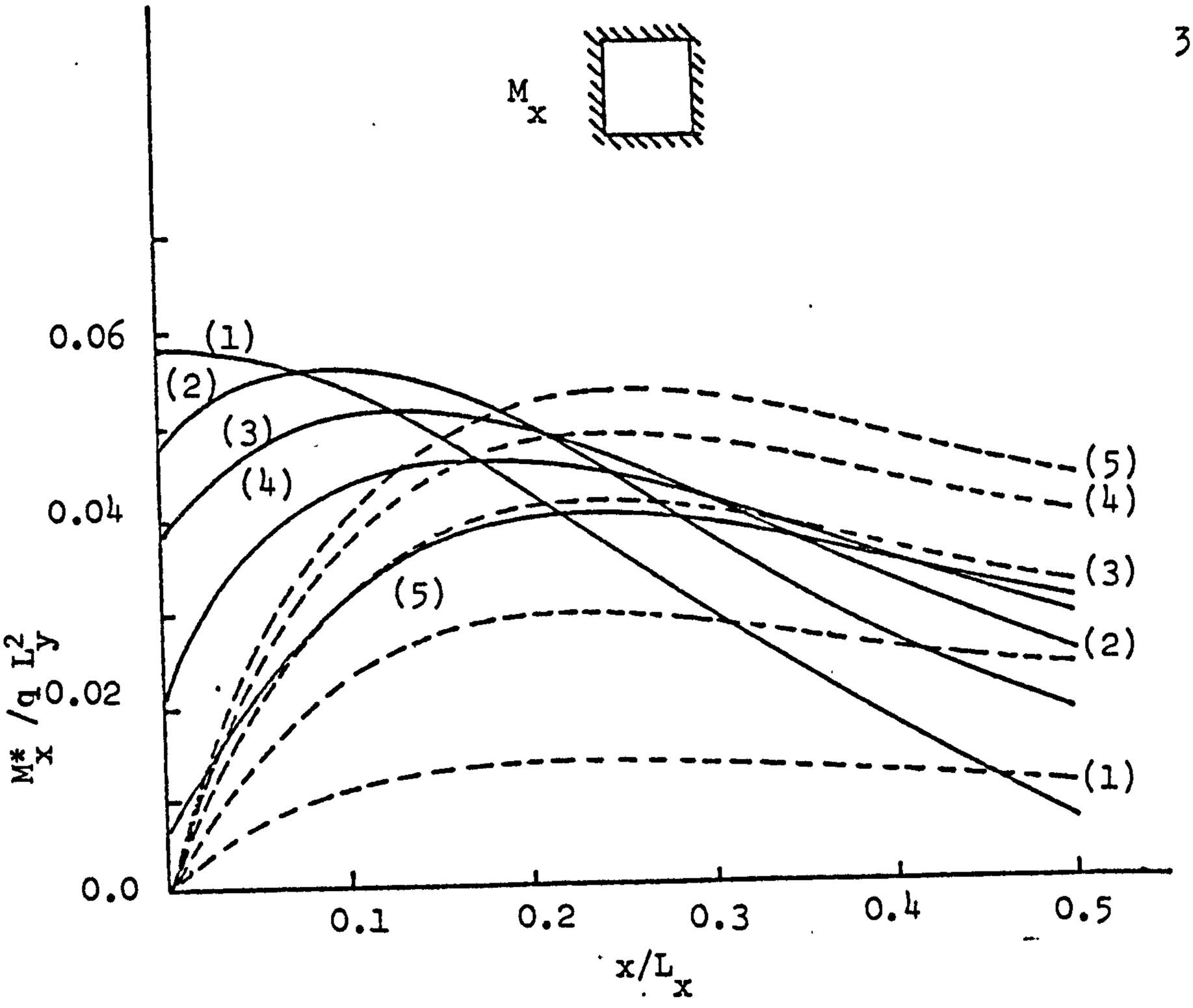

Figure (D5) Positive Moment M^*_x $(L_x/L_y = 2.0)$

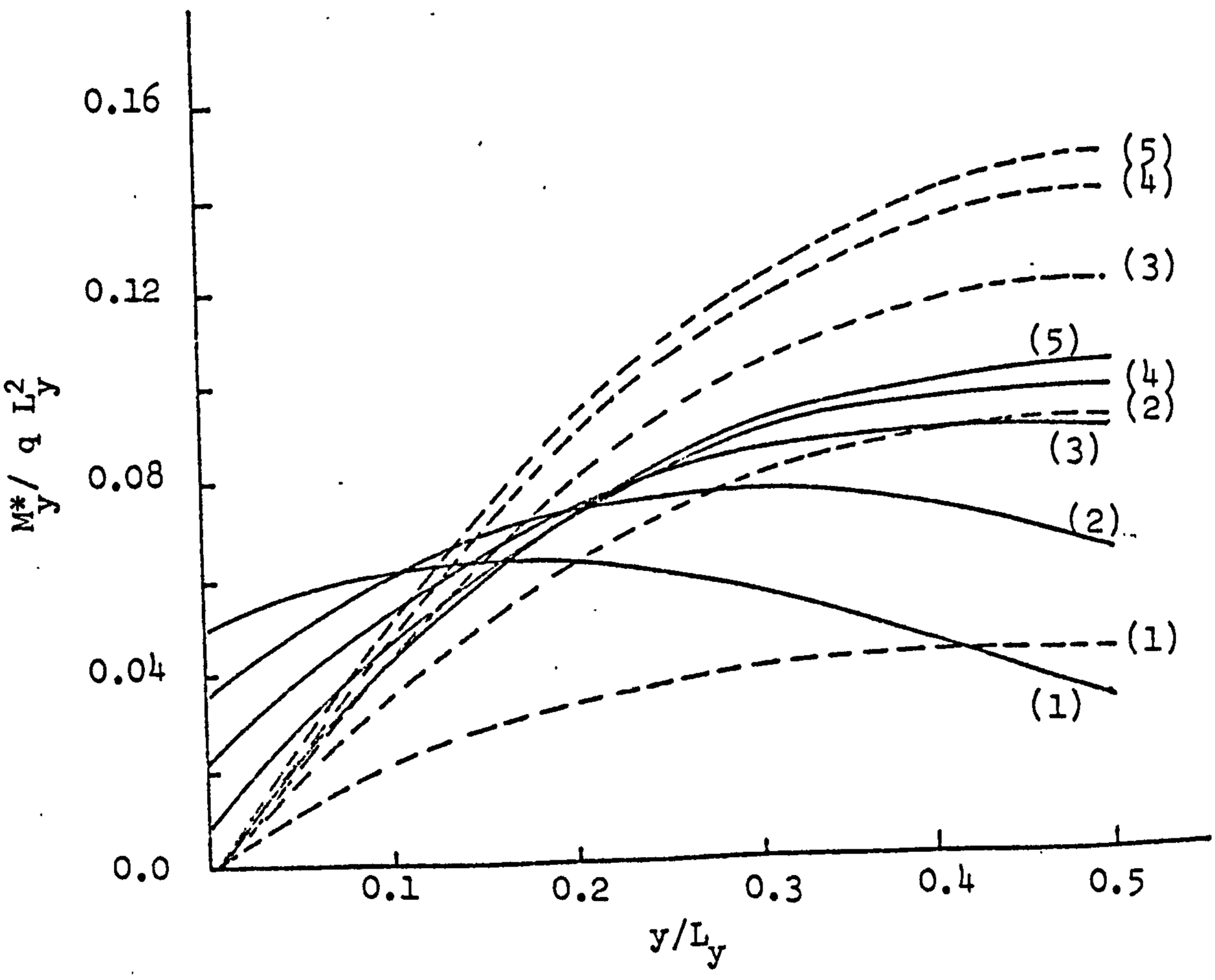

Figure (D.6) Positive Moment M^*_y $(L_x/L_y = 2.0)$

2

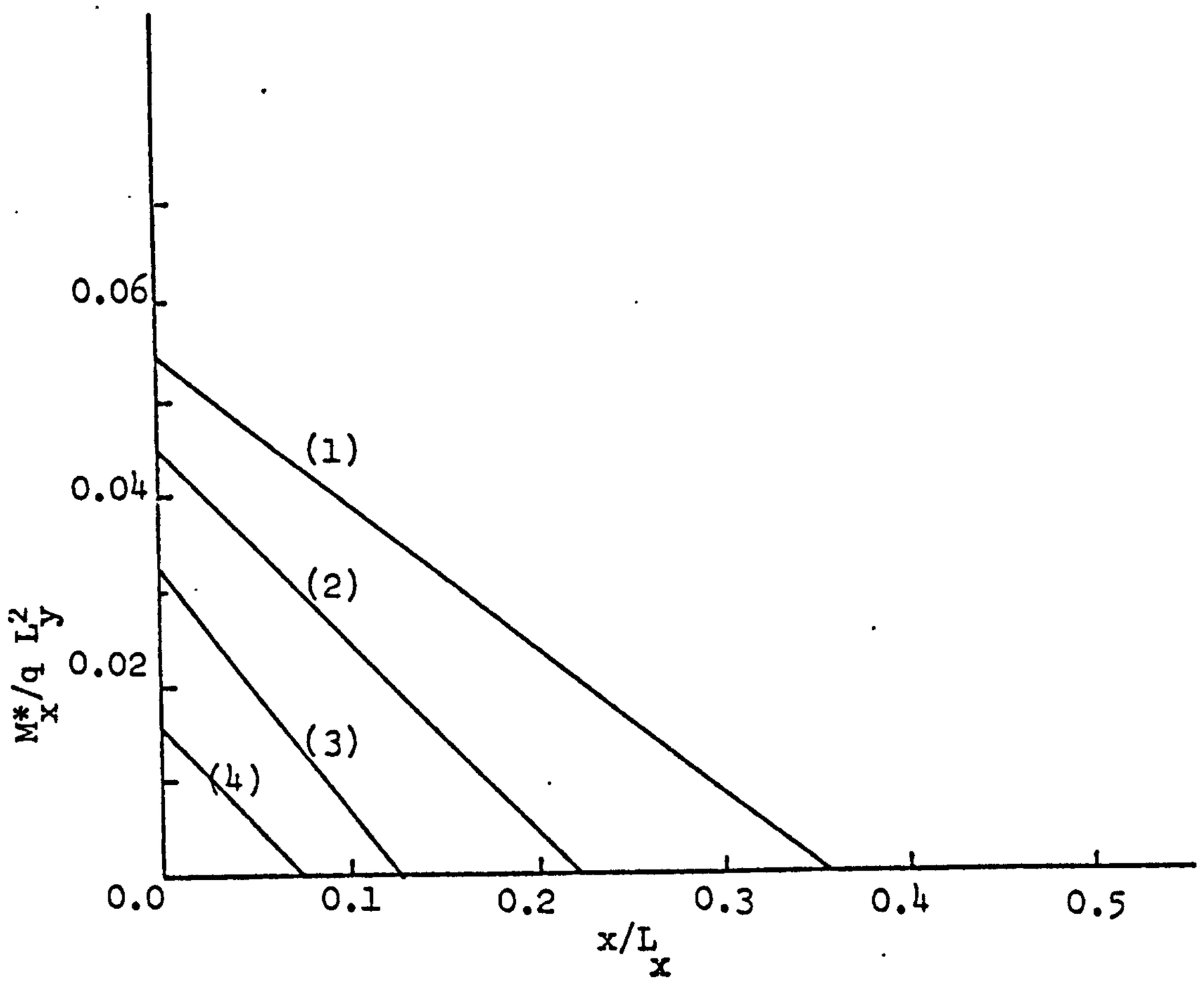

Figure (D7) Negative Moment M^*_x $(L_x/L_y = 2.0)$

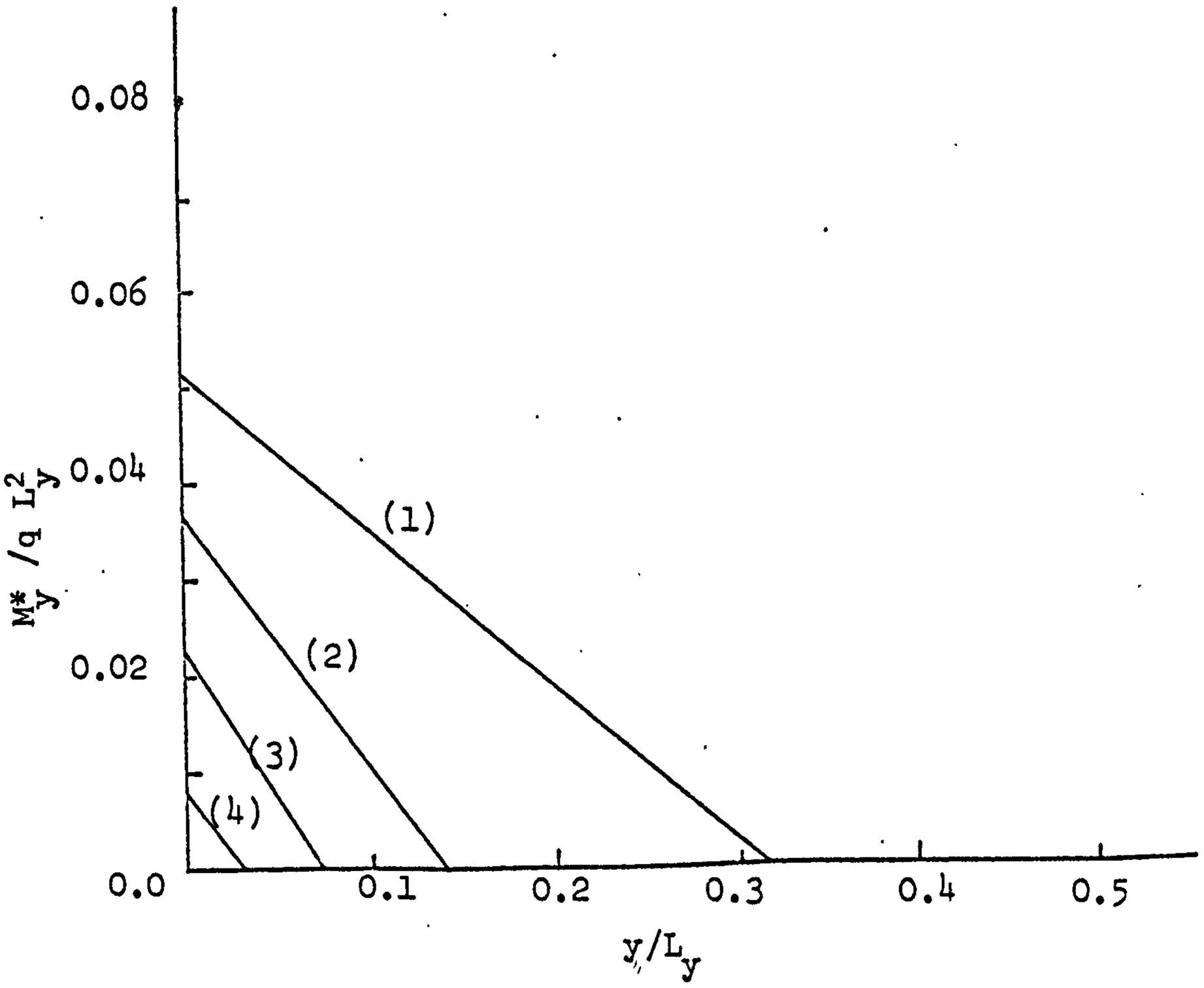

Figure (D8) Negative Moment M^*_y $(L_x/L_y = 2.0)$

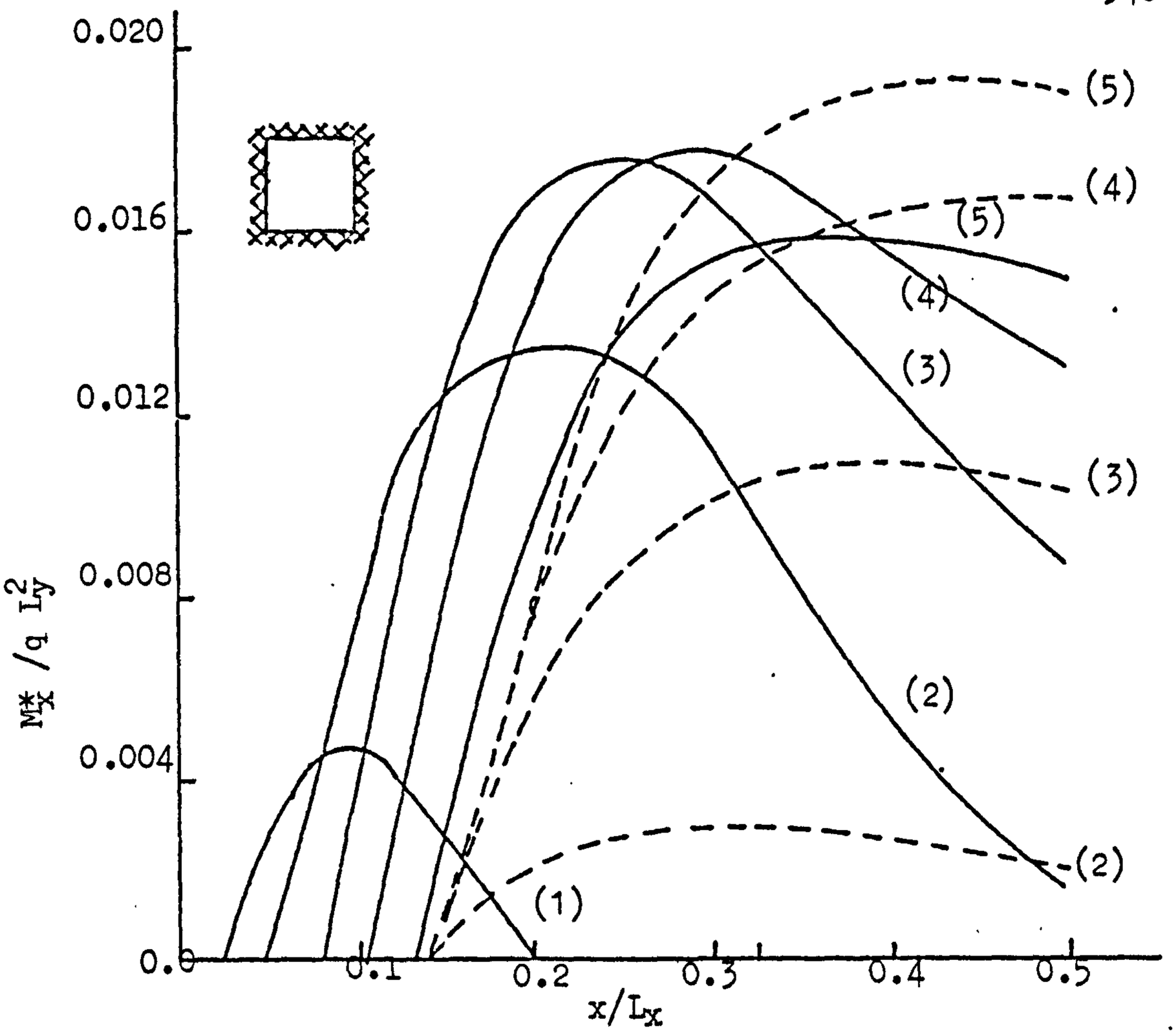

Figure (D9) Positive Moment M_x^* $(L_x/L_y = 1{\cdot}5)$

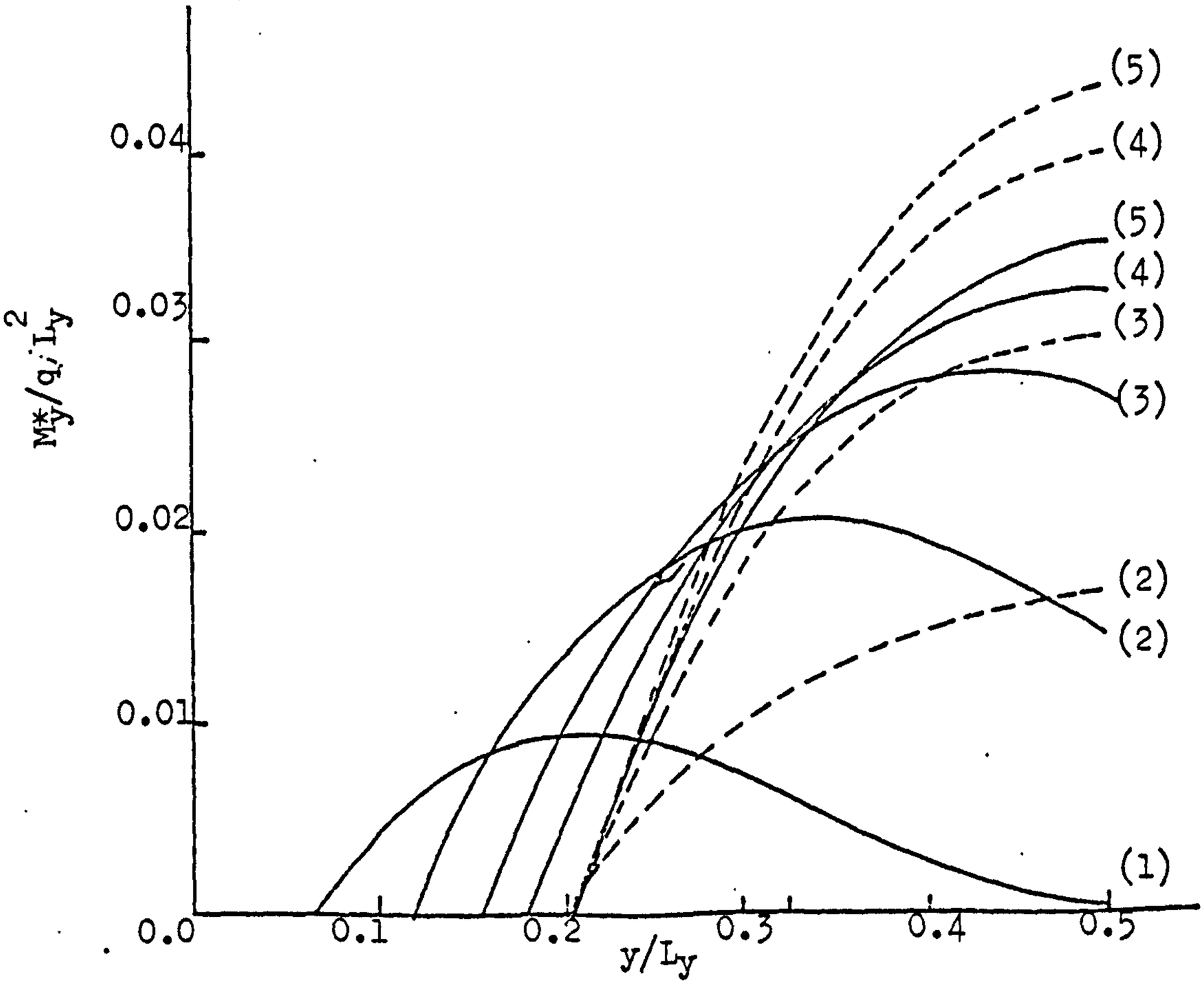

Figure (D10) Positive Moment M_y^* $(L_x/L_y = 1{\cdot}5)$

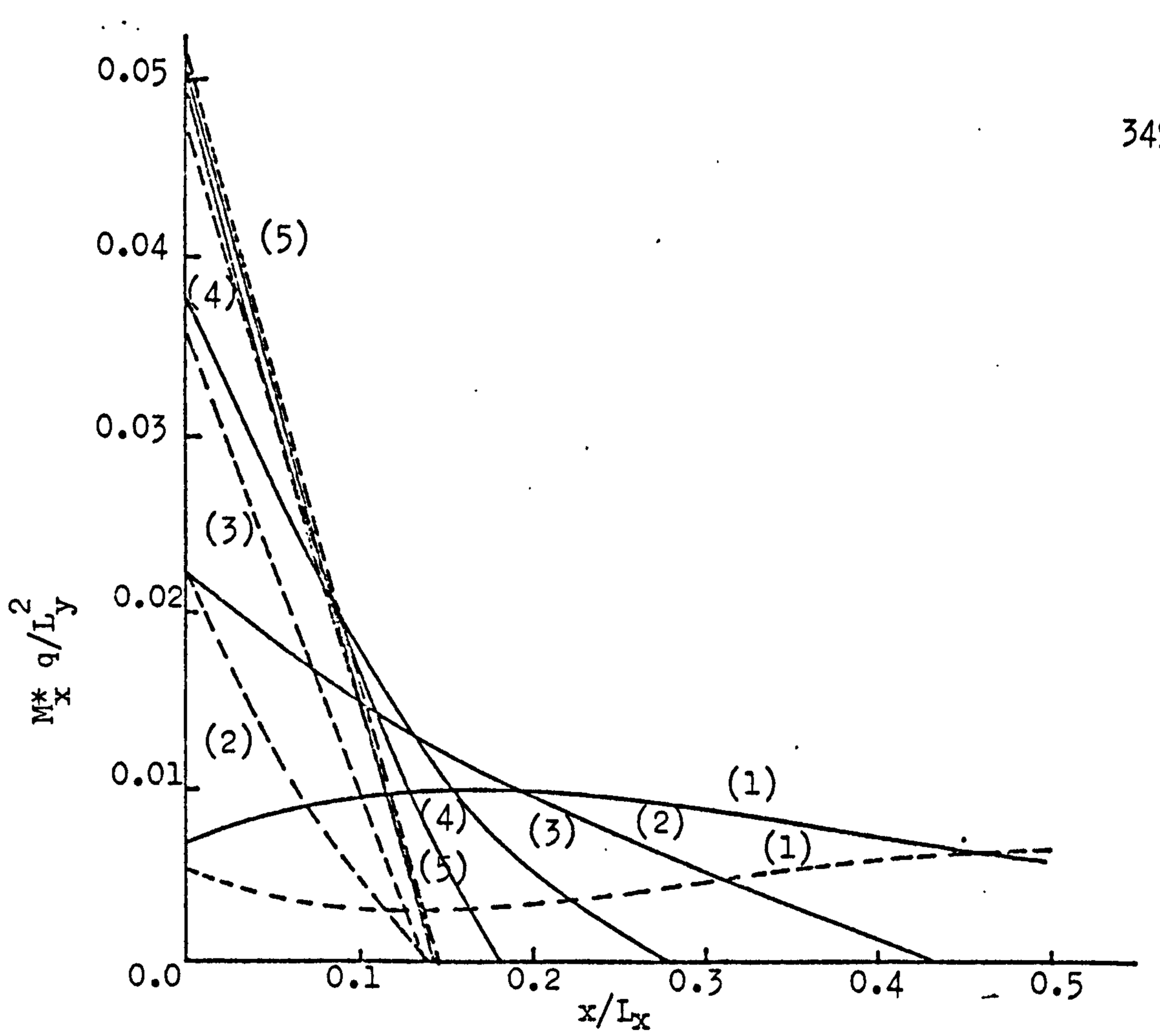

Figure (D11) Negative Moment M^*_x $(L_x/L_y = 1{\cdot}5)$

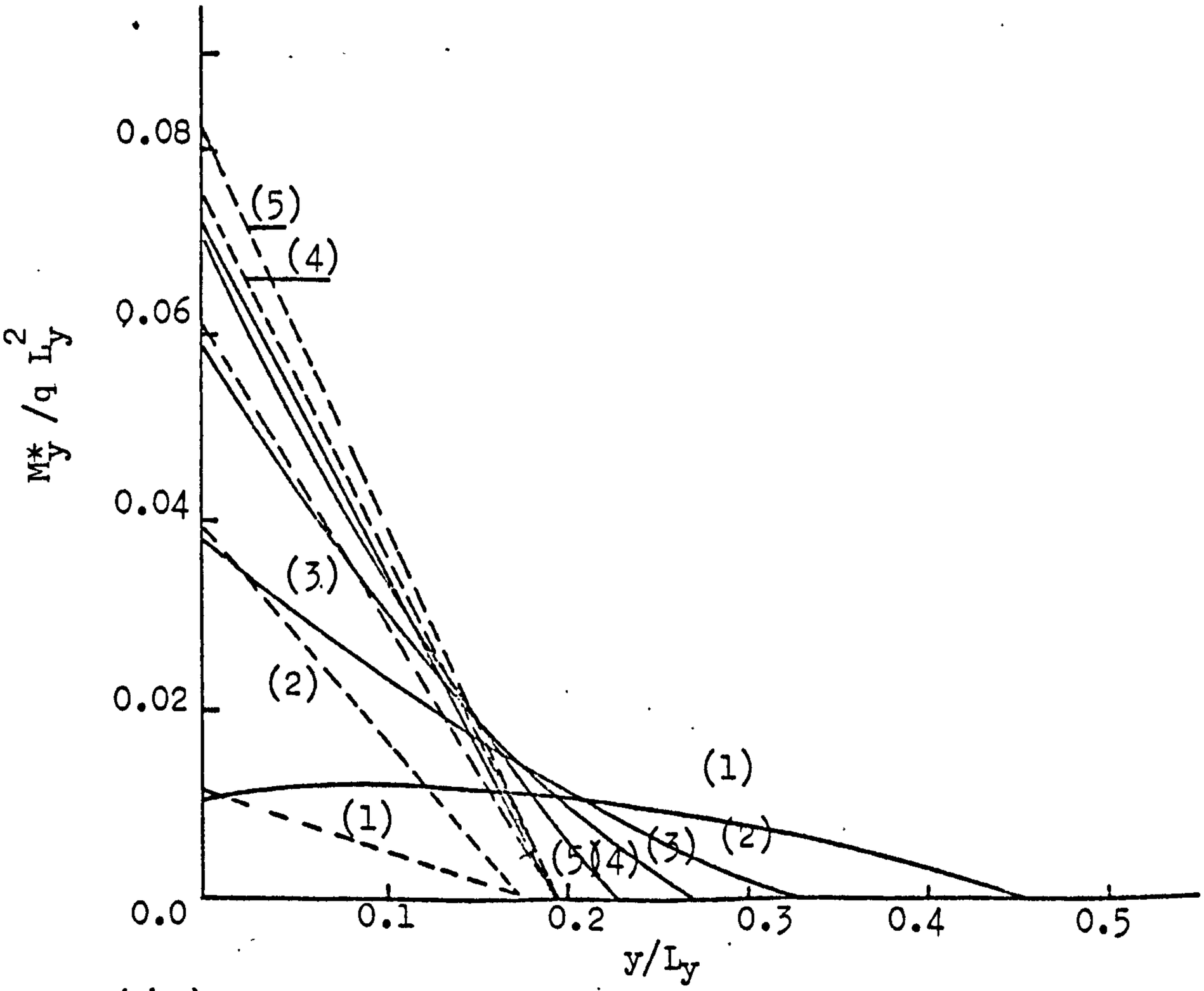

Figure (D12) Negative Moment M^*_y $(L_x/L_y = 1{\cdot}5)$

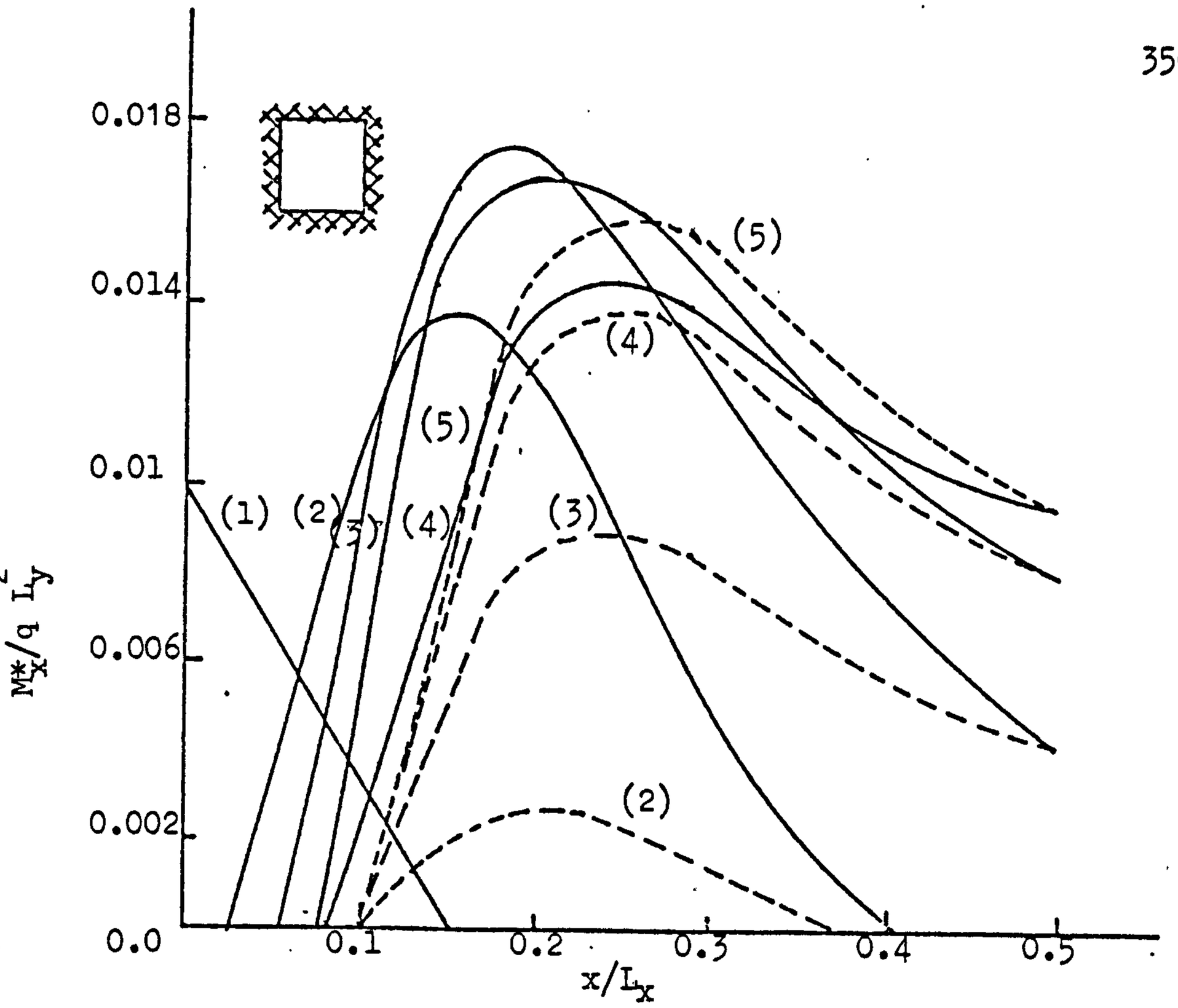

Figure (D13) Positive Moment M_x^* $(L_x/L_y = 2.0)$

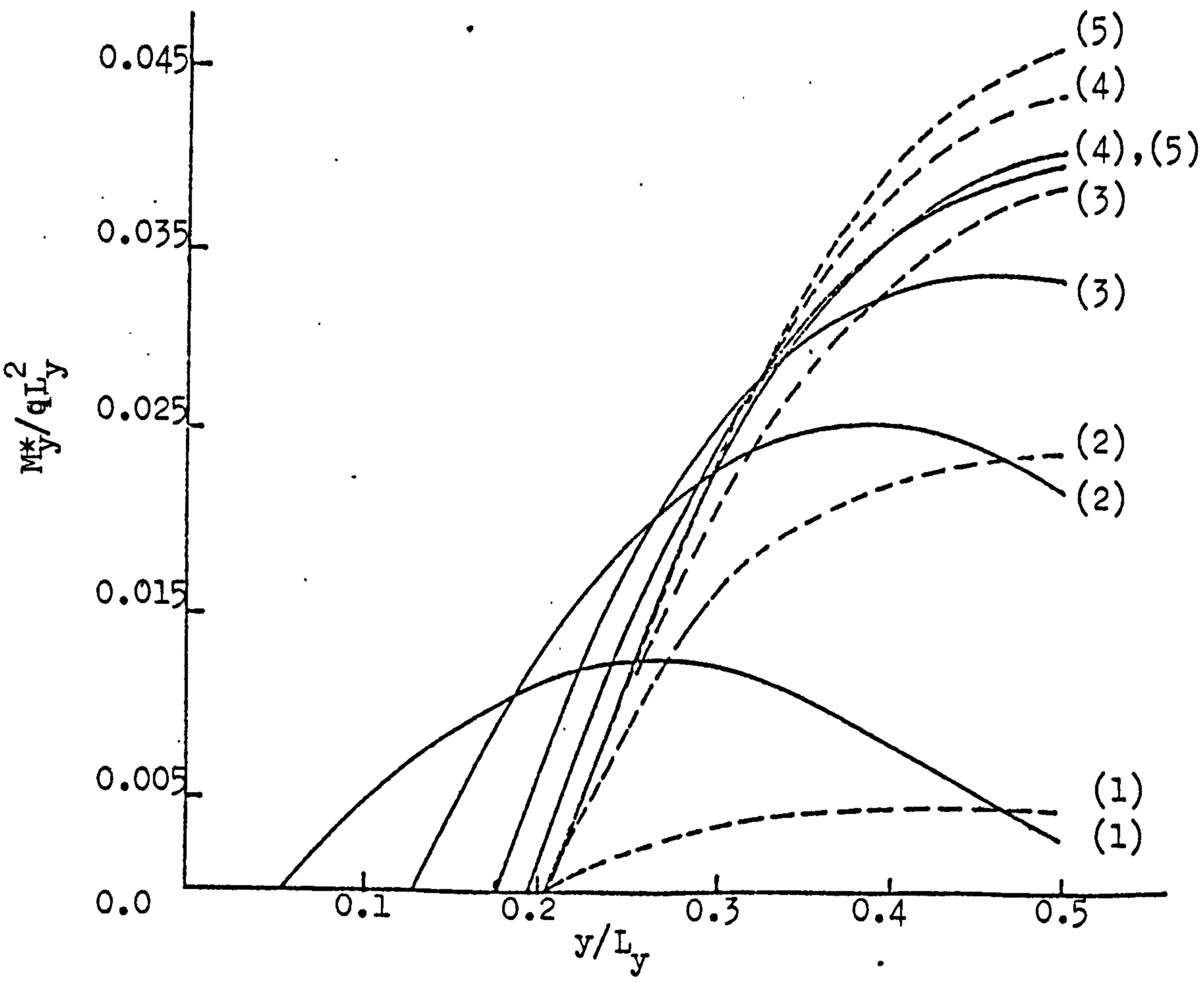

Figure (D14) Positive Moment M_y^* $(L_x/L_y = 2.0)$

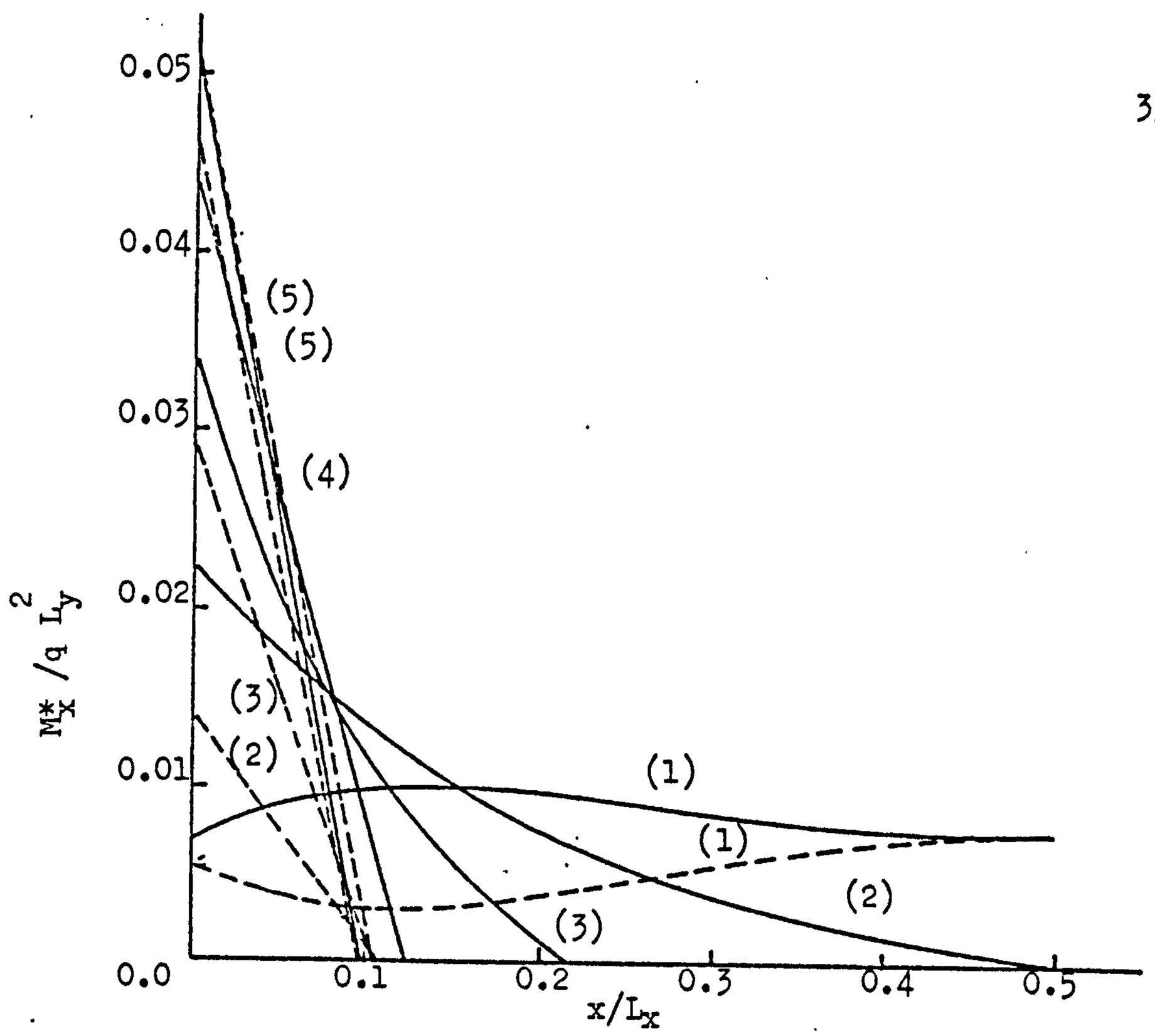

Figure (D15) Negative Moment M_x^* $(L_x/L_y = 2.0)$

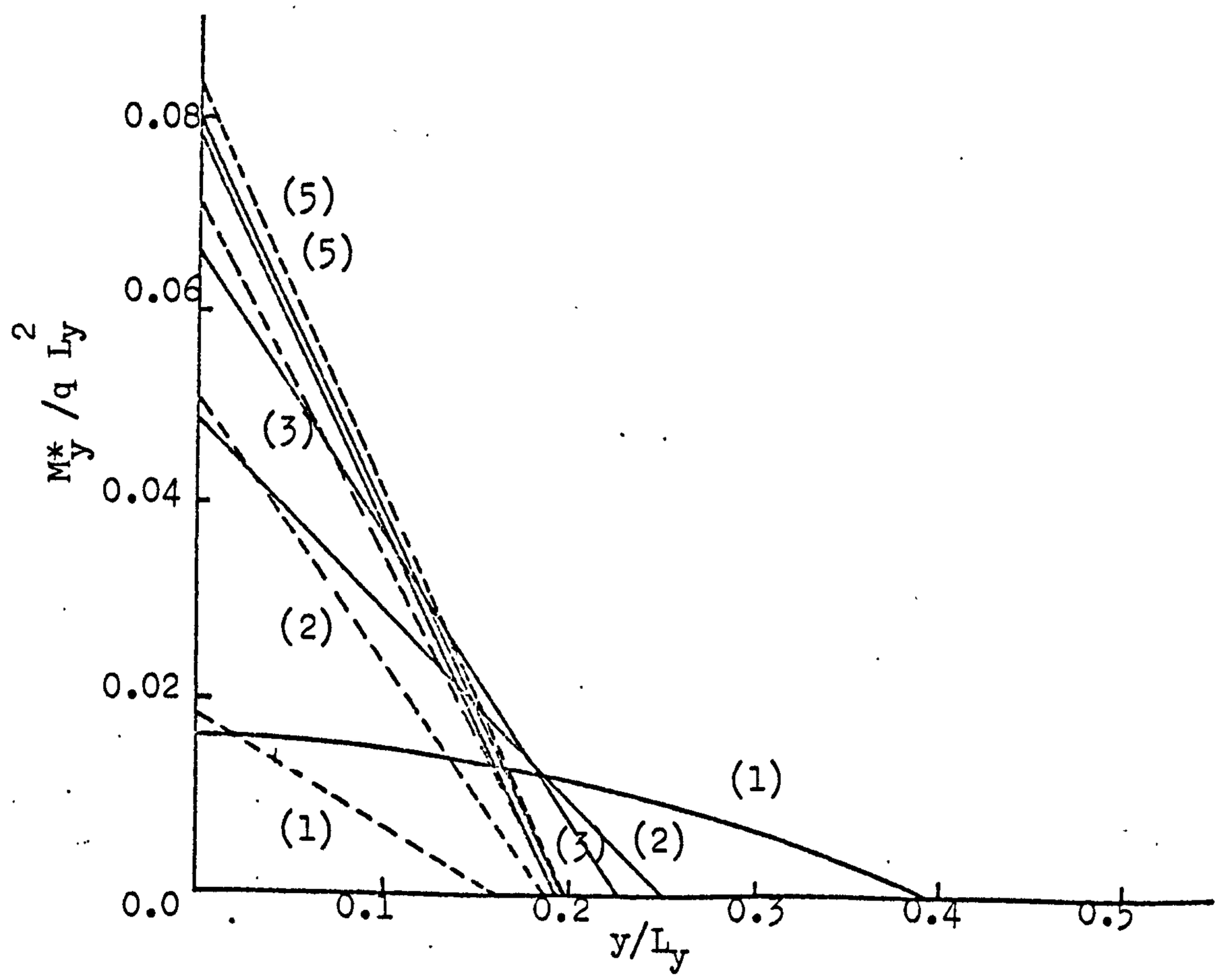

Figure (D16) Negative Moment M_x^* $(L_x/L_y = 2.0)$

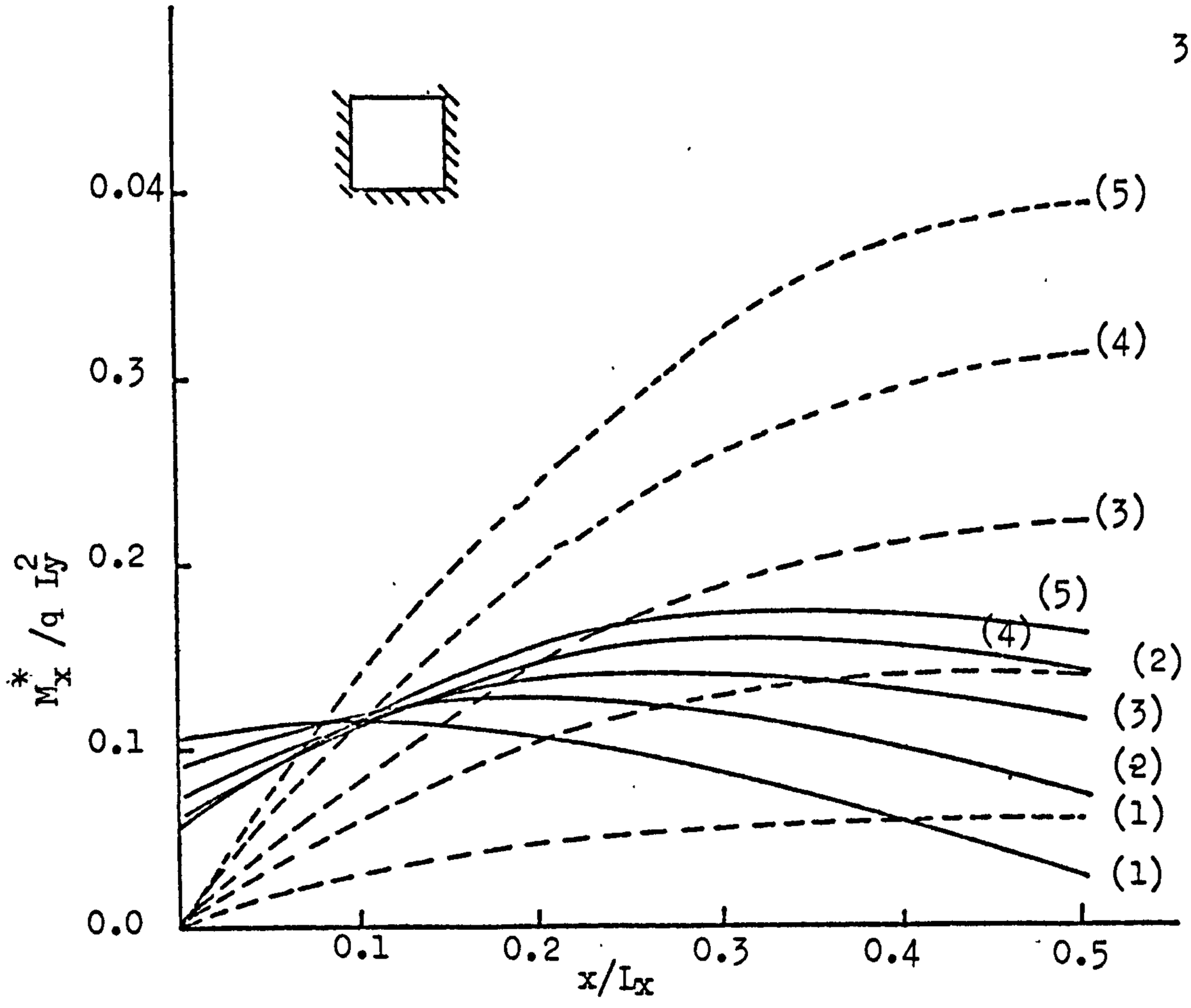

Figure (D17) Positive Moment M_x^* $(L_x/L_y = 1.5)$

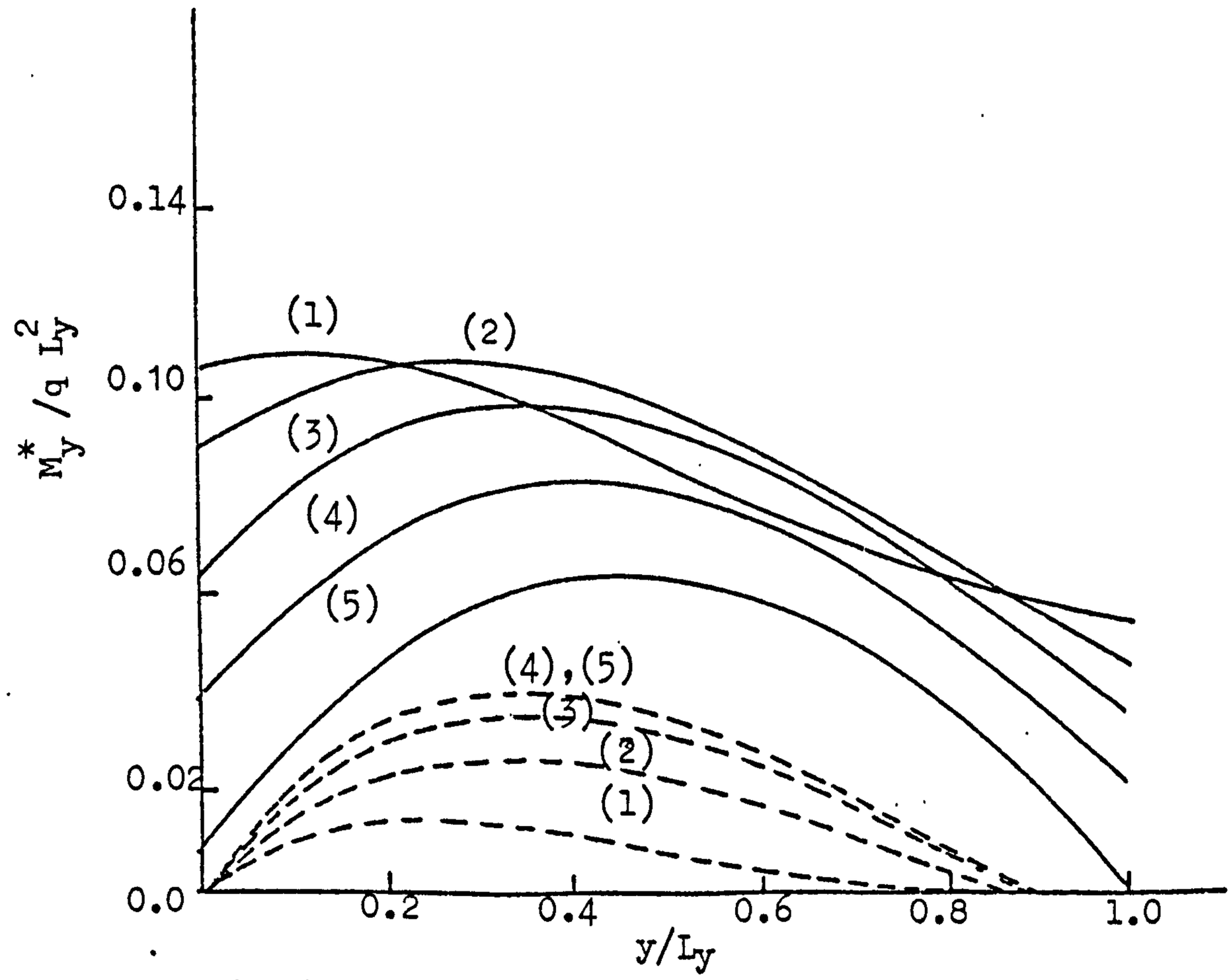

Figure (D18) Positive Moment M_y^* $(L_x/L_y = 1.5)$

DAMAGED PAGE(S)

P 353

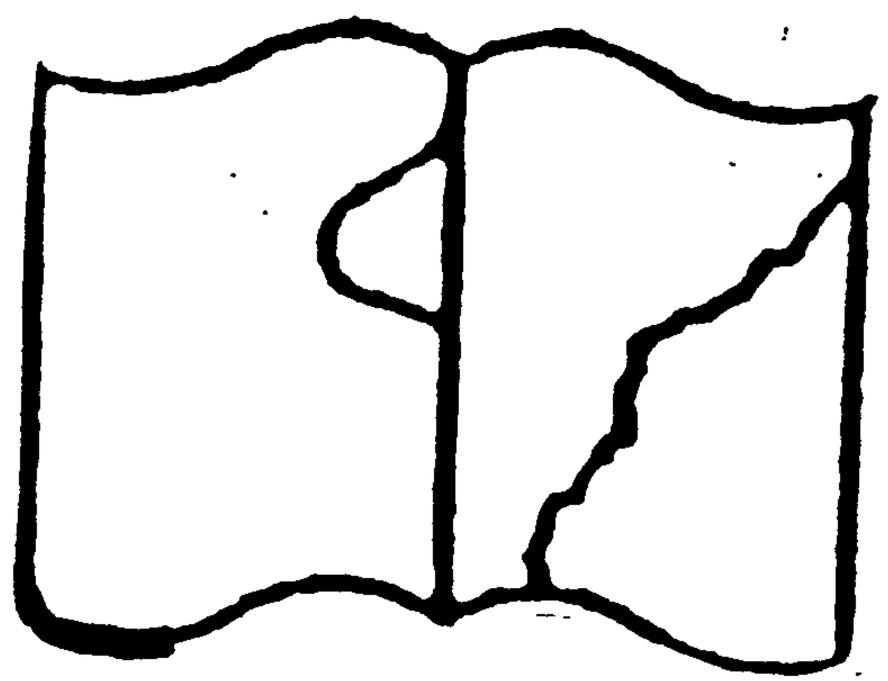

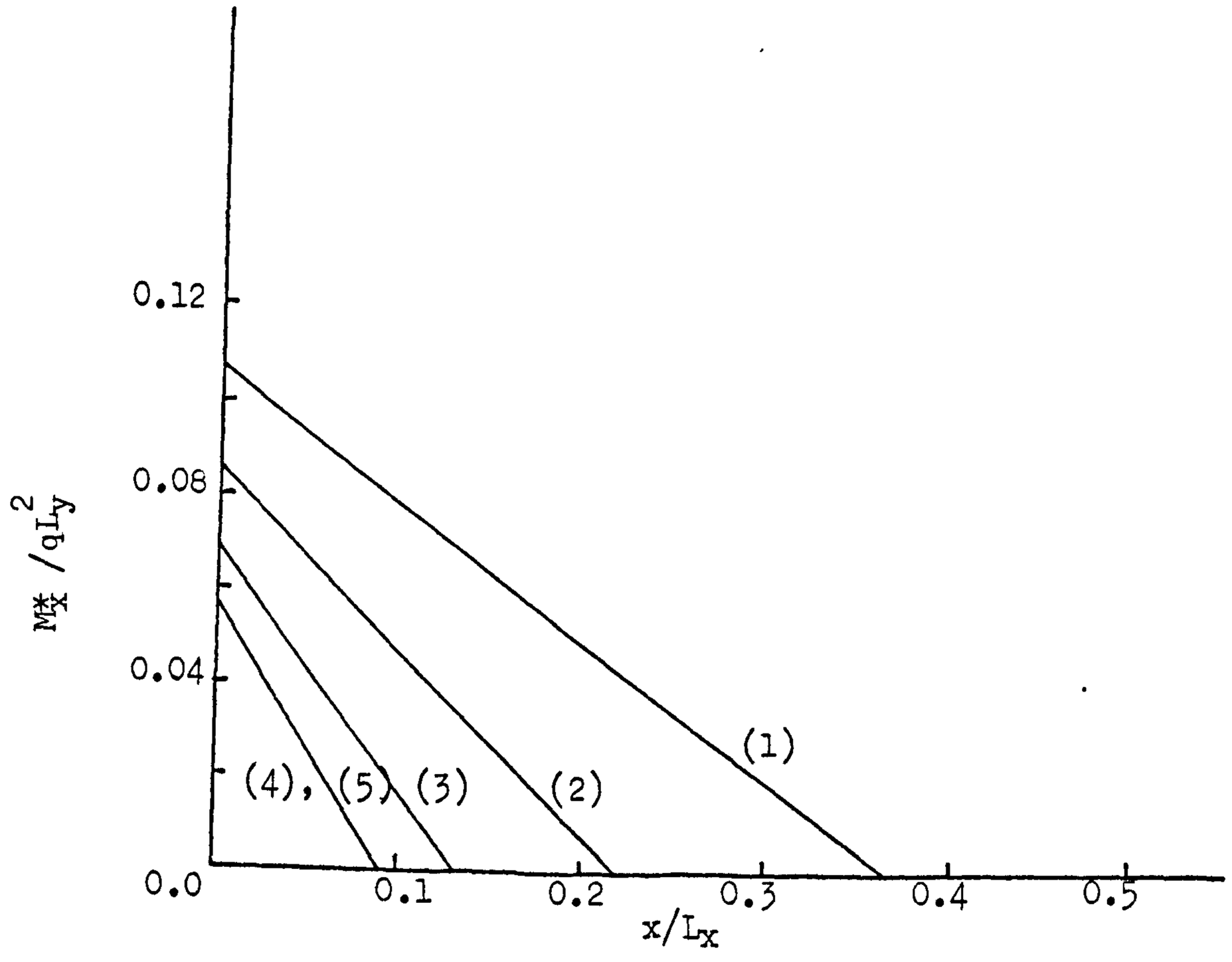

Figure (D19) Negative Moment M_x^* (L_x/L_y = 1.5)

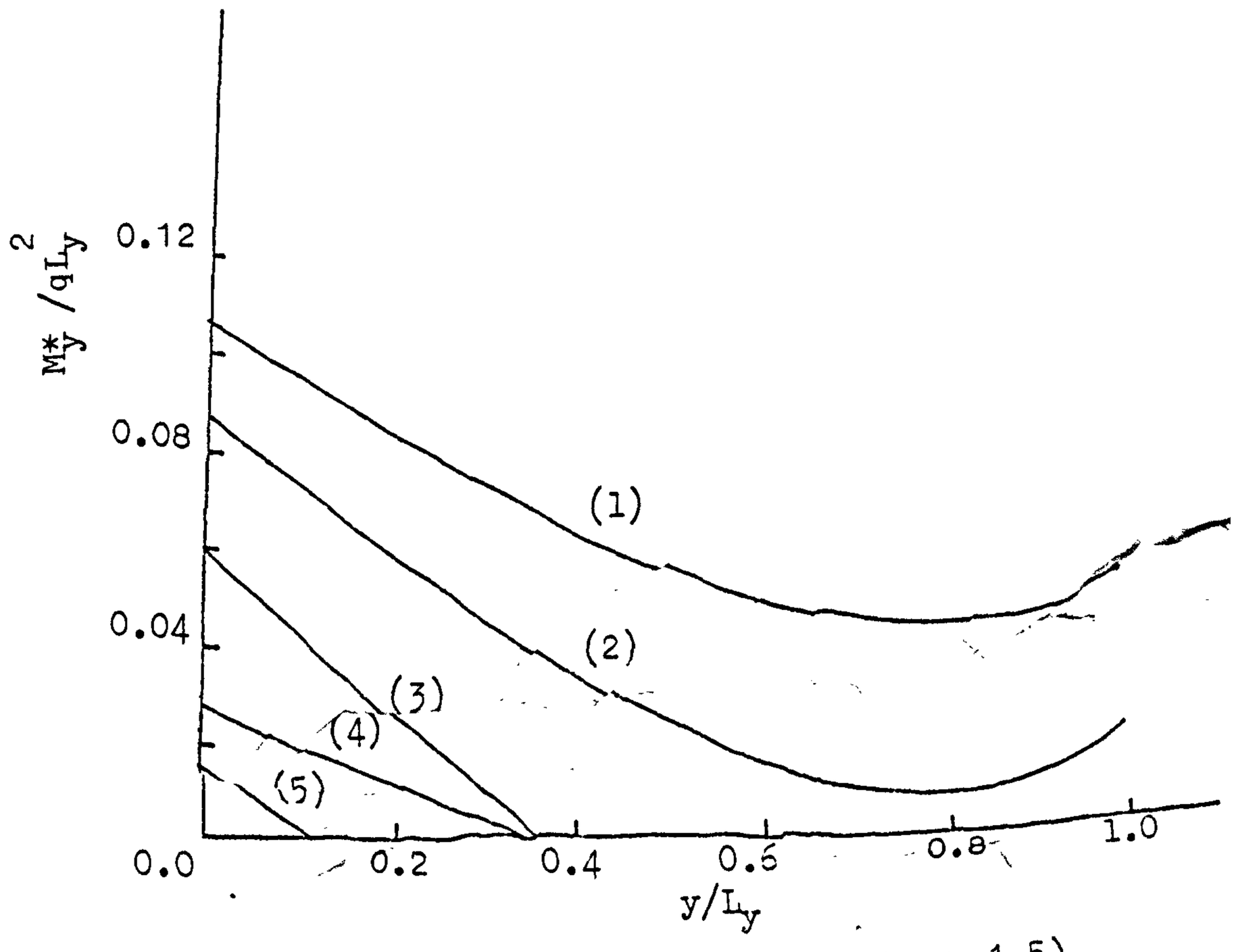

Figure (D20) Negative Moment M_x^* (L_x/L_y = 1.5)

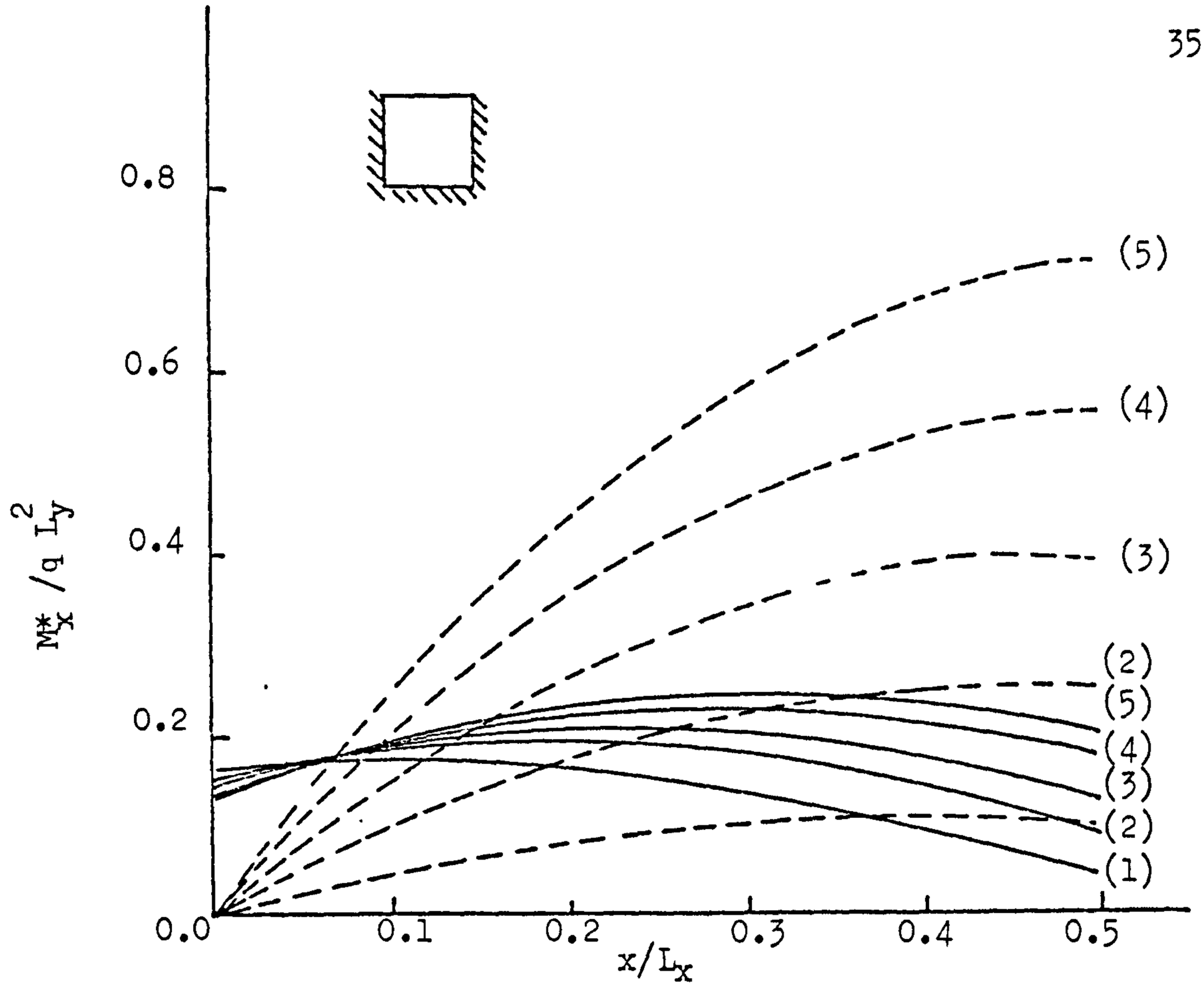

Figure (D21) Positive Moment M_x^* $(L_x/L_y = 2.0)$

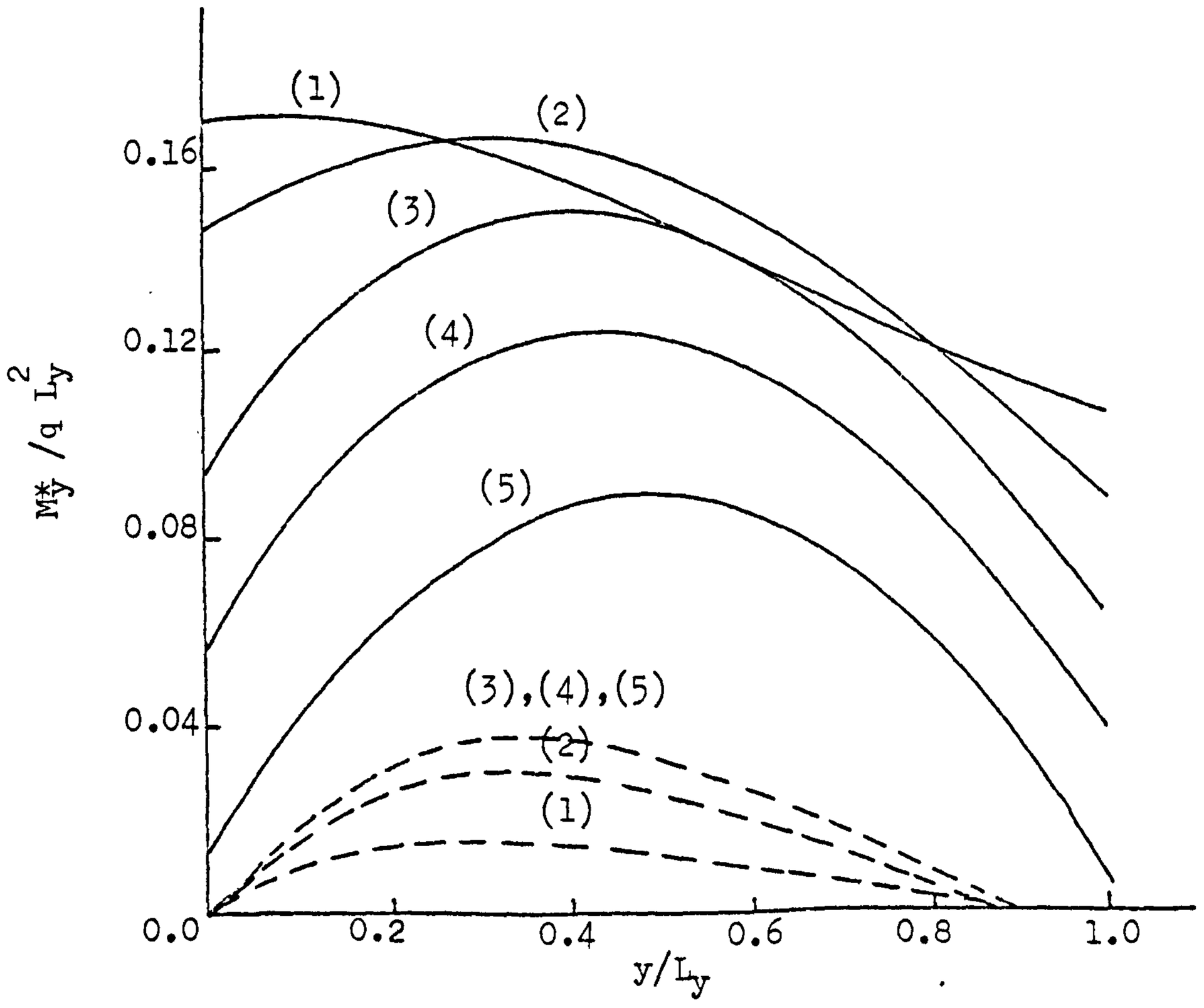

Figure (D22) Positive Moment M_y^* $(L_x/L_y = 2.0)$

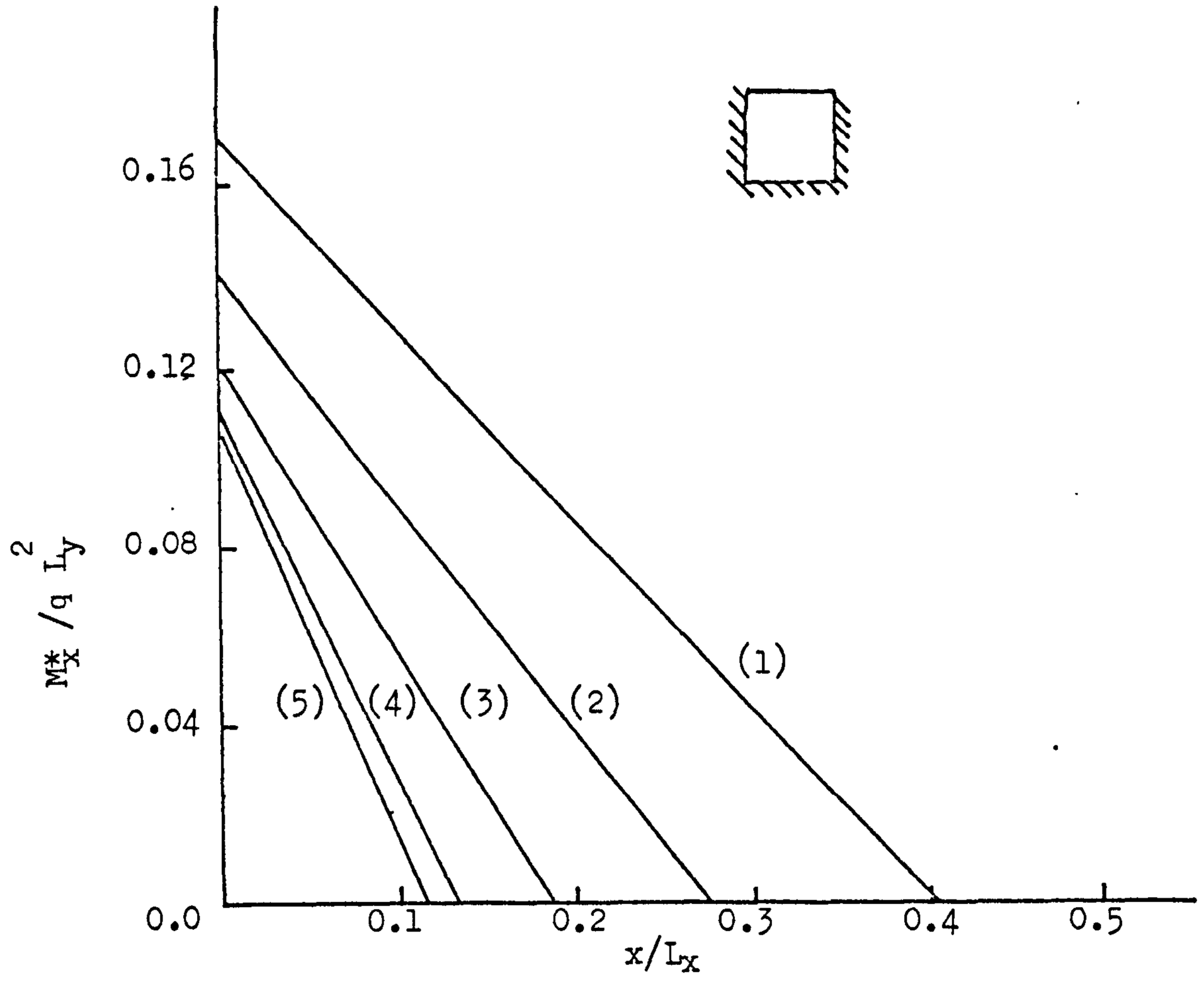

Figure (D23) Negative Moment M_x^* (L_x/L_y = 2.0)

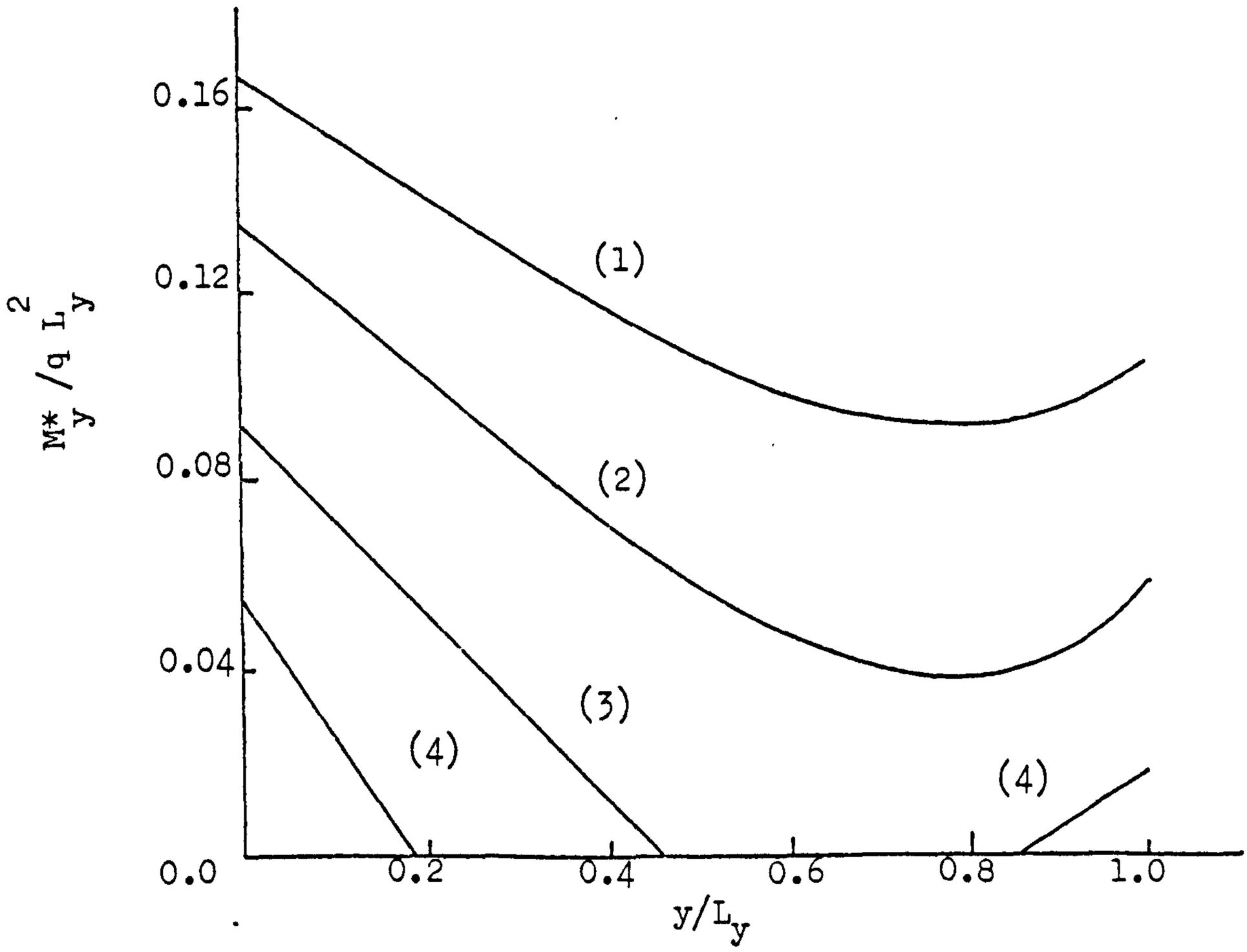

Figure (D24) Negative Moment M_y^* (L_x/L_y = 2.0)

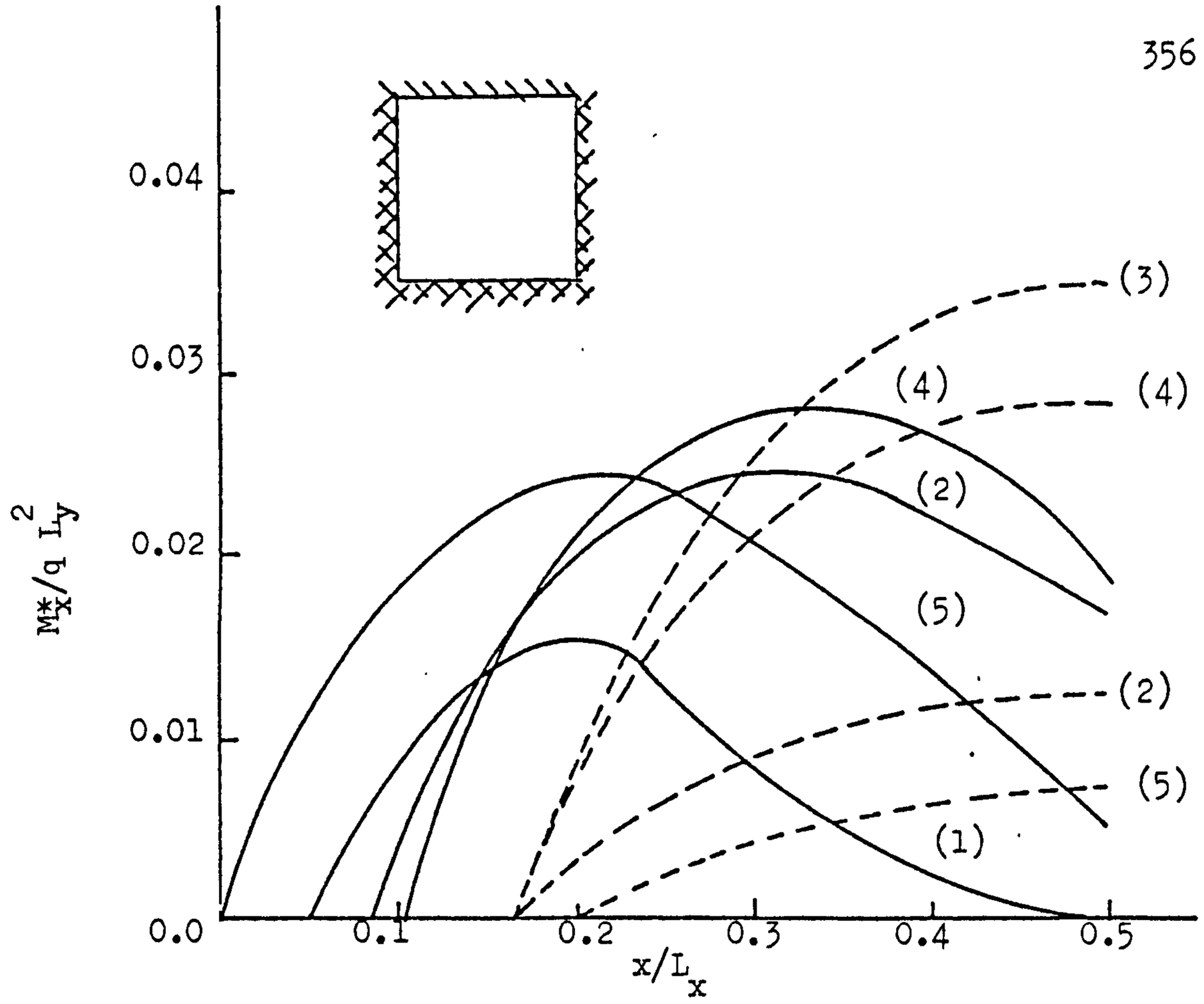

Figure (D25) Positive Moment M^*_x $(L_x/L_y = 1.5)$

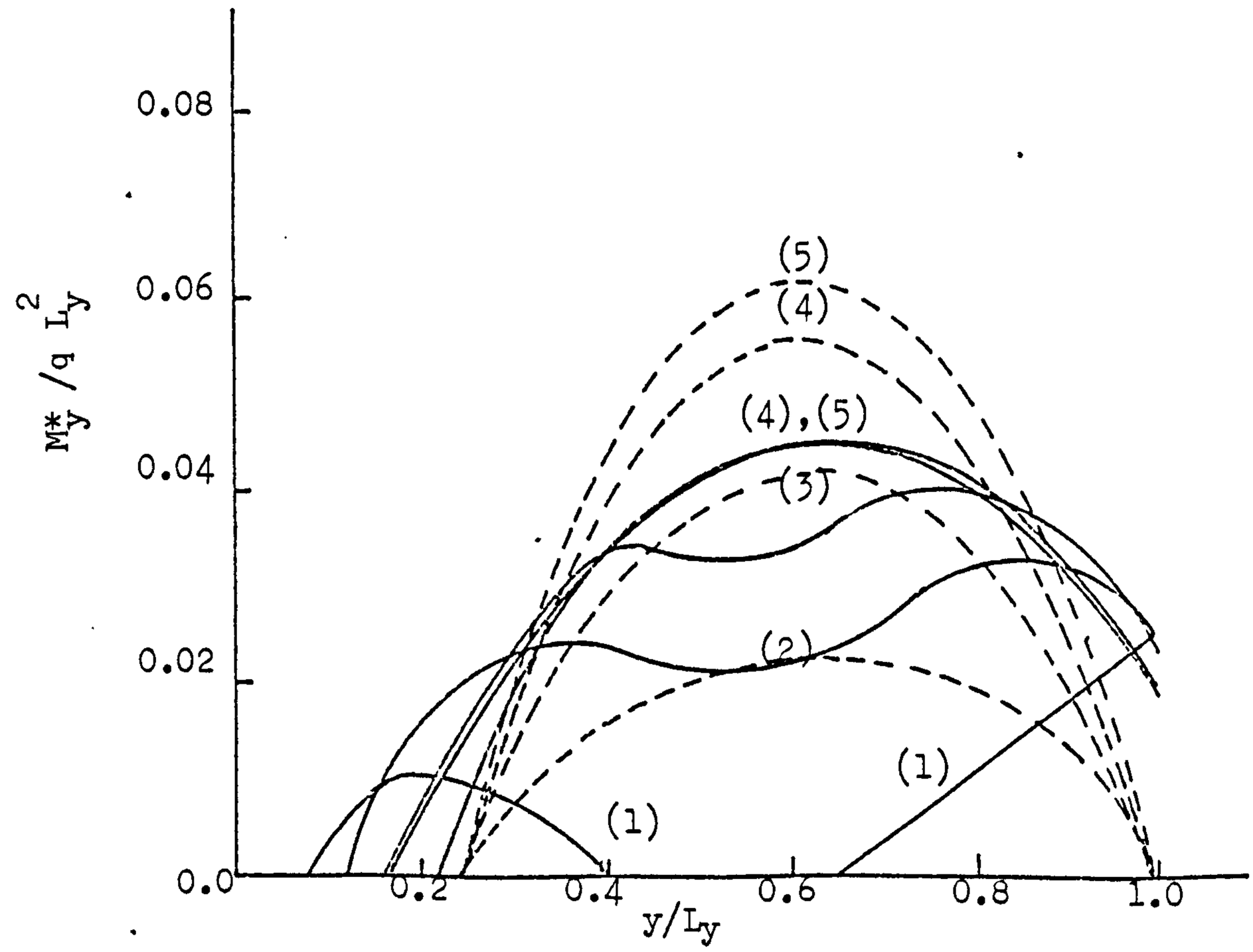

Figure (D26) Positive Moment M^*_y $(L_x/L_y = 1.5)$

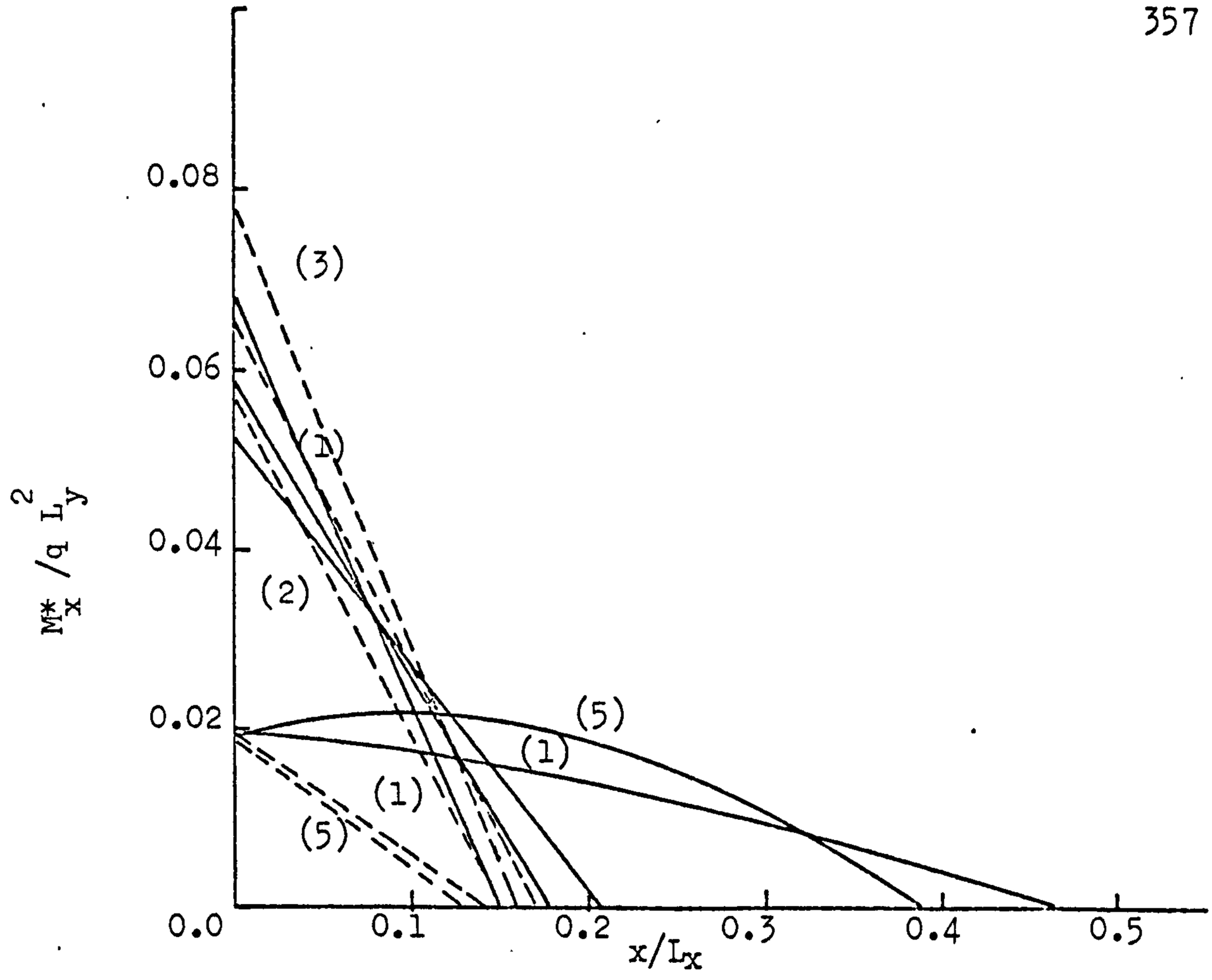

Figure (D27) Negative Moment M^*_x (L_x/L_y = 1.5)

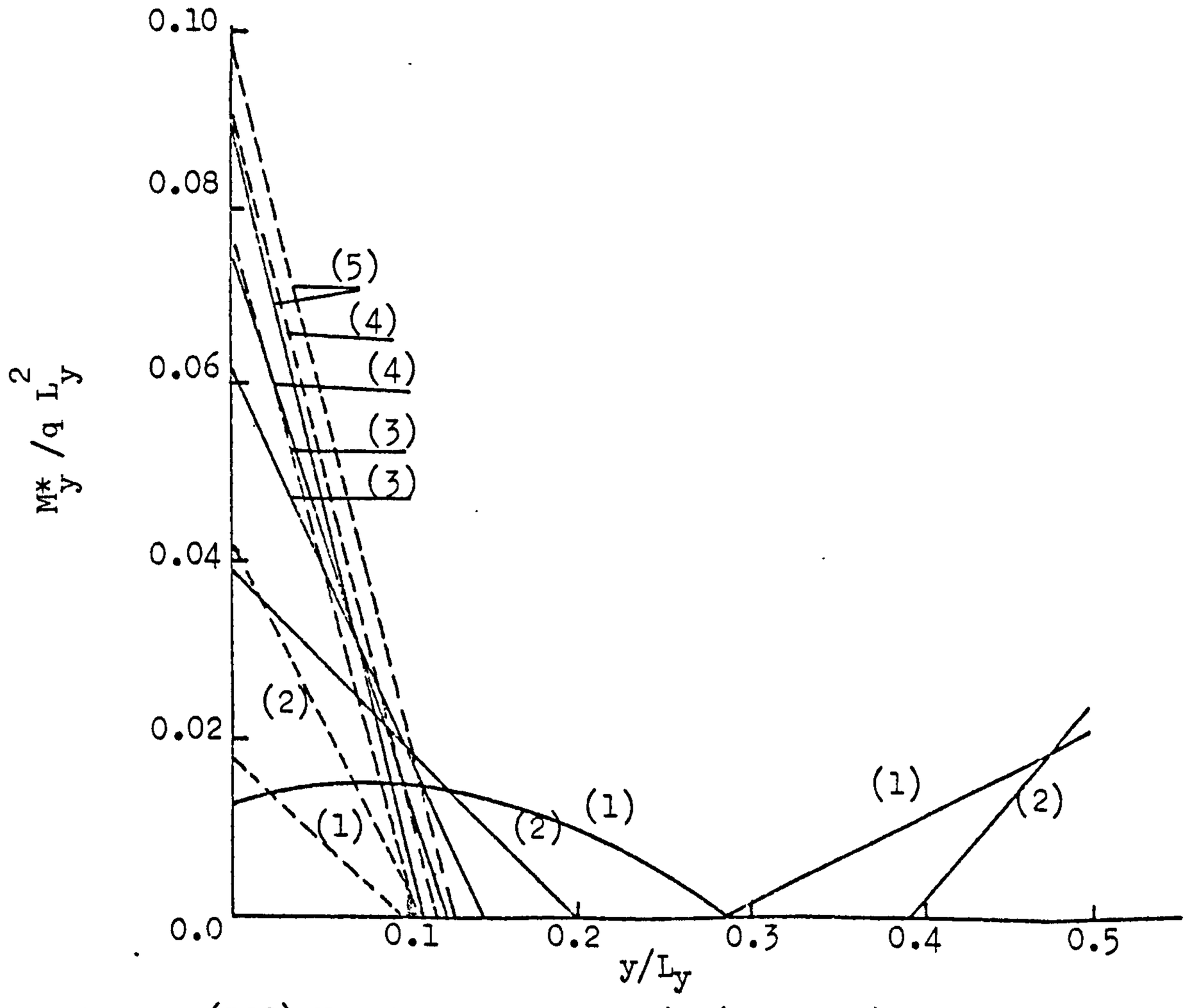

Figure (D28) Negative Moment M^*_y (L_x/L_y = 1.5)

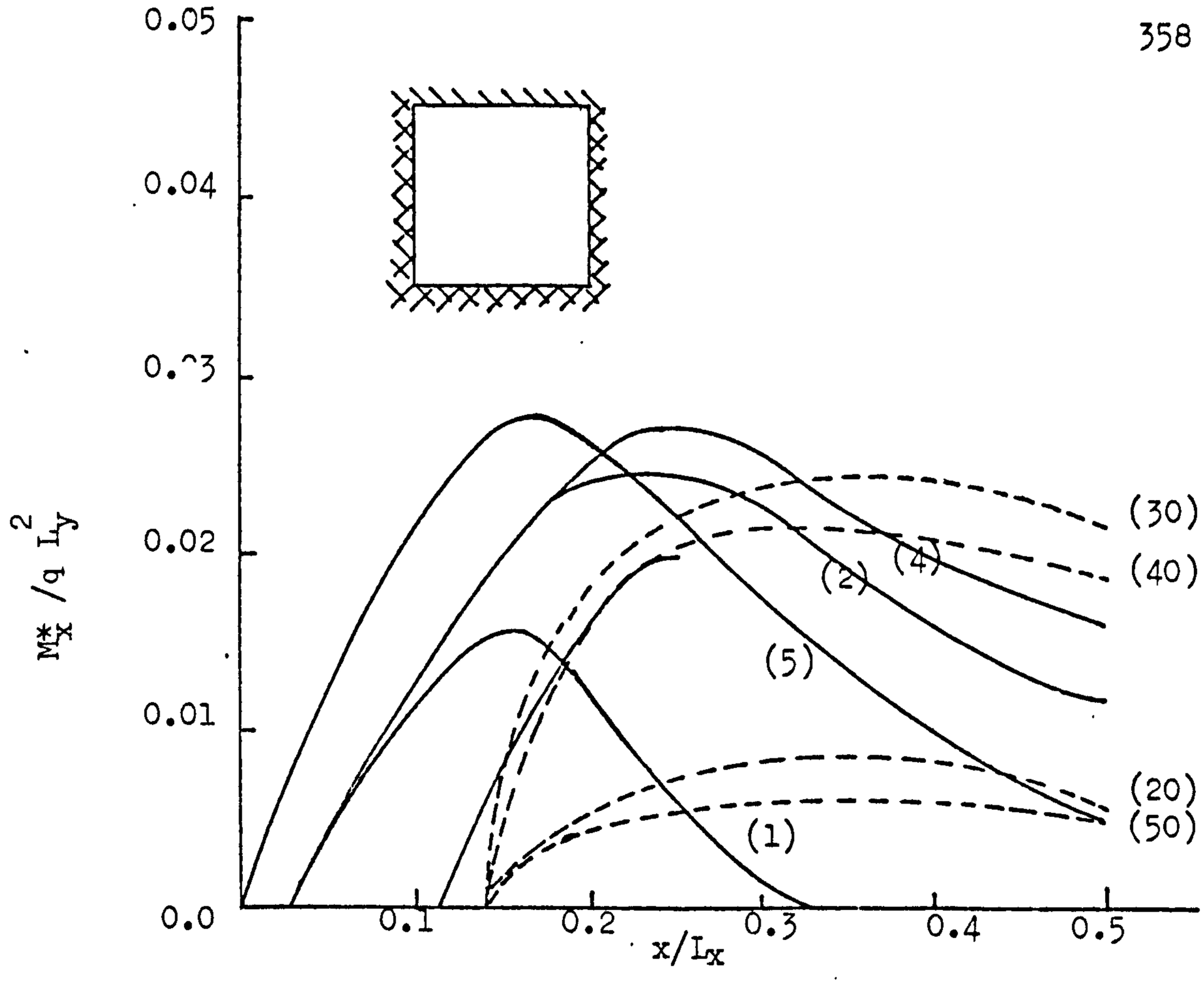

Figure (D29) Positive Moment M^*_x (L_x/L_y = 2.0)

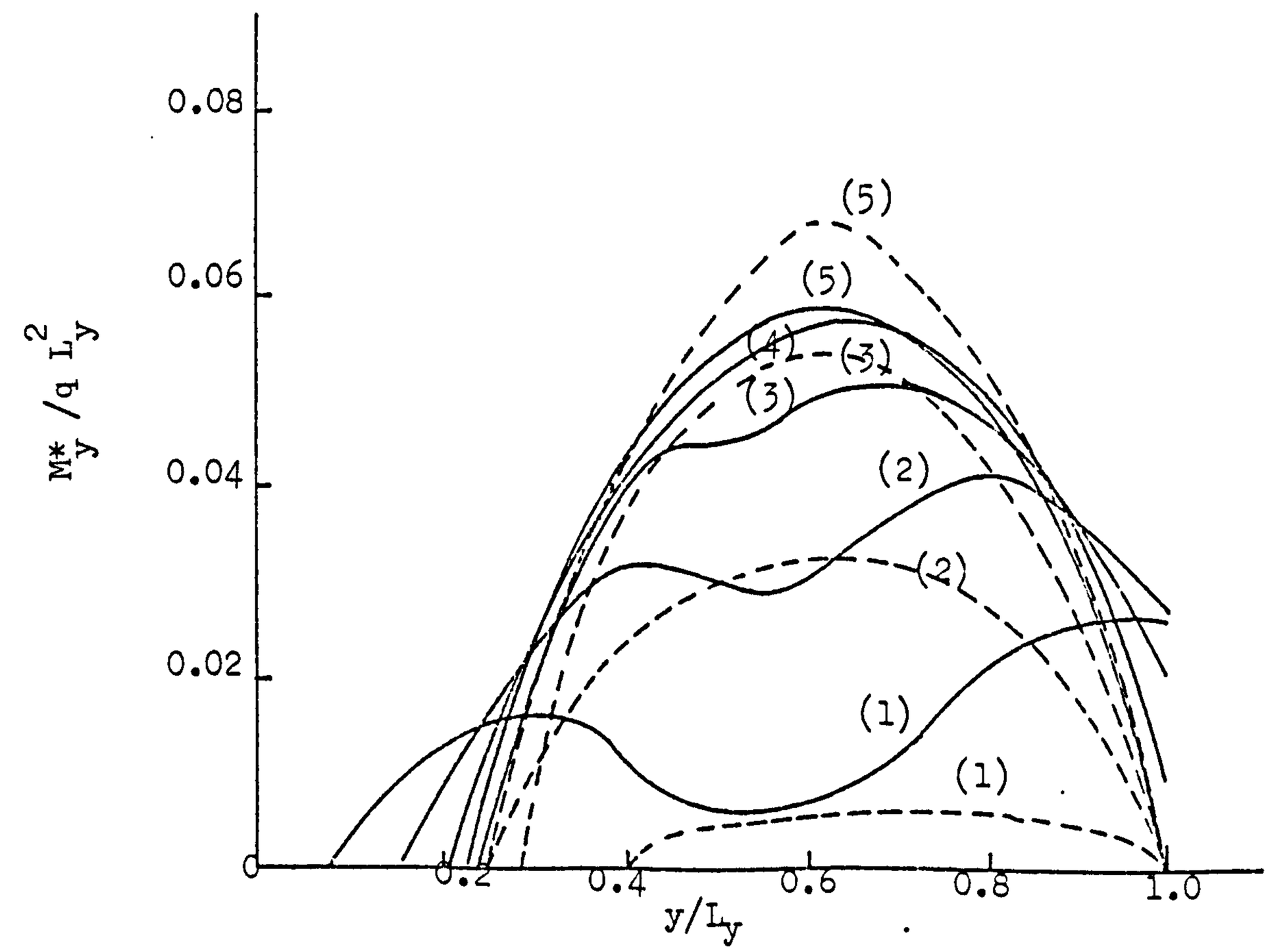

Figure (D30) Positive Moment M^*_y (L_x/L_y = 2.0)

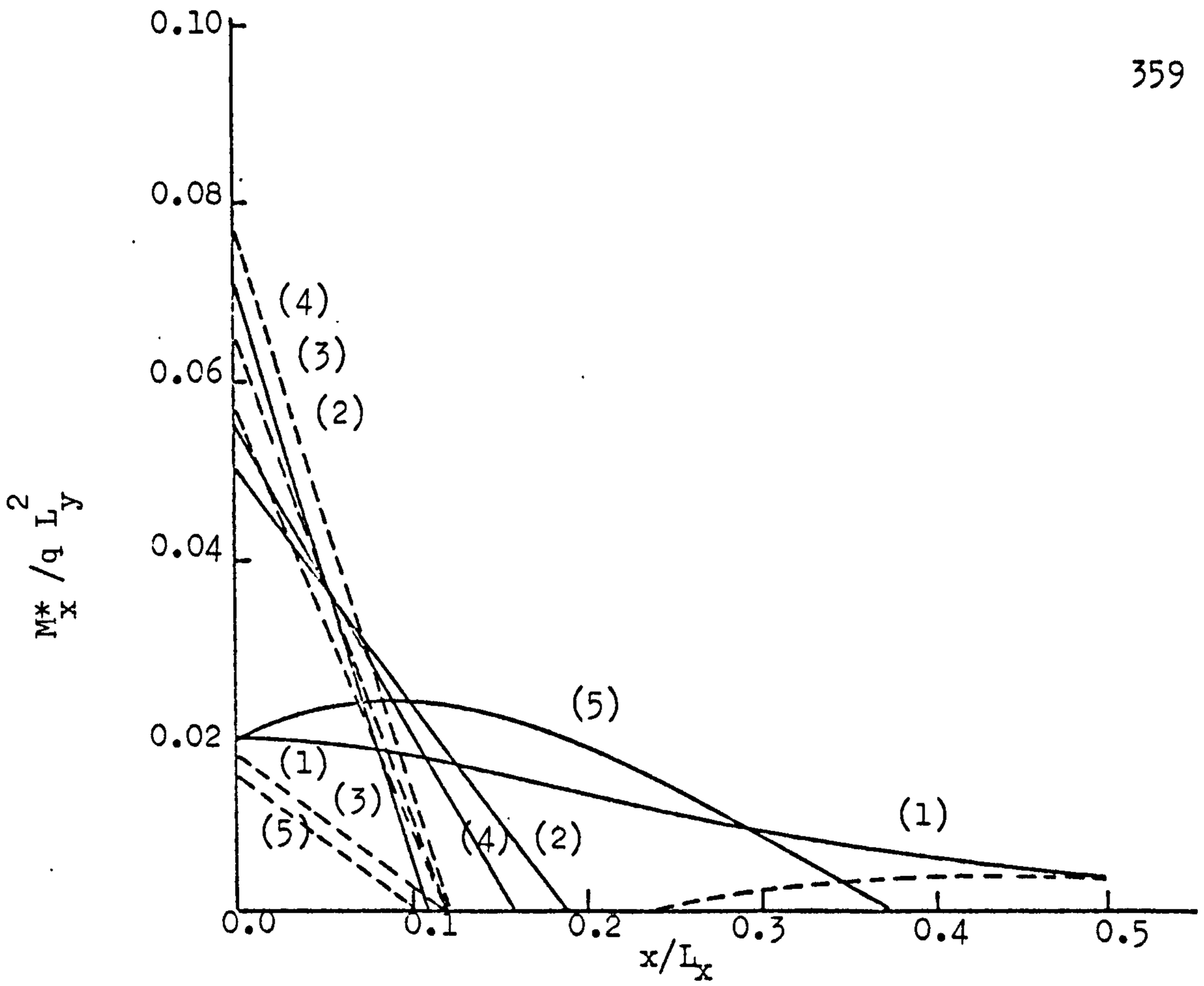

Figure (D31) Negative Moment M^*_x $(L_x/L_y = 2.0)$

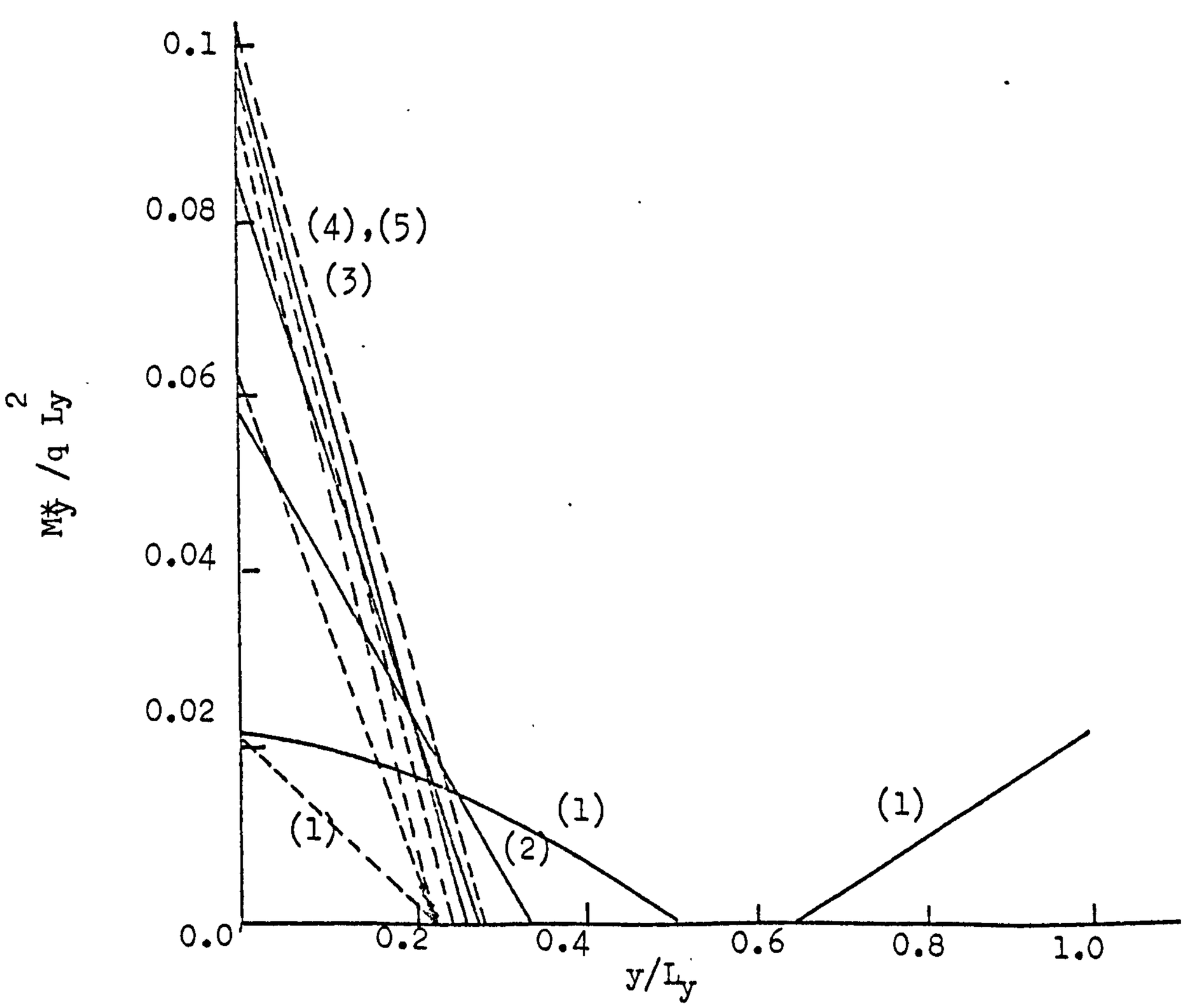

Figure (D32) Negative Moment M^*_y $(L_x/L_y = 2.0)$

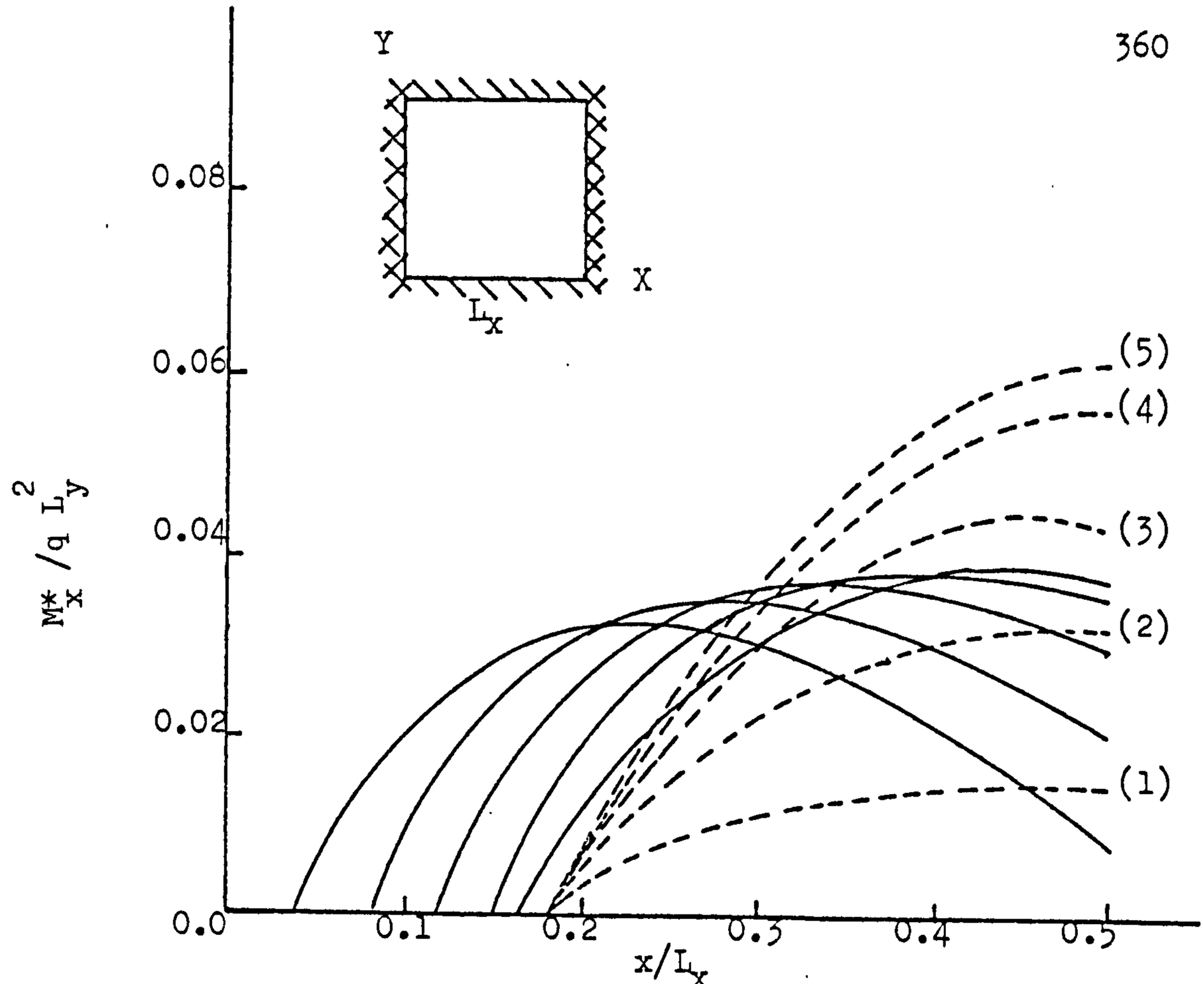

Figure (D33) Positive Moment M^*_x (L_x/L_y = 1.5)

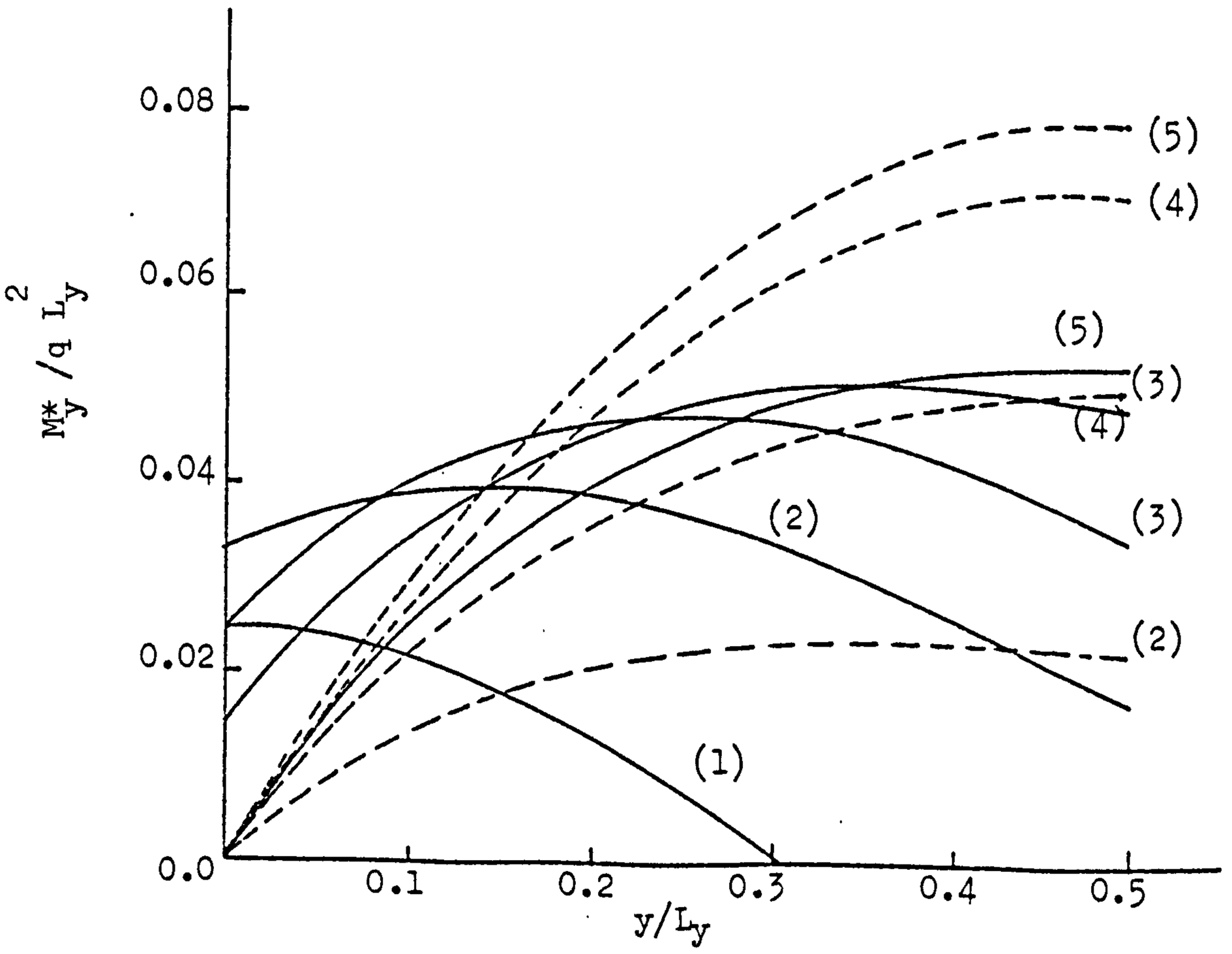

Figure (D34) Positive Moment M^*_y (L_x/L_y = 1.5)

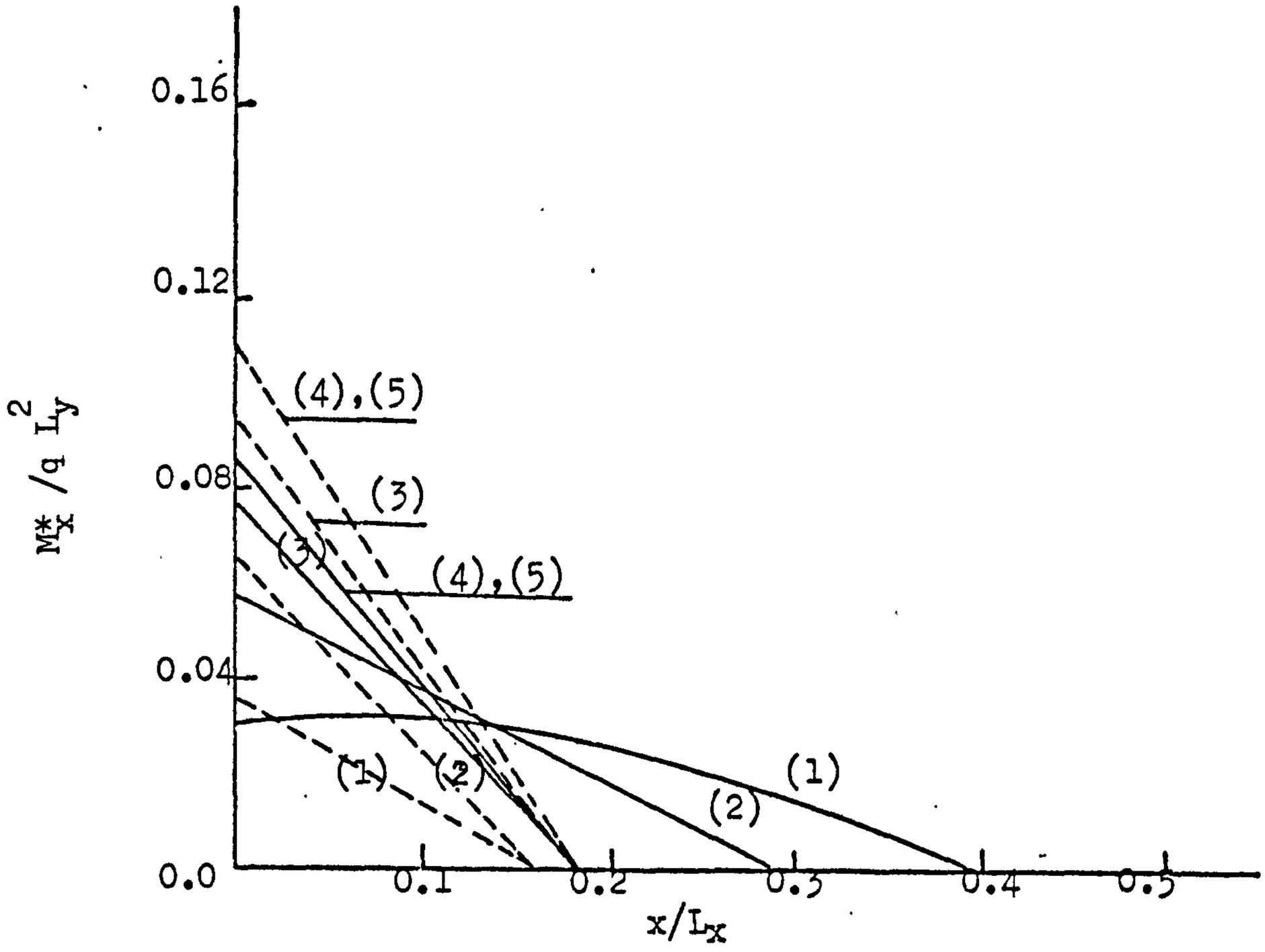

Figure (D35) Negative Moment M^*_x $(L_x/L_y = 1.5)$

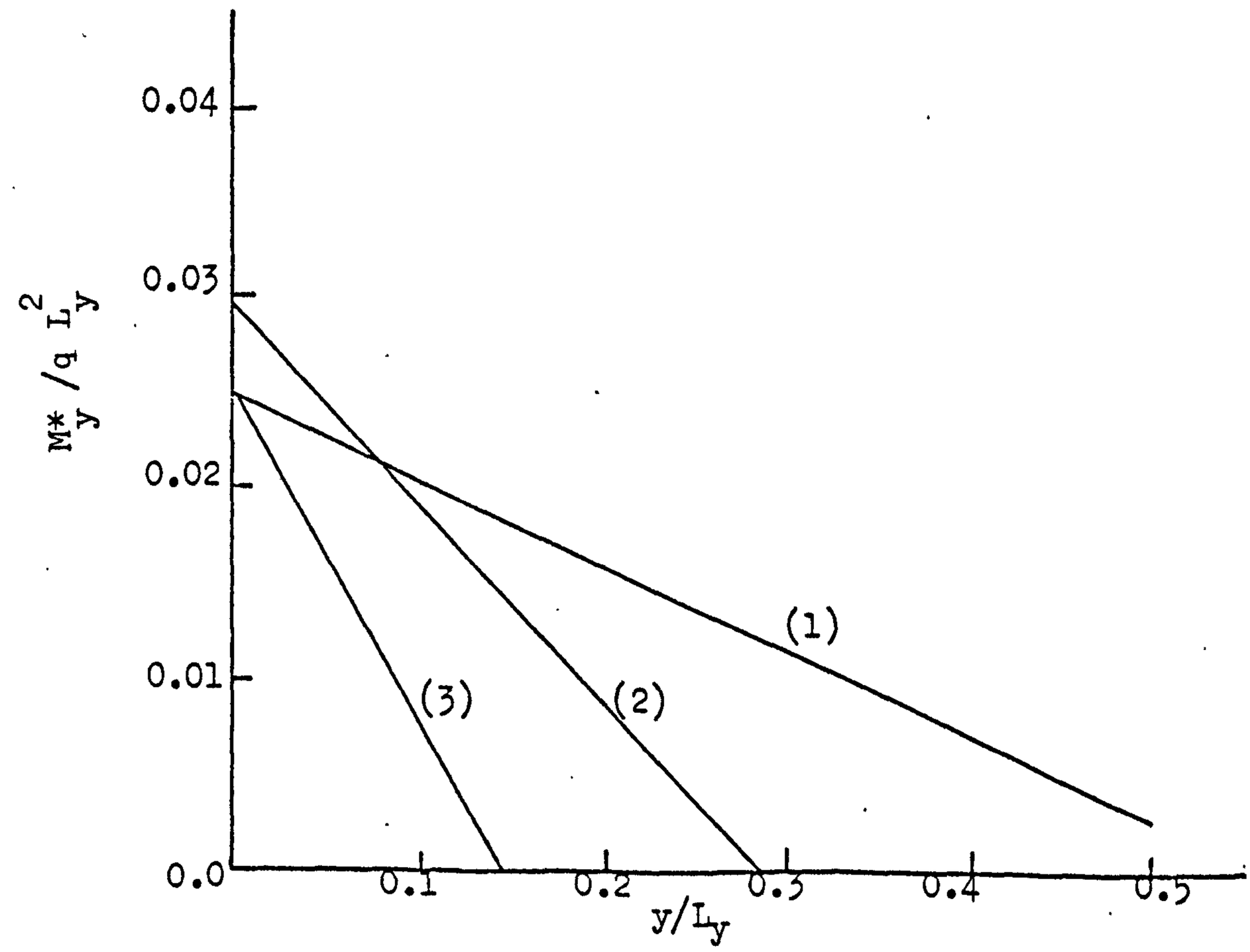

Figure (D36) Negative Moment M^*_y $(L_x/L_y = 1.5)$

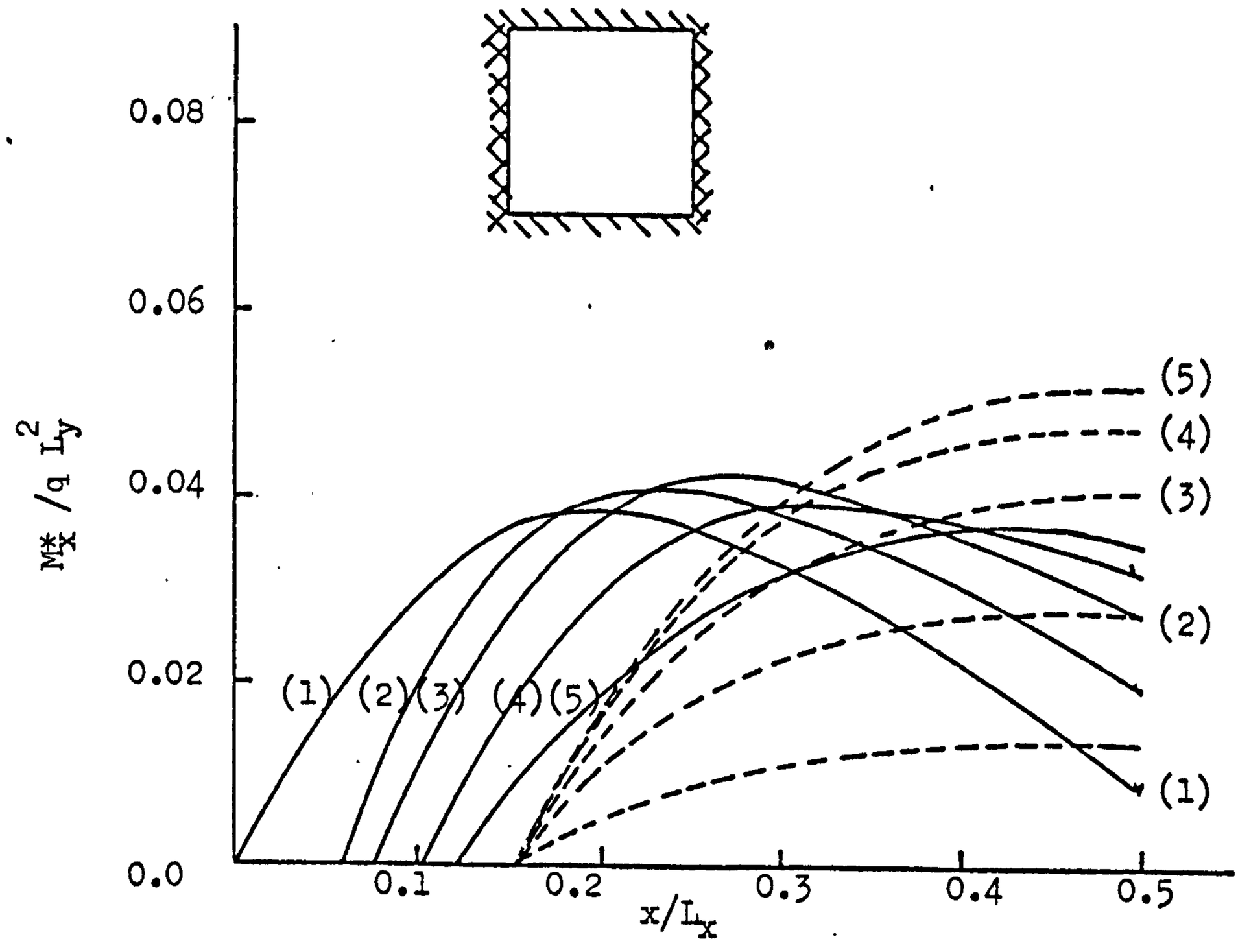

Figure (D37) Positive Moment M_x^* (L_x/L_y= 2.0)

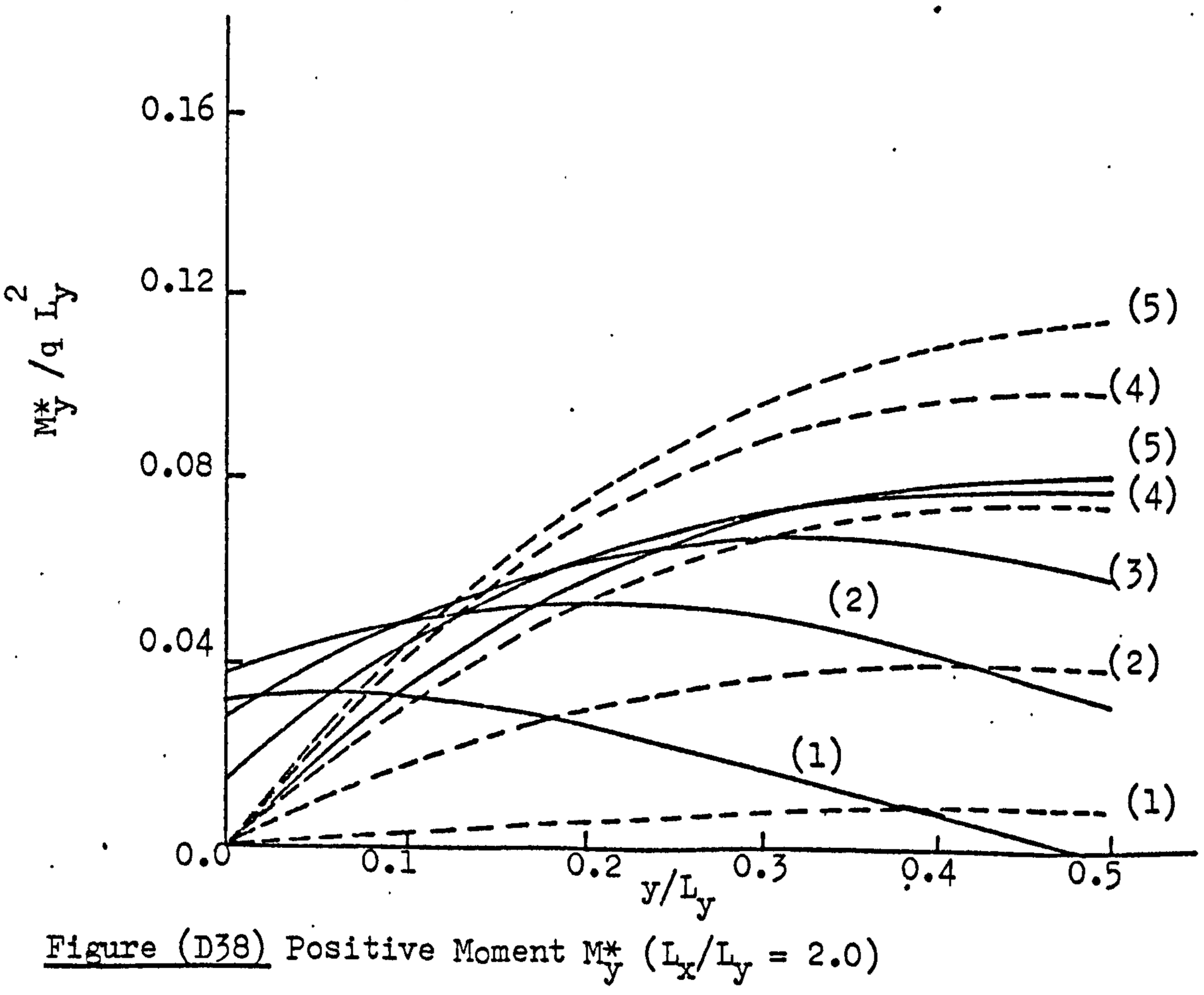

Figure (D38) Positive Moment M_y^* (L_x/L_y = 2.0)

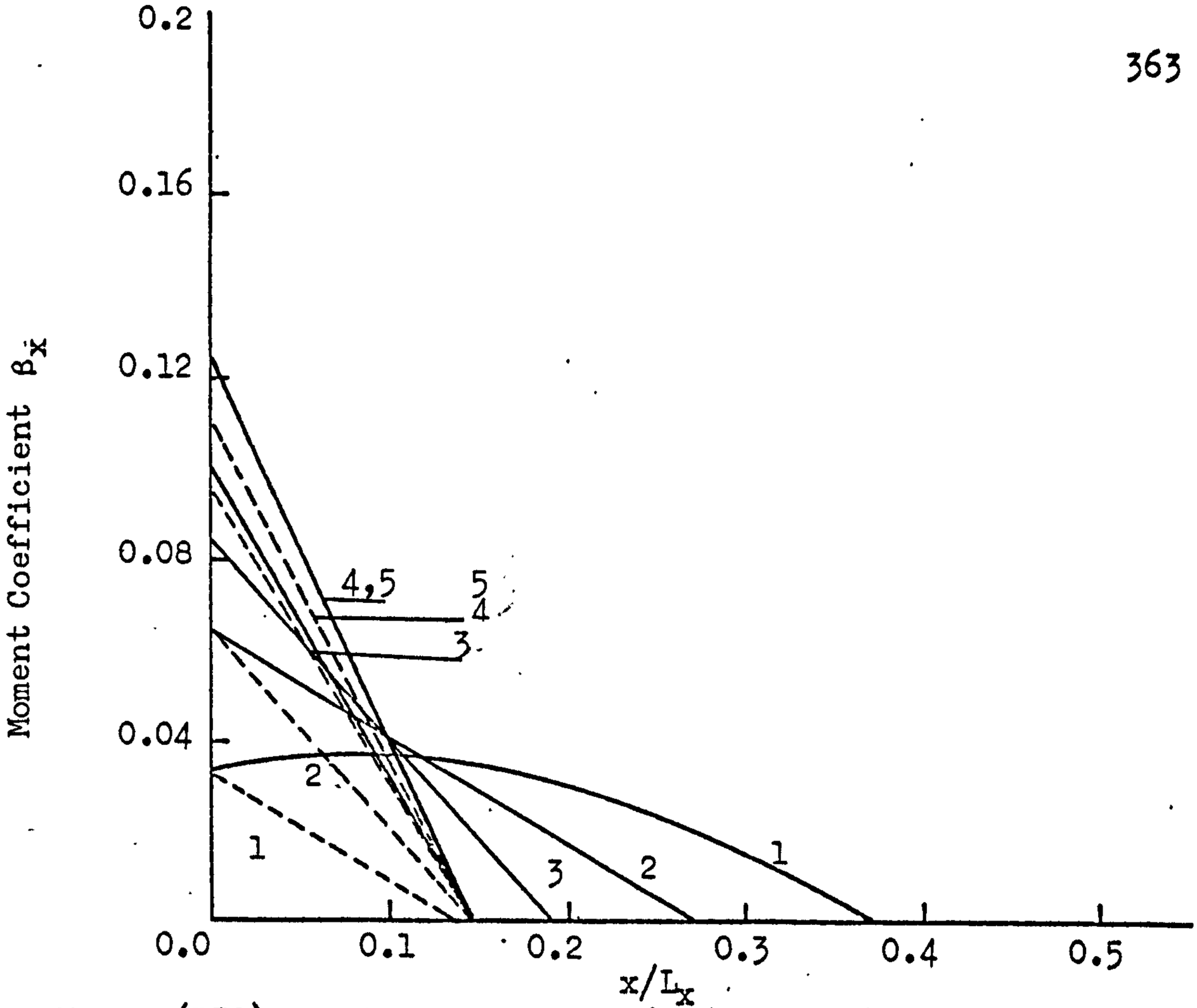

Figure (D39) Negative Moment M_x^* $(L_x/L_y = 2.0)$

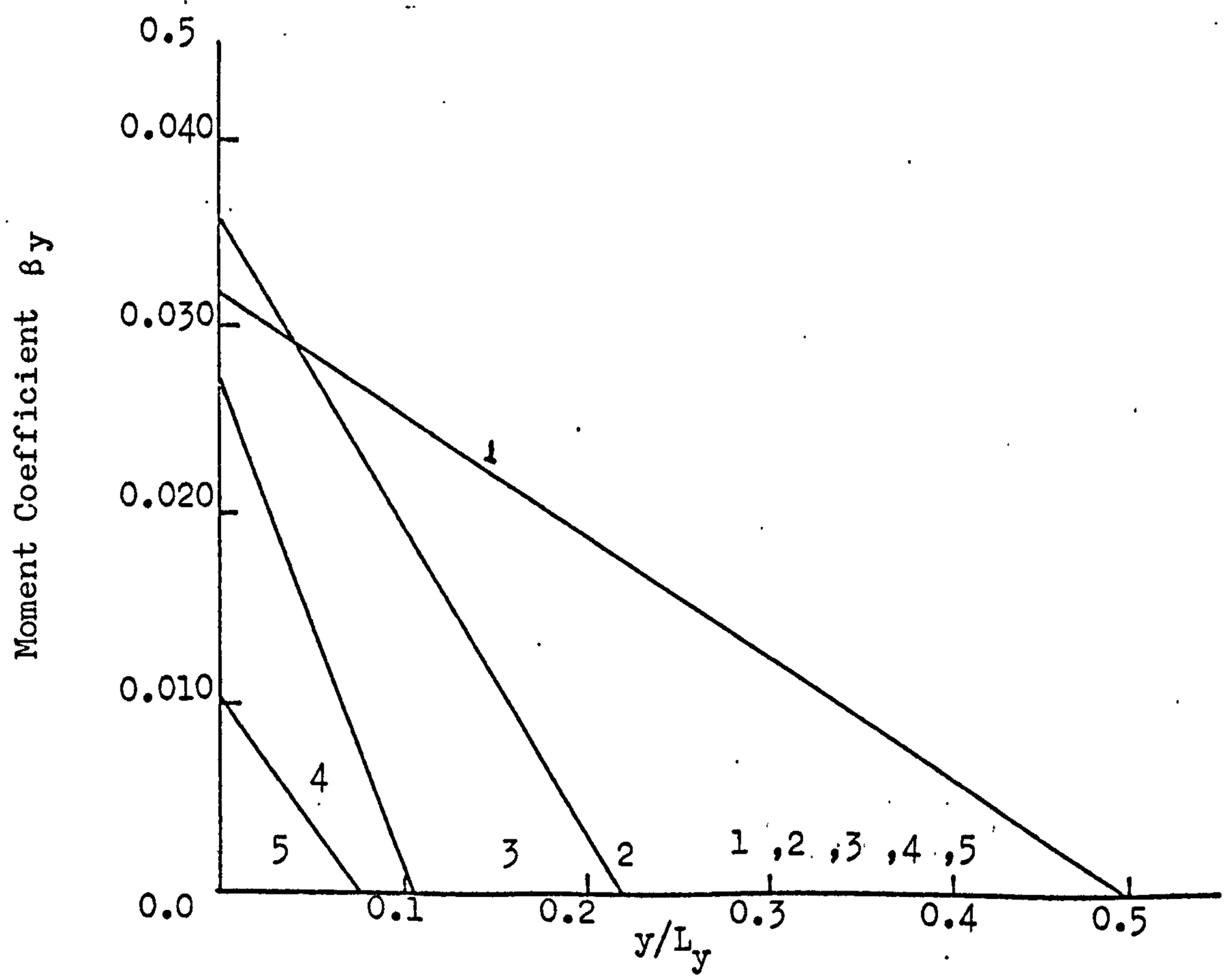

Figure (D40) Negative Moment M_y^* $(L_x/L_y = 2.0)$

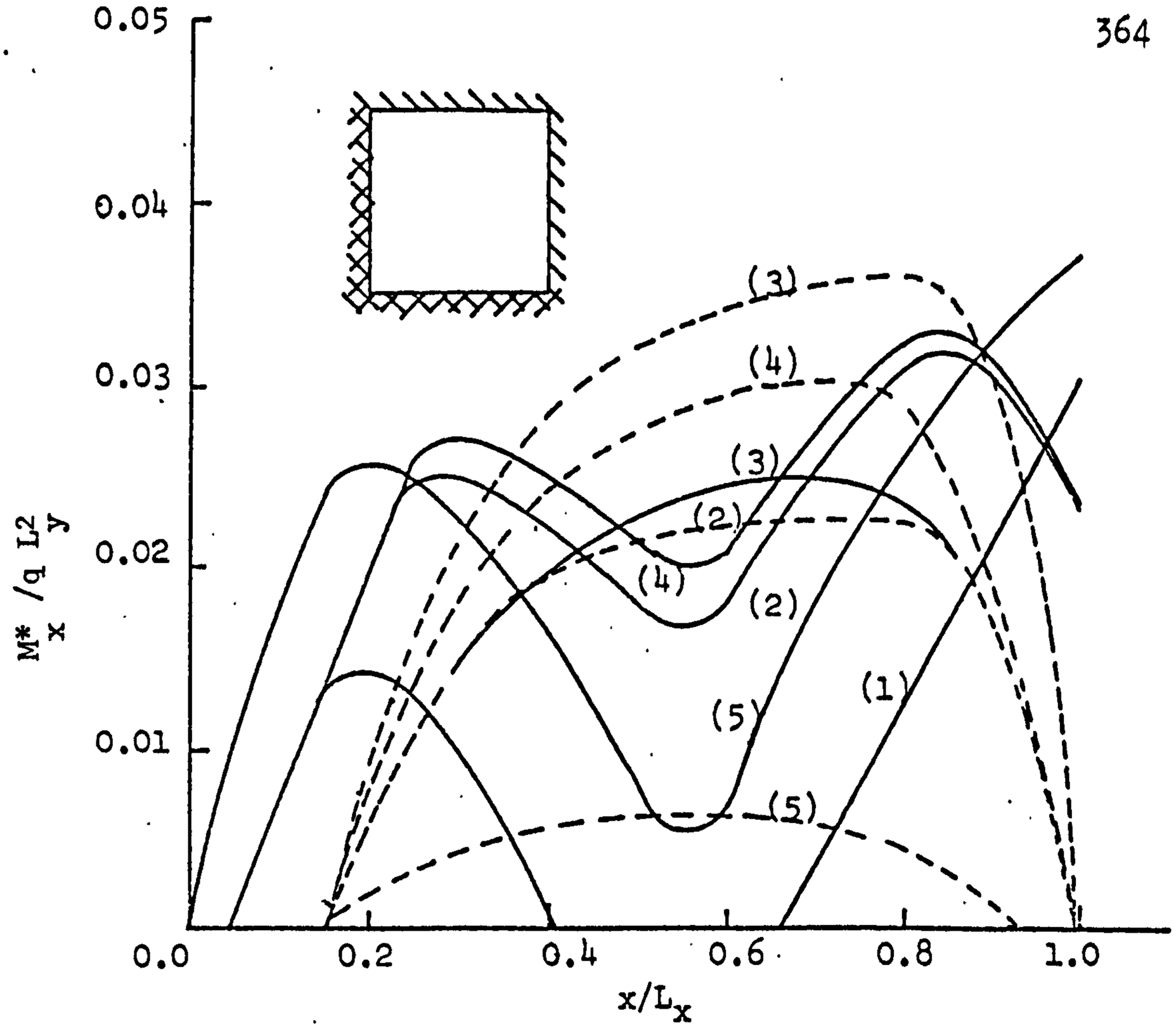

Figure (D41) Positive Moment M^*_x (L_x/L_y = 1.5)

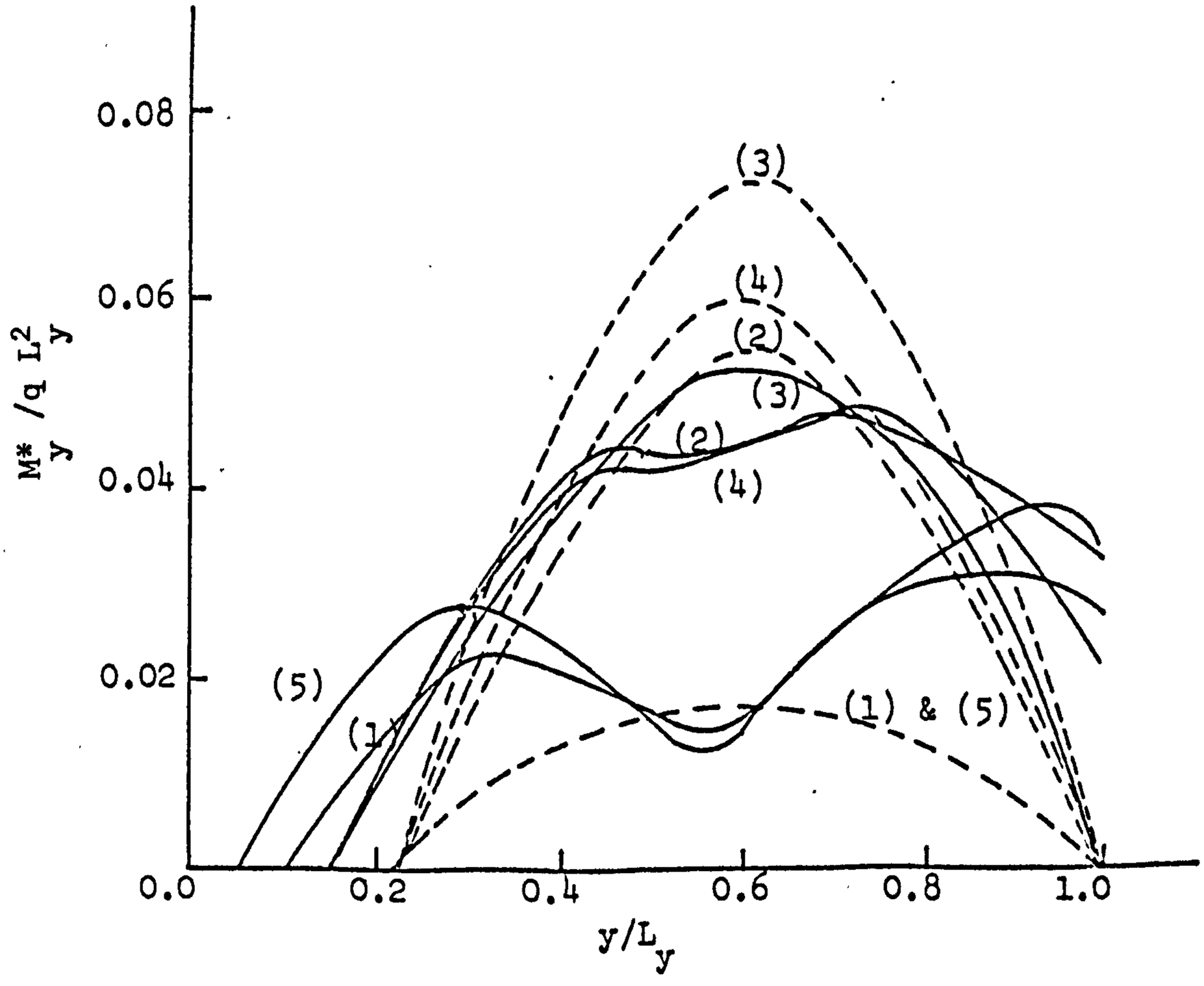

Figure (D42) Positive Moment M^*_y (L_x/L_y = 1.5)

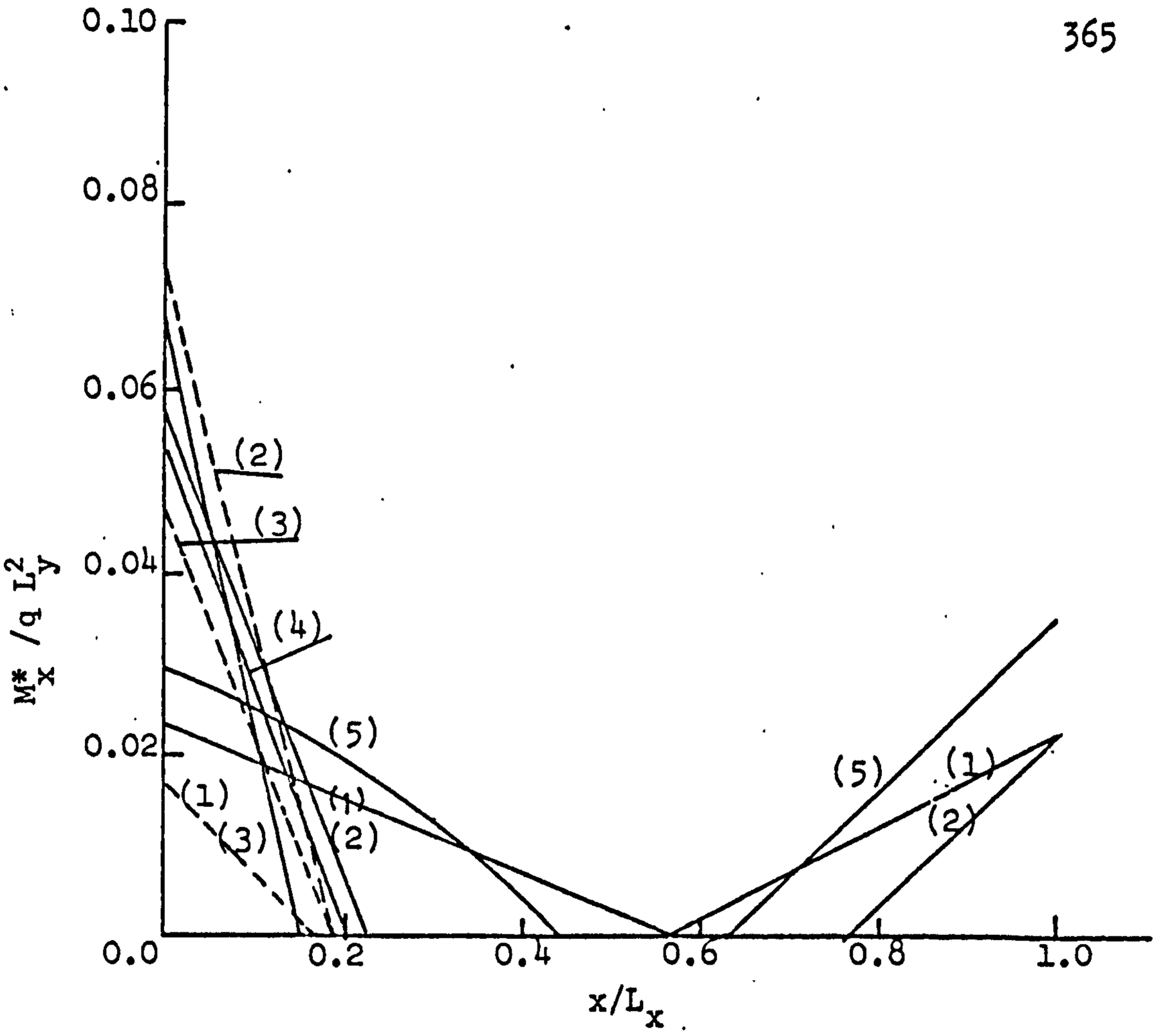

Figure (D43) Negative Moment M_x^* $(L_x/L_y = 1.5)$

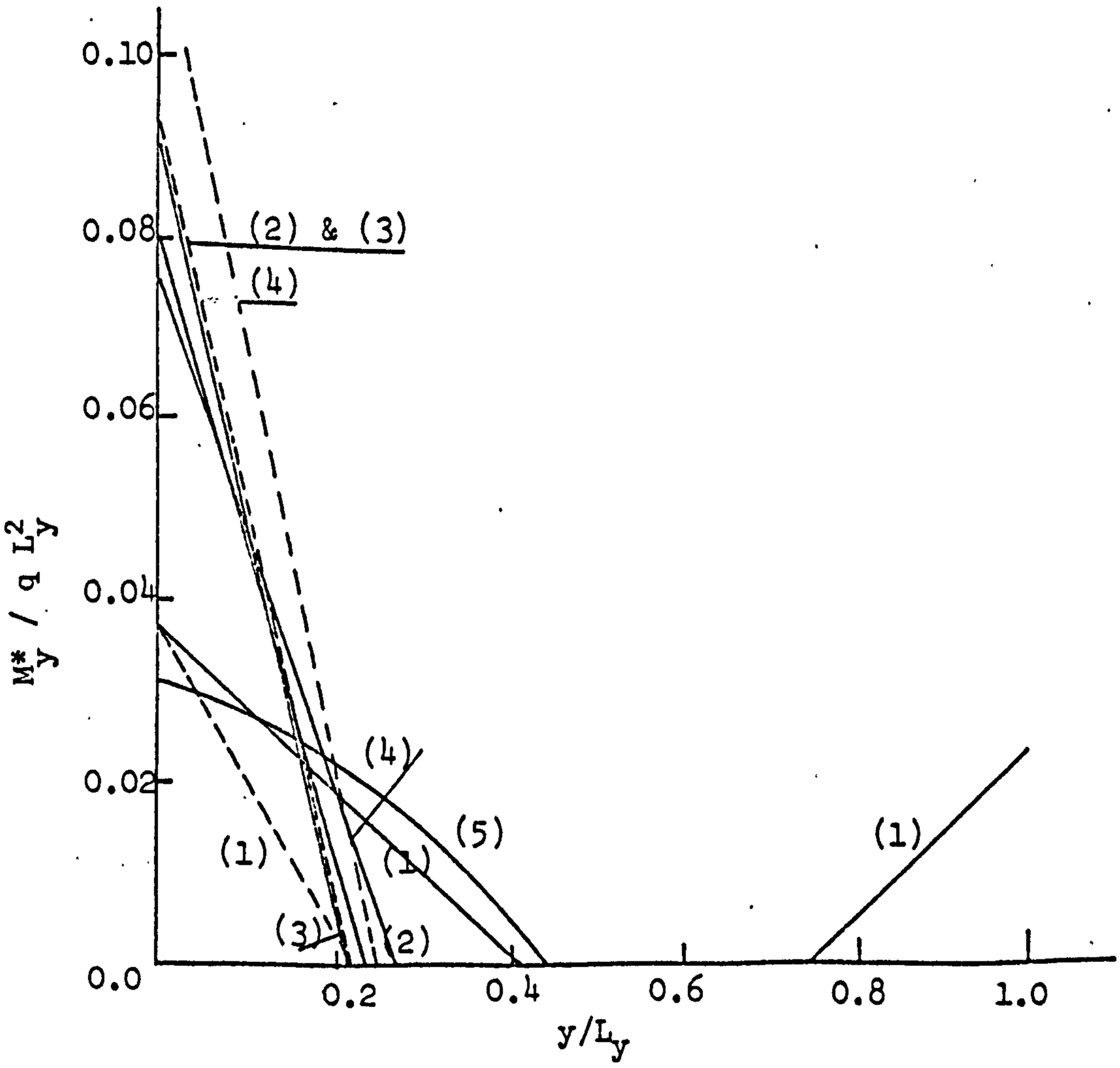

Figure (D44) Negative Moment M_y^* $(L_x/L_y = 1.5)$

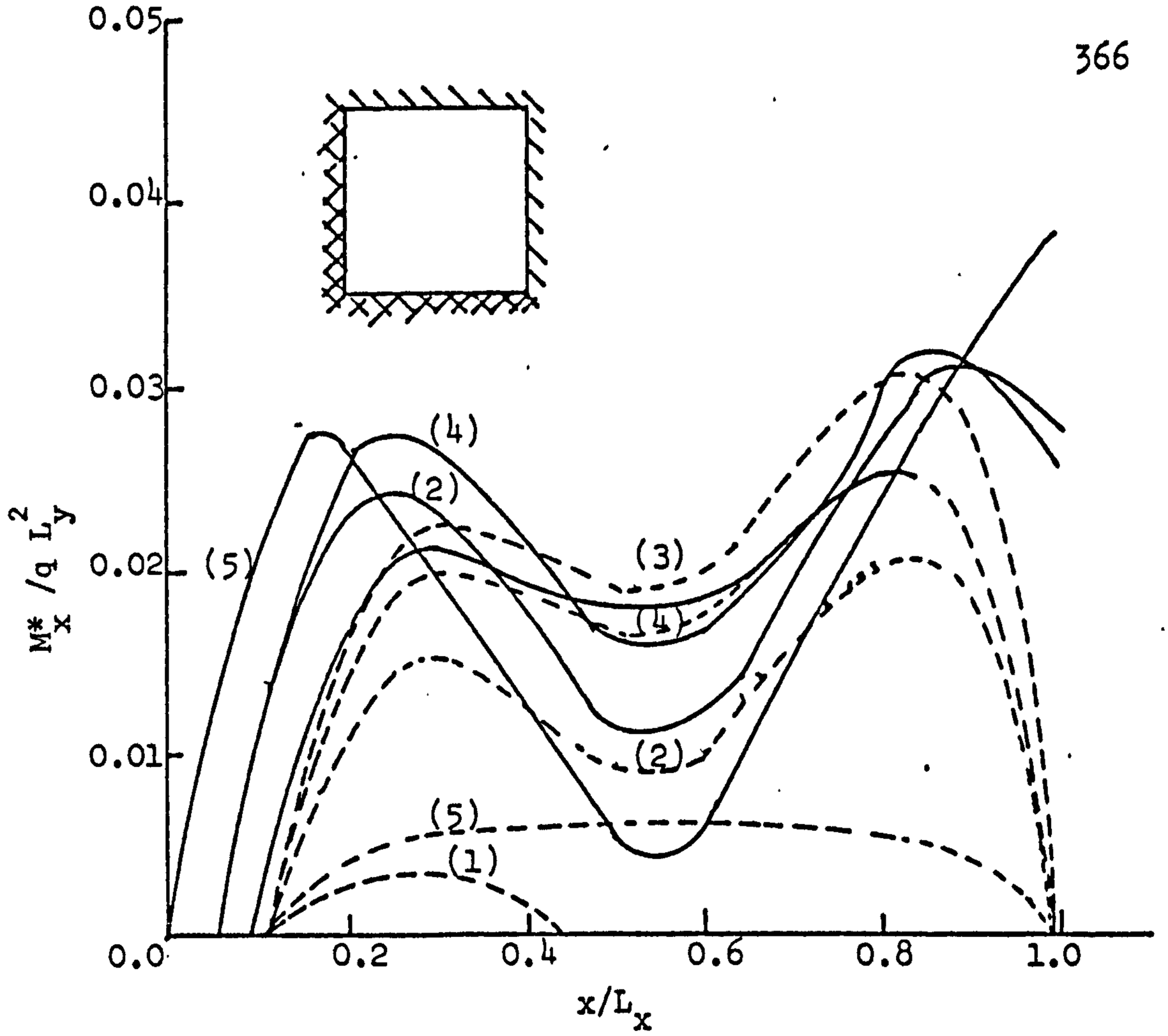

Figure (D45) Positive Moment M_x^* ($L_x/L_y = 2.0$)

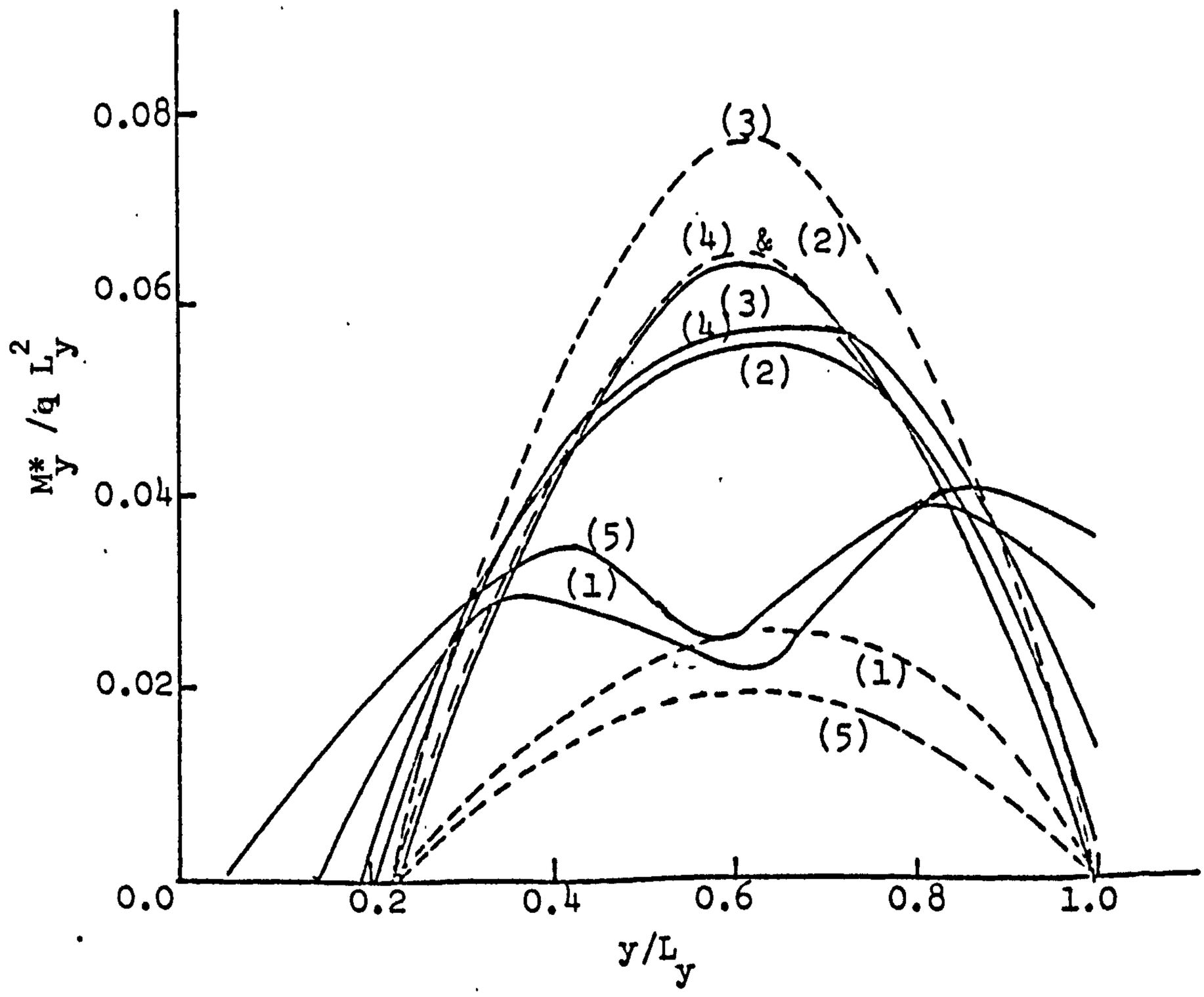

Figure (D46) Positive Moment M_y^* ($L_x/L_y = 2.0$)

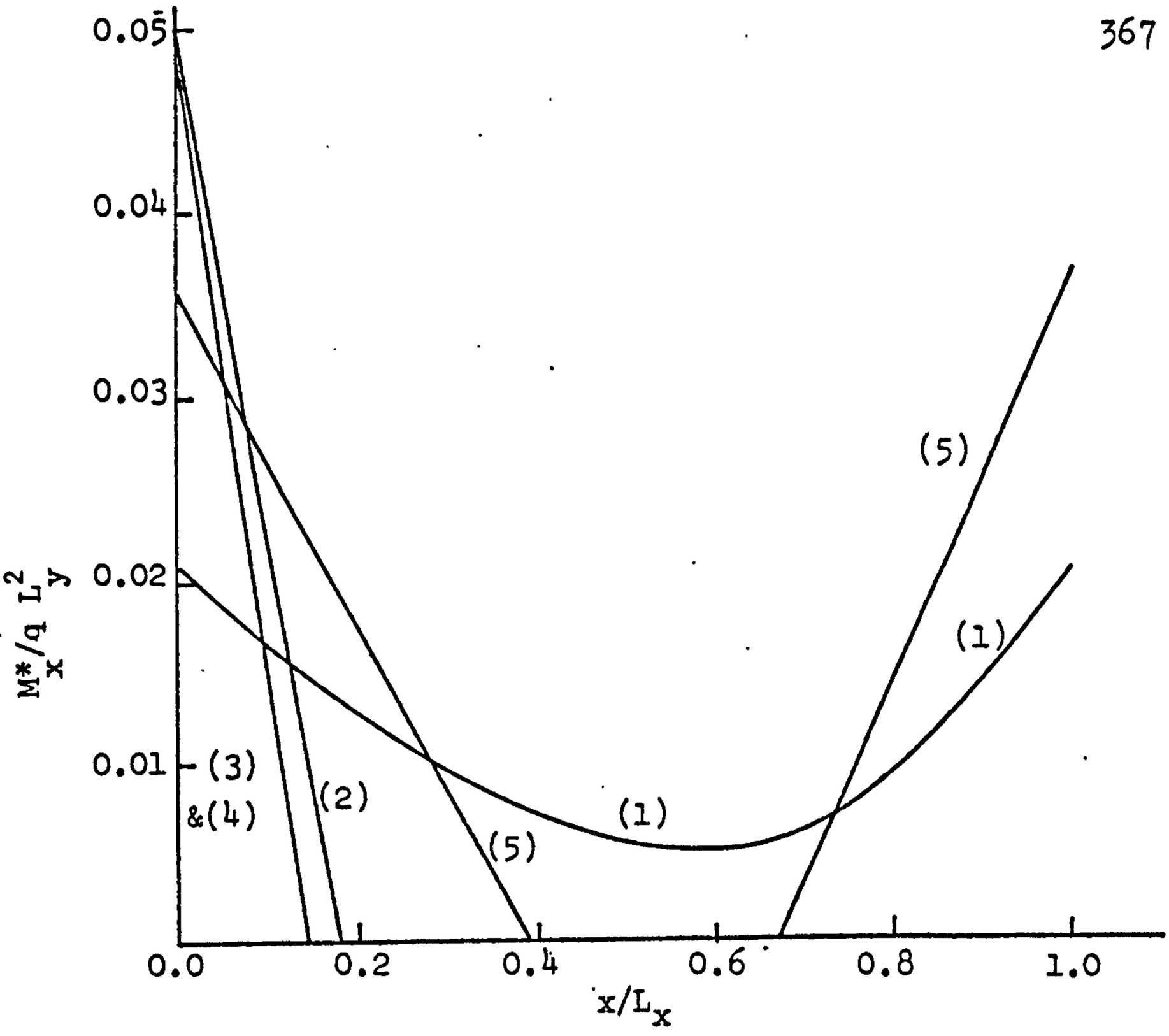

Figure (D47) Negative Moment M^*_x (L_x/L_y = 2.0)

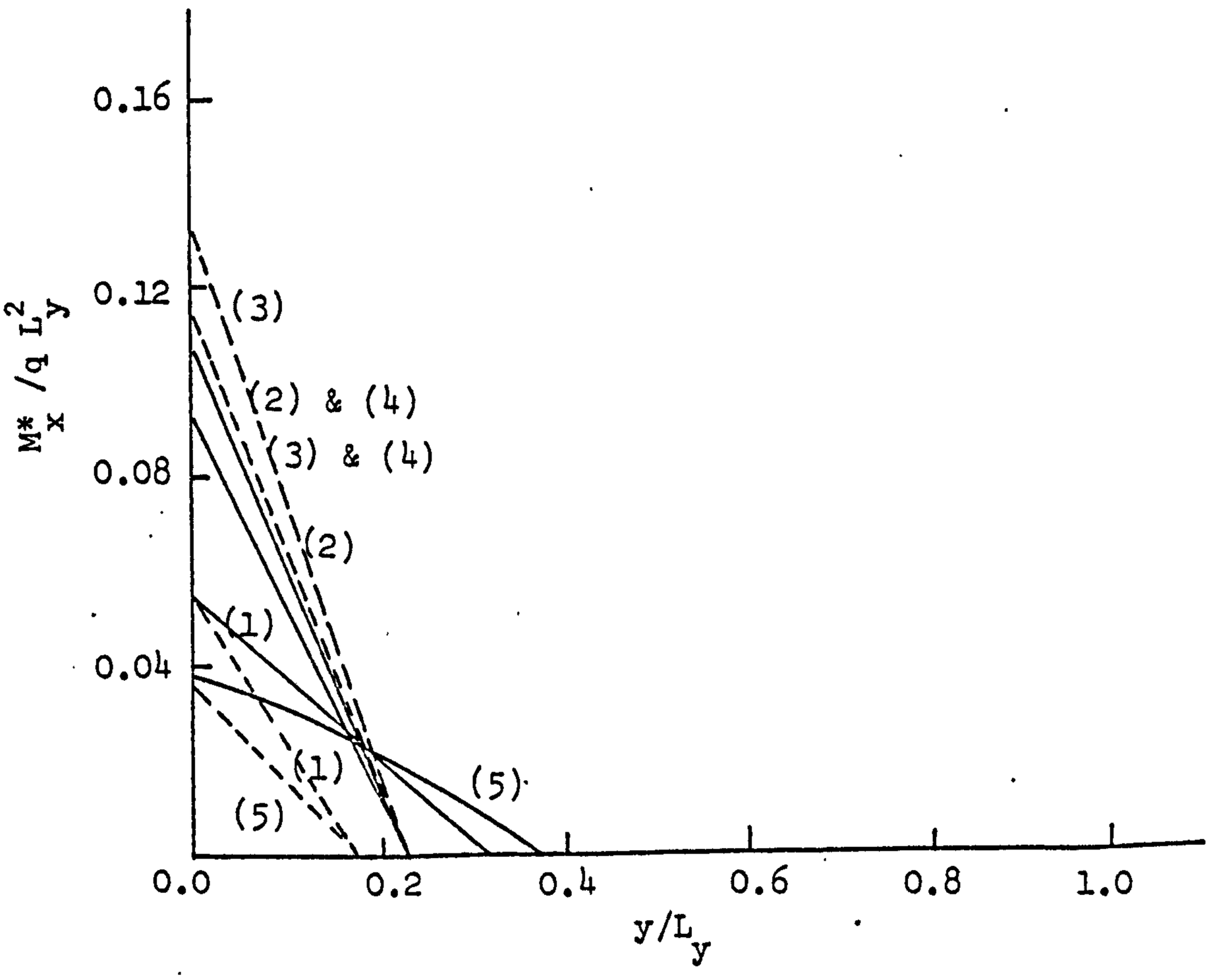

Figure (D.48) Negative Moment M^*_y (L_x/L_y = 2.0)

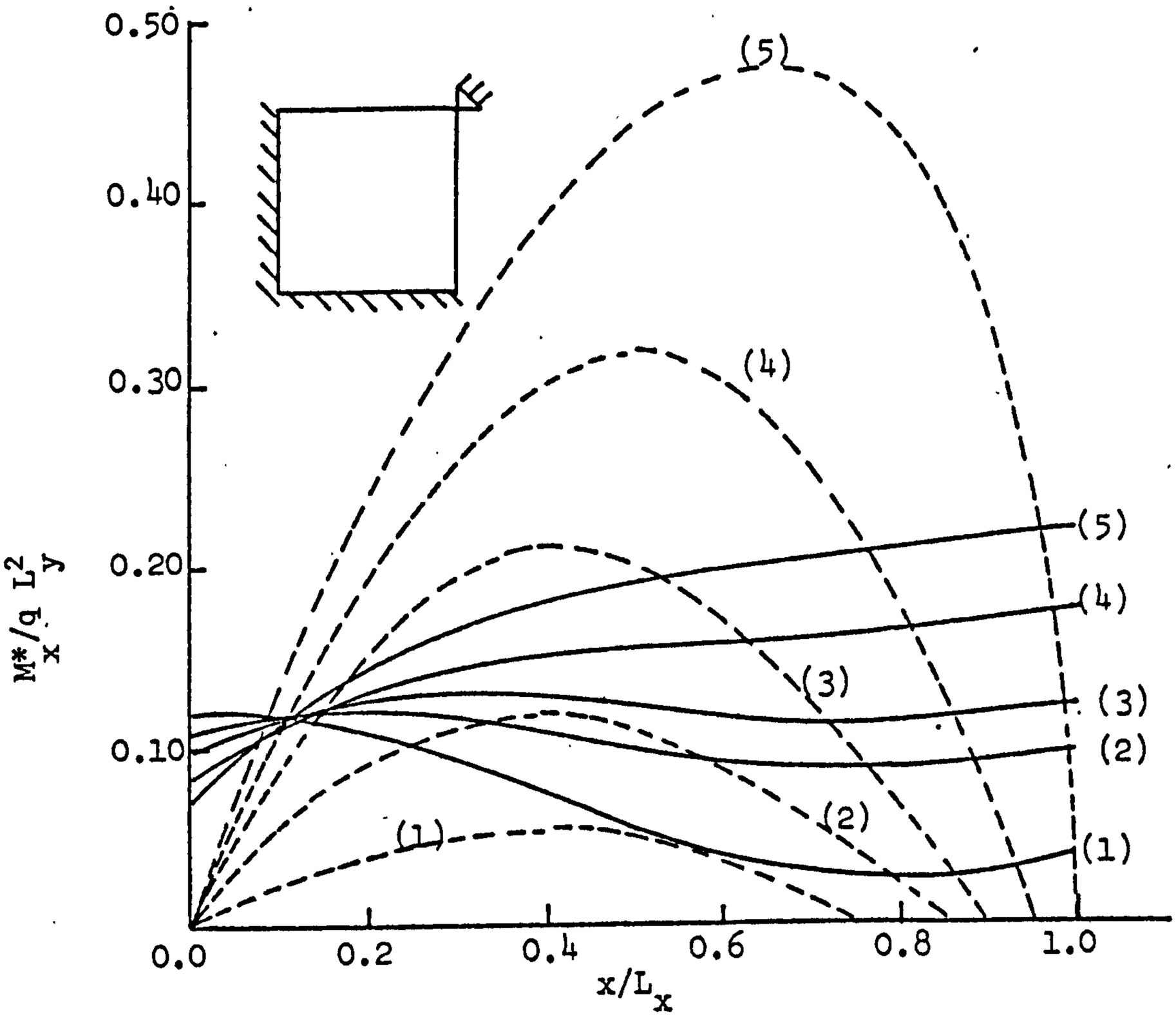

Figure (D49) Positive Moment M^*_x (L_x/L_y = 1.5)

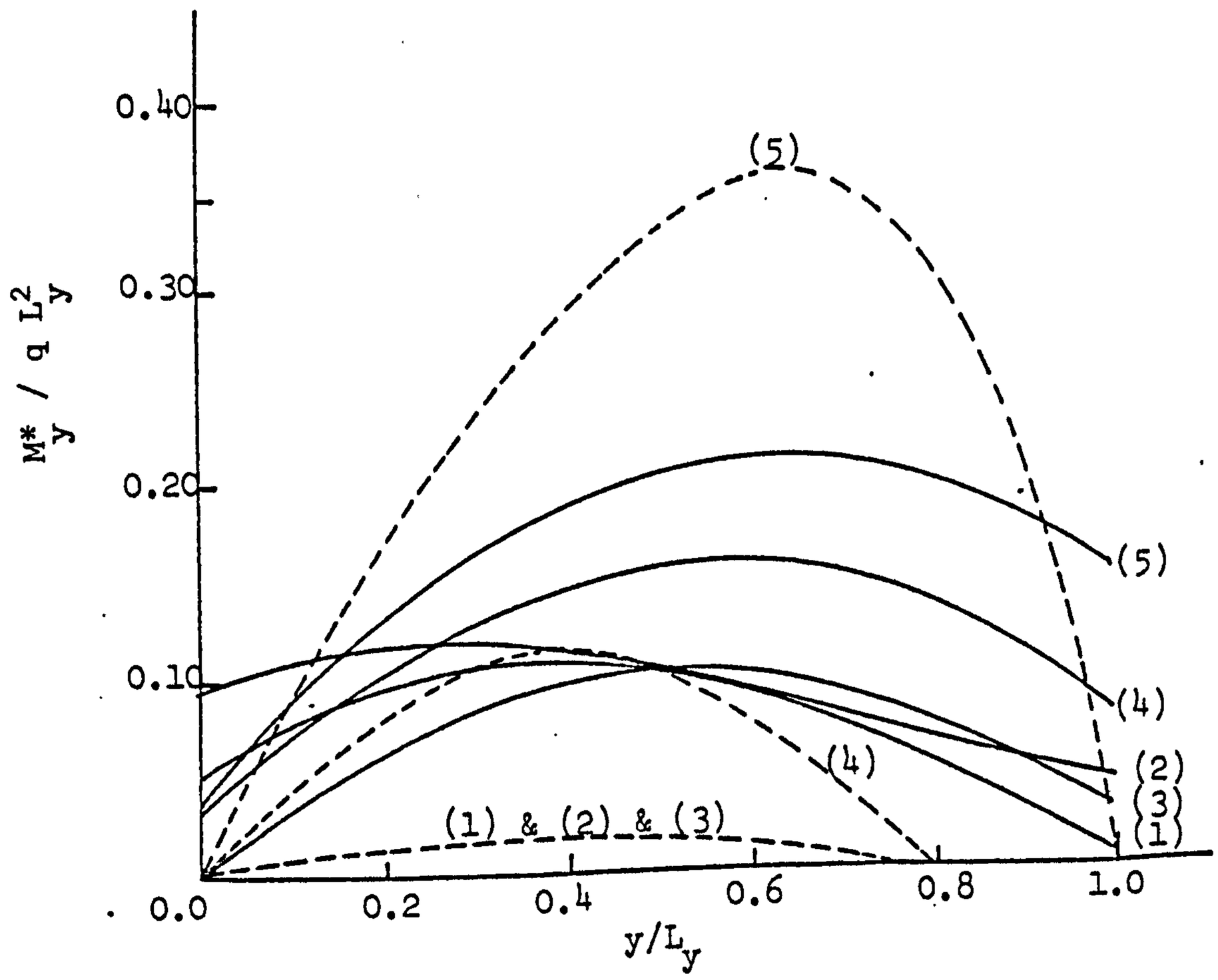

Figure (D50) Positive Moment M^*_y (L_x/L_y = 1.5)

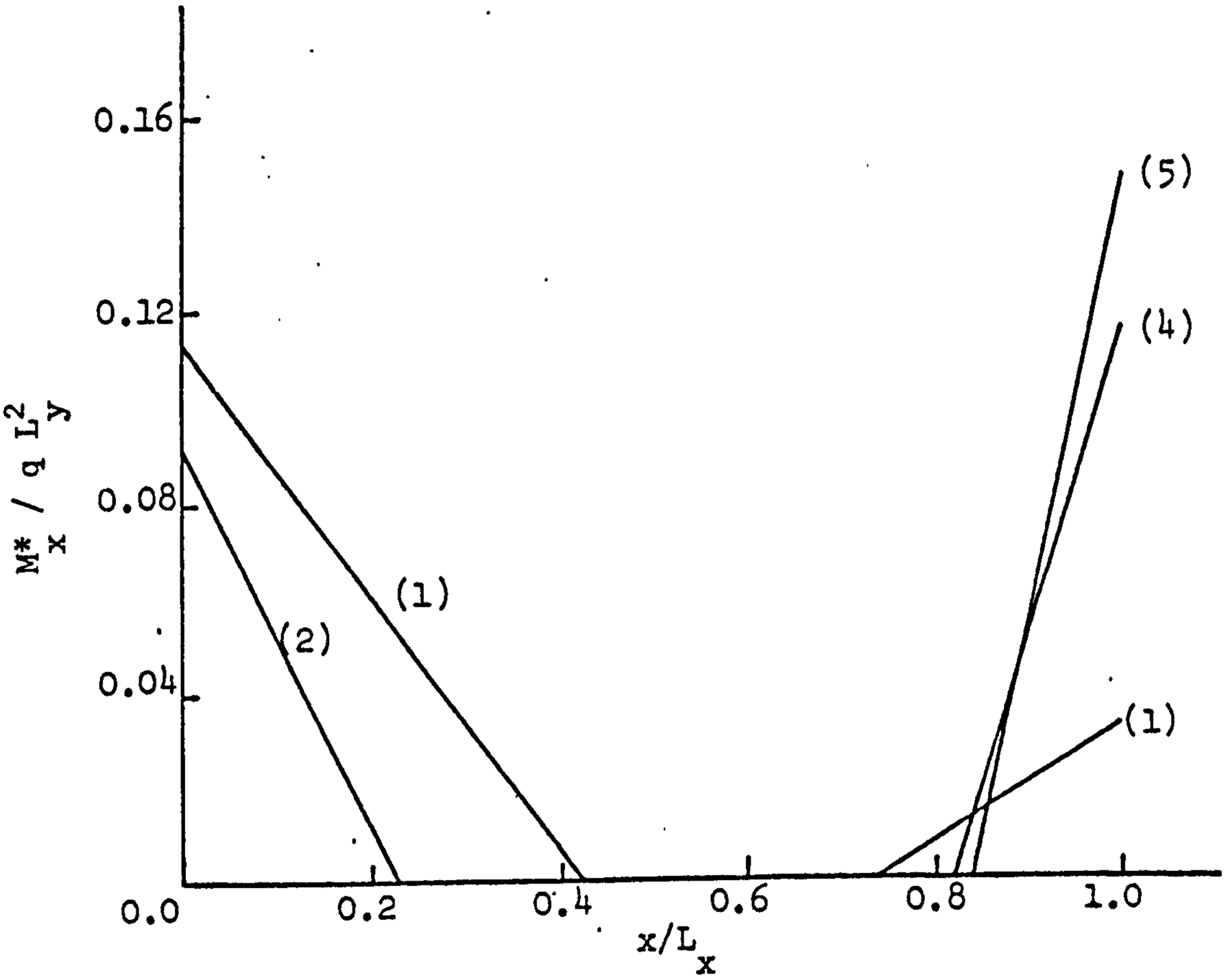

Figure (D51) Negative Moment M^*_x (L_x/L_y = 1.5)

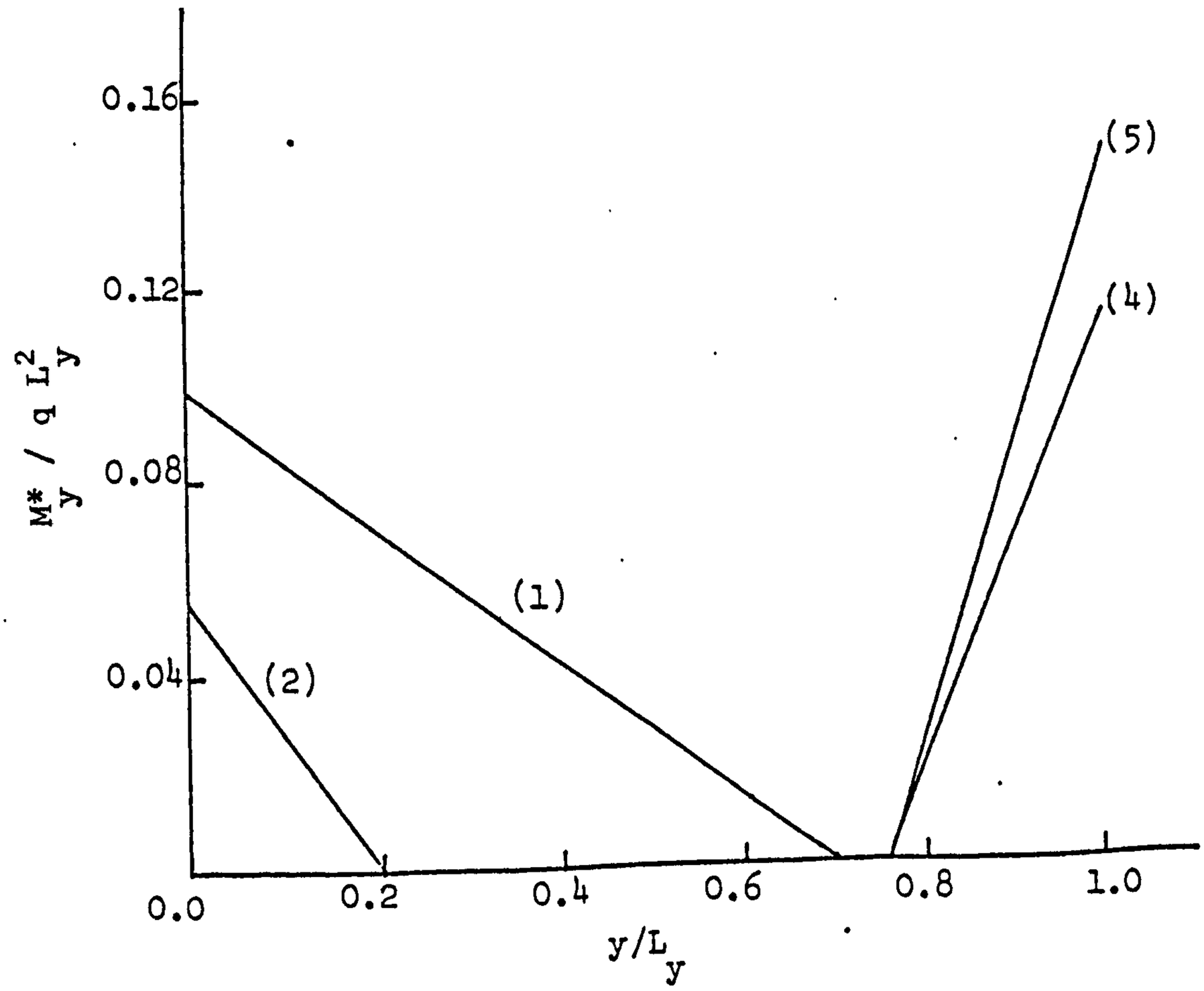

Figure (D52) Negative Moment M^*_y (L_x/L_y = 1.5)

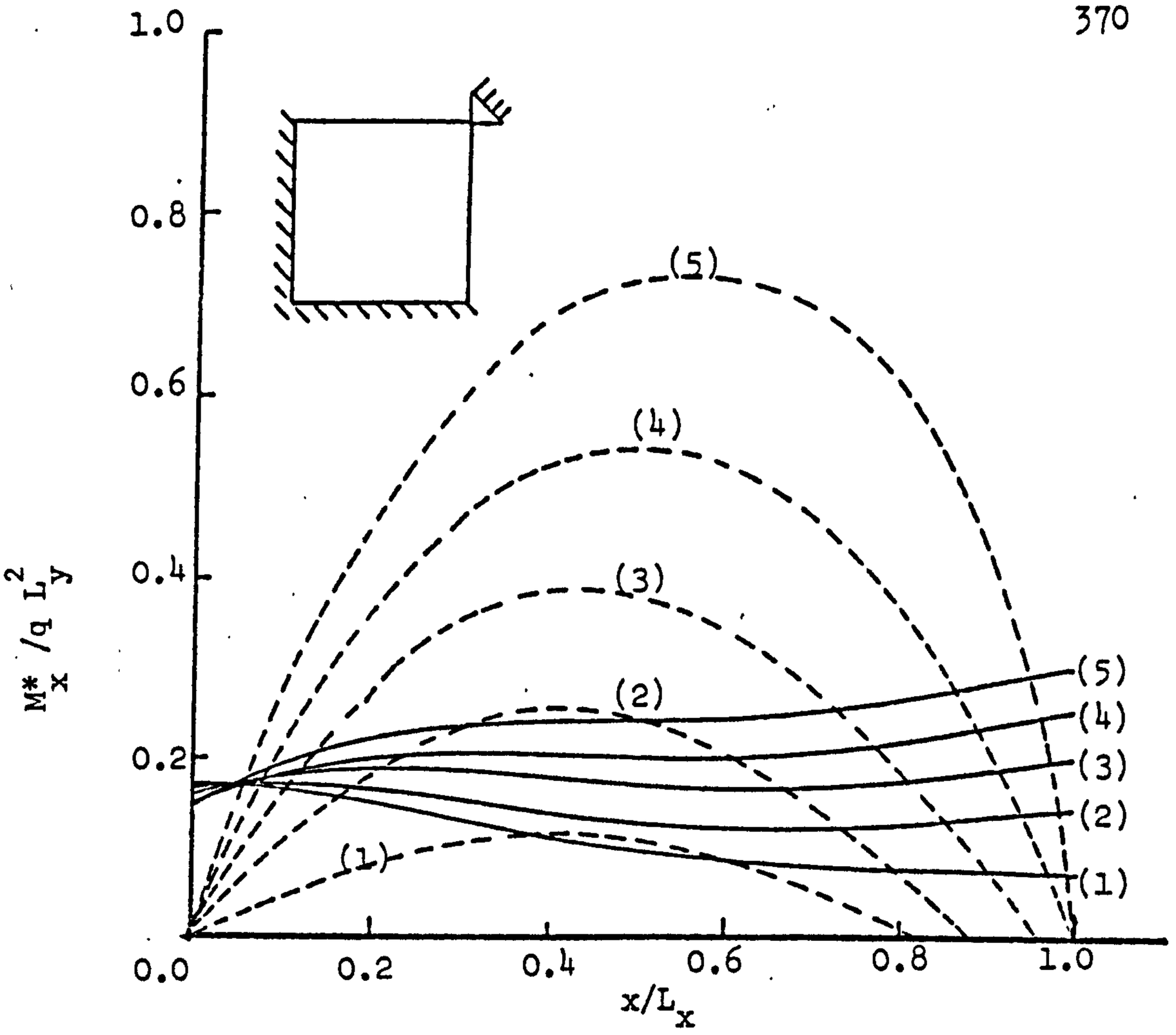

Figure (D53) Positive Moment M_x^* (L_x/L_y = 2.0)

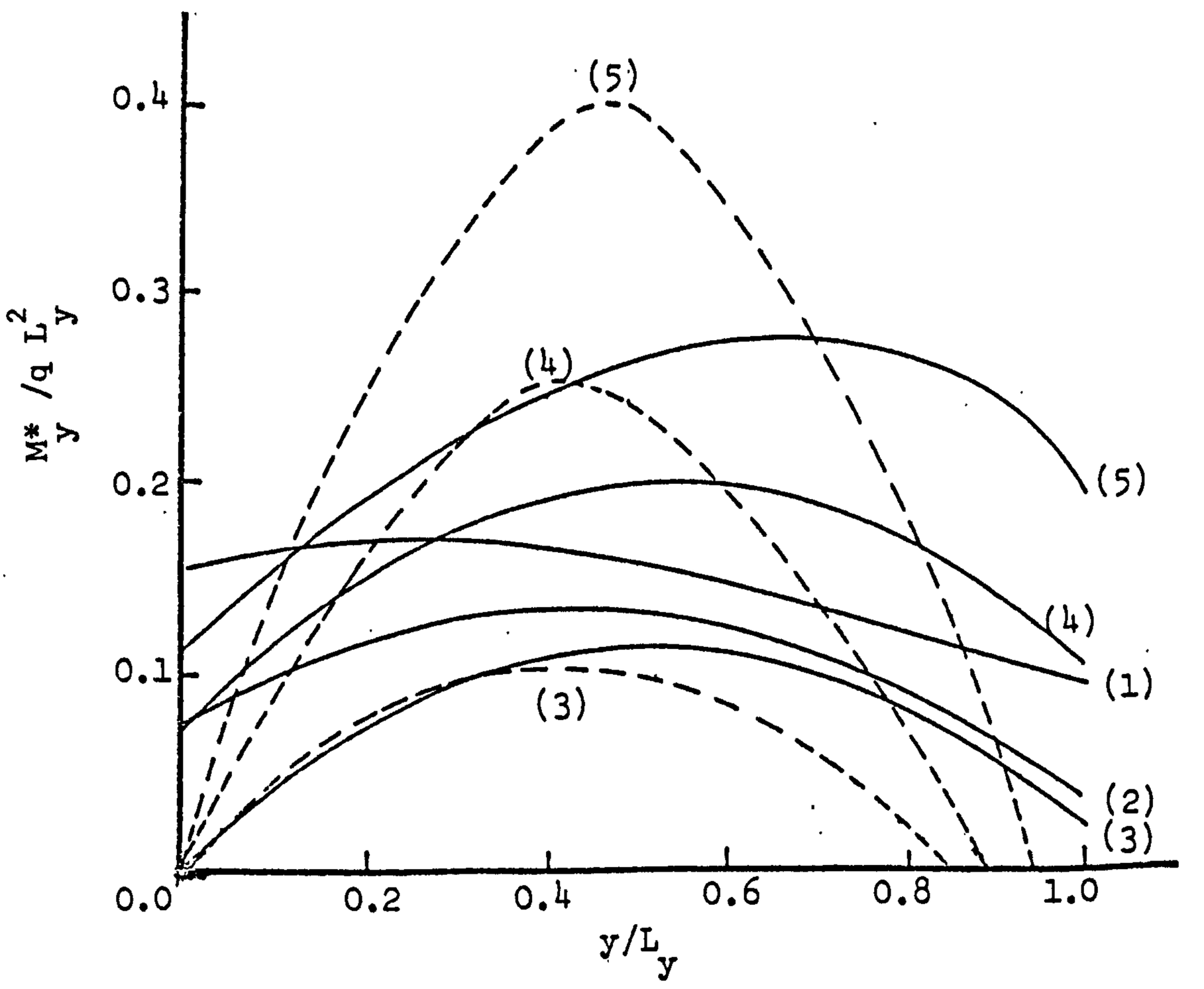

Figure (D54) Positive Moment M_y^* (L_x/L_y = 2.0)

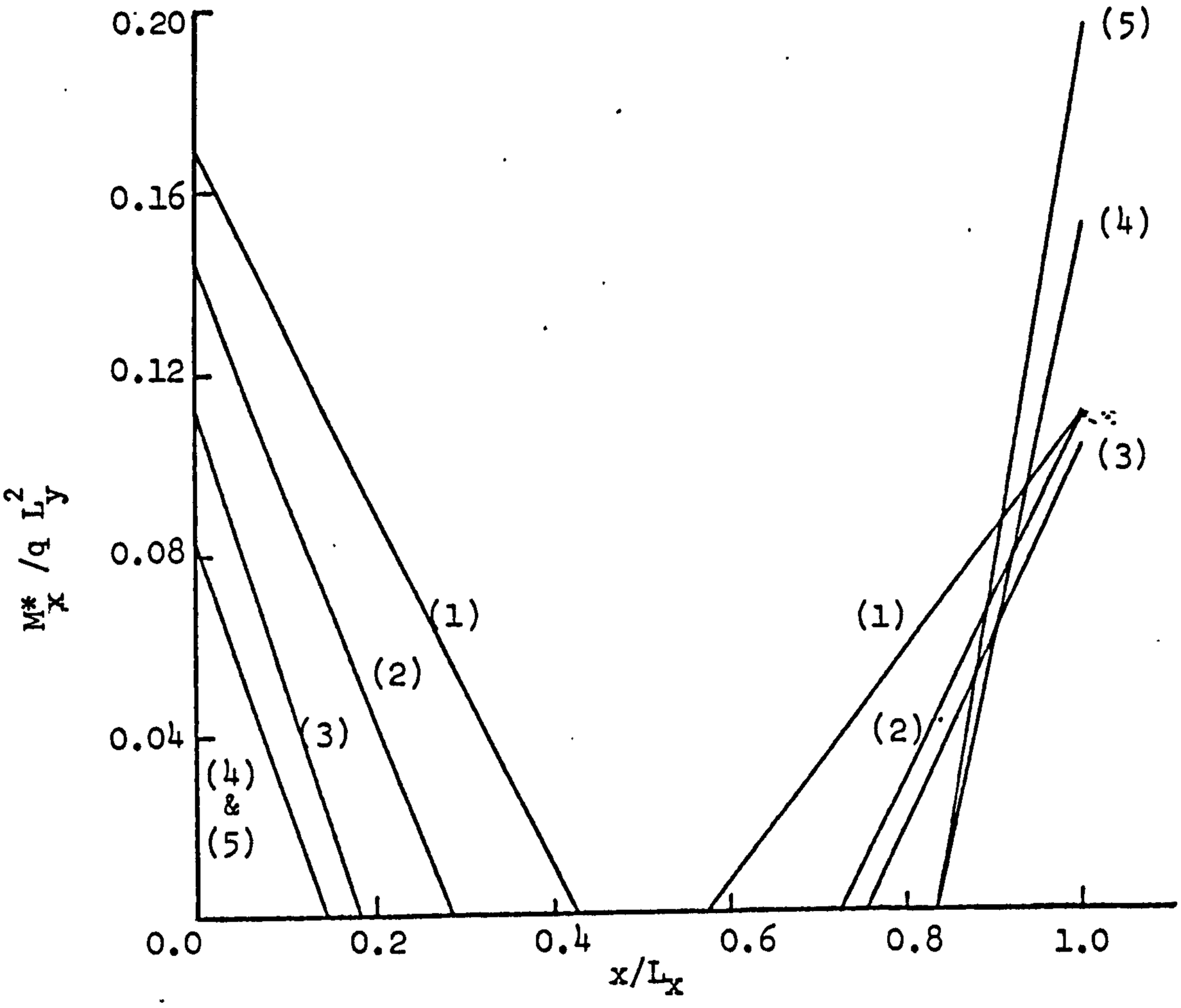

Figure (D55) Negative Moment M^*_x (L_x/L_y = 2.0)

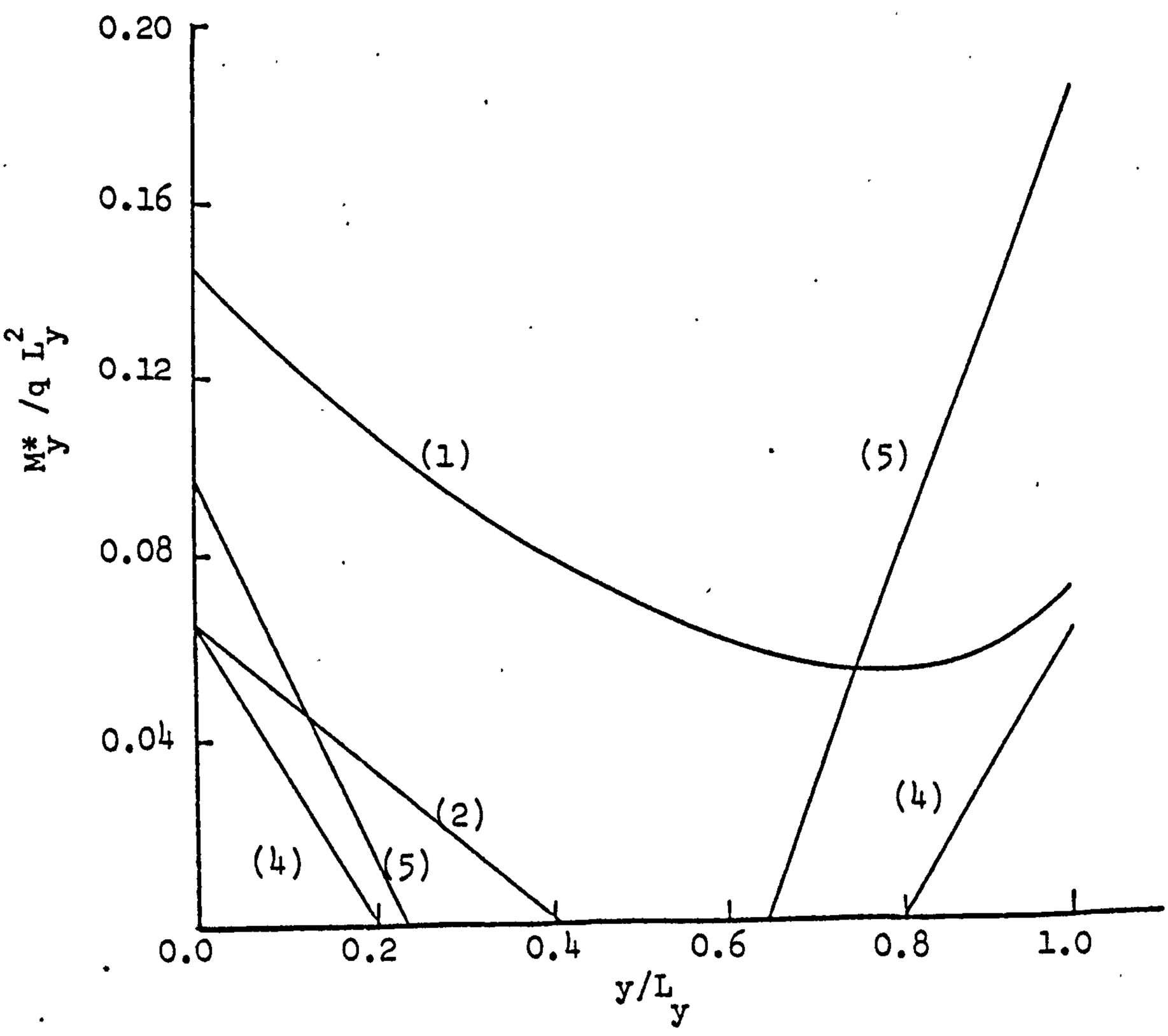

Figure (D56) Negative Moment M^*_y (L_x/L_y = 2.0)

APPENDIX(D1)

Additional torsional reinforcement at discontinuous edges according to CP110[5].

According to Section (3.4.3.2) in CP110, torsional steel has to be provided as four layers, as shown

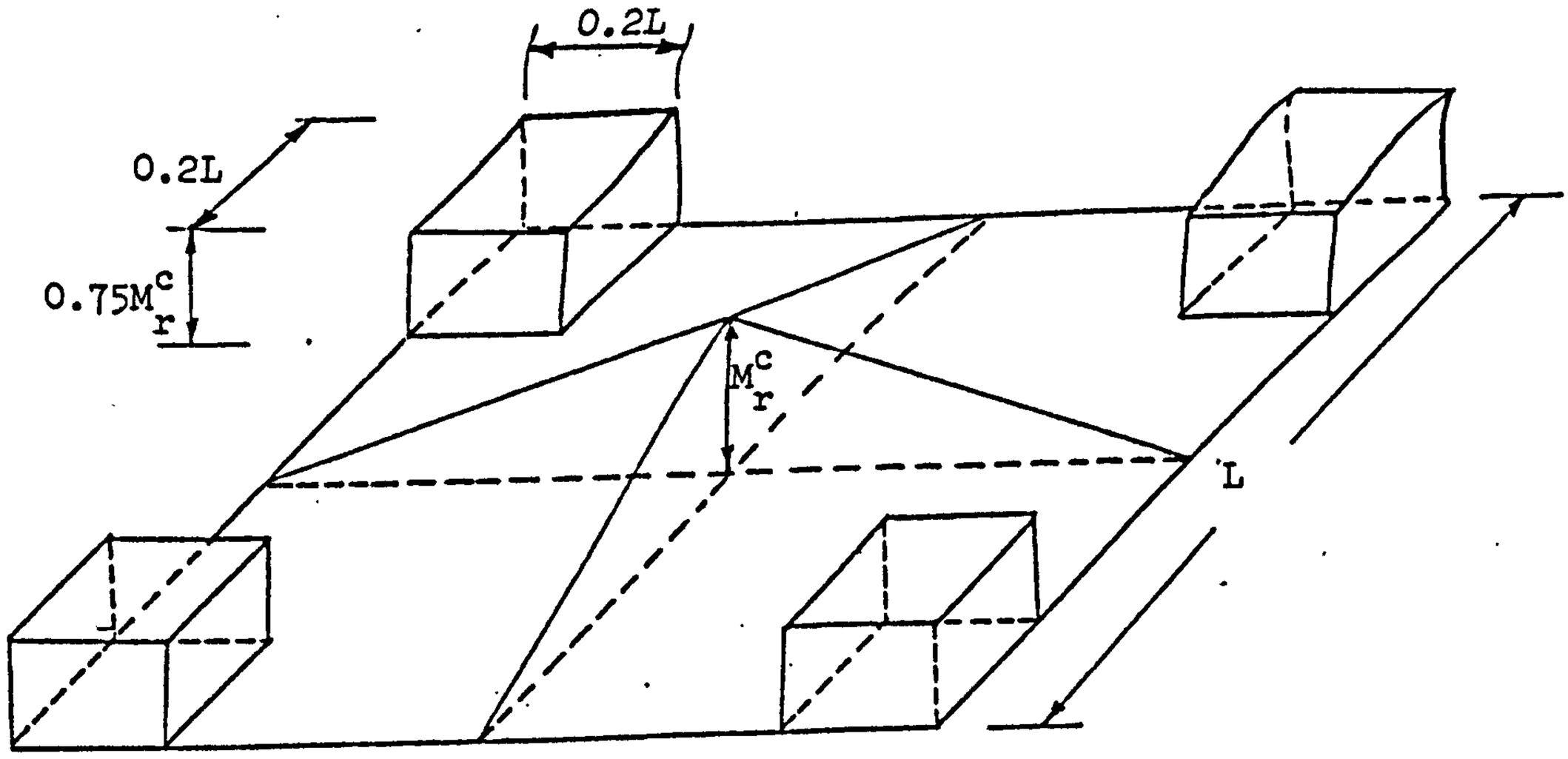

Where L = short span, M^c_r = design moment at centre.

Additional moment volume due to torsional steel:

$$V_a = 4 \times 0.75\ M^c_r \times (0.2L)^2$$
$$= 0.12\ M^c_r\ L^2$$

which is the moment volume due to torsional steel at one corner. In a simply supported slab with four corners

$$V_a = 4 \times 0.12\ M^c_r\ L^2 = 0.48\ M^c_r\ L^2$$

$$\therefore \quad \frac{V_a}{q\ L^4} = 0.48 \quad \frac{M^c_r}{q\ L^2} = 0.48\ \alpha$$

Where the moment coefficient $\alpha = \frac{M}{q\ L^2}$ can be obtained from Figures (5.3 to 5.9), and from the Appendix Figures D1 to D56.

APPENDIX E

CALCULATIONS FOR SERVICEABILITY

LIMIT STATES

Assumptions: Under the service load, the following assumptions are made.

1. Tension stiffening in cracked concrete is ignored.
2. Linear strain distribution across the depth of the section.
3. Linear elastic behaviour for concrete in compression.
4. Linear elastic behaviour for the reinforcing steel.
5. Uniaxial behaviour is assumed for concrete

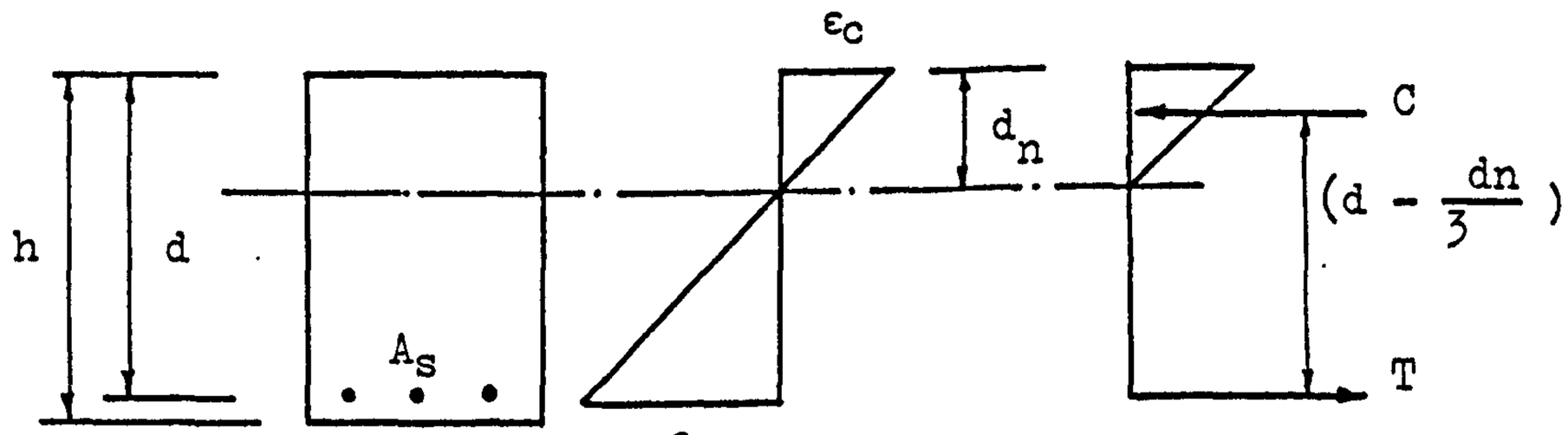

For equilibrium: $C = T$

$$\therefore \quad \tfrac{1}{2}\,\varepsilon_c\,E_c\,d_n = A_s\,E_s\,\varepsilon_s \qquad (1)$$

$$\therefore \quad d_n = 2\,\frac{E_s}{E_c}\cdot\frac{\varepsilon_s}{\varepsilon_c}\cdot A_s = 2\,mA_s\,\frac{\varepsilon_s}{\varepsilon_c} \qquad (2)$$

where m = modular ratio $= E_s/E_c$.

But from the strain diagram

$$\frac{\varepsilon_s}{\varepsilon_c} = \frac{d - d_n}{d_n} \qquad (3)$$

$$\therefore \quad d_n = 2\,m\,A_s\,(d - dn/dn)$$

arranging

$$\therefore \quad d_n^2 + 2m\,A_s\,d_n - 2m\,A_s\,d = 0 \qquad (4)$$

solving gives

$$d_n = (- mA_s + \sqrt{(mA_s)^2 + 2(mA_s)d} \qquad (5)$$

The gross moment of inertia is

$$I_g = \frac{b\,h^3}{12} + (m-1)\,A_s\,(d - \frac{h}{2})^2 \qquad (6)$$

and the fully cracked transformed section gives

$$I_{cr} = \frac{b\,d_n^3}{3} + m\,A_s\,(d - d_n)^2 \qquad (7)$$

then using the Branson's method, an effective moment of inertia is calculated from

$$I_{eff} = I_g\left(\frac{M_{cr}}{M}\right)^3 + I_{cr}\left[1 - \left(\frac{M_{cr}}{M}\right)^3\right] \qquad (8)$$

in which

M_{cr} = cracking moment = $2\,f_t\,I_g/h$

where h = total depth of section and

f_t = tensile strength of concrete.

The deflection under the service load is found from the elastic deflection as

$$\delta_s = \delta_e\,I_g/(\text{L.F.}\quad I_{eff}) \qquad (9)$$

where L.F. = average load factor for ultimate conditions.

R E F E R E N C E S

1. TIMOSHENKO S. and S. WOINOSKY-KRIEGER

   Theory of Plates and Shells. McGraw-Hill, New York, Second Edition 1959.

2. SZILARD R.

   Theory of Analysis of Plates, Classical and Numerical Methods. Prentice Hall, 1974.

3. PARK R. and GAMBLE W.L.

   Reinforced Concrete Slabs. Wiley, 1980.

4. WOOD R.H.

   Plastic and Elastic Design of Slabs and Plates. Thames and Hudson, London, 1967.

5. CP110 - PART 1: 1972

   The Structural Use of Concrete - B.S.I., London.

6. BELL J.C. and ELMS D.G.

   A Finite Element Approach to Post-Elastic Slab Behaviour. ACI Special Publications SP30-15, March 1971 PP325-344.

7. HUGHES B.P.

   Limit State Theory of Reinforced Concrete Design. Pitman, Second Edition, 1977,

8. SIMMONDS S.H. and GHALI A.

   Yield-Line Design of Slabs. Journal of the Structural Division, Proceedings of the American Society of Civil Engineers, Vol.102, No.ST1, Jan. 1976, PP109-123.

9. JONES L.L. and WOOD R.H.

   Yield-Line Analysis of Slabs. Thames and Hudson, Chatto and Windus, London, 1967.

10. MORLEY C.T.

The Minimum Reinforcement of Concrete Slabs. International Journal of Mechanical Sciences. Vol.8, 1966, PP305-319.

11. RANGAN B.V.

Lower Bound Solutions for Continuous Orthotropic Slabs. Journal of the Structural Division, Proceedings of the American Society of Civil Engineers, Vol.99, No.ST3, March 1973, PP443-452.

12. RANGAN B.V.

Limit States Design of Slabs using Lower Bound Approach. Journal of the Structural Division, Proceedings of the American Society of Civil Engineers, Vol.100, No.ST2, Feb.1974, PP373-389.

13. HILLERBORG A.

Strip Method of Design. A View Point Publication, 1975.

14. WOOD R.H. and ARMER G.S.T.

The Strip Method for Desigining Slabs. Proceedings of The Institution of Civil Engineers, Part 2, Vol.41, Oct.1968, PP285-311.

15. FERNANDO J.S. and KEMP K.O.

A Generalized Strip-Deflexion Method of Reinforced Concrete Slab Design. Proceedings of the Institution of Civil Engineers, Part 2, Vol.65, March 1978, PP163-174.

16. KEMP K.O. and FERNANDO J.S.

Reinforced Concrete Slab Design - A Generalized Strip Method Including Concentrated Loads and Supports. Advances in Concrete Slab Technology, Proceedings of the International Conference on Concrete Slabs, Dundee University 1979. Edited by Dhir and Munday, Pergamon Press, PP232-241.

17. WILBY C.B.

Computation of the Strip-Deflexion Method. Proceedings of the Institution of Civil Engineers, Part 2, Vol.69, June 1980, PP499-509.

18. BHATT P.

Discussion of Reference 15. Proceedings of the Institution of Civil Engineers, Part 2, Vol.65, Sept. 1978, PP719-724.

19. WOOD R.H.

The Reinforcement of Slabs in Accordance with a Pre-determined Field of Moments. Concrete, Vol.2, No.2, Feb.1968, PP69-76.

20. ARMER G.S.T.

Contribution to Discussion on Ref19. Concrete, Vol.2, No.8, Aug. 1968, PP319-320.

21. JOFRIET J.C. and McNEICE G.M.

Finite Element Analysis of Reinforced Concrete Slabs. Journal of the Structural Division, Proceedings of the American Society of Civil Engineers, Vol.97, No.ST3, March 1971, PP785-806.

22. DESAYI P. and MUTHU K.U.

Short-Time Deflexions of Rectangular Simply Supported Reinforced Concrete Slabs. Advances in Concrete Slab Technology - Proceedings of the International Conference on Concrete Slabs, Dundee University 1979, Pergamon Press, PP110-117,Edited by Dhir and Munday.

23. DESAYI P. and MUTHU K.U.

Short-Time Deflexions of Rectangular Restrained Reinforced Concrete Slabs. Technical Note TN221, Proceedings of the Institution of Civil Engineers, Part 2, Vol.67, June 1970, PP529-536.

24. BEEBY A.W.

An Investigation of Cracking in Slabs Spanning One Way. Technical Report, Cement and Concrete Association, RTA433, May 1970, PP31.

25. ORENSTEIN G.S. and NAWAY E.G.

Crack Width Control in Reinforced Concrete Two-way Slabs Subjected to Distributed Load. American Concrete Institution Vol.67, No.1, Jan 1970, PP57-61.

26. NAWAY E.G. and ORENSTEIN G.S.

Crack Width Control in Reinforced Concrete Two-way Slabs. Journal of the Structural Division, Proceedings of the American Society of Civil Engineers, Vol.96, No.ST3, March 1970, PP701-721.

27. DESAYI P. and KULKARNI A.B.

Determination of Maximum Crack Width in Two-way Reinforced Concrete Slabs. Proceedings of the Institution of Civil Engineers, Part 2, Vol.61, June 1976, PP343-349.

28. DESAYI P. and PRABHAKARA A.

Determination of Maximum Crack Width in Reinforced Concrete Skew and Rectangular Slabs. Proceedings of the Institution of Civil Engineers, Part 2, Vol.67, Dec.1979, PP1077-1090.

29. BHAUMIK A.K. and HANLEY J.T.

Elastoplastic Analysis by Finite Difference Method, Journal of the Structural Division, Proceedings of the American Society of Civil Engineers, Vol.93, No.ST5, Oct.1967, PP279-294.

30. MAY G.W. and GERSTLE K.H.

Elastoplastic Bending of Rectangular Plates. Journal of the Structural Division, Proceedings of the American Society of Civil Engineers, Vol.97, No.ST7, July 1971, PP1863-1878.

31. COOK R.D.

Concepts and Application of Finite Element Analysis, Wiley 1974.

32. BELL J.C. and ELMS D.G.

Nonlinear Analysis of Reinforced Concrete Slabs. Magazine of Concrete Research, Vol.24, No.79, June 1972, PP63-70.

33. PFRANG E.O., SIESS C.P. and SOZEN M.A.

Load-Moment-Curvature Characteristics of Reinforced Concrete Cross-sections. Journal of the American Concrete Institute, July 1964, PP763-778.

34. DESAI S.C. and ABEL J.F.

Introduction to the Finite Element Method. A Numerical Method for Engineering Analysis, van Nostrand, 1972.

35. JAIN O.P., TRIKHA D.N. and AGARWAL S.

A Finite Element Solution of Post Cracking Behaviour of Reinforced Concrete Slabs. Advances in Concrete Slab Technology, Proceedings of the International Conference on Concrete Slabs, Dundee University, 1979, PP129-139. Pergamon Press, Edited by Dhir and Munday.

36. SCHNOBRICH W.C.

Non-Linear Behaviour of Concrete Structures. Transport and Road Research Laboratory, Department of the Environment, Supplementary Report 164 UC-Structural Analysis-Nonlinear Behaviour Techniques, Proceedings of a Symposium held at the Transport and Road Research Laboratory, Crowthorne, December 1974.

37. SCHNOBRICH W.C.

Behaviour of Reinforced Concrete Structures predicted by the Finite Element Method, Computers and Structures, Vol.7, 1977, PP365-376.

38. SUIDAN M. and SCHNOBRICH, W.C.

Finite Element Analysis of Reinforced Concrete. Journal of the Structural Division, Proceedings of the American Society of Civil Engineers, Vol.99, No.ST10, Oct.1973, PP2109-2122.

39. RAO P.V.

Nonlinear Finite Element Analysis of Concrete Slab Structures, Ph.D. Thesis, Liverpool University, 1976.

40. WEGMULLER A.W.

Elasto-plastic Finite Element Analysis of Plates, Technical Note TN99, Proceedings of the Institution of Civil Engineers, Part 2, Vol.57, Sept. 1974, PP535-543.

41. WEGMULLER A.W.

Full-Range Analysis of Eccentrically Stiffened Plates, Journal of The Structural Division, Proceedings of the American Society of Civil Engineers, Vol.100, No.St1, Jan.1974, PP143-159.

42. HAND F.R., PECKNOLD D.A. and SCHNOBRICH W.C.

Nonlinear Layered Analysis of Reinforced Concrete Plates and Shells, Journal of the Structural Division, Proceedings of the American Society of Civil Engineers, Vol.99, No.ST7, July 1973, PP1491-1505.

43. JOHNARRY T.

Elasto-Plastic Analysis of Concrete Structures Using Finite Elements, Ph.D. Thesis, University of Strathclyde, May 1979.

44. DUNCAN W. and JOHNARRY T.

Further Studies on the Constant Stiffness Method of Nonlinear Analysis of Concrete Structures, Proceedings of the Institution of Civil Engineers, Part 2, Vol.67, Dec.1979, PP951-969.

45. COPE R.J. and RAO P.V.

Nonlinear Finite Element Analysis of Concrete Slab Structures, Proceedings of the Institution of Civil Engineers, Part 2, Vol.63, March 1977, PP159-179.

46. DOTREPPE J.C., SCHNOBRICH W.C. and PECKNOLD A.

Layered Finite Element Procedure for Inelastic Analysis of Reinforced Concrete Slabs. Publications of the International Association for Bridge and Structural Engineers, Vol.33, No.2, 1973, PP53-68.

47. WANCHOO M.K. and MAY G.W.

Cracking Analysis of Reinforced Concrete Plates. Journal of the Structural Division, Proceedings of the American Society of Civil Engineers, Vol.101, No.ST1, Jan.1975, PP201-215.

48. GILBERT R.I. and WARNER R.F.

Tension Stiffening in Reinforced Concrete Slabs. Journal of the Structural Division, Proceedings of the American Society of Civil Engineers, Vol.104, No.ST12, Dec.1978, PP1885-1900.

49. KLIEN D., KRISTJANSSON R., LINK G.M., and SCHÄFER H.

Finite Element Analysis of Reinforced Concrete Slabs - Special Problems of Material Nonlinearity. 3rd Post Conference on Computational Aspects of the Finite Element Method, Imperial College, London, Sept. 1975, PP337-358.

50. LIN C.S. and SCORDELIS A.C.

Nonlinear Analysis of Reinforced Concrete Shells of General Form, Journal of the Structural Division, Proceedings of the American Society of Civil Engineers, Vol.101, No.ST3, March 1975, PP523-538.

51. LABIB F. and EDWARDS A.D.

An Analytical Investigation of Cracking in Concentric and Eccentric Reinforced Concrete Tension Members, Proceedings of the Institution of Civil Engineers, Part 2, Vol.65, March 1978, PP53-70.

52. SINISALO H.S., TUOMALA M.T.E. and MIKKOLA M.J.

Nonlinear Finite Element Analysis of Reinforced Concrete Slabs Subjected to Transient Impulsive Loading. Advances in Concrete Slab Technology, Proceedings of International Conference on Concrete Slabs, Dundee University April 1979, PP140-148, Edited by Dhir and Munday.

53. SHIRAI N. and SATO T.

Inelastic Analysis of Reinforced Concrete Shear Wall Structures - Material Modelling of Reinforced Concrete, International Association for Bridge and Structural Engineers Colloquium - Delft 1981, PP197-210 Final Report.

54. RAZQPUR A.G. and GHALI A.

Shear Lag Analysis in Reinforced Concrete; Advanced Mechanics of Reinforced Concrete, International Association for Bridge and Structural Engineers Colloquium - Delft 1981 - PP671-686, Final Report.

55. HINTON E., ABDELRHMAN H.H. and ZIENKIEWICZ O.C.

Computational Models for Reinforced Concrete Slab Systems. Advanced Mechanics of Reinforced Concrete, International Association for Bridge and Structural Engineers Colloquium - Delft 1981, PP303-313, Final Report.

56. KUPFER H., HILSDORF H.K. and RUSCH H.

Behaviour of Concrete Under Biaxial Stresses. Proceedings of the American Concrete Institute, No.66-52, August 1969, PP656-666

57. KUPFER H., GERSTLE K.H.

Behaviour of Concrete under Biaxial Stresses. Journal of the Engineering Mechanics Division, Proceedings of the American Society of Civil Engineers, Vol.99, No.EM4, Aug.1973, PP853-866.

58. TASUJI M.E., SLATE F.O. and NILSON A.H.

Stress-Strain Response and Fracture of Concrete in Biaxial Loading, Proceedings of the American Concrete Institute, July 1978, PP.306-312.

59, TASUJI M.E., NILSON A.H. and SLATE F.O.

Biaxial Stress-Strain Relationships for Concrete, Magazine of Concrete Research, Vol.31, No.109,Dec.1979, PP217-224.

60. LIU T.C-Y, NILSON A.H. and SLATE F.O.

Stress-Strain Response and Fracture of Concrete in Uniaxial and Biaxial Compression. Proceedings of the American Concrete Institute, May 1972, PP291-295.

61. NEVILLE A.M.

Properties of Concrete, Pitman, Second Edition, 1978.

62. KOTSOVOS M.D. and NEWMAN J.B.

Behaviour of Concrete Under Multiaxial Stress. Proceedings of the American Concrete Institute, Sept.1977, PP443-446.

63. VALLIAPPAN S. and DOOLAN T.F.

Nonlinear Stress Analysis of Reinforced Concrete, Journal of the Structural Division, Proceedings of the American Society of Civil Engineers, Vol.98, No.ST4, April 1972, PP885-897.

64. PHILLIPS D.V. and ZIENKIEWICZ O.C.

Finite Element Nonlinear Analysis of Concrete Structures. Proceedings of the Institution of Civil Engineers, Part 2, Vol.61, March 1976, PP59-88.

65. PHILLIPS D.V.

Nonlinear Analysis of Structural Concrete by Finite Element Method. Ph.D. Thesis, University of Wales, Swansea 1973.

66. NADAI A.

Theory of Flow and Fracture of Solids, McGraw-Hill 1950, Chapter 15 PP175-228.

67. DARWIN D. and PECKNOLD D.

Analysis of Reinforced Concrete Shear Panels under Cyclic Loading, Journal of the Structural Division, Proceedings of the American Society of Civil Engineers, Vol.102, No.ST2, Feb.1976, PP355-369.

68. ZIENKIEWICZ O.C.

The Finite Element Method. Expanded and Revised Edition, London McGraw-Hill 1977.

69. KEMP K.O.

Optimum Reinforcement in a Concrete Slab Subjected to Multiple Loading, Publications of the International Association for Bridge and Structural Engineers, Vol.31, 1971, PP93-105.

70. GUPTA A.K. and SEN S.

Design of Flexural Reinfor-ement in Concrete Slabs. Journal of the Structural Division, Proceedings of the American Society of Civil Engineers, Vol.103, No.ST4, April 1977, PP793-804.

71. MORLEY C.T.

Skew Reinforcement of Concrete Slabs against Bending and Torsional Moments, Proceedings of the Institution of Civil Engineers, Part 2, Vol.42, Jan. 1969, PP57-74.

72. KEMP K.O.

The Yield Criterion for Orthotropically Reinforced Concrete Slabs, International Journal of Mechanical Sciences, Vol.7, 1965, PP737-746.

73. SAVE M.

A Consistent Limit-Analysis Theory for Reinforced Concrete Slabs, Magazine of Concrete Research, Vol.19, No.58, March 1967, PP3-12.

74. BRONDUM-NIELSEN T.

Optimum Design of Reinforced Concrete Shells and Slabs.

Structural Research Laboratory - Technical University of Denmark, Report NR R44-1974, PP190-200.

75. CLARK L.A.

The Provision of Tension and Compression Reinforcement to Resist Inplane Forces, Magazine of Concrete Research, Vol.28, No.94, March 1976, PP3-12.

76. MORLEY C.T. and GULVANESSIAN H.

Optimum Reinforcement of Concrete Slab Elements, Proceedings of the Institution of Civil Engineers, Part 2, Vol.63, June 1977, PP441-454.

77. LENSCHOW R. and SOZEN M.A.

A Yield Criterion for Reinforced Concrete Slabs. Proceedings of the American Concrete Institute, May 1967, PP266-273,Vol.64.

78. CHEN W.F. and TING E.C.

Constitutive Models for Concrete, Journal of the Engineering Mechanics Division, Proceedings of the American Society of Civil Engineers, Vol.106,No.EM1,Feb.1979, PP1-19.

79. TAYLOR R., MAHER D.R.H. and HAYES B.

Effect of the Arrangement of Reinforcement on the Behaviour of Reinforced Concrete Slabs Magazine of Concrete Research. Vol.18, No.55, June 1966, PP85-94.

80. CLARK L.A.

Tests on Slab Elements and Skew Slab Bridges Designed in Accordance with the Factored Elastic Moment Field, Cement and Concrete Association - Technical Report 42-474, Sept.1972, PP1-47.

81. GUPTA A.K.

Skew Reinforcement in Slabs, Technical Note. Journal of the Structural Division, Proceedings of the American Society of Civil Engineers, Vol.104, No.ST8, Aug. 1978, PP1317-1321.

82. BUYUKOZTURK O.

Nonlinear Analysis of Reinforced Concrete Structures, Computers and Structures, Pergamon Press, Vol.7, 1977, PP149-156.

83. LIN C.K.

Ultimate Strength of Deep Beams, M.Sc. Thesis, Glasgow University 1979.

84. HAYES B. and TAYLOR R.

Some Tests on Reinforced Concrete Beam-Slab Panels. Magazine of Concrete Research, Vol.21, No.67, June 1969, PP113-120.

85. NEVILLE A.M., HOUGHTON-EVANS W. and CLARKE C.V.

Deflection Control by Span/Depth Ratio, Magazine of Concrete Research, Vol.29, No.98, March 1977, PP31-41.

86. FERNANDO J.S. and KEMP K.O.

The Strip Method of Slab Design - Unique or Lower Bound? Magazine of Concrete Research, Vol.27,No.90,March 1975,PP23-43.

87. HARROP J.

Ultimate Load Design of Simply Supported Slab-Beam Systems. Building Science, Vol.4, 1969, PP145-150.

88. MORLEY C.T.

Optimum Reinforcement of Concrete Slab Elements Against Combinations of Moments and Membrane Forces, Magazine of Concrete Research: Vol.22, No.72, Sept. 1970, PP155-162.

89. PRINCE M.R. and KEMP K.O.

A New Approach to the Yield Criterion of Isotropically Reinforced Concrete Slabs, Magazine of Concrete Research: Vol.20, No.62, March 1968, PP13-20.

90. JAIN S.C. and KENNEDY J.B.

Yield Criterion for Reinforced Concrete Slabs. Journal of the Structural Division, Proceedings of the American Society of Civil Engineers, Vol.100, No.ST3, March 1974, PP631-644.

91. MORLEY C.T.

Yield Criteria for Elements of Reinforced Concrete Slabs. International Conference on Plasticity, International Association for Bridge and Structural Engineers, Copenhagen 1978, PP35-47.

92. CARDENAS A.E. and SOZEN M.A.

Flexural Yield Capacity of Slabs, Proceedings of the American Concrete Institute. Vol.70, Feb.1973, PP124-126.

93. BRANSON D.E.

Deformation of Concrete Structures, McGraw-Hill, 1977.

94. NIELSEN M.P.

Limit-Analysis of Reinforced Concrete Slabs. Acta Polytechnica Scandinica, Civil Engineering Construction Series, No.26, Copenhagen 1964.

95. LENKEI P.

Contribution to the Discussion of Ref.77. Proceedings of the American Concrete Institute, Vol.64, Nov.1967, PP786-789.

96. COPE R.J. and RAO P.V.

Discussion on Ref.44, Proceedings of the Institution of Civil Engineers, Part 2, Vol.69, Sept. 1980, PP873-874.

97. COPE R.J., RAO P.V. and EDWARDS K.R.

Nonlinear Finite Element Analysis Techniques for Concrete Slabs, Proceedings of the International Conference on Numerical Methods for Nonlinear Problems, Swansea, Sept. 1980, Pineridge Press, PP445-456.

98. PARK R.

The Lateral Stiffness and Strength required to Ensure Membrane Action at the Ultimate Load of a Reinforced Concrete Slab-Beam Floor, Magazine of Concrete Research, Vol.17, No.50, March 1965, PP29-38.

99. PARK R.

Further Tests on a Reinforced Concrete Floor Designed by Limit Procedures, Cracking, Deflections and Ultimate Load of Concrete Slab Systems - Symposium, American Concrete Institute Special Publications, Sp.30-11, March 1971, PP251-269.

100 NIELSEN, M.P.

On the strength of reinforced concrete discs. Aalborg, Danmarks Ingeniørakademi Bygningsafdelingen, 1971. Bulletin No.B2.

Reprinted from: Acta Polytechnica Scandinavica, Civil Engineering and Construction Series No.70, 1969. pp254.